Mathematical Models of Thrombin Generation

Matthew Owen

November 20, 2023

Acknowledgements

First and foremost, I would like to extend my deepest gratitude to my supervisors for their continuous guidance and support, and without whom this work would not have been possible. Prof. John King, who provided both mathematical insight and valuable critique of my writing, without which I would not have seen such improvement; Prof. Etienne Farcot, who provided insight into chemical kinetic models and first introduced me to Chemical Reaction Network Theory; Prof. Alison Goodall, who helped me to improve both my biological understanding and my writing; Dr Joy Wright, who answered my many questions on the data collection methods; Prof. Edward Tuddenham, who provided insight and clarification into the relevant biochemistry; and Dr Joanne Dunster, who provided both mathematical modelling insight and helped me to manage the inter-disciplinary side of this work.

I am incredibly thankful for the support of the MRC's IMPACT DTP, for funding this research and for the training they provided. I would like to give special thanks to Dr Karen Robinson, the University of Nottingham IMPACT DTP Lead, for making me feel so welcomed into the DTP.

I am grateful for access to the University of Nottingham's Augusta HPC service, which I make use of throughout this work.

I am also grateful for the mathematical insight and critique provided by Prof. Markus Owen and Prof. Ruediger Thul during the Annual Reviews.

I would also like to thank Prof. Andrea Cangiani, Prof. Edward Hall, and Prof. Jeremy Levesley, for first sending me down this path.

Finally, I would like to thank my Mum, Nan, and Granddad, for their support throughout my life, both as a student and before; my wife, Jessica Owen, for her unwavering confidence and tolerance, particularly in these final months; and my cats, Lily and Frankie, for their emotional support.

Abstract

Thrombin generation is a key step in the formation of a blood clot. It is the only enzyme able to cleave the protein fibrinogen into fibrin, which is vital to both the structure and stability of a clot. The formation of thrombin is the result of many positive and negative feedback loops, controlled by a series of proteins called coagulation factors, whose concentrations vary both between individuals and over time. It is the combined effects of all coagulation factors that regulate both the rate and amount of thrombin that is generated.

Many models have been developed to predict the rate of thrombin generation and how it varies under differing conditions. An accurate and reliable model could prove to be a vital tool in drug development, such as for antithrombotics, and could aid in improving our understanding of both haemophilia and cardiovascular disease. However, while these models are validated qualitatively against variation in a few coagulation factors, they have rarely been validated quantitatively under variation in all factors, matching the variation seen in patient data. This sets up the key questions of this work; can any of these models accurately predict thrombin generation across variation in all coagulation factors, and if not, what changes need to be made to achieve this?

In this work, we assess the accuracy of eight existing models against coagulation data from a large cohort of donors (n=348), showing none of these models are able to reliably reproduce thrombin generation. We then conduct multiple stages of exploratory analysis, identifying which reactions, reaction rates and coagulation factors control each of the model's predictions. Most notably, we observe a large amount of uncertainty in the reaction rates used to construct these models.

We construct a new model of thrombin generation that quantifies the uncertainty in its reaction rates and addresses other issues seen in the current models. We use this new model to show that the uncertainty in these reaction rates results in high levels of uncertainty in model outputs and that the use of parameter inference methods significantly reduces this uncertainty.

We conduct a simulation study, identifying improvements in the parameter inference methods we use and test assumptions made during model development.

Finally, we outline future improvements and key next steps in the development of these models, most prominently, how to analyse and address model discrepancy and improve model specification.

Contents

Chapter 1

Introduction

1.1 Biology

1.1.1 Haemostasis

Haemostasis is the process by which blood loss is limited upon damage to a blood vessel [1, 2]. Traditionally, haemostasis was separated into four distinct stages [3].

The first of these stages is vasoconstriction, in which the blood vessel narrows as a response to being damaged. This acts as a very rapid response where the muscles in the vessel walls constrict, reducing flow and thereby limiting the amount of blood that can be lost.

The second stage, commonly called primary haemostasis, is the formation of a platelet plug. In the seconds following damage to the vessel walls, platelets bind to vWF (von Willebrand Factor) and collagen is exposed to the blood. Over the next few minutes, these platelets can be activated by, among other things, collagen, damaged red blood cells, and ADP (Adenosine DiPhosphate) released from other activated platelets. Activation of platelets results in them becoming more adhesive, and in a change in their shape from discoid to round, followed by the development of pseudopodia. These changes allow them to adhere to the vessel wall and to aggregate together with other platelets by binding to the protein fibrinogen, forming the platelet plug. If the vessel damage is small enough, then this is sufficient to stop blood loss. For larger damage, it is necessary for coagulation to take place.

Coagulation, the third stage, involves a series of enzymatic reactions, initiated by collagen and Tissue Factor (TF), a protein present on the surface of sub-endothelial cells, which is exposed to the blood upon damage to the vessel wall. The goal of coagulation is to activate prothrombin into thrombin, which is able to cleave fibrinogen into fibrin monomers, which then bind together forming long fibrin polymers. These fibrin polymers, through cross-linking by factor XIII, form a complex fibrin mesh, trapping red blood cells and platelets, stabilising the platelet plug, and further reducing blood loss. Coagulation begins almost immediately upon damage to the vessel wall. However, this process takes multiple minutes to build up sufficient amounts of thrombin for a response to be noticeable

and is typically complete after around 30 minutes.

The final stage of haemostasis is fibrinolysis, which governs the breakdown of the formed clot. It also consists of a series of enzymatic reactions, although a much smaller system than for coagulation, which culminate in the production of the enzyme plasmin that is able to cleave fibrin, thus breaking the clot over the following couple of hours.

1.1.2 The Coagulation Cascade

The coagulation cascade consists of many protein-protein interactions culminating in the formation of fibrin.

The cascade model of coagulation remains similar in structure to the one originally proposed in 1964 [4, 5]. It consists of two pathways leading to thrombin activation, the extrinsic pathway which covers the reactions initiated by tissue factor, and the intrinsic pathway for the reactions resulting from contact activation. A simplified layout of the reactions in the coagulation cascade is given in Figure 1.1.

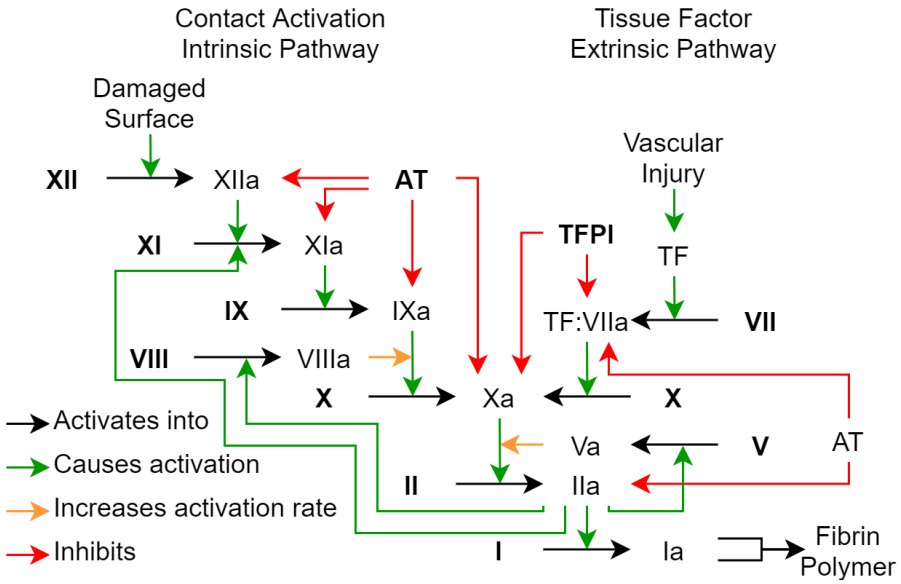

Figure 1.1: A network diagram demonstrating a basic form of the coagulation cascade for both tissue factor activation and contact activation as well as inhibitions caused by Antithrombin (AT) and Tissue Factor Pathway Inhibitor (TFPI). Factors present in the blood prior to coagulation are given in bold. Two or more fibrin monomers (FIa) can join together to form fibrin polymers. Acronyms are described in Table 1.1.

The most relevant proteins in the coagulation cascade are the coagulation factors, a collection of serine proteases and cofactors, with each protein given a roman

numeral, with an "a" appended to their name to denote the active form*. These are proteins, present in the blood plasma, six of which are serine proteases (factors II, VII, IX, X, XI, and XII) while the two cofactors are named factor V and factor VIII. In addition to these factors, there are two prominent inhibitors, a general inhibitor Antithrombin (AT) which inhibits all the serine proteases and a specific inhibitor Tissue Factor Pathway Inhibitor (TFPI) which inhibits only FXa and TF:VIIa. The names and their corresponding abbreviations are given in Table 1.1.

Names	Abbreviation
Tissue Factor	TF
Fibrinogen (Fibrin)	FI (FIa)
Prothrombin (Thrombin)	FII (FIIa)
Meizothrombin	mIIa
Factor V (Factor Va)	FV (FVa)
Factor VII (Factor VIIa)	FVII (FVIIa)
Factor VIII (Factor VIIIa)	FVIII (FVIIIa)
Factor IX (Factor IXa)	FIX (FIXa)
Factor X (Factor Xa)	FX (FXa)
Factor XI (Factor XIa)	FXI (FXIa)
Factor XII (Factor XIIa)	FXII (FXIIa)
Factor XIII (Factor XIIIa)	FXIII (FXIIIa)
Tissue Factor Pathway Inhibitor	TFPI
Antithrombin	AT
Protein C (Activated Protein C)	PC (APC)
Protein S	PS
von Willebrand Factor	vWF
Prothrombinase	Xa:Va
Extrinsic Tenase	TF:VIIa
Intrinsic Tenase	IXa:VIIIa

Table 1.1: The names and abbreviations for the proteins and complexes in the coagulation cascade.

After exposure of TF to these proteins in the blood plasma, FVIIa rapidly binds to TF to form the TF:VIIa complex. This TF:VIIa activates small amounts of FX into FXa which in turn activates FII (prothrombin) into FIIa (thrombin). This newly activated FIIa then begins a series of feedback loops, activating the serine protease FXI and the two cofactors FV and FVIII. FXIa begins activation of FIX to FIXa, which then binds to its cofactor FVIIIa to form the intrinsic tenase complex (IXa:VIIIa), increasing the rate of FIXa activation of FX. This large burst of FXa, along with its cofactor FVa, forms the prothrombinase complex (Xa:Va), which results in the rapid activation of large amounts of prothrombin into thrombin. As the system begins to deplete its levels of these coagulation factors, inhibition begins to take over, with sufficient levels of AT to inhibit all coagulation

*For notation, we will commonly write FV instead of Factor V. We also drop the F/Factor when describing complexes, like Xa:Va, or when writing out reactions.

factors.

1.1.3 The Cell-Based Model of Haemostasis

If these reactions occurred in solution, then the coagulation cascade would be an accurate description of the dynamics. However, many of these reactions occur on surfaces. This led to the proposal of a cell-based model of haemostasis [6], in which haemostasis occurs in three overlapping phases. In the first phase, initiation, coagulation begins on TF-bearing cells where factors Xa and IIa bind and are activated. The second phase, amplification, is where the small amounts of thrombin that were activated on the TF-bearing cells, move to and activate platelets. This phase contains the feedback for activation of FV and FVIII, that both bind to platelet surfaces, and FXI which is activated in solution. The third phase, propagation, is where the large amounts of thrombin generated lead to the formation of the fibrin mesh, which is cross-linked by FXIII, stabilising the clot. These three stages are demonstrated in Figure 1.2.

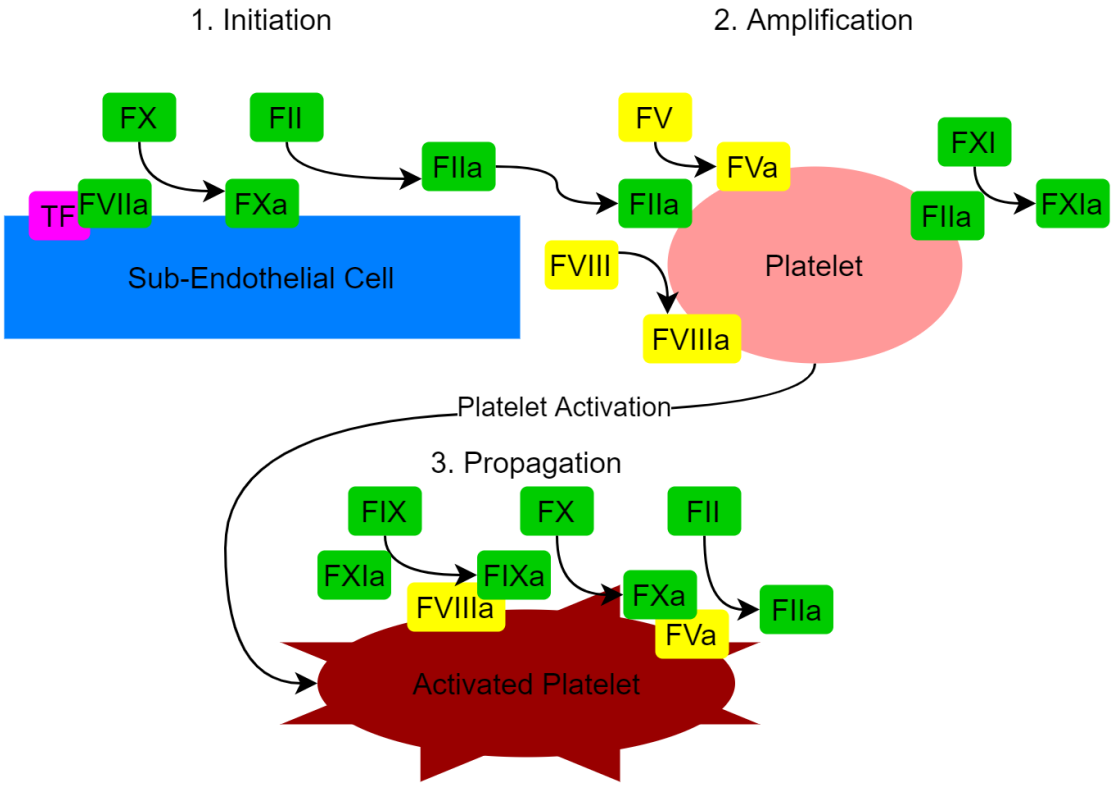

Figure 1.2: An overview of the cell-based model of haemostasis.

1.1.4 Phospholipids

Phospholipids make up the majority of the cell membrane [7]. Each phospholipid consists of a hydrophilic head and two hydrophobic tails. As shown in Figure 1.3, these phospholipids are grouped together in the cell membrane as a bilayer

with the hydrophilic heads pointing outwards and the hydrophobic tails pointing inwards. There are five key phospholipid groups, named based on the amino acid in their head group, phosphatidylethanolamine (PE), phosphatidylcholine (PC), phosphatidylglycerol (PG), phosphatidylinositol (PI) and phosphatidylserine (PS). PS and PE have negatively-charge head groups and are normally found on the inside of the cells. However, activated platelets, and membrane-bound microvesicles released from activated platelets and other cells, carry these negatively-charged phospholipids on the outside of their membranes, and this provides a surface for the coagulation factors to bind, accelerating their activation. When coagulation is measured in experimental laboratory assays, a phospholipid reagent comprising a mixture of phosphatidylcholine (PC) and the negatively charged phosphatidylserine (PS), typically shortened to PCPS, is frequently used in the form of phospholipid vesicles. These phospholipids provide a surface for many reactions in the coagulation cascade and are necessary for the prothrombinase complex which forms on negatively charged phospholipids like phosphatidylserine.

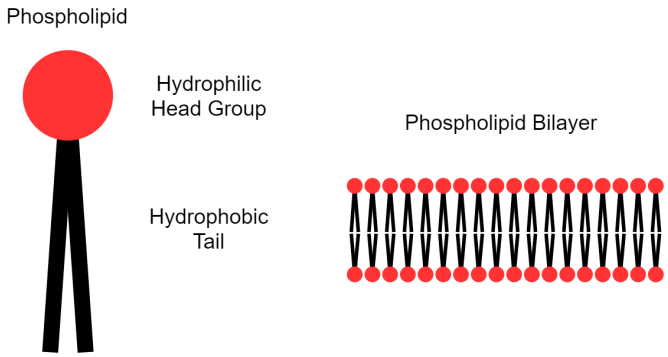

Figure 1.3: A demonstration of the phospholipid and bilayer structure.

1.1.5 Contact Activation

Factor XII can be activated in many ways with the two most prominent methods being contact with collagen at the site of vessel damage *in vivo* or activation through contact with a negatively charged surface *in vitro* [8]. This activated factor FXIIa then activates prekallikrein that then in turn activates more FXIIa resulting in a positive feedback loop for FXIIa activation. Factor XIIa is able to begin coagulation through its activation of FXI, beginning the intrinsic pathway. Historically, contact activation was thought of as the main method of coagulation activation *in vivo*. However, this has since shifted towards activation by TF with the role of FXIIa currently being questioned [9].

1.1.6 α-Inhibitors

There are a group of proteins we refer to here as the α inhibitors. These are the proteins α_1-Anti-Trypsin, α_2-Macroglobulin and α_2-Anti-Plasmin. These proteins are inhibitors of coagulation, ($\alpha_1 - AT$ inhibits FIIa, FXa, and FXIa; $\alpha_2 - M$

inhibits FIIa and FXIIa; $\alpha_2 - AP$ inhibits FXIa and FXIIa), however, they are not typically covered in descriptions of the coagulation cascade as they serve other roles outside of coagulation, most prominently in fibrinolysis.

1.1.7 Protein C

Protein C is a serine protease, however, unlike the other serine proteases in the coagulation cascade, it serves as an inhibitor of coagulation. Protein C, like the other proteases, circulates in the plasma in its zymogen form. It is activated by the surface-bound thrombin-thrombomodulin (IIa:TM) complex. As demonstrated in Figure 1.4, activation of protein C presents a strong negative feedback loop in the system in which high levels of thrombin results in high levels of activated protein C which inhibits the cofactors FVa and FVIIIa through cleavage, reducing the rate of activation of thrombin. Protein C is also able to increase its rate of inhibition through its cofactor protein S, however, unlike the cofactors FVa and FVIIIa, protein S does not need to be activated to inhabit its cofactor role.

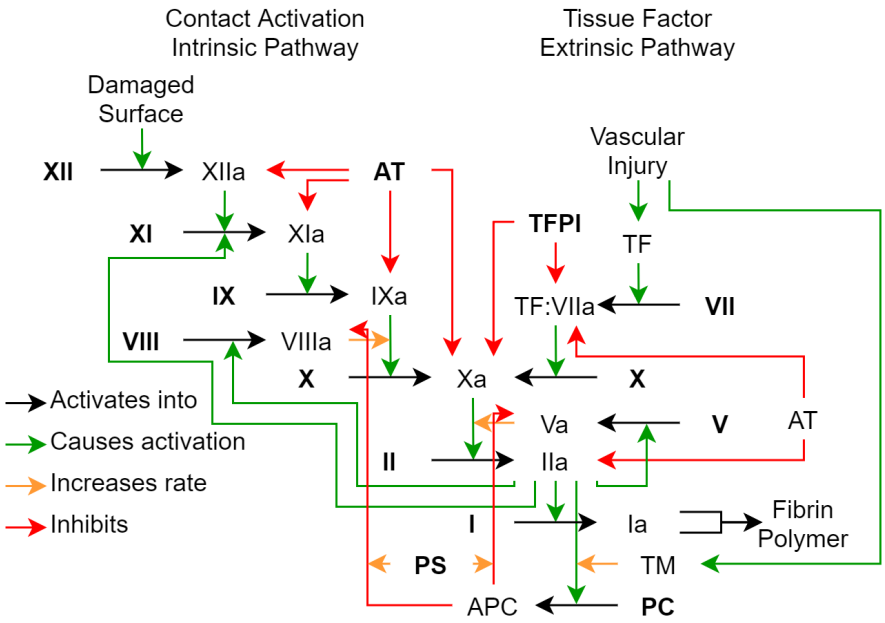

Figure 1.4: A network diagram demonstrating the coagulation cascade including the reactions for protein C. Factors present in the blood prior to coagulation are given in bold. Two or more fibrin monomers (FIa) can join together to form fibrin polymers. Acronyms are described in Table 1.1.

1.1.8 Clotting Measurements

Historically, the ability of an individual's blood to clot was measured using two clotting assays. The first, called a Prothrombin Time test (PT) [10], measures the function of the extrinsic system through the addition of TF to a patient's plasma and is measured as the time for the blood to clot (typically around 11-15 seconds). The second test, called an Activated Partial Thromboplastin Time test (aPTT or

PTT) [11], measures the intrinsic system similarly through addition of kaolin to activate FXII.

While these two assays have been, and are still routinely used in hospitals to check whether patients have a risk of bleeding, for example before they undergo surgery, they only measure ∼5% of the thrombin that is generated in the blood; enough to initiate coagulation. In recent years the Thrombin Generation Assay has been developed that measures the total amount of thrombin that can be generated in the blood plasma. While not yet used clinically, this assay monitors thrombin concentration over time. This gives a thrombin generation curve which is typically summarised using four key summary statistics: peak concentration, ttP (time to peak), lagtime (the time taken to reach 5% of the peak thrombin concentration[†]), and ETP (endogenous thrombin potential) which is the integral of the thrombin generation curve over the time-course of the thrombin generation assay [12]. These summary statistics are demonstrated in Figure 1.5, in addition to two other summary statistics we will make use of, the maximum increasing rate and minimum decreasing rate (most negative) of the thrombin concentration.

This assay can be performed using two similar methods. In the first of these [13], a chromogenic substrate, which is activated by thrombin, is added and the thrombin concentration at a given time is determined by measuring the levels of this chromogenic substrate. The activated chromogenic substrate concentration is measured as Optical Density[‡] which is proportional to its molar concentration. Due to the law of mass action, the thrombin concentration is proportional to the derivative of the molar concentration of activated chromogenic substrate and therefore proportional to the derivative of Optical Density. This results in ETP being proportional to the final value of the Optical Density curve. However, thrombin that has been inhibited by $\alpha_2 - M$ is still able to activate this chromogenic substrate. This makes measurements of free thrombin more complicated. The amount of IIa:$\alpha_2 - M$ can be determined at the end of the assay as only IIa:$\alpha_2 - M$ will activate the substrate, this effect can then be quantified and after accounting for the thrombin concentration over time, its effect can be removed from the whole time course. This form of the assay requires platelets to be removed beforehand and the formation of the fibrin mesh to be stopped.

The second method uses a fluorogenic substrate which is not affected by the presence of $\alpha_2 - M$ and, because it does not rely on the transmission of light through the reaction mixture, it can measure thrombin generation in plasma both in the presence of platelets and if fibrin is allowed to clot the blood. However, the fluorescent signal cannot be simply converted into a measurement of thrombin concentration. To resolve this, the fluorogenic substrate is added to a separate thrombin sample with a known and constant concentration and measured in par-

[†]Many sources use slightly different measures to find a lagtime summary statistic such as time to 2% or 5% of peak value or time to 2nM FIIa concentration.

[‡]Optical Density is measured by shining a light source on the sample. The activated chromogenic substrate has revealed chromophores which will absorb the light, and re-emit it at a particular wavelength. The Optical Density is a measurement of the intensity of the light at this wavelength.

allel with the samples being analysed. This method is known as a Calibrated Automated Thrombogram (CAT).

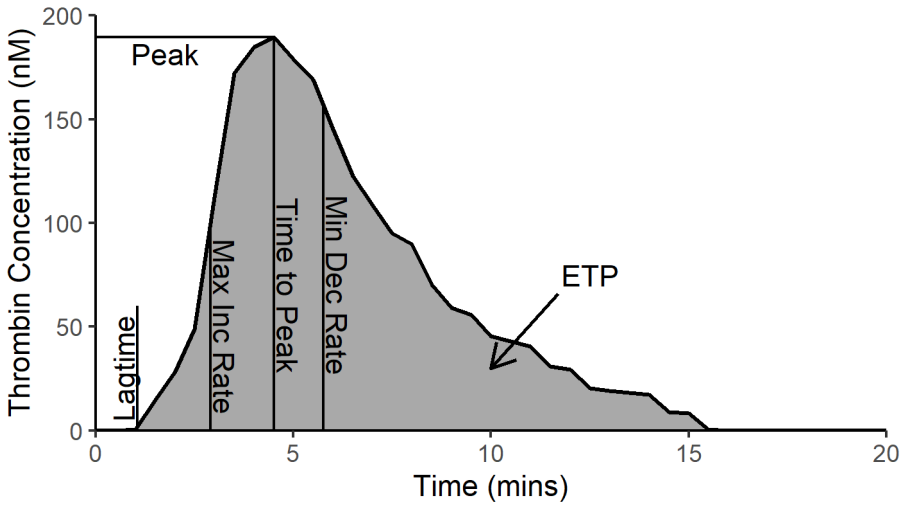

Figure 1.5: An example thrombin generation assay curve labelling the key summary statistics used for describing a thrombin generation curve.

1.1.9 Coagulation Disorders

Coagulation disorders are normally split into two groups, hypercoagulable disorders, also called thrombophilia, which results in excessive clotting and can lead to heart attacks and strokes, and bleeding disorders.

Hypercoagulable disorders [14] come from either genetic defects in key coagulation factor genes resulting in conditions, such as factor V Leiden [15], in which a single point mutation in factor V renders it no longer able to be inhibited by protein C, or variations in the FII gene that lead to higher levels of prothrombin, or reduced concentrations of inhibitors, namely antithrombin, protein C, or protein S.

While these deficiencies and mutations collectively affect around 0.4% of the general population [14], heart disease and strokes are the two leading causes of death worldwide, accounting for over a quarter of all deaths in 2019 (16% and 11% respectively), both of which are caused by blood clots blocking blood vessels [16].

A common type of bleeding disorder is haemophilia, split into three different types: haemophilia A (deficiency in FVIII), haemophilia B (deficiency in FIX), and haemophilia C (deficiency in FXI) [17]. There are also other bleeding disorders caused by deficiencies in other coagulation factors, including FX and FV as well as deficiency of von Willebrand Factor [18], which acts as a carrier for FVIII in the blood, protecting it from being degraded.

Haemophilia affects a smaller proportion of the population (around 0.3% of newborn males) with haemophilia A being the most common [19]. Unfortunately,

mortality rates for those diagnosed with haemophilia are increased by 40% relative to the general population [20], even with recent improvements in treatment [17].

1.1.10 Data

In this work, we make use of a large coagulation data set [21] measured on the PRAMIS (Platelet Reactivity And Myocardial Infarction Study) cohort [22]. These data are from 162 patients who suffered a myocardial infarction before the age of 50 and 186 age, sex and smoking-status matched healthy controls. Laboratory analysis of plasma samples from each of these individuals provided measurements of the level of the coagulation factors (factors I, II, V, VII, VIII, IX, X, XI, and XII), the inhibitors (AT, protein C, protein S, and TFPI), the key haemostatic proteins TF and vWF, as well as the output from a thrombin generation assay (both ETP and Optical Density curves), and a handful of health related measures (concentration of low and high density lipoproteins, concentration of C-reactive protein, and demographic data on each individual such as age, sex, smoking status, etc.). Figure 1.6 gives histograms of the coagulation factors and inhibitors, as well as a plot demonstrating the variance in the Optical Density curves throughout the data set. The concentrations of the coagulation factors vary across a wide range between individuals and thrombin generation provides a response as a combination of all of these factors.

Thrombin generation was measured in platelet-poor plasma using a chromogenic substrate, Pefachrome TG, with the addition of a small peptide that prevents the cross-linking of fibrin, allowing the plasma to remain clear (unclotted) to allow the passage of light to the photoreceptor in the analyser. Phospholipid was added to each sample as well as 2mM calcium chloride to initiate the coagulation reaction and each plasma sample was analysed with and without the addition of 5pM exogenous TF. This produces the measured Optical Density curves and ETP, both of which are recorded relative to a 20-donor pooled plasma sample, which provides a standard to compare against, reducing inter-assay variability. Both the Optical Density curves and the measured ETP for each individual are expressed as a percentage of the pooled plasma ETP, given as the final value of the OD curve. The concentrations of FII, FV, FVII, FVIII, FIX, FX, FXI, FXII, AT, protein C, protein S, and vWF were also all given as a percentage of the 20-donor plasma pool. The concentration of endogenous TF[§] was reported in pM, TFPI was given in Units/ml (a measure of activity), and fibrinogen is given in g/L. Where patient-level factor concentrations were missing, they were assumed to be at a healthy reference concentration.

[§]This TF is not present normally in the blood stream but is instead a result of the venepuncture during sample collection.

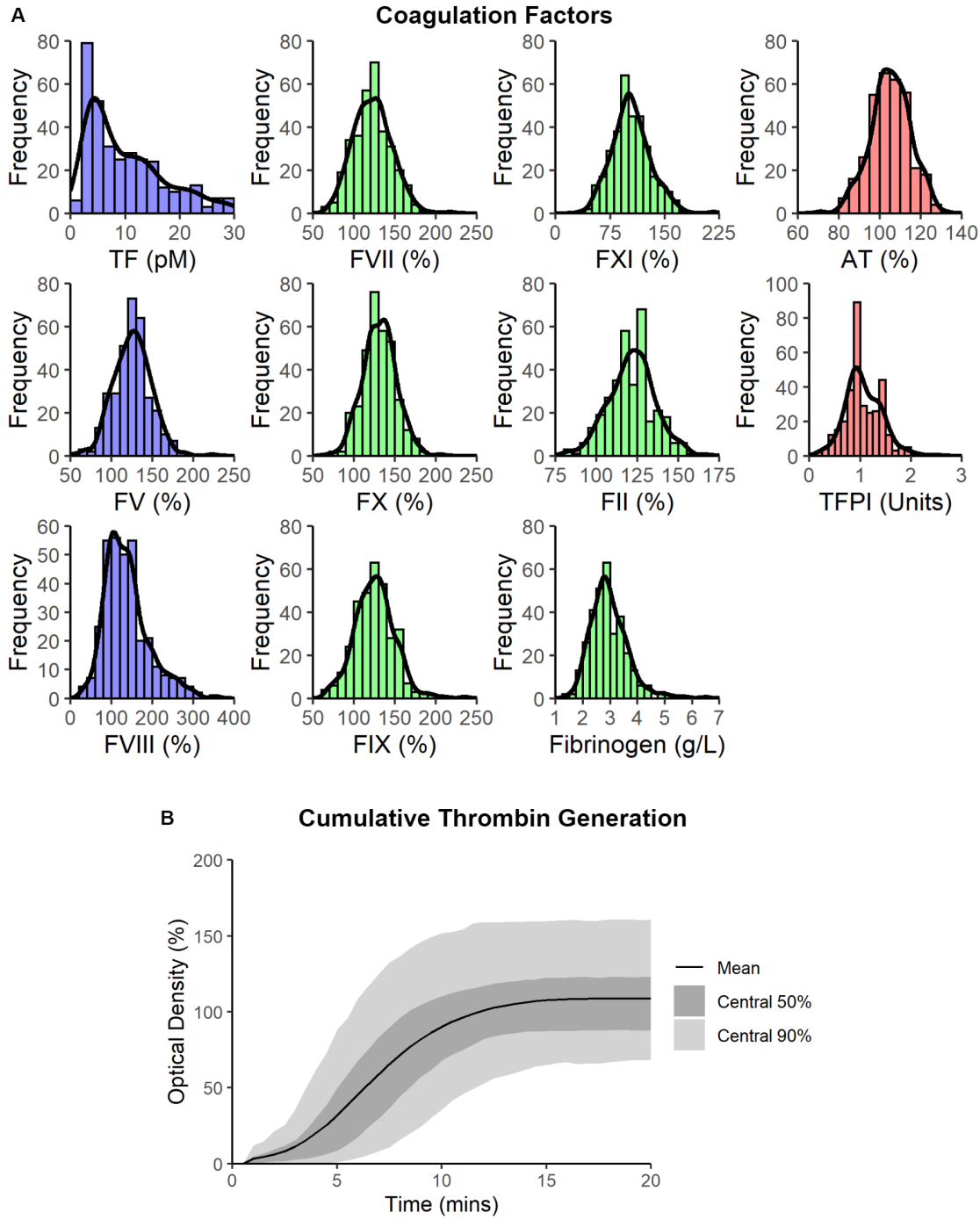

Figure 1.6: A: Histograms of the coagulation factor concentrations at the start of the thrombin generation assay. Where units are expressed as percentages, they are given compared to the 20-donor plasma pool. B: The mean Optical Density curves across the patients for the with added Tissue Factor data cut. The central 50% and 90% regions are also given (using the 5th, 25th, 75th, and 95th percentiles).

1.2 Mathematical Modelling

Thrombin generation can be modelled through chemical reaction networks. These models produce a system of ODEs (Ordinary Differential Equations), for a given

set of chemical reactions and reaction rates, which describe how the concentrations of each species in the system changes over time. This system of ODEs can then be solved numerically, for a given set of initial concentrations, to model the dynamics of the system.

Here, we present a formalisation of the process for generating these ODEs through Chemical Reaction Network Theory, followed by a short introduction of two mathematical modelling techniques we later make use of in Section 2.7.

1.2.1 Chemical Reaction Networks

A chemical reaction network is given by $N = (S, C, R)$, where S is the set of n species in the network, C is the set of combinations of species that appear in the network represented as vectors of length n, and $R \subset C \times C$ is the set of reactions in the network consisting of ordered pairs (C_i, C_j) representing the reaction which goes from combination C_i to C_j [23].

Rate Law

The rate law gives a description of how each species in the network should change over time based of the reactions it is involved in. Each reaction, $C_i \to C_j$, has a rate constant $k_{i,j}$ and occurs with reaction rate $\kappa_{i,j} = k_{i,j} \prod_{m=1}^{n} s_m^{\alpha_{i,j,m}}$ where $s_m \in S$ and $\alpha_{i,j,m} \in \mathbb{N}_0$. This gives us:

$$\frac{dS}{dt} = \sum_{C_i \to C_j \in R} \kappa_{i,j} Y_{i,j}$$

where $Y_{i,j}$ denotes the reaction vector $C_j - C_i$.

Law of Mass Action

The law of mass action is the most common rate law applied in chemical reactions [24]. In mass action kinetics, the values of $\alpha_{i,j,m}$ are set as the stoichiometric coefficient for species m in combination C_i. This results in the rate of reaction, $\kappa_{i,j}$, being proportional to the product of the concentrations of the reactants.

Example

Consider a system consisting of four species, A, B, C, and D, with the following reactions:

$$A + B \to A + 2C, \;\; C + D \to A + C, \;\; A + 2C \to B + C$$

Converting this system into the form $N = (S, C, R)$ gives:

$$S = \{A, B, C, D\},$$

$$C = \{A + B, A + 2C, C + D, A + C, B + C\},$$
$$R = \{(A + B, A + 2C), (C + D, A + C), (A + 2C, B + C)\}$$

If this system is assumed to follow the mass action rate law, with reaction rates p, q, and r for the reactions $A+B \to A+2C$, $C+D \to A+C$, and $A+C \to B+C$, respectively, we can derive the ODEs given as follows:

$$\begin{aligned}
\frac{dA}{dt} &= qCD - rAC^2 \\
\frac{dB}{dt} &= -pAB + rAC^2 \\
\frac{dC}{dt} &= 2pAB - rAC^2 \\
\frac{dD}{dt} &= -qCD
\end{aligned}$$

Michaelis Menten Kinetics

A typical enzymatic reaction for an enzyme E converting a substrate S into the product P through the intermediate step of a complex C is defined as $E + S \underset{k_-}{\overset{k_+}{\rightleftharpoons}} C \overset{q}{\to} E + P$. Following mass action kinetics, this gives us the following system:

$$\begin{aligned}
\frac{dE}{dt} &= k_-C - k_+ES + qC \\
\frac{dS}{dt} &= k_-C - k_+ES \\
\frac{dC}{dt} &= k_+ES - k_-C - qC \\
\frac{dP}{dt} &= qC
\end{aligned}$$

This system can be simplified into a single reaction by assuming that $\frac{dC}{dt} = 0$. The steps in this simplification are given below, where $K_m = \frac{q+k_-}{k_+}$ and $E_T = E+C$ is the total concentration of the enzyme E.

$$k_+ES = (k_- + q)C = k_+(E_T - C)S \Rightarrow C = \frac{k_+E_TS}{q + k_- + k_+S} = \frac{E_TS}{K_m + S}$$

This gives us a direct reaction from S to P with Michaelis Menten [25, 26] rate $\frac{dP}{dt} = -\frac{dS}{dt} = \frac{qE_TS}{K+S}$.

Further Approximations

We now demonstrate two approximations that can be applied to Michaelis Menten kinetics, the first of which is frequently used in mathematical models for thrombin generation.

If $S << K_m$, then we can simplify the rate to $\frac{q}{K_m} E_T S$ which is equivalent to a mass action law reaction of $E + S \overset{\frac{q}{K_m}}{\rightarrow} E + P$. This approximation is used very frequently in the published models.

The other approximation is for the case of $S >> K_m$, or over-saturation of species S. In this case the rate simplifies to qE_T and is independent of the concentration of S.

Michaelis Menten with Competitive Inhibition

An aspect of chemical kinetics that the Michaelis Menten rate law does not capture is competitive inhibition. This is where the enzyme is bound to one substrate and therefore cannot bind to another to begin activation. This effect can be modelled into the rate law with a simple modification, however. For the enzymatic reaction $S \overset{E}{\rightarrow} P$, where enzyme E can also activate, and therefore bind to, species I_i, we scale the parameter K_m by the constant $1 + \sum_i I_i/K_i$ where $K_i = \frac{k_-}{k_+}$ is the ratio of the backwards and forwards binding rates for species I_i [27, 28].

Standard Notation

For enzymatic reactions cleaving substrate S into product P through enzyme E with intermediate complex E:S, we denote them either in mass action form $E + S \leftrightarrow E{:}S \rightarrow E + P$ with k_+ to represent the forwards association rate, k_- to represent the backwards disassociation rate and k_{cat} to represent the rate of complex $E : S$ releasing product P, or in the Michaelis Menten form $S \overset{E}{\rightarrow} P$ specified by reaction rate parameters $K_m = \frac{k_- + k_{\text{cat}}}{k_+}$ and k_{cat}.

For reversible reactions between two species A and B, we denote them by a reaction $A + B \leftrightarrow A{:}B$ where A:B denotes the complex of A and B and the reaction rates k_+ and k_- are used to denote the forwards association and backwards disassociation rates, respectively. We may also summarise this reaction with the rate $K_d = \frac{k_-}{k_+}$.

1.2.2 Nondimensionalisation

Nondimensionalisation is the process of removing physical dimensions from a system through variable substitution. Each variable is separated into two constituent parts, consisting of a dimensional scaling constant and a dimensionless variable. By carefully choosing the values for these dimensional scaling constants (taking

them to be functions of parameters in the model), we can reduce the number of parameters in the model while maintaining the same dynamics. Typically, the dimensional scaling constants are chosen to either reduce the number of parameters by as much as possible, set all variables to be $O(1)$, or some combination of the two.

The Buckingham π theorem [29] states that at least p parameters can be removed through nondimensionalisation where p is the number of linearly independent dimensions in the system. For the purposes of our work $p = 2$, with the fundamental dimensions being time (typically expressed in seconds) and count (typically expressed in moles), coming from the units of the reaction rates, s^{-1} and $M^{-1}s^{-1}$ for mass action kinetics and s^{-1} and M for Michaelis Menten kinetics.

1.2.3 Timescale Analysis

Timescale analysis is the process of separating the dynamics of a model or system into timescales, such that reduced sub-models can accurately predict the dynamics of the full model on their corresponding timescale. The sub-models can then be more easily analysed due to their smaller size. This is typically done through asymptotic analysis and has been performed previously on a model of thrombin generation [30].

The process by which a model is separated into timescales is given as follows. First, the model is nondimensionalised aiming for all variables to be O(1). A small dimensionless parameter ε is then introduced as some function of the dimensionless parameters in the system. All dimensionless parameters then have some power of ε taken out as a factor, resulting in a product between a power of ε and an O(1) dimensionless parameter. The model can then be solved on separate timescales given by the various powers of ε using methods from Perturbation Theory [31, 32, 33].

1.3 Statistics

In this section, we outline the statistical and data analysis methods we make use of for this work. We begin by giving an overview of the performance metrics we use to evaluate model predictions against patient data. We then give a short introduction to Bayesian statistics, before introducing the two parameter inference methods we use, gradient descent with the interior point algorithm and Approximate Bayesian Computation (ABC). The final methods we use to analyse the models are two methods in uncertainty quantification, forward propagation of uncertainty and sensitivity analysis. Finally, we detail the data analysis methods we use. These are principal component analysis and the varimax transformation, k-means clustering using the Gap statistic, regression trees and the Gini index, and functional data analysis.

1.3.1 Performance Metrics

For the majority of this work, we make use of two metrics for comparing model predictions to patient level ETP. The model predictions for ETP are reported in $nM \cdot min$ while patient level ETP is reported as a percentage of pooled plasma ETP. In order to compare between these two units, we make use of two transformations, one linear and one affine (linear plus a constant). A linear relationship is expected, since both an ETP of 0 in both units, would only occur if no thrombin was generated. A affine relationship is included compare without the need for the assumption of a linear relationship.

The first metric we use to compare these values is R^2, given by Equation (1.1), where $\hat{y}$ is given by the line of best fit (an affine transformation, the line $y = mx+c$ where m and c minimise the sum of squared errors, y represents the experimental ETP measurement in % of pooled plasma, and x represents the model-derived ETP in $nM \cdot min$). This gives a dimensionless value between 0 (no linear correlation) and 1 (perfect linear correlation). Values above 0.7 are commonly considered to represent a high level of correlation while values below 0.4 are commonly considered to represent a low level or weak correlation.

$$R^2 = 1 - \frac{\sum_i (y_i - \hat{y}_i)^2}{\sum_i (y_i - \bar{y})^2} \tag{1.1}$$

The second metric we use is Root Mean Squared Error (RMSE), given by Equation (1.2), where $\hat{y}$ is given by the line of proportionality (a linear transformation, the line $y = mx$ where m minimises the sum of squared errors). This gives a value in the same units as y that can be considered as an measure of the average error in predictions.

$$\text{RMSE} = \sqrt{\frac{\sum_{i=1}^{n} (\hat{y}_i - y_i)^2}{n}} \tag{1.2}$$

Other metrics, such as those to compare model predicted OD curves and patient level OD curves, are to be introduced later in Chapter 3.

1.3.2 Bayesian Statistics

In frequentist statistics, parameters are thought of as having true values which we try to approximate. However, in Bayesian statistics parameters are thought of as random variables with an unknown distribution. This allows us to consider a probability distribution for a parameter θ, $\pi(\theta)$, called a prior. This is the distribution which summarises our current beliefs about θ. We can then update these beliefs with some new data y to get the posterior distribution $\pi(\theta \mid y) = \frac{p(y|\theta)\pi(\theta)}{m(y)}$ where $p(y \mid \theta)$ is the probability model for the likelihood of the data y given the parameter θ and $m(y)$ is the marginal density function of the data y. Given that $m(y)$ is typically intractable, it is sufficient to note that $\pi(\theta \mid y) \propto p(y \mid \theta)\pi(\theta)$

since $\pi(\theta \mid y)$ is a probability distribution.

The benefit of treating parameters as probability distributions rather than point values is that it allows us to easily encode information about uncertainty into the prior distribution of the parameter and also assess how this uncertainty is changed through posterior distributions.

1.3.3 Parameter Inference

Parameter inference is the method by which parameters are optimised to best fit a data set. It generally consists of defining a cost function, which measures the error between model predictions and the data set, which is then optimised, possibly under some constraints or conditions. We make use of two methods, both introduced here, gradient descent with the interior point algorithm and Approximate Bayesian Computation - Sequential Monte Carlo.

Gradient Descent

Gradient Descent is a simple but powerful parameter inference method. It consists of beginning at an initial point in parameter space and calculating the gradient of the cost function at that point, typically by finite differences. We then move from the initial point in the direction opposite of the gradient, with step size proportional to the magnitude of the gradient, to achieve a lower cost. This process is then repeated, typically until the magnitude of the gradient is sufficiently small.

There are many alterations to the basic premise of gradient descent, such as line search [34], stochastic gradient descent [35], and gradient descent with momentum [36]. We will make use of an alteration called the interior point algorithm [37]. This algorithm allows us to specify upper and lower bounds. In the case relevant to our work in Chapter 3 and onward, where all parameters (reaction rates) need to remain positive, the cost function $f(x)$ is replaced by the barrier function $B(x, \mu)$ given by Equation (1.3). This barrier function is then minimised using gradient descent and after each iteration, the barrier parameter μ is decreased towards zero. As shown in Figure 1.7, the barrier function increases rapidly as any of the parameters x_i approach zero, however, as the barrier parameter μ approaches zero, the barrier function approaches $f(x)$ $\forall x > 0$ and therefore represents its local minimums accurately.

$$B(x, \mu) = f(x) - \mu \sum_i \log(x_i) \tag{1.3}$$

For upper bounds, and also non-zero lower bounds, we apply a transform on the parameters to map the position of the bound to result in an infinite cost from the barrier function. To achieve this, for an upper bound of a, we include the term $-\mu \log(a - x_i)$ into the barrier function. For a non-zero lower bound of b, we include the term $-\mu \log(x_i - b)$ into the barrier function.

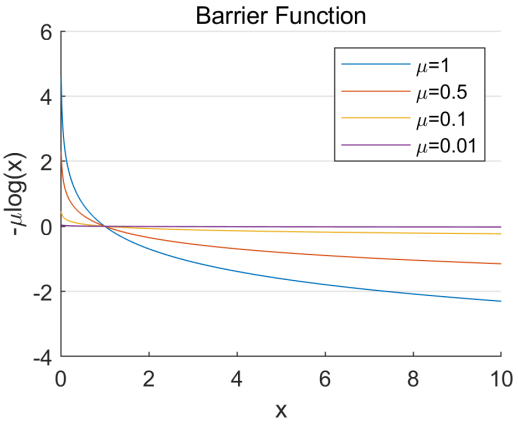

Figure 1.7: A plot of the barrier function $-\mu \log(x)$ for varying values of μ.

Approximate Bayesian Computation

Approximate Bayesian Computation (ABC) methods [38] aim to approximate the posterior distribution in situations where the likelihood function $p(y|\theta)$ is too computationally expensive to evaluate. This approximation is achieved by replacing the likelihood function with a comparison between simulated and observed data. The general steps of an ABC algorithm are as follows:

1. Sample a particle (parameter or parameter vector) of θ^* from the prior $\pi(\theta)$
2. Generate a simulated data set y^* based on the parameter θ^*
3. Compare the simulated data set y^* with the observed data y_0 through the use of a distance function $d(y_0, y^*)$. If $d(y_0, y^*) < \epsilon$ then accept θ^*, where ϵ is a given tolerance.

This allows us to sample from the distribution $\pi(\theta \mid d(y_0, y^*) < \epsilon)$ which should give a good approximation of $\pi(\theta \mid y_0)$ for sufficiently small ϵ. The distance metric is commonly defined using a set of summary statistics and evaluates the distance between the summary statistics of the simulated data set and that of the observed data set.

ABC Rejection Sampler

The ABC Rejection Sampler [38] is the simplest ABC algorithm and is defined in Algorithm 1.

The ABC Rejection Sampler has a very low acceptance rate if the prior and the posterior are very different and so it struggles with uninformative priors.

ABC Markov Chain Monte Carlo

The ABC-MCMC algorithm [38] aims to avoid the issues from the ABC Rejection Sampler for uninformative priors by instead using a proposal distribution $q(\theta|\theta_i)$

Algorithm 1: ABC Rejection

Input: Number of particles N, prior π, model simulator l, data y and tolerance ϵ.
Output: A set of sampled particles Θ.
for *i=1:N* **do**
  while *True* **do**
    $\theta^* \sim \pi(\cdot)$;
    $y^* \sim l(\cdot|\theta^*)$;
    if $d(y, y^*) < \epsilon$ **then**
      $\Theta(i) = \theta^*$;
      break;
    end
  end
end

to form a Markov chain of parameters and is defined in Algorithm 2.

Algorithm 2: ABC-MCMC

Input: Initial estimate θ_1, number of particles N, proposal distribution $q(\theta|\theta_i)$, prior π, model simulator l, data y and tolerance ϵ.
Output: A set of sampled particles Θ.
$\Theta(1) = \theta_1$;
for *i=1:N* **do**
  $\theta^* \sim q(\theta|\Theta(i))$;
  $y^* \sim l(\cdot|\theta^*)$;
  if $d(y, y^*) < \epsilon$ **then**
    $\alpha = \min\left(1, \frac{\pi(\theta^*)q(\Theta(i)|\theta^*)}{\pi(\Theta(i))q(\theta^*|\Theta(i))}\right)$;
    if $rand() < \alpha$ **then**
      $\Theta(i+1) = \theta^*$;
    else
      $\Theta(i+1) = \Theta(i)$;
    end
  else
    $\Theta(i+1) = \Theta(i)$;
  end
end

This gives us a Markov chain with a stationary distribution of $\pi(\theta \mid d(y_0, y^*) < \epsilon)$. The two main disadvantages of ABC-MCMC are that the sampled parameters are heavily correlated with one another and that the algorithm can get stuck in areas of low probability for a long time as θ_{i+1} can only change if we have that $d(y_0, y^*) < \epsilon$.

ABC Sequential Monte Carlo

In ABC-SMC [38], we have a list of tolerances $\epsilon_1, \ldots, \epsilon_T$ such that $\epsilon_1 > \ldots > \epsilon_T > 0$ and take a sample of N particles for each ϵ_t. This allows us to avoid one of the disadvantages of ABC-MCMC where we can get stuck in areas of low probability for a long time. The algorithm is defined in Algorithm 3.

Algorithm 3: ABC Sequential Monte Carlo

Input: Number of populations T, number of particles per population N, prior π, model simulator l, family of perturbation kernels $K_t(\theta|\theta^*)$ and a descending sequence of tolerances $\epsilon_1, \ldots, \epsilon_T$

Output: Particles and weights $\{(\theta_t^{(i)}, w_t^{(i)})\}_{i=1}^N$ for each population t

for *t=1:T* **do**
  for *i=1:N* **do**
    while *True* **do**
      if *t=1* **then**
        $\theta^{**} \sim \pi(\cdot)$;
      else
        $\theta^* \sim \{\theta_{t-1}^{(i)}\}_{i=1,\ldots,N}$ with weights $\{w_{t-1}^{(i)}\}_{i=1,\ldots,N}$;
        $\theta^{**} \sim K_t(\theta|\theta^*)$
      end
      $y^* \sim l(\cdot|\theta^{**})$;
      if $\pi(\theta^{**}) > 0$ *AND* $d(y^*, y) < \epsilon_t$ **then**
        break;
      end
    end
    $\theta_t^{(i)} = \theta^{**}$;
    if *t=1* **then**
      $w_t^{(i)} = 1$;
    else
      $w_t^{(i)} = \frac{\pi(\theta_t^{(i)})}{\sum_{j=1}^N w_{t-1}^{(j)} K_t(\theta_{t-1}^{(j)}|,\theta_t^{(i)})}$;
    end
  end
  $w_t = w_t / \sum_i (w_t^{(i)})$
end

1.3.4 Uncertainty Quantification

Uncertainty quantification is the field of characterisation and measurement of uncertainty and its effect on models. For this work, we focus on parameter uncertainty in both the reaction rates used to construct a chemical kinetic model and the coagulation factor concentrations. We make use of two uncertainty quantification methods, sensitivity analysis and forward propagation of uncertainty.

Sensitivity Analysis

Sensitivity analysis is a method for understanding how variation in particular model inputs influences variation in the output. In Section 2.5, we introduce a local, variance-based sensitivity analysis method. A local sensitivity analysis method aims to quantify variation in model output as inputs are varied close to their original or typical values, usually performed by varying each parameter independently of the others. This is in comparison to a global sensitivity analysis method which explores the whole parameter space. To quantify variation in the model output, one of two common methods are typically used. The first of these methods, the one that we make use of, is through calculating the variance in a set of summary statistics. The second method is to estimate the derivative of the summary statistics with respect to changes in the parameters, usually calculated with finite differences.

Many sensitivity analysis methods have been applied to different models of thrombin generation, including both global and local methods, with almost all methods being variance-based and only a single derivative-based method [39, 40, 41, 42, 43, 44, 45].

Forward Propagation of Uncertainty

Although the prior distributions are defined on the model parameters, we can also investigate model outputs under variation across these priors. This can be done analytically for simpler models but we will instead do this through a Monte Carlo approach. We can randomly sample parameters from the prior distributions and simulate them in the models. This will give us model outputs, which if we repeat many times, can be used to infer the distribution of these model outputs. This can be helpful to understand if a large uncertainty in a few key parameters (which may have low sensitivity) results in large uncertainty in model outputs.

1.3.5 Principal Component Analysis

Principal Component Analysis (PCA) is a method commonly used in high dimension data sets for dimensionality reduction [46]. It provides a linear coordinate transform which, when the data is projected upon, maximises the variance in the data under the condition that all coordinate axes, called principal components, are perpendicular.

The first principal component is calculated as the line that passes through the mean of the data and maximises the sum of the squared distances between the data points projected onto the line and the mean. All later principal components are given as the line which is perpendicular to all preceding principal components and maximises the squared distances between the data points projected onto the line and the mean. Each principal component can be assigned a percentage of explained variance, measured using the sum of the squared distances between the data points and the mean projected onto that principal component, reported as a

proportion of the sum of squared distances between the data points and the mean.

PCA is commonly formulated through vector notation. If X is the $m \times n$ data matrix with n observations of m variables (after subtracting the mean for each variable), then the eigenvectors of XX^T are the principal components, given in the order of largest to smallest eigenvalue. The explained variance for each principal component is given as the ratio between the corresponding eigenvalue and the sum of the eigenvalues [46].

The Varimax rotation is a common tool in PCA [46]. It applies a rotation to the first k principal component vectors such that the components emphasise variation in a few variables while maintaining the same amount of explained variance as the first k principal components. Due to this transform the components will no longer be perpendicular to one another. However, being able to emphasise a smaller number of variables can greatly aid interpretation.

1.3.6 Clustering

Clustering is an unsupervised data analysis method to group data together into clusters, such that the data in each cluster are more similar to one another than to the data in the other clusters. A common method for this, the one we make use of, is k-means clustering. In the k-means clustering algorithm, k data points are randomly selected to be the cluster centre points. Each data point is then classified into the cluster whose centre point is closest. The cluster centres are then recalculated to be the mean of the data classified into that cluster. This centring-reclassification loop is then repeated until the classifications no longer change.

Determining the optimal number of clusters, k, can be a challenging task. We make use of a metric called the Gap statistic which compares the clustering for a given value of k to the performance of clustering uniform data [47].

To calculate the gap statistic, we first calculate the dispersion metric W_k, the pooled within-cluster sum of squares around the cluster means (given by Equation (1.4), where d_{ij} is the squared Euclidean distance between observation i and observation j and C_r is the set, of size n_r, of observations in cluster r), for each value of k we wish to investigate. We then generate B reference data sets, sampled from a uniform distribution over the hypercube defined by the ranges of the data after performing PCA. We then calculate the dispersion metric for each of these reference data sets, denoted as W^*_{kb}. The gap statistic, $\mathrm{Gap}(k)$, and its standard deviation sd_k are then given by Equations (1.5) and (1.6), respectively.

$$W_k = \sum_{r=1}^{k} \frac{1}{2n_r} \sum_{i,j \in C_r} d_{ij} \tag{1.4}$$

$$\text{Gap}(k) = \frac{1}{B}\sum_b (\log(W^*_{kb}) - \log(W_k)) \tag{1.5}$$

$$\text{sd}_k = \sqrt{\frac{1}{B}\sum_b \left(\log(W^*_{kb}) - \frac{1}{B}\sum_b \log(W^*_{kb})\right)^2} \tag{1.6}$$

There are still multiple ways of choosing the optimal value of k from the values of the gap statistic. It was first defined as the smallest k such that $\text{Gap}(k) \geq \text{Gap}(k+1) - \text{sd}_{k+1}$ [47] and then later defined by another group as the smallest k such that $\text{Gap}(k) \geq \text{Gap}(p) - \text{sd}_p$ where $p = \arg\max_k(\text{Gap}(k))$, i.e. the smallest value of k that is within one standard deviation of the global maximum [48]. Here, we define the optimal value for k as the smallest value that is within one standard deviation of the first local maximum of the gap statistic.

1.3.7 Regression Tree

Regression trees are a data analysis tool used to identify which variables may have an important influence on a particular output (regression trees for continuous output, decision trees for categorical output) [49]. The tree consists of a series of branching binary questions (such as "Is the FII concentration > 95?") such that both the variable (FII concentration) and the cutoff (95%) are optimal in separating high and low values of the output variable. The full tree can then be used to estimate the variable of interest, knowing only the answers to a set of binary questions regarding other variables. An example regression tree to predict ETP is given in Figure 1.8.

The optimal questions and cutoffs are determined by minimising the sum of squared errors [49]. For every possible combination of question and cutoff, two sub-nodes are generated. Each sub-node is assigned a predictive value corresponding to the average of the data points that are sorted into that sub-node. The sum of squared errors is then calculated, taking the error as the difference between the output variable for a data point and the predictive value given by the sub-node that data point is sorted into. The optimal question and cutoff are given as those that minimise this sum of squared errors.

For decision trees, there are a handful of metrics that can be used to determine the optimal questions. Here, we will introduce the Gini Index [50], which we will make use of for determining optimal cutoffs in Chapter 4. The Gini, defined by Equation (1.7), is calculated for all possible questions (all variable-cutoff combinations) for each of the two sub-nodes. The variable p_i is the probability of each class being sampled from a given node. For example, if there are two classes that the decision tree is differentiating between, pass and fail, and n samples that fall into a sub-node, then the Gini of the sub-node is $1 - (\frac{\#\text{passes}}{n})^2 - (\frac{\#\text{fails}}{n})^2$. The weighted average of these two Gini scores (weighting by the number of samples that are classified into each of the two sub-nodes) gives the Gini Index, also called the Gini Impurity, of that variable-cutoff combination. The question which gives

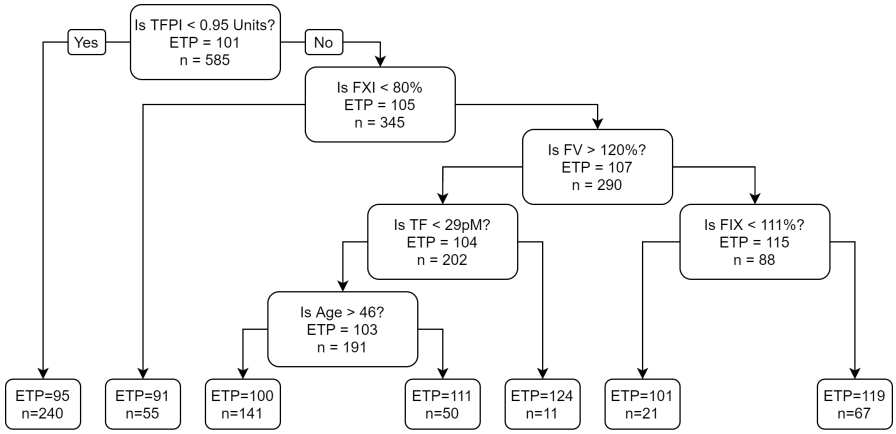

Figure 1.8: An example regression tree for predicting ETP. Each cell is labelled with the average ETP of the samples that pass through it and the number of samples n. Calculations were done using the rpart package in R.

the lowest Gini Index is chosen for that node. This process is repeated for each sub-node until either all sub-nodes have a Gini Index of 0 (perfect classification), or some other termination criteria is reached.

$$\text{Gini} = 1 - \sum_i (p_i)^2 \tag{1.7}$$

1.3.8 Functional Data Analysis

In Functional Data Analysis (FDA), data functions are represented in the form of a linear combination of basis functions. This form then grants the ability to perform common data analysis methods such as linear models, PCA, and clustering.

Common basis functions to use in FDA include monomials, Fourier series and splines. Here, we will focus on the use of splines as the basis functions as this is what we make use of in Chapter 4. To identify the splines which best fit a given set of data points, we evaluate the residual sum of squares ($\sum_j [y_j - \hat{y}(x_j)]$ where y_j are the data points at x_j and $\hat{y}$ is the linear combination to be evaluated). In order to better handle noise in the experimental data, a roughness penalty can be included. This penalty is typically defined as proportional to the curvature of the functional representation (the square of the second derivative). Through a cost function, given as the sum of the residual sum of squares and the roughness penalty, the functional representations of the data can be derived. From these functional representations, linear models, PCA, and clustering, among other methods, can be performed [51, 52].

1.4 Thesis Outline

We begin with Chapter 2, split up into many smaller sections, covering the exploratory analysis of eight published mathematical models of thrombin generation.

These sections are detailed below.

- Section 2.1 selects eight published models to analyse, chosen to best match the thrombin generation data set.
- Section 2.2 validates our implementation of these models.
- Section 2.3 investigates the accuracy of these models in their predictions of patient level ETP across the cohort.
- Section 2.4 compares the differences in model predictions for many factors throughout the coagulation cascade and identifies the primary cause for these differences.
- Section 2.5 introduces a sensitivity analysis method which is then applied to each of the eight models, investigating changes in their response under variation in both the coagulation factor concentrations and the reaction rates used in the construction of these models.
- Section 2.6 explores the different choices of reaction rates between the models, identifying the original sources for each reaction rate in each model.
- Section 2.7 conducts a numerical timescale analysis on two of the models, identifying which reactions are relevant in the models and how these change over time.

We develop upon the results found through the exploratory analysis of these eight models to develop a new model, named the Unified Model, in Chapter 3.

In order to further improve the predictions of the Unified Model, Chapter 4 covers the analysis of the thrombin generation data. While ideally this work would have been completed earlier, the discoveries made in Chapter 2 demonstrated a clear weakness in the models that we chose to investigate first.

Chapter 5 aims to implement the improvements identified in Chapter 4 into a new version of the Unified Model.

Chapter 6 details the results of a simulation study, exploring the parameter inference methods used in the construction of the Unified Model and other modelling assumptions made during its development.

Chapter 7 concludes with a summary of the findings of this work and discusses future steps in the development of mathematical models of thrombin generation.

Following this a glossary of key terms and the bibliography are given.

The Appendix provides ODEs for each of the models implemented in this work, reaction rates to simulate the models where not specified in the main body of the thesis, supplementary data concerning the exploratory analysis of the models, and further information on the Unified Model.

The key results explored in the thesis are the discovery of the importance of FXI in model predictions, made in Section 2.4, and the limitations surrounding the choice of sources for the reaction rates, particularly the uncertainty driven by differing experimental conditions, explored in Section 2.6 and Chapters 3 and 5.

Chapter 2

Existing Models

2.1 Thrombin Generation Models

There are many mathematical models for thrombin generation, each with different descriptions of the coagulation cascade. Here, we focus on models that describe coagulation as it occurs in the *in vitro* thrombin generation assay rather than *in vivo* where surfaces, flow and diffusion all play large roles. The earliest descriptions of the coagulation cascade, describing reactions but not reaction rates, proposed simple enzyme cascades from FXII down to fibrinogen [4, 5]. As the understanding of coagulation improved and more interactions between the coagulation factors were uncovered, new chemical kinetic models (mathematical models that could simulate coagulation using both reactions and their corresponding rates) that aimed to predict thrombin generation were developed, with a shift in focus from contact activation towards TF activation [53, 54]. These earlier models have been improved iteratively, producing a wide variety of available models. A timeline presenting the development of these models is given in Figure 2.1.

To aid in explanation, each model is named after the surname of the first author in its publication, with publication year used to differentiate when necessary.

The earliest mathematical models of thrombin generation, such as Khanin 1989 [54] and Willems [55], featured heavily simplified dynamics with only a handful of the coagulation factors being included. Newer models sought to improve upon the previous ones through inclusion of more coagulation factors and more reactions, expanding the range of predictions the models could make and better aligning them with the understanding of coagulation at the time. This led to the inclusion of factors VIII and IX into the models [56, 57] and more detailed descriptions of TF:VIIa formation [53, 58]. One of these groups, the group that developed the Jones model [53], then continued the development of their model, updating it to include AT and TFPI, producing the Hockin model [59]. This model then became a baseline for continued work by the same group [42, 60] and others [39, 45, 61]. In addition, there have also been many models developed independently [62, 63, 64, 65, 66, 67, 68]. As these later models were developed, they began to focus on different aspects of the cascade, such as the effect of phospholipids in the Bungay model [62], or the differences between the intrinsic and extrinsic pathways in the Zhu model [68]. Table 2.1 presents the components contained in each of the

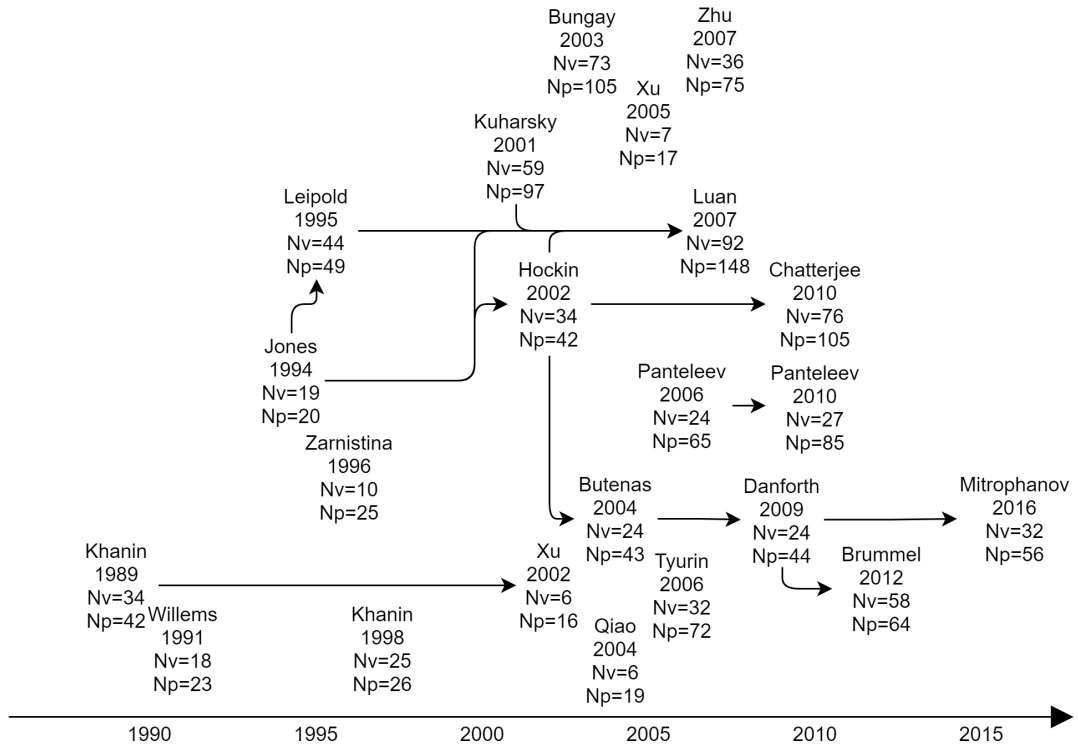

Figure 2.1: A timeline of *in vitro* thrombin generation models. The arrows demonstrate where models have utilised the reactions or reaction rates of a previous model. The size of the model is given by Nv and Np. Nv denotes the number of variables in the model and Np denotes the number of parameters in the model.

mathematical models of the thrombin generation assay.

All of these models use chemical kinetics to form a system of ordinary differential equations (with the exception of [64] which uses partial differential equations to describe the rate of diffusion in the thrombin generation assay and its effect on a plasma that is not well-mixed). This system of ODEs is defined using a set of reactions and their corresponding reaction rates. The simulation of these models is then performed numerically, with initial coagulation factor concentrations specified as the model input and concentrations of all coagulation factors over time (although typically only thrombin is analysed) forming the output of the model.

Some of these models have been validated qualitatively against data for a 'normal' donor under varying concentrations of a few coagulation factors, with the remaining models not being validated against any data (in which case the models are assumed to be representative of general dynamics of the system). However, these models are still used to make predictions about the thrombin generation assay [72]. The use of the models in this way has been questioned. Hemker, who developed many of the current methods for the thrombin generation assay [13, 73, 74, 75], believes that there is too much uncertainty in both the reaction schemes and reaction rates for the models to generate useful predictions [76]. Mann, who aided in the development of these models [53, 59], believes that these models are still useful due to their high level of transparency compared with biological assays

Model	TF Pathway	Common Pathway	XI	XII	AT	TFPI	PC	Platelets	Spatial
Khanin 1989 [54]	VII	X, V, II							
Willems [55]	-	X, V, II			✓		✓		
Jones [53]	TF, VII	X, V, II, IX, VIII							
Leipold [56]	TF:VIIa only	X, V, II, IX, VIII							
Zarnitsina [57]	-	X, V, II, IX, VIII	✓		✓		✓		
Khanin 1998 [58]	TF, VII	X, V, II, IX, VIII			✓	✓			
Kuharsky [69]	TF, VII	X, V, II, IX, VIII			✓	✓	✓	✓	
Hockin [59]	TF, VII	X, V, II, IX, VIII			✓	✓			
Xu 2002 [70]	TF:VIIa only	X, V, II, IX, VIII			✓	✓		✓	
Bungay [62]	TF, VII	X, V, II, IX, VIII	✓		✓	✓	✓		
Butenas [71]	TF, VII	X, V, II, IX, VIII			✓	✓			
Qiao [65]	-	X, V, II, IX, VIII					✓		
Xu 2005 [67]	TF:VIIa only	X, II, IX, VIII				✓			
Tyurin [66]	TF, VII	X, V, II, IX, VIII	✓	✓	✓	✓	✓		
Panteleev 2006 [64]	TF, VII	X, V, II, IX, VIII	✓		✓	✓	✓	✓	✓
Zhu [68]	TF, VII	X, V, II, IX, VIII	✓	✓	✓	✓	✓		
Luan [45]	TF, VII	X, V, II, IX, VIII			✓	✓	✓	✓	
Danforth [42]	TF, VII	X, V, II, IX, VIII			✓	✓			
Panteleev 2010 [63]	TF, VII	X, V, II, IX, VIII	✓		✓	✓	✓		
Chatterjee [39]	TF, VII	X, V, II, IX, VIII	✓	✓	✓	✓		✓*	
Brummel [60]	TF, VII	X, V, II, IX, VIII			✓	✓	✓		
Mitrophanov [61]	TF, VII	X, V, II, IX, VIII			✓	✓			

Table 2.1: Details of *in vitro* thrombin generation models. The chosen models are in bold. Models that include a specific component (for example, factor XI) are ticked in the corresponding column. *The Chatterjee model only treats platelets as an activation surface so is still included.

and cheap computational cost [77].

Recent attempts of modelling focus on validating these complex models against patient data. A previous group have shown that a subset of these models failed to reproduce patient data for a cohort of 112 male subjects, 40 of which had haemophilia A, 32 with haemophilia B and 40 healthy controls [78]. They then explored reparametrising one of these models, specifically the Hockin model [59], on a per-patient basis. However, it has been suggested that thrombin generation curves can be efficiently summarised in five parameters and fitting more than this, on a per-patient level, will result in an unidentifiable model [79]. Due to this fact, they fit all reaction rates across the cohort (one value per reaction rate for all individuals), and then fit three reaction rates on a per-patient level. From this, they are able to achieve a good match between model predictions and patient data, however, it is still unclear if these reaction rates truly vary on a patient specific level across such a broad range or if this is a result of over-fitting. We believe that, assuming there are no mutations in these proteins, then the rates of these reactions should be identical between individuals. Differences in thrombotic potential between individuals, for example between different ages or sexes [21], then comes about due to differences in the concentrations of these proteins. Under this assumption, a single set of reaction rates should be sufficient for all individuals.

In this work, we focus on mathematical models for the thrombin generation assay. However, models have also been developed to capture thrombin generation *in vivo*. These models typically include the effects of flow, clot formation and its effect on blood flow, and platelets with both their activation and aggregation [43, 80, 81, 82, 83, 84]. These models use partial differential equations for both the flow of the blood and the coagulation factor concentrations but vary in the techniques used for modelling platelets, typically coupled through multiscale modelling. These models have already been used to identify new interactions in the regulation of coagulation *in vivo*. Most notably, that the reduction in coagulation seen in patients with haemophilia A (deficiency in FVIII) is improved if that patient also has low levels of FV, which was discovered through a global sensitivity analysis of a mathematical model of *in vivo* coagulation [44].

We aim to select the models that should be best at reproducing the data from the PRAMIS cohort. As such, we select the models that satisfy the following five conditions.

- They should include both TF and FVII to specify the initiation of coagulation;
- They should contain factors X, V, IX, VIII, and II to accurately capture their effects on thrombin generation;
- They should contain the inhibitors AT and TFPI;
- They should not model spatial effects as this data is not available; and

- They should not include platelets as the data was collected in platelet poor plasma.

There are eleven models that satisfy these conditions, namely Hockin [59], Danforth [42], Chatterjee [39], Brummel [60], Bungay [62], Panteleev [63], Tyurin [66], Zhu [68], Mitrophanov [61], Butenas [71], and Khanin 1998 [58]. Of these eleven models, the Mitrophanov model [61] was excluded as it is identical to the Danforth model for the reactions that are relevant to our work, the Butenas model [71], a precursor to the Danforth model and developed from the Hockin model, was removed due to its similarity to both of these models. Finally, the Khanin 1998 model [58] was also removed as the specified ODEs violated typical conservation laws and allowed negative concentrations. This leaves us with eight remaining models that satisfy these conditions, varying in size between 24 and 81 ODEs (Panteleev and Chatterjee, respectively) and 42 to 110 parameters (Hockin and Bungay, respectively).

Each of these models are converted to ODEs and implemented in Matlab. These ODEs are then solved with the ode23tb numerical ODE solver to extract model outputs.

2.1.1 Hockin Model

The Hockin model [59] is the simplest model that we consider. It built upon the Jones model [53] by adding AT and TFPI and utilises a simple form of the coagulation cascade consisting of 31 reactions (12 of which are reversible) which all use mass action law kinetics. This model was validated against thrombin generation curves under varying prothrombin concentrations for an average donor [85], where it was able to reproduce the general shape of thrombin generation curves but not a specific curve. The reactions and rate constants are given in Table 2.3. When the model is solved along with the non-zero initial conditions listed in Table 2.2, we can plot the thrombin generation curve, given in Figure 2.2. The ODEs are presented in Appendix A.

Substrate	Initial Concentration (M)
TF	10×10^{-12}
II	1.4×10^{-6}
V	2.0×10^{-8}
VII	1.0×10^{-8}
VIIa	1.0×10^{-10}
VIII	7×10^{-10}
IX	9.0×10^{-8}
X	1.6×10^{-7}
TFPI	2.5×10^{-9}
AT	3.4×10^{-6}

Table 2.2: The non-zero initial concentrations for the Hockin model [59].

Index	Reaction	$k_{+,ind}$	$k_{-,ind}$
1	TF + VII $\leftrightarrow$ TF:VII	3.2×10^6	3.1×10^{-3}
2	TF + VIIa $\leftrightarrow$ TF:VIIa	2.3×10^7	3.1×10^{-3}
3	TF:VIIa + VII $\rightarrow$ TF:VIIa + VIIa	4.45×10^5	-
4	Xa + VII $\rightarrow$ Xa + VIIa	1.3×10^7	-
5	IIa + VII $\rightarrow$ IIa + VIIa	2.3×10^4	-
6	TF:VIIa + X $\leftrightarrow$ TF:VIIa:X	2.5×10^7	1.05
7	TF:VIIa:X $\rightarrow$ TF:VIIa:Xa	-	6
8	TF:VIIa + Xa $\leftrightarrow$ TF:VIIa:Xa	2.2×10^7	19
9	TF:VIIa + IX $\leftrightarrow$ TF:VIIa:IX	1.0×10^7	2.45
10	TF:VIIa:IX $\rightarrow$ TF:VIIa + IXa	-	1.8
11	Xa + II $\rightarrow$ Xa + IIa	7.5×10^3	-
12	IIa + VIII $\rightarrow$ IIa + VIIIa	2.0×10^7	-
13	VIIIa + IXa $\leftrightarrow$ IXa:VIIIa	1.0×10^7	5.0×10^{-3}
14	IXa:VIIIa + X $\leftrightarrow$ IXa:VIIIa:X	1.0×10^8	1.0×10^{-3}
15	IXa:VIIIa:X $\rightarrow$ IXa:VIIIa + Xa	-	8.2
16	$VIIIa_1L$ + $VIIIa_2$ $\leftrightarrow$ VIIIa	2.2×10^4	6.0×10^{-5}
17	IXa:VIIIa:X $\rightarrow$ $VIIIa_1L$ + $VIIIa_2$ + X + IXa IXa:VIIIa $\rightarrow$ $VIIIa_1L$ + $VIIIa_2$ + IXa	-	1.0×10^{-3}
18	IIa + V $\rightarrow$ IIa + Va	2.0×10^7	-
19	Xa + Va $\leftrightarrow$ Xa:Va	4.0×10^8	0.2
20	Xa:Va + II $\leftrightarrow$ Xa:Va:II	1.0×10^8	103
21	Xa:Va:II $\rightarrow$ Xa:Va + mIIa	-	63.5
22	mIIa + Xa:Va $\rightarrow$ IIa + Xa:Va	1.5×10^7	-
23	Xa + TFPI $\leftrightarrow$ Xa:TFPI	9.0×10^5	3.6×10^{-4}
24	TF:VIIa:Xa + TFPI $\leftrightarrow$ TF:VIIa:Xa:TFPI	3.2×10^8	1.1×10^{-4}
25	TF:VIIa + Xa:TFPI $\rightarrow$ TF:VIIa:Xa:TFPI	5.0×10^7	-
26	Xa + AT $\rightarrow$ Xa:AT	1.5×10^3	-
27	mIIa + AT $\rightarrow$ mIIa:AT	7.1×10^3	-
28	IXa + AT $\rightarrow$ IXa:AT	4.9×10^2	-
29	IIa + AT $\rightarrow$ IIa:AT	7.1×10^3	-
30	TF:VIIa + AT $\rightarrow$ TF:VIIa:AT	2.3×10^2	-

Table 2.3: The reaction scheme and rate constants used for the Hockin model [59]. The reaction rate $k_{-,17}$ is used for 2 reactions and should remain so during any changes for sensitivity analysis or parameter fitting. The units for all $k_{+,ind}$ and $k_{-,ind}$ reaction rates are $M^{-1}s^{-1}$ and s^{-1}, respectively.

2.1.2 Danforth Model

The Danforth model [42] is an update to the Butenas model [71] which itself is an update to the Hockin model [59]. The result of these changes, when compared with the Hockin model, are two updated reaction rates and two new reactions. This model has not been validated against data. However, the Butenas model was compared to data in which small concentrations of active coagulation factors (such as FXa and FIXa) were used to initiate the system in the absence of TF

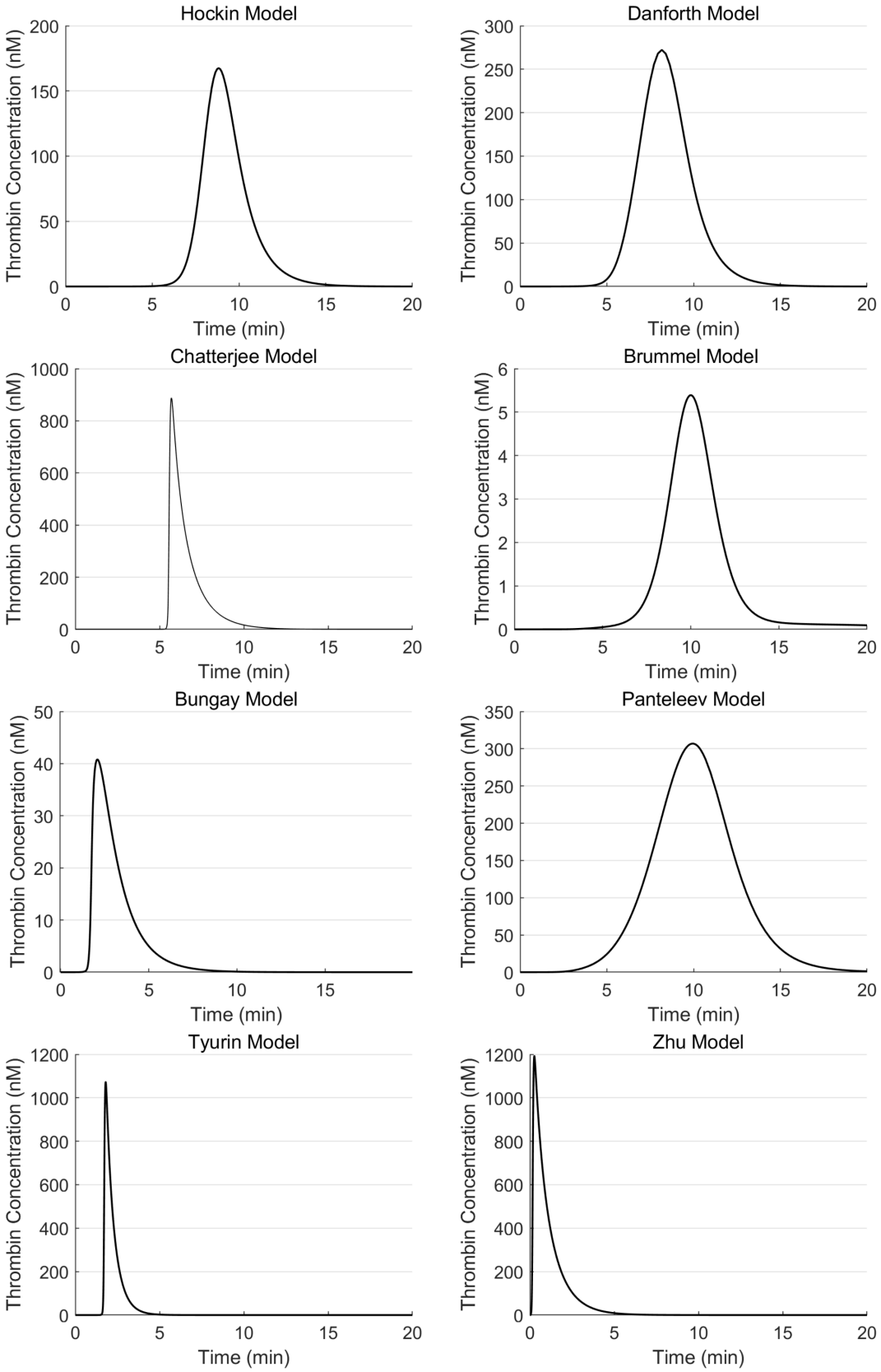

Figure 2.2: Thrombin generation curves for each of the models.

for an average donor. The two new reactions and their rates are given in Table 2.4 and the two updated reaction rates are given in Table 2.5. The thrombin generation curve, given using the initial conditions in Table 2.6, is in Figure 2.2. The Danforth model produces a similar thrombin generation curve to the Hockin model, featuring a slightly higher peak height and a slightly reduced lagtime. The ODEs are presented in Appendix A.

Index	Reaction	$k_{+,ind}$ $(M^{-1}s^{-1})$
31	IXa + X $\rightarrow$ IXa + Xa	5.7×10^3
32	mIIa + V $\rightarrow$ mIIa + Va	3.0×10^6

Table 2.4: The two new reactions that were added to the Hockin model for the Danforth Model as well as their corresponding rate constants.

Index	Reaction	$k_{+,ind}$ $(M^{-1}s^{-1})$
22	mIIa + Xa:Va $\rightarrow$ IIa + Xa:Va	2.3×10^8
26	Xa + AT $\rightarrow$ Xa:AT	4.2×10^3

Table 2.5: The two reaction rates that were updated and their corresponding reactions.

Substrate	Initial Concentration (M)
TF	5×10^{-12}
II	1.4×10^{-6}
V	2.0×10^{-8}
VII	1.0×10^{-8}
VIIa	1.0×10^{-10}
VIII	7×10^{-10}
IX	9.0×10^{-8}
X	1.6×10^{-7}
TFPI	2.5×10^{-9}
AT	3.4×10^{-6}

Table 2.6: The non-zero initial concentrations for the Danforth model [42].

2.1.3 Chatterjee Model

The Chatterjee model [39] consists of 75 mass action law reactions (29 of which are reversible). The main goal of this model was to capture the effects of platelet activation on the coagulation cascade. To do this, they expanded upon the Hockin model and added in reactions for kallikreins, FXI, FXII, CTI (Corn Trypsin Inhibitor), Boc-VPR-AMC (a fluorogenic substrate), $\alpha_1 - AT$, $\alpha_2 - M$ and $\alpha_2 - AP$ (α_1-Anti-Trypsin, α_2-Macroglobulin and α_2-Anti-Plasmin). On top of this, they

added a parameter, ε, to model instantaneous platelet activation and scale a handful of reaction rates based on its current value. The definition of ε is given by Equation (2.1) where $\varepsilon_{max_0} = 0.01$ and $k = 0.005$ and $\varepsilon(t = 0) = 0.01$.

$$\begin{aligned} \frac{d\varepsilon}{dt} &= k(\varepsilon_{max} - \varepsilon) \\ \varepsilon_{max} &= \varepsilon_{max_0} + (1 - \varepsilon_{max_0}) \times f([IIa*(t)]) \\ f([IIa*(t)]) &= \frac{[IIa*(t)]^{1.6123}}{[IIa*(t)]^{1.6123} + (2.45279 \times 10^9)^{1.6123}} \\ [IIa*(t)] &= \max_{t' \in [0,t]} ([IIa(t')]) \end{aligned} \tag{2.1}$$

This model was validated against the same data as the Butenas model [71] as well as new data, also using active coagulation factors to initiate coagulation, described for this model [39].

When the reactions are solved using the initial conditions given in Table 2.8, we can plot a thrombin generation curve, given in Figure 2.2 and a plot of ε, the instantaneous platelet activation, is given in Figure 2.3. The ODEs are presented in Appendix A.

The thrombin generation curve produced by the Chatterjee model is very different to the Hockin and Danforth models. It features a similar lagtime to these models but with much more rapid activation once this lagtime is reached, culminating in a peak height much larger than both of these models. We will investigate the reason for these differences in Section 2.4.

Index	Reaction	$k_{+,ind}$	$k_{-,ind}$
1	TF + VII $\leftrightarrow$ TF:VII	3.2×10^6	3.1×10^{-2}
2	TF + VIIa $\leftrightarrow$ TF:VIIa	2.3×10^7	3.1×10^{-5}
3	TF:VIIa + VII $\rightarrow$ TF:VIIa + VIIa	4.45×10^5	-
4	Xa + VII $\rightarrow$ Xa + VIIa	1.3×10^7	-
5	IIa + VII $\rightarrow$ IIa + VIIa	2.3×10^4	-
6	TF:VIIa + X $\leftrightarrow$ TF:VIIa:X	2.5×10^7	$0.0105^\dagger$
7	TF:VIIa:X $\rightarrow$ TF:VIIa:Xa	-	6
8	TF:VIIa + Xa $\leftrightarrow$ TF:VIIa:Xa	2.2×10^7	19
9	TF:VIIa + IX $\leftrightarrow$ TF:VIIa:IX	1.0×10^7	2.45
10	TF:VIIa:IX $\rightarrow$ TF:VIIa + IXa	-	1.8
11	II + Xa $\rightarrow$ IIa + Xa	7.5×10^3	-
12	IIa + VIII $\rightarrow$ IIa + VIIIa	2.0×10^7	-
13	VIIIa + IXa $\leftrightarrow$ IXa:VIIIa	1.0×10^7	$1.0 \times 10^{-4\dagger}$
14	IXa:VIIIa + X $\leftrightarrow$ IXa:VIIIa:X	1.0×10^8	$1.0 \times 10^{-5\dagger}$
15	IXa:VIIIa:X $\rightarrow$ IXa:VIIIa + Xa	-	8.2
16	$VIIIa_1L$ + $VIIIa_2$ $\leftrightarrow$ VIIIa	2.2×10^4	$6.0 \times 10^{-5\dagger}$
17	IXa:VIIIa:X $\rightarrow$ $VIIIa_1L$ + $VIIIa_2$ + X + IXa IXa:VIIIa $\rightarrow$ $VIIIa_1L$ + $VIIIa_2$ + IXa	-	1.0×10^{-3}

18	IIa + V → IIa + Va	2.0×10^7	-
19	Xa + Va ↔ Xa:Va	4.0×10^8	$0.008^\dagger$
20	Xa:Va + II ↔ Xa:Va:II	1.0×10^8	$2.06^\dagger$
21	Xa:Va:II → Xa:Va + mIIa	-	63.5
22	Xa:Va + mIIa → Xa:Va + IIa	1.5×10^7	-
23	Xa + TFPI ↔ Xa:TFPI	9.0×10^5	$3.6 \times 10^{-4\dagger}$
24	TF:VIIa:Xa + TFPI ↔ TF:VIIa:Xa:TFPI	3.2×10^8	1.1×10^{-2}
25	TF:VIIa + Xa:TFPI → TF:VIIa:Xa:TFPI	5.0×10^7	-
26	Xa + AT → Xa:AT	1.5×10^3	-
27	mIIa + AT → mIIa:AT	7.1×10^3	-
28	IXa + AT → IXa:AT	4.9×10^2	-
29	IIa + AT → IIa:AT	7.1×10^3	-
30	TF:VIIa + AT → TF:VIIa:AT	2.3×10^2	-
31	BocVPRMCA + IIa ↔ BocVPRMCA:IIa	1.0×10^8	6.1×10^3
32	BocVPRMCA:IIa → BocVPR + AMC + IIa	-	53.8
33	XII → XIIa	-	5.0×10^{-4}
34	XIIa + XII ↔ XIIa:XII	1.0×10^8	$750^\dagger$
35	XIIa:XII → XIIa + XIIa	-	3.3×10^{-2}
36	XIIa + PK ↔ XIIa:PK	1.0×10^8	$3.6 \times 10^{3\dagger}$
37	XIIa:PK → XIIa + K	-	40
38	XII + K ↔ XII:K	1.0×10^8	$45.3^\dagger$
39	XII:K → XIIa + K	-	5.7
40	PK + K → K + K	2.7×10^4	-
41	K → Kinh	-	1.1×10^{-2}
42	XIIa + CTI ↔ XIIa:CTI	1.0×10^8	2.45
43	XIIa + C1-inh → XIIa:C1-inh	3.6×10^3	-
44	XIIa + AT → XIIa:AT	21.6	-
45	XI + IIa ↔ XI:IIa	1.0×10^8	5
46	XI:IIa → XIa + IIa	-	1.3×10^{-4}
47	XIIa + XI ↔ XIIa:XI	1.0×10^8	$200^\dagger$
48	XIIa:XI → XIIa + XIa	-	5.7×10^{-4}
49	XIa + XI → XIa + XIa	3.19×10^6	-
50	XIa + AT → XIa:AT	3.2×10^2	-
51	XIa + C1-inh → XIa:C1-inh	1.8×10^3	-
52	XIa + α_1AT → XIa:α_1AT	1.0×10^2	-
53	XIa + α_2AP → XIa:α_2AP	4.3×10^3	-
54	XIa + IX ↔ XIa:IX	1.0×10^8	$41^\dagger$
55	XIa:IX → XIa + IXa	-	7.7
56	IXa + X ↔ IXa:X	1.0×10^8	$0.64^\dagger$
57	IXa:X → IXa + Xa	-	7.0×10^{-4}
58	Xa + VIII ↔ Xa:VIII	1.0×10^8	$2.1^\dagger$
59	Xa:VIII → Xa + VIIIa	-	0.023
60	VIIa + IX ↔ VIIa:IX	1.0×10^8	0.9
61	VIIa:IX → VIIa + IXa	-	3.6×10^{-5}
62	VIIa + X ↔ VIIa:X	1.0×10^8	210
63	VIIa:X → VIIa + Xa	-	1.6×10^{-6}
64	Fbg + IIa ↔ Fbg:IIa	1.0×10^8	636
65	Fbg:IIa → Fbn1 + IIa + FPA	-	84

66	Fbn1 + IIa $\leftrightarrow$ Fbn1:IIa	1.0×10^8	742.6
67	Fbn1:IIa $\rightarrow$ Fbn2 + IIa + FPB	-	7.45
68	Fbn1 + Fbn1 $\leftrightarrow$ $(Fbn1)_2$	1.0×10^6	6.45×10^{-2}
69	$(Fbn1)_2$ + IIa $\leftrightarrow$ $(Fbn1)_2$:IIa	1.0×10^8	701
70	$(Fbn1)_2$:IIa $\rightarrow$ $(Fbn2)_2$ + IIa + FPB	-	49
71	Fbn2 + IIa $\leftrightarrow$ Fbn2:IIa	1.0×10^8	1.0×10^3
72	$(Fbn1)_2$:IIa + AT $\rightarrow$ $(Fbn1)_2$:IIa:AT	1.6×10^4	-
73	Fbn1:IIa + AT $\rightarrow$ Fbn1:IIa:AT	1.6×10^4	-
74	Fbn2:IIa + AT $\rightarrow$ Fbn2:IIa:AT	1.0×10^4	-

Table 2.7: The reaction scheme and rate constants used for the Chatterjee model [39]. The reaction rate $k_{-,17}$ is used for 2 reactions and should remain so during any changes for sensitivity analysis or parameter fitting. The units for all $k_{+,ind}$ and $k_{-,ind}$ reaction rates are $M^{-1}s^{-1}$ and s^{-1}, respectively.

Substrate	Initial Concentration (M)
TF	10×10^{-12}
II	1.4×10^{-6}
V	2.0×10^{-8}
VII	1.0×10^{-8}
VIIa	1.0×10^{-10}
VIII	7×10^{-10}
IX	9.0×10^{-8}
X	1.6×10^{-7}
XI	3.1×10^{-8}
XII	3.4×10^{-7}
Fbg	9×10^{-6}
PK	4.5×10^{-7}
TFPI	2.5×10^{-9}
AT	3.4×10^{-6}
C1-inh	2.5×10^{-6}
CTI	4.2×10^{-6}
$\alpha_1 - AT$	4.5×10^{-5}
$\alpha_2 - AP$	1×10^{-6}
BocVPRMCA	1×10^{-5}

Table 2.8: The non-zero initial concentrations for the Chatterjee model as reported in [39].

2.1.4 Brummel Model

The Brummel model [60] is an extension to the Danforth model. It consists of the original 33 reactions of the Danforth model with an additional 39 reactions (16 of which are reversible) to capture the effects of protein C and Thrombomodulin.

[†]These unbinding reaction rates are be divided by ε.

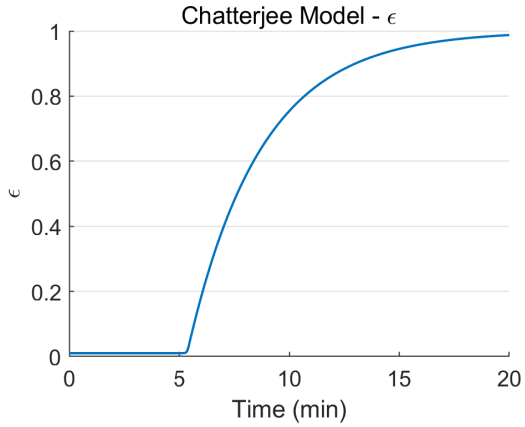

Figure 2.3: Time course for the parameter ε (instantaneous platelet activation) for the Chatterjee model.

The effects of protein C are highly detailed, even modelling the effects of FVa being partially cleaved. The model also contains a large number of parameters which are meant to remain identical across multiple reactions (like was seen for $k_{-,17}$ in the Hockin model). The protein C reactions were validated against data under varying concentrations of activated protein C [86].

When the reactions in Table 2.10 and parameter values in Table 2.11 are solved with the non-zero initial conditions given in Table 2.9, we can plot a thrombin generation curve, given in Figure 2.2. The ODEs are presented in Appendix A.

The thrombin generation curve produced by the Brummel model is similar in shape to the Hockin and Danforth models, but greatly reduced in scale, possibly due to the inclusion of the inhibitor protein C.

Substrate	Initial Concentration (M)
TF	5×10^{-12}
VII	1.0×10^{-8}
VIIa	1.0×10^{-10}
X	1.6×10^{-7}
IX	9.0×10^{-8}
II	1.4×10^{-6}
VIII	7×10^{-10}
V	2.0×10^{-8}
TFPI	2.5×10^{-9}
AT	3.6×10^{-6}
TM	1.0×10^{-9}
PC	6.5×10^{-8}

Table 2.9: The initial conditions that we used for the Brummel model. All values were reported in [60] except for FVIIa, TM and PC where values from the Bungay model [62] were used.

Reaction	k_+	k_-
TF + VII $\leftrightarrow$ TF:VII	k_2	k_1
TF + VIIa $\leftrightarrow$ TF:VIIa	k_4	k_3
TF:VIIa + VII $\rightarrow$ TF:VIIa + VIIa	k_5	-
Xa + VII $\rightarrow$ Xa + VIIa	k_6	-
IIa + VII $\rightarrow$ IIa + VIIa	k_7	-
TF:VIIa + X $\leftrightarrow$ TF:VIIa:X	k_9	k_8
TF:VIIa:X $\rightarrow$ TF:VIIa:Xa	k_{10}	-
TF:VIIa + Xa $\leftrightarrow$ TF:VIIa:Xa	k_{12}	k_{11}
TF:VIIa + IXa $\leftrightarrow$ TF:VIIa:IX	k_{14}	k_{13}
TF:VIIa:IX $\rightarrow$ TF:VIIa + IXa	k_{15}	-
Xa + II $\rightarrow$ Xa + IIa	k_{16}	-
IIa + VIII $\rightarrow$ IIa + VIIIa	k_{17}	-
VIIIa + IXa $\leftrightarrow$ IXa:VIIIa	k_{19}	k_{18}
IXa:VIIIa + X $\leftrightarrow$ IXa:VIIIa:X	k_{21}	k_{20}
IXa:VIIIa:X $\rightarrow$ IXa:VIIIa + Xa	k_{22}	-
VIIIa $\leftrightarrow$ VIIIa1L + VIIIa2	k_{24}	k_{23}
IXa:VIIIa:X $\rightarrow$ VIIIa1L + VIIIa2 + X + IXa	k_{25}	-
IXa:VIIIa $\rightarrow$ VIIIa1L + VIIIa2 + IXa	k_{25}	-
IIa + V $\rightarrow$ IIa + Va	k_{26}	-
Xa + Va $\leftrightarrow$ Xa:Va	k_{28}	k_{27}
Xa:Va + II $\leftrightarrow$ Xa:Va:II	k_{30}	k_{29}
Xa:Va:II $\rightarrow$ Xa:Va + mIIa	k_{31}	-
mIIa + Xa:Va $\rightarrow$ IIa + Xa:Va	k_{32}	-
Xa + TFPI $\leftrightarrow$ Xa:TFPI	k_{34}	k_{33}
TF:VIIa:Xa + TFPI $\leftrightarrow$ TF:VIIa:Xa:TFPI	k_{36}	k_{35}
TF:VIIa + Xa:TFPI $\rightarrow$ TF:VIIa:Xa:TFPI	k_{37}	-
Xa + AT $\rightarrow$ Xa:AT	k_{38}	-
mIIa + AT $\rightarrow$ mIIa:AT	k_{39}	-
IXa + AT $\rightarrow$ IXa:AT	k_{40}	-
IIa + AT $\rightarrow$ IIa:AT	k_{41}	-
TF:VIIa + AT $\rightarrow$ TF:VIIa:AT	k_{42}	-
TM + IIa $\leftrightarrow$ TM:IIa	k_{44}	k_{43}
TM:IIa + PC $\leftrightarrow$ TM:IIa:PC	k_{46}	k_{45}
TM:IIa:PC $\rightarrow$ TM:IIa + APC	k_{47}	-
TM:IIa + AT $\rightarrow$ IIa:AT + TM	k_{48}	-
APC + Va $\leftrightarrow$ APC:Va	k_{50}	k_{49}
APC:Va $\rightarrow$ APC + Va5	k_{51}	-
APC:Va $\rightarrow$ APC + Va3	k_{52}	-
APC + Va5 $\leftrightarrow$ APC:Va5	k_{50}	k_{49}
APC + Va3 $\leftrightarrow$ APC:Va3	k_{50}	k_{49}
APC:Va3 $\rightarrow$ APC + Va53	k_{51}	-
APC:Va5 $\rightarrow$ APC + Va53	k_{52}	-
Va3 $\rightarrow$ HCF + LCA1	k_{53}	-
Va53 $\rightarrow$ HCF + LCA1	k_{53}	-
APC + LCA1 $\leftrightarrow$ APC:LCA1	k_{50}	k_{49}
APC + TM:IIa $\leftrightarrow$ TM:IIa:APC	k_{46}	k_{45}

Xa + Va5 ↔ Xa:Va5	k_{28}	k_{54}
Xa + Va3 ↔ Xa:Va3	k_{28}	k_{54}
Xa:Va5 + II ↔ Xa:Va5:II	k_{30}	k_{29}
Xa:Va5:II → Xa:Va5 + mIIa	k_{55}	-
Xa:Va3 + II ↔ Xa:Va3:II	k_{30}	k_{29}
Xa:Va3:II → Xa:Va3 + mIIa	k_{56}	-
Xa:Va5 + mIIa → IIa + Xa:Va5	k_{57}	-
Xa:Va3 + mIIa → IIa + Xa:Va3	k_{58}	-
Xa:Va3 → HCF + LCA1 + Xa	k_{59}	-
Xa:Va3:II → HCF + LCA1 + Xa + II	k_{59}	-
IXa + X → IXa + Xa	k_{60}	-
mIIa + V → mIIa + Va	k_{61}	-
TM + mIIa ↔ TM:mIIa	k_{44}	k_{43}
TM:mIIa + PC ↔ TM:mIIa:PC	k_{46}	k_{45}
TM:mIIa:PC → TM:mIIa + APC	k_{47}	-
TM:mIIa + AT → mIIa:AT + TM	k_{48}	-
Xa + Va53 ↔ Xa:Va53	k_{28}	k_{54}
Xa:Va53 + II ↔ Xa:Va53:II	k_{30}	k_{29}
Xa:Va53:II → Xa:Va53 + mIIa	k_{56}	-
Xa:Va53 + mIIa → IIa + Xa:Va53	k_{58}	-
Xa:Va53:II → HCF + LCA1 + Xa + II	k_{59}	-
II + Va ↔ II:Va	k_{63}	k_{62}
Xa:Va5 + APC → Xa:Va53 + APC	k_{64}	-

Table 2.10: The reaction scheme used for the Brummel model. Parameter names are listed instead of parameter values because many of the later parameters are reused across multiple reactions. The values for each of the parameters are given in Table 2.11.

Parameter	Parameter Value	Parameter	Parameter Value
k_1	$3.10 \times 10^{-3} s^{-1}$	k_2	$3.20 \times 10^{6} M^{-1} s^{-1}$
k_3	$3.10 \times 10^{-3} s^{-1}$	k_4	$2.30 \times 10^{7} M^{-1} s^{-1}$
k_5	$4.450 \times 10^{5} M^{-1} s^{-1}$	k_6	$1.30 \times 10^{7} M^{-1} s^{-1}$
k_7	$2.30 \times 10^{4} M^{-1} s^{-1}$	k_8	$1.05 s^{-1}$
k_9	$2.50 \times 10^{7} M^{-1} s^{-1}$	k_{10}	$6 s^{-1}$
k_{11}	$19 s^{-1}$	k_{12}	$2.20 \times 10^{7} M^{-1} s^{-1}$
k_{13}	$2.45 s^{-1}$	k_{14}	$1.00 \times 10^{7} M^{-1} s^{-1}$
k_{15}	$1.8 s^{-1}$	k_{16}	$7.50 \times 10^{3} M^{-1} s^{-1}$
k_{17}	$2.00 \times 10^{7} M^{-1} s^{-1}$	k_{18}	$5.00 \times 10^{-3} s^{-1}$
k_{19}	$1.00 \times 10^{7} M^{-1} s^{-1}$	k_{20}	$1.00 \times 10^{-3} s^{-1}$
k_{21}	$1.00 \times 10^{8} M^{-1} s^{-1}$	k_{22}	$8.2 s^{-1}$
k_{23}	$2.20 \times 10^{4} M^{-1} s^{-1}$	k_{24}	$6.00 \times 10^{-3} s^{-1}$
k_{25}	$1.00 \times 10^{-3} s^{-1}$	k_{26}	$2.00 \times 10^{7} M^{-1} s^{-1}$
k_{27}	$0.075 s^{-1}$	k_{28}	$1.50 \times 10^{8} M^{-1} s^{-1}$
k_{29}	$103 s^{-1}$	k_{30}	$1.00 \times 10^{8} M^{-1} s^{-1}$
k_{31}	$63.5 s^{-1}$	k_{32}	$2.30 \times 10^{8} M^{-1} s^{-1}$
k_{33}	$3.60 \times 10^{-4} s^{-1}$	k_{34}	$9.00 \times 10^{5} M^{-1} s^{-1}$

k_{35}	$1.10 \times 10^{-4} s^{-1}$	k_{36}	$3.20 \times 10^{8} M^{-1} s^{-1}$
k_{37}	$5.00 \times 10^{7} M^{-1} s^{-1}$	k_{38}	$4.20 \times 10^{3} M^{-1} s^{-1}$
k_{39}	$7.10 \times 10^{3} M^{-1} s^{-1}$	k_{40}	$4.90 \times 10^{2} M^{-1} s^{-1}$
k_{41}	$7.10 \times 10^{3} M^{-1} s^{-1}$	k_{42}	$2.30 \times 10^{2} M^{-1} s^{-1}$
k_{43}	$0.33 s^{-1}$	k_{44}	$1.00 \times 10^{8} M^{-1} s^{-1}$
k_{45}	$100 s^{-1}$	k_{46}	$1.00 \times 10^{8} M^{-1} s^{-1}$
k_{47}	$0.41 s^{-1}$	k_{48}	$7.10 \times 10^{3} M^{-1} s^{-1}$
k_{49}	$0.7 s^{-1}$	k_{50}	$1.00 \times 10^{8} M^{-1} s^{-1}$
k_{51}	$1 s^{-1}$	k_{52}	$0.192 s^{-1}$
k_{53}	$0.028 s^{-1}$	k_{54}	$0.15 s^{-1}$
k_{55}	$10.3 s^{-1}$	k_{56}	$10.3 s^{-1}$
k_{57}	$4.60 \times 10^{7} M^{-1} s^{-1}$	k_{58}	$4.60 \times 10^{7} M^{-1} s^{-1}$
k_{59}	$0.0035 s^{-1}$	k_{60}	$5.70 \times 10^{3} M^{-1} s^{-1}$
k_{61}	$3.00 \times 10^{6} M^{-1} s^{-1}$	k_{62}	$70 s^{-1}$
k_{63}	$1.00 \times 10^{8} M^{-1} s^{-1}$	k_{64}	$4.05 \times 10^{6} M^{-1} s^{-1}$

Table 2.11: The parameter values given for the Brummel model [60].

2.1.5 Bungay Model

The Bungay model [62] consists of 49 reactions (26 of which are reversible) governed by mass action law kinetics. The aim of the model was to capture the reliance of the coagulation cascade on phospholipid binding sites where many of these reactions occur. This was achieved by considering a lipid head group species which can bind to many of the species in the model (indicated by a subscript of L) and then considering any reactions that only occur on a phospholipid surface to be modelled by a reaction between lipid bound species. The lipid binding reactions for a species S are given by Equation (2.2), where LBS_S is the number of lipid binding sites available for species S. LBS_S is given by $\frac{[Lipid]}{n_S}$ where $[Lipid]$ is the concentration of lipid head groups and n_S is the number of head groups that are required to bind species S, which was assumed to be 100 for all species.

$$S_f + LBS_S \leftrightarrow S_L \tag{2.2}$$

This model, like the Hockin model, was validated qualitatively against data for an average donor with varied prothrombin concentrations [85]. These reactions are given in Table 2.12 and the model is then completed by including reactions to represent the lipid binding and unbinding reactions which are given in Table 2.13.

When the model is solved using the non-zero initial conditions given in Table 2.14, we can then plot a thrombin generation curve for the Bungay model, given in Figure 2.2. The ODEs are presented in Appendix A.

The thrombin generation curve for the Bungay model is different to all the previous models. Its shape falls somewhere between that of the Chatterjee model and the others. It has the shortest lagtime of the models so far, but the second lowest peak height.

Index	Reaction	$k_{+,ind}$	$k_{-,ind}$
1	$TF_L + VIIa_L \leftrightarrow TF{:}VIIa_L$	5×10^8	0.005
2	$TF_L + VII_L \leftrightarrow TF{:}VII_L$	5×10^6	0.005
3	$TF{:}VIIa_L + IX_L \leftrightarrow TF{:}VIIa{:}IX_L$	1×10^7	2.09
4	$TF{:}VIIa{:}IX_L \rightarrow TF{:}VIIa_L + IXa_L$	-	0.34
5	$TF{:}VIIa_L + X_L \leftrightarrow TF{:}VIIa{:}X_L$	1×10^8	32.5
6	$TF{:}VIIa{:}X_L \rightarrow TF{:}VIIa{:}Xa_L$	-	1.5
7	$TF{:}VIIa{:}Xa_L \rightarrow TF{:}VIIa_L + Xa_L$	-	1
8	$TF{:}VII_L + Xa_L \leftrightarrow TF{:}VII{:}Xa_L$	5×10^7	44.8
9	$TF{:}VII{:}Xa_L \rightarrow TF{:}VIIa_L + Xa_L$	-	15.2
10	$IXa_L + VIIIa_L \leftrightarrow IXa{:}VIIIa_L$	1×10^8	0.2
11	$Xa_L + Va_L \leftrightarrow Xa{:}Va_L$	1×10^9	1
12	$IXa{:}VIIIa_L + X_L \leftrightarrow IXa{:}VIIIa{:}X_L$	1×10^8	10.7
13	$IXa{:}VIIIa{:}X_L \rightarrow IXa{:}VIIIa_L + Xa_L$	-	8.3
14	$V_L + Xa_L \leftrightarrow V{:}Xa_L$	1×10^8	1
15	$V{:}Xa_L \rightarrow Va_L + Xa_L$	-	0.043
16	$VIII_L + Xa_L \leftrightarrow VIII{:}Xa_L$	1×10^8	2.1
17	$VIII{:}Xa_L \rightarrow VIIIa_L + Xa_L$	-	0.023
18	$V_L + IIa_f \leftrightarrow V{:}IIa_L$	1×10^8	6.94
19	$V{:}IIa_L \rightarrow Va_L + IIa_f$	-	0.23
20	$VIII_L + IIa_f \leftrightarrow VIII{:}IIa_L$	1×10^8	13.8
21	$VIII{:}IIa_L \rightarrow VIIIa_L + IIa_f$	-	0.9
22	$Xa{:}Va_L + II_L \leftrightarrow Xa{:}Va{:}II_L$	1×10^8	100
23	$Xa{:}Va_L + mIIa_L \leftrightarrow Xa{:}Va{:}mIIa_L$	1×10^8	66
24	$Xa{:}Va{:}II_L \rightarrow Xa{:}Va{:}mIIa_L$	-	13
25	$Xa{:}Va{:}mIIa_L \rightarrow Xa{:}Va_L + IIa_f$	-	15
26	$VII_L + Xa_L \leftrightarrow VII{:}Xa_L$	5×10^7	44.8
27	$VII{:}Xa_L \rightarrow VIIa_L + Xa_L$	-	15.2
28	$XI_f + IIa_f \leftrightarrow XI{:}IIa_f$	1×10^8	10
29	$XI{:}IIa_f \rightarrow XIa_f + IIa_f$	-	1.453
30	$APC{:}PS_L + VIIIa_L \leftrightarrow APC{:}PS{:}VIIIa_L$	1×10^8	1.6
31	$APC{:}PS{:}VIIIa_L \rightarrow APC{:}PS_L + VIIIai_L$	-	0.45
32	$APC{:}PS_L + Va_L \leftrightarrow APC{:}PS{:}Va_L$	1×10^8	1.6
33	$APC{:}PS{:}Va_L \rightarrow APC{:}PS_L + Vai_L$	-	0.45
34	$TFPI_f + Xa_f \leftrightarrow TFPI{:}Xa_f$	1.6×10^7	0.00033
35	$TFPI{:}Xa_f + TF{:}VIIa_L \leftrightarrow TFPI{:}Xa{:}TF{:}VIIa_L$	1×10^7	0.0011
36	$IXa_f + AT_f \rightarrow IXa{:}AT_f$	4.9×10^2	-
37	$Xa_f + AT_f \rightarrow Xa{:}AT_f$	2.3×10^3	-
38	$IIa_f + AT_f \rightarrow IIa{:}AT_f$	6.83×10^4	-
39	$V_L + mIIa_L \leftrightarrow V{:}mIIa_L$	1×10^8	6.94
40	$V{:}mIIa_L \rightarrow Va_L + mIIa_L$	-	1.035
41	$VIII_L + mIIa_L \leftrightarrow VIII{:}mIIa_L$	1×10^8	13.8
42	$VIII{:}mIIa_L \rightarrow VIIIa_L + mIIa_L$	-	0.9
43	$IIa_f + TM_L \leftrightarrow TM{:}IIa_L$	1×10^9	0.5
44	$TM{:}IIa_L + PC_L \leftrightarrow TM{:}IIa{:}PC_L$	1×10^8	6.45
45	$TM{:}IIa{:}PC_L \rightarrow TM{:}IIa_L + APC_L$	-	3.6
46	$mIIa_f + AT_f \rightarrow mIIa{:}AT_f$	6.83×10^3	-

47	$APC_L + PS_L \leftrightarrow APC{:}PS_L$	1×10^8	0.5
48	$XIa_f + IX_L \leftrightarrow XIa{:}IX_L$	1×10^7	1.4517
49	$XIa{:}IX_L \rightarrow XIa_f + IXa_L$	-	0.183

Table 2.12: The reaction scheme for the Bungay model and their corresponding rate values. The units for all $k_{+,ind}$ and $k_{-,ind}$ reaction rates are $M^{-1}s^{-1}$ and s^{-1}, respectively.

Index	Substrate	$k_{on_{ind}}$ $(M^{-1}s^{-1})$	$k_{off_{ind}}$ (s^{-1})
1	II	4.3×10^6	1
2	mIIa	5×10^7	0.4575
3	V	5×10^7	0.145
4	Va	5.7×10^7	0.17
5	VII	5×10^7	0.66
6	VIIa	5×10^7	0.227
7	VIII	5×10^7	0.1
8	VIIIa	5×10^7	0.335
9	IX	5×10^7	0.115
10	IXa	5×10^7	0.115
11	X	1×10^7	1.9
12	Xa	2.9×10^7	3.3
13	APC	5×10^7	3.5
14	PS	5×10^7	0.2
15	VIIIai	5×10^7	0.335
16	Vai	5.7×10^7	0.17
17	PC	5×10^7	11.5

Table 2.13: The species that can bind to lipids in the Bungay model and their binding and unbinding rates.

Substrate	Initial Concentration (M)
TF	5×10^{-12}
II	1.4×10^{-6}
V	2×10^{-8}
VII	1×10^{-8}
VIIa	1×10^{-10}
VIII	7×10^{-10}
IX	9×10^{-8}
X	1.7×10^{-7}
XI	3×10^{-8}
TFPI	2.5×10^{-9}
AT	3.4×10^{-6}
TM	1×10^{-9}
PC	6×10^{-8}
PS	3×10^{-7}

Table 2.14: The non-zero initial concentrations for the Bungay model [62].

2.1.6 Panteleev Model

The Panteleev model [63] is based on a spatial flow model used in earlier work by Panteleev [64], that was subsequently simplified to remove the spatial components, platelets and thrombomodulin. This model is defined differently to others by featuring some additional assumptions. Binding to phospholipids and of enzyme substrate complexes is assumed to be rapid so the concentrations of these is given as a fraction of the total levels of the substrates. Additionally, the concentrations of some inhibitors ($\alpha_1 - AT$, $\alpha_2 - AP$, $\alpha_2 - M$, PCI, C1-inh, heparin and PS) were assumed to be constant. This model was validated against data on fibrin concentration in normal and factor V deficient plasma for varying TF concentrations where it was able to reproduce the experimental data accurately.

The model was originally defined only as an ODE system which we have translated into an equivalent set of mass action law and non-mass action law reactions given in Table 2.16 and 2.17, respectively. The instant binding equations are given in Table 2.15 where S^B denotes substrate S is bound to lipids and S^F denotes the free concentration of substrate S that is not bound to an enzyme or cofactor. The ^{B} and ^{F} qualifiers have been added to the reaction scheme in any places where it effects a reaction rate.

When the model is solved using the non-zero initial conditions given in Table 2.19, we can then plot a thrombin generation curve for the Panteleev model which is given in Figure 2.2. The ODEs are presented in Appendix A.

The Panteleev model produces a very smooth thrombin generation curve, with its activation appearing almost identical to its inhibition. Its peak height is similar to (although slightly larger than) the Danforth model.

Reaction
$[\text{TF:VIIa}^F] = \frac{[TF:VIIa]}{1+[IX]/K_4+[X]/K_6}$
$[\text{TF:VIIa:Xa}] = \frac{k_6}{K_6 \cdot k_{-19}} \cdot [X][TF:VIIa^F]$
$[\text{IXa}^{BF}] = \frac{[IXa]p \cdot n_{20}}{K_{20}+[IXa]}$
$[\text{VIIIa}^{BF}] = \frac{[VIIIa]p \cdot n_{21}}{(K_{21}+VIIIa) \cdot (1+\frac{[X^B]}{p \cdot K_{10}}) \cdot (1+[PS]/K_{22})}$
$[\text{Xa:Va}^B] = \frac{[Xa] \cdot [Va^B]}{K_{23}(1+[PS]/K_{24}+[Xa]/K_{23})+Va^B}$
$[\text{Xa}^F] = [\text{Xa}]\text{-}[\text{XaVa}^B]$
$[\text{X}^B] = \frac{[X]p \cdot n_{25}}{K_{25}(1+[X]/K_{25}+[II]/K_{26})}$
$[\text{IIa}^F] = \frac{[IIa]}{1+\frac{[Ia]+[I]}{K_{14}}}$
$[\text{II}^B] = \frac{[II]p \cdot n_{25}}{K_{26}(1+[X]/K_{25}+[II]/K_{26})}$
$[\text{Va}^B] = \frac{[Va]p \cdot n_{27}}{K_{27}+[Va]}$
$[\text{Va}^{BF}] = [\text{Va}^B]\text{-}[\text{Xa:Va}^B]$

Table 2.15: The Panteleev model's equations for the levels of free and lipid bound substrate.

Reaction	Reaction rate
$\mathrm{TF} + \mathrm{VII} \leftrightarrow \mathrm{TF{:}VII}$	k_1, k_{-1}
$\mathrm{TF} + \mathrm{VIIa} \leftrightarrow \mathrm{TF{:}VIIa}^F$	k_1, k_{-1}
$\mathrm{TF{:}VII} + \mathrm{IIa}^F \rightarrow \mathrm{TF{:}VIIa} + \mathrm{IIa}$	k_2
$\mathrm{TF{:}VII} + \mathrm{Xa}^F \rightarrow \mathrm{TF{:}VIIa} + \mathrm{Xa}$	k_3
$\mathrm{VII} + \mathrm{IIa}^F \rightarrow \mathrm{VIIa} + \mathrm{IIa}$	k_2
$\mathrm{TF{:}VIIa}^F + \mathrm{Xa{:}TFPI} \rightarrow \mathrm{TF{:}VIIa{:}Xa{:}TFPI}$	h_1
$\mathrm{TF{:}VIIa{:}Xa} + \mathrm{TFPI} \rightarrow \mathrm{TF{:}VIIa{:}Xa{:}TFPI}$	h_2
$\mathrm{IX} + \mathrm{TF{:}VIIa}^F \rightarrow \mathrm{IXa} + \mathrm{TF{:}VIIa}$	k_4/K_4
$\mathrm{IXa} + \mathrm{AT} \rightarrow \mathrm{IXa{:}AT}$	h_3
$\mathrm{X} + \mathrm{TF{:}VIIa}^F \rightarrow \mathrm{Xa} + \mathrm{TF{:}VIIa}$	k_6/K_6
$\mathrm{X}^B + \mathrm{IXa}^{BF} \rightarrow \mathrm{Xa} + \mathrm{IXa}$	$\frac{k_7}{p \cdot K_7}$
$\mathrm{X}^B + \mathrm{IXa}^{BF} + \mathrm{VIIIa}^{BF} \rightarrow \mathrm{Xa} + \mathrm{IXa} + \mathrm{VIIIa}$	$\frac{k_8}{p^2 \cdot K_8 \cdot K_9}$
$\mathrm{Xa}^F + \mathrm{TFPI} \leftrightarrow \mathrm{Xa{:}TFPI}$	k_{11}, k_{-11}
$\mathrm{Xa}^F + \mathrm{AT} \rightarrow \mathrm{Xa{:}AT}$	h_4
$\mathrm{Xa}^F + \alpha_2 - M \rightarrow \mathrm{Xai} + \alpha_2 - M$	h_5
$\mathrm{Xa}^F + \alpha_1 - AT \rightarrow \mathrm{Xai} + \alpha_1 - AT$	h_6
$\mathrm{Xa}^F + \mathrm{PCI} \rightarrow \mathrm{Xai} + \mathrm{PCI}$	h_7
$\mathrm{XaVa}^B + \mathrm{AT} \rightarrow \mathrm{Xa{:}AT} + \mathrm{Va}$	h_8
$\mathrm{II} + \mathrm{Xa}^F \rightarrow \mathrm{IIa} + \mathrm{Xa}$	$k_{12} \cdot p$
$\mathrm{II}^B + \mathrm{XaVa}^B \rightarrow \mathrm{IIa} + \mathrm{XaVa}$	k_{13}/p
$\mathrm{IIa}^F + \mathrm{AT} \rightarrow \mathrm{IIa{:}AT}$	h_9
$\mathrm{IIa}^F + \alpha_2 - M \rightarrow \mathrm{IIai} + \alpha_2 - M$	h_{10}
$\mathrm{IIa}^F + \alpha_1 - AT \rightarrow \mathrm{IIai} + \alpha_1 - AT$	h_{11}
$\mathrm{IIa}^F + \mathrm{PCI} \rightarrow \mathrm{IIai} + \mathrm{PCI}$	h_{12}
$\mathrm{IIa}^F + \mathrm{hep} \rightarrow \mathrm{IIai} + \mathrm{hep}$	h_{13}
$\mathrm{Fbg} + \mathrm{IIa}^F \rightarrow \mathrm{Fbn} + \mathrm{IIa}$	k_{14}/K_{14}
$\mathrm{VIIIa} \rightarrow \mathrm{VIIIai}$	h_{14}
$\mathrm{Va}^{BF} + \mathrm{APC} \rightarrow \mathrm{Vai} + \mathrm{APC}$	h_{15}
$\mathrm{XI} + \mathrm{IIa}^F \rightarrow \mathrm{XIa} + \mathrm{IIa}$	$k_{17} \cdot p$
$\mathrm{XIa} + \mathrm{AT} \rightarrow \mathrm{XIa{:}AT}$	h_{16}
$\mathrm{XIa} + \alpha_2 - AP \rightarrow \mathrm{XIai} + \alpha_2 - AP$	h_{17}
$\mathrm{XIa} + \alpha_1 - AT \rightarrow \mathrm{XIai} + \alpha_1 - AT$	h_{18}
$\mathrm{XIa} + \mathrm{PCI} \rightarrow \mathrm{XIai} + \mathrm{PCI}$	h_{19}
$\mathrm{XIa} + \mathrm{C1inh} \rightarrow \mathrm{XIai} + \mathrm{C1inh}$	h_{20}
$\mathrm{PC} + \mathrm{IIa}^F \rightarrow \mathrm{APC} + \mathrm{IIa}$	k_{18}
$\mathrm{APC} + \alpha_2 - M \rightarrow \mathrm{APCi} + \alpha_2 - M$	h_{21}
$\mathrm{APC} + \alpha_2 - AP \rightarrow \mathrm{APCi} + \alpha_2 - AP$	h_{22}
$\mathrm{APC} + \alpha_1 - AT \rightarrow \mathrm{APCi} + \alpha_1 - AT$	h_{23}
$\mathrm{APC} + \mathrm{PCI} \rightarrow \mathrm{APCi} + \mathrm{PCI}$	h_{24}

Table 2.16: Mass action law reactions for the Panteleev model [63].

Reaction	Reaction rate (M/s)
IX $\overset{XIa}{\rightarrow}$ IXa	$\frac{k_5[IX][XIa]}{K_5+[IX]}$
VIII $\overset{IIa^F}{\rightarrow}$ VIIIa	$\frac{k_{15}[VIII][IIa^F]}{K_{15}+[IIa^F]}$
V $\overset{IIa^F}{\rightarrow}$ Va	$\frac{k_{16}[V][IIa^F]}{K_{16}+[IIa^F]}$

Table 2.17: The non-mass action law reactions and their reaction rate functions for the Panteleev model [63].

Parameter	Parameter Value
k_1	$7 \times 10^7 M^{-1} s^{-1}$
k_{-1}	$0.0183 s^{-1}$
k_2	$2.33 \times 10^4 M^{-1} s^{-1}$
k_3	$6.67 \times 10^6 M^{-1} s^{-1}$
k_4	$0.25 s^{-1}$
K_4	$2.1 \times 10^{-7} M$
k_5	$0.097 s^{-1}$
K_5	$2 \times 10^{-7} M$
k_6	$7.25 s^{-1}$
K_6	$2.38 \times 10^{-7} M$
k_7	$1 \times 10^{-3} s^{-1}$
K_7	230 molecules/platelet
k_8	$105.8 s^{-1}$
K_8	1216 molecules/platelet
K_9	278 molecules/platelet
K_{10}	1655 molecules/platelet
k_{11}	$8.67 \times 10^5 M^{-1} s^{-1}$
k_{-11}	$3.33 \times 10^{-4} s^{-1}$
k_{12}	$7.5 \times 10^{17} M^{-2} s^{-1}$
k_{13}	$0.024 s^{-1}$
k_{14}	$84 s^{-1}$
K_{14}	$7.2 \times 10^{-6} M$
k_{15}	$0.9 s^{-1}$
K_{15}	$1.47 \times 10^{-7} M$
k_{16}	$0.23 s^{-1}$
K_{16}	$7.17 \times 10^{-8} M$
k_{17}	$5 \times 10^{14} M^{-2} s^{-1}$
k_{18}	$3.33 \times 10^2 M^{-1} s^{-1}$
k_{-19}	$12.83 s^{-1}$
n_{20}	260 sites/platelet
K_{20}	$2.57 \times 10^{-9} M$
n_{21}	750 sites/platelet
K_{21}	$1.5 \times 10^{-9} M$
K_{22}	$1.5 \times 10^{-7} M$
K_{23}	$1.18 \times 10^{-10} M$
K_{24}	$2 \times 10^{-7} M$
n_{25}	16000 sites/platelet
K_{25}	$3.2 \times 10^{-7} M$
K_{26}	$4.7 \times 10^{-7} M$
n_{27}	2700 sites/platelet
K_{27}	$2.9 \times 10^{-9} M$
h_1	$7.33 \times 10^6 M^{-1} s^{-1}$
h_2	$1 \times 10^8 M^{-1} s^{-1}$
h_3	$1.37 \times 10^2 M^{-1} s^{-1}$
h_4	$2.5 \times 10^3 M^{-1} s^{-1}$
h_5	$6.67 \times 10^2 M^{-1} s^{-1}$

h_6	$2.27 \times 10^2 M^{-1}s^{-1}$
h_7	$2 \times 10^4 M^{-1}s^{-1}$
h_8	$3.67 \times 10^2 M^{-1}s^{-1}$
h_9	$6.83 \times 10^3 M^{-1}s^{-1}$
h_{10}	$1.67 \times 10^3 M^{-1}s^{-1}$
h_{11}	$50 M^{-1}s^{-1}$
h_{12}	$6.17 \times 10^3 M^{-1}s^{-1}$
h_{13}	$1.05 \times 10^3 M^{-1}s^{-1}$
h_{14}	$5.83 \times 10^{-3} s^{-1}$
h_{15}	$1.28 \times 10^8 M^{-1}s^{-1}$
h_{16}	$3.17 \times 10^2 M^{-1}s^{-1}$
h_{17}	$4.33 \times 10^2 M^{-1}s^{-1}$
h_{18}	$1 \times 10^2 M^{-1}s^{-1}$
h_{19}	$9 \times 10^4 M^{-1}s^{-1}$
h_{20}	$2.33 \times 10^3 M^{-1}s^{-1}$
h_{21}	$1 \times 10^2 M^{-1}s^{-1}$
h_{22}	$1 \times 10^2 M^{-1}s^{-1}$
h_{23}	$11.7 M^{-1}s^{-1}$
h_{24}	$6.5 \times 10^3 M^{-1}s^{-1}$
p	$7.5 \times 10^{-14} M/(\text{sites/platelet})$

Table 2.18: The parameter values given for the Panteleev model [63].

Substrate	Initial Concentration (M)
TF	5×10^{-12}
II	1.4×10^{-6}
V	2×10^{-8}
VII	1×10^{-8}
VIIa	1×10^{-10}
VIII	7×10^{-10}
IX	9×10^{-8}
X	1.7×10^{-7}
XI	3×10^{-8}
Fbg	7.6×10^{-6}
TFPI	2.5×10^{-9}
AT	3.4×10^{-6}
PC	6×10^{-8}
PS	3.46×10^{-7}
PCI	8.8×10^{-8}
C1-inh	1.7×10^{-6}
hep	1.4×10^{-6}
$\alpha_1 - AT$	4×10^{-5}
$\alpha_2 - AP$	1.1×10^{-6}
$\alpha_2 - M$	3×10^{-6}

Table 2.19: The non-zero initial concentrations for the Panteleev model [63].

2.1.7 Tyurin Model

The Tyurin model [66] consists of 48 reactions (22 of which follow Michaelis Menten kinetics and 26 follow mass action law with two of the mass action law reactions being reversible). This model included many new features such as contact activation (which was modelled using a fixed concentration of factor XIIa present initially), many new inhibitors such as $\alpha_1 - AT$, $\alpha_2 - M$, $\alpha_2 - AP$ (α_1-Anti-Trypsin, α_2-Macroglobulin and α_2-Anti-Plasmin), protein C (in a more simplified set of reactions than those in Brummel) and PCI (Protein C Inhibitor). The model was produced for the purpose of evaluating optimal initial concentrations of the various coagulation factors. The model uses Michaelis Menten with competitive inhibition and mass action law rather than exclusively mass action law that was used in the work by Hockin [59], Danforth [42], Chatterjee [39], Brummel [60] and Bungay [62]. This model was not validated against any experimental data. The Michaelis Menten reactions are given in Table 2.20 and the mass action law reactions are given in 2.21.

Index	Reaction	$k_{cat_{ind}}(\mathrm{s}^{-1})$	$k_{m_{ind}}(M)$
1	XI $\overset{XIIa}{\rightarrow}$ XIa	0.35	5×10^{-8}
2	XI $\overset{IIa}{\rightarrow}$ XIa	1.43	5×10^{-8}
3	XI $\overset{XIa}{\rightarrow}$ XIa	0.13	5×10^{-8}
4	IX $\overset{XIa}{\rightarrow}$ IXa	1.25	3.55×10^{-7}
5	IX $\overset{VIIa}{\rightarrow}$ IXa	$1.8 \times 10^{-}4$	9×10^{-9}
6	IX $\overset{TF:VIIa}{\rightarrow}$ IXa	0.7	1×10^{-7}
7	X $\overset{IXa}{\rightarrow}$ Xa	6.7×10^{-4}	1×10^{-6}
8	X $\overset{IXa:VIIIa}{\rightarrow}$ Xa	25	1.6×10^{-7}
9	X $\overset{VIIa}{\rightarrow}$ Xa	2.45×10^{-3}	2.5×10^{-7}
10	X $\overset{TF:VIIa}{\rightarrow}$ Xa	1.8	2.2×10^{-7}
11	II $\overset{Xa}{\rightarrow}$ IIa	0.0375	5.8×10^{-6}
12	II $\overset{Xa:Va}{\rightarrow}$ IIa	28.3	1.03×10^{-6}
13	V $\overset{IIa}{\rightarrow}$ Va	0.23	7.17×10^{-8}
14	V $\overset{Xa}{\rightarrow}$ Va	0.043	1.04×10^{-8}
15	VII $\overset{Xa}{\rightarrow}$ VIIa	0.05	5×10^{-8}
16	TF:VII $\overset{Xa}{\rightarrow}$ TF:VIIa	0.66	9.3×10^{-9}
17	VIII $\overset{IIa}{\rightarrow}$ VIIIa	0.36	2.0×10^{-8}
18	PC $\overset{TM:IIa}{\rightarrow}$ APC	88.3	5.9×10^{-6}
19‡	Va $\overset{APC}{\rightarrow}$ Vai	0.4	2.0×10^{-8}
20‡	VIIIa $\overset{APC}{\rightarrow}$ VIIIai	0.4	2.0×10^{-8}
21‡	IXa:VIIIa $\overset{APC}{\rightarrow}$ VIIIai + IXa	0.4	2.0×10^{-8}
22‡	Xa:Va $\overset{APC}{\rightarrow}$ Vai + Xa	0.4	2.0×10^{-8}

Table 2.20: The Michaelis Menten reactions and rate constants for the Tyurin model [66].

Index	Reaction	k_{ind}
1	Va + Xa $\rightarrow$ Xa:Va	1.67×10^8
2	VIIIa + IXa $\rightarrow$ VIIIa:IXa	1.67×10^8
3	VIIa + TF $\rightarrow$ TF:VIIa	5×10^4
4	TF:VIIa $\rightarrow$ VIIa + TF	3.33×10^{-5}
5	VII + TF $\rightarrow$ TF:VII	3.33×10^4
6	TF:VII $\rightarrow$ VII + TF	3.33×10^{-6}
7	TF:VIIa + TFPI:Xa $\rightarrow$ TF:VIIa:TFPI:Xa	1.08×10^7
8	TF:VIIa + AT $\rightarrow$ TF:VIIa:AT	450
9	IIa + AT $\rightarrow$ IIa:AT	7.08×10^3
10	IIa + $\alpha_1 - AT$ $\rightarrow$ IIa:$\alpha_1 - AT$	78.3
11	IIa + $\alpha_2 - M$ $\rightarrow$ IIa:$\alpha_2 - M$	488
12	IIa + PCI $\rightarrow$ IIa:PCI	1.67×10^4
13	Xa + AT $\rightarrow$ Xa:AT	3.13×10^3
14	Xa + $\alpha_1 - AT$ $\rightarrow$ Xa:$\alpha_1 - AT$	262
15	Xa + TFPI $\rightarrow$ Xa:TFPI	1.6×10^7
16	Xa:Va + $\alpha_1 - AT$ $\rightarrow$ Xa:$\alpha_1 - AT$ + Va	262
17	Xa:Va + AT $\rightarrow$ Xa:AT + Va	1.67×10^3
18	IXa + AT $\rightarrow$ IXa:AT	490
19	VIIIa:IXa + AT $\rightarrow$ IXa:AT + VIIIa	500
20	XIa + C1-inh $\rightarrow$ XIa:C1-inh	16.7
21	XIa + $\alpha_1 - AT$ $\rightarrow$ XIa:$\alpha_1 - AT$	66.7
22	XIa + AT $\rightarrow$ XIa:AT	167
23	XIa + $\alpha_2 - AP$ $\rightarrow$ XIa:$\alpha_2 - AP$	500
24	XIa + PAI-1 $\rightarrow$ XIa:PAI-1	2.1×10^5
25	IIa + TM $\rightarrow$ TM:IIa	5×10^5
26	TM:IIa + PCI $\rightarrow$ TM:IIa:PCI	1×10^6
27	APC + PCI $\rightarrow$ APC:PCI	2.5×10^3
28	APC + $\alpha_1 - AT$ $\rightarrow$ APC:$\alpha_1 - AT$	10

Table 2.21: Mass action law reactions and reaction rate constants for the Tyurin model [66]. All units are $M^{-1}s^{-1}$ except for k_4 and k_6 which are both s^{-1}.

When this system is solved with the initial conditions given in Table 2.22, we get the thrombin generation curve given in Figure 2.2. The ODEs are presented in Appendix A.

The thrombin generation curve of the Tyurin model appears similar in shape to the Chatterjee model, with very rapid activation up to a very large peak height once it passes the lagtime. The lagtime is shorter than the Chatterjee model, similar to the Bungay model, and its peak height is larger.

[‡]The parameters for these reactions are identical to one another and should remain so during any changes for sensitivity analysis or approximate Bayesian computation.

[§]These initial conditions are not stated in the description of the model and are added to ensure that all reactions in the model can occur.

Substrate	Initial Concentration (M)
TF	1×10^{-8}
II	1.4×10^{-6}
V	2.1×10^{-8}
VII	1×10^{-8}
VIIa[§]	1×10^{-10}
VIII	7×10^{-10}
IX	9×10^{-8}
X	1.33×10^{-7}
XI[§]	3×10^{-8}
XIIa[§]	2.3×10^{-11}
TFPI	2.5×10^{-9}
AT	5×10^{-6}
TM[§]	1×10^{-9}
PC	6.45×10^{-8}
PCI	7×10^{-8}
C1-inh[§]	2.1×10^{-6}
PAI-1[§]	4.6×10^{-10}
$\alpha_1 - AT$	4×10^{-5}
$\alpha_2 - AP$	9.5×10^{-7}
$\alpha_2 - M$	3×10^{-6}

Table 2.22: The non-zero initial conditions for the Tyurin model as reported in [66]. Some initial conditions were not given so values have been used from other models.

2.1.8 Zhu Model

The Zhu model [68] consists of 55 reactions (of which 35 follow mass action law kinetics and 20 follow Michaelis Menten kinetics). They separated the model into contact activation and tissue factor activation to investigate the differences between them. This meant the model has a very detailed contact activation pathway which included kallikreins, an activator for FXII, and a simplified set of protein C reactions. This model was not validated against any experimental data. The Michaelis Menten reactions are reported in Table 2.23 and the mass action law reactions are given in Table 2.24.

When these reactions are solved with the non-zero initial conditions given in Table 2.25, we observe the thrombin generation curve given in Figure 2.2. The ODEs are presented in Appendix A.

The Zhu model has the largest peak height of all the models and the smallest lagtime. It is most similar in shape to the Tyurin and Chatterjee models.

Index	Reaction	$k_{cat_{ind}}(\mathrm{s}^{-1})$	$k_{m_{ind}}(M)$
1	XII $\overset{XIIa}{\rightarrow}$ XIIa	0.033	1.1×10^{-5}
2	PK $\overset{XIIa}{\rightarrow}$ K	3.6	9.1×10^{-8}
3	PK $\overset{XIIf}{\rightarrow}$ K	40	3.7×10^{-5}
4	XII $\overset{K}{\rightarrow}$ XIIa	5.7	5.1×10^{-7}
5	XIIa $\overset{K}{\rightarrow}$ XIIf	5.7×10^{-3}	5×10^{-7}
6	XI $\overset{XIIa}{\rightarrow}$ XIa	5.7×10^{-4}	2×10^{-6}
7	XII $\overset{XIa}{\rightarrow}$ XIIa	0.57	5×10^{-7}
8	IX $\overset{XIa}{\rightarrow}$ IXa	3.75	3.5×10^{-7}
9	X $\overset{IXa}{\rightarrow}$ Xa	6.7×10^{-4}	2×10^{-6}
10	X $\overset{IXa:VIIIa}{\rightarrow}$ Xa	29	1.9×10^{-7}
11	II $\overset{Xa}{\rightarrow}$ IIa	0.0375	5.8×10^{-8}
12	II $\overset{Xa:Va}{\rightarrow}$ IIa	28.3	1×10^{-6}
13	V $\overset{IIa}{\rightarrow}$ Va	0.23	7.17×10^{-8}
14	V $\overset{Xa}{\rightarrow}$ Va	0.043	1.04×10^{-8}
15	VIII $\overset{IIa}{\rightarrow}$ VIIIa	1	2×10^{-8}
16	Fbg $\overset{IIa}{\rightarrow}$ Fbn	84	7.2×10^{-6}
17	TF:VII $\overset{Xa}{\rightarrow}$ TF:VIIa	0.66	9.3×10^{-9}
18	X $\overset{TF:VIIa}{\rightarrow}$ Xa	1.72	3.8×10^{-7}
19	IX $\overset{TF:VIIa}{\rightarrow}$ IXa	0.57	1.33×10^{-7}
20	PC $\overset{TM:IIa}{\rightarrow}$ APC	0.33	7.7×10^{-6}

Table 2.23: The Michaelis Menten reactions and rate constants for the Zhu model [68].

Index	Reaction	k_{ind}
1	Xa + Va $\rightarrow$ Xa:Va	1.67×10^8
2	VIIIa + IXa $\rightarrow$ VIIIa:IXa	1.67×10^8
3	IIa + AT $\rightarrow$ IIa:AT	5833
4	IIa + $\alpha_1 - AT \rightarrow$ IIa:$\alpha_1 - AT$	78.3
5	IIa + $\alpha_2 - M \rightarrow$ IIa:$\alpha_2 - M$	488
6	Xa + AT $\rightarrow$ Xa:AT	1833
7	Xa + $\alpha_1 - AT \rightarrow$ Xa:$\alpha_1 - AT$	262
8	Xa + TFPI $\rightarrow$ Xa:TFPI	1.6×10^7
9	IXa + AT $\rightarrow$ IXa:AT	490
10	XIa + C1-inh $\rightarrow$ XIa:C1-inh	16.7
11	XIa + $\alpha_1 - AT \rightarrow$ XIa:$\alpha_1 - AT$	66.7
12	XIa + AT $\rightarrow$ XIa:AT	167
13	XIa + $\alpha_2 - AP \rightarrow$ XIa:$\alpha_2 - AP$	500
14	XIa + PAI-1 $\rightarrow$ XIa:PAI-1	2.1×10^5
15	XIIa + C1-inh $\rightarrow$ XIIa:C1-inh	3667
16	XIIa + $\alpha_2 - AP \rightarrow$ XIIa:$\alpha_2 - AP$	183
17	XIIa + $\alpha_2 - M \rightarrow$ XIIa:$\alpha_2 - M$	83
18	XIIa + AT $\rightarrow$ XIIa:AT	21.7
19	XIIa + PAI-1 $\rightarrow$ XIIa:PAI-1	1.6×10^4
20	XIIf + C1-inh $\rightarrow$ XIIf:C1-inh	3083
21	XIIf + $\alpha_2 - AP \rightarrow$ XIIf:$\alpha_2 - AP$	152
22	XIIf + AT $\rightarrow$ XIIf:AT	53.3
23	K + C1-inh $\rightarrow$ K:C1-inh	1.67×10^4
24	K + $\alpha_2 - M \rightarrow$ K:$\alpha_2 - M$	4833
25	K + PAI-1 $\rightarrow$ K:PAI-1	6×10^4
26	K + AT $\rightarrow$ K:AT	160
27	VII + TF $\rightarrow$ TF:VII	3.3×10^4
28	TF:VIIa + AT $\rightarrow$ TF:VIIa:AT	450
29	TF:VIIa + Xa:TFPI $\rightarrow$ TF:VIIa:Xa:TFPI	1.1×10^7
30	APC + Va $\rightarrow$ APC:Va	2×10^7
31	APC + VIIIa $\rightarrow$ APC:VIIIa	2×10^7
32	APC + Xa:Va $\rightarrow$ APC:Xa:Va	2×10^7
33	APC + VIIIa:IXa $\rightarrow$ APC:VIIIa:IXa	2×10^7
34	TM + IIa $\rightarrow$ TM:IIa	6.7×10^6
35	XI $\rightarrow$ XIa	1.3×10^{-4}

Table 2.24: Mass action law reactions and reaction rate constants for the Zhu model [68]. All units are $M^{-1}s^{-1}$ except for k_{35} which has units of s^{-1}

Substrate	Initial Concentration (M)
TF	5×10^{-7}
II	1.4×10^{-6}
V	2.1×10^{-8}
VII	1.8×10^{-8}
TF:VIIa	5×10^{-9}
VIII	7×10^{-10}
IX	9×10^{-8}
X	1.33×10^{-7}
XI	2.5×10^{-8}
XII	3×10^{-7}
XIIa	2.3×10^{-11}
Fbg	8.3×10^{-6}
PK	5.8×10^{-7}
TFPI	2.5×10^{-9}
AT	3.4×10^{-6}
TM	2.2×10^{-10}
PC	6.4×10^{-8}
C1-inh	1.7×10^{-6}
PAI-1	4.6×10^{-10}
$\alpha_1 - AT$	2.45×10^{-5}
$\alpha_2 - AP$	9×10^{-7}
$\alpha_2 - M$	3.5×10^{-6}

Table 2.25: The non-zero initial conditions for the Zhu model [68].

2.1.9 Model Components

Figure 2.4 presents the components in each of the models in the form of a Venn diagram.

Alongside the default species required for the tissue factor activation pathway, protein C and thrombomodulin are commonly used in models as well as including the contact activation pathway. Although protein C is featured in many of these models, its cofactor protein S is only included in two models.

There is still clearly large disagreement between models on which components are relevant to predicting thrombin generation. Over the following sections, we will investigate these differences between the models, with the end goal of identifying what is necessary, what may be removed, and where we can improve upon them.

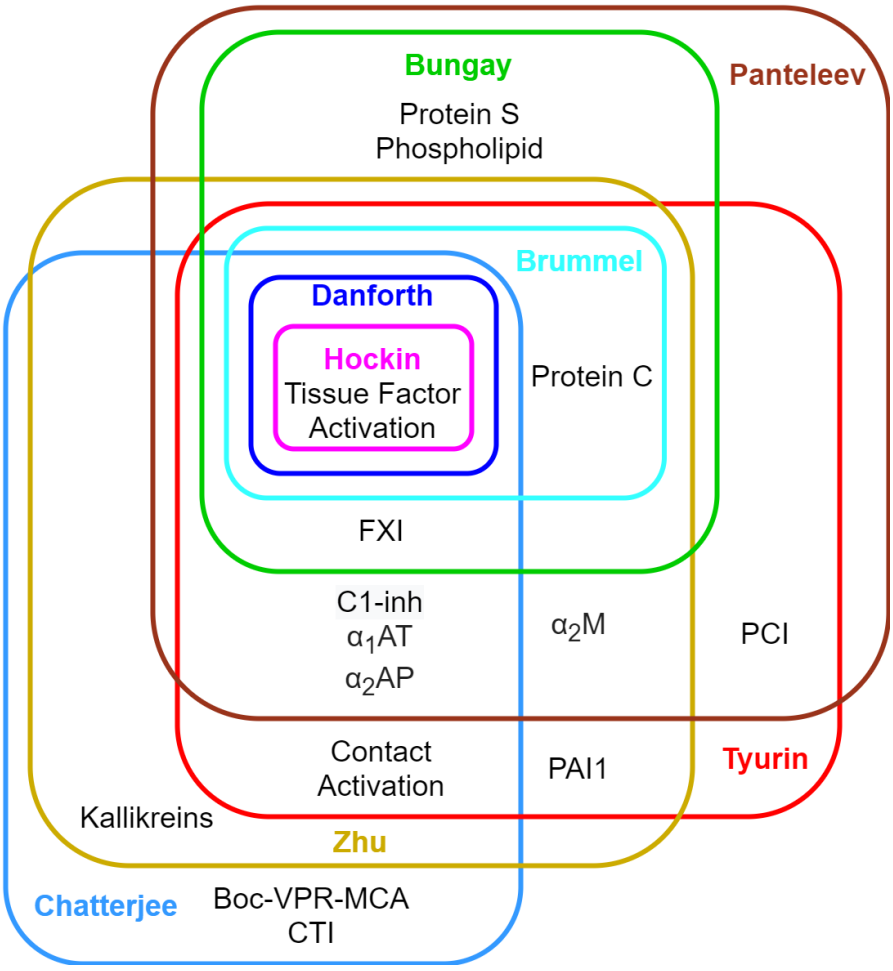

Figure 2.4: A Venn diagram comparing the species used in each of the models.

2.2 Model Validation

To ensure our implementation of the models is accurate, for each model we utilise, our code is validated against available code on BioModels [87] and figures and plots available in the original papers.

2.2.1 Hockin Model

The code for the Hockin model is validated against the auto-generated MATLAB BioModels code (Version 2 of the Hockin Model; BIOMD0000000335) and by reproducing Figure 3 from the original paper [59].

To produce easily comparable figures the BioModels time interval is changed from [0,100] to [0,700] and the AbsTol (ODE solver absolute tolerance) is reduced to 10^{-10}. This is then compared against our thrombin generation curve in Figure 2.5*. We also reproduce Figure 3 from the original paper [59], which demonstrates total thrombin generation curves ([IIa] + 1.2[mIIa]) for varying initial levels of tissue factor, presented in Figure 2.6. In both cases we are able to reproduce the results of the model accurately.

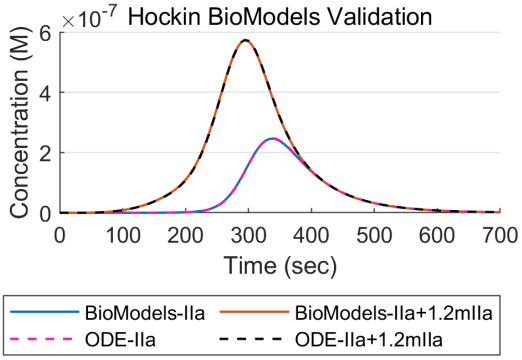

Figure 2.5: A comparison between the BioModels and our code (labelled ODE) for the Hockin model.

2.2.2 Danforth Model

The code for the Danforth model is validated against Figure 1 from the original paper [42], with the comparison given in Figure 2.7. There appears to be a slight discrepancy in time to peak which lead us to compare another figure, specifically Figure 2B in the original paper [42]. As demonstrated in Figure 2.8, this also presented minor discrepancies that become more apparent at large changes to the parameter values.

*This validation was performed using an initial TF concentration of 25pM.

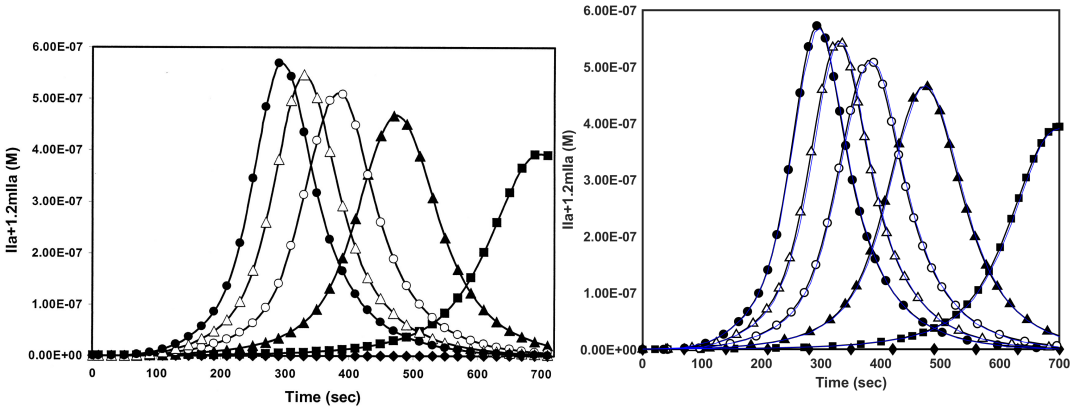

(a) Copied from the original paper.

(b) Generated using our Hockin model code. Blue curves are used for the digitized curves from the original figure.

Figure 2.6: A comparison between Figure 3 from the original paper [59] and the same figure generated using our code for the Hockin model.

We have verified that, after reversing the changes between the Danforth model and Hockin model in our code, we reproduce the results of the Hockin model but we are unable to identify a cause for these discrepancies. This leads us to believe there are differences between the reactions and rates described in the supplemental information of the paper and the implementation of the model used to generate the figures in the paper.

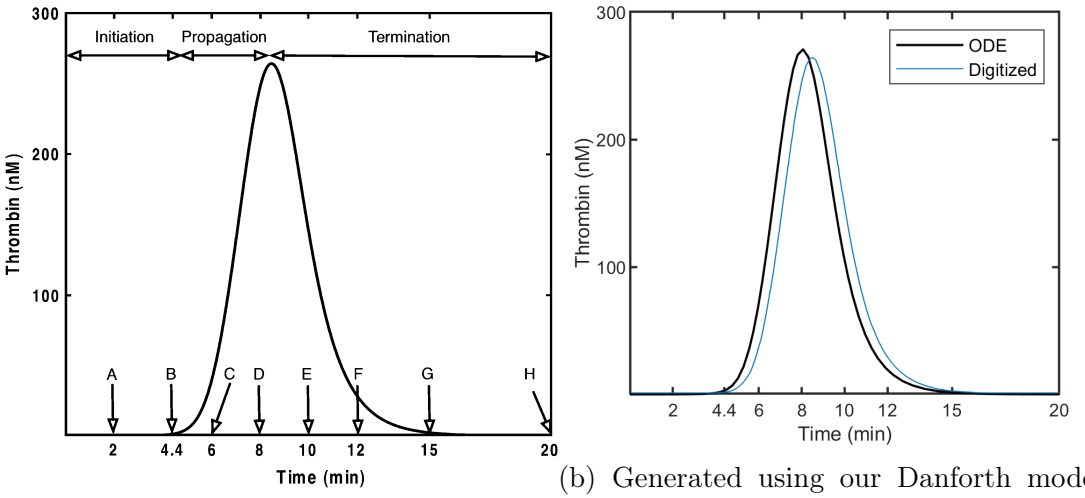

(a) Plot from original paper.

(b) Generated using our Danforth model. Blue curves are used a digitized curve from the original figure.

Figure 2.7: A comparison between Figure 1 from the original Danforth paper [42] and the same figure generated by our Danforth model code.

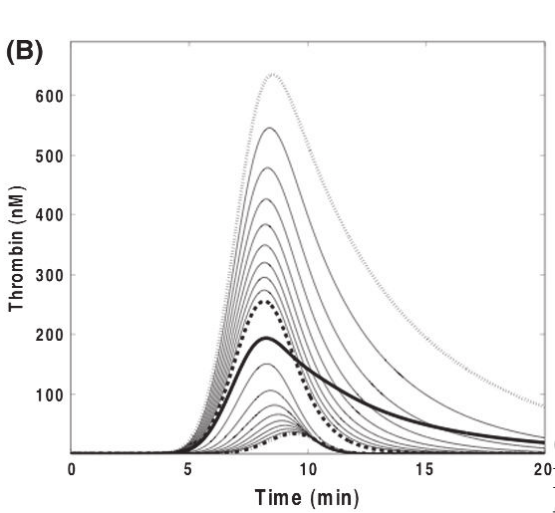

(a) Plot from original paper.

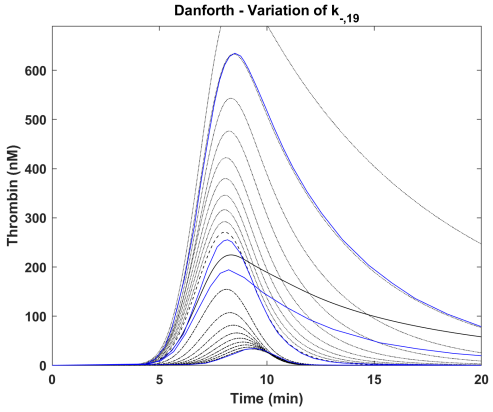

(b) Generated using our Danforth model. Blue curves are used for four digitized curves from the original figure (only the thick black line and the three dotted lines are reproduced).

Figure 2.8: A comparison between Figure 2B from the original Danforth paper [42] and the same figure generated by our Danforth model code for the variation of parameter $k_{-,19}$ (referred to as k_{41} in the Danforth paper [42]).

2.2.3 Chatterjee Model

The code for the Chatterjee model is validated against the BioModels auto-generated MATLAB code (MODEL1108260014). The dilution event* that is used frequently in the paper, and also in the BioModels code, is unnecessary for our work so is removed from the BioModels code to produce the thrombin generation curve. There is also an error caused by the auto-generation program which only uses parameters in the default of local scope and the parameter which represents [IIa·(t)] (global_par_parameter_1) needs to be global for the code to update ε correctly, so this is also changed. This code is then compared against our thrombin generation curve in Figure 2.9 where we are able to reproduce the results.

2.2.4 Brummel Model

The code for the Brummel model is validated against the BioModels SBML file (Version 2; MODEL1807180002) which is then analysed using the SimBiology application in MATLAB. There are two discrepancies between the SBML BioModels file and our MATLAB code which are the lack of an initial concentration for FVIIa in the SBML file and the parameter k_{17} which uses a value of 2×10^7 in our code and 237 in the SBML file. After checking the parameter value in the description of the model given by Brummel [60], it is reported as 2×10^7 and therefore corrected in the SBML file. Although initial conditions are not specified by Brummel in the model description, a non-zero initial FVIIa concentration is required for thrombin generation so this is also added to the SBML file as 1×10^{-10}M. The thrombin

*The dilution event is a part of the SBML file, and therefore also the auto-generated code, in which the volume of the system is changed to capture an experimental assay being diluted.

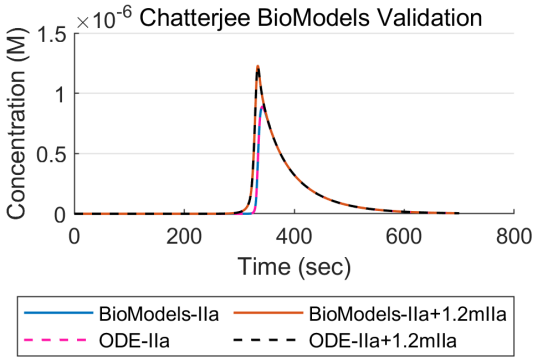

Figure 2.9: A comparison between the BioModels and our code (labelled ODE) for the Chatterjee model.

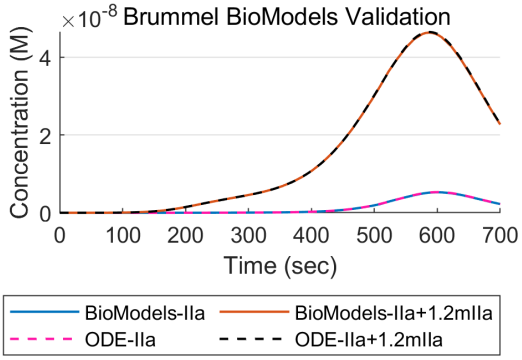

Figure 2.10: A comparison between the BioModels and our code (labelled ODE) for the Brummel model.

generation curves are then compared to one another in Figure 2.10 where we are able to match the results of this edited SBML file.

2.2.5 Bungay Model

The code for the Bungay model is validated against the BioModels auto-generated MATLAB file (Version 2; BIOMD0000000334) as well as Figure 4 from the original paper [62]. To produce easily comparable figures, the BioModels time interval is changed from [0,100] to [0,700] and the AbsTol is reduced to 10^{-10}. This is compared against our thrombin generation curve in Figure 2.11. The comparison to Figure 4 from the original paper [62] is given in Figure 2.12 and in both cases we produce matching figures.

2.2.6 Panteleev Model

The code for the Panteleev model is validated against two figures from the paper [63] (Figures 4A and 4D). The comparison between the original figures and our

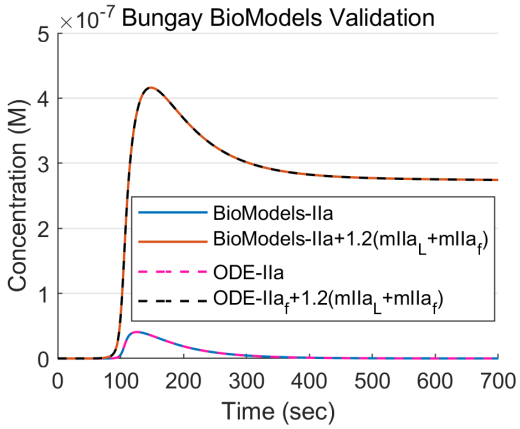

Figure 2.11: A comparison between the BioModels and our code (labelled ODE) for the Bungay model.

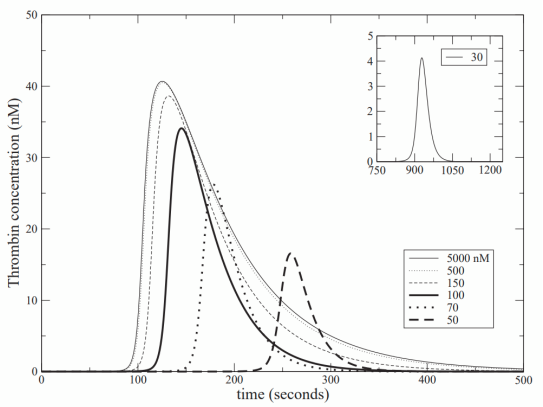

(a) Plot from the original paper.

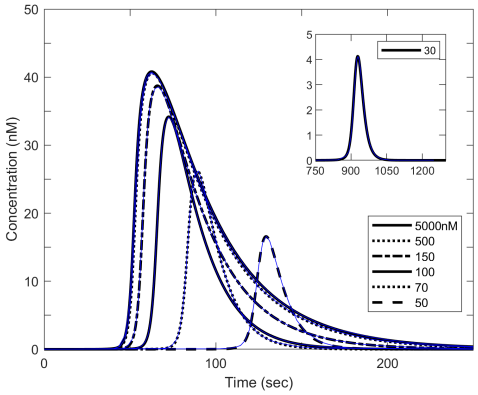

(b) Generated using our Bungay code. Blue curves are used for the digitized curves from the original figure.

Figure 2.12: A comparison between the thrombin generation curves for different vesicle concentrations from Figure 4 of the original paper and our code for the Bungay model.

code is given in 2.14. All curves appear to match except for the 4pM of TF curve where it appears slightly slower in the original compared to our predictions. We were unable to identify the cause of this discrepancy so we compared our code to the BioModels code (BIOMD0000000740; which also fails to reproduce the original Figure 4A, although in a different way) and found a handful of discrepancies between these two implementations. All discrepancies were due to errors in the BioModels code (using k_8 instead of K_8 in the FX and FXa ODEs and using i_3, Xa:TFPI, instead of i_1, AT, in the FIXa ODE). After fixing these mistakes and including an initial FV concentration, our code matches the edited BioModels code as demonstrated in Figure 2.13.

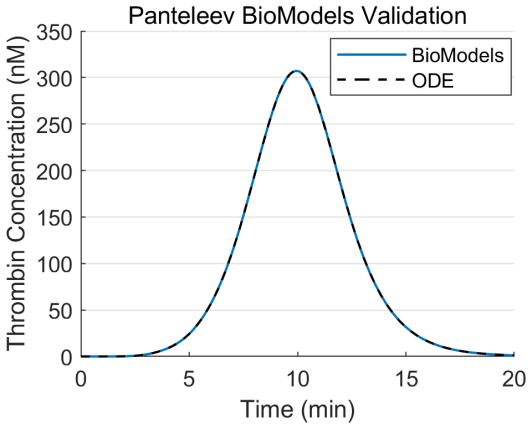

Figure 2.13: A comparison between the BioModels and our code (labelled ODE) for the Panteleev model.

2.2.7 Tyurin Model

The Tyurin model's original paper [66] lacks any figures or results that can be easily used for verifying our code and there is not a version of the model available on BioModels. As such, we rebuilt the model in the SimBiology MATLAB app to verify against minor implementation mistakes[†]. The thrombin generation curves are given in Figure 2.15.

2.2.8 Zhu Model

We are unable to validate our code against the figures given in the original paper. Additionally, no code is given with the paper and there are no implementations on BioModels. The model is given as a set of 55 reactions, but in the ODEs and figures these reactions are separated into intrinsic, extrinsic or both. Unfortunately, the only statement of which reactions are in each group is given in the ODEs which contain multiple errors. These mistakes are fairly simple to resolve, such as the rate of FIIa inhibition by $\alpha_2 - M$ being given as $-k_{21}[\alpha_2 - M][Xa]$. However, implementing these ODEs with or without these mistakes still fails to reproduce the results seen in the paper (See Figure 2.17). We are able to verify that, after fixing the mistakes in the ODEs, we replicated the results of our previous code (when the intrinsic and extrinsic reactions are merged together). Additionally, to further ensure that there are no mistakes in our model's code we reproduced the model in SimBiology and then verify our code against it. The thrombin generation curves are given in Figure 2.16.

2.2.9 Conclusions

We are able to accurately reproduce the Hockin, Chatterjee, Brummel, and Bungay models. The Danforth and Panteleev models appears to have a small discrep-

[†]This is focused on avoiding mistakes in the typing of the ODEs which are unlikely to be repeated. This does not ensure that our implementation matches the one used in the paper.

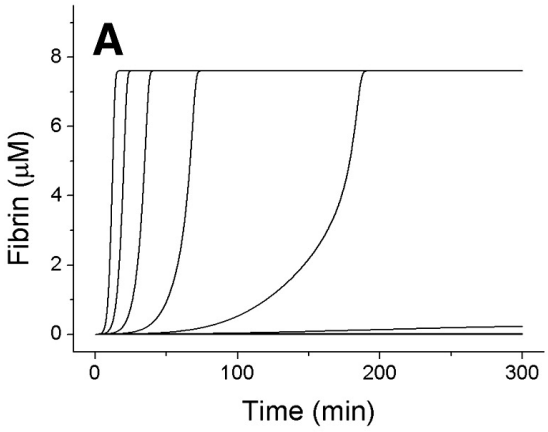

(a) Figure 4A from [63].

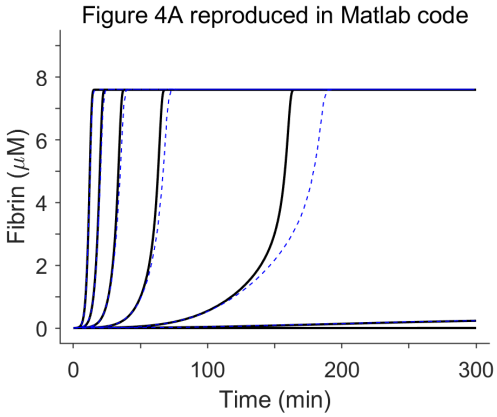

(b) Generated using our Panteleev code. Blue curves are used for the digitized curves from the original figure.

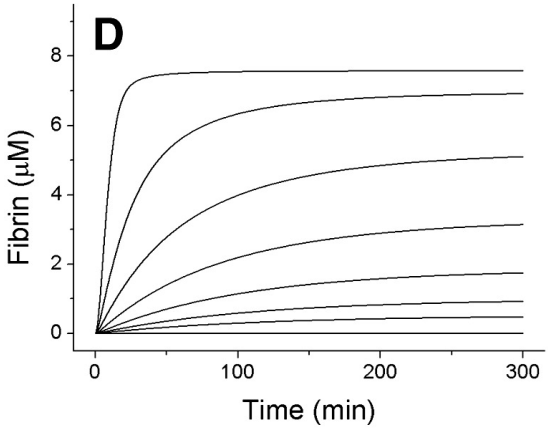

(c) Figure 4D from [63].

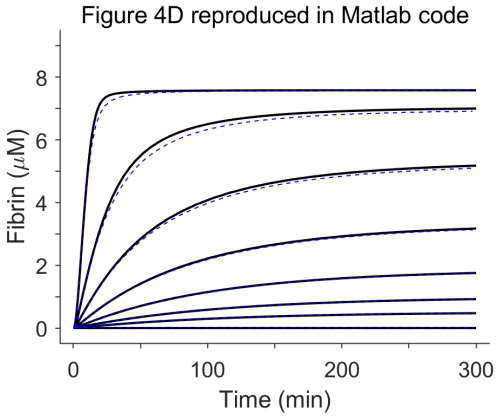

(d) Generated using our Panteleev code. Blue curves are used for the digitized curves from the original figure.

Figure 2.14: A comparison between the fibrin curves from the original paper [63] and our Panteleev model code. Figure 4A uses 0.64, 0.32, 0.16, 0.08, 0.04, 0.02, 0.01 and 0pM as the initial concentration of TF and Figure 4D uses 64, 32, 16, 8, 4, 2, 1 and 0pM of TF with no initial V concentration.

ancy between our implementation and the results in the paper. In the case of the Panteleev model, we were able to validate against the available model on BioModels. The Tyurin model does not present any methods for a simple validation so we have verified our implementation against minor mistakes. We were unable to reproduce the results of the Zhu model, so we have also verified our implementation against minor mistakes. In the interest of clarity and reproducibility, we have presented the ODEs we use to implement the models in Appendix A.

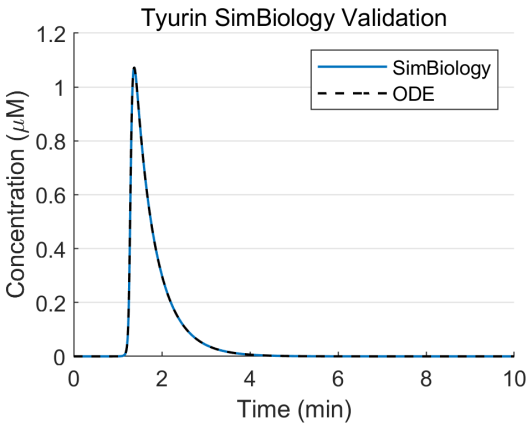

Figure 2.15: A comparison between our SimBiology implementation and our ODE implementation for the Tyurin model.

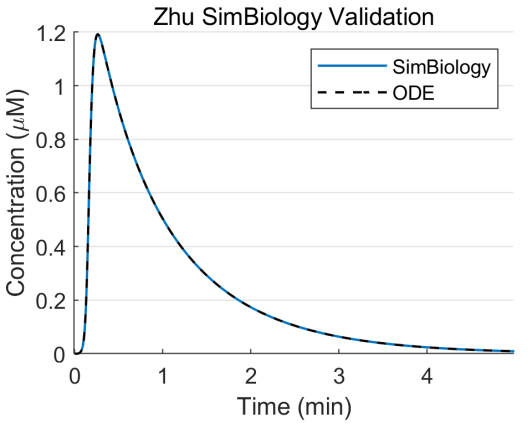

Figure 2.16: A comparison between our SimBiology implementation and our ODE implementation for the Zhu model.

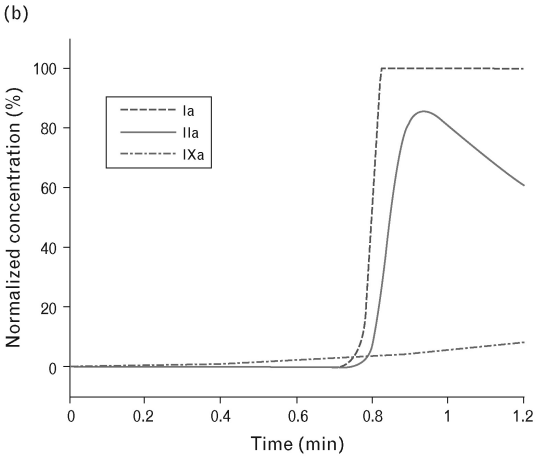

Kinetics of (a) proenzyme consumption and (b) enzyme formation during the second stage of the intrinsic pathway.

(a) Plot for intrinsic pathway from the original paper.

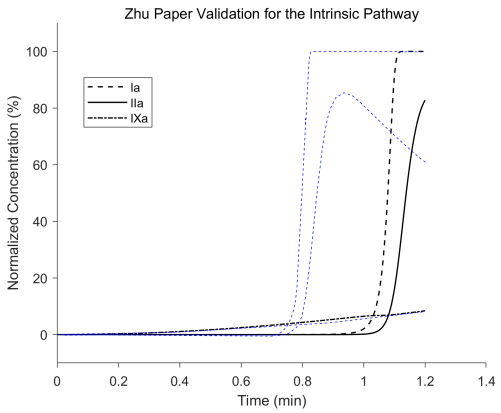

(b) Generated using our Zhu code for the intrinsic pathway. Blue curves are used for the digitized curves from the original figure.

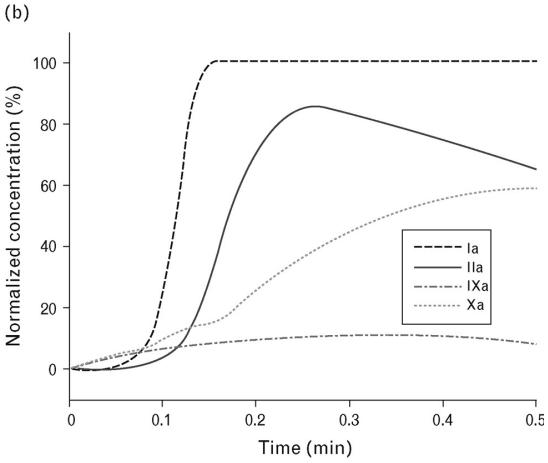

Kinetics of (a) proenzyme consumption and (b) enzyme formation during the extrinsic pathway.

(c) Plot for extrinsic pathway from the original paper.

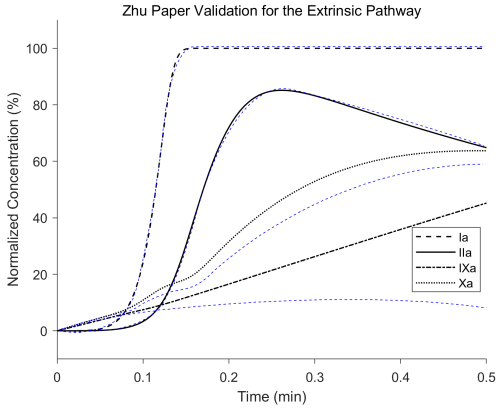

(d) Generated using our Zhu code for the extrinsic pathway. Blue curves are used for the digitized curves from the original figure.

Figure 2.17: A comparison between the figures from the original paper and the same figures made using our implementation of the ODEs after fixing the mistakes.

2.3 Correlation

The models have been validated qualitatively against thrombin generation data, under which the concentrations of at most two coagulation factors are varied. It has previously been shown that a subset of the models we consider (Hockin, Chatterjee, Bungay, Tyurin and Zhu) failed to reproduce ETP from patient data for a cohort of 112 individuals [78]. We will expand on this work, both in the number of models and the number of patients. We will then assess some similarities and differences between the predictions made by the models. Finally, we will conclude by identifying the cause of a discrepancy in one of the model's predictions of ETP that was found when comparing the models to patient data.

In this chapter, we assess the models as they were originally described. Later, in Chapter 3, we will assess one of these models after optimising the reaction rates to best fit the PRAMIS data.

2.3.1 Correlation with Patient Data

As previously described in Section 1.1, the data set we use consists of measured values for factor concentrations and ETP from a cohort of 348 individuals (162 premature myocardial infarction cases and 186 age, sex and smoking-status matched healthy controls). The thrombotic potential, given as ETP, was measured through a chromogenic assay with the Pefachrome-TG substrate. From this assay, ETP was reported as a percentage of a 20-donor plasma pool. Additionally, the measured concentrations of factors II, V, VII, VIII, IX, X, XI and the inhibitor AT are also reported relative to a 20-donor plasma pool. The concentration of TF is recorded in pM and TFPI is recorded in Units. We convert the TFPI concentration to a percentage using the mean TFPI concentration of the controls. The chromogenic assay was performed twice, using both the reported concentration of TF and with an additional 5pM of exogenous TF added.

A set of baseline initial conditions were taken as the median of the initial conditions given by each of the models, which coincides with previously reported healthy figures [59]. These baseline initial conditions are given in Table 2.26. We use the patient specific factor concentrations (given as a percentage of pooled plasma) to scale these baseline concentrations, giving us the patient specific factor concentration in moles that can be simulated in the models. The rate constants for each model are fixed at their original values, so only the initial concentrations of the coagulation factors vary between individuals.

The patient specific factor concentrations are simulated in each of the models and the ETP is extracted from the resulting model-predicted thrombin generation curve. The units for model predicted ETP, $mol \cdot sec$, cannot be easily compared to the units recorded in the data, percentage of pooled plasma. This is because while we had standard reference values to assume were present in the pooled plasma

*The Zhu model does not feature a FVIIa species so the TF:VIIa is used in its place.

Species	Baseline Initial Concentration (M)
II	1.4×10^{-6}
V	2×10^{-8}
VII	1×10^{-8}
VIII	7×10^{-10}
IX	9×10^{-8}
X	1.6×10^{-7}
XI	3×10^{-8}
VIIa	[VII]/100*
AT	3.4×10^{-6}
TFPI	2.5×10^{-9}
PCI	7.9×10^{-8}
$\alpha_1 - AT$	4×10^{-5}
$\alpha_2 - M$	3×10^{-6}
$\alpha_2 - AP$	9.75×10^{-7}
PAI1	4.6×10^{-10}
C1-inh	1.7×10^{-6}
Lipid	4×10^{-6}

Table 2.26: The baseline non-zero initial concentrations to be used as standard values. These values are gathered as a median from the models and coincides with the healthy figures reported in [59]. The lipid concentration used matches that in our assay rather than from the models.

(which we scale by the patient data in % of pooled plasma to derive patient specific values), the ETP in $mol \cdot sec$ for pooled plasma is dependent on the assay and its setup. As such, we evaluate model performance using scatter plots, with the accuracy quantified through the RMSE of a line of proportionality. We focus on the line of proportionality as we still expect zero ETP in the assay (which can only occur if no thrombin is formed) to correspond to zero ETP in the model. This method is presented diagrammatically in Figure 2.18.

Only the initial coagulation factor concentrations are varied between individuals while the reactions and reaction rates are kept fixed for each of the models.

Factor XII is not included in the model simulations to provide the best match to the data, for which FXII activation is minimal. Additionally, CTI, Boc-VPR-MCa, TM, and protein C are not included as they are not present in the assay (protein C is present but will not be significantly activated due to the lack of TM).

The ETP scatter plots for each of the models are given in Figure 2.19. All models were poor predictors of ETP (RMSE: 27.6-32.5) with the Panteleev model giving marginally the best RMSE. For comparison, a linear model, trained using the same factor concentrations as used by the models to predict ETP gives a RMSE of 25.7[†], considerably better than all models.

[†]The linear model was trained to predict ETP using the initial concentrations of factors II,

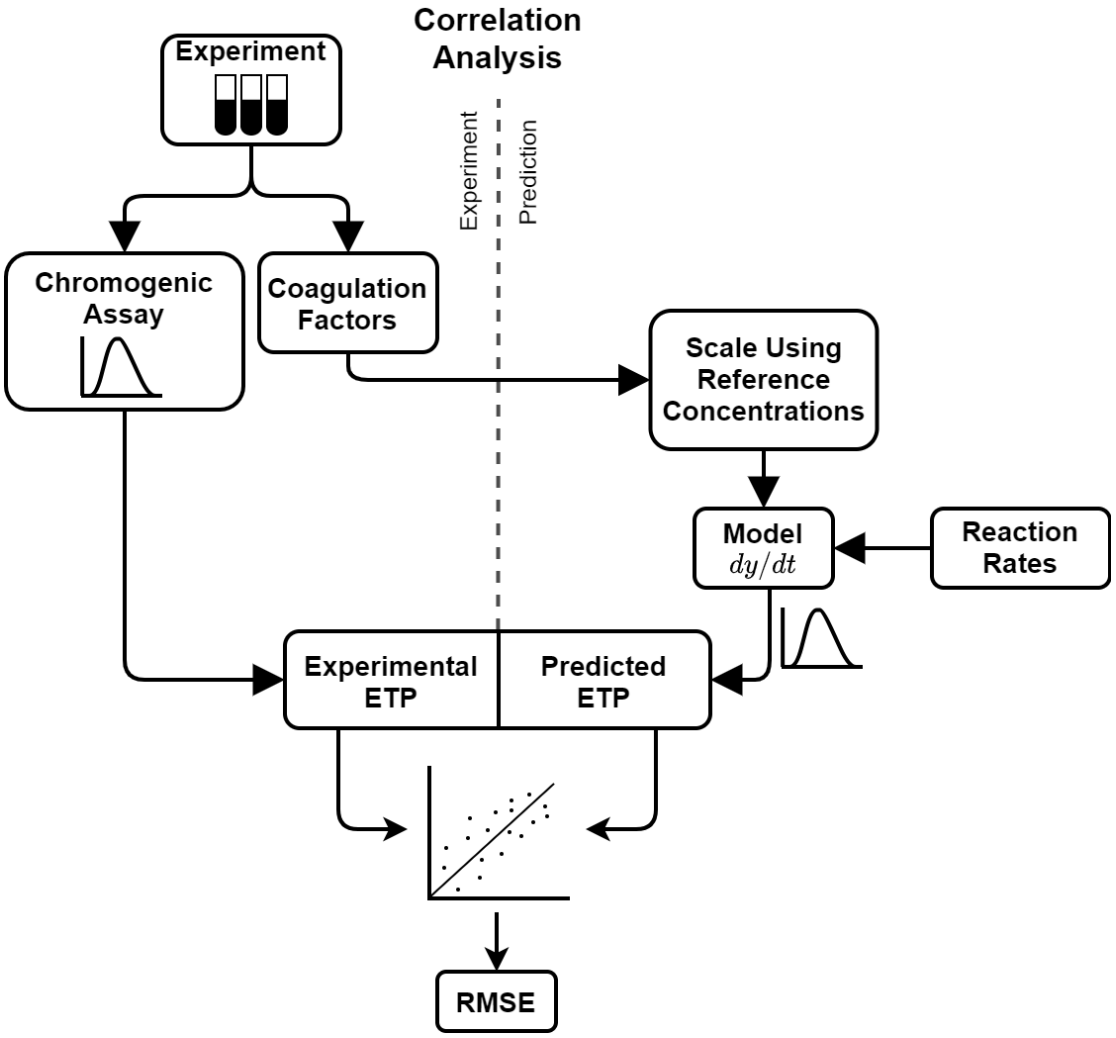

Figure 2.18: A diagram of the steps taken to perform the correlation analysis.

Model predictions have also been compared to the optical density time course data. The cohort is sorted by the absolute value of the residuals of the lines of proportionality given in Figure 2.19. For each model, the individual that gave the largest and smallest absolute residual, for their with TF sample, were taken to be compared against model time courses. The individuals model predicted thrombin generation curve is converted into an optical density curve by taking the cumulative integral, as given by Equation (2.3). This is then scaled from nM $\cdot$ min into % of pooled plasma using the gradient of the line of proportionality in Figure 2.19.

$$OD(t = k) = \int_{t=0}^{k} [FIIa](t)dt \tag{2.3}$$

Figure 2.20 presents the model predicted optical density curves for the best ETP predicted individuals. Only the Danforth and Brummel models present a similar OD curve as the data with all other models showing different shapes and

V, VII, VIII, IX, X, and XI, AT, TFPI, and TF. The RMSE was evaluated using 5-fold cross validation to avoid skewing the results due to overfitting.

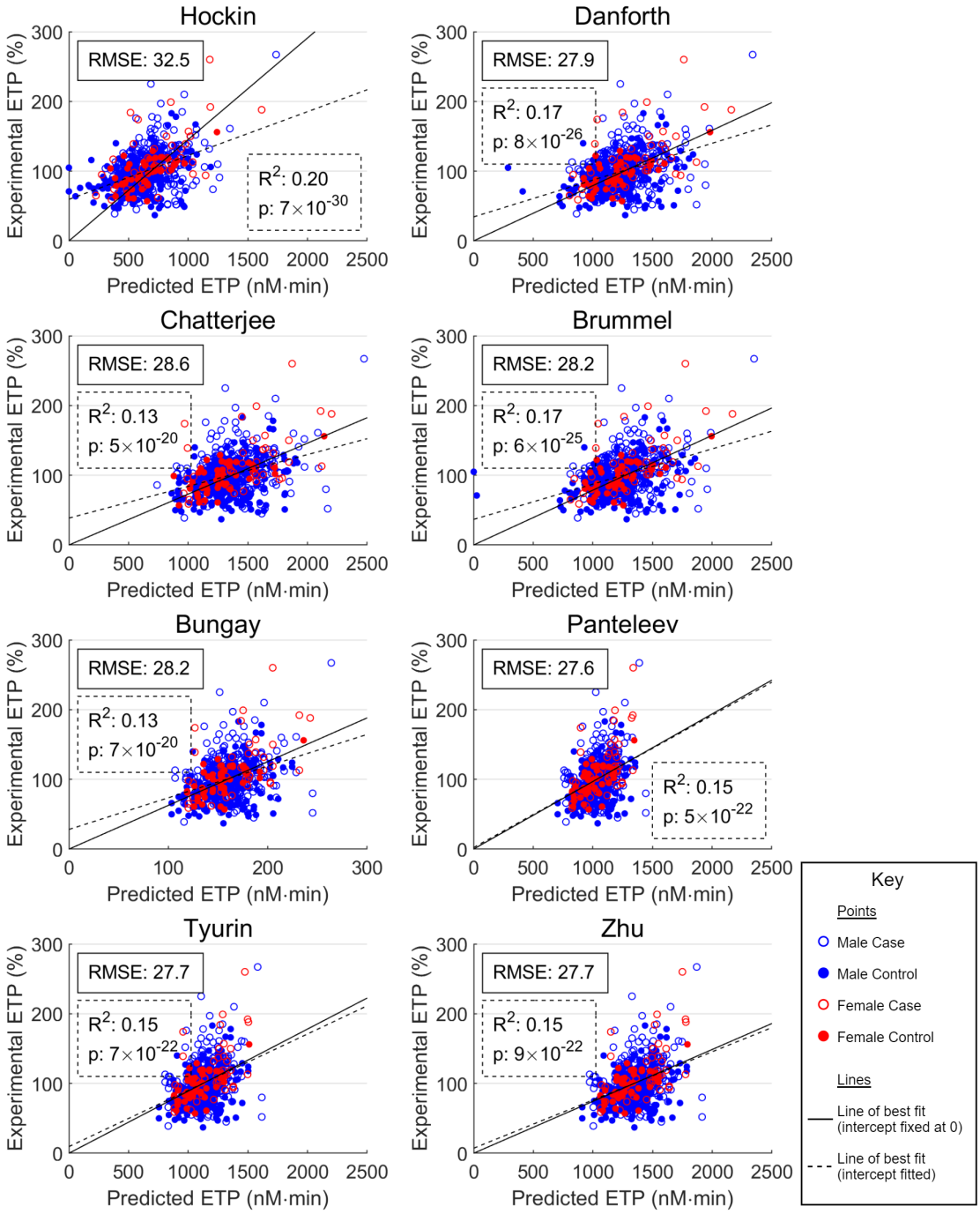

Figure 2.19: Scatter plots of predicted ETP against measured ETP, separated by cases/control (open/closed) and male/female (blue/red). RMSE measured the error using the line of proportionality (solid line) and R^2 measures the correlation using the line of best fit (dashed line).

lagtimes. However, even these two models then fail when looking at other individuals. It seems clear that the models fail to reproduce experimental data across the cohort.

Figure 2.21 presents similar results but for the worst predicted donor of each model (largest absolute residual of the line of proportionality). Interestingly, for most of the models this is the same individual. In all cases, the models significantly under-predict ETP. All three of these individuals show increased levels of all factors, particularly FVIII. It seems that the models struggle to reproduce the large ETPs seen in the data.

2.3.2 Inter-Model Correlation

We have shown the models correlate poorly with patient data in which many coagulation factors are varied simultaneously. However, it is difficult to identify from the scatter plots if the predictions of the models are similar to one another. To identify models with similar predictions, we will compare the predicted patient specific ETP values from the models to one another. The R^2 correlation coefficient, between each of the models predicted patient data sets, is given in the heatmap in Figure 2.22.

There is much stronger correlation between the different models than there was between the models and the patient data, with all inter-model $R^2 > 0.5$, compared with the largest R^2 to the patient data of $R^2 = 0.20$ for the Hockin model. Even still, there is significant variation in the strength of the correlations between different pairings of models. The Hockin model generally has the weakest correlation to the other models, with its most correlated models being that of Danforth ($R^2 = 0.87$) and Brummel ($R^2 = 0.86$), both models which utilise the Hockin model to build upon. Other than the Hockin model, all show strong correlation with one another ($R^2 > 0.75$) with the Danforth-Brummel pairing and the Tyurin-Zhu-Panteleev triplet all being almost perfectly correlated with one another ($R^2 > 0.99$). The Tyurin and Zhu models are the most strongly correlated with $R^2 = 0.9998$.

The ETP inter-model correlation would suggest that most model predictions are highly similar. However, comparing different summary statistics (those given previously in Figure 1.5) shows much greater separation between the models. Heatmaps of R^2 for each of the summary statistics are given in Figure 2.22.

The Hockin-Danforth-Brummel triplet are even more strongly correlated ($R^2 > 0.95$) for the other summary statistics, except for lagtime, where only Danforth and Brummel remain strongly correlated. The Panteleev model appears to be most strongly correlated with the Hockin-Danforth-Brummel triplet, although slightly weaker than seen between the models in this triplet. The Bungay model does not have significant correlations with any models across all the summary statistics. The Tyurin and Zhu models remain significantly correlated for all of the summary statistics and, while the Chatterjee model is correlated with the Tyurin-Zhu pair

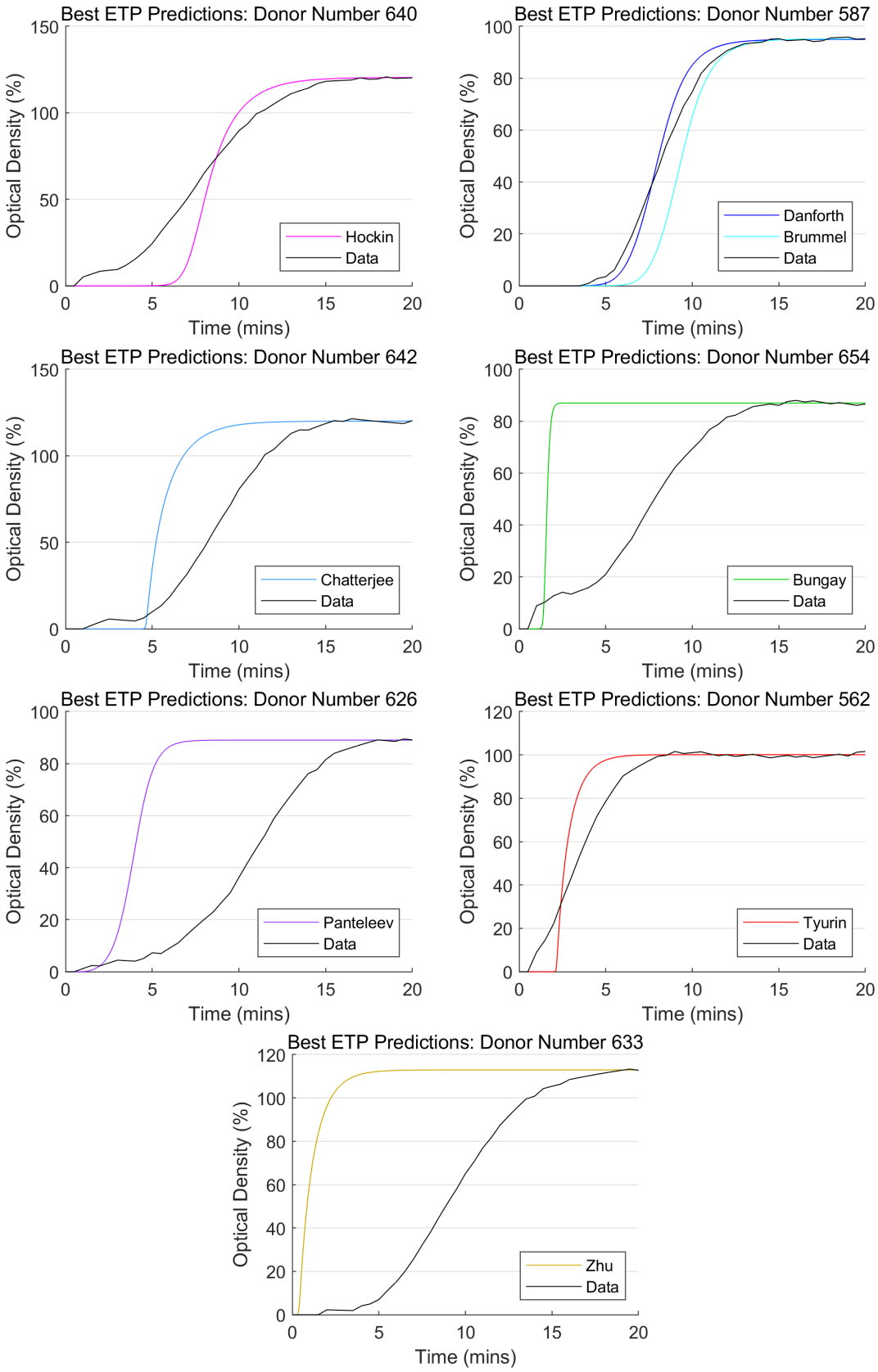

Figure 2.20: Optical Density plots for the best predicted individuals of each model. Model predicted OD curves are given by cumulative integral of the thrombin generation curves, scaled according to the lines of proportionality from Figure 2.19. The experimentally determined OD curves are given in black and labelled 'Data'.

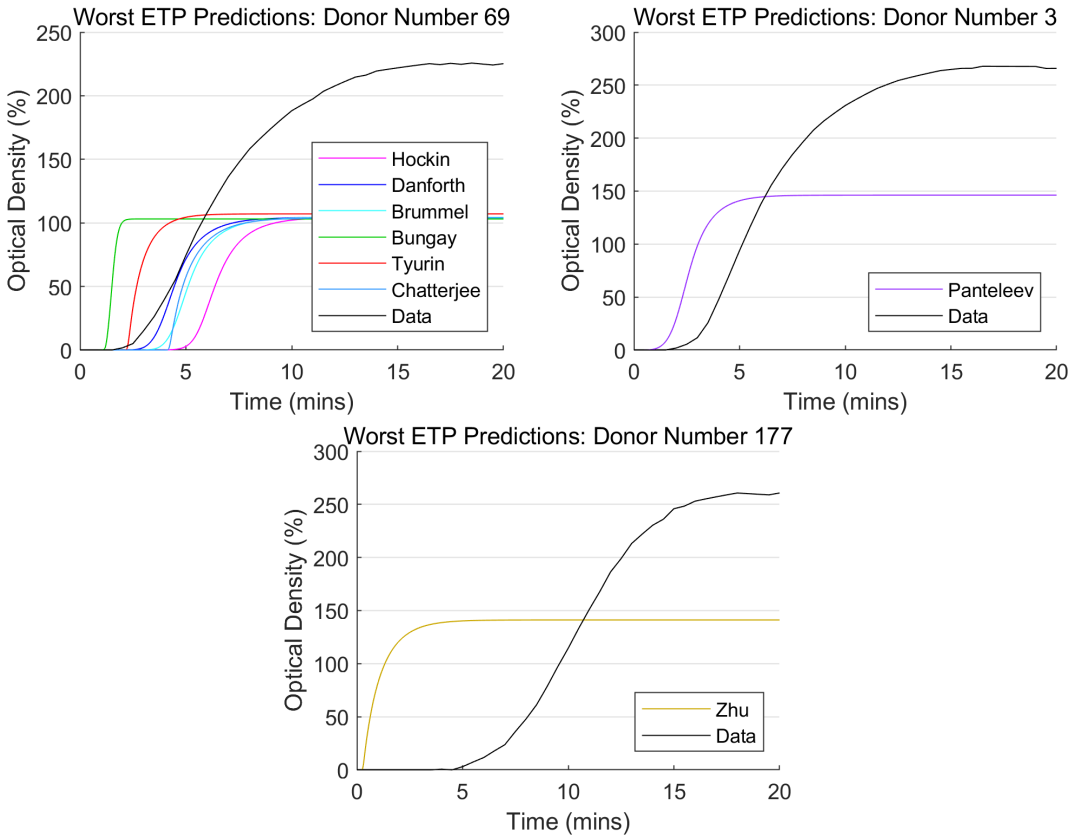

Figure 2.21: Optical Density plots for the worst predicted individuals of each model. Model predicted OD curves are given by cumulative integral of the thrombin generation curves, scaled according to the lines of proportionality from Figure 2.19. The experimentally determined OD curves are given in black and labelled 'Data'.

for some summary statistics (peak, maximum increasing rate, and minimum decreasing rate), it is poorly correlated with these models for lagtime and time to peak.

The correlation between the Hockin, Danforth, and Brummel models is to be expected since the Danforth and Brummel models are derived by expanding the Hockin and Danforth models, respectively. The similarity between the Tyurin and Zhu models is likely because they both make use of the rates in the Kogan [88] and Khanin [58] models, leading to many identical rates between the Tyurin and Zhu models.

2.3.3 Low ETP Predictions

The Hockin model (and to a lesser extent, the Brummel and Danforth models) predicted exceptionally low ETP for a handful of individuals (seen in Figure 2.19). By exploring the mean values for each initial conditions for small and large predicted ETPs for the Hockin model, we aim to find a cause for the low ETP predictions. The average initial factor concentrations for those that predicted ETP

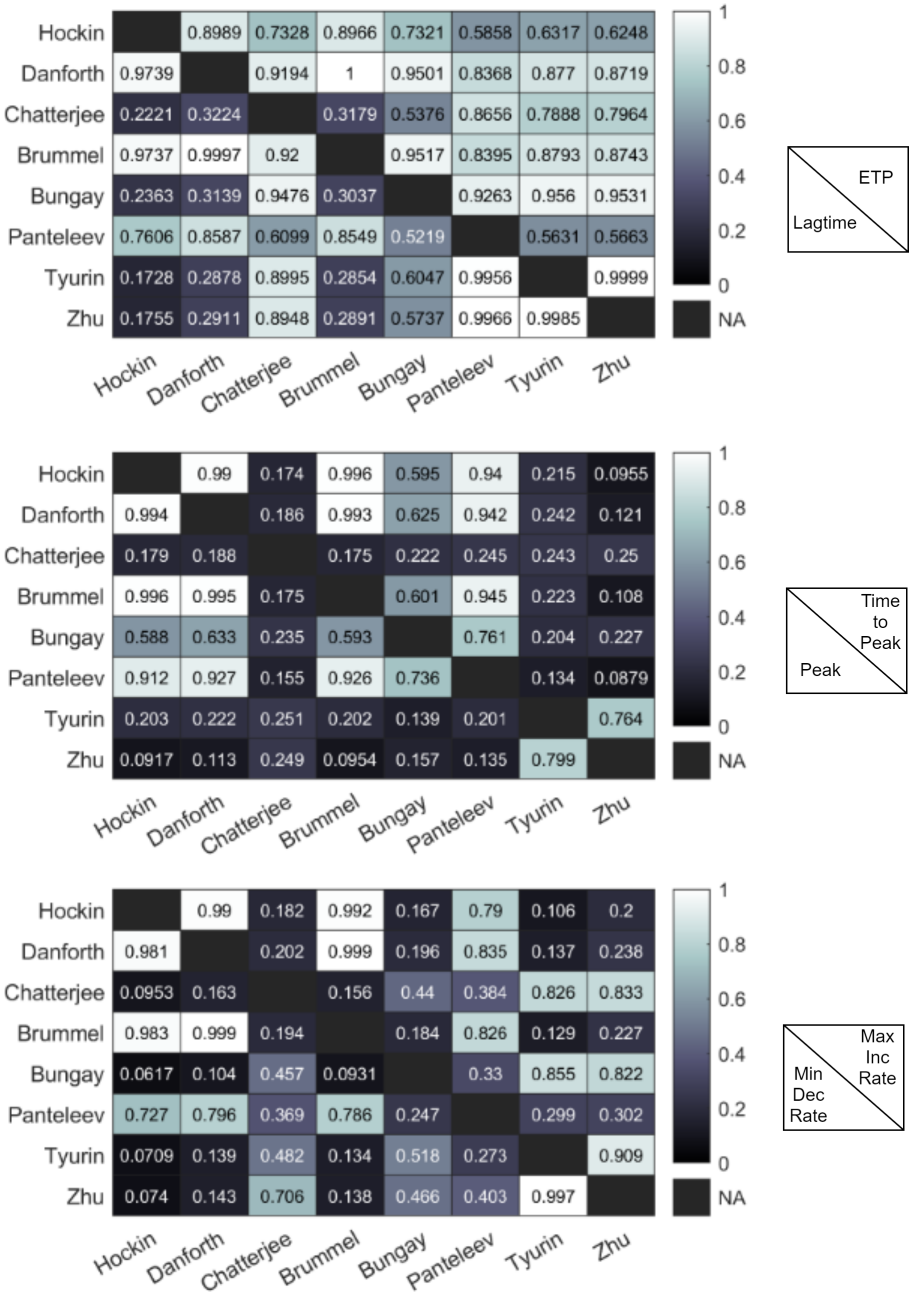

Figure 2.22: The R^2 correlation between the predicted summary statistics of the models. Each heatmap is split into an upper-right half, showing the correlation for one summary statistic, and a lower-left half showing the correlation for another summary statistic. Which summary statistics are used is given to the right of each heatmap.

below 250nM $\cdot$ min and for ETP larger than 250nM $\cdot$ min are given in Table 2.27.

Initial Condition	Mean for small ETP (n=12)	Mean for large ETP (n=573)
Tissue Factor	$2.81pM$	$10.64pM$
II	110.75%	121.94%
V	111.83%	125.18%
VII	117.08%	122.90%
VIII	109.00%	137.45%
IX	101.00%	124.82%
X	124.83%	130.93%
XI	90.25%	103.37%
TFPI	1.41 Units	1.06 Units

Table 2.27: The mean initial factor concentrations, split by whether the Hockin model predicts an ETP of greater or less than 250nM $\cdot$ min.

The initial condition for tissue factor is significantly different between the two groups. To verify this is the only cause for the low ETP or if there are others, our ETP correlation plot for the Hockin model is coloured based on the initial level of tissue factor on the left-hand side of Figure 2.23.

All individuals with a low predicted ETP also had a low TF concentration. Further investigation into the thrombin generation curves predicted by the Hockin model for these individuals revealed that a long lagtime for these individuals resulted in thrombin generation that did not complete in the 20-minute simulation time. The ETP correlation for the Hockin model was performed again with an extended simulation time of four hours[‡]. The results are demonstrated on right-hand side of Figure 2.23. These longer simulations reveals that this was the only cause of low predicted ETP individuals in the Hockin model.

[‡]This time far exceeds the time used in the experimental assay of 20 minutes. This is done to verifiy that it is the cut-off time to which the Hockin model is sensitive.

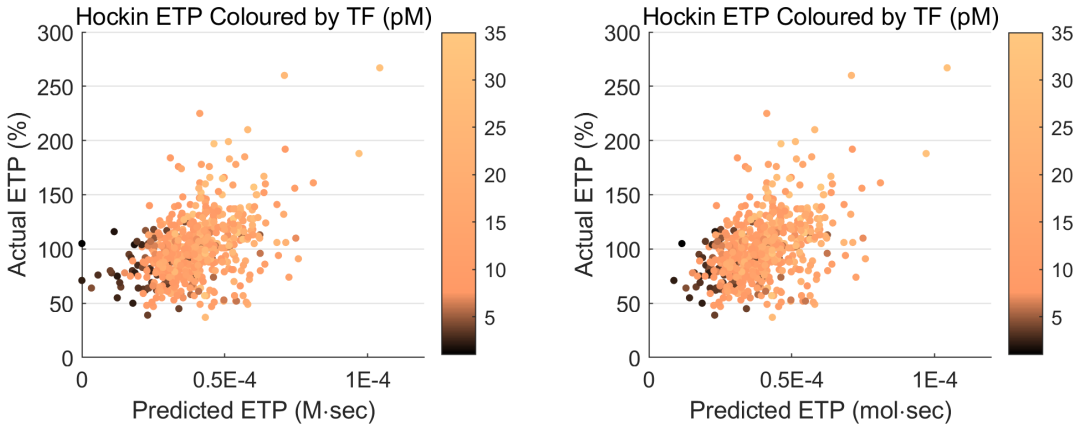

Figure 2.23: Scatter plot of predicted ETP (from the Hockin model) against measured ETP, coloured by the initial level of TF in pM. Followed by an identical figure for an extended 4-hour simulation time.

2.4 Model Comparison

In the previous section, we demonstrated that the models are poorly correlated with patient data and are more strongly correlated with one another. Here, we will further explore the differences between these models and identify the causes that give rise to them. We will investigate the differences in the thrombin generation curves predicted by the models, demonstrating that the models fall into two groups; the differences in reaction rates between two of the models; and the differences in the reactions used in each of the models. Finally, we will demonstrate the differences in the predictions of the models for other coagulation factors and identify the underlying cause for these two groups of models.

2.4.1 Differences in Thrombin Generation Curves

First, we will look at the thrombin generation curves predicted by each of the models. The same coagulation factors are used for the initial conditions for each of the models (Table 2.26). The predicted thrombin generation curves for all the models are given in Figure 2.24, followed by similar figures for the predicted thrombin generation curves of three patients, a high ETP individual (199% ETP), a medium ETP individual (100% ETP), and a low ETP individual (51%). These patient level predicted curves are given in Figure 2.25.

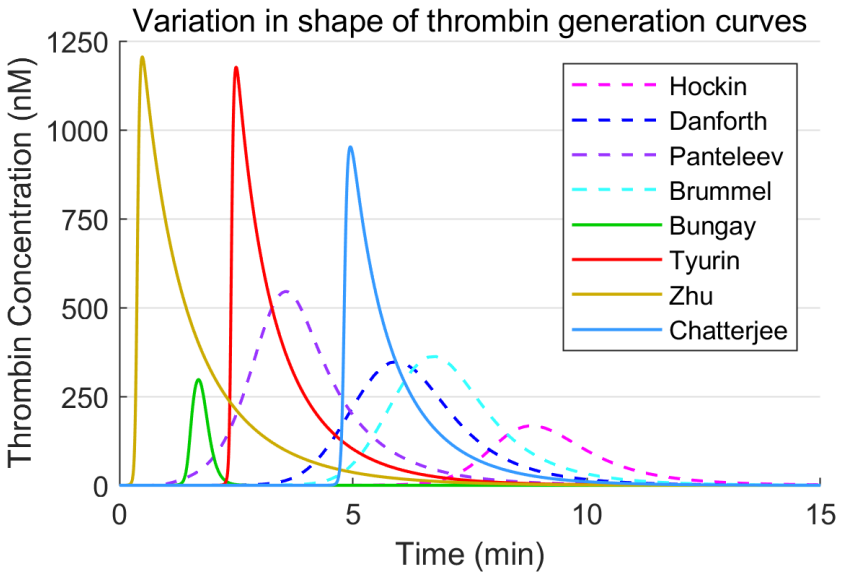

Figure 2.24: The thrombin generation curve given by each model for the baseline initial conditions given in Table 2.26.

The models all show vastly different predicted thrombin generation curves. There appears to be two distinct shapes for the model predicted thrombin generation curves. The curves predicted by Zhu, Tyurin and Chatterjee all show very rapid thrombin activation after the lagtime, continuing up to a large peak height. The Panteleev, Hockin, Danforth and Brummel models all predict smoother, more symmetrical shapes for the thrombin generation curves. We will term these groups

the Quick group and the Symmetrical group, respectively, to aid with later comparisons. The Bungay model most closely matches that of the Quick group so we will include it there, while also taking note of its much smaller peak height and slightly less sharp activation compared with the other members of the Quick group.

Figure 2.25 shows only minor changes between the predicted thrombin generation curves for each of the three individuals. Mostly, these changes appear to be stretching or shifting the thrombin generation curves, while the underlying shape of the curves remains consistent between these three individuals.

2.4.2 Are Model Differences the Result of the Reactions, Reaction Rates, or Both?

We will now begin looking into the construction of the models themselves. All the models feature both differences in the reaction schemes they use and in their reaction rates. First, we will attempt to separate the influences of the reaction rates from the reactions. To do this, we will replace the reaction rates of the Hockin model with the corresponding rates from the Tyurin model, wherever possible. The reactions that appear in both models and their corresponding reaction rates (in a reduced form) are given in Table 2.28*. Replacing the reaction rates in the Hockin model with those from the Tyurin model wherever possible produces the model given in Table 2.29.

Reaction	Model	Reaction Rates
TF + VII $\leftrightarrow$ TF:VII	Hockin	$k_+ = 3.2 \times 10^6 M^{-1}s^{-1}$, $k_- = 3.1 \times 10^{-3}s^{-1}$
	Tyurin	$k_+ = 3.33 \times 10^4 M^{-1}s^{-1}$, $k_- = 3.33 \times 10^{-6}s^{-1}$
TF + VIIa $\leftrightarrow$ TF:VIIa	Hockin	$k_+ = 2.3 \times 10^7 M^{-1}s^{-1}$, $k_- = 3.1 \times 10^{-3}s^{-1}$
	Tyurin	$k_+ = 5 \times 10^4 M^{-1}s^{-1}$, $k_- = 3.3 \times 10^{-5}s^{-1}$
VII $\overset{Xa}{\rightarrow}$ VIIa	Hockin	$\frac{k_{\text{cat}}}{K_m} = 1.3 \times 10^7 M^{-1}s^{-1}$
	Tyurin	$\frac{k_{\text{cat}}}{K_m} = 1 \times 10^6 M^{-1}s^{-1}$
X $\overset{TF:VIIa}{\rightarrow}$ Xa	Hockin	$K_m = 2.14 \times 10^{-7} M$, $k_{\text{cat}} = 4.56s^{-1}$
	Tyurin	$K_m = 2.2 \times 10^{-7} M$, $k_{\text{cat}} = 1.8s^{-1}$

*The reduced form of the reaction rates are K_m, K_d, k_{cat} and $\frac{k_{\text{cat}}}{K_m}$. If there is only a single forward reaction involved (such as AT inhibition) then only that parameter is reported. These parameters are used to allow easy comparison between the models due to their different rate laws.

IX $\overset{TF:VIIa}{\rightarrow}$ IXa	Hockin	$K_m = 4.25 \times 10^{-7}M$, $k_{\text{cat}} = 1.8s^{-1}$
	Tyurin	$K_m = 1 \times 10^{-7}M$, $k_{\text{cat}} = 0.7s^{-1}$
II $\overset{Xa}{\rightarrow}$ IIa	Hockin	$\frac{k_{\text{cat}}}{K_m} = 7.5 \times 10^3 M^{-1}s^{-1}$
	Tyurin	$\frac{k_{\text{cat}}}{K_m} = 6.5 \times 10^3 M^{-1}s^{-1}$
VIII $\overset{IIa}{\rightarrow}$ VIIIa	Hockin	$\frac{k_{\text{cat}}}{K_m} = 2.0 \times 10^7 M^{-1}s^{-1}$
	Tyurin	$\frac{k_{\text{cat}}}{K_m} = 1.8 \times 10^7 M^{-1}s^{-1}$
VIIIa + IXa → IXa:VIIIa	Hockin	$k_+ = 1 \times 10^7 M^{-1}s^{-1}$
	Tyurin	$k_+ = 1.67 \times 10^8 M^{-1}s^{-1}$
X $\overset{IXa:VIIIa}{\rightarrow}$ Xa	Hockin	$K_m = 8.2 \times 10^{-8}M$, $k_{\text{cat}} = 8.2s^{-1}$
	Tyurin	$K_m = 1.6 \times 10^{-7}M$, $k_{\text{cat}} = 25s^{-1}$
V $\overset{IIa}{\rightarrow}$ Va	Hockin	$\frac{k_{\text{cat}}}{K_m} = 2 \times 10^7 M^{-1}s^{-1}$
	Tyurin	$\frac{k_{\text{cat}}}{K_m} = 3.2 \times 10^6 M^{-1}s^{-1}$
Xa + Va → Xa:Va	Hockin	$k_+ = 4 \times 10^8 M^{-1}s^{-1}$
	Tyurin	$k_+ = 1.67 \times 10^8 M^{-1}s^{-1}$
Xa + TFPI → Xa:TFPI	Hockin	$k_+ = 9.5 \times 10^5 M^{-1}s^{-1}$
	Tyurin	$k_+ = 1.6 \times 10^3 M^{-1}s^{-1}$
TF:VIIa + Xa:TFPI → TF:VIIa:Xa:TFPI	Hockin	$k = 5 \times 10^7 M^{-1}s^{-1}$
	Tyurin	$k = 1.08 \times 10^7 M^{-1}s^{-1}$
Xa + AT → Xa:AT	Hockin	$k = 1.5 \times 10^3 M^{-1}s^{-1}$
	Tyurin	$k = 3.13 \times 10^3 M^{-1}s^{-1}$
IXa + AT → IXa:AT	Hockin	$k = 490M^{-1}s^{-1}$
	Tyurin	$k = 490M^{-1}s^{-1}$
IIa + AT → IIa:AT	Hockin	$k = 7.1 \times 10^3 M^{-1}s^{-1}$
	Tyurin	$k = 7.08 \times 10^3 M^{-1}s^{-1}$
TF:VIIa + AT → TF:VIIa:AT	Hockin	$k = 230M^{-1}s^{-1}$
	Tyurin	$k = 450M^{-1}s^{-1}$

Table 2.28: Comparison between the reaction rates used in the Hockin and Tyurin models for their common reactions.

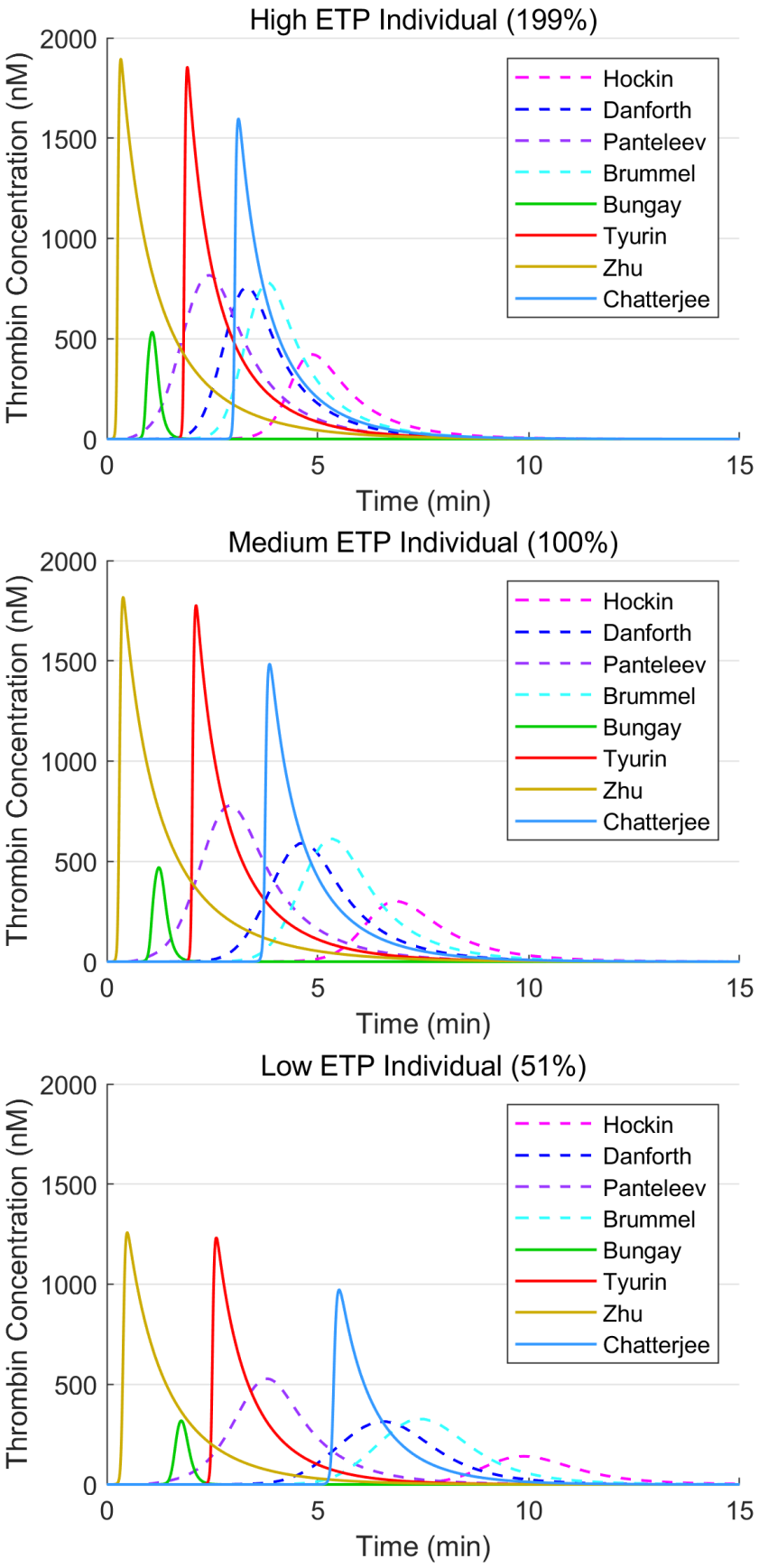

Figure 2.25: Thrombin generation curves for each of the models using initial conditions from high, medium and low ETP individuals.

Index	Reaction	$k_{+,ind}$	$k_{-,ind}$
1	TF + VII $\leftrightarrow$ TF:VII	$\underline{3.33 \times 10^4}$	$\underline{3.33 \times 10^{-6}}$
2	TF + VIIa $\leftrightarrow$ TF:VIIa	$\underline{5 \times 10^4}$	$\underline{3.33 \times 10^{-5}}$
3	TF:VIIa + VII $\rightarrow$ TF:VIIa + VIIa	4.45×10^5	-
4	Xa + VII $\rightarrow$ Xa + VIIa	$\underline{1 \times 10^6}$	-
5	IIa + VII $\rightarrow$ IIa + VIIa	2.3×10^4	-
6	TF:VIIa + X $\leftrightarrow$ TF:VIIa:X	2.5×10^7	$\underline{4.09}$
7	TF:VIIa:X $\rightarrow$ TF:VIIa:Xa	$\underline{1.99}$	-
8	TF:VIIa + Xa $\leftrightarrow$ TF:VIIa:Xa	2.2×10^7	19
9	TF:VIIa + IX $\leftrightarrow$ TF:VIIa:IX	1.0×10^7	$\underline{0.3}$
10	TF:VIIa:IX $\rightarrow$ TF:VIIa + IXa	$\underline{0.7}$	-
11	Xa + II $\rightarrow$ Xa + IIa	$\underline{6.47 \times 10^3}$	-
12	IIa + VIII $\rightarrow$ IIa + VIIIa	$\underline{1.8 \times 10^7}$	-
13	VIIIa + IXa $\leftrightarrow$ IXa:VIIIa	$\underline{1.67 \times 10^8}$	$\underline{8.35 \times 10^{-2}}$
14	IXa:VIIIa + X $\leftrightarrow$ IXa:VIIIa:X	2.0×10^8	$\underline{7}$
15	IXa:VIIIa:X $\rightarrow$ IXa:VIIIa + Xa	$\underline{25}$	-
16	VIIIa $\leftrightarrow$ $VIIIa_1L$ + $VIIIa_2$	6.0×10^{-3}	2.2×10^4
17	IXa:VIIIa:X $\rightarrow$ $VIIIa_1L$ + $VIIIa_2$ + X + IXa IXa:VIIIa $\rightarrow$ $VIIIa_1L$ + $VIIIa_2$ + IXa	1.0×10^{-3}	-
18	IIa + V $\rightarrow$ IIa + Va	$\underline{3.21 \times 10^6}$	-
19	Xa + Va $\leftrightarrow$ Xa:Va	$\underline{1.67 \times 10^8}$	$\underline{8.35 \times 10^{-2}}$
20	Xa:Va + II $\leftrightarrow$ Xa:Va:II	1.0×10^8	103
21	Xa:Va:II $\rightarrow$ Xa:Va + mIIa	63.5	-
22	mIIa + Xa:Va $\rightarrow$ IIa + Xa:Va	1.5×10^7	-
23	Xa + TFPI $\leftrightarrow$ Xa:TFPI	$\underline{1.6 \times 10^3}$	$\underline{6.4 \times 10^{-7}}$
24	TF:VIIa:Xa + TFPI $\leftrightarrow$ TF:VIIa:Xa:TFPI	3.2×10^8	1.1×10^{-4}
25	TF:VIIa + Xa:TFPI $\rightarrow$ TF:VIIa:Xa:TFPI	$\underline{1.08 \times 10^7}$	-
26	Xa + AT $\rightarrow$ Xa:AT	$\underline{3.13 \times 10^3}$	-
27	mIIa + AT $\rightarrow$ mIIa:AT	7.1×10^3	-
28	IXa + AT $\rightarrow$ IXa:AT	4.9×10^2	-
29	IIa + AT $\rightarrow$ IIa:AT	$\underline{7.08 \times 10^3}$	-
30	TF:VIIa + AT $\rightarrow$ TF:VIIa:AT	$\underline{4.5 \times 10^2}$	-

Table 2.29: The reaction scheme and reaction rates for the altered Hockin model, made to more closely match the Tyurin model. The units for the reaction rates are s^{-1} and $M^{-1}s^{-1}$ for first and second order rates, respectively. Reaction rates that have been changed are underlined.

When applying these changes to the Hockin model, a very minimal amount of TF:VIIa is produced which is not able to lead to producing significant quantities of thrombin. The Tyurin model includes activations using FVIIa, in addition to TF:VIIa, which can account for the lack of TF:VIIa produced in the model. After the reaction for the activation of FX by FVIIa was included, the thrombin generation curves produced (given in Figure 2.26) are more similar to the Hockin model than the Tyurin model, featuring an even longer lagtime and more symmetrical thrombin generation curve than the Hockin model.

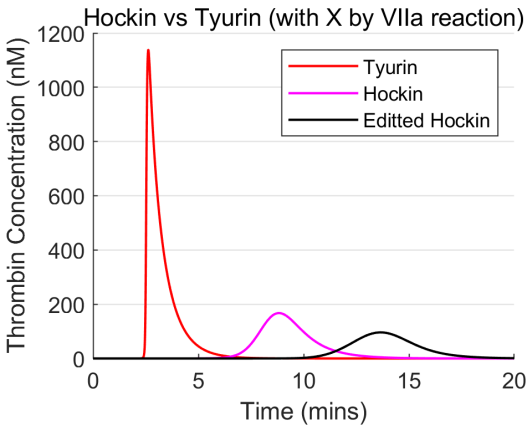

Figure 2.26: The thrombin generation curves for the Tyurin model as well as the edited Hockin model

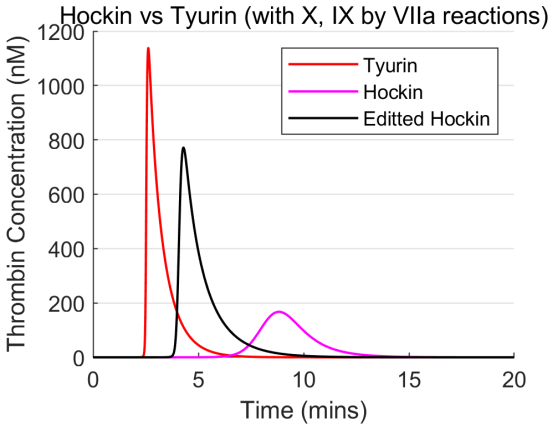

Figure 2.27: The thrombin generation curves for the Tyurin model as well as the edited Hockin model

As shown in Figure 2.27, addition of a single extra reaction, FIX activation by FVIIa, produces thrombin generation curves resembling the Tyurin model with a slightly longer lagtime and lower peak height. This suggests that there are some significant differences between the reaction rates of the models, hence the lack of TF:VIIa produced by the Tyurin model. However, this is not the cause of the disparity in the shape of the thrombin generation curves which appears to be more closely linked with activation of FIX.

2.4.3 Differences in Reaction Schemes

To help explain the differences seen in the thrombin generation curves, we now compare the reaction schemes used by the models. To aid comparison between the reaction schemes, the enzymatic reactions in the models that exclusively use mass action kinetics were reduced down to a simpler form, for example using X $\overset{\text{IXa:VIIIa}}{\rightarrow}$ Xa to denote the three-step reaction X + IXa:VIIIa $\leftrightarrow$ IXa:VIIIa:X $\rightarrow$ IXa:VIIIa + Xa.

The reactions that are featured in all models are given in Table 2.30. The reactions that are missing from a single model and those that are contained in only a single model are given in Tables 2.31 and 2.32, respectively.

Reaction
$TF + VII \rightarrow TF{:}VII$
$X \overset{TF:VIIa}{\rightarrow} Xa$
$IX \overset{TF:VIIa}{\rightarrow} IXa$
$Xa + Va \rightarrow Xa{:}Va$
$V \overset{IIa}{\rightarrow} Va$
$VIII \overset{IIa}{\rightarrow} VIIIa$
$X \overset{IXa:VIIIa}{\rightarrow} Xa$
$IIa + AT \rightarrow IIa{:}AT$
$IXa + AT \rightarrow IXa{:}AT$
$Xa + AT \rightarrow Xa{:}AT$
$Xa + TFPI \rightarrow Xa{:}TFPI$
$TF{:}VIIa + Xa{:}TFPI \rightarrow TF{:}VIIa{:}Xa{:}TFPI$

Table 2.30: The reduced reactions that are contained in all the models.

Reaction	Missing From?
$II \overset{Xa}{\rightarrow} IIa$	Bungay
$TF + VII \leftarrow TF{:}VII$	Zhu
$TF + VIIa \leftrightarrow TF{:}VIIa$	Zhu
$IXa + VIIIa \rightarrow IXa{:}VIIIa$	Panteleev

Table 2.31: The reduced reactions that are missing from only one of the models.

Reaction	Included In?
$II + Va \leftrightarrow II{:}Va$	Brummel
$XI \rightarrow XIa$	Zhu
$VIII \overset{mIIa}{\rightarrow} VIIIa$	Bungay
$TF{:}VIIa + Xa{:}TFPI \leftarrow TF{:}VIIa{:}Xa{:}TFPI$	Bungay
$IXa{:}VIIIa + AT \rightarrow IXa{:}VIIIa{:}AT$	Tyurin

Table 2.32: The reduced reactions that are only included in a single model.

One notable reaction that is not contained in the Bungay model, but is featured in all other models, is $II \overset{Xa}{\rightarrow} IIa$. This reaction is necessary for the initial activation of FIIa. Instead, the Bungay model activates FII exclusively by Xa:Va, which is initially formed using FV activated by FXa. This was thought to be an explanation of the low ETP predictions by the Bungay model, however, including

this reaction (using the reaction rate in the Hockin model) does not produce a significant effect on the thrombin generation curve (as seen in Figure 2.28).

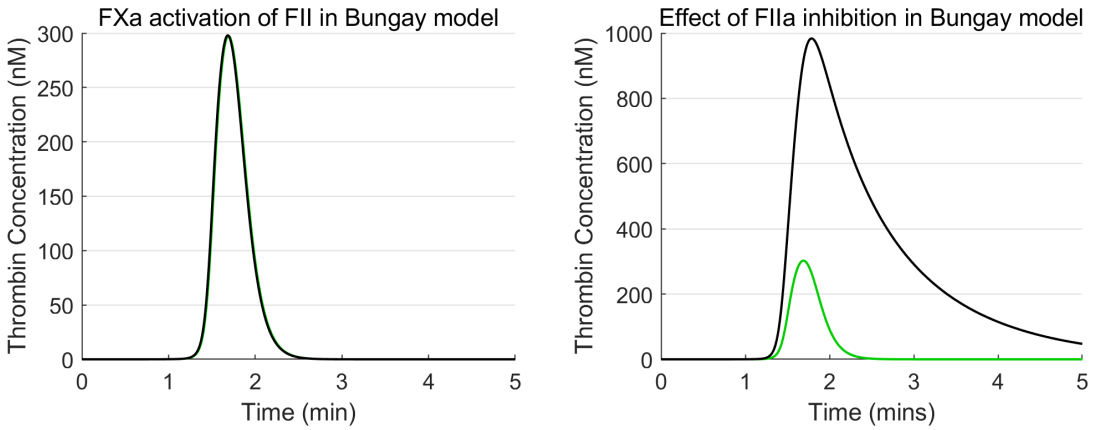

Figure 2.28: The Bungay model both before (green) and after (black) undergoing two edits. On the left the edited curve shows the inclusion of an extra reaction for activation of FII by FXa (using reaction rates from the Hockin model). On the right shows the thrombin generation curves for a decreased rate of FIIa inhibition by AT (using reaction rates from the Hockin model).

Further investigation into the Bungay model and its rates revealed that it has a much higher rate of FIIa inhibition by AT than the other models ($6.83\times10^4 M^{-1}s^{-1}$ for Bungay vs $7.1 \times 10^3 M^{-1}s^{-1}$ for Hockin). If this rate is adjusted to match the other models, as is given in Figure 2.28, then the Bungay model produces similar peaks heights to the other models in the Quick group.

There is a lack of reactions for the formation of TF:VIIa in the Zhu model. This model lacks a FVIIa species, which is normally used as an initial condition so TF:VIIa had to be used to initiate coagulation instead, resulting in an excess of TF.

The Brummel model's additional reaction, II + Va $\leftrightarrow$ II:Va, does not appear to have much purpose other than reducing the amount of free FII and FVa. However, this does still seem to have a significant effect on the thrombin generation curve as this reaction is the only difference between the Danforth and Brummel models once the effects of protein C are removed.

The Panteleev model is missing a reaction for IXa:VIIIa formation. This model instead keeps these factors separate and uses third order reactions, for example, X + IXa + VIIIa $\rightarrow$ Xa + IXa + VIIIa.

The auto-activation of FXI in the Zhu model is heavily simplified as it does not require any activated factors to form FXIa and begin coagulation. The Bungay model is the only model to include mIIa activation of FVIII, in addition to that by FIIa. The Tyurin model includes AT reactions for the complexes Xa:Va and IXa:VIIIa to inhibit FXa and FIXa, respectively.

The remaining reactions are all used at least twice and left out at least twice. These reactions and the models in which they are used, are given in Appendix C.

2.4.4 Exploring Model Predictions for Other Factors

We have investigated the differences between the models in both their reaction schemes and their reaction rates. However, we have been unable to identify the cause for the differences in the shape of their thrombin generation curves. We have demonstrated a potential link between the shape and activation of FIX by FVIIa in the Tyurin model but the lack of this reaction in the other models of the Quick group shows this description of the differences is not complete. We will now look at model predictions of coagulation factors other than thrombin to help explore this difference.

Figure 2.29 gives plots of TF:VIIa, XIa, II, mIIa, TFPI and AT concentration. Notably, all prothrombin is converted into thrombin in all the models, in opposition to the thrombin generation assay where only $\approx 90\%$ of the prothrombin is converted to thrombin [89]. This may explain why the models struggled to produce the extreme ETPs seen in the data (Figure 2.21). If all prothrombin is always converted, an increase in the rate of prothrombin conversion will have limited effect on ETP compared with if faster prothrombin conversion was able to convert more prothrombin.

Additionally, we identify the delayed formation of TF:VIIa in the Tyurin model, where little TF:VIIa is formed at the early timescales, where it is normally most impactful. The models clearly separate into the Quick and Symmetrical groups in the depletion of TFPI. Since TFPI can only be depleted in its inhibition of FXa, then the models must make distinct predictions for FX activation.

In Figure 2.30, we present similar plots but with a focus on FXa and its activation. We observe the models separating into the Quick and Symmetrical groups in the plots of FIX, FX, Xa:Va and IXa:VIIIa. This leads us to conclude that the differences are due to the Quick group activating significantly more FIXa than the Symmetrical group, resulting in higher levels of IXa:VIIIa, which in turn activates larger amounts of FXa so more Xa:Va is formed. These larger amounts of Xa:Va in the Quick group then cause the differences in the shape of the thrombin generation curves. The differences in activation of FIX are likely predominantly due to the presence of FXI in the Quick group. Although the Zhu model does not activate FXI as significantly as the other models, it still activates all FIX, likely through its activation by TF:VIIa, of which it has a significant excess.

However, the Panteleev model does not match this trend as it features significant FXI activation, but sees much less FIXa than the Quick group. This is due to its significantly slower rates for FXIa activation of FIX (Panteleev: $\frac{k_{\text{cat}}}{K_m} = 4.9 \times 10^5 M^{-1} s^{-1}$, Chatterjee: $\frac{k_{\text{cat}}}{K_m} = 1.6 \times 10^7 M^{-1} s^{-1}$). It does still activate far more FX than the other Symmetrical group models, but does not result in full depletion of FX.

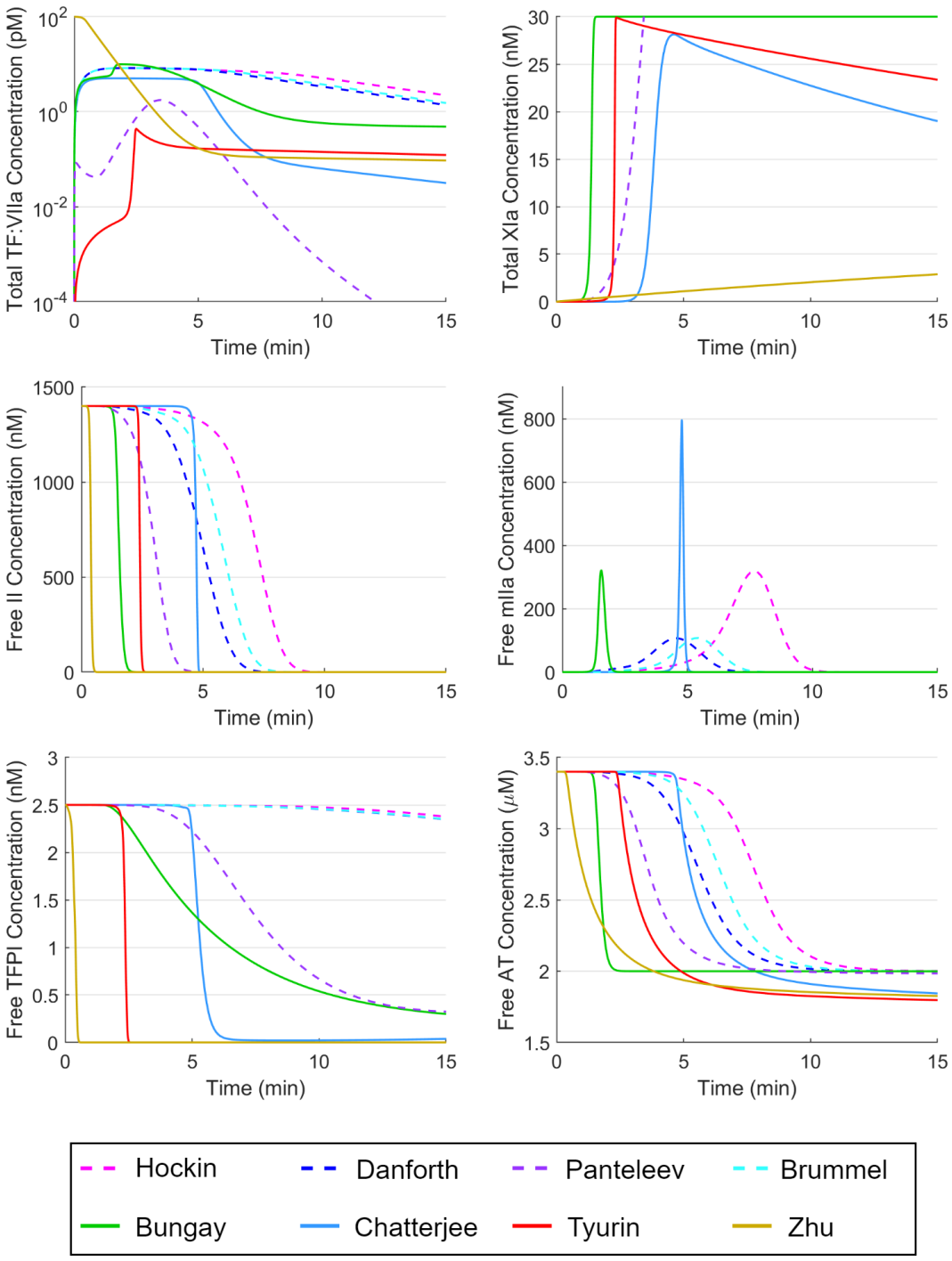

Figure 2.29: Plots of coagulation factor concentrations (TF:VIIa, XIa, II, mIIa, TFPI, AT) over time, for identical initial conditions (Table 2.26). The Symmetrical group of models are given in dashed line while the Quick group of models are given in solid lines.

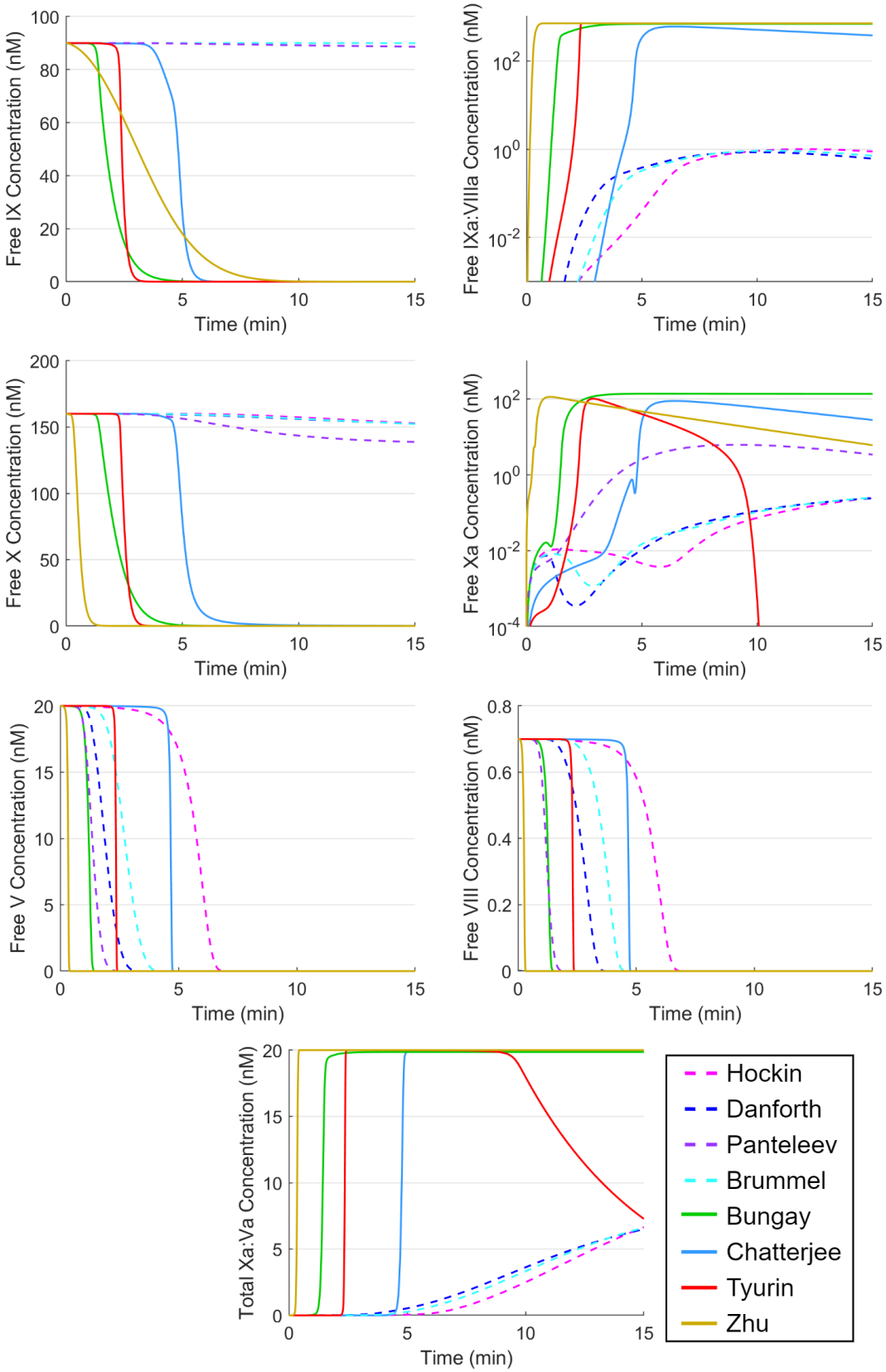

Figure 2.30: Plots of coagulation factor concentrations (those related to FX activation; FIX, IXa:VIIIa, FX, FXa, FV, FVIII, Xa:Va) over time, for identical initial conditions (Table 2.26). The Symmetrical group of models are given in dashed line while the Quick group of models are given in solid lines.

To verify the claim that FIX activation, predominantly through FXIa, is the cause for the different shapes of the predicted thrombin generation curves, we have given thrombin generation curves in Figure 2.31 with FXI included and then excluded. There is a dramatic shift in the shape of the curves predicted by the models of Tyurin, Chatterjee and Bungay. The Tyurin model still resembles its original shape more closely than that of the Symmetrical group, however, this is likely due to activation of FIX by FVIIa, as explored in the Hockin vs Tyurin section earlier. Both the Zhu and Panteleev models remain similar to their original curves, with a slight shift in the Panteleev model and no noticeable change in the Zhu model.

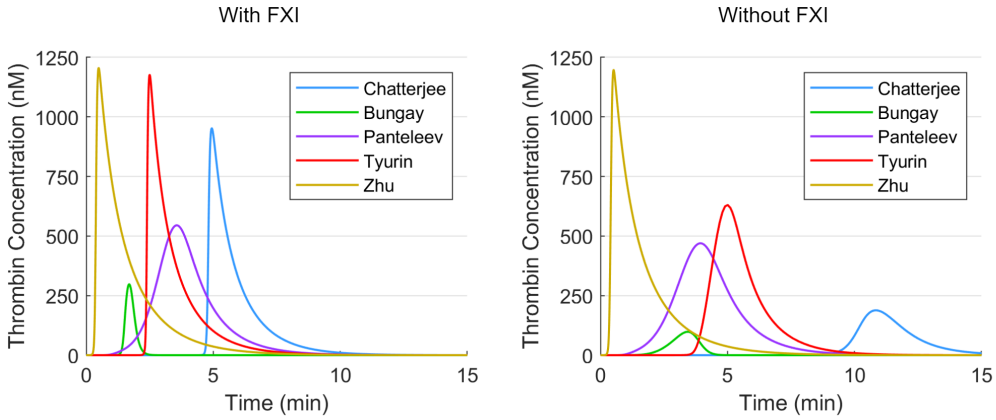

Figure 2.31: Thrombin generation curves for the five models that feature FXI (Chatterjee, Bungay, Panteleev, Tyurin and Zhu), with FXI included and then excluded.

2.4.5 Conclusions

We have seen that the differences in reaction rates between the models give rise to differences in the thrombin generation curves, but not in their shape. The differences in shape are instead due to FIX activation, most commonly by FXIa (Figure 2.31), which after several steps, significantly changes the levels of Xa:Va. Additionally, there are many differences in the reaction schemes of these models, with some models missing significant reactions.

All the models predicted that all the prothrombin is converted into thrombin, contrary to expectation [89]. This may be, at least in part, due to the lack of reactions for inhibiting Xa:Va. The only models which feature a reaction like this are the models of Tyurin and Panteleev, both of which feature a reaction that releases the FVa and only inhibits the FXa part of the complex. Since there is significantly more FX than FV, this will result in Xa:Va being present for significantly longer than if FVa was also inhibited.

2.5 Sensitivity Analysis

In the previous sections, we have seen that the models vary significantly in their predictions, with both reactions and reaction rates having significant influences over particular parts of the models. We will continue this investigation into their predictions through the use of a variance-based, local sensitivity analysis. This allows us to test which components of the cascade have the greatest influence on the predictions of the models and therefore need to be implemented most accurately. We will perform this sensitivity analysis on both the initial coagulation factor concentrations, to compare the significance of general areas of the cascade, and on the reaction rates, to pinpoint individual reaction rates which have particularly strong or weak influence on the model predictions. Rather than comparing to experimental data and drawing conclusions through comparison to a ground truth, this section will be purely focused on the predictions of the models and comparing them to one another, identifying if these models behave similarly under variation in reaction rates and coagulation factor concentrations.

2.5.1 Sensitivity to Coagulation Factor Concentrations

Method

To quantify the sensitivity of the models to each of the coagulation factors, we introduce a new sensitivity analysis method and apply it to these models. This method, demonstrated in Figure 2.33, uses summary statistics to quantify a thrombin generation curve and measures the variance in these summary statistics as the sensitivity.

The concentration of each coagulation factor is varied, one at a time, across eleven linearly spaced points between 50% and 150% of their default value, given as a reduced set of initial concentrations in Table 2.33. A reduced set of coagulation factors is used, removing the inhibitors $\alpha_1 - AT$, $\alpha_2 - AP$, $\alpha_2 - M$, PAI-1, PCI, and C1-inh to improve comparability between the models. We then calculate the six summary statistics (lagtime, peak height, time to peak, ETP, maximum increasing rate and minimum decreasing rate), demonstrated in Figure 2.32, for each resulting thrombin generation curve. The standard deviation for the variation in each summary statistic is calculated and then normalised using the value of the summary statistic at the 100% initial condition. We will then calculate the sensitivity to each coagulation factor as the norm of the vector of normalised standard deviations. Finally, we report the normalised sensitivity of each coagulation factor scaled such that the sum of the sensitivities for a model is one*. The sensitivity analysis method is presented in Figure 2.33. These normalised sensitivities are presented in a heatmap in Figure 2.34.

*This means if a model has a sensitivity of one to a particular factor, and therefore a sensitivity of zero to all other factors, then its predicted thrombin generation curves are entirely determined by that single factor and varying the other factors will not change the thrombin generation curves.

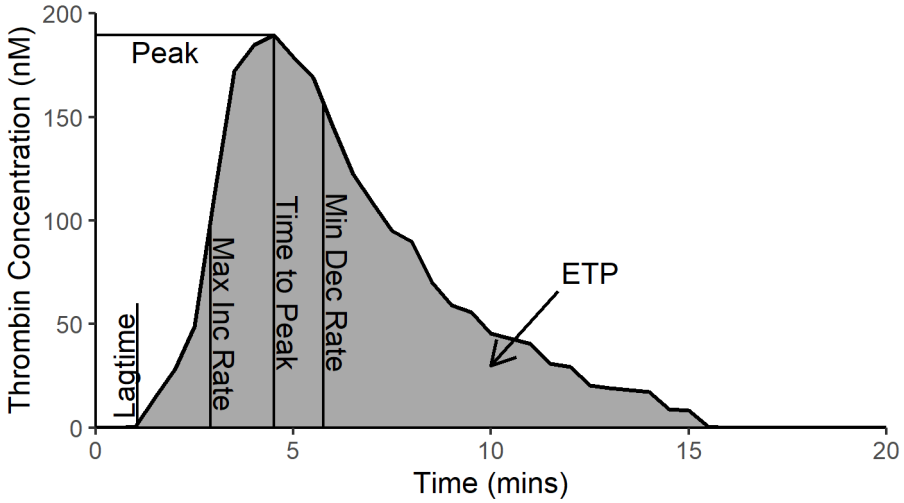

Figure 2.32: The summary statistics that are used for the sensitivity analysis, demonstrated on a thrombin generation curve. Peak height is the maximum of the thrombin generation curve and time to peak is the time taken to reach this maximum. Lagtime is the time to reach 5% of the peak height. ETP is the integral of the thrombin generation curve. Maximum increasing rate and minimum decreasing rate are given as the gradient at the steepest increase and decrease of the curve respectively.

Species	Baseline Initial Concentration (M)
TF	1×10^{-11}
II	1.45×10^{-6}
V	2×10^{-8}
VII	1×10^{-8}
VIII	7×10^{-10}
IX	9×10^{-8}
X	1.6×10^{-7}
XI	3×10^{-8}
VIIa	1×10^{-10}
AT	3.45×10^{-6}
TFPI	2.5×10^{-9}
Lipid	4×10^{-6}

Table 2.33: The baseline non-zero initial concentrations to be used in the sensitivity analysis. These values are gathered as a median from the models and coincide with the healthy figures reported in [59]. The lipid concentration used matches that in our assay rather than from the models.

Results

The predictions of all models are significantly influenced by initial FII and AT concentrations. The Bungay model is also sensitive to the FV concentration. Interestingly, only the Chatterjee model appears to be significantly affected by variance in the FXI concentration. The Symmetrical group (Hockin, Danforth, Brummel and Panteleev) are all more sensitive to the TF and TFPI concentra-

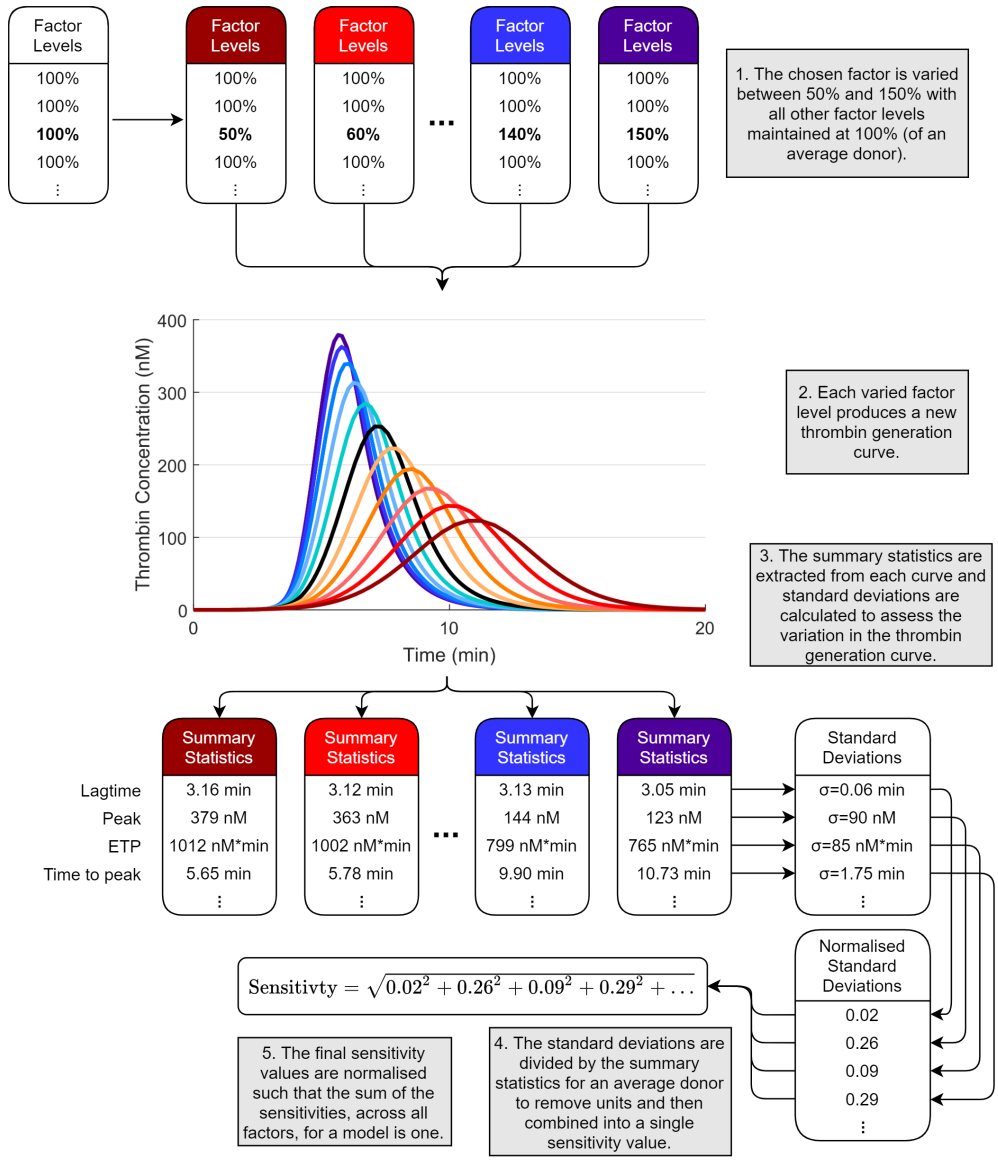

Figure 2.33: A flowchart of the sensitivity analysis method. For each coagulation factor, the concentration is varied between 50% and 150% and the resulting thrombin generation curves are calculated. The six summary statistics are then calculated for each thrombin generation curve and the standard deviation for each summary statistic is found. These standard deviations are normalised by the corresponding summary statistic value for the curve of the 100% initial concentration. The final sensitivity value is calculated as the norm of the vector of normalised standard deviations.

tions than the Quick group (Chatterjee, Bungay, Tyurin and Zhu).

The sensitivities are also given for the individual summary statistics. These are reported in Figure 2.35 as the normalised standard deviations, then scaled such that the sum across the coagulation factors, for each model, is one. ETP is only significantly influenced by the FII and AT concentrations for all models, however, the other summary statistics are much more varied.

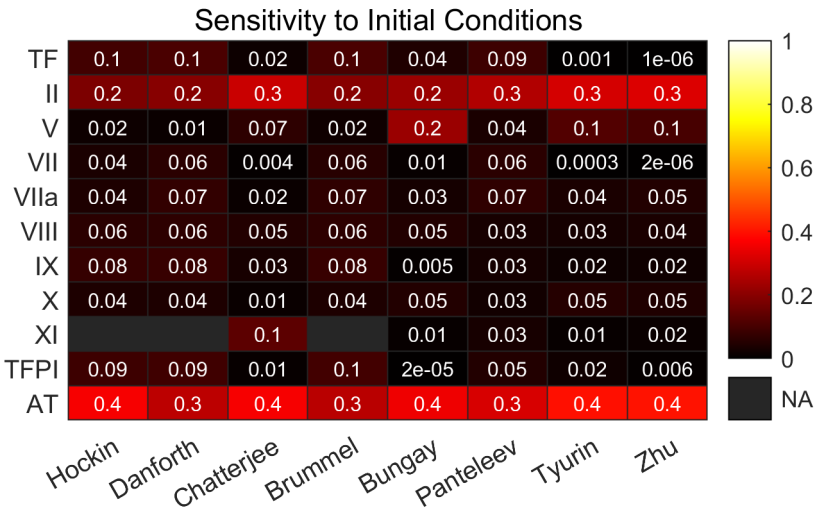

Figure 2.34: A heatmap demonstrating the sensitivity of the models to variation in the coagulation factors. The sensitivities are normalised such that the sum of the sensitivities for a given model is one.

The predictions of lagtime in the Chatterjee model are predominantly driven by FXI, while the other Hockin based models (Hockin, Danforth and Brummel) are influenced by TF, VII, VIIa, TFPI and AT. The Panteleev model is similar to the Hockin, Danforth and Brummel models except, instead of being significantly influenced by AT, it is influenced by FV. The lagtime predictions of the Tyurin and Zhu models are sensitive to FVIIa but not sensitive to TF or FVII, as expected from previous results concerning TF:VIIa in these models.

The time to peak sensitivities are similar to the ones for lagtime with no meaningful changes between the two. Lagtime and time to peak are likely to be strongly correlated with one another and, unsurprisingly, this results in similar sensitivity distributions.

The peak height is most sensitive to FII and AT, similarly to the ETP sensitivity, but the Chatterjee, Tyurin and Zhu models show much lower sensitivity to AT and greater sensitivity to FII whereas previously, all models were more sensitive to AT than FII. Additionally, the Bungay model is again sensitive to FV.

The sensitivities of the maximum increasing rate appear to focus on AT (for which Hockin, Danforth, Brummel, Bungay and Panteleev are particularly sensitive), FII (for which all models are sensitive) and FV (for which Bungay, Tyurin and Zhu are most sensitive). The minimum decreasing rate behaves similarly, with the same models sensitive to FII and FV. However, the minimum decreasing rates of the Danforth and Brummel models are not sensitive to AT while the minimum decreasing rates of the Chatterjee, Tyurin and Zhu models are sensitive to AT.

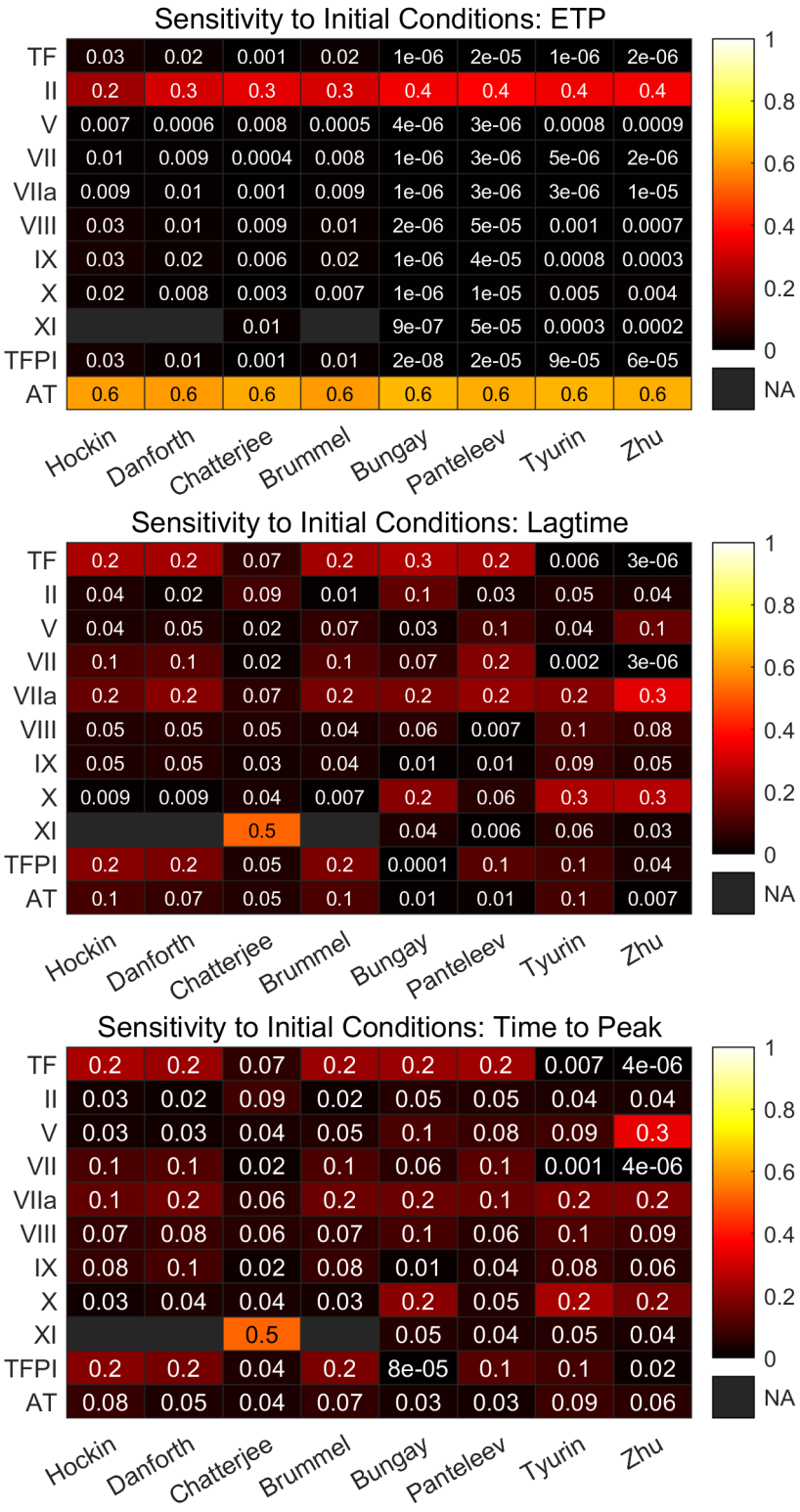
Sensitivity to Initial Conditions: ETP
TF 0.03 0.02 0.001 0.02 1e-06 2e-05 1e-06 2e-06
II 0.2 0.3 0.3 0.3 0.4 0.4 0.4 0.4
V 0.007 0.0006 0.008 0.0005 4e-06 3e-06 0.0008 0.0009
VII 0.01 0.009 0.0004 0.008 1e-06 3e-06 5e-06 2e-06
VIIa 0.009 0.01 0.001 0.009 1e-06 3e-06 3e-06 1e-05
VIII 0.03 0.01 0.009 0.01 2e-06 5e-05 0.001 0.0007
IX 0.03 0.02 0.006 0.02 1e-06 4e-05 0.0008 0.0003
X 0.02 0.008 0.003 0.007 1e-06 1e-05 0.005 0.004
XI 0.01 9e-07 5e-05 0.0003 0.0002
TFPI 0.03 0.01 0.001 0.01 2e-08 2e-05 9e-05 6e-05
AT 0.6 0.6 0.6 0.6 0.6 0.6 0.6 0.6
Hockin Danforth Chatterjee Brummel Bungay Panteleev Tyurin Zhu
1 0.8 0.6 0.4 0.2 0 NA
Sensitivity to Initial Conditions: Lagtime
TF 0.2 0.2 0.07 0.2 0.3 0.2 0.006 3e-06
II 0.04 0.02 0.09 0.01 0.1 0.03 0.05 0.04
V 0.04 0.05 0.02 0.07 0.03 0.1 0.04 0.1
VII 0.1 0.1 0.02 0.1 0.07 0.2 0.002 3e-06
VIIa 0.2 0.2 0.07 0.2 0.2 0.2 0.2 0.3
VIII 0.05 0.05 0.05 0.04 0.06 0.007 0.1 0.08
IX 0.05 0.05 0.03 0.04 0.01 0.01 0.09 0.05
X 0.009 0.009 0.04 0.007 0.2 0.06 0.3 0.3
XI 0.5 0.04 0.006 0.06 0.03
TFPI 0.2 0.2 0.05 0.2 0.0001 0.1 0.1 0.04
AT 0.1 0.07 0.05 0.1 0.01 0.01 0.1 0.007
Hockin Danforth Chatterjee Brummel Bungay Panteleev Tyurin Zhu
1 0.8 0.6 0.4 0.2 0 NA
Sensitivity to Initial Conditions: Time to Peak
TF 0.2 0.2 0.07 0.2 0.2 0.2 0.007 4e-06
II 0.03 0.02 0.09 0.02 0.05 0.05 0.04 0.04
V 0.03 0.03 0.04 0.05 0.1 0.08 0.09 0.3
VII 0.1 0.1 0.02 0.1 0.06 0.1 0.001 4e-06
VIIa 0.1 0.2 0.06 0.2 0.2 0.1 0.2 0.2
VIII 0.07 0.08 0.06 0.07 0.1 0.06 0.1 0.09
IX 0.08 0.1 0.02 0.08 0.01 0.04 0.08 0.06
X 0.03 0.04 0.04 0.03 0.2 0.05 0.2 0.2
XI 0.5 0.05 0.04 0.05 0.04
TFPI 0.2 0.2 0.04 0.2 8e-05 0.1 0.1 0.02
AT 0.08 0.05 0.04 0.07 0.03 0.03 0.09 0.06
Hockin Danforth Chatterjee Brummel Bungay Panteleev Tyurin Zhu
1 0.8 0.6 0.4 0.2 0 NA

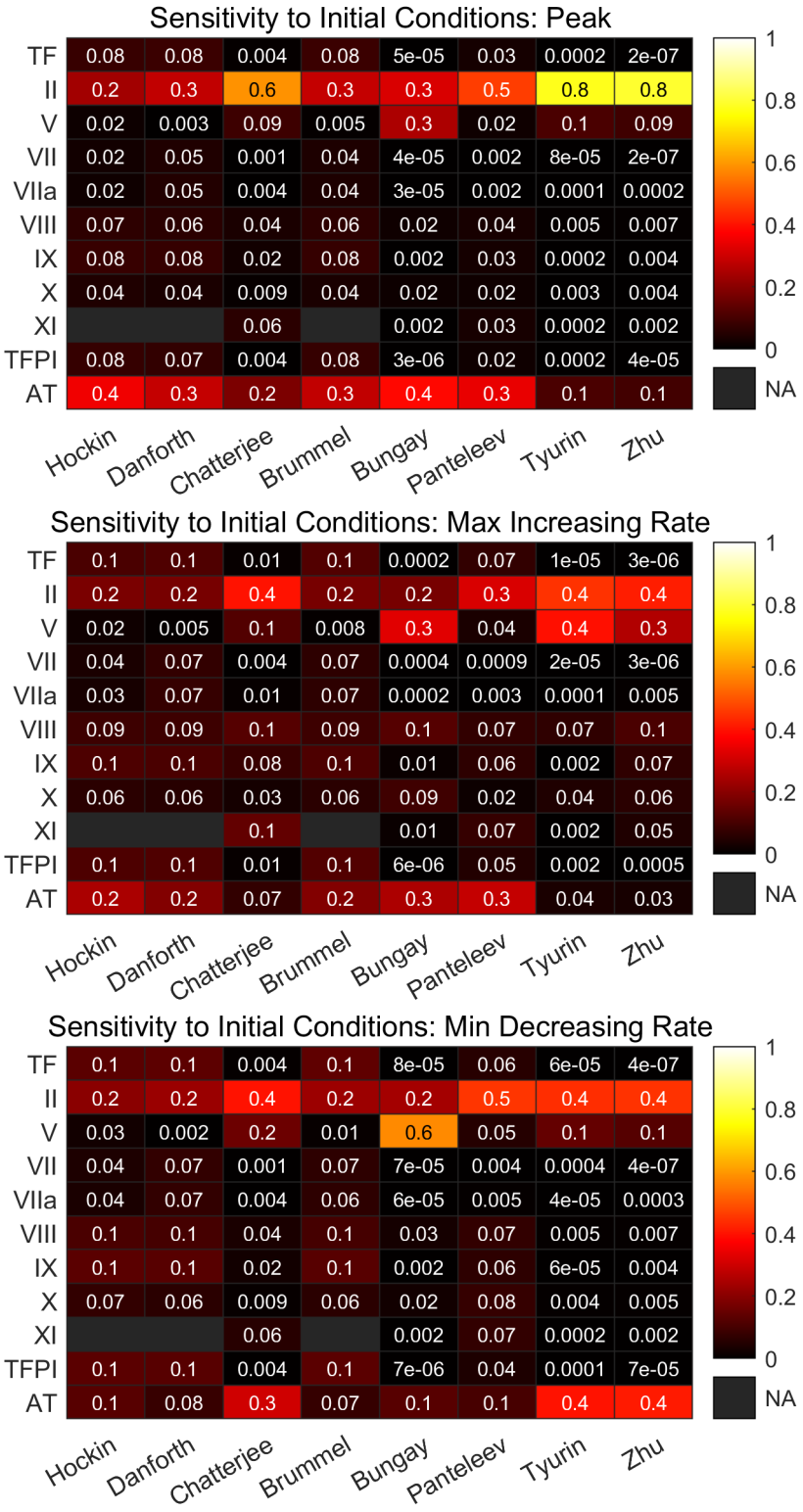

Figure 2.35: Heatmaps of sensitivity of each model to variation in the initial concentration of the coagulation factors. A separate heatmap is given for each summary statistic.

2.5.2 Sensitivity to Reaction Rates

The same sensitivity analysis method can be used on the reaction rates. We vary each reaction rate between 50% and 150% of its value, calculating thrombin generation curves for each variation and the sensitivity similarly. These sensitivities are then presented in reaction network diagrams, isolated to the reactions relevant to the initial conditions given in Table 2.33. Enzymatic activations, which are represented as multiple mass action law reactions in some of the models, are reduced to a single reaction in the network diagrams, with the sensitivity given as the largest reaction rate sensitivity of the mass action law reactions that compose it. All sensitivities are reported as a percentage of the largest reaction rate sensitivity for that model.

As seen in Figure 2.36, the Hockin model's most sensitive reactions commonly involve TF:VIIa (including its formation, its activation of both FIX and FX, and its inhibition by TFPI) or FIIa (its activation from mIIa and both FIIa and mIIa inhibition by AT). Many of the least sensitive reactions are the reverse direction of reversible reactions or the activations of FVII by FIIa and TF:VIIa. Interestingly, even though TF:VIIa inhibition by TFPI (through inhibition of the TF:VIIa:Xa complex) is a sensitive reaction, TF:VIIa inhibition by AT is not a sensitive reaction.

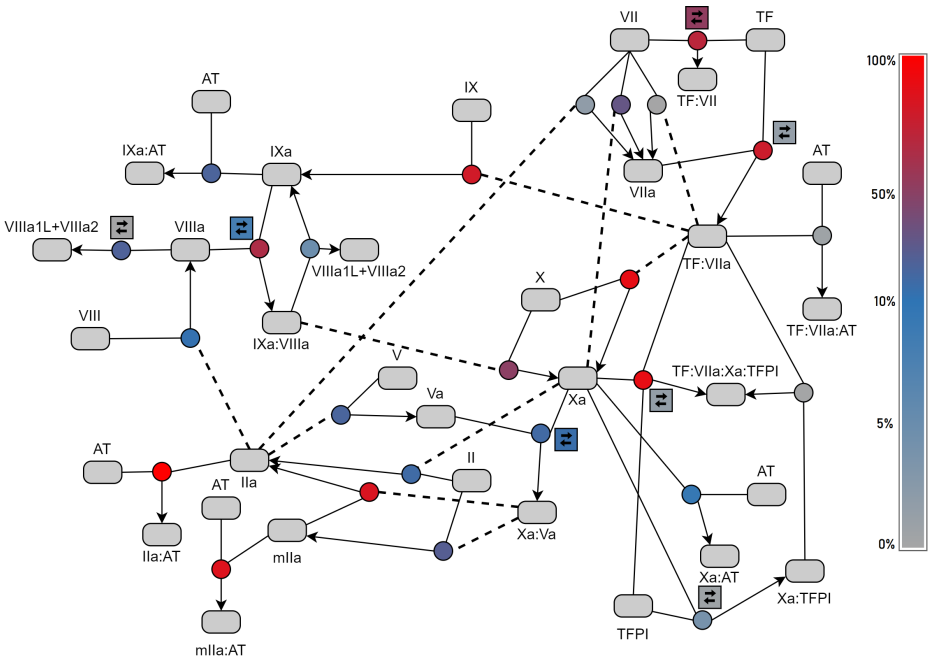

Figure 2.36: The reaction rate sensitivity analysis results for the Hockin model, given as a network diagram coloured by sensitivity as a proportion of the most sensitive reaction rate. Sensitive reactions are coloured in red, while insensitive reactions are given in grey. Reactions with an average level of sensitivity ($\approx 10\%$) are coloured in blue.

The reaction rate sensitivity distribution for the Danforth model is given in Figure 2.37. None of the changes in the Danforth model, inclusion of activation

of FX by FIXa and FV by mIIa and changes to the reaction rates for mIIa conversion into FIIa and FXa inhibition by AT, produce sensitive reactions. Instead, the sensitivity is reduced for mIIa conversion into FIIa when compared with the Hockin model and the additional reaction of FX activation by FIXa is insensitive in the Danforth model. However, these changes to the model do produce a different sensitivity distribution in the other reactions. All but FIIa inhibition by AT have a reduced sensitivity, likely due to an increased sensitivity to FIIa inhibition by AT, resulting in other sensitivities being lower in proportion.

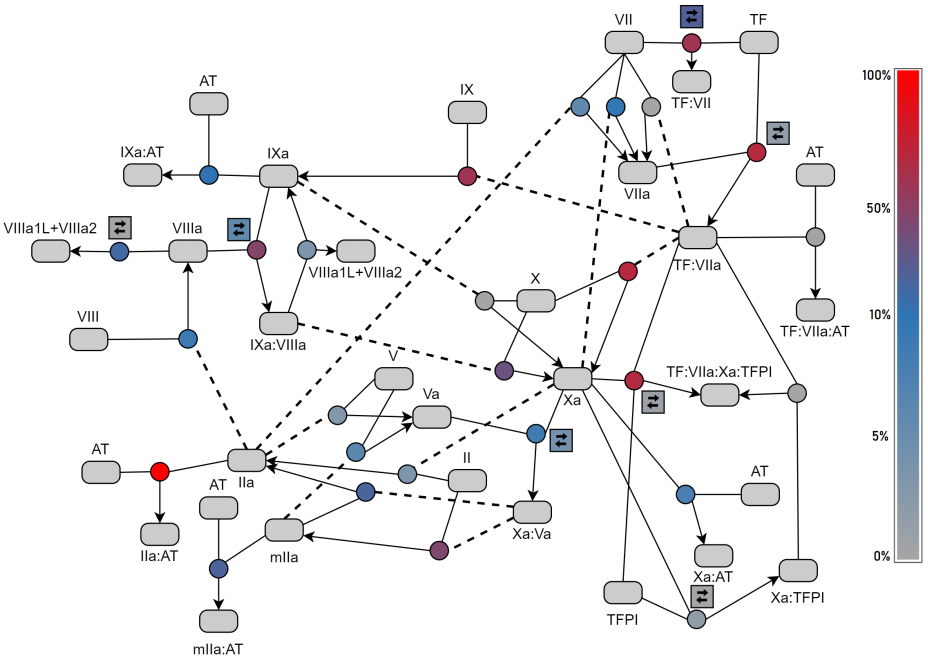

Figure 2.37: The reaction rate sensitivity analysis results for the Danforth model, given as a network diagram coloured by sensitivity as a proportion of the most sensitive reaction rate. Sensitive reactions are coloured in red, while insensitive reactions are given in grey. Reactions with an average level of sensitivity ($\approx 10\%$) are coloured in blue.

As demonstrated in Figure 2.38, the Chatterjee model features only three sensitive reactions. The first two of these are similar to previous models (mIIa conversion into FIIa and FIIa inhibition by AT), however, the third reaction, FXI activation by FXIa, has not appeared as a sensitive reaction in any other model. Many inhibitions by AT are insensitive, including those for TF:VIIa, FXIa, FIXa and FXa. All FVII activations and the reverse direction of reversible reactions are also insensitive throughout the model.

The results of the Brummel model, given in Figure 2.39, are identical to those of the Danforth model. The additional reactions in the Brummel model (FII and FVa binding and unbinding) have an average level of sensitivity.

The most sensitive reactions in the Bungay model, as seen in Figure 2.40, are those involving FIIa, in particular activation of FII into mIIa and mIIa into FIIa by Xa:Va and FIIa inhibition by AT. The model is insensitive to most reactions,

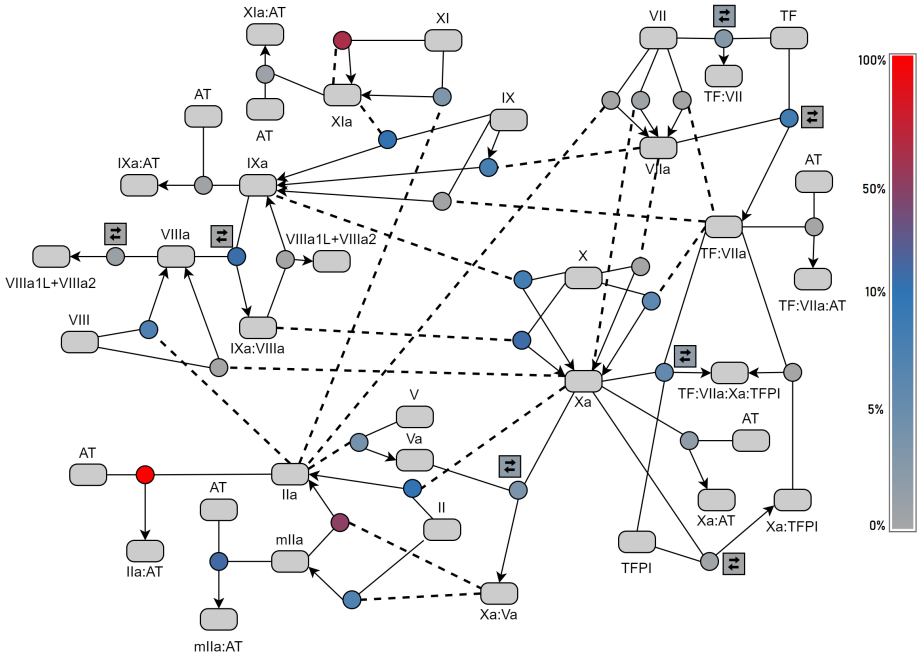

Figure 2.38: The reaction rate sensitivity analysis results for the Chatterjee model, given as a network diagram coloured by sensitivity as a proportion of the most sensitive reaction rate. Sensitive reactions are coloured in red, while insensitive reactions are given in grey. Reactions with an average level of sensitivity ($\approx 10\%$) are coloured in blue.

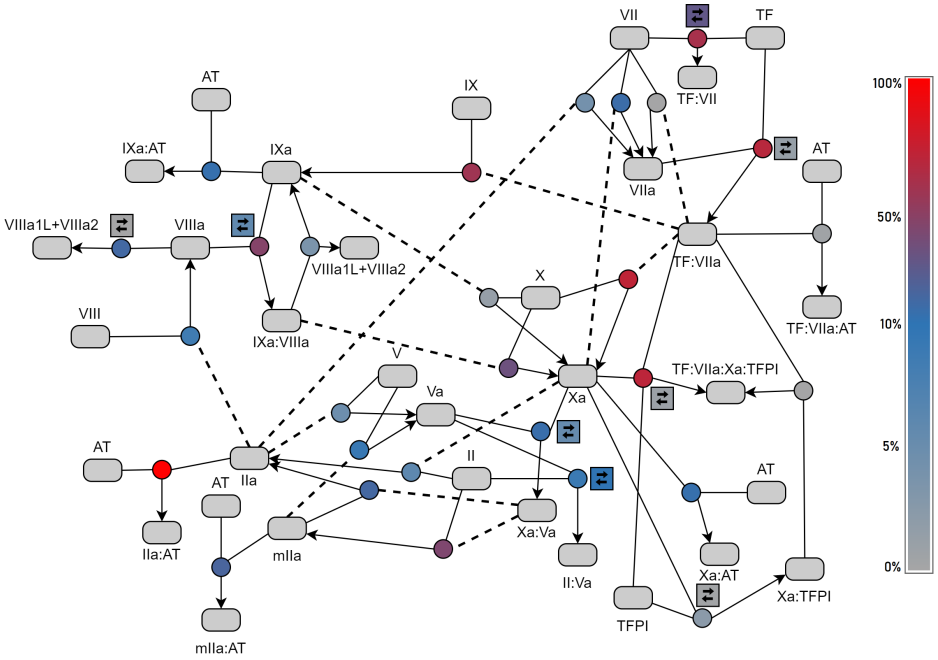

Figure 2.39: The reaction rate sensitivity analysis results for the Brummel model, given as a network diagram coloured by sensitivity as a proportion of the most sensitive reaction rate. Sensitive reactions are coloured in red, while insensitive reactions are given in grey. Reactions with an average level of sensitivity ($\approx 10\%$) are coloured in blue.

including TFPI; activation of FVII; inhibition of mIIa; Xa and IXa by AT; and some activations of FV and FVIII (insensitive to FVIII activation by FIIa and FXa and to FV activation by FIIa).

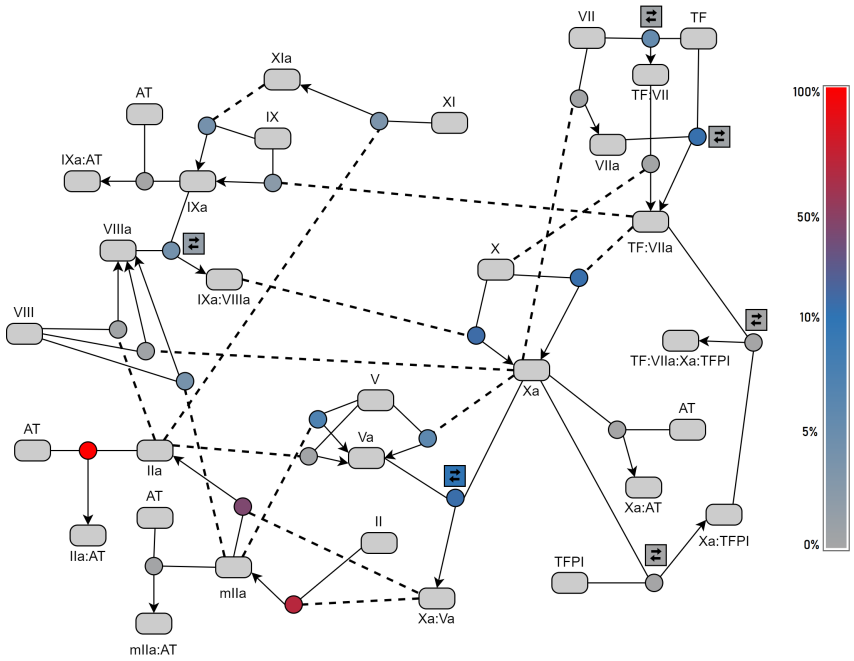

Figure 2.40: The reaction rate sensitivity analysis results for the Bungay model, given as a network diagram coloured by sensitivity as a proportion of the most sensitive reaction rate. Sensitive reactions are coloured in red, while insensitive reactions are given in grey. Reactions with an average level of sensitivity ($\approx 10\%$) are coloured in blue.

The reaction rate sensitivity distribution for the Panteleev model is given in Figure 2.41. This model has FII activation by Xa:Va and FIIa inhibition by AT as its only sensitive reactions. Almost all reactions have an average sensitivity of around 10%. The insensitive reactions include inhibition of FXIa, FIXa and Xa:Va by AT, some of the TFPI reactions and activation of FX by FIXa.

As seen in Figure 2.42, the Tyurin model is most sensitive to FII activation by Xa:Va and FIIa inhibition by AT. There are many insensitive reactions in the Tyurin model, including all inhibitions other than FIIa by AT and FXa by TFPI. Additionally, all reactions involving the formation of TF:VIIa or activation by TF:VIIa were insensitive, further demonstrating the lack of involvement of TF:VIIa in the predictions of the Tyurin model.

As demonstrated in Figure 2.43, the conclusions of the Zhu model are similar to those of the Tyurin model, sensitive reactions for FII activation by Xa:Va and FIIa inhibition by AT with low sensitivities for all other inhibitions and formation of TF:VIIa. However, activations by TF:VIIa are significant in the Zhu model since it still relies of TF:VIIa (featuring no FVIIa to otherwise initiate coagulation) but features sufficient high TF:VIIa initially set that it no longer requires more to be formed.

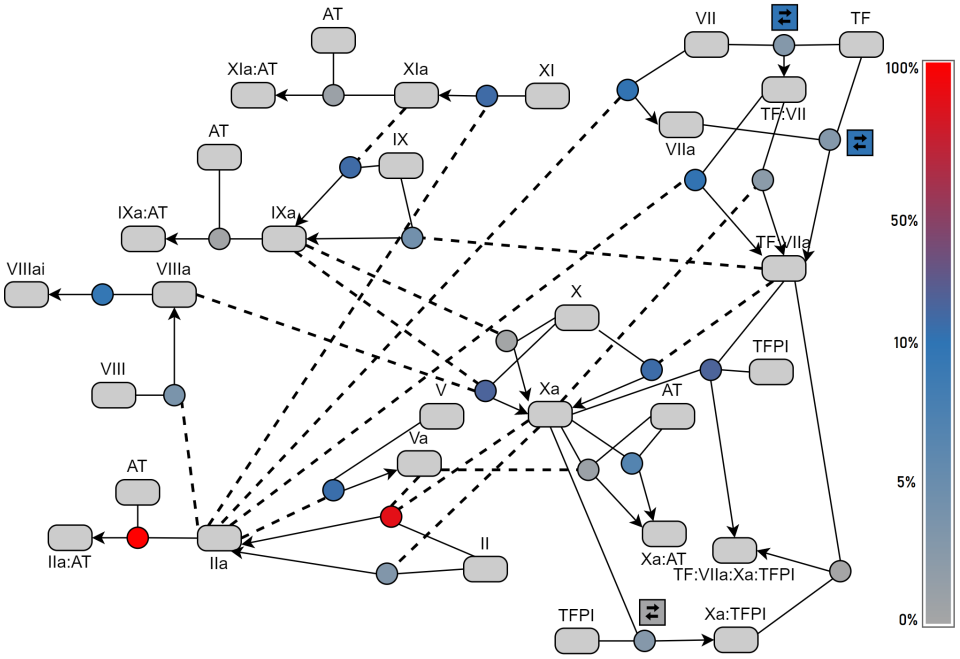

Figure 2.41: The reaction rate sensitivity analysis results for the Panteleev model, given as a network diagram coloured by sensitivity as a proportion of the most sensitive reaction rate. Sensitive reactions are coloured in red, while insensitive reactions are given in grey. Reactions with an average level of sensitivity ($\approx 10\%$) are coloured in blue.

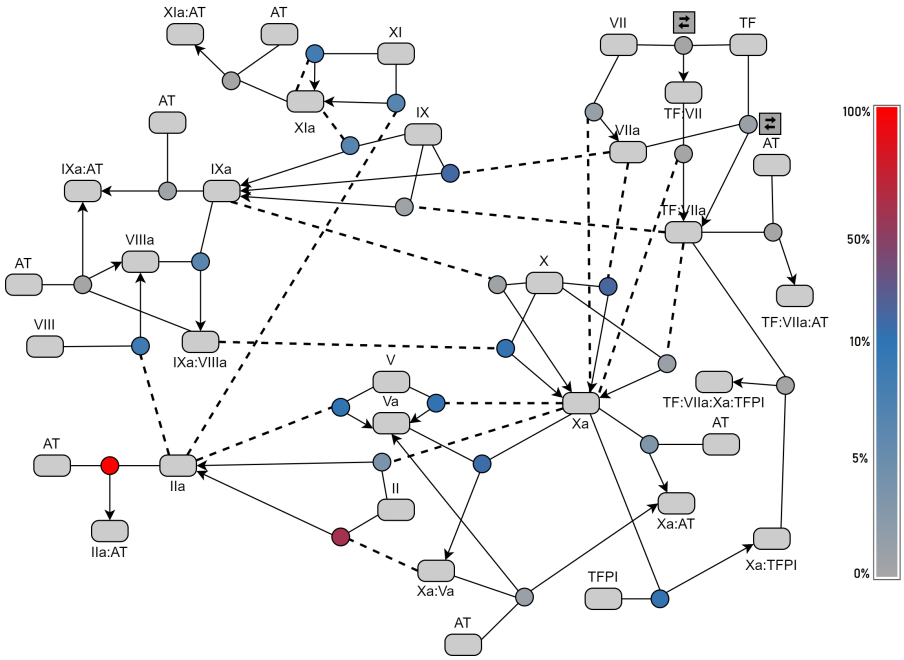

Figure 2.42: The reaction rate sensitivity analysis results for the Tyurin model, given as a network diagram coloured by sensitivity as a proportion of the most sensitive reaction rate. Sensitive reactions are coloured in red, while insensitive reactions are given in grey. Reactions with an average level of sensitivity ($\approx 10\%$) are coloured in blue.

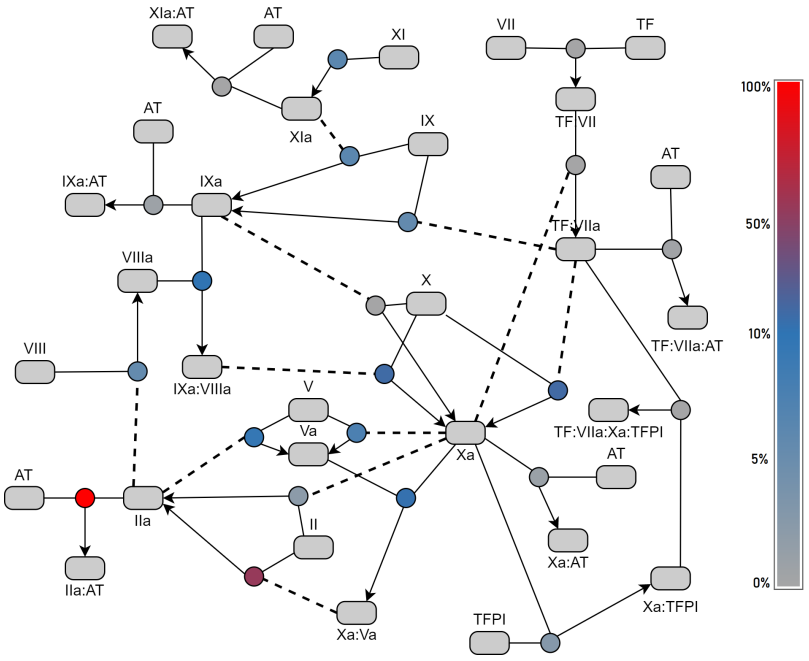

Figure 2.43: The reaction rate sensitivity analysis results for the Zhu model, given as a network diagram coloured by sensitivity as a proportion of the most sensitive reaction rate. Sensitive reactions are coloured in red, while insensitive reactions are given in grey. Reactions with an average level of sensitivity ($\approx$ 10%) are coloured in blue.

2.5.3 Conclusions

In this section, we have explored how model predictions vary in response to variations in coagulation factors and reaction rates. The Hockin, Danforth and Brummel models were generally similar in sensitivity distributions for both methods, being sensitive to FII, AT, TF and TFPI as well as most reactions involving those factors. The Bungay model appears sensitive to FV in both methods, possibly linked to the high rate of FIIa inhibition by AT where predictions will be heavily influenced by how much and how quickly prothrombinase can be formed. The Chatterjee model was the only model to appear sensitive to FXI (particularly its auto-activation). The Tyurin and Zhu models again appeared similar in their predictions, this time having similar sensitivity distributions in all coagulation factors and all comparable reaction rates except for activation by TF:VIIa for which only the Zhu model is sensitive.

The most sensitive reaction rate in all models was FIIa inhibition by AT and all models were sensitive to some form of FIIa activation by Xa:Va (II to mIIa, mIIa to IIa or II to IIa), although they disagreed on which specific step in the activation was the most sensitive. The models also varied in their sensitivity to TFPI with some models, such as the Hockin model, being incredibly sensitive to TFPI reactions and others, such as Bungay, where all TFPI reactions are insensitive. Finally, we found that inhibition of many coagulation factors (FIXa, FXa,

FXIa and TF:VIIa) were frequently insensitive reactions.

2.6 Parameter Sources

The values of the reaction rates used by the models has been shown to vary significantly depending on the source that is used [76]. Additionally, many of the models cite earlier models as the source of their reaction rates. Understanding the accuracy of the reaction rates that are used, what changes have been made, and where any assumptions have been used will inform the process by which we can develop a new model. We have investigated the sources given for all reaction rates in the Hockin, Danforth, Chatterjee, Brummel, Bungay, Tyurin and Zhu models*. This included identifying the original source for each reaction rate, changes that have been made since that source was measured and the reason for those changes, where given. We will provide an overview here, with the tables detailing the values, sources and notes for all reaction rates given in the Appendix D.

2.6.1 Hockin Model

The Hockin model predominantly uses reaction rates from the Jones model [53]. This includes some reaction rates that were tweaked from their measured values through fitting to data and some that were entirely derived through fitting. For example, [90] gives a $K_d = 2nM$ for TF:VII association and dissociation which was used as a base to fit both k_+ and k_- using data from [91]. All enzyme substrate binding reactions feature a common rate of $1 \times 10^8 M^{-1}s^{-1}$ and a handful of rates are assumed to be the same as similar reactions, such as activation of FVIII by FIIa which is assumed to be the same as for FV activation by FIIa.

2.6.2 Danforth Model

Of the four changes made to the Hockin model by Danforth, two of the changes are not given a citation (the two reaction rate changes). Since the Danforth model is built upon the Hockin model, many of the comments there are still relevant in the Danforth model, including that it contains fitted reaction rates from the Jones model [53].

2.6.3 Chatterjee Model

The first 31 reactions, and their reaction rates, in the Chatterjee model come from the Hockin model. Many of these reaction rates have been scaled based on reports using varied phospholipid concentrations. This includes the fitted reaction rates, some of which are scaled but the underlying values are still based on the fitting performed by Jones [53]. The enzyme substrate binding reactions are assumed to be diffusion limited ($k_+ = 1 \times 10^8 M^{-1}s^{-1}$ [69]). This was likely also the source used for the Hockin model even though it was not cited as such. A thoroughly validated model for fibrin is used [92] and all inhibitions of kallikrein are combined

*The Panteleev model was not included as all of its rates are derived for the spatial model and, as such, as less easily compared to the other models.

into a single first order rate.

2.6.4 Brummel Model

The comments on the Danforth model are also applicable to the Brummel model. Many of the new reactions and their rates come from the model of Bravo [86], which itself gets many of its reactions and rates from an earlier, protein C model by Hockin [93]. There are some reaction rates which are not given a source in these models and some with incorrect citations, leaving many reaction rates without an experimental source.

2.6.5 Bungay Model

The Bungay model features a handful of reaction rates that utilise measured values of multiple sources to average over. The source for activation of FXI by FIIa [94] has been retracted since the Bungay model was published [95], which demonstrates another potential pitfall of using previous models as the source of reaction rates. The sources of two reaction rates are reported as "Not Available" with no reason given. Four reaction rates are assumed to be the same as similar reactions, for example activation of FVIII by mIIa is assumed to occur at the same rate as activation by FIIa.

2.6.6 Tyurin Model

The Tyurin model features many reaction rates that are defined as an average over multiple sources. They appear to have used the models of Kogan [88] and Khanin [58] (which both use multiple sources frequently) for many of their rates, although they typically cited the original sources rather than the models. The Tyurin model also uses the same retracted source as Bungay for its activation of FXI by FIIa [94, 95].

2.6.7 Zhu Model

The Zhu model also features many rates from Kogan [88] and Khanin [58] which use multiple sources. Some of the rates in these earlier models were derived through fitting or estimated and are then reused in the Zhu model. The reaction rate for activation of FXI is first order and is calculated using data of its activation by FIIa [96].

2.6.8 Conclusions

We have identified several potential issues in the reaction rates for these models. A breakdown of how these reaction rates have been derived for each model is given

in Table 2.34. Of the 504 reaction rates across the models, 32% use estimated values, roughly half of which are due to a lack of rate constants for enzyme substrate binding. Only 10% of the reaction rates use multiple sources when determining the values to use in the models with all other reaction rates using a single experimental source. It has already been shown that there exists significant variation between different sources for the same reaction rate [76], likely due to the different experimental conditions each laboratory uses. This may mean that using a single source for each reaction rate is insufficient, and the uncertainty in these reaction rates leads to large amounts of uncertainty in the resulting model predictions.

Model	Estimated Rates		Measured Rates	
	Diffusion Limited[†]	Other	Single Source	Multiple Sources
Hockin	4	10	24	4
Danforth	4	11	25	4
Chatterjee	20	15	58	4
Brummel	7	19	33	7
Bungay	36	15	52	6
Tyurin	0	13	45	13
Zhu	0	8	54	13

Table 2.34: Each reaction rate in the models has been grouped into either "Estimated Rates" or "Measured Rates", which are then further separated into the subgroups of "Diffusion Limited" or "Other", and "Single Source" or "Multiple Sources". The total number of reaction rates which fall into each of these groups are given for each model.

[†]This includes a handful of rates that are assumed to be $1 \times 10^7 M^{-1}s^{-1}$, or other similar values, rather than $1 \times 10^8 M^{-1}s^{-1}$.

2.7 Timescale Analysis and Nondimensionalization

We have seen many differences in the predictions of the models, such as formation of TF:VIIa; the shape of the thrombin generation curves; and their inhibition schemes for the complexes Xa:Va and IXa:VIIIa (Section 2.4). We now aim to investigate the models across various timescales (Figures 2.29 and 2.30, on pages 89 and 90, respectively, highlight significantly different dynamics between the early and late timescales) to identify accuracies and inaccuracies in their predictions across the three standard phases of coagulation: initiation, propagation, and inhibition.

The first model we investigated was the Danforth model. This was chosen as it contains relatively few reactions and performed significantly better in the correlation analysis than the model with the fewest reactions, the Hockin model (Section 2.3 and Figure 2.19).

Due to the size of the models (44 parameters across 34 ODEs), typical timescale analysis methods such as asymptotic analysis would be challenging to implement. This led us to attempt to reduce the complexity of the models through nondimensionalization, hoping to remove a significant number of the parameters to make the timescale analysis work easier. Unfortunately, we found it was not possible to remove more than two parameters from the model (the minimum number already guaranteed by the Buckingham π theorem [29]), and therefore we were unable to significantly reduce its complexity.

In this section, will demonstrate the reason why we were unable to remove more than two parameters from the model. Then given the complexity of these models, we will perform a computational timescale analysis on both the Danforth and Tyurin models, skipping the nondimensionalization.

2.7.1 Nondimensionalization

After attempting the nondimensionalize the Danforth model to remove a significant number of parameters, we found we were unable to remove more than two (with removal of two parameters guaranteed by the Buckingham π theorem [29]). To understand why this is the case we will break down the model into first and second order reactions.

- First order reaction rates can only be removed through the time scaling and as such only one can be removed.
- Second order reaction rates cannot be removed if one of the concentration scalings for a reactant has already been set.

For notation, we will use $\tilde{a}$ to denote the dimensionless version of the variable a and a_0 to denote the dimensional scaling used for the variable a giving us $a = a_0\tilde{a}$.

First Order Reactions

First order reactions are those that only contain a single reactant*. An example reaction of this form would be $x \to x_1 + x_2$. This reaction would give an ODE for x, x_1 and x_2 with the ODE for x given as $\frac{dx}{dt} = -k \cdot x$ where k is the reaction rate parameter. By nondimensionalizing this ODE, we reach $\frac{d\tilde{x}}{d\tilde{t}} = -k \cdot t_0 \cdot \tilde{x}$. From this we can see that the only way to remove the parameter k is to set the value of t_0. Since this can only be done once for the whole system then we can only remove a single first order reaction rate.

Second Order Reactions

There are two types of second order reactions present in the Danforth model, binding reactions of the form $x + y \to z$ and enzymatic reactions of the form $x + y \to x + z$.

For the binding reactions, with reaction rate p, we get the ODE system below.

$$\begin{aligned}\frac{dx}{dt} &= -p \cdot x \cdot y \\ \frac{dy}{dt} &= -p \cdot x \cdot y \\ \frac{dz}{dt} &= p \cdot x \cdot y\end{aligned}$$

After nondimensionalizing this system, we get the following.

$$\begin{aligned}\frac{d\tilde{x}}{d\tilde{t}} &= -p \cdot t_0 \cdot y_0 \cdot \tilde{x}\tilde{y} \\ \frac{d\tilde{y}}{d\tilde{t}} &= -p \cdot t_0 \cdot x_0 \cdot \tilde{x}\tilde{y} \\ \frac{d\tilde{z}}{d\tilde{t}} &= p \cdot t_0 \cdot \frac{x_0 \cdot y_0}{z_0}\tilde{x}\tilde{y}\end{aligned}$$

To remove the parameter p from the system we require $x_0 = y_0 = z_0 = \frac{1}{t_0 \cdot p}$ (up to multiples of other nondimensional parameters).

Then suppose we have another reaction which uses one of x, y or z as a reactant. Without loss of generality, we will assume this reaction uses x and is of the form $x + a \to b$ with reaction rate q. The nondimensionalized ODE system for this reaction is given below.

*The model contains first order reactions both with one and two products. However, we will see the number of products is not relevant and the same properties hold.

$$\frac{d\tilde{x}}{d\tilde{t}} = -q \cdot t_0 \cdot a_0 \cdot \tilde{x}\tilde{a}$$
$$\frac{d\tilde{a}}{d\tilde{t}} = -q \cdot t_0 \cdot x_0 \cdot \tilde{x}\tilde{a}$$
$$\frac{d\tilde{b}}{d\tilde{t}} = q \cdot t_0 \cdot \frac{x_0 \cdot a_0}{b_0}\tilde{x}\tilde{a}$$

Since x_0 is already defined then, from the ODE for $\tilde{a}$, we now have a nondimensional parameter of $\frac{q}{p}$ which cannot be removed, and we are forced to choose $a_0, b_0 = \frac{1}{t_0 \cdot p}$ (up to multiples of other nondimensional parameters) to avoid introducing further parameters.

Similarly, any first order reactions of the form $x \to c$ or $x \to c + d$ (system given below), where the scaling for x_0 is already defined, require that the scalings c_0 and d_0 are the same as x_0 (up to multiples of other nondimensional parameters) in order to not introduce more nondimensional parameters into the system.

$$\frac{d\tilde{x}}{d\tilde{t}} = -r \cdot t_0 \cdot \tilde{x}$$
$$\frac{d\tilde{c}}{d\tilde{t}} = r \cdot t_0 \cdot \frac{x_0}{c_0} \cdot \tilde{x}$$
$$\frac{d\tilde{d}}{d\tilde{t}} = r \cdot t_0 \cdot \frac{x_0}{d_0} \cdot \tilde{x}$$

These two properties are enough to show that whichever species's scaling is chosen first, it is not possible to remove further parameters by setting the other scalings in the Danforth model. This is with the exception of the scalings V_0 and $VIII_0$ which only appear as the species y in reactions of the form $x + y \to x + z$. Unfortunately, it is not possible to remove parameters through these scalings either. Any reactions of the form $x + y \to x + z$ (system given below), where the scalings x_0 and z_0 are already set, requires that $y_0 = z_0$ (up to multiples of other nondimensional parameters).

$$\frac{d\tilde{y}}{d\tilde{t}} = -s \cdot t_0 \cdot x_0 \cdot \tilde{x}\tilde{y}$$
$$\frac{d\tilde{z}}{d\tilde{t}} = s \cdot t_0 \cdot \frac{x_0 \cdot y_0}{z_0} \cdot \tilde{x}\tilde{y}$$

This means that, regardless of which scaling is used to remove a parameter, no more parameters can be removed from the system. This, along with the fact that time scaling can only remove one first order reaction rate, is why we can only remove a maximum of two parameters through nondimensionalization.

2.7.2 Timescale Analysis - Danforth

To assess the various timescales in the Danforth model, we have extracted the *intervals of influence* for each term in the ODE system. This is the time interval that a particular term has a meaningful influence on a given species ODE. The process by which we did this is presented in Figure 2.44.

The intervals of influence take into account cancelling any reactions in equilibrium and whether the current value of the ODE is significant to the system as a whole. For example, the reaction TF:VIIa + AT → TF:VIIa:AT is the dominant reaction on AT for very early times (in the first 5 seconds). However, the AT concentration does not change significantly during this time meaning it will have no meaningful influence on the levels of free AT in the system so this reaction is not considered influential to AT. The decision as to whether a small change to a species is influential requires knowledge about the roles each species plays in the system. For example, FIIa is only activated by FXa at early times which produces what would appear as a negligible change in FIIa concentration but due to the strong positive feedback loops in FIIa concentration if this reaction is deemed negligible then no FIIa will be produced in the system at the later timescales. The intervals of influence for each reaction on each species is given in Table 2.35.

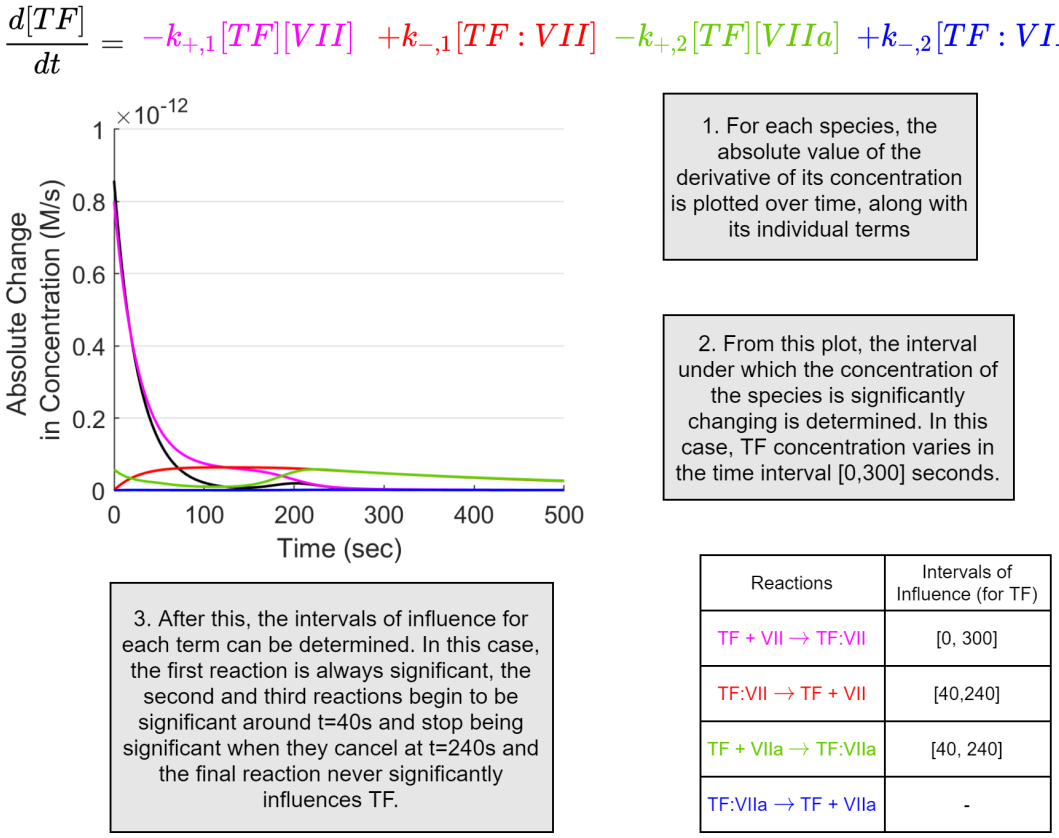

Figure 2.44: The steps taken to determine the intervals of influence. An example is given for determining the intervals of influence, on TF, for the four reactions that affect it.

Species	Reaction	Interval of Influence (s)
TF	TF + VII → TF:VII	(0,300)
	TF:VII → TF + VII	(40,240)
	TF + VIIa → TF:VIIa	(40,240)
	TF:VIIa → TF + VIIa	-
TF:VII	TF + VII → TF:VII	(0,300)
	TF:VII → TF + VII	(40,700)
VII	TF + VII → TF:VII	(0,30)
	TF:VII → TF + VII	-
	TF:VIIa + VII → TF:VIIa + VIIa	-
	Xa + VII → Xa + VIIa	(10,150)∪(340,700)
	IIa + VII → IIa + VIIa	(130,460)
TF:VIIa	TF + VIIa → TF:VIIa	(0,700)
	TF:VIIa → TF + VIIa	(15,700)
	TF:VIIa + X → TF:VIIa:X	(0,700)
	TF:VIIa:X → TF:VIIa + X	(0,700)
	TF:VIIa + Xa → TF:VIIa:Xa	(250,700)
	TF:VIIa:Xa → TF:VIIa + Xa	(0,700)
	TF:VIIa + IX → TF:VIIa:IX	(7,700)
	TF:VIIa:IX → TF:VIIa + IX	(7,700)
	TF:VIIa:IX → TF:VIIa + IXa	(7,700)
	TF:VIIa + Xa:TFPI → TF:VIIa:Xa:TFPI	(250,700)
	TF:VIIa + AT → TF:VIIa:AT	(50,700)
VIIa	TF + VIIa → TF:VIIa	(0,5)
	TF:VIIa → TF + VIIa	-
	TF:VIIa + VII → TF:VIIa + VIIa	-
	Xa + VII → Xa + VIIa	(2,150)∪(340,700)
	IIa + VII → IIa + VIIa	(130,420)
Xa	TF:VIIa + Xa → TF:VIIa:Xa	-
	TF:VIIa:Xa → TF:VIIa + Xa	(0,460)
	IXa:VIIIa:X → IXa:VIIIa + Xa	(100,150)∪(300,700)
	Xa + Va → Xa:Va	(25,140)∪(320,700)
	Xa:Va → Xa + Va	(25,140)∪(320,700)
	Xa + TFPI → Xa:TFPI	(500,700)
	Xa:TFPI → Xa + TFPI	-
	Xa + AT → Xa:AT	(10,700)
	IXa + X → IXa + Xa	-
IIa	Xa + II → Xa + IIa	(0,100)
	Xa:Va + mIIa → Xa:Va + IIa	(85,350)
	IIa + AT → IIa:AT	(30,700)

TF:VIIa:X	TF:VIIa + X → TF:VIIa:X	(0,700)
	TF:VIIa:X → TF:VIIa + X	(0,700)
	TF:VIIa:X → TF:VIIa:Xa	(0,700)
X	TF:VIIa + X → TF:VIIa:X	(0,140)
	TF:VIIa:X → TF:VIIa + X	-
	IXa:VIIIa + X → IXa:VIIIa:X	(100,700)
	IXa:VIIIa:X → IXa:VIIIa + X	-
	IXa:VIIIa:X → IXa + X + $VIIIa_1L$ + $VIIIa_2$	-
	IXa + X → IXa + Xa	-
TF:VIIa:Xa	TF:VIIa:X → TF:VIIa:Xa	(0,700)
	TF:VIIa + Xa → TF:VIIa:Xa	(200,700)
	TF:VIIa:Xa → TF:VIIa + Xa	(0,700)
	TF:VIIa:Xa + TFPI → TF:VIIa:Xa:TFPI	(0,700)
	TF:VIIa:Xa:TFPI → TF:VIIa:Xa + TFPI	(50,700)
IX	TF:VIIa + IX → TF:VIIa:IX	(0,700)
	TF:VIIa:IX → TF:VIIa + IX	(0,700)
TF:VIIa:IX	TF:VIIa + IX → TF:VIIa:IX	(0,700)
	TF:VIIa:IX → TF:VIIa + IX	(0,700)
	TF:VIIa:IX → TF:VIIa + IXa	(0,700)
IXa	TF:VIIa:IX → TF:VIIa + IXa	(0,700)
	IXa + VIIIa → IXa:VIIIa	(110,700)
	IXa:VIIIa → IXa + VIIIa	(120,700)
	IXa:VIIIa:X → IXa + X + $VIIIa_1L$ + $VIIIa_2$	(350,700)
	IXa:VIIIa → IXa + $VIIIa_1L$ + $VIIIa_2$	(350,700)
	IXa + AT → IXa:AT	(50,700)
II	Xa + II → Xa + IIa	-
	Xa:Va + II → Xa:Va:II	(40,350)
	Xa:Va:II → Xa:Va + II	(40,350)
VIII	IIa + VIII → IIa + VIIIa	(40,170)
VIIIa	IIa + VIII → IIa + VIIIa	(20,170)
	IXa + VIIIa → IXa:VIIIa	-
	IXa:VIIIa → IXa + VIIIa	-
	VIIIa → $VIIIa_1L$ + $VIIIa_2$	(120,700)
	$VIIIa_1L$ + $VIIIa_2$ → VIIIa	-
IXa:VIIIa	IXa + VIIIa → IXa:VIIIa	(80,700)
	IXa:VIIIa → IXa + VIIIa	(120,700)
	IXa:VIIIa + X → IXa:VIIIa:X	(80,700)
	IXa:VIIIa:X → IXa:VIIIa + X	(170,700)
	IXa:VIIIa:X → IXa:VIIIa + Xa	(80,700)
	IXa:VIIIa → IXa + $VIIIa_1L$ + $VIIIa_2$	(170,700)

IXa:VIIIa:X	IXa:VIIIa + X → IXa:VIIIa:X	(80,700)
	IXa:VIIIa:X → IXa:VIIIa + X	(170,700)
	IXa:VIIIa:X → IXa:VIIIa + Xa	(80,700)
	IXa:VIIIa:X → IXa + X + $VIIIa_1L$ + $VIIIa_2$	(170,700)
$VIIIa_1L$	VIIIa → $VIIIa_1L$ + $VIIIa_2$	(80,700)
	$VIIIa_1L$ + $VIIIa_2$ → VIIIa	-
	IXa:VIIIa:X → IXa + X + $VIIIa_1L$ + $VIIIa_2$	-
	IXa:VIIIa → IXa + $VIIIa_1L$ + $VIIIa_2$	-
V	IIa + V → IIa + Va	(10,30)∪(100,170)
	mIIa + V → mIIa + Va	(25,170)
Va	IIa + V → IIa + Va	(10,30)∪(100,170)
	Xa + Va → Xa:Va	(25,700)
	Xa:Va → Xa + Va	(170,700)
	mIIa + V → mIIa + Va	(25,170)
Xa:Va	Xa + Va → Xa:Va	(25,700)
	Xa:Va → Xa + Va	(25,700)
	Xa:Va + II → Xa:Va:II	(25,360)
	Xa:Va:II → Xa:Va + II	(25,360)
	Xa:Va:II → Xa:Va + mIIa	(25,360)
Xa:Va:II	Xa:Va + II → Xa:Va:II	(25,360)
	Xa:Va:II → Xa:Va + II	(25,360)
	Xa:Va:II → Xa:Va + mIIa	(25,360)
mIIa	Xa:Va:II → Xa:Va + mIIa	(25,360)
	Xa:Va + mIIa → Xa:Va + IIa	(120,360)
	mIIa + AT → mIIa:AT	(40,340)
TFPI	Xa + TFPI → Xa:TFPI	(10,700)
	Xa:TFPI → Xa + TFPI	-
	TF:VIIa:Xa + TFPI → TF:VIIa:Xa:TFPI	(0,360)
	TF:VIIa:Xa:TFPI → TF:VIIa:Xa + TFPI	-
Xa:TFPI	Xa + TFPI → Xa:TFPI	(0,700)
	Xa:TFPI → Xa + TFPI	-
	TF:VIIa + Xa:TFPI → TF:VIIa:Xa:TFPI	-
TF:VIIa: Xa:TFPI	TF:VIIa:Xa + TFPI → TF:VIIa:Xa:TFPI	(0,700)
	TF:VIIa:Xa:TFPI → TF:VIIa:Xa + TFPI	-
	TF:VIIa + Xa:TFPI → TF:VIIa:Xa:TFPI	-
AT	Xa + AT → Xa:AT	-
	mIIa + AT → mIIa:AT	(70,270)
	IXa + AT → IXa:AT	-
	IIa + AT → IIa:AT	(180,700)
	TF:VIIa + AT → TF:VIIa:AT	-

Table 2.35: Intervals of influence for each reaction, on each of the species that the reaction affects, for the Danforth model.

Based on the intervals of influence, five interval timescales were chosen which are reported in seconds. The $t = O(1s)$ dynamics are demonstrated by the significant reactions on the (0,5) time interval; the $t = O(10s)$ dynamics are governed by the (5,40) significant reactions; the $t = O(100s)$ dynamics are split across two timescales, covering the amplification on the interval (40,170) and the switch from amplification to inhibition on the (170,460) interval; and the $t = O(1000s)$ dynamics are demonstrated by the significant reactions on the (460,1200) interval. Each timescale will be demonstrated using a reduced network diagram and simulations. We only look on the interval (0,1200) since this corresponds to the timescale in which relevant reactions are occurring in the experiment (20 minutes). A network diagram for the Danforth model, containing all reactions, is given in Figure 2.45. The ODEs for each of the Danforth timescale-reduced models are given in Appendix A.

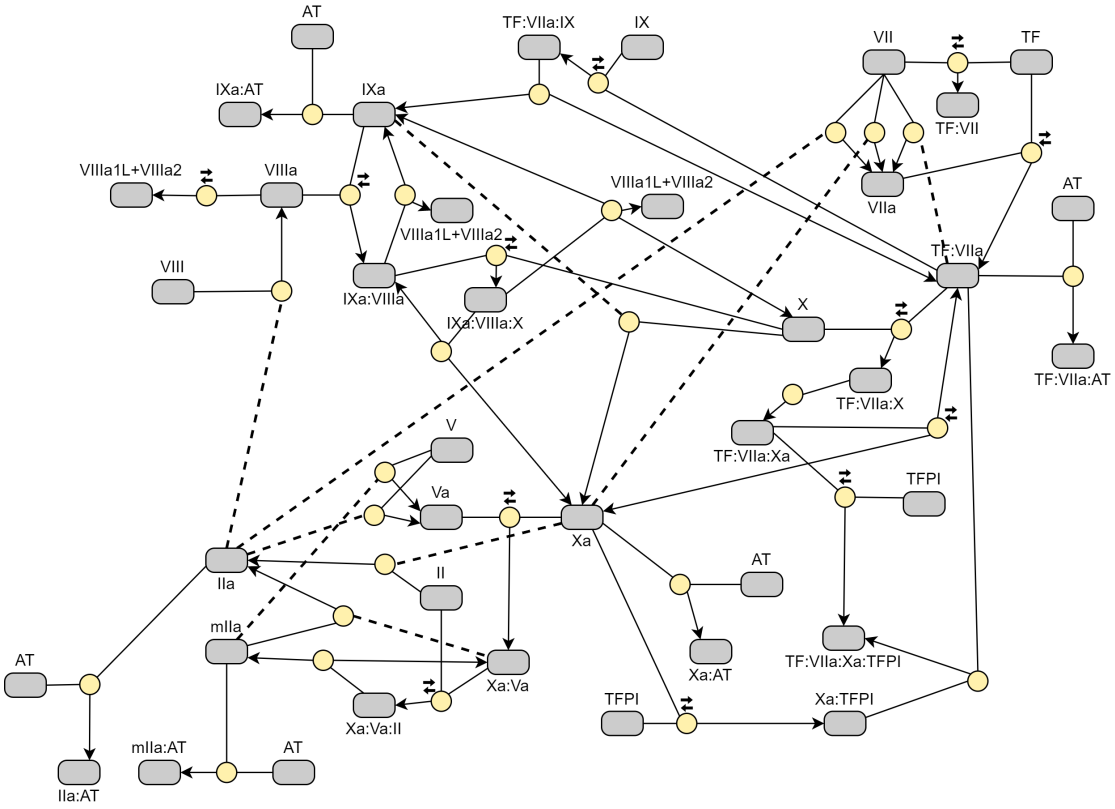

Figure 2.45: A reaction network diagram of the Danforth model. Grey nodes correspond to individual species. Yellow nodes correspond to reactions and each reaction node is connected to its products (arrows), reactants (solid lines) and species which are both products and reactants (dotted lines). Reaction nodes next to a pair of arrows indicate that the reaction is reversible. The species nodes for AT, TFPI and $\text{VIIIa}_1\text{L}+\text{VIIIa}_2$ have been repeated in multiple places to simplify the network diagram.

The First Timescale

The first interval timescale is (0,5) and contains the reactions that begin almost immediately in the system. A reduced network diagram for the reactions which are significant on this timescale is given in Figure 2.46 and simulations of this reduced model are given in Figure 2.47 for TF:VIIa, FXa, FIXa and FIIa. We observe a surprisingly large number of reactions being involved at this timescale. TF:VIIa, FIXa, FXa and FIIa are all being formed immediately as well as the feedback from FXa activating FVII. We also observe TFPI beginning to regulate TF:VIIa and TF:VIIa:Xa. We can see good predictions in the (0,5) timescale with differences only starting to appear at around $t = 10s$ and onward, when the AT inhibitions start to become more relevant resulting in all species being over predicted. The initial conditions used for these simulations are the original Danforth initial conditions given in Table 2.2.

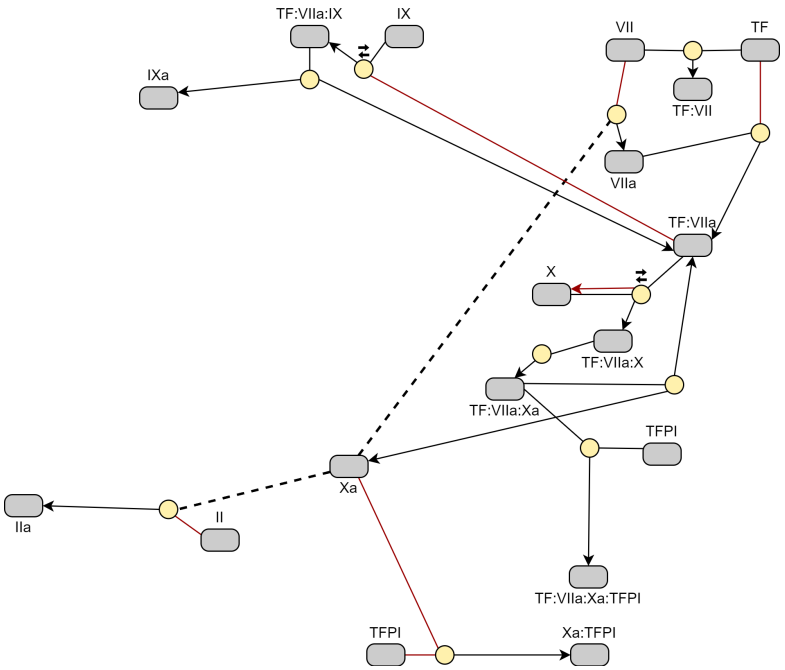

Figure 2.46: A reaction network diagram of the reduced Danforth model for the (0,5) timescale. Red lines and arrows indicate a species that is not significantly affected by a reaction, but the reaction still has a significant effect on other species. If only one direction in a reversible reaction is insignificant, then an additional red arrow is used to demonstrate that direction.

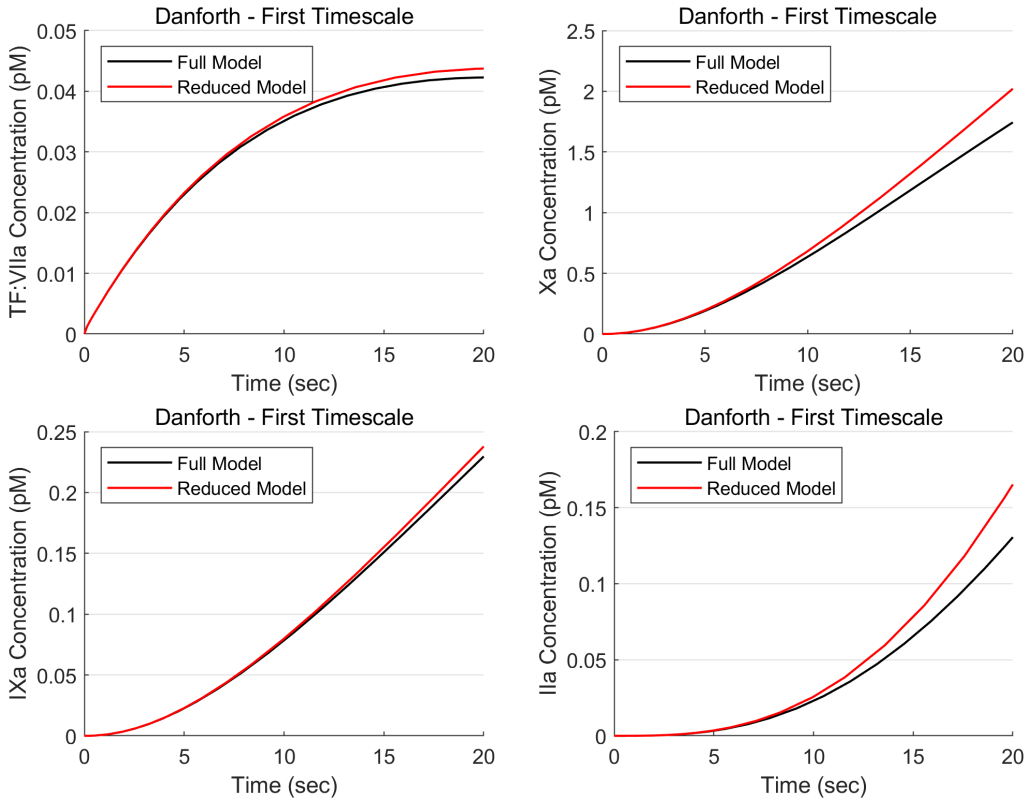

Figure 2.47: Comparison between the reduced Danforth for the first timescale and the full Danforth model.

The Second Timescale

The second interval timescale is (5,40) and governs the reactions that may not begin immediately but do still play a role in the initiation of the system. A reduced network diagram for the reactions which are significant on this timescale is given in Figure 2.48. Simulations of this model are given in Figure 2.49 for TF:VIIa, FXa, FIXa, FIIa and FVa concentrations. The initial conditions for the system are taken from the first timescale model at $t = 5s$. This timescale adds in reactions for AT inhibition and activation of FV by FIIa to then move into production of prothrombinase in the later timescales. We see good agreement up to $t = 45s$ where mIIa conversion into FIIa becomes significant, slightly surpassing the required (5,40) time interval.

The Third Timescale

The third interval timescale is (40,170) and begins amplification. A reduced network diagram for the reactions which are significant on this timescale is given in Figure 2.50 and simulations of this model are given in Figure 2.51 for TF:VIIa, FXa, FIXa, FIIa and FVa. The initial conditions used are from the second timescale model at $t = 40s$. This model now includes most of the full model with FVIII now being activated and IXa:VIIIa being formed. TF:VIIa seems to no longer have a significant effect on the system. The third timescale model stays valid for longer than required with good predictions up to $t = 200s$. The initial

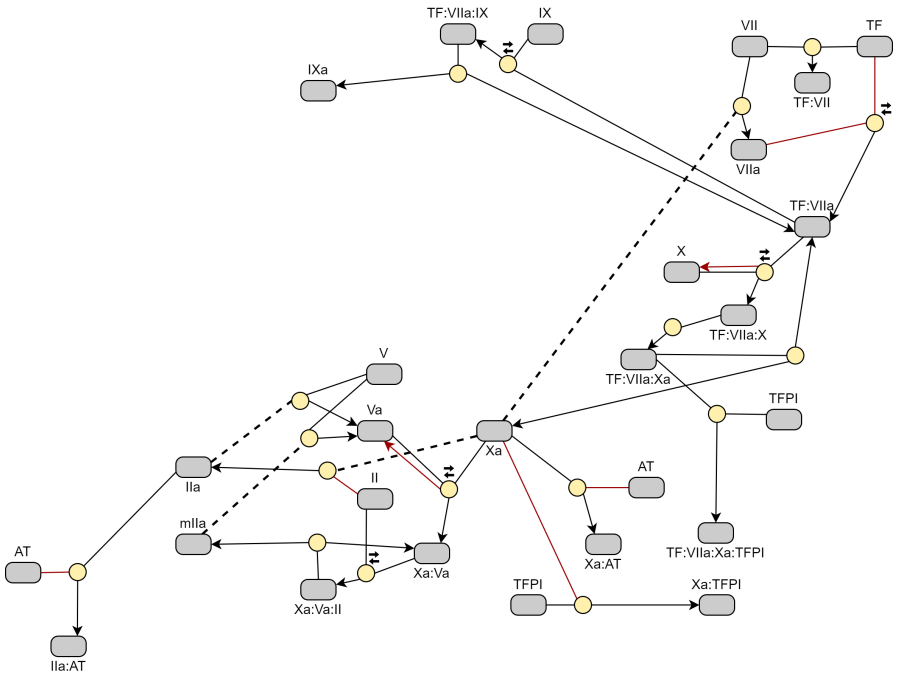

Figure 2.48: A reaction network diagram of the reduced Danforth model for the (5,40) timescale. Red lines and arrows indicate a species that is not significantly affected by a reaction, but the reaction still has a significant effect on other species. If only one direction in a reversible reaction is insignificant, then an additional red arrow is used to demonstrate that direction.

condition for FXa appears to be slightly off, however, this does not significantly affect the results on this timescale. The levels of FVa are the first to show differences between the models, where the full model begins to drift downwards at around $t = 150s$, which is not followed by the reduced model, corresponding to the prothrombinase formation reaction starting to significantly affect the FVa concentration.

The Fourth Timescale

The fourth interval timescale is (170,460) and covers the end of amplification and the beginning of initiation. A reduced network diagram for the reactions which are significant on this timescale is given in Figure 2.52 and simulations are given in Figure 2.53, beginning with the initial conditions defined by the third timescale model at $t = 170s$. Factors VIII and V are no longer being activated. This model has the largest set of reactions, and this allows it to capture the results of the later timescales accurately. There is a slight drift between the reduced model and the full model which is due to earlier timescales as the shapes of the concentration curves matches very well.

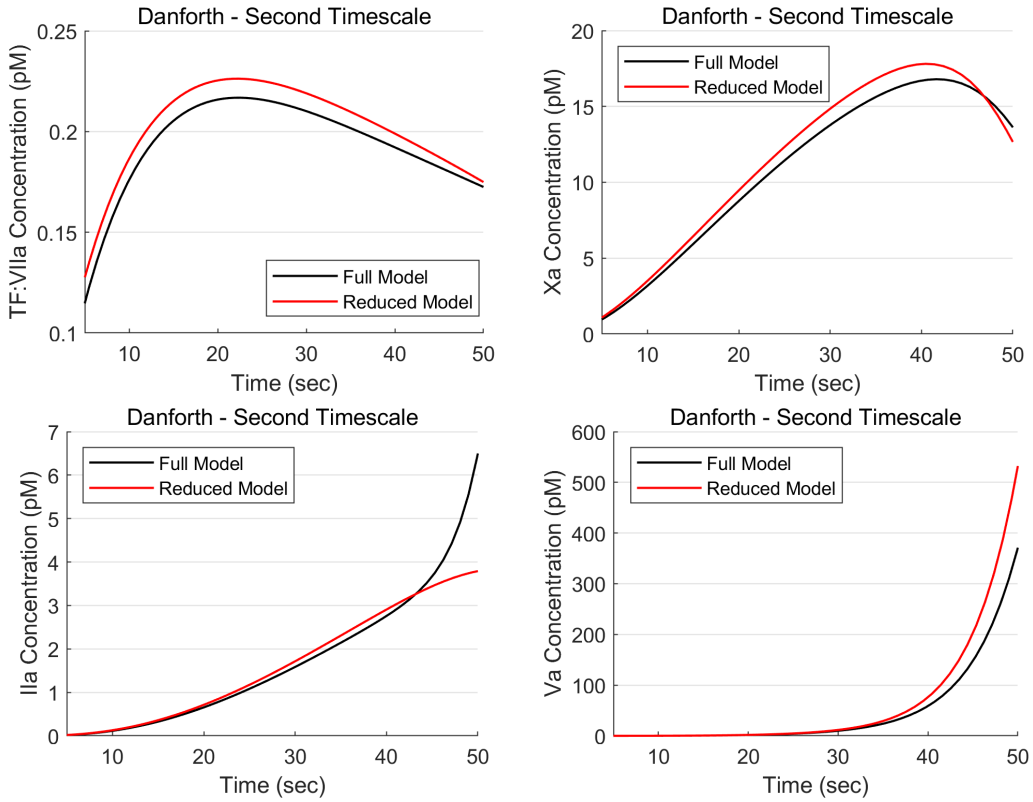

Figure 2.49: Comparison between the reduced Danforth for the second timescale and the full Danforth model.

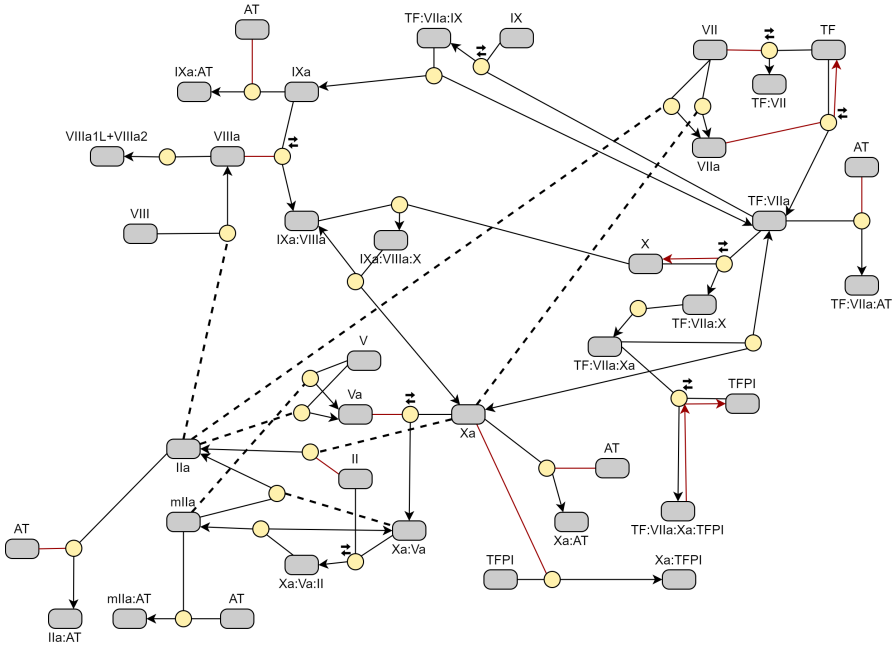

Figure 2.50: A reaction network diagram of the reduced Danforth model for the (40,170) timescale. Red lines and arrows indicate a species that is not significantly affected by a reaction, but the reaction still has a significant effect on other species. If only one direction in a reversible reaction is insignificant, then an additional red arrow is used to demonstrate that direction.

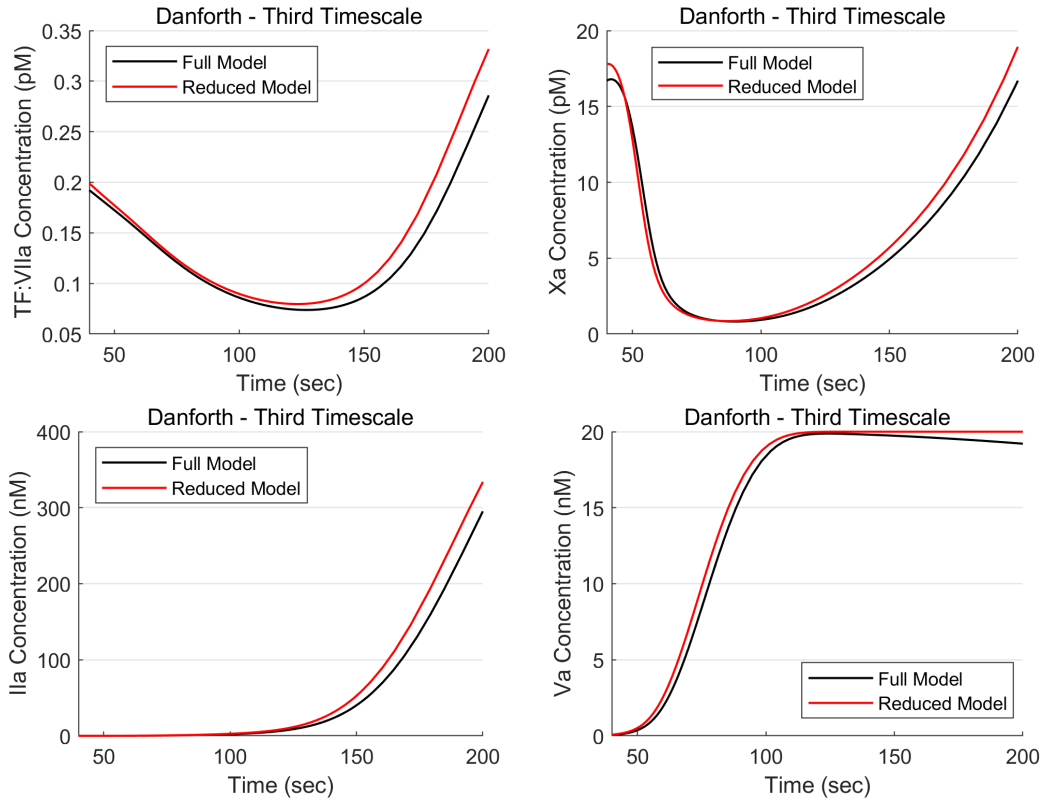

Figure 2.51: Comparison between the reduced Danforth for the third timescale and the full Danforth model.

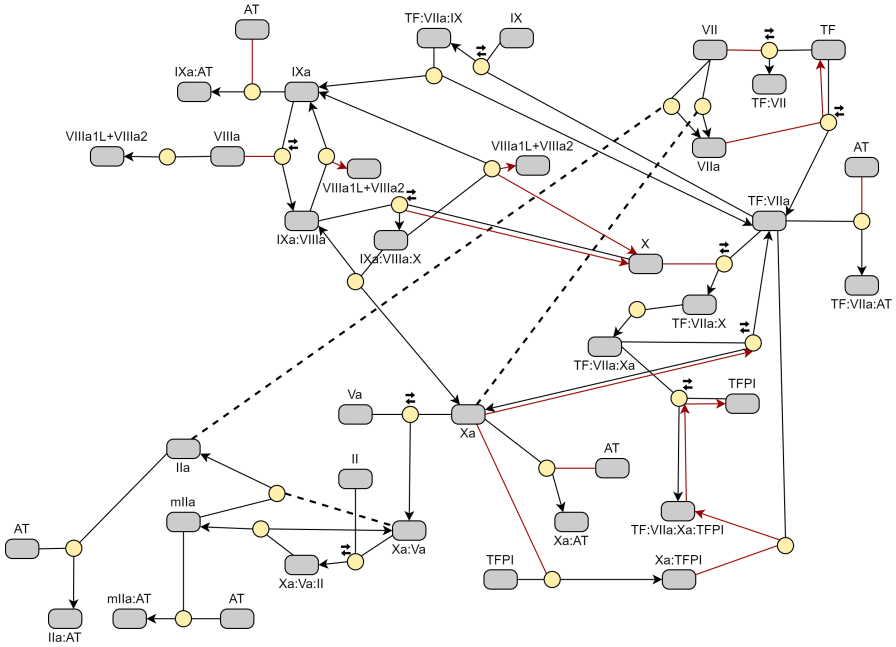

Figure 2.52: A reaction network diagram of the reduced Danforth model for the (170,460) timescale. Red lines and arrows indicate a species that is not significantly affected by a reaction, but the reaction still has a significant effect on other species. If only one direction in a reversible reaction is insignificant, then an additional red arrow is used to demonstrate that direction.

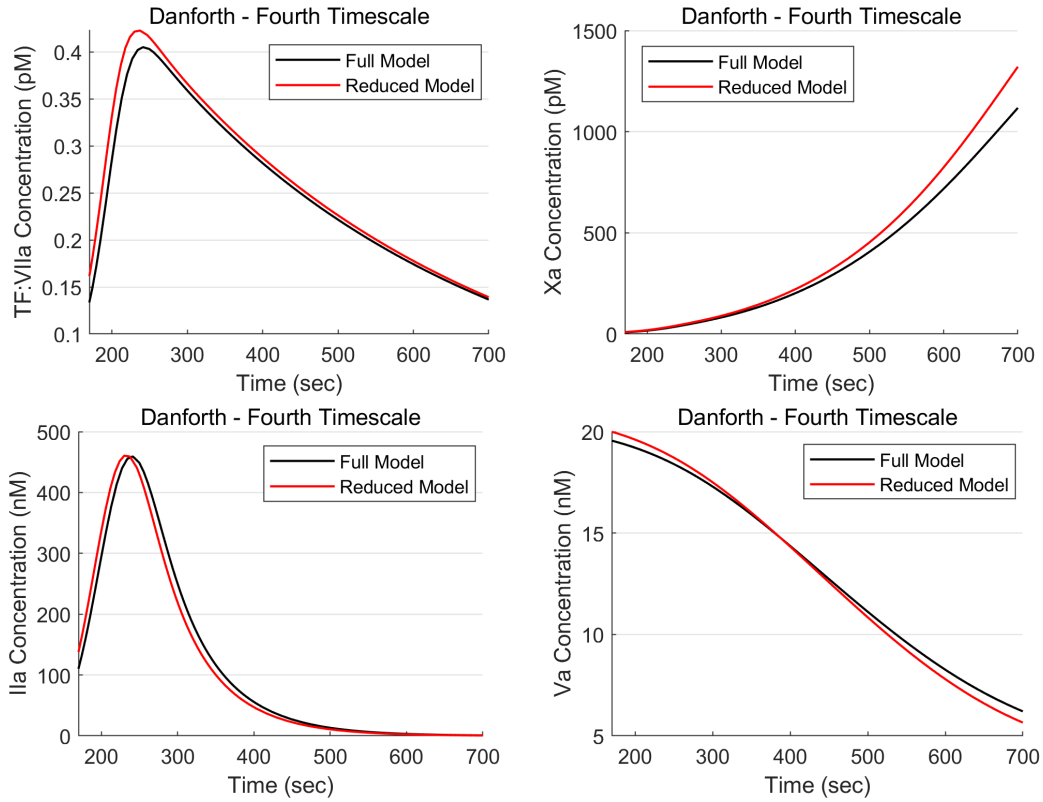

Figure 2.53: Comparison between the reduced Danforth for the fourth timescale and the full Danforth model.

The Fifth Timescale

The fifth interval timescale is (460,1200) and governs the inhibitions. A reduced network diagram for the reactions which are significant on this timescale is given in Figure 2.54. The simulation for the fifth timescale model only tracks FIIa and AT levels and is given in Figure 2.55 using the initial conditions from the fourth timescale model at $t = 460s$. No new thrombin is being activated which means, if only thrombin is of interest, the system reduces dramatically to only AT inhibition of FIIa. Most of the reactions on this timescale are inhibitions or are only changing due to inhibitions such as the balance of prothrombinase levels as FXa is inhibited by TFPI and AT. However, there are still significant activations for FVII, FIX and FX. The FIIa concentration is able to follow the shape of the curve well with the only error appearing to be due to the initial conditions from previous timescales. The fifth timescale model is small enough to be solved for thrombin concentration, as is given below.

$$\frac{d[IIa]}{dt} = \frac{d[AT]}{dt} = -k[IIa][AT]$$

This will give us a solution of the following form:

$$[AT] = [IIa] + c$$

The ODE for [IIa] can then be solved by separation of variables using this substitution to give the equation below, with the constants $c = [AT] - [IIa]$ and d

which can be found from the initial concentration of FIIa.

$$[IIa] = \frac{ce^{cd}}{e^{kct} - e^{cd}}$$

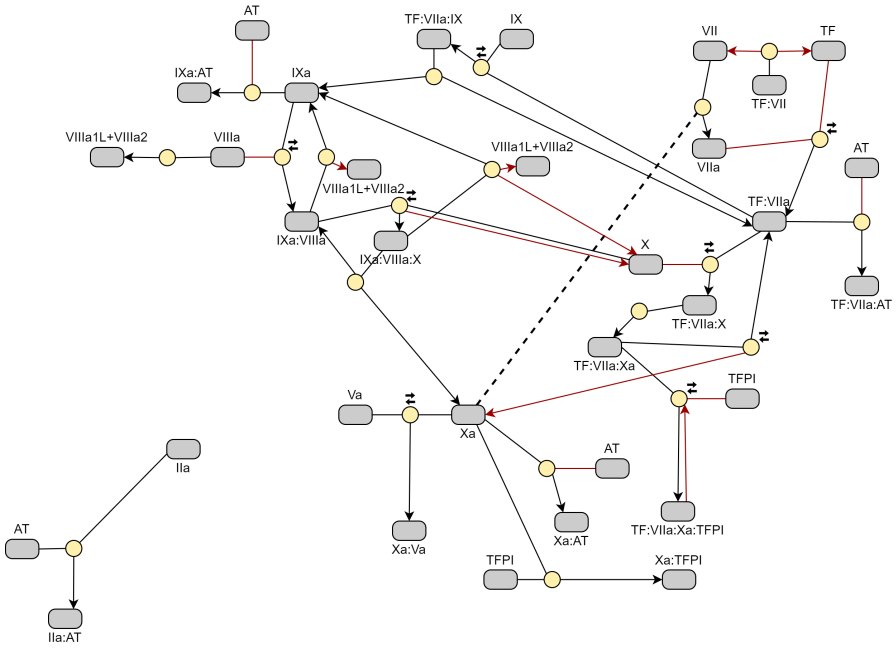

Figure 2.54: A reaction network diagram of the reduced Danforth model for the (460,1200) timescale. Red lines and arrows indicate a species that is not significantly affected by a reaction, but the reaction still has a significant effect on other species. If only one direction in a reversible reaction is insignificant, then an additional red arrow is used to demonstrate that direction.

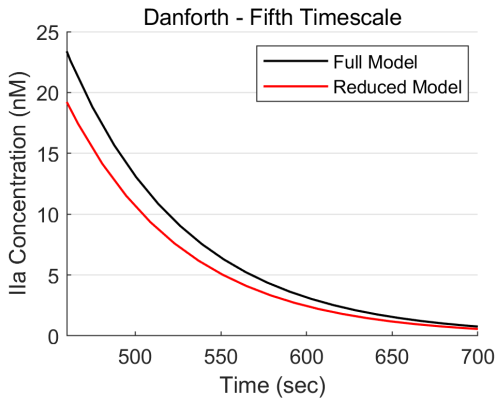

Figure 2.55: Comparison between the reduced Danforth for the fifth timescale and the full Danforth model.

Unnecessary Reactions

Four reactions, given in Table 2.36, are insignificant for all species on all timescales and can therefore be removed from the model. These reactions being insignificant

matches well with the biology, FVII is predominantly activated by FXa; and FX can be activated by FIXa without the need for FVIIIa to be present but the activation is much weaker. The two remaining unnecessary reactions are both reversible reactions, but due to their tight binding (fast association and slow disassociation), the disassociation does not occur in significant amounts.

Reaction
VII + TF:VIIa → VIIa + TF:VIIa
$VIIIa_1L + VIIIa_2 \rightarrow VIIIa$
Xa:TFPI → Xa + TFPI
X + IXa → Xa + IXa

Table 2.36: The reactions in the Danforth model that are negligible across all timescales.

2.7.3 Timescale Analysis - Tyurin

To complement the analysis of the Danforth model, we have conducted the same analysis on the Tyurin model, after removing the reactions for species not used in this section (chosen as it contains many of the reactions that are missing from the Danforth model, such as FXI). The intervals of influence, for each reaction, are given in Table 2.37. The dynamics on both $t = O(1s)$ and $t = O(10s)$ utilise similar reactions so are jointly covered by the reactions significant on the (0,40) time interval; the shift between the $t = O(10s)$ and $t = O(100s)$ timescales are governed by the reactions which are significant on the (40,130) time interval; the $t = O(100s)$ dynamics are shown on the (130,180) interval; the switch between the $t = O(100s)$ and $t = O(1000s)$ timescales are given on the (180,500) interval; and the $t = O(1000s)$ dynamics are given by the reactions which are significant on the (500,1200) interval. The ODEs for each of the Tyurin timescale-reduced models are given in Appendix A.

Species	Reaction	Interval of Influence (s)
TF	TF + VIIa → TF:VIIa	(150,1200)
	TF + VII → TF:VII	(0,230)
	TF:VIIa → TF + VIIa	-
	TF:VII → TF + VII	-
TF:VII	TF:VII $\overset{Xa}{\rightarrow}$ TF:VIIa	(130,220)
	TF + VII → TF:VII	(0,220)
	TF:VII → TF + VII	-

TF:VIIa	TF:VII $\overset{Xa}{\rightarrow}$ TF:VIIa	(110,220)
	TF + VIIa $\rightarrow$ TF:VIIa	(0,140)$\cup$(160,1200)
	TF:VIIa + Xa:TFPI $\rightarrow$ TF:VIIa:Xa:TFPI	(165,1200)
	TF:VIIa + AT $\rightarrow$ TF:VIIa:AT	(10,150)$\cup$(70,1200)
	TF:VIIa $\rightarrow$ TF + VIIa	-
VIIa	VII $\overset{Xa}{\rightarrow}$ VIIa	(0,260)
	TF + VIIa $\rightarrow$ TF:VIIa	(0,100)
	TF:VIIa $\rightarrow$ TF + VIIa	-
VII	VII $\overset{Xa}{\rightarrow}$ VIIa	(100,260)
	TF + VII $\rightarrow$ TF:VII	(0,130)
	TF:VII $\rightarrow$ TF + VII	-
Xa	X $\overset{IXa}{\rightarrow}$ Xa	-
	X $\overset{IXa:VIIIa}{\rightarrow}$ Xa	(60,250)
	X $\overset{VIIa}{\rightarrow}$ Xa	(0,120)
	X $\overset{TF:VIIa}{\rightarrow}$ Xa	(20,90)
	Xa + Va $\rightarrow$ Xa:Va	(140,620)
	Xa + AT $\rightarrow$ Xa:AT	(20,90)$\cup$(150,600)
	Xa + TFPI $\rightarrow$ Xa:TFPI	(0,180)
X	X $\overset{IXa}{\rightarrow}$ Xa	-
	X $\overset{IXa:VIIIa}{\rightarrow}$ Xa	(80,240)
	X $\overset{VIIa}{\rightarrow}$ Xa	(0,100)
	X $\overset{TF:VIIa}{\rightarrow}$ Xa	-
Va	V $\overset{IIa}{\rightarrow}$ Va	(40,170)
	V $\overset{Xa}{\rightarrow}$ Va	(0,165)
	Xa + Va $\rightarrow$ Xa:Va	(150,180)$\cup$(540,620)
	Xa:Va + AT $\rightarrow$ Xa:AT + Va	(155,180)$\cup$(540,1200)
V	V $\overset{IIa}{\rightarrow}$ Va	(40,170)
	V $\overset{Xa}{\rightarrow}$ Va	(0,160)
Xa:Va	Xa + Va $\rightarrow$ Xa:Va	(0,170)$\cup$(560,620)
	Xa:Va + AT $\rightarrow$ Xa:AT + Va	(165,170)$\cup$(560,1200)
XIa	XI $\overset{IIa}{\rightarrow}$ XIa	(0,165)
	XI $\overset{XIa}{\rightarrow}$ XIa	(10,155)
	XIa + AT $\rightarrow$ XIa:AT	(160,1200)
XI	XI $\overset{IIa}{\rightarrow}$ XIa	(0,165)
	XI $\overset{XIa}{\rightarrow}$ XIa	(10,155)

IXa	$IX \overset{XIa}{\rightarrow} IXa$	(20,240)
	$IX \overset{VIIa}{\rightarrow} IXa$	(0,40)
	$IX \overset{TF:VIIa}{\rightarrow} IXa$	-
	$IXa + VIIIa \rightarrow IXa:VIIIa$	-
	$IXa + AT \rightarrow IXa:AT$	(170,1200)
IX	$IX \overset{XIa}{\rightarrow} IXa$	(20,240)
	$IX \overset{VIIa}{\rightarrow} IXa$	(0,40)
	$IX \overset{TF:VIIa}{\rightarrow} IXa$	-
VIIIa	$VIII \overset{IIa}{\rightarrow} VIIIa$	(0,170)
	$IXa + VIIIa \rightarrow IXa:VIIIa$	(60,1200)
	$IXa:VIIIa + AT \rightarrow IXa:AT + VIIIa$	(160,200)
VIII	$VIII \overset{IIa}{\rightarrow} VIIIa$	(0,165)
IXa:VIIIa	$IXa + VIIIa \rightarrow IXa:VIIIa$	(60,200)
	$IXa:VIIIa + AT \rightarrow IXa:AT + VIIIa$	(130,200)
IIa	$II \overset{Xa}{\rightarrow} IIa$	(0,40)
	$II \overset{Xa:Va}{\rightarrow} IIa$	(20,180)
	$IIa + AT \rightarrow IIa:AT$	(20,120)∪(160,700)
II	$II \overset{Xa}{\rightarrow} IIa$	(0,40)
	$II \overset{Xa:Va}{\rightarrow} IIa$	(20,180)
TFPI	$Xa + TFPI \rightarrow Xa:TFPI$	(10,30)∪(130,180)
Xa:TFPI	$TF:VIIa + Xa:TFPI \rightarrow TF:VIIa:Xa:TFPI$	(170,1200)
	$Xa + TFPI \rightarrow Xa:TFPI$	(0,180)
AT	$TF:VIIa + AT \rightarrow TF:VIIa:AT$	-
	$IIa + AT \rightarrow IIa:AT$	(150,600)
	$Xa + AT \rightarrow Xa:AT$	(220,500)
	$Xa:Va + AT \rightarrow Xa:AT + Va$	-
	$IXa + AT \rightarrow IXa:AT$	(300,1200)
	$IXa:VIIIa + AT \rightarrow IXa:AT + VIIIa$	-
	$XIa + AT \rightarrow XIa:AT$	-

Table 2.37: Intervals of influence for each reaction, on each of the species that the reaction effects, for the Tyurin model.

The First Timescale

The first interval timescale, (0,40), covers the initiation. A reduced network diagram is given in Figure 2.58 and model simulations are given in Figure 2.58. The initial conditions used are the original Tyurin initial conditions in Table 2.22. Due to the slower TF:VII and TF:VIIa binding in the Tyurin model, most activation is performed by FVIIa instead. This timescale covers activation of FX and FIX by FVIIa, activation of FII by FXa, activation of FV by FXa and FVIII by FIIa,

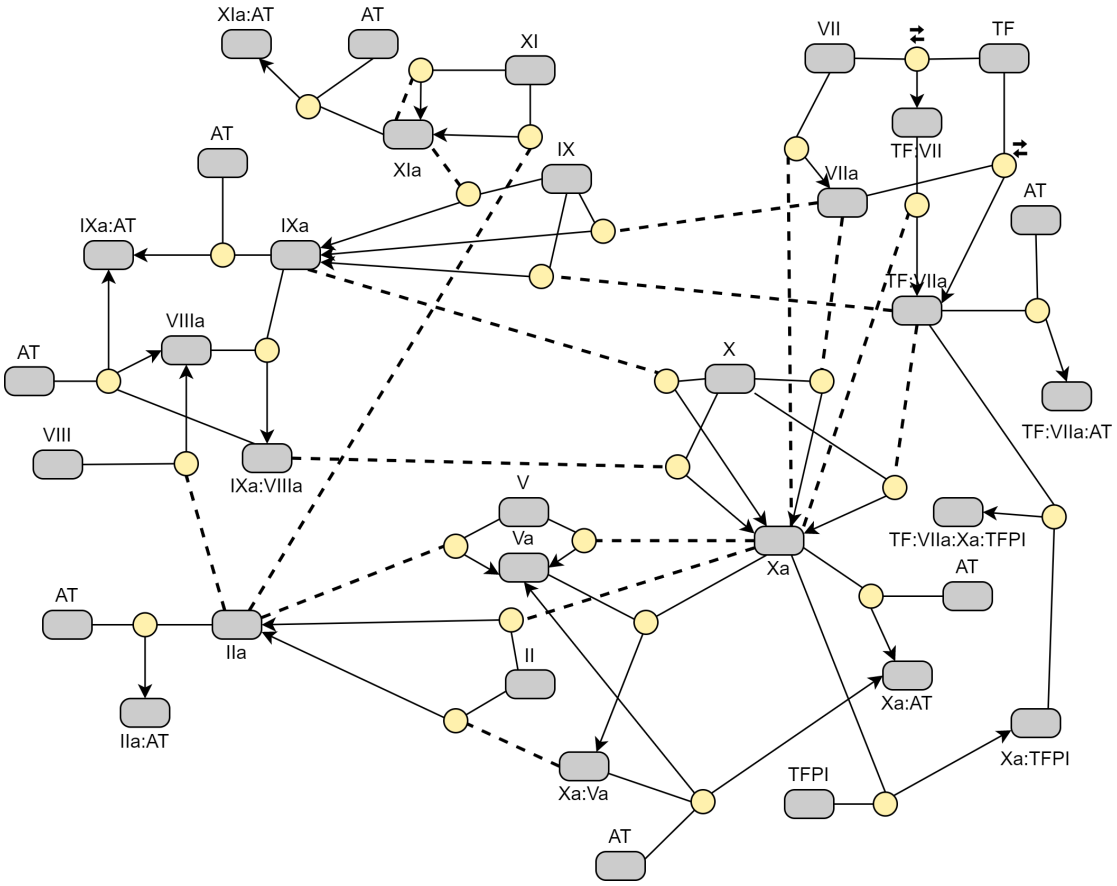

Figure 2.56: A reaction network diagram of the Tyurin model. Grey nodes correspond to individual species. Yellow nodes correspond to reactions and each reaction node is connected to its products (arrows), reactants (solid lines) and species which are both products and reactants (dotted lines). Reaction nodes next to a pair of arrows indicate that the reaction is reversible. The species nodes for AT have been repeated in multiple places to simplify the network diagram.

and the beginning of Xa:Va formation and its activation of FIIa. The simulations of the reduced model are able to reproduce the full model up to $t = 60s$, where activation of FX by IXa:VIIIa becomes significant.

The Second Timescale

The second interval timescale, (40,130), covers the end of initiation and leads into amplification. A reduced network diagram is given in Figure 2.60 and model simulations are given in Figure 2.60. The initial conditions are taken from the first timescale model at $t = 40s$. We now include activation of FV by FIIa and activation of FX by IXa:VIIIa. This results in most factors seeing rapid exponential growth through this timescale.

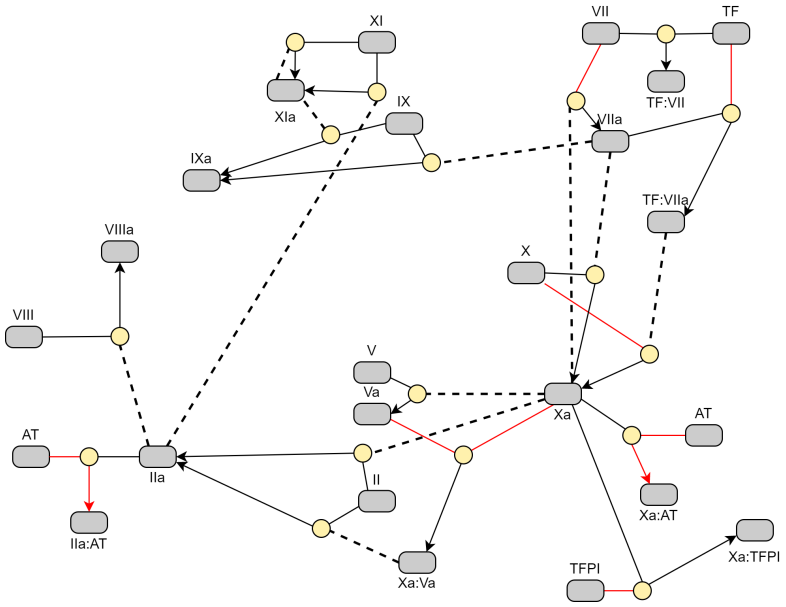

Figure 2.57: A reaction network diagram of the reduced Tyurin model for the (0,40) timescale. Red lines and arrows indicate a species that is not significantly affected by a reaction, but the reaction still has a significant effect on other species. If only one direction in a reversible reaction is insignificant, then an additional red arrow is used to demonstrate that direction.

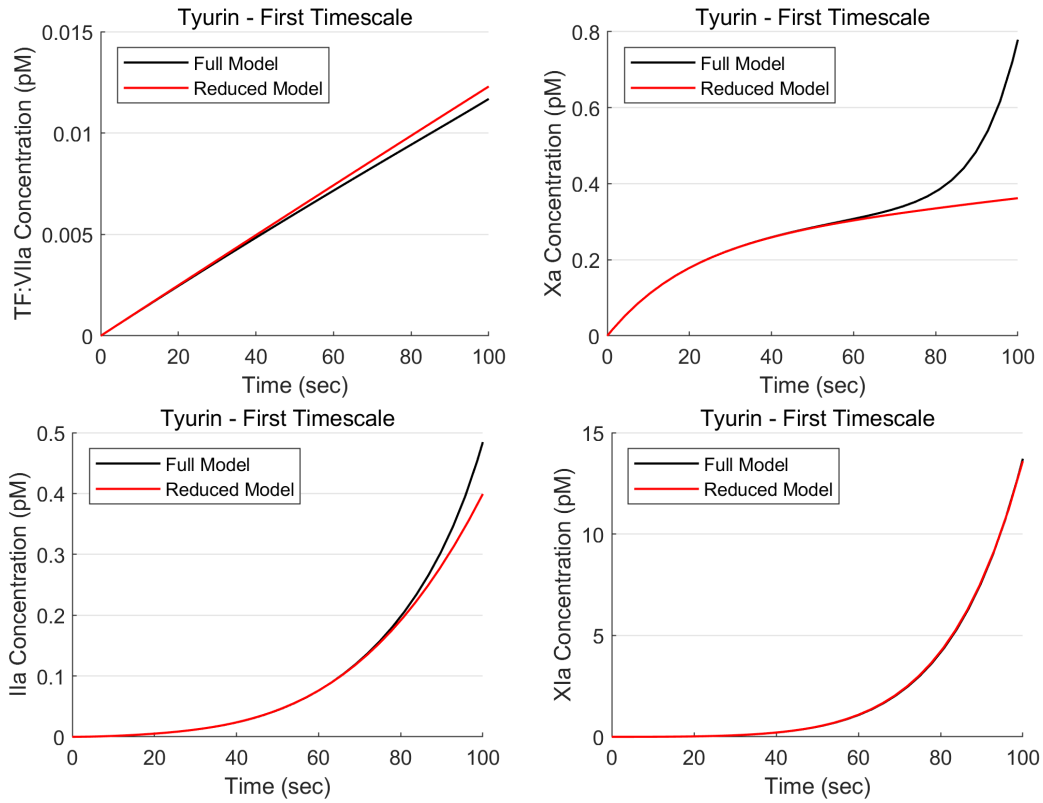

Figure 2.58: Comparison between the reduced Tyurin for the first timescale and the full Tyurin model.

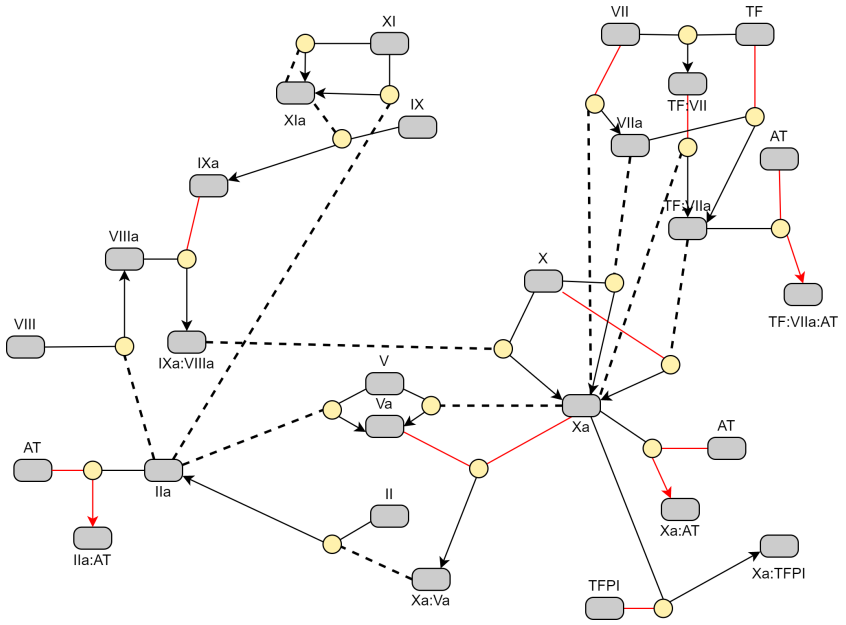

Figure 2.59: A reaction network diagram of the reduced Tyurin model for the (40,130) timescale. Red lines and arrows indicate a species that is not significantly affected by a reaction, but the reaction still has a significant effect on other species. If only one direction in a reversible reaction is insignificant, then an additional red arrow is used to demonstrate that direction.

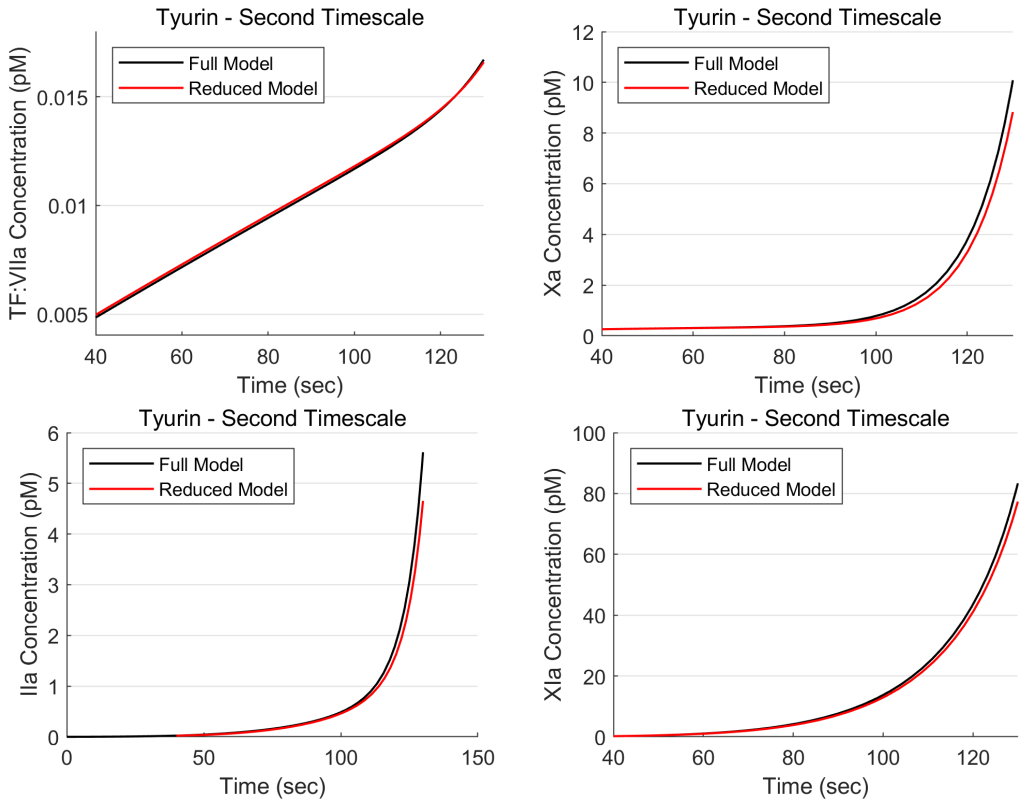

Figure 2.60: Comparison between the reduced Tyurin for the second timescale and the full Tyurin model.

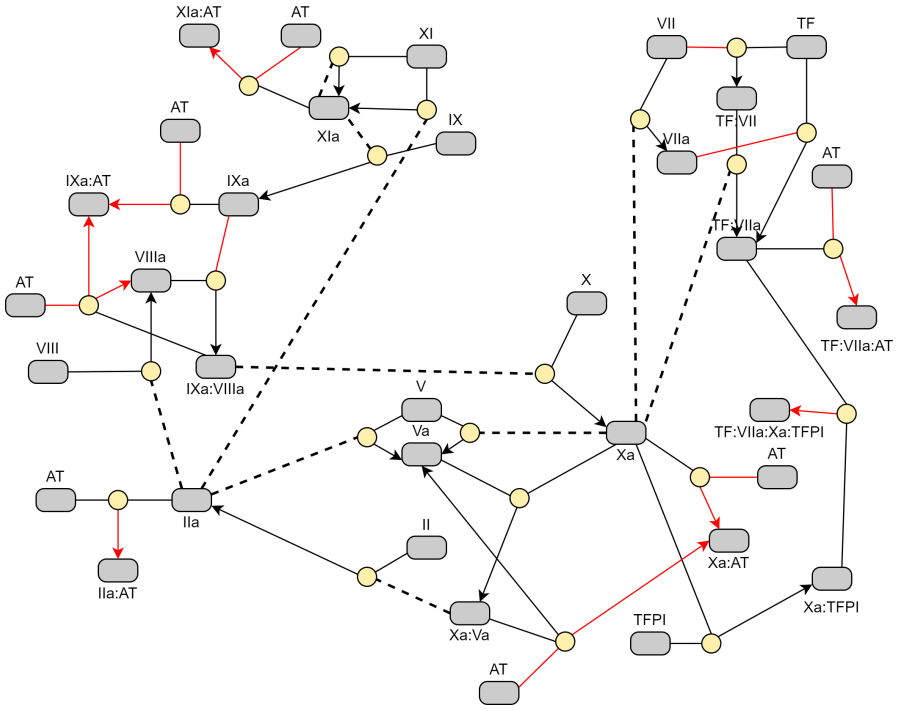

Figure 2.61: A reaction network diagram of the reduced Tyurin model for the (130,180) timescale. Red lines and arrows indicate a species that is not significantly affected by a reaction, but the reaction still has a significant effect on other species. If only one direction in a reversible reaction is insignificant, then an additional red arrow is used to demonstrate that direction.

The Third Timescale

The third interval timescale, (130,180), is quite short and covers the rapid amplification up to peak thrombin and towards inhibition. A reduced network diagram is given in Figure 2.62 and model simulations are given in Figure 2.62. The initial conditions are taken from the second timescale model at $t = 130s$. This timescale includes most reactions and subsequent timescales have a reduced number of reactions. Prothrombinase formation is now happening rapidly enough to significantly affect the levels of FVa and FXa. All inhibitions are now significant.

The Fourth Timescale

The fourth interval timescale, (180,500), covers most of the inhibition. A reduced network diagram is given in Figure 2.64 and model simulations are given in Figure 2.64. The initial conditions are taken from the third timescale model at $t = 180s$. There is still significant activation occurring, with FIX activation by FXIa and activation of FX by IXa:VIIIa, FVIIa and TF:VIIa. However, this remaining activation does not continue to activate more thrombin, due to all prothrombin being depleted. The model simulations continue to match well as the factors are strongly inhibited.

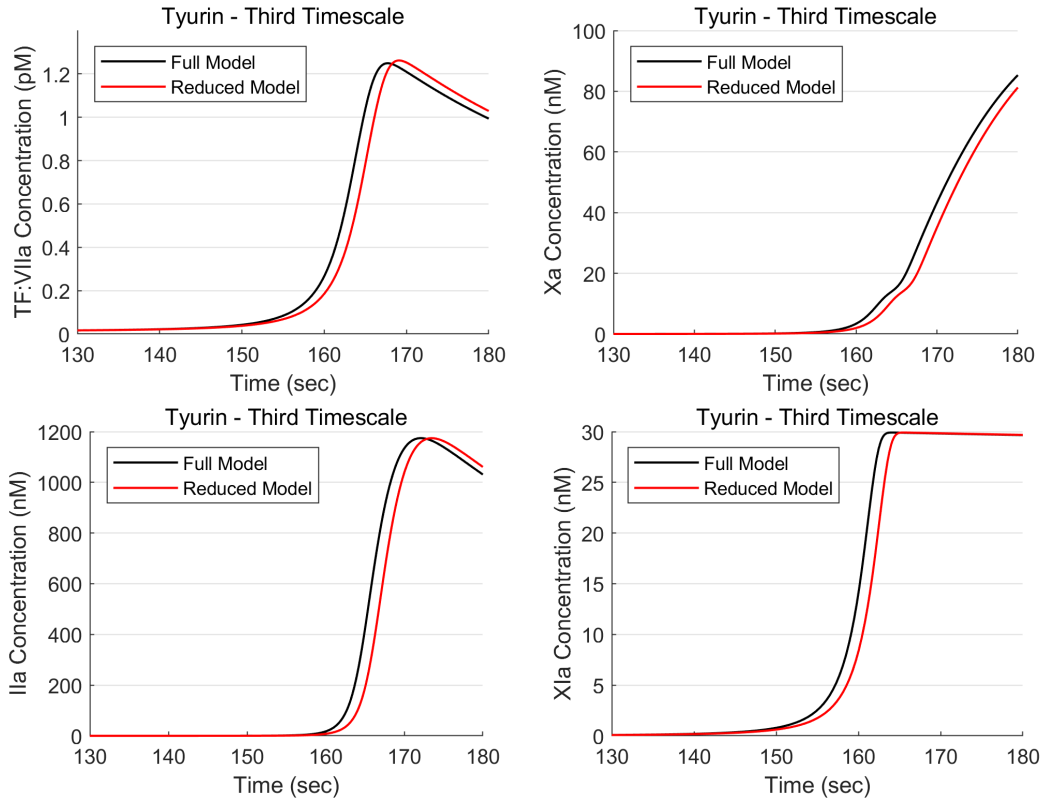

Figure 2.62: Comparison between the reduced Tyurin for the third timescale and the full Tyurin model.

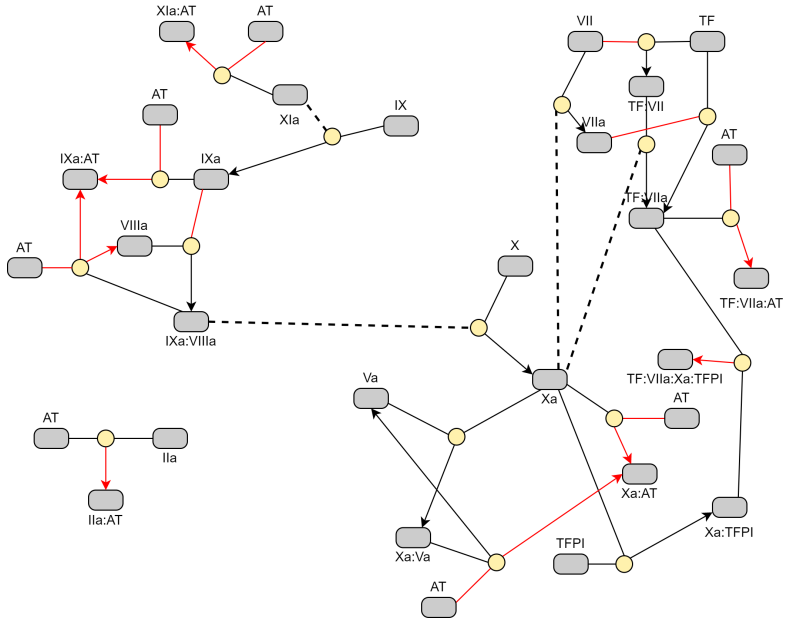

Figure 2.63: A reaction network diagram of the reduced Tyurin model for the (180,500) timescale. Red lines and arrows indicate a species that is not significantly affected by a reaction, but the reaction still has a significant effect on other species. If only one direction in a reversible reaction is insignificant, then an additional red arrow is used to demonstrate that direction.

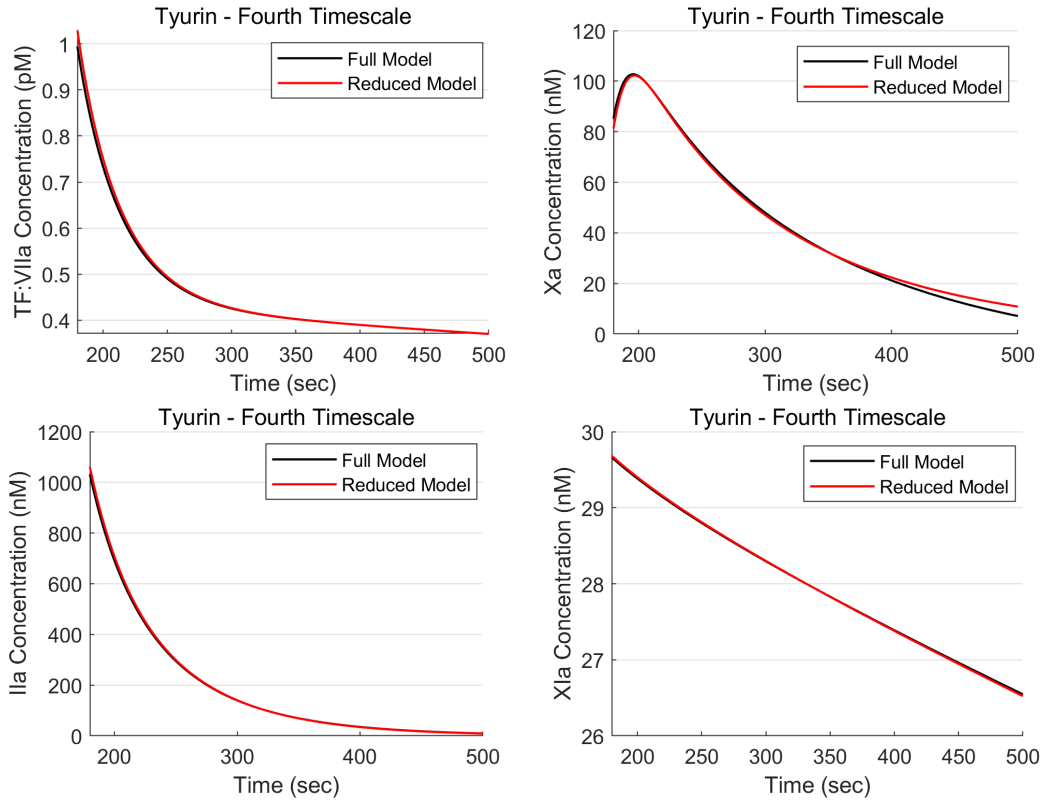

Figure 2.64: Comparison between the reduced Tyurin for the fourth timescale and the full Tyurin model.

The Fifth Timescale

The fifth interval timescale, (500,1200), covers the final inhibitions of the system for the longest lasting species. A reduced network diagram is given in Figure 2.66 and model simulations are given in Figure 2.66. The initial conditions are taken from the fourth timescale model at $t = 500s$. No more activation is occurring and the only reactions are inhibitions, or reversible reactions balancing as inhibition takes place.

Unnecessary Reactions

There are four reactions that are insignificant for all species on all timescales and can be removed from the model, these reactions are given in Table 2.38. The activation of FX by FIXa, as seen previously for the Danforth model, is insignificant across all timescales. The remaining reactions could all be put down to the poor production of TF:VII and TF:VIIa in the Tyurin model, hence FIXa activation by TF:VIIa is insignificant but activation by FVIIa remains significant.

2.7.4 Conclusions

The two models show fairly significant differences in their initiation of the system. This is covered in the first and second timescales for the Danforth model and the

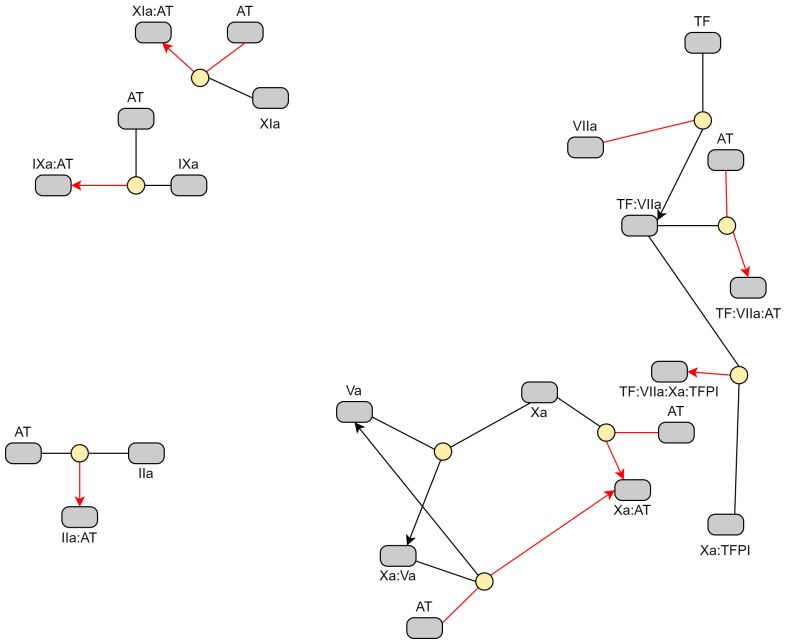

Figure 2.65: A reaction network diagram of the reduced Tyurin model for the (500,1200) timescale. Red lines and arrows indicate a species that is not significantly affected by a reaction, but the reaction still has a significant effect on other species. If only one direction in a reversible reaction is insignificant, then an additional red arrow is used to demonstrate that direction.

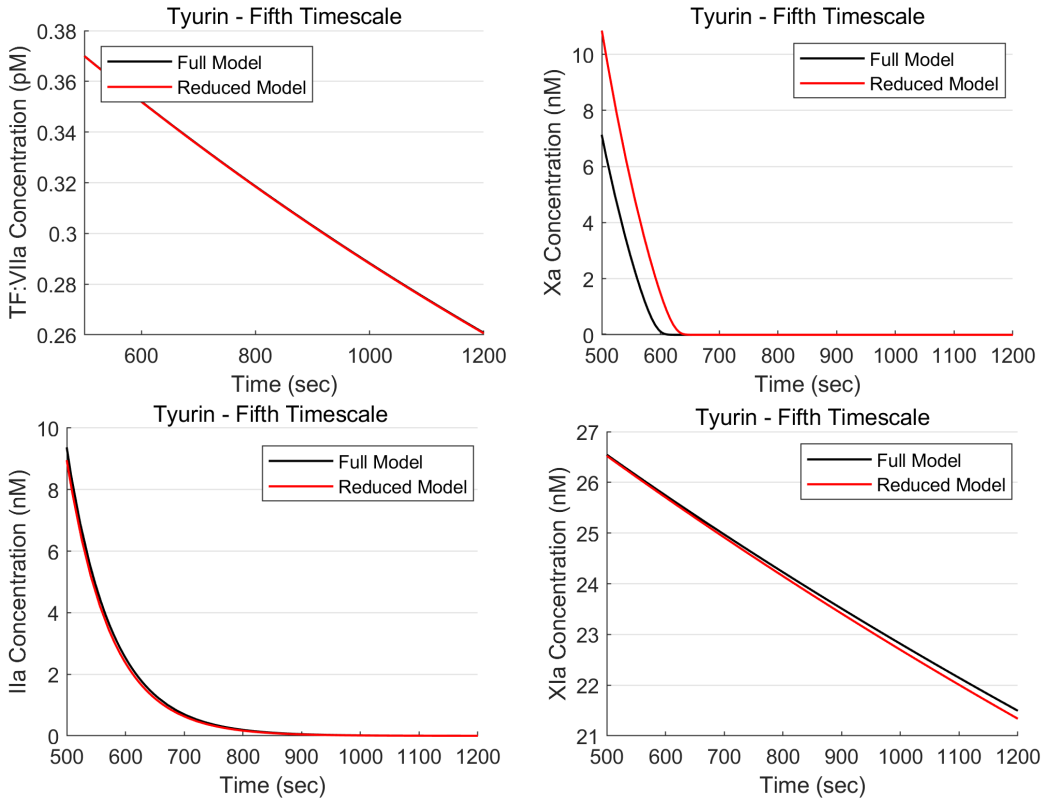

Figure 2.66: Comparison between the reduced Tyurin for the fifth timescale and the full Tyurin model.

Reaction
$IX \overset{TF:VIIa}{\rightarrow} IXa$
$X \overset{IXa}{\rightarrow} Xa$
TF:VIIa $\rightarrow$ TF + VIIa
TF:VII $\rightarrow$ TF:VII

Table 2.38: The reactions in the Tyurin model that are negligible across all timescales.

first timescale for the Tyurin model. The Danforth model has a very rapid first timescale, (0,5), that captures rapid binding of FVIIa to TF and leads to small amounts of FIIa. The second timescale for the Danforth model, (5,40), then begins formation of Xa:Va and its activation of thrombin. In the Tyurin model, all of these reactions are included in the first timescale, (0,40), as this model more heavily relies on activation by FVIIa and less so on TF:VIIa.

The two models both show similar dynamics for amplification, covered in the third timescale for Danforth, (40,170), and the second for Tyurin, (40,130). Both models begin formation of the IXa:VIIIa and use this to activate larger amounts of FX into FXa. The only significant difference between these two is the presence of FXI in the Tyurin model which is entirely absent from the Danforth model and therefore not included in this timescale.

The peak of thrombin comes after amplification in the fourth timescale for Danforth, (170,460), and the third timescale for Tyurin, (130,180). For both models this occurs when both inhibition and activation are significant.

The final stages of the system are inhibition. For the Danforth model, this occurs on the fifth timescale, (460,1200), in which thrombin decouples from the majority of the system and is then only inhibited by AT. This decoupling does not occur until there is below 25nM of thrombin in the system. Contrary to this, in the Tyurin model, inhibition occurs across the fourth, (180,500), and fifth, (500,1200), timescales, both of which decouple thrombin starting at around 1000nM of thrombin in the system. The fifth timescale covers the slower inhibitions in the system and the coagulation factors which are activated in significant numbers.

During the inhibition phase, both models still presented significant amounts of prothrombinase so they could only be reduced to FIIa inhibition by AT if prothrombin had been fully depleted. This suggests that, in order to not fully deplete prothrombin, the models require a stronger inhibition of prothrombinase.

Almost all reactions, in both the Danforth and Tyurin models, were significant at least one timescale. Of the handful that were not significant at any timescale, FX activation by FIXa was insignificant in both models. The remaining insignificant reactions were model specific, with Tyurin's related to the lack of TF:VIIa formation and Danforth's focusing on the strongly bound but reversible reactions that are not present in the Tyurin model.

2.8 Conclusions

In this chapter, we conducted many stages of exploratory analysis on eight models of thrombin generation. We showed that none of these models could accurately and reliably predict thrombin generation over the whole cohort (Section 2.3). We were able to show that the models can be separated into two groups, the Quick group and the Symmetrical group, based on the shape of their thrombin generation curves and we identified the presence or absence of FXI in the models as the most common cause for this difference (Section 2.4).

We found high levels of sensitivity in the models (Section 2.5), with the most sensitive reaction rates and coagulation factors differing between the models. This led us to investigate the original sources for each of the reaction rates in the models (Section 2.6), exploring how they were changed from their original values. We found large variability in the reaction rates between the models for the same reactions, with few reaction rates in the models determined using multiple experimental sources.

Finally, we conducted a timescale analysis on the Danforth and Tyurin models (Section 2.7). We found that almost all of the reactions in the model were significant on at least one timescale. Most conclusions of the timescale analysis were similar between the two models, with Danforth having shorter early timescales due to differences in the predictions of the models for TF:VII(a) association. We had previously identified this difference, where the Tyurin model has much less TF:VII and TF:VIIa during the early stages, in Section 2.4. Using the work from Section 2.6, we were able to show that this was caused by the Tyurin model being the only model to use an experimental source for TF:VII and TF:VIIa association rather than an approximation using an experimental source for $K_d = \frac{k_-}{k_+}$.

Looking forward to the development of a new model, it seems clear that the choice of reaction rates for the model will be important. The high variability between experimental sources for the same reaction rates and low variability in repeated measurements within the same source suggests that the variability is likely a result of changes in the experimental conditions between different sources. This makes it complex to choose reaction rates which match the experimental conditions of our assay. Further, there are still minor differences between the models in their reaction schemes that need to be resolved.

A qualitative result of partial prothrombin conversion, something that is known to occur in the assay but is not observed in any of the models (Figure 2.29), should also likely be a focus of this work. Inhibition of the prothrombinase complex is likely a requirement for this result, however, as seen in the Tyurin model, this alone is not sufficient to predict partial prothrombin conversion.

Finally, it would be worth evaluating model performance beyond just measures of ETP. We have seen differences in the predictions of lagtime, both in the average case (Section 2.4) and in the lagtime sensitivity under variation in different coagulation factors (Section 2.5). Measuring performance through the Optical Density

curves would allow us to investigate the accuracy of other summary statistics such as lagtime.

Chapter 3

Unified Model

3.1 Introduction

Previously, in Section 2.3, we showed that the current mathematical models of thrombin generation fail to predict patient data across a large cohort of donors. The models were found to have many differences in the reaction schemes they use, with some models missing crucial parts of the cascade. Additionally, there is significant variation between the models in both the reaction rates and the sources they use which vary in pH, temperature, phospholipids levels and even species (with many measurements using bovine coagulation factors in place of human; Section 2.6). These differences not only result in issues when the models are compared between one another but also produce inconsistencies within the individual models themselves with no clear experimental setting that the models are trying to simulate. This chapter will attempt to resolve these issues to build a more accurate model of thrombin generation.

As seen in Section 2.5, the current models of thrombin generation are very sensitive to changes in the reaction rates with changes in even a single reaction rate, of which the models contain between 50 and 150, being sufficient to significantly change the predictions of a model, as seen in the Chatterjee model with its FXI auto-activation reaction rate. In addition to this, the reaction rates are known to vary across multiple orders of magnitude between different sources [76]. This combination of features poses a problem in the construction of the models: if even a single reaction rate is significantly different to the experimental conditions, then this could result in the model having significantly reduced accuracy. In an attempt to resolve this, the reaction rates will be fitted to better match the data set and by extension, the experimental conditions.

In an attempt to resolve these three issues (differences in the reaction schemes, large variation in reaction rates, and differing experimental conditions between the reaction rates), we introduce a three-step process for building a new model. As part of this process, we also remove any reactions that are not relevant to the PRAMIS data set, including contact activation and protein C.

1. Form the model reaction scheme as the union of previous models, including additional reactions for consistency where applicable.

2. Build reaction rate prior distributions by collecting a wide number of values from different sources.

3. Use the reaction rate prior distributions to fit to a large data set in order to best identify a set of reaction rates that match a single experimental setting.

The ODEs and reaction rates for the models not given in this chapter are presented in Appendices A and B.

3.1.1 Optical Density Data

Experimental data provided by Glenfield Hospital and the University of Leicester describes the haemostatic profile of 333 donors (162 of whom suffered a myocardial infarction up to the age of 50), consisting of measurements of coagulation factor levels (TF; factors II, V, VII, VIII, IX, X, and XI; and the inhibitors AT and TFPI) and optical density curves measured during the thrombin generation assay.

The optical density curves are standardised against a fixed pooled plasma sample to limit inter-assay variation. In order to best match this data, we include the chromogenic substrate used in the assay into the model (allowing us to capture any competitive inhibitory effects it may have) and use the concentration of the active substrate in place of optical density. Additionally, we simulate a pooled plasma curve using the reference concentrations given in Table 3.1 and use the final concentration of the active substrate to determine the pooled plasma ETP, which we then use to normalise all patient-specific, model predicted optical density curves.

Figure 3.1 gives examples of a thrombin generation curve and an optical density curve and the relationship between the two and an example of the data that is available for each of the 333 individuals.

Species	Baseline Initial Concentration (M)
TF	1.5×10^{-11}
II	1.4×10^{-6}
V	2×10^{-8}
VII	1×10^{-8}
VIII	7×10^{-10}
IX	9×10^{-8}
X	1.6×10^{-7}
XI	3×10^{-8}
VIIa	[VII]/100
AT	3.4×10^{-6}
TFPI	2.5×10^{-9}

Table 3.1: The initial coagulation factor concentrations used for the pooled plasma simulation.

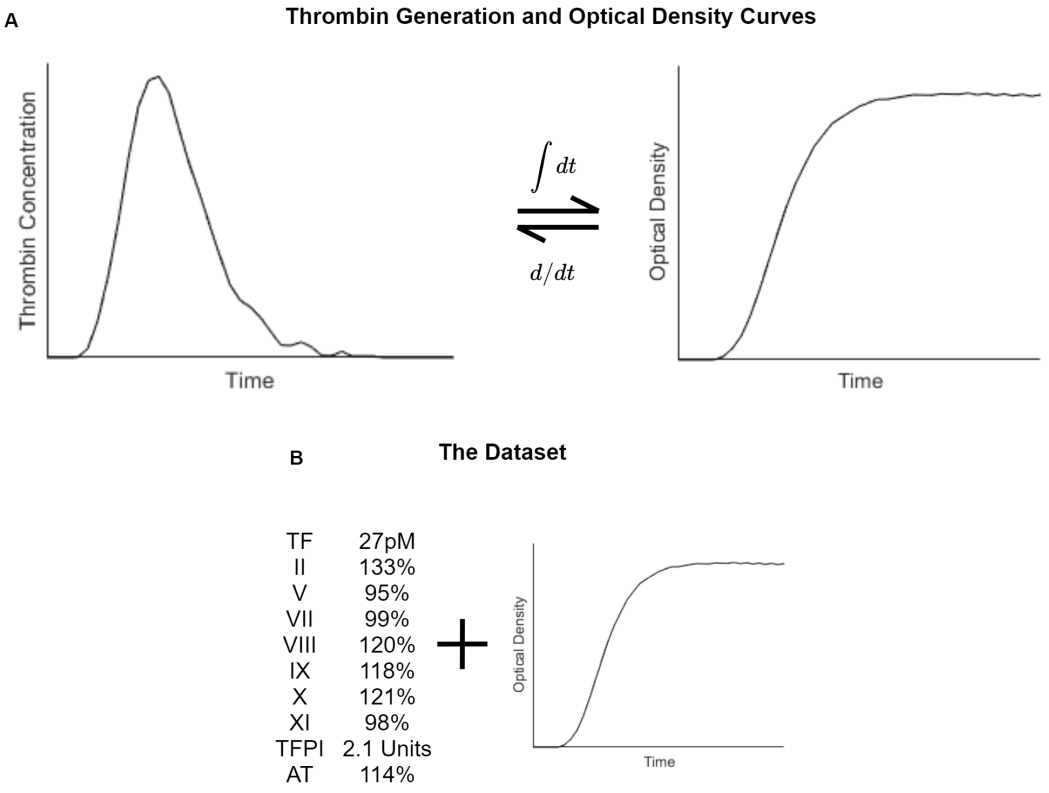

Figure 3.1: A: An example thrombin generation curve, an optical density curve and a demonstration of the relationship between them. B: An example of the data available for each individual.

3.2 Methods

In this section, we detail the steps taken in the construction of a new model, named the Unified Model. We begin with the introduction of the modules and other tools we make use of to simplify the model construction. Following this, we demonstrate the method used to combine the reaction schemes of the previous models into the reaction scheme for the Unified Model. We then detail the methods used to collect the reaction rates and form the prior distributions. Finally, we demonstrate how we utilise the fitting methods to produce the final model. An overview of this method is given in Figure 3.2.

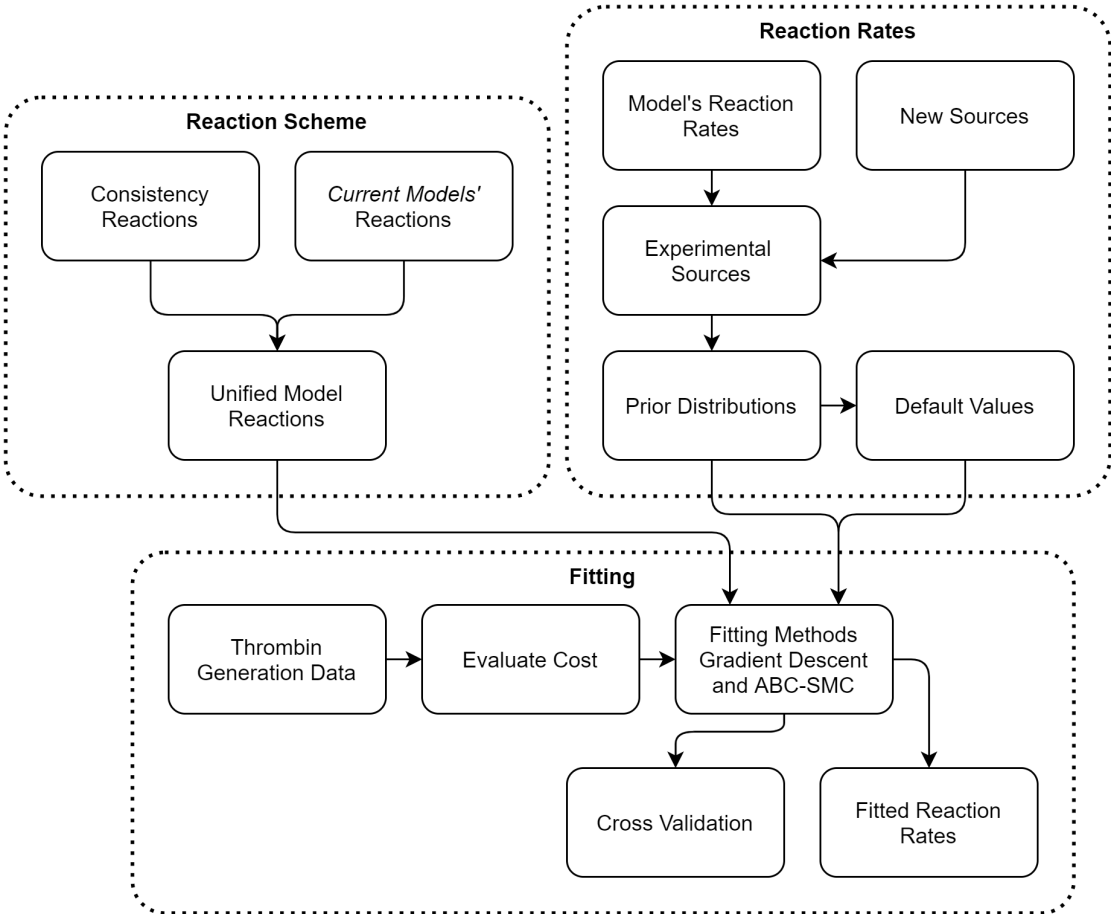

Figure 3.2: A flowchart demonstrating the method used in the Unified Model construction, separated into the construction of the reaction scheme, the prior distributions, and the fitting methods.

3.2.1 Modules

To reduce the complexity of the model, the coagulation cascade has been separated into modules (groupings of reactions) in which each module has a clear, biologically important goal (the TF:VIIa module has the goal of producing TF:VIIa, so includes reactions for factor VII activation, binding of factors VII and VIIa to TF, and inhibition of TF:VIIa; the Xa:Va module includes reactions for FX and

FV activation, their binding into Xa:Va and inhibition of FXa and Xa:Va; the FIIa module contains the reactions for FII activation by FXa and Xa:Va and its inhibition by AT; the FXIa module contains the reactions for FXI activation by FXIa and FIIa and FXIa inhibition by AT; the IXa:VIIIa module contains the reactions for activation of FVIII and FIX, their binding to form IXa:VIIIa, inhibition of FIXa and IXa:VIIIa by AT, and degradation of FVIIIa; and the TFPI module contains the reactions for inhibition of FXa by TFPI and TF:VIIa by Xa:TPFI). Each module has an associated PDF document, given in Appendix E, which contains information about the reaction schemes used by each model, the reaction rates used in the models, and the original values of the reaction rates that were reported. Finally, they detail the reaction scheme, reaction rates and prior distributions used in the Unified Model.

3.2.2 Development of the Reaction Scheme

The models make use of different rate laws and therefore represent the enzymatic reactions in different forms. To better compare the reaction schemes of each of the models, we describe their enzymatic reactions in a simplified form. For example, the reactions TF:VIIa + X $\leftrightarrow$ TF:VIIa:X $\rightarrow$ TF:VIIa + Xa are reduced to the form X $\overset{\text{TF:VIIa}}{\rightarrow}$ Xa. This process is applied to all the models, with the resulting reduced reaction schemes for each model given in Figure 3.3. There are five inhibitors that we do not have patient-specific concentrations for (namely $\alpha_1 - AT$, $\alpha_2 - AP$, $\alpha_2 - M$, C1-inh and PAI-1). These inhibitors have weaker effects than the likes of AT or TFPI. This leads us to ignore these inhibitors to favour model simplicity, at least with this initial construction. The Unified Model reaction scheme, given in Figure 3.4, is chosen by combining the simplified reaction schemes from these models, along with any other reactions which are necessary to produce a consistent model. Finally, the enzymatic reactions are then expanded into the standard three reaction mass action law system to produce the final Unified Model reaction scheme. We use exclusively mass action kinetics, as has been recommended [43], in order to capture all competitive inhibitory effects. A summary of this method for building the Unified Model reaction scheme is given in Figure 3.5.

Meizothrombin (mIIa) is the intermediate for prothrombin activation by prothrombinase. Unlike some other intermediates, it has comparable levels of activity to the fully active form, thrombin [97]. However, it has not been included in the model due to the limited number of sources that determine the reaction rates in multiple steps (with an intermediate) compared with assuming it is a single step reaction.

3.2.3 Choice of Reaction Rates

As explained in Section 2.1, we believe a single set of reaction rates should be sufficient for a model to predict all individuals in this cohort. This is because the experimental conditions should be consistent across all samples and there should not be any differences in the proteins between individuals. This means none of

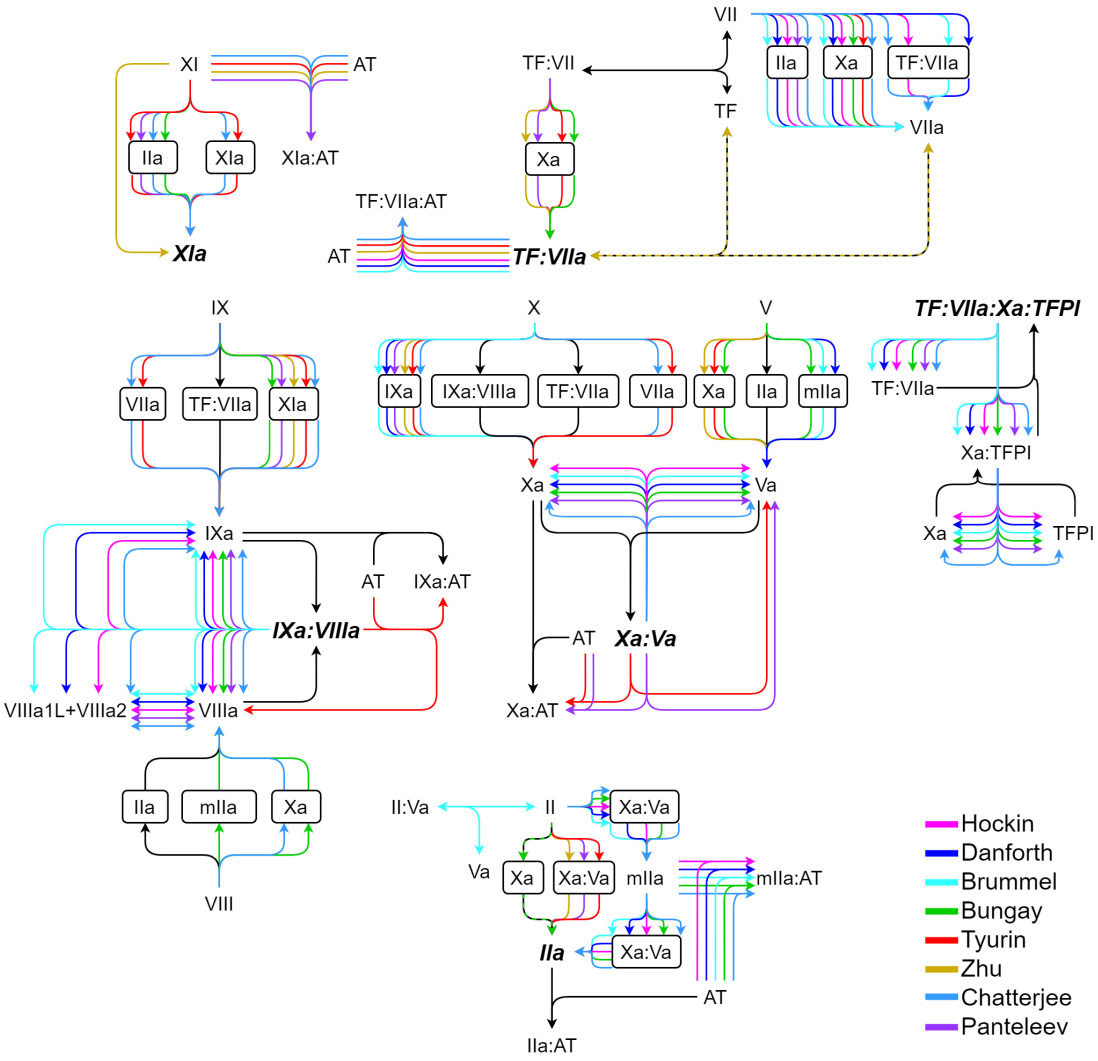

Figure 3.3: A comparison of reduced form of the reaction schemes for the eight models. The reactions are separated to best compare with the modules for the Unified Model, as seen in Figure 3.4.

the parameters will be fitted patient specifically.

To build the prior distributions, we want to make use of multiple sources for each reaction rate. To begin, we use the original sources in each of the models, as found in Section 2.6. Any reaction rates which have two or fewer sources are then investigated and new sources are added where they can be found. Details on each source are then collected such as temperature; pH; where the coagulation factors were sourced from; whether non-human factors are used; the concentration and type of phospholipids that were used, if applicable; and anything else notable about the experimental conditions used for the reaction rate measurements. There is insufficient data to identify the shape of these distributions, however we do know that they are all bounded from below by zero. For this reason, log-normal distributions are fitted to the reaction rate values and the geometric mean (median of the log-normal distribution) is used as the point estimate for the reaction rates. Any sources which are considered too different from the experimental setting of

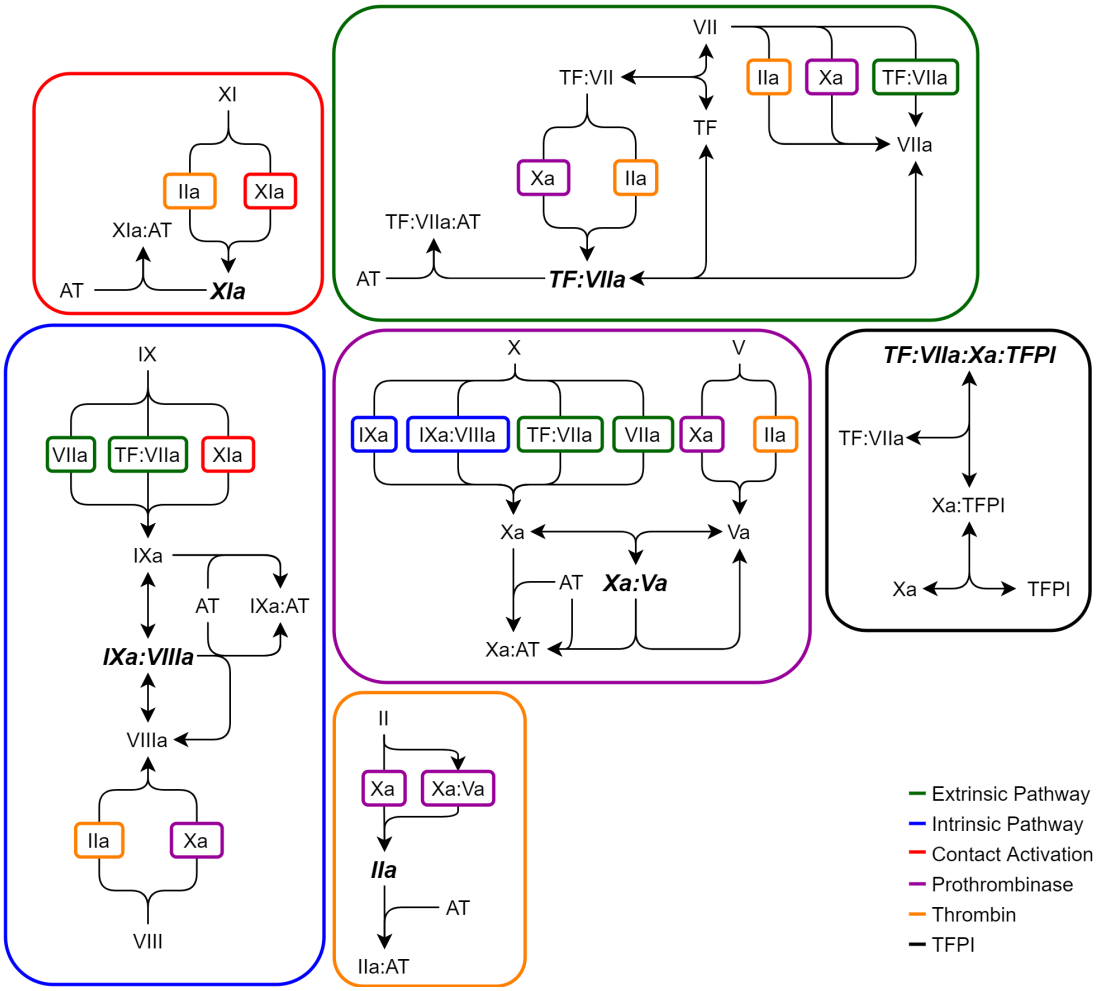

Figure 3.4: The simplified reaction scheme for the Unified Model, separated into the individual modules.

the thrombin generation assay, or appear unreliable, are ignored. These details are recorded in the module documents in Appendix E.

The reaction rates are described in a standard from, here named the prior form. This uses K_m and k_{cat} to describe the enzymatic reactions; K_d and k_+ to describe the association and dissociation reactions; and k_+ for the association reactions. This allows us to implement the prior distributions using the form most commonly used in the original sources that identify them.

To simulate the model, the set of reaction rates is converted from prior form to mass action form. This form of the reaction rates uses k_+, k_-, and k_{cat} to describe the enzymatic reactions; k_+ and k_- to describe the association and dissociation reactions; and k_+ for the association reactions. To convert the prior form for enzymatic reactions (K_m and k_{cat}) into the mass action form (k_+, k_-, and k_{cat}), k_+ is assumed to be diffusion limited at a rate of $1 \times 10^8 M^{-1} s^{-1}$ [69]. Equation 3.1 presents the formulas for the disassociation constant and Michaelis Menten constant which we can rearrange into the form given by Equation 3.2 to derive equations for k_- in both of these contexts.

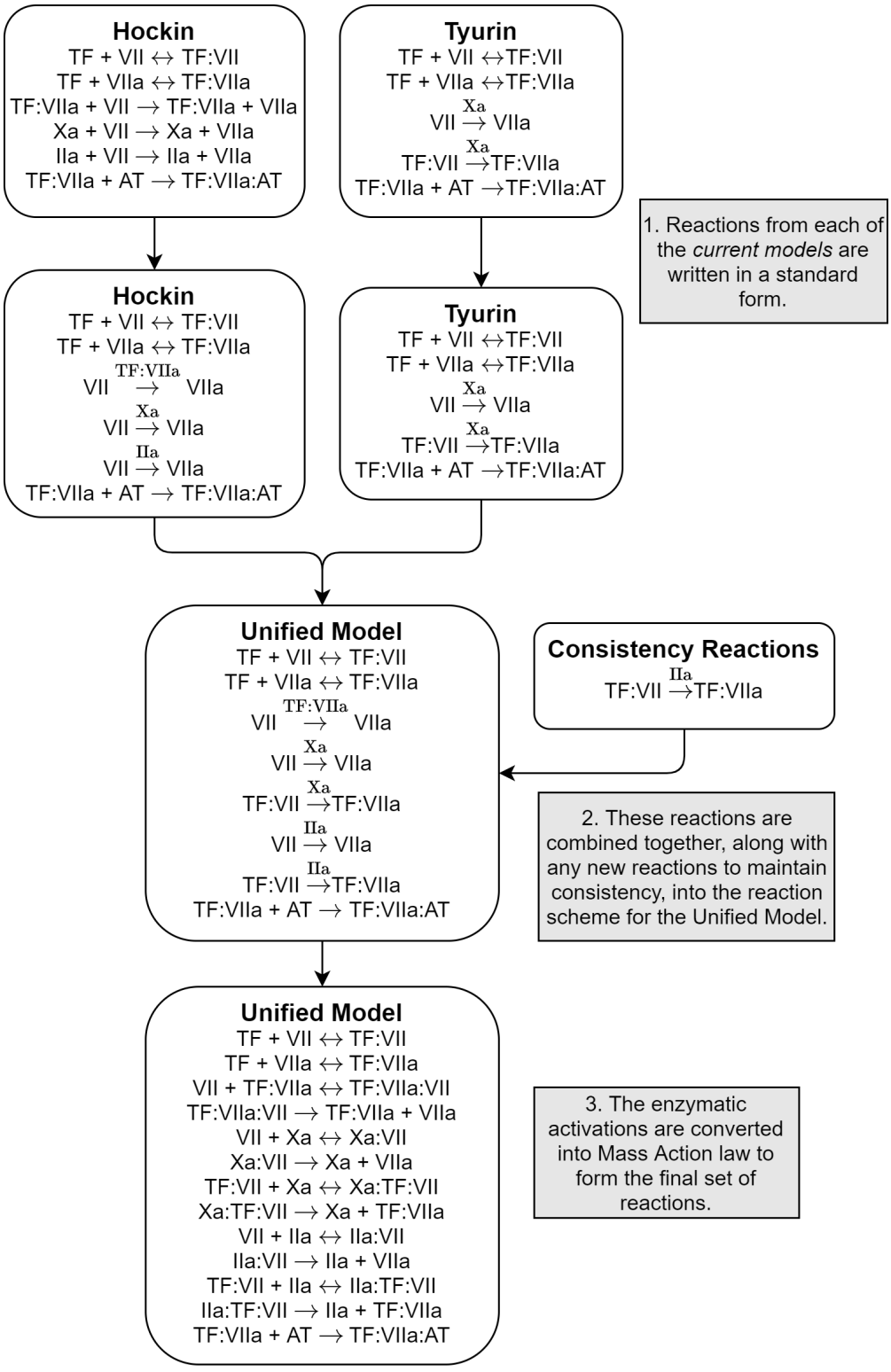

Figure 3.5: A summary of the method used to build the Unified Model reaction scheme.

$$K_d = \frac{k_-}{k_+}$$
$$K_m = \frac{k_- + k_{\text{cat}}}{k_+} \tag{3.1}$$

$$k_- = K_d \times k_+$$
$$k_- = K_m \times k_+ - k_{\text{cat}} \tag{3.2}$$

Sometimes a given pair of values for K_m and k_{cat} cannot be used with the on rate of $k_+ = 1 \times 10^8 M^{-1} s^{-1}$ as it will result in a negative value of k_-. To resolve this, the value of k_+ will be iteratively increased by a factor of 10 until a positive value of k_- is found. This is ensures all values in the prior can be simulated.

This conversion from prior to mass action form for the reaction rates alters the shape of some of the distributions. In prior form, all distributions are log-normal. In mass action form, any binding/unbinding reactions (those using K_d and k_+ in the prior form) will find that k_- is still a log-normal distribution since the product of two log-normal distributions is also log-normal. For the enzymatic activations, we see that $k_- = K_m \times k_+ - k_{\text{cat}}$. The difference between two log-normal distributions does not appear to produce any typical distribution, and considering that k_+ here is a discontinuous function of K_m and k_{cat}, it seems unlikely that anything useful can be derived about the shape of the distribution for k_- in enzymatic activations.

If a reaction rate has no experimental sources, we use an assumed rate and set the log-normal standard deviation to 2.5. If a reaction rate has a single experimental source, we use this value as the median of the log-normal distribution and set the log-normal standard deviation to 2.5. A log-normal standard deviation of 2.5 was chosen since it is larger than the largest standard deviation of 1.5. This puts 95% of the distribution within a factor of 10^5 up or down, avoiding a reliance on values in which we are least certain.

An example of a table in the module documents that is used to form the prior distributions is given in Table 3.2. A summary of the method to build the prior distributions is given in Figure 3.6.

3.2.4 Parameter Fitting Overview

Our previous work in Section 2.5 shows that the models are highly sensitive, with even small discrepancies in the reaction rates resulting in significantly different model outputs. To mitigate the effect this has on the final model, the reaction rates are fitted to the data set. This is done using Gradient Descent and Approximate Bayesian Computation - Sequential Monte Carlo. These two fitting methods are utilised to compare between the quality of fit reached when a prior

TF + VII ↔ TF:VII		
Citation	Rates	Notes
[98]	$K_d = 13.2nM$	Temperature: 37°C. Bovine FVII. Purified bovine brain TF. Egg PC lipid from Supleco, Bellefonte, PA. pH: 7.5. Measures with different binding schemes for varying PS% (not taken into account here for consistency with other binding/unbinding reactions).
[99]	$K_d = 1nM$, $k_+ = 5 \times 10^4 M^{-1}s^{-1}$, $k_- = 6 \times 10^{-5}s^{-1}$	Room temp. Human FVII. Human TF from American Diagnostic Inc, Greenwich, CT, USA. pH: 7.4. Phospholipids not used as the surface. Separate association and disassociation rates are given. Also gives rates for AT.
[90]	$K_d = 2nM$, $k_+ = 3.14 \times 10^5 M^{-1}s^{-1}$, $k_- = 6.29 \times 10^{-4}s^{-1}$	Soluble truncated TF_{1-219} gift from Dr. D. L. Eaton, Greentech Inc., South San Francisco, CA. Separate association and disassociation rates are given. Also gives activation of FX. pH: 7.3.
Chosen values: $K_d = 3nM(10 \wedge N(-8.55, 0.58^2), 5\% = 3.28 \times 10^{-10}, 95\% = 2.66 \times 10^{-8}), k_+ = 1.25 \times 10^5 M^{-1}s^{-1}(10 \wedge N(5.10, 0.56^2), 5\% = 1.51 \times 10^4, 95\% = 1.05 \times 10^6)$ therefore $k_- = 3.75 \times 10^{-4}s^{-1}$		

Table 3.2: An example reaction rate table for the reaction TF + VII ↔ TF:VII. $10 \wedge N(\mu, \sigma^2)$ denotes a log-normal distribution with parameters μ and σ. The remaining reaction rate tables can be found in Appendix E.

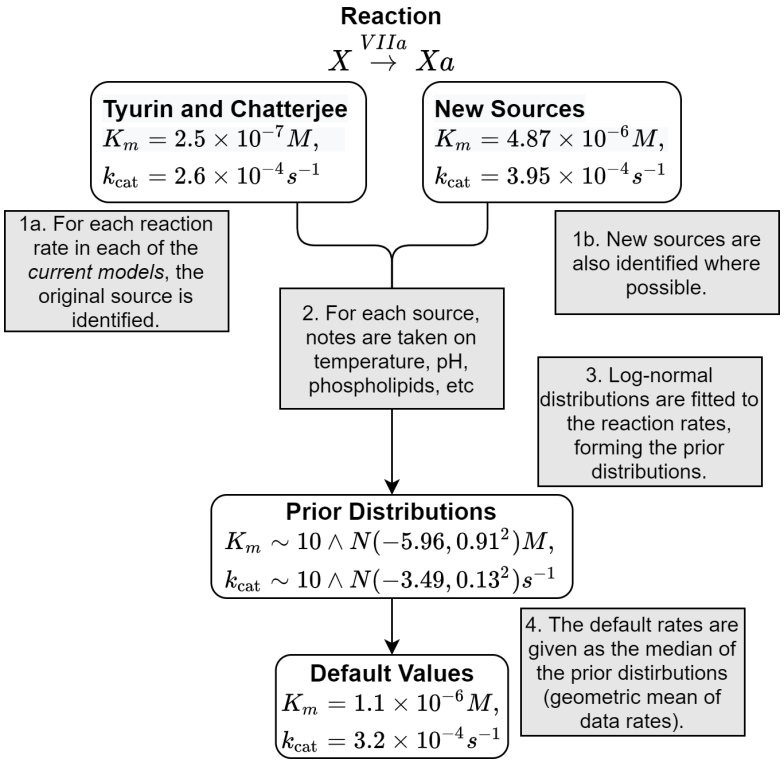

Figure 3.6: A summary of the method used to build the Unified Model reaction rate prior distributions.

is stipulated, encouraging reaction rates to remain in a biologically relevant range (ABC-SMC), and a fitting method where any positive values for the reaction rates can be used (Gradient Descent). The use of two methods allows us to infer additional information based on differences in the two sets of fitted reaction rates. For example, if the Gradient Descent algorithm finds much more improvement than the ABC-SMC by using a reaction rate for thrombin inhibition by AT much larger than would be biologically plausible (which can be determined from the prior distributions), then it can be inferred that the reaction scheme may need more inhibitors (such as $\alpha_2 - M$) to be added whereas if they both find similar sets of reaction rates then greater trust can be placed in the fitted values.

3.2.5 Parameter Identifiability

To avoid reaction rates which have insignificant effects on model output undergoing an effectively random selection during the fitting process, any reaction rates with an insignificant effect on the OD curves have not been fitted and are instead maintained at their default rates (the median of the priors) throughout the fitting process. To identify which reaction rates do not have a significant effect on optical density, the model is simulated using the reaction rates at the 5th and 95th percentiles of the prior distribution for that reaction rate, keeping all other reaction rates at their default rates. If there is no noticeable difference between the model predicted OD curves, then we do not fit that reaction rate. This is then repeated for all reaction rates.

3.2.6 Data Set and Cross Validation

Although the data contain measurements at forty time points, each optical density curve can be very efficiently summarised by a small number of parameters [79]. Due to the large number of reaction rates we will be fitting, and the fact that each OD curve can be summarised in only a few parameters, it will be useful to perform cross validation to ensure that any improvement in model accuracy is not a result of over-fitting. As such, we use 5-fold stratified cross validation, maintaining consistent ratios of males to females and cases to controls across all folds. This is implemented using Matlab's cvpartition function.

In 5-fold cross validation, the data is cut into five folds. The model is trained on four of these folds and then tested against the fifth fold. This is repeated to use each fold as a test set once. This allows exploration into model accuracy on data that was not used for training, allowing diagnosis of over-fitting.

3.2.7 Evaluating Model Fit

We define four metrics to evaluate model accuracy, the first of which is cost. This metric, as defined by Equation (3.3), finds the sum of squared errors between the experimentally determined OD curve for a given individual and the model predicted OD curve. This patient-specific squared error measure is then averaged across all individuals and square rooted.

$$\text{cost} = \sqrt{\frac{\sum_{i=1}^{n}[\sum_{j=1}^{40}((modelOD_{i,j} - dataOD_{i,j})^2)]}{n}} \tag{3.3}$$

The model performance for ETP predictions are evaluated using three methods. To match the ETP correlation results seen previously, we use the R^2 of the line of best fit and the RMSE of the line of proportionality (renamed to RMSE_{fit}). In addition, since ETP can now be measured in units of % of pooled plasma, it is also possible to investigate the RMSE for ETP predictions using a direct 1:1 match (intercept fixed at 0 and gradient fixed at 1), labelled as $\text{RMSE}_{1:1}$.

3.2.8 Approximate Bayesian Computation

Using the log-normal distribution priors for each reaction rate, the model is fitted using ABC-SMC with Early Rejection [100] with a minor alteration*. The perturbation kernel uses a multivariate log-normal distribution with a covariance matrix equal to one-fourth of the empirical covariance matrix measured in the log of the previous population of particles. To get a pointwise estimate of the reaction rates the most repeated particle in the final population is used. Pseudocode of the ABC-SMC algorithm we use is given in Algorithm 4.

The ABC-SMC method is run with 2000 particles per population, 200 of which

*In the original algorithm, the first set of particles, those that are selected from the prior, are sampled freely which can result in a large initial tolerance and increase in computation time

are unique, using an initial tolerance of 250. The ABC-SMC algorithm is run for seven days across twelve cores, after which the tolerances for each iteration are checked to ensure convergence.

3.2.9 Gradient Descent Fitting

MATLAB's fmincon (using a gradient descent method with the interior point algorithm) is used to fit the reaction rates, utilising a lower bound of zero to ensure all reaction rates remain positive. An increased finite difference step size of 1×10^{-3} is specified to ensure a significant change is made in the reaction rates for the errors in the ODE solver to be insignificant in the gradient calculation. Additionally, the step size calculation is adjusted to use normalised reaction rates (all initially set to one) to ensure changes in small reaction rates, those $< 10^{-6}$, are not considered too small and result in an early termination of the algorithm.

3.3 Results

3.3.1 Previous Models

Since we make use of a different data set in this chapter (only 333 individuals, all of whom have 5pM of added TF vs. the full 348 individuals, both with and without added TF), one which the previous models have not been tested against, we present their performance here. The performance of the previous models is presented in Table 3.3. To calculate the cost metric, the OD curves are calculated as given previously in Equation (2.3) (Section 2.3) and again below for clarity. For comparison with the cost metric, assuming a mean OD curve for all individuals results in a cost of 185. The $\text{RMSE}_{1:1}$ metric shows the Panteleev model as the best at predicting ETP, with the Hockin model performing significantly worse. The cost metric shows the Brummel model as performing best, however, all models perform worse than a mean OD curve.

$$OD(t = k) = \int_{t=0}^{k} [FIIa](t)dt$$

3.3.2 Unified Model Fitting

There were 44 significant reaction rates (determined using the method in Subsection 3.2.5) to be fitted. The results of the fitting are given in Table 3.4. After fitting, there is a decrease in cost from 291 to 175. The cross validation also demonstrates that the fitting is robust against over-fitting with similar training costs and test costs given for both methods.

of the algorithm. Initially restricting the first tolerance to select N particles that meet this tolerance helped improve computation time and improve consistency between runs.

Algorithm 4: ABC-SMC with Early Rejection

Input: Number of particles N, desired number of unique particles U, prior π, model simulator l, initial tolerance ϵ_{init} and final tolerance ϵ_{end}

Output: Particles, costs and Weights $\{(\theta_t^{(i)}, x_t^{(i)}, w_t^{(i)})\}_{i=1}^N$ for each population t

for *i=1:N* **do**
  while *True* **do**
    $\theta^* \sim \pi(\cdot)$;
    $x^* \sim l(\cdot|\theta^*)$;
    if $d(y, x^*) < \epsilon_{init}$ **then**
      $\theta_0^{(i)} = \theta^*$;
      $x_0^{(i)} = x^*$;
      $w_0^{(i)} = \frac{1}{N}$;
      break;
    end
  end
end
$\epsilon_0 = \max_i d(y, x_0^{(i)})$;
$t = 0$;
while $\epsilon_t > \epsilon_{end}$ **do**
  $v \sim U[0,1]^N$, to be used in resampling
  Use bisection to choose ϵ_{t+1} s.t. there are U unique particles after reweighting and resampling (using fixed random numbers v)
  for *i=1:N* **do**
    $\tilde{w}_{t+1}^{(i)} = w_t^{(i)} \mathbb{I}(d(y, x_0^{(i)}) < \epsilon_{t+1})$;
  end
  $w_{t+1}^{(\cdot)} = \tilde{w}_{t+1}^{(\cdot)} / \sum_{i=1}^N (\tilde{w}_{t+1}^{(i)})$;
  Resample using random draws v
  for *i=1:N* **do**
    $\theta_{t+1}^{(i)} = \theta_t^{(i)}, x_{t+1}^{(i)} = x_t^{(i)}$;
    $\theta^* \sim q(\cdot|\theta_0^{(i)})$;
    $u \sim U[0,1]$;
    if $u < \frac{\pi(\theta^*) q(\theta_t^{(i)}|\theta^*)}{\pi(\theta_t^{(i)}) q(\theta^*|\theta_t^{(i)})}$ **then**
      $x^* \sim l(\cdot|\theta^*)$;
      if $d(y, x^*) < \epsilon_{t+1}$ **then**
        $\theta_{t+1}^{(i)} = \theta^*, x_{t+1}^{(i)} = x^*$;
      end
    end
  end
  $t = t + 1$;
end

Model	Cost	R^2	RMSE_{fit}	$\text{RMSE}_{1:1}$
Hockin	286.2	0.23	32.4	44.5
Danforth	250.3	0.22	27.8	32.8
Chatterjee	242.0	0.21	28.1	33.0
Brummel	238.2	0.22	27.8	32.7
Bungay	393.8	0.20	27.9	31.8
Panteleev	296.0	0.22	27.4	29.6
Tyurin	323.1	0.22	27.4	30.2
Zhu	384.1	0.22	27.4	30.0

Table 3.3: The performance of the previous models against the OD data set for the metrics we use to evaluate the Unified Model.

Fitting Method		Training Cost	Test Cost
No fitting		N/A	291.3
Gradient Descent	Cross Validation	173.2±5.4	174.0±25.9
	Full	175.2	N/A
ABC-SMC	Cross Validation	172.9±5.9	173.4±24.7
	Full	174.7	N/A

Table 3.4: The results from the Unified Model fitting process. Cross validation costs are given as mean$\pm\frac{1}{2}\times$range from the five folds.

Thrombin Generation Curves and Optical Density Curves

The thrombin generation curves for each of the reaction rate sets (default, gradient descent fitted, and ABC-SMC fitted) are given in Figure 3.7, using the initial conditions given in Table 3.1. Optical density curves from the chromogenic substrate are given for six randomly selected individuals in Figure 3.8.

After fitting, the thrombin generations curves shift to have a shorter lagtime and a longer tail. This allows the model to better predict the shape of an average OD curve. As seen from the OD curves in Figure 3.8, most of the cost improvement comes from correcting this shape, with the model predicting close to an average curve for all individuals. The minor deviations from an average curve then allow the cost to reduce slightly further than the mean OD curve cost (175 vs. 185).

ETP Correlation

The ETP correlation scatter graphs (as seen with the previous models), for the default and the fitted reaction rates, and the ETP correlation metrics are given in Figure 3.9 and Table 3.5, respectively. The ETP correlation appears similar to the previous models, showing minor improvement in R^2 and RMSE_{fit}. The fitting provides small improvements in all metrics.

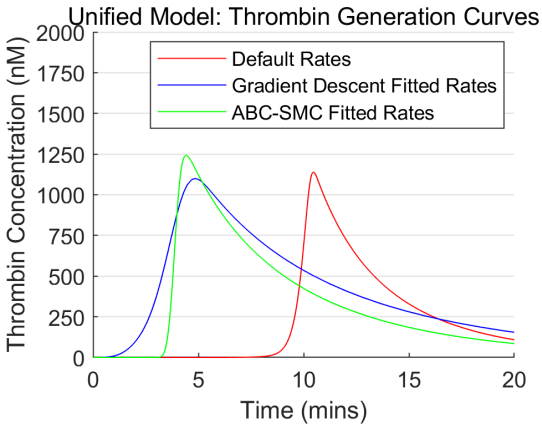

Figure 3.7: The thrombin generation curves for each of the three reaction rate sets, default, gradient descent fitted, and ABC-SMC fitted.

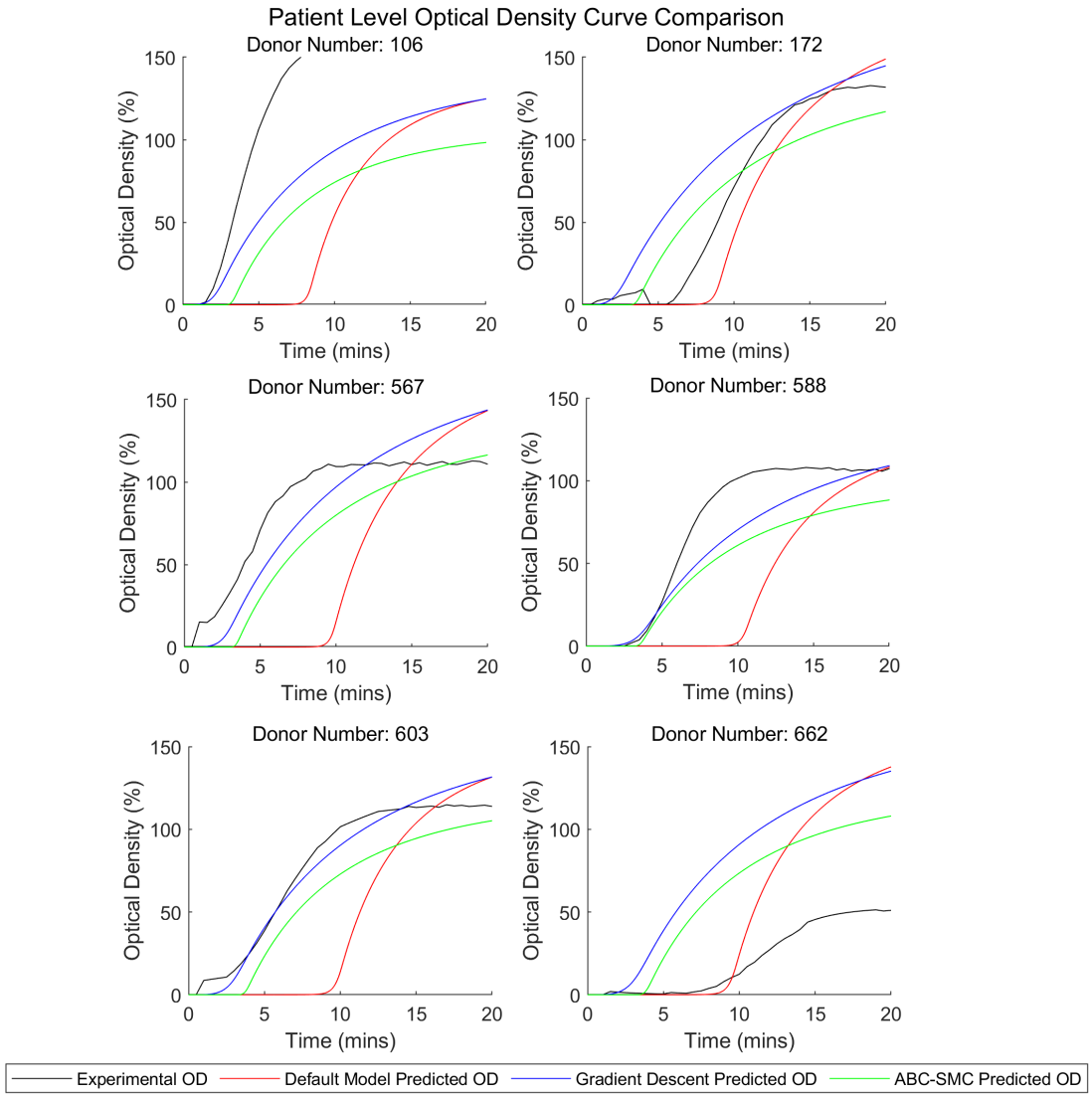

Figure 3.8: A comparison of optical density curves of six randomly selected individuals. The experimentally determined OD curves are given in black. The model predicted OD curves are given in red, blue, and green for the default, gradient descent fitted, and ABC-SMC fitted reaction rates, respectively.

The OD curves, both experimental and model predicted, for the individuals with the best and worst ETP predictions are given in Figure 3.10. Whereas previously we had to scale the OD curves by the gradient of the line of proportionality to convert the units of nM · min to % of pooled plasma, we now use the model to simulate a pooled plasma sample for the scaling.

Compared with the previous models (Figures 2.20 and 2.21), the Unified Model is able to better match lagtime but the shape, even for the curve with the best ETP prediction, still does not match the experimental data. Interestingly, the same individual that many of the previous models found most difficult to predict was also the most difficult for the Unified Model. We had originally put this result, at least partially, down to the models predicting all prothrombin is always converted, reducing the amount of variability allowed in model predicted ETP.

	Fitting Method	R^2	RMSE_{fit}	$\text{RMSE}_{1:1}$
Unified Model	No fitting	0.22	27.17	30.3
	Gradient Descent	0.23	26.96	29.9
	ABC-SMC	0.23	26.93	30.1

Table 3.5: The accuracy of the Unified Model predicted ETP, as assessed using the metrics of R^2, RMSE_{fit} and $\text{RMSE}_{1:1}$.

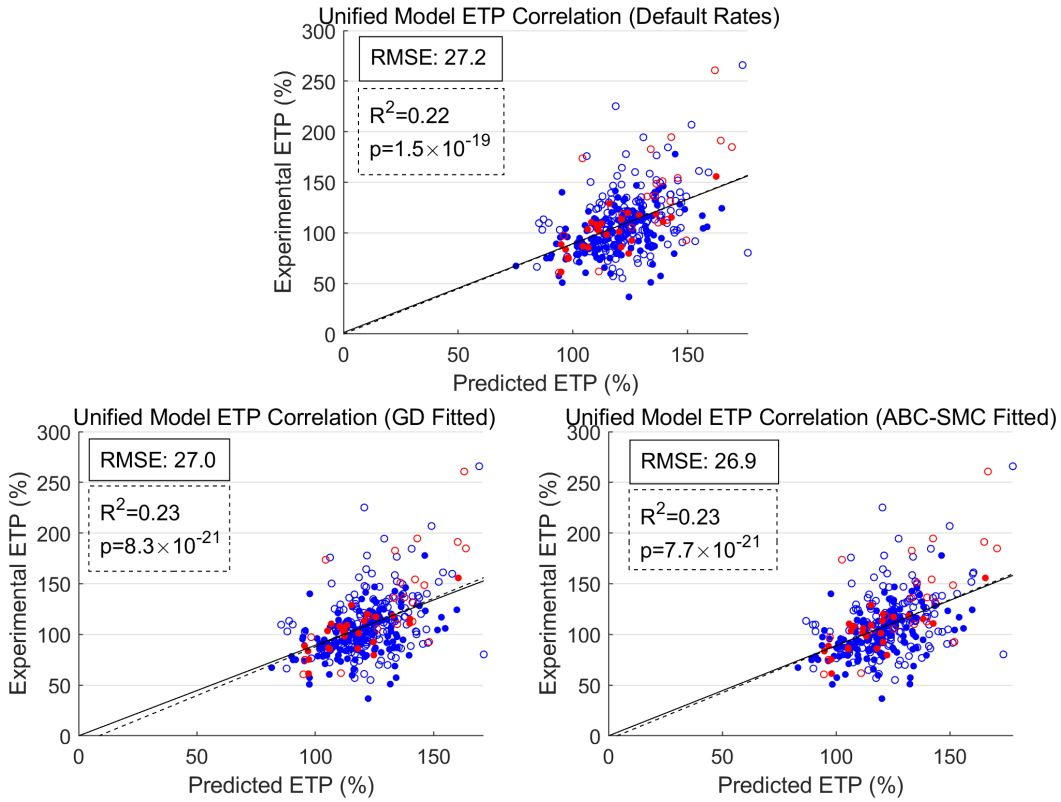

Figure 3.9: The ETP correlation scatter graph for the default, gradient descent fitted, and ABC-SMC fitted reaction rates.

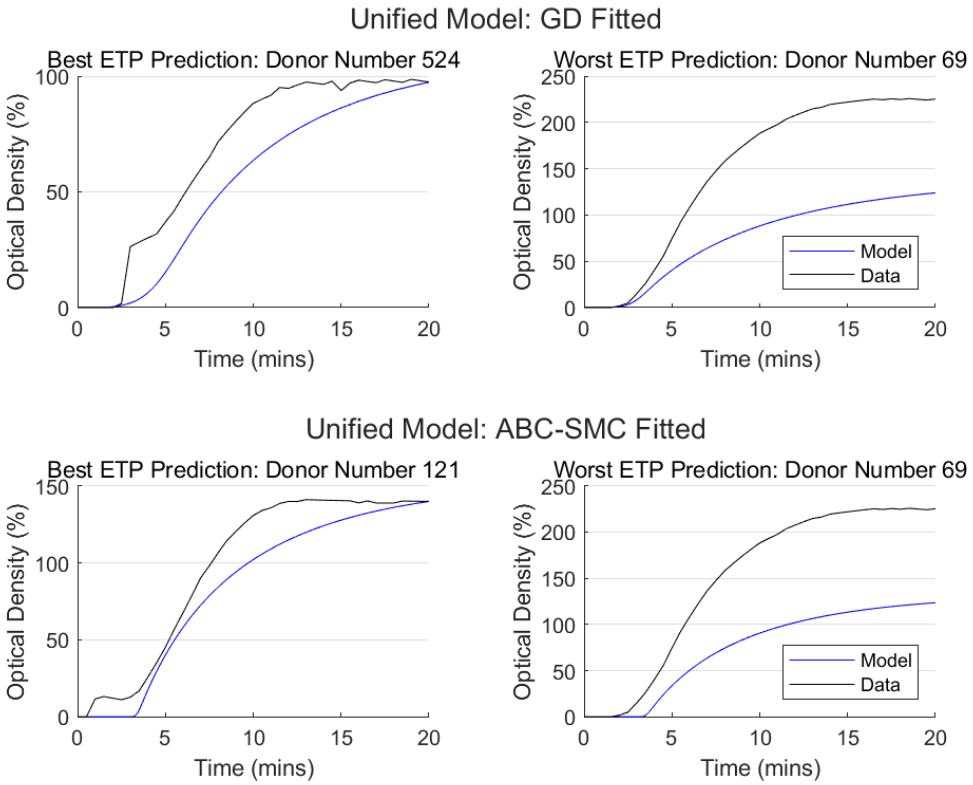

Figure 3.10: The Unified Model predicted OD curve and the experimental OD curve for the individuals with the best and worst predicted ETP, separated by the Gradient Descent (top) and ABC-SMC (bottom) fitted rates.

Parameter Changes

In Tables 3.6 and 3.7, the default reaction rates used by the model are given, followed by the changes from the gradient descent and ABC-SMC fitting.

The Gradient Descent algorithm changes many reaction rates to be an extreme value (outside of the central 90% of the prior distributions) with multiple k_{cat} rates reaching magnitudes of $1000s^{-1}$. The ABC-SMC is more successful at maintaining a realistic set of reaction rates with only a handful of reaction rates falling outside of the central 90% of the prior distributions. Most of these rate changes most strongly affect the lagtime and could be the reason that the gradient descent achieves a shorter lagtime than the ABC-SMC fitting.

Reaction	Default Reaction Rates		Gradient Descent		ABC-SMC	
	K_d (M)	k_+ $(M^{-1}s^{-1})$	K_d (M)	k_+ $(M^{-1}s^{-1})$	K_d (M)	k_+ $(M^{-1}s^{-1})$
TF + VII $\leftrightarrow$ TF:VII	2.95×10^{-9}	1.26×10^{5}	Default	Default	Default	Default
TF + VIIa $\leftrightarrow$ TF:VIIa	3.16×10^{-9}	1.29×10^{5}	Default	$1.49 \times 10^{7\dagger}$	Default	1.33×10^{5}
TF:VIIa + AT $\rightarrow$ TF:VIIa:AT	-	9.55×10^{2}	-	$3.78 \times 10^{5\dagger}$	-	2.71×10^{2}
Xa + Va $\leftrightarrow$ Xa:Va	1.78×10^{-10}	1.58×10^{9}	$2.26 \times 10^{-13\dagger}$	Default	1.02×10^{-9}	Default
Xa + AT $\rightarrow$ Xa:AT	-	1.82×10^{3}	-	$3.26 \times 10^{5\dagger}$	-	5.06×10^{3}
Xa:Va + AT $\rightarrow$ Xa:AT + Va	-	1.07×10^{3}	-	Default	-	Default
IIa + AT $\rightarrow$ IIa:AT	-	6.17×10^{3}	-	$3.04 \times 10^{3\dagger}$	-	$4.28 \times 10^{3\dagger}$
XIa + AT $\rightarrow$ XIa:AT	-	3.98×10^{2}	-	Default	-	Default
IXa + VIIIa $\leftrightarrow$ IXa:VIIIa	1.62×10^{-9}	1.00×10^{7}	Default	1.71×10^{9}	Default	8.45×10^{6}
IXa + AT $\rightarrow$ IXa:AT	-	4.90×10^{2}	-	1.11×10^{5}	-	9.48×10^{5}
IXa:VIIIa + AT $\rightarrow$ IXa:AT + VIIIa	-	4.90×10^{2}	-	1.24×10^{5}	-	3.93
Xa + TFPI $\leftrightarrow$ Xa:TFPI	9.33×10^{-11}	3.80×10^{6}	Default	$5.34 \times 10^{8\dagger}$	Default	1.36×10^{6}
TF:VIIa + Xa:TFPI $\leftrightarrow$ TF:VIIa:Xa:TFPI	1.51×10^{-10}	8.91×10^{6}	Default	Default	Default	Default

Table 3.6: The reaction rates for the Unified Model and the changed reaction rates for the non-enzymatic reactions made by the fitting processes. Default is used to denote a rate that is fixed at the default rates for the fitting.

Reaction	Default Reaction Rates		Gradient Descent		ABC-SMC	
	K_m (M)	k_{cat} (s^{-1})	K_m (M)	k_{cat} (s^{-1})	K_m (M)	k_{cat} (s^{-1})
VII $\overset{Xa}{\rightarrow}$ VIIa	1.20×10^{-6}	15.1	3.14×10^{-4}	4.10×10^{3}	2.69×10^{8}	1.82×10^{-2}
TF:VII $\overset{Xa}{\rightarrow}$ TF:VIIa	1.05×10^{-7}	3.16	2.21×10^{-6}	$2.21 \times 10^{3\dagger}$	$1.16 \times 10^{-4\dagger}$	54.9
VII $\overset{IIa}{\rightarrow}$ VIIa	2.69×10^{-6}	6.17×10^{-2}	9.62×10^{-4}	8.08	6.11×10^{-8}	0.165

†These fitted reaction rates fall outside the central 90% of the prior distributions.

TF:VII $\overset{IIa}{\rightarrow}$ TF:VIIa	2.69×10^{-6}	6.17×10^{-2}	1.40×10^{-3}	10.4	4.60×10^{-9}	0.267
VII $\overset{IXa}{\rightarrow}$ VIIa	1.70×10^{-6}	3.24×10^{-1}	4.68×10^{-4}	79.3	1.83×10^{-5}	$2.04 \times 10^{5\dagger}$
TF:VII $\overset{IXa}{\rightarrow}$ TF:VIIa	1.70×10^{-6}	3.24×10^{-1}	4.35×10^{-4}	88.6	$3.46 \times 10^{-2\dagger}$	4.86×10^{-3}
VII $\overset{TF:VIIa}{\rightarrow}$ VIIa	3.24×10^{-6}	1.41	7.93×10^{-4}	Default	1.26×10^{-8}	Default
X $\overset{TF:VIIa}{\rightarrow}$ Xa	3.16×10^{-7}	6.03	8.89×10^{-7}	$5.54 \times 10^{2\dagger}$	4.84×10^{-8}	6.81
X $\overset{VIIa}{\rightarrow}$ Xa	1.10×10^{-6}	3.24×10^{-4}	$2.46 \times 10^{-4\dagger}$	Default	2.36×10^{-6}	Default
X $\overset{IXa:VIIIa}{\rightarrow}$ Xa	8.51×10^{-8}	3.39	Default	$3.00 \times 10^{2\dagger}$	Default	4.45
X $\overset{IXa}{\rightarrow}$ Xa	7.94×10^{-8}	2.82×10^{-4}	$1.04 \times 10^{-5\dagger}$	Default	3.57×10^{-7}	Default
V $\overset{IIa}{\rightarrow}$ Va	7.24×10^{-8}	2.95×10^{-1}	1.18×10^{-5}	Default	1.34×10^{-6}	Default
V $\overset{Xa}{\rightarrow}$ Va	1.05×10^{-8}	4.27×10^{-2}	Default	14.2	Default	0.170
II $\overset{Xa}{\rightarrow}$ IIa	1.32×10^{-6}	9.33×10^{-3}	$5.45 \times 10^{-4\dagger}$	Default	2.50×10^{-6}	Default
II $\overset{Xa:Va}{\rightarrow}$ IIa	6.92×10^{-7}	35.5	$4.19 \times 10^{-4\dagger}$	$4.46 \times 10^{3\dagger}$	1.70×10^{-6}	25.5
XI $\overset{IIa}{\rightarrow}$ XIa	5.01×10^{-8}	1.29×10^{-4}	2.21×10^{-5}	1.11×10^{-4}	7.45×10^{-11}	1.88×10^{-3}
XI $\overset{XIa}{\rightarrow}$ XIa	5.01×10^{-8}	1.29×10^{-4}	1.48×10^{-5}	3.34×10^{-2}	1.08×10^{-8}	0.185
IX $\overset{TF:VIIa}{\rightarrow}$ IXa	1.62×10^{-7}	5.37×10^{-1}	Default	Default	Default	Default
IX $\overset{VIIa}{\rightarrow}$ IXa	8.91×10^{-9}	3.63×10^{-5}	1.52×10^{-6}	5.55×10^{-5}	9.71×10^{-11}	7.75×10^{-3}
IX $\overset{XIa}{\rightarrow}$ IXa	4.17×10^{-7}	7.41×10^{-1}	$9.86 \times 10^{-5\dagger}$	$60.0^{\dagger}$	7.10×10^{-7}	1.99
VIII $\overset{IIa}{\rightarrow}$ VIIIa	2.00×10^{-7}	1.00	7.65×10^{-6}	$3.02 \times 10^{2\dagger}$	1.86×10^{-9}	0.532
VIII $\overset{Xa}{\rightarrow}$ VIIIa	2.00×10^{-7}	2.19×10^{-1}	5.39×10^{-5}	57.9	1.09×10^{-8}	4.86
Substrate $\overset{IIa}{\rightarrow}$ Activated Substrate	1.95×10^{-3}	1.91	Default	Default	Default	Default

Table 3.7: The reaction rates for the Unified Model and the changed reaction rates of the enzymatic activations made by the fitting processes. Default is used to denote a rate that is fixed at the default rates for the fitting.

In order to test various different hypotheses that could limit the predictive capabilities of the model, for the remainder of this chapter we will only make use of gradient descent (the quicker of the two fitting methods) and we will not perform cross validation. If we are able to improve model accuracy, then we can return to using both of these methods.

Perturbed Fitting

Noisy data can sometimes present problems in fitting. Noise can introduce bias in the optimal parameter values. As a step to validate the fitting process, the model has been fitted to its own output, using the default reaction rates, with perturbations added to replicate experimental noise. The model is simulated for the coagulation factor data for each individual and the OD curves are recorded. These OD curves are then perturbed by a normal distribution (mean zero and standard deviation one, in units of % of pooled plasma) at each point and any negative values were set to 0. The model is then fitted to this perturbed model output using gradient descent to assess the change in the optimal parameter values.

The cost sees only a minor decrease after fitting from 5.5908 for the default rates to 5.5882 for the gradient descent fitted rates. The largest relative changes in the reaction rates after fitting are a reduction by 0.5% and an increase by 0.25%. This suggests that the fitting process should be resilient to data noise.

ETP Fitting

The Unified Model fitting showed much greater improvement in the cost metric than in the ETP correlation metrics. To verify that this is not due to the current cost metric weighting accurate lagtimes too heavily over the ETP predictions, we have performed the gradient descent fitting to optimise the $\mathrm{RMSE}_{1:1}$ metric.

The thrombin generation curve predicted for the reference factor concentrations using the fitted rates, the ETP correlation scatter graph, and model performance metrics are given in Figure 3.11, Figure 3.12, and Table 3.8, respectively.

The ETP fitting presents a very rapid thrombin generation curve (almost all fitted reaction rates are scaled to $\times 1000$ the original values). The $\mathrm{RMSE}_{\mathrm{fit}}$ comes out higher than for the default reaction rates. There is only minor improvements in $\mathrm{RMSE}_{1:1}$ and it is clear that the fitting is not working as intended and accurately predicting ETP from the coagulation factors, but is instead trying to approximate a linear model from FII and AT concentration by removing the effects of the other factors. This is further demonstrated in Figure 3.13 with the OD curves of the individuals with the best and worst ETP predictions.

	Fitting Method	R^2	RMSE_{fit}	$\text{RMSE}_{1:1}$
Unified Model	No fitting	0.22	27.17	30.3
	Gradient Descent (ETP)	0.22	27.38	29.1

Table 3.8: The ETP prediction results from the ETP fitted Unified Model.

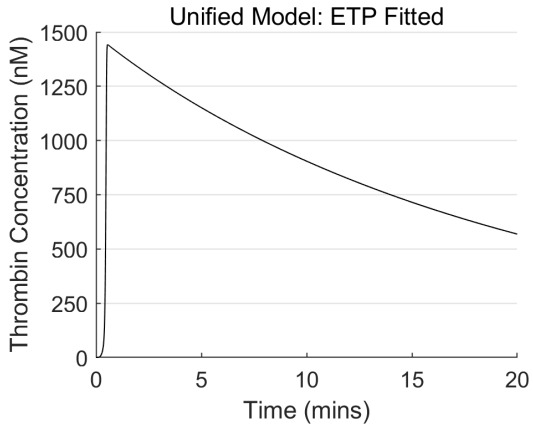

Figure 3.11: The thrombin generation curve for the ETP fitted reaction rates.

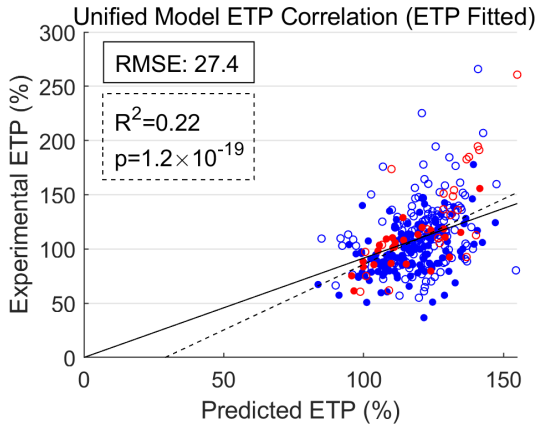

Figure 3.12: The ETP correlation scatter graph for the reaction rates found through fitting to ETP only.

3.3.3 Chatterjee Model Fitting

To help understand what components could be missing from the model, a current model which gives good coverage over the reactions in the coagulation cascade has been fitted. The Chatterjee model was chosen as it contains the largest reaction scheme and its main problem is in the reaction rate for FXI auto-activation, which can be easily accounted for in fitting.

Since priors are not available for the reaction rates in the Chatterjee model, parameter identifiability is performed by varying each mass action reaction rate between 0.1 and 10 times its value and assessing for changes in the resulting thrombin generation curves. This leads us to find 33 significant reaction rates to fit. The cost is evaluated as described previously in Equation (2.3).

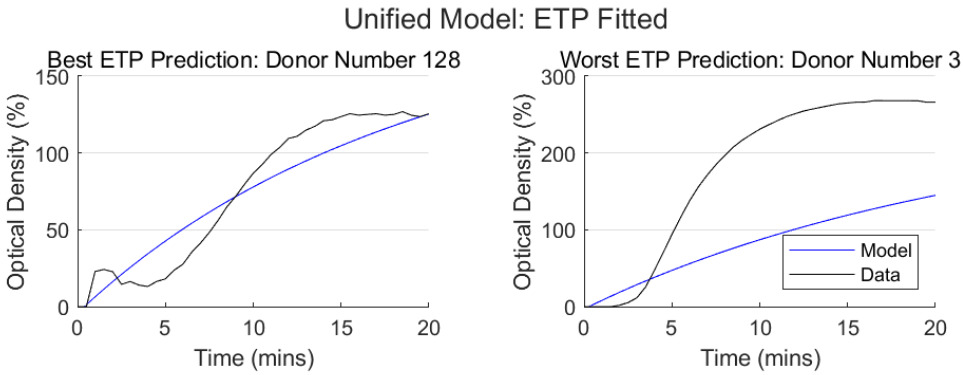

Figure 3.13: The Unified Model predicted OD curve and the experimental OD curve for the individuals with the best and worst predicted ETP for the gradient descent fitted rates, fitted to ETP.

Again, the fitting reduced the model predicted lagtime, as shown in Figure 3.14. The cost was lowered from 190.8 to 167.7 after fitting, achieving a slightly lower cost than the Unified Model. The ETP correlation, presented in Table 3.9 and Figure 3.15, appears similar to the Unified Model. After fitting, the RMSE is lower than that achieved by the Unified Model but, again, there is no substantial improvement.

The Chatterjee model shows improvement in all measures after fitting but is still an unreliable predictor of ETP.

Figure 3.16 shows the OD curves for the individuals with the best and worst ETP predictions. Compared with the previous results for the Chatterjee model (Figures 2.20 and 2.21), the Chatterjee model's worst donor is the same individual but the predictions have generally improved, both in shape and lagtime.

This suggests that there may be minor improvements to be found by including some of the features of the Chatterjee model, but even inclusion of these will not result in a significant improvement in model accuracy.

	Fitting Method	R^2	RMSE_{fit}	$\text{RMSE}_{1:1}$	Cost
Chatterjee Model	No fitting	0.22	27.48	31.6	190.8
	Gradient Descent	0.26	26.49	28.2	167.7

Table 3.9: The predictive accuracy of the Chatterjee model.

3.3.4 Expanded Unified Model

In the process of building the Unified Model, some inhibitors and other reactions which were thought to be smaller in effect size were ignored in order to keep the

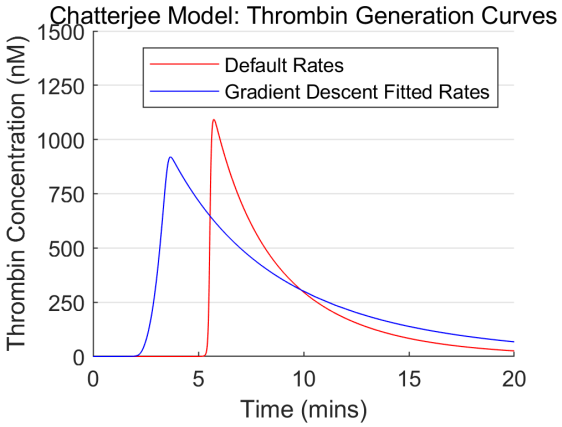

Figure 3.14: The thrombin generation curves of the Chatterjee model for the default and gradient descent fitted reaction rates.

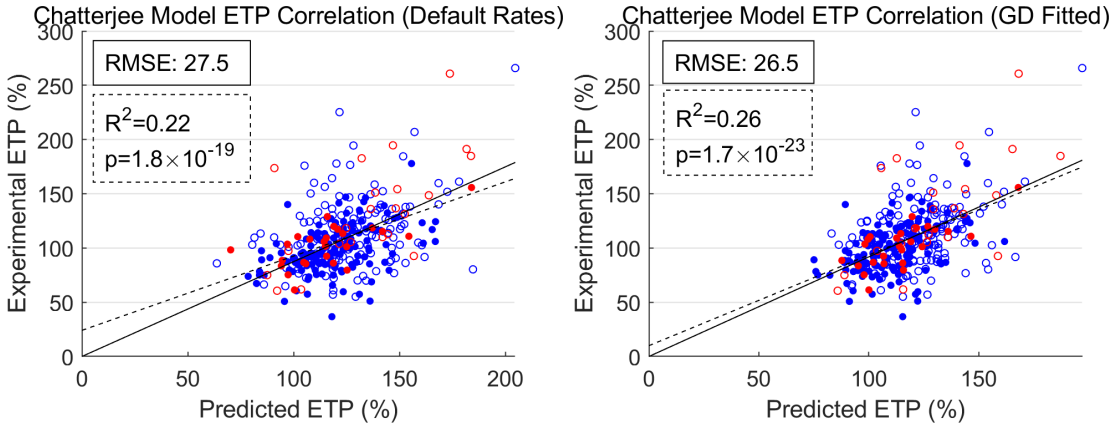

Figure 3.15: The ETP correlation scatter graph for the Chatterjee model with the default and gradient descent fitted reaction rates.

model simple. The poor fitting of the Unified Model, and its robustness to overfitting (shown in Section 3.3.2), suggests that it may be relevant to include these additional components. In this section, we will construct the Expanded Unified Model which will include these reactions. This model also incorporates a more detailed reaction scheme for TFPI inhibition which includes protein S as a cofactor and the slow-tight binding interaction between TFPI and Xa [101, 102]. A list of the additional reactions that were included into the Unified Model to form the Expanded Unified Model, alongside their corresponding rates, is given in Table 3.11.

The same $0.1\times$ and $10\times$ parameter identifiability, as was used in the Chatterjee fitting, is used for the Expanded Unified model (as the new reactions do not feature full prior distributions) on the prior form of the rates. The new inhibitors added are included at fixed concentrations given in Table 3.10. Protein S is included using the patient data, scaled against a reference concentration of $350nM$ [101].

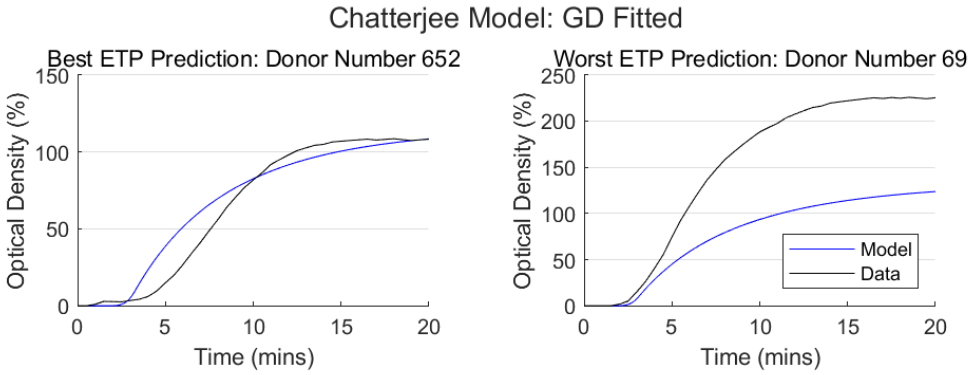

Figure 3.16: The Chatterjee Model predicted OD curve and the experimental OD curve for the individuals with the best and worst predicted ETP for the gradient descent fitted rates.

Species	Reference Initial Concentration (M)
$\alpha_1 - AT$	4×10^{-5}
$\alpha_2 - AP$	9.5×10^{-7}
$\alpha_2 - M$	3.25×10^{-6}
C1-inh	2.1×10^{-6}
PAI1	4.6×10^{-10}

Table 3.10: The coagulation factor concentrations for the new inhibitors used for all individuals. The reference concentrations are taken from the previous models [66, 68, 39, 63].

Reactions	Rates
TF:VIIa + Xa ↔ TF:VIIa:Xa	$K_d = 8.64 \times 10^{-7} M$, $k_+ = 2.2 \times 10^7 M^{-1} s^{-1}$
IIa + a1AT → IIa:a1AT	$k = 78.3 M^{-1} s^{-1}$
Xa + a1AT → Xa:a1AT	$k = 262 M^{-1} s^{-1}$
Xa:Va + a1AT → Xa:a1AT + Va	$k = 262 M^{-1} s^{-1}$
XIa + a1AT → XIa:a1AT	$k = 66.7 M^{-1} s^{-1}$
XIa + a2AP → XIa:a2AP	$k = 500 M^{-1} s^{-1}$
IIa + a2M → IIa:a2M	$k = 488 M^{-1} s^{-1}$
XIa + C1inh → XIa:C1inh	$k = 16.7 M^{-1} s^{-1}$
XIa + PAI1 → XIa:PAI1	$k = 2.1 \times 10^5 M^{-1} s^{-1}$
VIIIa ↔ $VIIIa_1L$ + $VIIIa_2$	$K_d = 2.6 \times 10^{-7} M$, $k_+ = 5.85 \times 10^{-3} s^{-1}$
IXa:VIIIa → IXa + $VIIIa_1L$ + $VIIIa_2$	$k = 1.4 \times 10^{-3} s^{-1}$
IXa + VIII ↔ IXa:VIII → IXa + VIIIa	$K_m = 2 \times 10^{-7} M$, $k_{cat} = 0.22 s^{-1}$
TFPI + Xa ↔ Xa:TFPI	$K_d = 4.4 \times 10^{-9} M$, $k_+ = 3.8 \times 10^6 M^{-1} s^{-1}$
Xa:TFPI ↔ Xa=TFPI	$k_+ = 4.15 \times 10^{-2} s^{-1}$, $k_- = 5 \times 10^{-4} s^{-1}$
Xa:TFPI + TF:VIIa ↔ TF:VIIa:Xa:TFPI	$K_d = 1.51 \times 10^{-10} M$, $k_+ = 8.91 \times 10^6 M^{-1} s^{-1}$
Xa=TFPI + TF:VIIa ↔ TF:VIIa:Xa=TFPI	Same rates as for Xa:TFPI
TF:VIIa:Xa + TFPI → TF:VIIa:Xa:TFPI	$k = 8.91 \times 10^6 M^{-1} s^{-1}$
TF:VIIa:Xa:TFPI ↔ TF:VIIa:Xa=TFPI	Same as Xa:TFPI to Xa=TFPI
PS + TFPI ↔ TFPI:PS	$K_d = 5 \times 10^{-9} M$, $k_+ = 1 \times 10^8 M^{-1} s^{-1}$‡
TFPI:PS + Xa ↔ Xa:TFPI:PS	$K_d = 5 \times 10^{-10} M$, $k_+ = 3.8 \times 10^6 M^{-1} s^{-1}$
Xa:TFPI:PS ↔ Xa=TFPI:PS	$k_+ = 1.2 \times 10^{-2} s^{-1}$, $k_- = 4.67 \times 10^{-4} s^{-1}$
Xa:TFPI:PS + TF:VIIa ↔ TF:VIIa:Xa:TFPI:PS	Same as without PS
Xa=TFPI:PS + TF:VIIa ↔ TF:VIIa:Xa=TFPI:PS	Same as without PS
TF:VIIa:Xa + TFPI:PS → TF:VIIa:Xa:TFPI:PS	Same as without PS
TF:VIIa:Xa:TFPI:PS ↔ TF:VIIa:Xa=TFPI:PS	Same as Xa:TFPI:PS to Xa=TFPI:PS
Xa:TFPI + PS ↔ Xa:TFPI:PS	Same as for PS and TFPI alone
Xa=TFPI + PS ↔ Xa=TFPI:PS	Same as for PS and TFPI alone
TF:VIIa:Xa:TFPI + PS ↔ TF:VIIa:Xa:TFPI:PS	Same as for PS and TFPI alone
TF:VIIa:Xa=TFPI + PS ↔ TF:VIIa:Xa=TFPI:PS	Same as for PS and TFPI alone

Table 3.11: The additional reactions and reactions rates that have been added into the Unified Model to form the Expanded Unified Model. "=" is used to denote a strong binding between the TFPI and FXa compared with the weaker ":" binding. Reaction rates are defined from the previous models for previously defined reactions and from the literature for reactions that have not previously been included in the models.

The thrombin generation curves, ETP correlation scatter graphs, and ETP correlation metrics are given in Figure 3.17, Figure 3.18, and Table 3.12, respectively. The thrombin generation curves continue to present a delayed lagtime which is then fixed through fitting. The cost is improved from 301.6 to 168.8. There is only a minor improvement in RMSE_{fit} after fitting compared with the original Unified Model (26.96 vs. 26.92). Equivalent results are seen for the R^2 metric (0.22 vs. 0.24), with the largest improvement coming from $\text{RMSE}_{1:1}$ (29.6 vs. 29.0).

	Fitting Method	R^2	RMSE_{fit}	$\text{RMSE}_{1:1}$	Cost
Expanded Unified Model	No fitting	0.22	27.16	29.6	301.6
	Gradient Descent	0.24	26.92	29.0	168.8

Table 3.12: The predictive accuracy of the Expanded Unified Model.

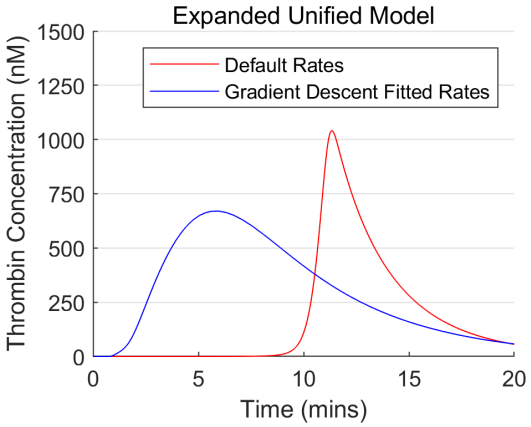

Figure 3.17: The thrombin generation curves for the two reaction rate sets for the Expanded Unified Model.

Figure 3.19 shows the OD curves for the individuals with the best and worst ETP predictions. The lagtime is accurately predicted for the best individual but the shape does not match, with a poorer match than the original Unified Model (Figure 3.10).

[‡]These rates are taken for protein C and protein S binding. Multiple sources have attempted to, but have been unable to, find rates for binding between TFPI and PS [103, 104, 105].

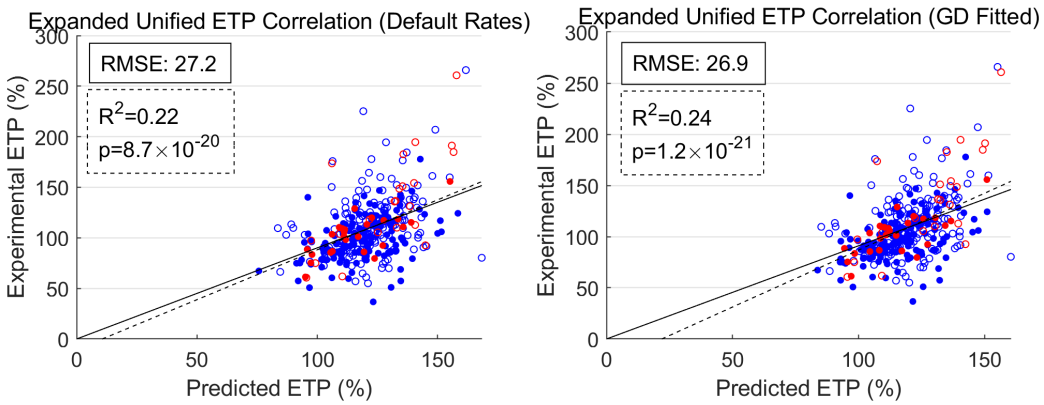

Figure 3.18: The ETP correlation scatter graph for the Expanded Unified Model with the default and gradient descent fitted reaction rates.

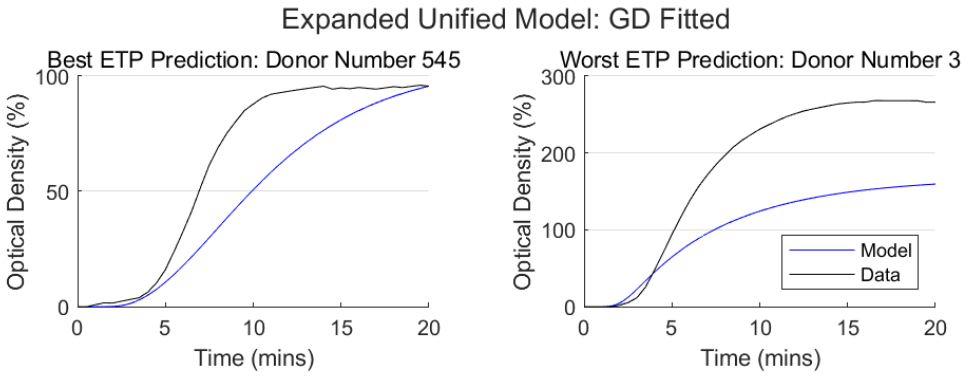

Figure 3.19: The Expanded Unified Model predicted OD curve and the experimental OD curve for the individuals with the best and worst predicted ETP for the gradient descent fitted rates.

3.3.5 Partial Prothrombin Conversion

The current models (including both previous versions of the Unified Model) predict that all prothrombin is converted into thrombin (see Section 2.4, Figure 2.29). This issue had been noted by us in Section 2.4 and by others [76] (data show only around 90% of prothrombin is converted into thrombin [89]) but it is not clear whether this is an issue with inaccurate reaction rates or missing elements of the reaction scheme. It is possible for the Expanded Unified Model to predict partial prothrombin conversion through amplifying its AT inhibition rates; however, this is not achieved through the fitting process.

Protein C

A potential cause of this effect could be protein C as this inhibitor needs to be first activated by thrombin (specifically thrombin which is bound to thrombomodulin). This means protein C can be a strong inhibitor without affecting lagtime as it is only significantly activated after the lagtime during the amplification phase.

Protein C was originally ignored from the Unified Model and Expanded Unified Model because the assay lacks the surface-bound thrombomodulin, which is needed, as a cofactor, to activate significant amounts of protein C. However, there is a weaker, soluble form of thrombomodulin found in the plasma which could be the cause of partial prothrombin conversion in the assay. A simple protein C reaction scheme using soluble thrombomodulin (sTM), given in Table 3.13, was added to the Expanded Unified Model as well as $0.228nM$ of sTM for all individuals (16.9ng/ml [106] at a molecular weight of 74kDa [107]). Data for the sTM reaction rates is used from multiple sources [108, 109, 110].

Reaction	Rates
IIa + sTM $\rightarrow$ IIa:sTM	$K_d = 1 \times 10^{-8}M, k_+ = 1 \times 10^{8}M^{-1}s^{-1}$
$PC \overset{IIa:sTM}{\rightarrow} APC$	$K_m = 9.8 \times 10^{-7}M, k_{cat} = 14.5s^{-1}$
$Va \overset{APC}{\rightarrow} Vai$	$K_m = 2 \times 10^{-8}M, k_{cat} = 0.4s^{-1}$
$Xa : Va \overset{APC}{\rightarrow} Xa + Vai$	$K_m = 2 \times 10^{-8}M, k_{cat} = 0.4s^{-1}$
$VIIIa \overset{APC}{\rightarrow} VIIIai$	$K_m = 2 \times 10^{-8}M, k_{cat} = 0.4s^{-1}$
$IXa : VIIIa \overset{APC}{\rightarrow} IXa + VIIIai$	$K_m = 2 \times 10^{-8}M, k_{cat} = 0.4s^{-1}$

Table 3.13: The additional reactions for the Expanded Unified Model to include protein C inhibition.

As shown in Figure 3.23, inclusion of protein C was successful in stopping all prothrombin being converted, however this made the model dramatically less accurate (Figure 3.21) and produced 'normal' thrombin generation curves similar to the Expanded Unified Model (Figure 3.20). Prior to fitting, the model output was very strongly dependent on the individual's concentration of protein C ($R^2 = 0.113$), much more so than the data predicted ($R^2 = 0.0022$) and protein C would inhibit the system well before 90% of the prothrombin had been converted. After fitting, the model would return to activating all prothrombin so long as there was at least ~10pM of TF ($R^2 = 0.064$ after fitting) and perform slightly worse than the original Expanded Unified Model. The lack of correlation between protein C and ETP in the data make it clear protein C is an unlikely explanation for the system to stop before all prothrombin is converted.

Figure 3.22 shows the OD curves for the individuals with the best and worst ETP predictions. For the best individual, the model predicted lagtime is significantly shorter than the data with the shape of the OD curve being much smoother in the model.

3.3.6 Fibrinogen and Fibrin

It is typical for the thrombin generation assay to be in defibrinated plasma (all fibrinogen is removed) as the fibrin polymer mesh network can interfere with the OD measurements [13]. However, the assay still included fibrinogen and instead blocked the mesh network formation at the point of fibrin which is kept in a

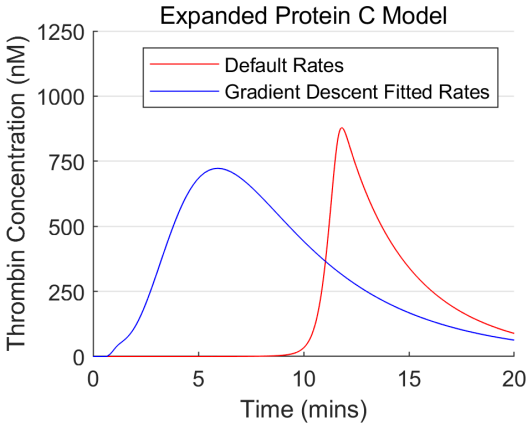

Figure 3.20: The thrombin generation curves for each of the reaction rate sets for the Expanded Unified Model with Protein C.

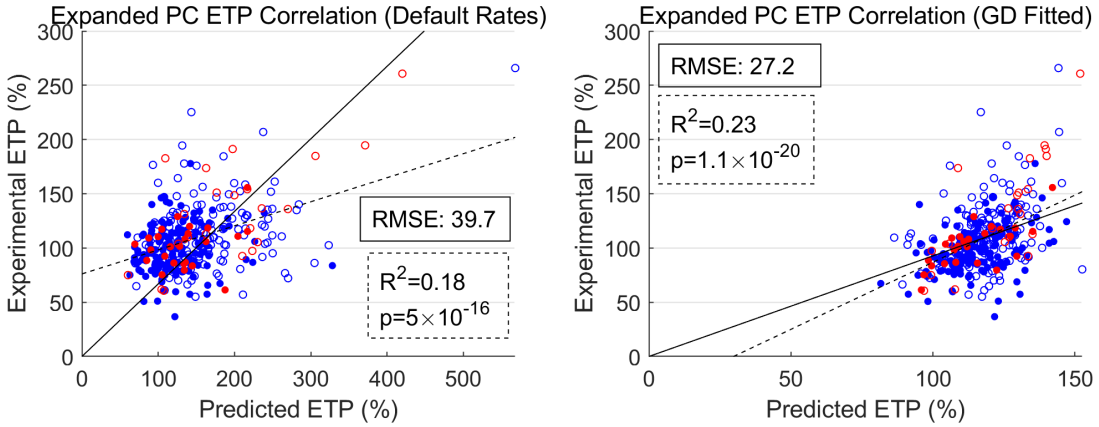

Figure 3.21: The ETP correlation scatter graph for the Expanded Unified Model with Protein C for the default and gradient descent fitted reaction rate sets.

monomer state and stopped from polymerising. This means fibrinogen still has a competitive inhibitory effect on FIIa which may be relevant to include in the model.

The reaction scheme and rates are defined using a model of fibrinogen conversion given in [92]. This model has then been reduced to remove polymerisation, with the final form of the reactions added to the Expanded Unified Model given in Table 3.14.

Fibrinogen concentration is measured on an individual level in g/L. This is converted into moles using a molecular weight of 340kDa [111]. For the pooled plasma simulation, a fibrinogen concentration of $8.65 \times 10^{-6} M$ is used (the average concentration across all individuals).

The thrombin generation curves, ETP correlation scatter graphs, and ETP correlation metrics are given in Figure 3.24, Figure 3.25, and Table 3.15, respectively. The thrombin generation curves still present a delayed lagtime when using the default rates which is then fixed by gradient descent. The model performance

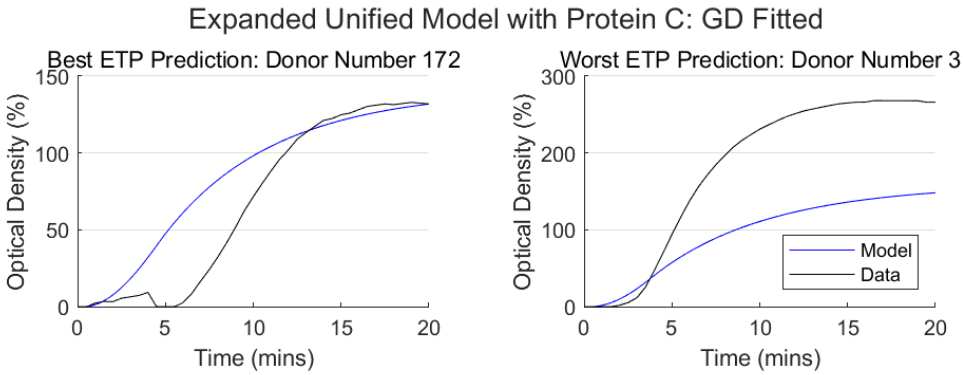

Figure 3.22: The Expanded Unified Model with Protein C predicted OD curve and the experimental OD curve for the individuals with the best and worst predicted ETP for the gradient descent fitted rates.

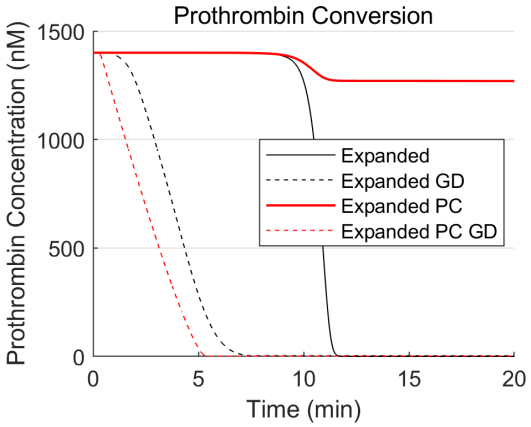

Figure 3.23: Plots of prothrombin conversion for the Expanded Unified Model (black) and Expanded Protein C Model (red), with the corresponding default (solid) and gradient descent (dashed) reaction rates.

Reaction	Rates
Fbg + IIa $\leftrightarrow$ Fbg:IIa $\rightarrow$ Fbn1 + FPA	$K_m = 7.2 \times 10^{-6} M, k_{cat} = 84 s^{-1}$
Fbn1 + IIa $\leftrightarrow$ Fbn1:IIa $\rightarrow$ Fbn2 + FPB	$K_m = 7.5 \times 10^{-6} M, k_{cat} = 7.45 s^{-1}$
Fbn2 + IIa $\leftrightarrow$ Fbn2:IIa	$K_d = 1 \times 10^{-5} M$

Table 3.14: The additional reactions to include fibrinogen and fibrin into the Expanded Unified Model.

metrics are similar to those seen in the Expanded Unified Model with a cost reduction from 321.0 to 169.6.

Figure 3.26 shows the OD curves for the individuals with the best and worst ETP predictions. The best predicted individual is an almost perfect match, with only a slightly shorter lagtime in the model. The lagtime is also slightly shorter, but still close, in the worst individual.

	Fitting Method	R^2	RMSE_{fit}	$\text{RMSE}_{1:1}$	Cost
Fibrinogen Unified Model	No fitting	0.20	27.46	30.2	321.0
	Gradient Descent	0.24	26.90	28.9	169.6

Table 3.15: The predictive accuracy of the Expanded Unified Model with fibrinogen.

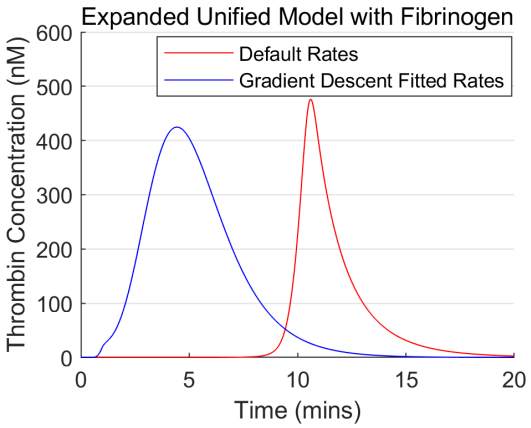

Figure 3.24: The thrombin generation curves for the default and gradient descent fitted reaction rates for the Expanded Unified Model with Fibrinogen.

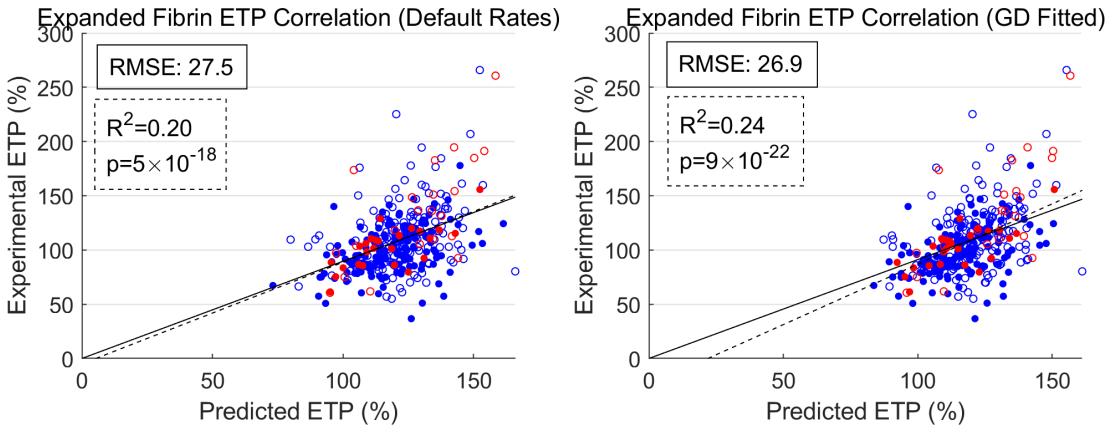

Figure 3.25: The ETP correlation scatter graph for the Expanded Unified Model with Fibrinogen with the default and gradient descent fitted reaction rates.

3.3.7 Lagtime

The different versions of the Unified Model have consistently predicted a long lagtime, which is then fixed through fitting. For the original Unified Model, this was fixed by increasing or decreasing reaction rates far outside of a biologically relevant range. This section investigates which components of the coagulation cascade result in the long lagtime and investigates if the reaction rates they correspond to are known accurately.

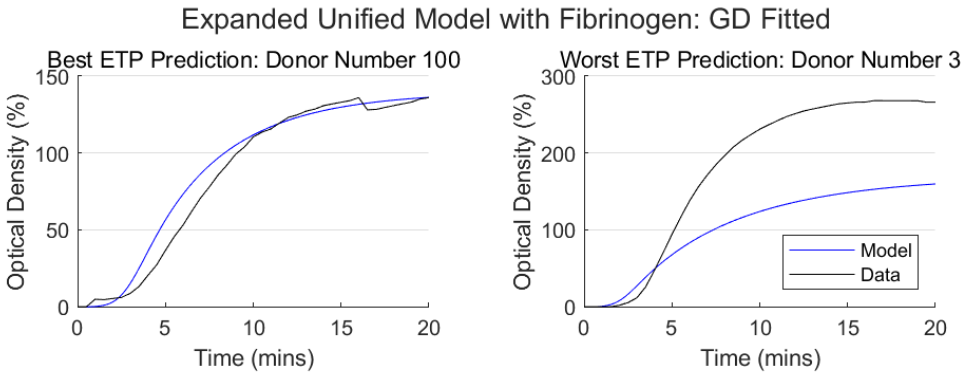

Figure 3.26: The Expanded Unified Model with Fibrinogen predicted OD curve and the experimental OD curve for the individuals with the best and worst predicted ETP for the gradient descent fitted rates.

Which Factors are Slow to Activate?

Figure 3.27 gives time course plots (on a log scale) of the coagulation factors that control the lagtime (grey). There is a rapid burst for TF:VIIa and FXa initially with another burst once significant amounts of thrombin are produced. The lagtime of this system is around 9 minutes. Prior to this, the is a long period of exponential growth from around 1 minute until 10 minutes (straight line on the log plots). Since this is the shape we expect from a simple feedback loop between FVa and FIIa, it seems likely there are no other factors producing significant effects on FVa or FIIa. Since the lagtime is marked by reaching a specific FIIa concentration, and we think the main thing driving the FIIa concentration are FIIa itself, FVa and Xa:Va then it seems reasonable to conclude that if we want to reduce the lagtime, either one of FIIa, FVa, Xa:Va need to start the feedback at higher concentrations, or the feedback needs to be stronger (larger gradient).

A larger initial value of FXa, hopefully leading to a larger value of Xa:Va at 1 minute in at the start of the feedback. A larger gradient would be a result of stronger feedback, so either a greater rate of activation of FV by FIIa or FII by Xa:Va.

The reaction rates for FIIa action of FV and Xa:Va activation of FII are known very accurately with many sources measuring them and identifying similar values in each of the sources. This suggests that any inaccuracies should lie in the amount of FIIa activated by FXa in the initial burst.

Fitting for Realistic Lagtime

To investigate whether a model can fit with realistic values (within the central 90% of the prior distributions) for all reaction rates, the original Unified Model is fitted using gradient descent and upper and lower bounds on all reaction rates are stipulated at the 5th and 95th percentiles of their corresponding prior distribution. The cost improves from 291.3 to 172.8 and the quality of fit appears similar to the

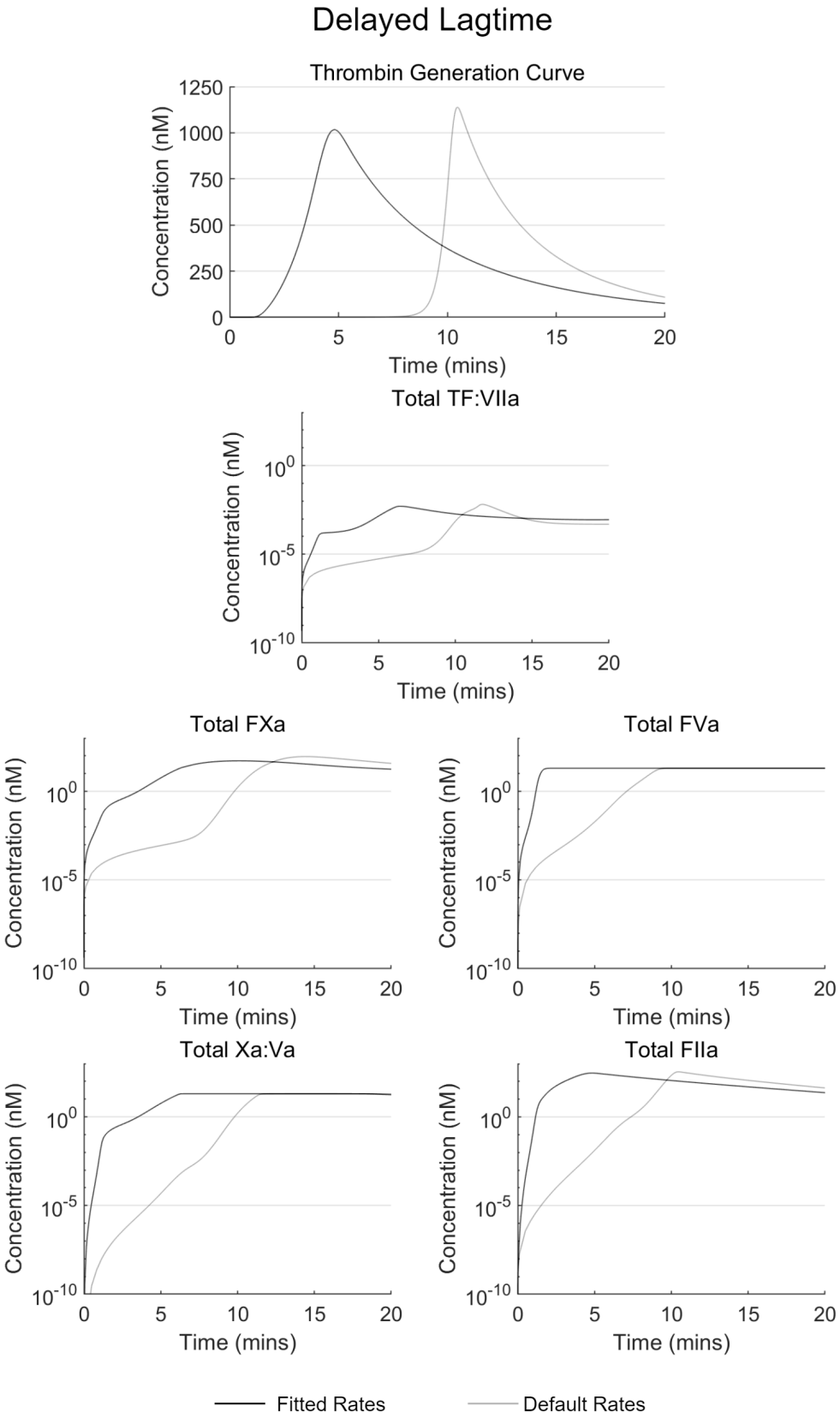

Figure 3.27: Plots of the total levels of the coagulation factors TF:VIIa, FXa, FVa, Xa:Va and FIIa found from the original Unified Model with its default and fitted reaction rates (fitted as described in Section 3.3.7) in grey and black, respectively.

fittings performed previously.

Figure 3.27 also shows the concentration plots after fitting (black). There is a decrease in lagtime given in the thrombin generation curve that aligns with more significant amounts of FXa produced in the initial burst. The three reaction rates k_{cat} for TF:VII activation by FXa, K_m for FX activation by TF:VIIa, and inhibition of FIIa by AT were fitted to be very close to their upper or lower bounds suggesting either the reaction rates for these reactions have poor accuracy in the sources or the reactions involving TF:VIIa and FXa are not properly captured by the model. The sources for FX activation by TF:VIIa are very consistent with one another. There are only two rates for TF:VII activation by FXa which disagree by several orders of magnitude (both present similar values for $\frac{k_{\text{cat}}}{K_m}$ suggesting the overall rates of activation will be similar but with differences in the strength of the binding for activation). As such, it seems likely that a poor understanding of this reaction rate is the cause of the long lagtime in the default reaction rates.

3.4 Reduced Unified Model

So far we have been unable to find a model that is able to match the data well. To move ahead with future work, however, we still require a model. We will take the Expanded Unified Model with Fibrinogen[§] and perform the model reduction algorithm described in Section 2.7. Specifically, instead of looking at which reactions are significant at various timescales, we will identify reactions which are significant across the full simulation time of 20 minutes and remove any reactions which are never significant in this interval.

The Reduced Unified Model is given in Tables 3.16 and 3.17 (mass action and enzymatic reactions, respectively) and the reactions that were found to be insignificant are given in Table 3.18.

3.5 Conclusions

In this chapter, we built a new mathematical model of thrombin generation, targeted for a specific example of the thrombin generation assay. Unfortunately, we were unable to achieve a significant improvement in model accuracy compared with the previous models (in fact, if the previous models undergo similar fitting, then they achieve similar results; Section 3.3.3). We then constructed another version of this model, testing various hypotheses. We were able to show the fitting process is robust against over-fitting (Table 3.4) and experimental noise (Section

[§]Protein S has been removed and the TFPI module reactions were reverted back to the original form used in the first Unified Model as the assumption of TFPI and PS having similar on and off rates as that of PS and PC seems too strong (all TFPI and PS quickly bind at the start and no TFPI is left unbound from PS). Unless an accurate measurement of the K_d between TFPI and PS can be made it seems as though this more complex form of the TFPI module cannot be used.

Reaction	K_d (M)	k_+ $(M^{-1}s^{-1})$
TF + VII $\leftrightarrow$ TF:VII	2.95×10^{-9}	1.26×10^{5}
TF + VIIa $\leftrightarrow$ TF:VIIa	3.16×10^{-9}	1.29×10^{5}
TF:VIIa + AT $\rightarrow$ TF:VIIa:AT	-	9.55×10^{2}
Xa + Va $\leftrightarrow$ Xa:Va	1.78×10^{-10}	1.58×10^{9}
Xa + AT $\rightarrow$ Xa:AT	-	1.82×10^{3}
Xa:Va + AT $\rightarrow$ Xa:AT + Va	-	1.07×10^{3}
IIa + AT $\rightarrow$ IIa:AT	-	6.17×10^{3}
XIa + AT $\rightarrow$ XIa:AT	-	3.98×10^{2}
IXa + VIIIa $\leftrightarrow$ IXa:VIIIa	1.62×10^{-9}	1.00×10^{7}
IXa + AT $\rightarrow$ IXa:AT	-	4.90×10^{2}
IXa:VIIIa + AT $\rightarrow$ IXa:AT + VIIIa	-	4.90×10^{2}
Xa + TFPI $\leftrightarrow$ Xa:TFPI	9.33×10^{-11}	3.80×10^{6}
TF:VIIa + Xa:TFPI $\leftrightarrow$ TF:VIIa:Xa:TFPI	1.51×10^{-10}	8.91×10^{6}
TF:VIIa + Xa $\leftrightarrow$ TF:VIIa:Xa	8.64×10^{-7}	2.20×10^{7}
IIa + a1AT $\rightarrow$ IIa:a1AT	-	78.3
Xa + a1AT $\rightarrow$ Xa:a1AT	-	262
Xa:Va + a1AT $\rightarrow$ Xa:a1AT + Va	-	262
XIa + a1AT $\rightarrow$ XIa:a1AT	-	66.7
XIa + a2AP $\rightarrow$ XIa:a2AP	-	50
IIa + a2M $\rightarrow$ IIa:a2M	-	488
XIa + PAI1 $\rightarrow$ XIa:PAI1	-	2.10×10^{5}
VIIIa $\rightarrow$ $VIIIa_1L$ + $VIIIa_2$	-	5.85×10^{-3}
IXa:VIIIa $\rightarrow$ IXa + $VIIIa_1L$ + $VIIIa_2$	-	1.40×10^{-3}

Table 3.16: The mass action reactions used in the Reduced Unified Model and their corresponding reaction rates.

3.3.2).

Expanding the reaction scheme to include the inhibitors $\alpha_1 - AT$, $\alpha_2 - AP$, $\alpha_2 - M$, and PAI-1 did affect model predictions so should be included in future iterations of the model (Section 3.3.4). It may be the case that patient-specific concentrations of these inhibitors are necessary for an accurate model to be used. We end up testing this in Section 5.6.4.

All forms of the Unified Model, except for that with protein C, predicted total prothrombin conversion. Unfortunately, the inclusion of protein C (through the use of soluble thrombomodulin) significantly weakened model accuracy and, if the model were to predict partial prothrombin conversion, would produce ETP which was significantly more correlated with the protein C concentration than the data suggests (Section 3.3.5). It appears unlikely that protein C is the cause for the partial prothrombin conversion in the assay.

Inclusion of fibrinogen in the model produced different predictions compared with its exclusion, suggesting its competitive inhibitory effects are significant in their effect on model output and fibrinogen should be included in future iterations

Reaction	K_m (M)	k_{cat} (s^{-1})
VII $\overset{Xa}{\rightarrow}$ VIIa	1.20×10^{-6}	15.1
TF:VII $\overset{Xa}{\rightarrow}$ TF:VIIa	1.05×10^{-7}	3.16
VII $\overset{IIa}{\rightarrow}$ VIIa	2.69×10^{-6}	6.17×10^{-2}
TF:VII $\overset{IIa}{\rightarrow}$ TF:VIIa	2.69×10^{-6}	6.17×10^{-2}
VII $\overset{IXa}{\rightarrow}$ VIIa	1.70×10^{-6}	3.24×10^{-1}
TF:VII $\overset{IXa}{\rightarrow}$ TF:VIIa	1.70×10^{-6}	3.24×10^{-1}
X $\overset{TF:VIIa}{\rightarrow}$ Xa	3.16×10^{-7}	6.03
X $\overset{VIIa}{\rightarrow}$ Xa	1.10×10^{-6}	3.24×10^{-4}
X $\overset{IXa:VIIIa}{\rightarrow}$ Xa	8.51×10^{-8}	3.39
X $\overset{IXa}{\rightarrow}$ Xa	7.94×10^{-8}	2.82×10^{-4}
V $\overset{IIa}{\rightarrow}$ Va	7.24×10^{-8}	2.95×10^{-1}
V $\overset{Xa}{\rightarrow}$ Va	1.05×10^{-8}	4.27×10^{-2}
II $\overset{Xa}{\rightarrow}$ IIa	1.32×10^{-6}	9.33×10^{-3}
II $\overset{Xa:Va}{\rightarrow}$ IIa	6.92×10^{-7}	35.5
XI $\overset{IIa}{\rightarrow}$ XIa	5.01×10^{-8}	1.29×10^{-4}
XI $\overset{XIa}{\rightarrow}$ XIa	5.01×10^{-8}	1.29×10^{-4}
IX $\overset{TF:VIIa}{\rightarrow}$ IXa	1.62×10^{-7}	5.37×10^{-1}
IX $\overset{VIIa}{\rightarrow}$ IXa	8.91×10^{-9}	3.63×10^{-5}
IX $\overset{XIa}{\rightarrow}$ IXa	4.17×10^{-7}	7.41×10^{-1}
VIII $\overset{IIa}{\rightarrow}$ VIIIa	2.00×10^{-7}	1.00
VIII $\overset{Xa}{\rightarrow}$ VIIIa	2.00×10^{-7}	2.19×10^{-1}
Substrate $\overset{IIa}{\rightarrow}$ Activated Substrate	1.95×10^{-3}	1.91

Table 3.17: The enzymatic reactions used in the Reduced Unified Model and their corresponding reaction rates.

Insignificant Reactions
VII + TF:VIIa $\leftrightarrow$ VII:TF:VIIa $\rightarrow$ VIIa + TF:VIIa
VIII + IXa $\leftrightarrow$ VIII:IXa $\rightarrow$ VIIIa + IXa
$VIIIa_1L$ + $VIIIa_2$ $\rightarrow$ VIIIa
XIa + C1-inh $\rightarrow$ XIa:C1-inh

Table 3.18: The insignificant reactions removed from the Reduced Unified Model.

of the Unified Model (Section 3.3.6). This happens since thrombin is required to bind to fibrinogen to order to activate it into fibrin. While it is bound, it cannot bind to and activate any other factors, thus acting as a kind of temporary inhibitor.

The default reaction rates produce a large lagtime which is then fixed in fitting. By fitting the Unified Model, with biologically relevant upper and lower bounds, and then investigating plots of the concentration of multiple factors leading up

to the lagtime, we were able to link this long lagtime to the reactions and reaction rates corresponding to the interactions between TF:VIIa and FXa (Section 3.3.7). In particular, we suggest that poor knowledge of the reaction rates for TF:VII activation by FXa is the cause of this long lagtime with the default reaction rates. This modelling work suggests that the K_m values for this reaction should be smaller and its k_{cat} values should be larger than what is observed.

To ascertain where improvements in the model may be most useful, in the following chapters we will perform a stage of data analysis, and then using the results of this data analysis, we will return to build a definitive version of the Unified Model.

Chapter 4

Data Analysis

4.1 Introduction

In the previous chapter, we introduced the Unified Model, building multiple versions with different reaction schemes. Unfortunately, we failed to identify a model which would fit the data sufficiently accurately. In this chapter, we perform a stage of data analysis to help explain where the model can be improved. We begin this chapter with functional data analysis, exploring both principal component analysis and data clustering. Following this, we identify which variables are most closely linked with model error. We also compare the correlation of different variables between model predictions and experimental data, aiming to identify which variables may be able to be linked to an increase in predictive power. Finally, we answer some questions that arise from these analyses such as differing effects between endogenous and exogenous TF and the possibility of filtering the data to improve the fitted model accuracy.

4.2 Functional Data Analysis

4.2.1 Introduction

To begin our functional data analysis, we first find a functional representation of the OD curves in the form of a linear combination of a set of basis functions. The resulting curves can then be differentiated to find functional representations of the thrombin generation curves. We then investigate properties of these thrombin generation curves using Principal Component Analysis and k-means clustering.

4.2.2 Curve Smoothing

To convert the measured OD curve values (recorded every 30 seconds during the 20-minute assay) into a single smooth curve, we first define a set of basis functions. We will use quartic splines as the set of basis functions as they will grant us smooth cubic splines for the final thrombin generation curves. The curve smoothing is performed in the fda [112] package in R. The quartic splines used for the basis functions are defined using 21 knots (placed at one minute intervals) for a

total of 24 basis functions, plotted in Figure 4.1. In addition to fitting to the experimental data, the curve smoothing process uses a roughness penalty, given as the square of the third derivative (curvature of the thrombin generation curve). This roughness penalty helps to minimise over-fitting that would result in noisy oscillations in the thrombin generation curves. Additionally, the curve fitting makes use of linearly decreasing weights, from 21 to 1, applied to the data points which emphasise the lagtime that is otherwise poorly matched to favour smoother curves.

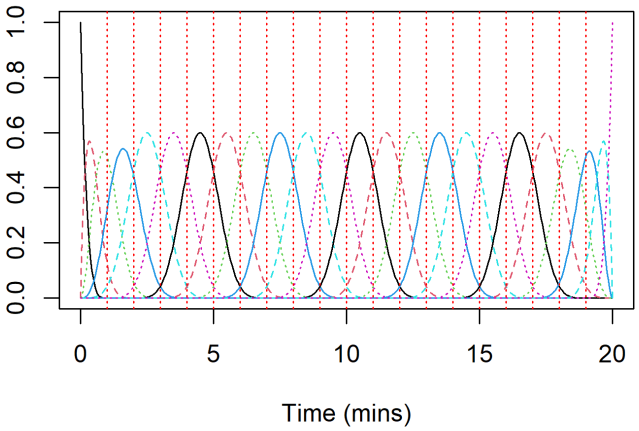

Figure 4.1: A plot of the 24 quartic splines that make up the set of basis functions.

Figure 4.2 shows the OD data before smoothing while Figure 4.3 contains a plot of the smoothed OD curves with the mean OD and its 95% confidence interval marked. We now take the derivative of these smoothed curves to investigate the thrombin generation curves, plotted in Figure 4.4.

There is a lot of variation between the thrombin generation curves, in particular there appears to be substantial amounts of thrombin present initially. This does not appear as clearly in the OD curves (present as an initial positive gradient) and is likely just a result of experimental noise in the early stages of the assay.

Additionally, some smoothed thrombin generation curves show negative concentrations. This comes from the raw OD data being noisy and therefore not monotonically increasing. While the fda package we use for the smoothing does allow us to constrain the smoothing to be monotonic through a transform on the linear combination of basis functions, and therefore force positive thrombin concentrations, it is not possible to perform principal component analysis on the resulting transformed smooth curves in the fda package [112]. The same applies if the smoothing was constrained to force an initial gradient of zero in the OD curves (which would ensure the thrombin generation curves start at zero).

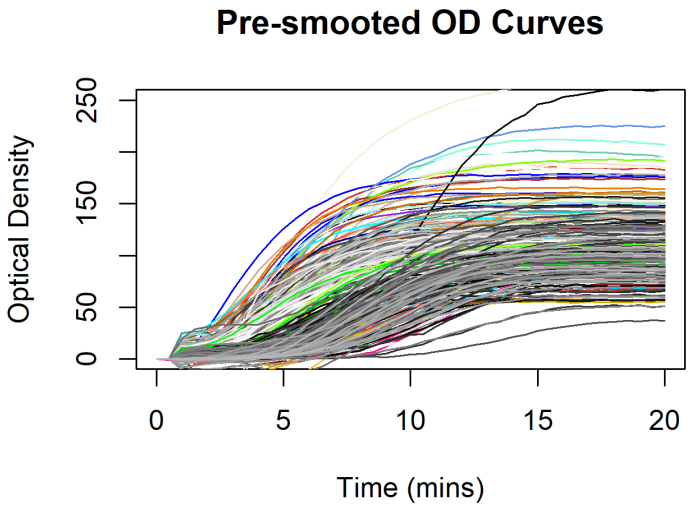

Figure 4.2: The OD curves for all patients before smoothing.

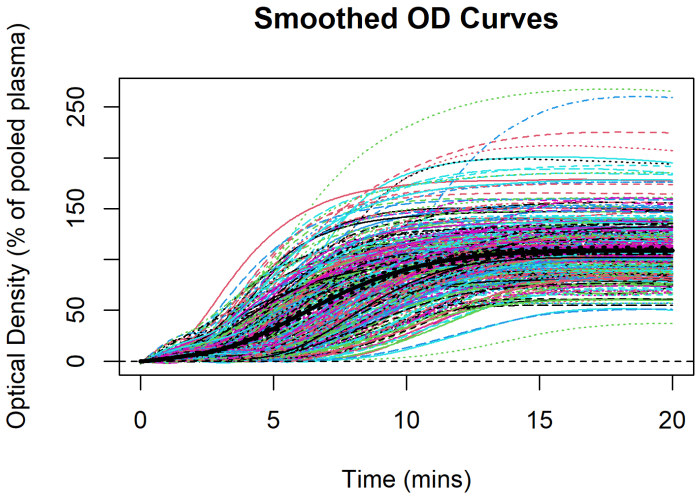

Figure 4.3: The smoothed OD curves for all patients. The mean (solid) and its 95% confidence interval (dashed) plotted in black.

4.2.3 Principal Component Analysis

We have performed Functional Principal Component Analysis on the thrombin generation curves to better understand their distribution. This is done using the same fda package in R (using the function pca.fd), which is applying a standard PCA algorithm to the basis coefficients but with adjusted weights to account for the shape and overlap of the basis functions. The four principal components (that explain 95% of the variance) are given in Figure 4.5. We have then performed a Varimax rotation (this provides components that explain the same amount of total variation but focuses the variation onto a smaller time interval at the cost of the components becoming correlated) in order to better identify which summary statistics produce the most variation in Figure 4.6.

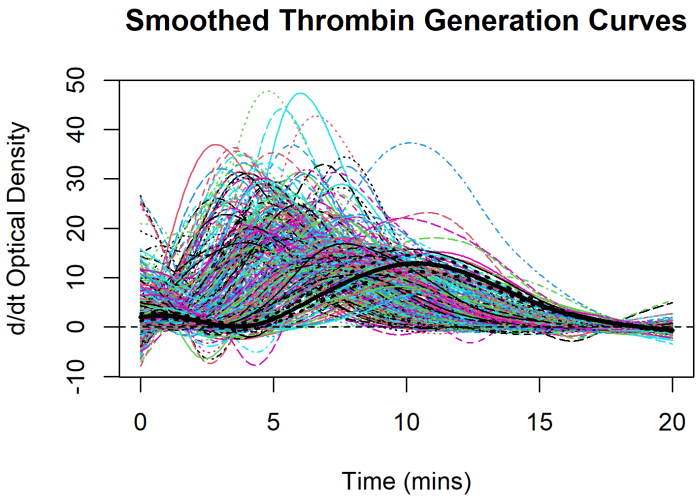

Figure 4.4: The smoothed thrombin generation curves with the mean and its 95% confidence interval plotted in bold.

The effects of the principal component directions can be seen by where the perturbed curves deviate most from the mean curve. The first principal component demonstrates how rapid the activation is and influences ttP, lagtime and peak. The second principal component seems more closely related to total activation capacity and influences peak and ETP. The third principal component controls how wide the curve is and influences the two gradient summary statistics of maximum increasing rate and minimum decreasing rate. The fourth principal component influences the appearance of an early peak. It is useful to know that this early peak is uncorrelated from the majority of the rest of the curve with only a small correlation with ttP. The Varimax transformed curves show similar effects with the summary statistics.

4.3 Clustering

4.3.1 Introduction

To further understand the distributions in the data, we performed k-means clustering on the factor levels (TF, FII, FV, FVII, FVIII, FIX, FX, FXI, TFPI, AT, protein C, protein S, vWF and fibrinogen) and the thrombin generation curves (represented as summary statistics, basis coefficients, and principal component scores), aiming to find groups of individuals, who can be identified either from the concentration data or their thrombin generation curves, who are accurately predicted by mathematical models, possibly pointing in the direction where the greatest improvement in accuracy can be found.

There are a few predefined groups in the PRAMIS cohort that it is worth remembering for this section. The cohort is already split into cases (who suffered

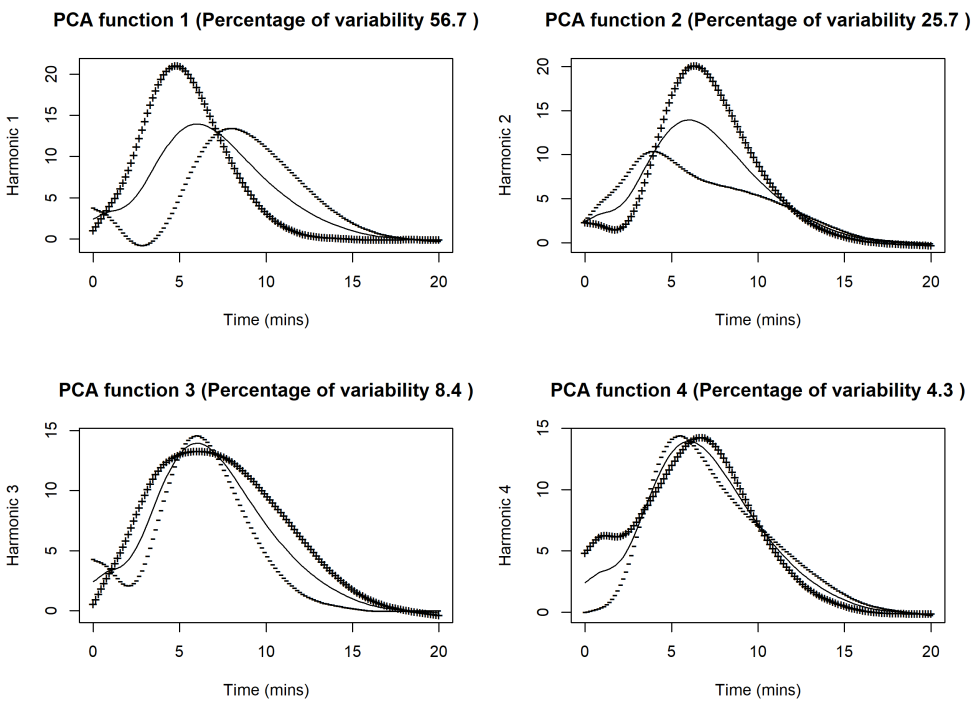

Figure 4.5: Plots of the mean thrombin generation curve (solid), overlaid with the effect of the variation in each of the four principal component directions. + is used to show the effect of perturbing the mean thrombin generation curve by increasing it in the principal component direction while - shows a decrease in the principal component direction. The titles of each subplot show the percentage of the variability that is explained by that principal component.

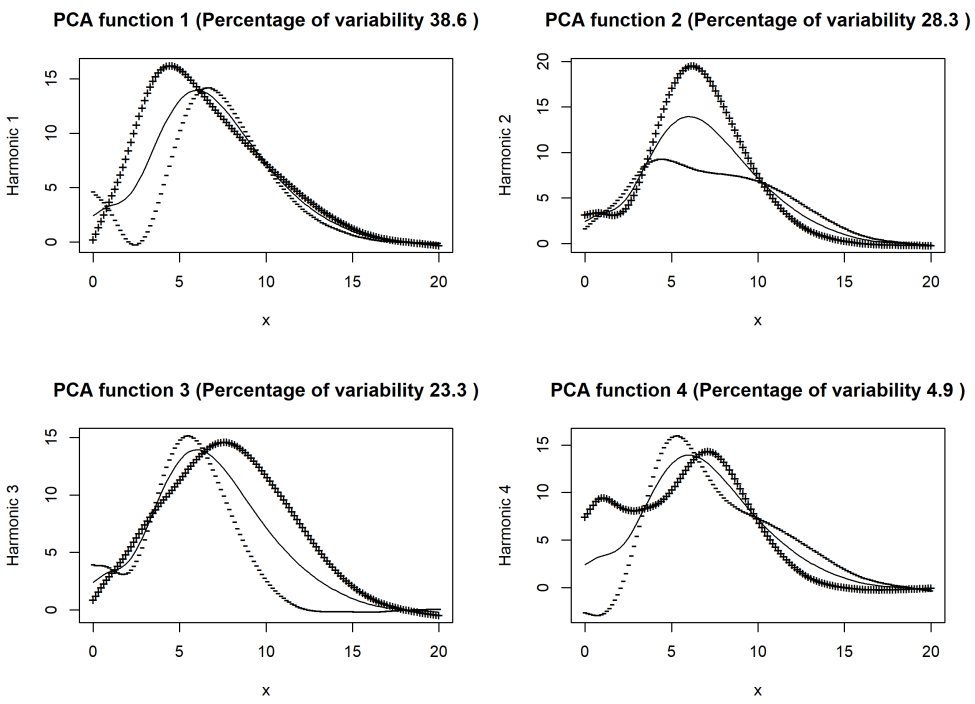

Figure 4.6: Plots of the mean thrombin generation curve (solid), overlaid with the effect of the variation in each of the four Varimax transformed component directions. + is used to show the effect of perturbing the mean thrombin generation curve by increasing it in the principal component direction while - shows a decrease in the principal component direction. The titles of each subplot show the percentage of the variability that is explained by that principal component.

a myocardial infarction before the age of 50) and controls (who are age, sex, and smoking status matched to the cases population). Age is similar among the whole cohort (mean of 47 years, standard deviation of 6 years) but other demographics, such as sex (86:14, male:female), will still separate individuals into predefined groups. These groups are significantly different in ETP [21], but we believe this should be entirely explained by their differences in coagulation factor concentrations. The proteins themselves should be identical between individuals.

Definitions of Summary Statistics

Before we begin the clustering, we first define the summary statistics for the functional representations of the thrombin generation curves. Since many thrombin generation curves are initially non-zero (sometimes quite significantly), there are issues trying to define the lagtime as there may be no time point such that the value of the curve is below 5%. In addition, there are some curves where the peak height is at, or close to, the start of the curve. Due to these issues, it is necessary to give clear definitions of peak, ttP and lagtime. Peak and ttP both use the global maximum, regardless of its location. Lagtime is defined as the first time with a thrombin concentration = 5% of the peak height, and if there is no such value, or the value is larger than the ttP, then the lagtime is reported as missing.

4.3.2 Gap Statistic

In order to assess whether or not clusters are present in the data and if so, the optimal value for k in the k-means clustering, we have used the gap statistic [47]. The gap statistic uses bootstrapping (1000 samples) to determine its standard error which allows us to assess if improvements in the gap statistic from larger values of k are significant. The plots of the gap statistic for values of k between one and ten, along with the optimal value of k, are given in Figure 4.7. The optimal value of k is chosen as the smallest value of k such that its gap statistic is within one standard error of the gap statistic at the first local maximum.

For the initial conditions, summary statistics, and PCA scores, there are no significant clusters ($k = 1$ is optimal). However, when clustering using the basis coefficients, there is a clear set of seven clusters.

4.3.3 Thrombin Generation Curve Clusters

We now investigate the differences between these seven clusters defined by the thrombin generation curve basis coefficients. The mean values of the summary statistics in each cluster, as well as the mean thrombin generation curves for each cluster, are used to determine names for each of the clusters. The names, reasoning behind the names and the size of each cluster are given in Table 4.1. The mean values for each summary statistic, split by cluster, are given in Table 4.2. Finally, plots of the thrombin generation curves in each cluster, the raw OD data (before smoothing) in each cluster, and the mean curves for each cluster are given

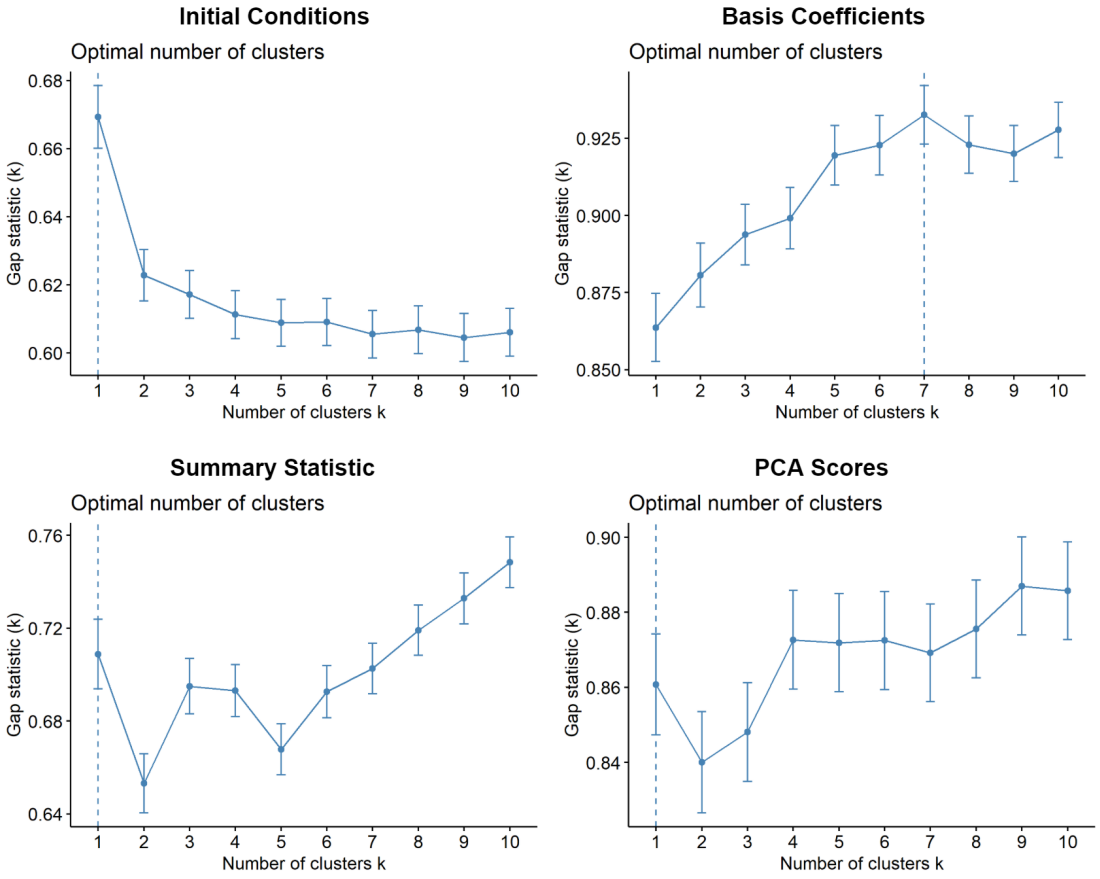

Figure 4.7: Plots of the gap statistic for clustering the initial conditions and the thrombin generation curve summary statistics, basis coefficients and principal component scores. The dashed vertical line shows the optimal number of clusters.

in Figures 4.8, 4.9 and 4.10, respectively.

Most of the clusters feature clear differences from the average in some summary statistics giving them obvious names (Big, Quick, Small, No Lag and Late Peak). However, the Double Bump cluster is instead named due to the shape of its thrombin generation curves which appear to show a high initial thrombin concentration that subsequently decreases before then giving a normally shaped curve. This is likely due to the initial OD reading at $t = 0$ being low due to experimental noise, resulting in an initial positive gradient in the OD curve as it returns to normal. Although the majority of the curve is likely still accurate, it may be the case that this shape interferes with the fitting process as it produces curves that the models are unable to reproduce.

Looking at the OD data before smoothing in Figure 4.9 appears to confirm this conclusion. While the artefacts, such as double bumps, are not a result of the smoothing process, they are exaggerated by it. This means that when fitting to the OD data, they likely have little influence.

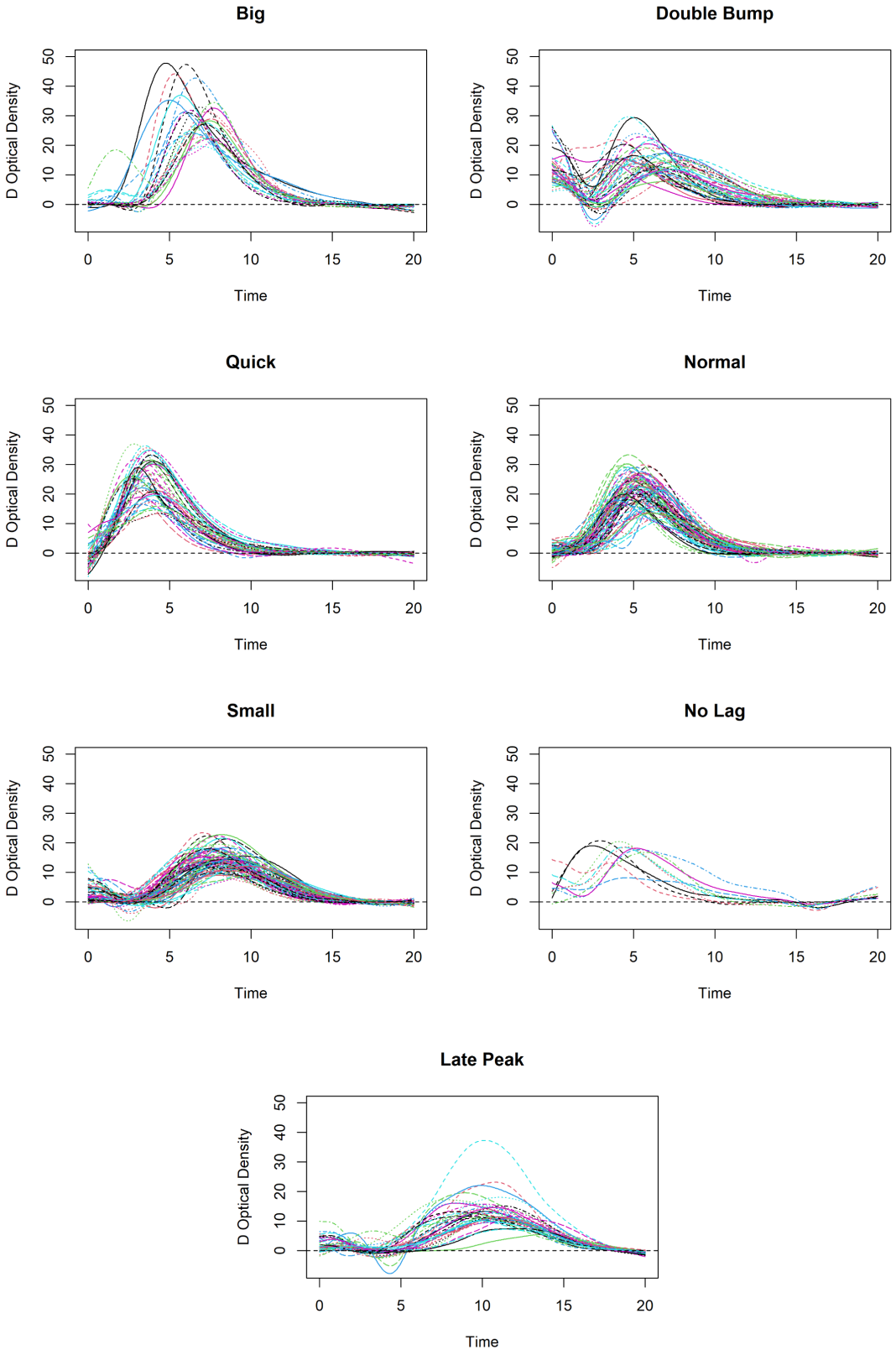

Figure 4.8: All thrombin generation curves, separated into the seven clusters.

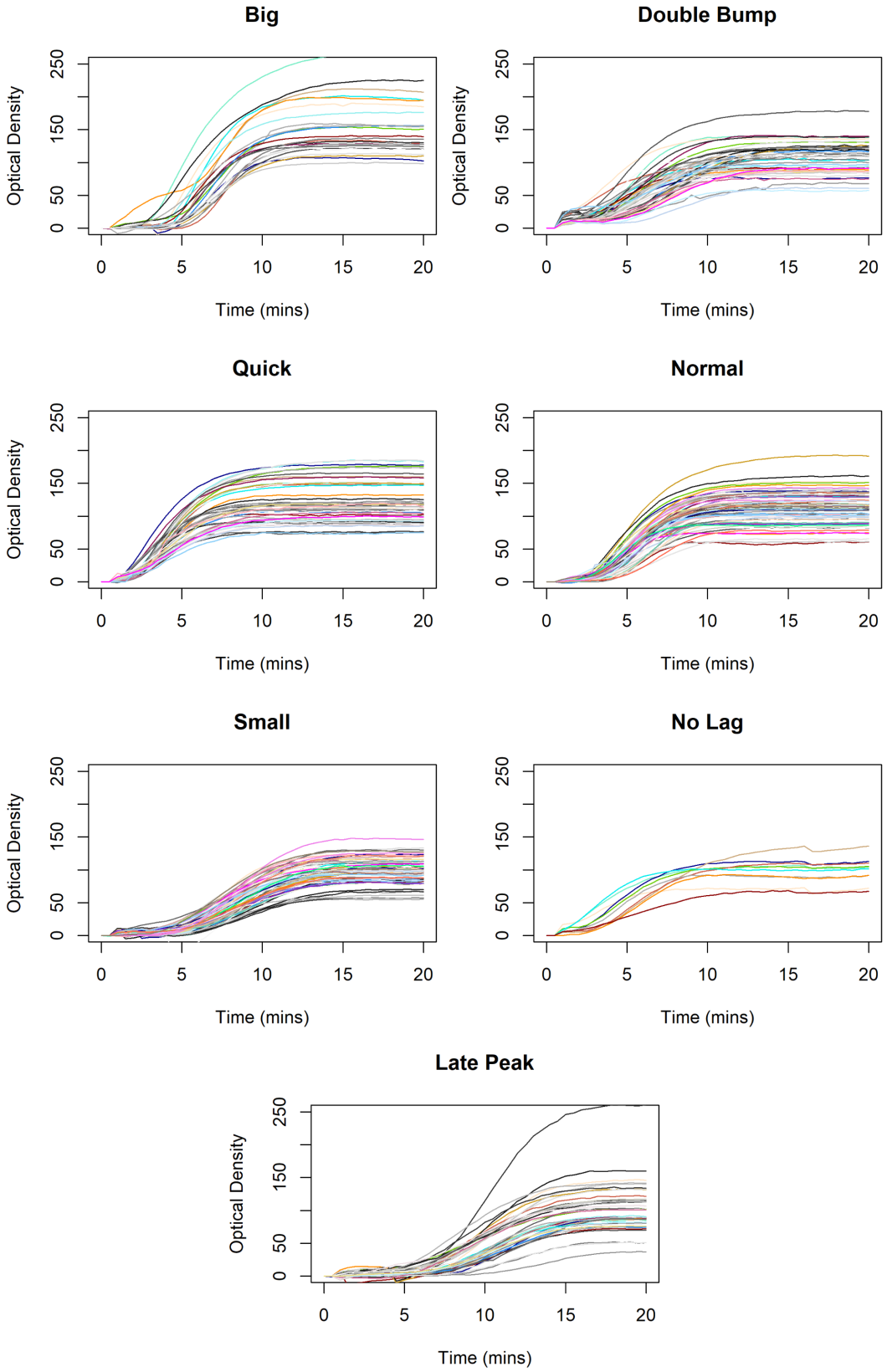

Figure 4.9: The raw OD curves (before smoothing), separated into the seven clusters.

Cluster Names	Name Reasoning	Cluster Size
Big	Largest ETP, Peak, Max Inc Rate and Min Dec Rate	25
Double Bump	Summary statistics appear normal, name from thrombin generation curves	45
Quick	Smallest Lagtime and ttP	45
Normal	Summary statistics appear normal, name from thrombin generation curves	81
Small	Smallest ETP (fairly small Max Inc Rate and Min Dec Rate)	86
No Lag	All bar one lagtime value is missing due to large initial value	10
Late Peak	Largest Lagtime, ttP. Smallest Peak, Max Inc Rate and Min Dec Rate	41

Table 4.1: The names given to identify each cluster, the reasons for each name and the size of each cluster.

Cluster	ETP	Lagtime	Peak	ttP	Max Inc Rate	Min Dec Rate
Big	150.8	2.40	31.0	6.68	13.5	8.5
Double Bump	106.0	3.33	17.4	4.47	6.6	6.8
Quick	120.3	0.47	25.2	3.66	11.8	6.7
Normal	109.9	1.05	21.8	5.32	8.8	6.0
Small	96.0	2.42	14.5	7.92	4.9	3.6
No Lag	100.0	0.52	17.3	3.94	7.0	4.0
Late Peak	102.2	3.80	13.5	10.31	4.0	3.4

Table 4.2: The mean summary statistics for each cluster.

4.3.4 ANOVA and Between Cluster Differences

To understand the possible influences in the different thrombin generation curve shapes, we have used ANOVA and Fisher's Exact Test to test significance between cluster means. The variables used in the ANOVA are the concentrations of FII, FV, FVII, FVIII, FIX, FX, FXI, TF, TFPI, AT, protein C, protein S, fibrinogen, and vWF; the age of each individual; the absolute value of the Unified Model's ETP error for that individual (with and without GD); and an estimate of the pooled plasma ETP that was used to normalise the sample. The categorical variables that used Fisher's Exact Test were Event and Sex. Further details of these variables can be found in Table 4.5. The variables that were found to be significant, and their corresponding p-values, are given in Table 4.3.

One of the assumptions of the ANOVA method is that the data must be normally distributed. While this is true for the majority of these variables, there are a handful, such as the TF concentration, for which this is not true (see Figure 1.6). However, since this is restricted to only a few variables, ANOVA is generally robust against violations to the normality assumption [113], and the resulting p-

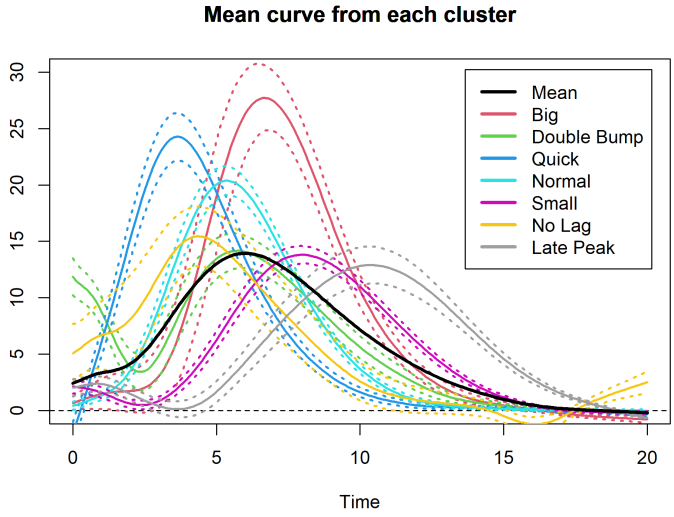

Figure 4.10: The mean thrombin generation curves, and their 95% confidence intervals, for each cluster.

values are of less importance here than the relative significance between variables (since we are looking to identify which variables are most different between the clusters), we believe an ANOVA will suffice for our purposes.

Variable	p-value
FII	0.0028
FVIII	6.7e-6
FIX	0.0027
FX	0.0066
FXI	0.025
TF	0.00012
Fibrinogen	0.00097
vWF	0.019
Unified Model error	2.8e-5
Unified Model error (GD)	3.4e-5
pooledOD.ETP	2.8e-6
Event	0.00022
Sex	0.00027

Table 4.3: The variables with a significant difference in means between the clusters and their corresponding p-values.

The Normal cluster gives significantly lower absolute model ETP error than the other clusters with the Late Peak and Big clusters having the highest error. The Big cluster features very high levels of all of the significant factor levels. FVIII appears to be a very big influence in the size and shape of the thrombin generation curves, being highest in the Big, Quick and No Lag clusters and lowest in the Small cluster. We have seen previously that the size and shape of model predicted

Variable	Cluster Means						
	Big	Double Bump	Quick	Normal	Small	No Lag	Late Peak
FII (%)	133	118	121	120	120	124	126
FVIII (%)	160	134	161	142	117	173	127
FIX (%)	139	124	130	120	122	135	131
FX (%)	139	130	133	126	131	146	137
FXI (%)	112	107	105	101	99	117	105
TF (pM)	17.3	9.8	11.0	10.1	8.9	7.7	7.8
Fibrinogen (g/L)	3.61	3.06	3.06	2.89	2.78	2.98	2.98
vWF (%)	123	102	111	105	96	94	105
Unified Model error	30.0	20.3	22.0	15.8	26.5	22.8	34.9
Unified Model error (GD)	30.0	19.8	21.8	15.6	26.1	23.1	34.5
pooledOD.ETP	57.4	45.3	53.5	55.7	53.8	46.5	50.2
Control Percentage (%)	16	51	36	59	64	40	51
Female Percentage (%)	24	11	20	23	5	30	2

Table 4.4: The mean values of variables that are significantly different between the clusters. Details on each of the variables are given in Table 4.5.

thrombin generation curves are heavily dependent on activation of FIX. It may be the case that FVIII is a more limiting factor in IXa:VIIIa formation that the models would suggest.

4.4 Model Error Analysis

4.4.1 Introduction

In this section, we aim to identify the individuals that the model predicts poorly and explore the variables that are the most influential in determining model accuracy. To achieve this, we construct a regression tree to predict model error.

4.4.2 Regression Tree

The regression tree is trained using the variables listed in Table 4.5 and aims to predict absolute model error from the Unified Model (using the default rates). We use absolute error rather than square error as we want to be able to more closely separate smaller errors rather than larger ones. The resulting regression tree is then presented in Figure 4.11.

Three variables seem to stand out quite strongly in their effect on model error. The most important separation the regression tree makes is the distinction between samples with or without added TF. Of the samples with added TF (the choice that gave the lower error), the next check is that the ETP of the pooled OD

Variable	Details
TF.tot	Initial total TF concentration in pM, including both endogenous TF and added exogenous TF.
FII	Initial individuals FII concentration in % of pooled plasma.
FV	Initial individuals FV concentration in % of pooled plasma.
FVII	Initial individuals FVII concentration in % of pooled plasma.
FVIII	Initial individuals FVIII concentration in % of pooled plasma.
FIX	Initial individuals FIX concentration in % of pooled plasma.
FX	Initial individuals FX concentration in % of pooled plasma.
FXI	Initial individuals FXI concentration in % of pooled plasma.
TFPI	Initial individuals TFPI concentration in Units.
AT	Initial individuals AT concentration in % of pooled plasma.
ProteinC	Initial individuals protein C concentration in % of pooled plasma.
ProteinS	Initial individuals protein S concentration in % of pooled plasma.
vWF	Initial individuals von Willebrand Factor concentration in % of pooled plasma.
Fibrinogen	Initial individuals Fibrinogen concentration in g/L.
CRP	Health related measure. C-reactive protein concentration in mmol/L. High levels are an indicator of recent injury.
LDL	Health related measure. Low density lipoprotein concentration in mmol/L.
HDL	Health related measure. High density lipoprotein concentration in mmol/L.
Age	Age of the individual in years.
Sex	Binary representation of the sex of each individual. 1=Male, 2=Female.
Event	Binary representation of whether an individual was a case or control, ie. whether or not the individual suffered a MI before the age of 50. 1=Case, 2=Control.
addedTF	Binary representation of whether or not that thrombin generation assay used an additional 5pM of exogenous TF.
pooledOD.ETP	An estimate of the pooled plasma ETP that was used to normalise the sample.

Table 4.5: The variable names and further details on their definitions and purpose.

was not large (typical range of 40-60, split at <68), a possible anomaly in the data. If a sample was compared against an artificially raised pooled OD ETP, through a mistake in the experimental setup, the measured sampled would be reported as lower than it should be (as a percentage of pooled plasma). Finally, the average absolute error reduces again if we remove the samples with a high prothrombin concentration (remove those with FII>143%). Average absolute error decreases from 27 to 21 for the samples measured with added TF, at an average pooledOD.ETP (typical range of 40-60), and at an average FII concentration. There are 310 samples (53%) that satisfy all three of these conditions. It is interesting to

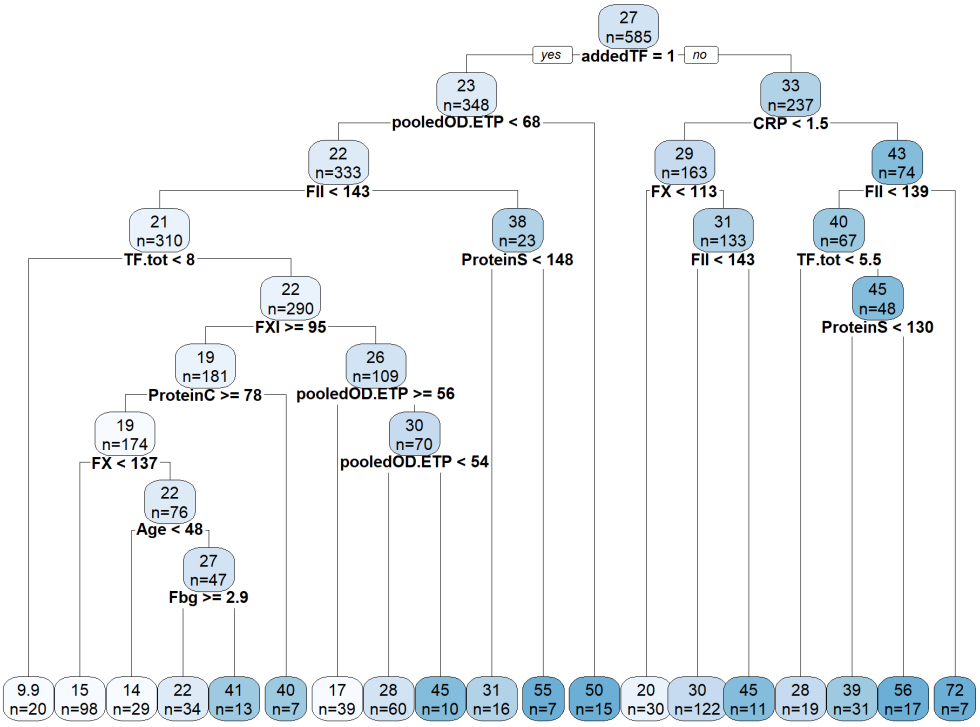

Figure 4.11: The regression tree fitted to predict absolute model error (Unified Model without fitting). Each cell shows the average absolute model error of the samples that satisfy its requirements as well as the number of samples n.

note that it is the addition of exogenous TF that separates the groups rather than total TF concentration. It may be the case that there is differing effects between the endogenous and exogenous TF.

4.5 Side by Side Factor Correlations

The clustering showed us that FVIII is influential in the magnitude of thrombin generation, however the previous models suggested that FIX activation is the rate limiting component of IXa:VIIIa formation. It may be useful to compare other factors correlation with both the model predicted ETP and the experimental ETP to identify other areas with similar discrepancies. Plots of ETP (predicted by Unified Model, Unified Model with Gradient Descent and from the data) against various factors are given in Figure 4.12. These plots can tell us which factors differ in importance between the models and the data. For example, if FV is more strongly correlated with the data than with the model predictions, it would suggest the model is missing some interaction involving FV.

It is clear there is more variation in the data that is not present in the predictions of the model. However, there does not appear to be a clear factor which produces this variation in the data. There is a clear correlation in the model with

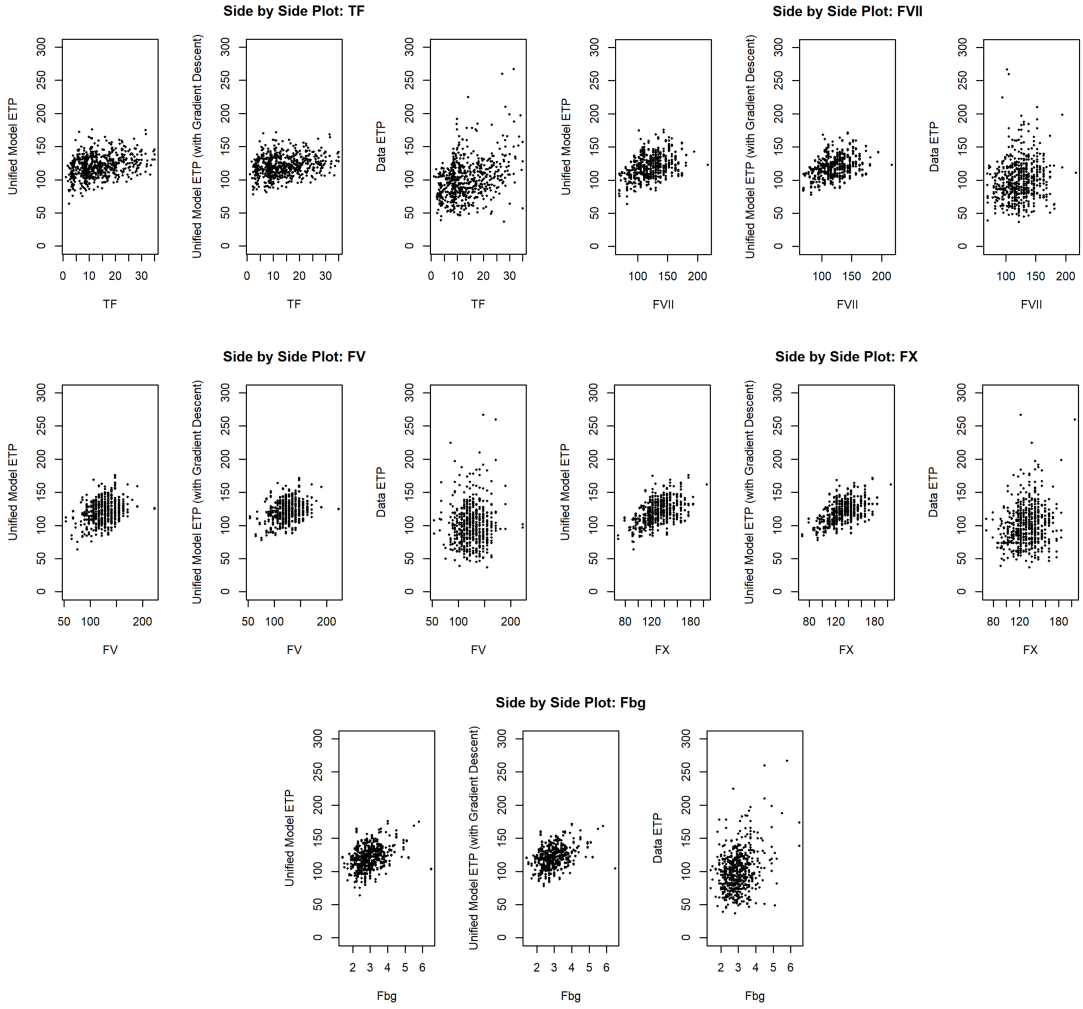

Figure 4.12: Scatter plots of model predicted ETP (Unified Model with and without gradient descent) and data ETP against various factor levels. Each factor, labelled under a heading "Side by Side Plot", has three scatter plots associated with it. The first scatter plot looks at the correlation between the concentration of that factor and the ETP predicted by the Unified Model using the default rates, the second figure uses the gradient descent fitted rates, and the third figure compares the correlation between the concentration of that factor and the ETP given experimentally for that individual.

factor VII concentration that is not present in the data (Figure 4.12, heading "Side by Side Plot: FVII") which could suggest that the assumed FVIIa concentration may not be valid. There are also correlations in FV, FX and fibrinogen that are not present in the data and the correlation with FV appears to be reduced by gradient descent.

4.6 Added TF vs Higher TF

The regression tree trained on model error predicted that whether a sample included the added 5pM of exogenous TF produced the best separation in errors, with the added TF reducing the absolute model error. It is interesting that the additional TF was a more relevant predictor than total TF. This suggests that there may be some difference in adding 5pM of exogenous TF compared with 5pM higher endogenous TF. To assess this, we will compare the mean change in ETP from adding 5pM of exogenous TF with 5pM higher concentration of endogenous TF as predicted through linear regression.

4.6.1 Added TF

The mean change in ETP between the added TF and no added TF groups is 23.99% of pooled plasma (95% CI: 21.18%, 26.80%; measured with a t-test).

4.6.2 Higher TF

To assess the effect of higher levels of endogenous TF, we have trained a simple linear regression model (ETP=m×TF+c) to predict ETP using total TF concentration for the full dataset and the two data cuts of added TF and no added TF. The gradient, and its confidence interval, are then scaled to find the effect of increasing endogenous TF by 5pM on average. These results are given in given in Table 4.6.

Data	Change in ETP from increasing TF (95% CI)
Added TF	6.82% (4.63%, 9.00%)
No added TF	3.73% (1.76%, 5.69%)
Full data	7.01% (5.50%, 8.53%)

Table 4.6: The average change in ETP from increasing TF by 5pM for the 3 data cuts, those measured with the 5pM of added TF, those measured without the 5pM of added TF, and the full dataset.

The exogenous TF clearly has a much larger effect on ETP than the endogenous TF. Since the TF proteins should be identical for endogenous and exogenous TF, there is no clear reason for this difference. It may be an error in the calibration of the TF measurements (either to determine the 5pM or the endogenous TF in a sample) or there may be a difference in the sizes of the phospholipids between that the exogenous and endogenous TF are expressed upon.

4.7 Data Filtering

4.7.1 Introduction

We have seen that model error is significantly different between the thrombin generation curve clusters and that some of the curve clusters represent thrombin generation curves that the models cannot predict (non-zero initial thrombin concentration). The Unified Model may be able to fit better to a subset of the data which do not exhibit these shapes.

4.7.2 Filtering

To filter the data, we first search through the smoothed curves by hand, identifying which curves demonstrate a particular property we are aiming to remove. Once these curves are identified, a measure of this property is defined and the optimal cut-off for this measure is determined using the Gini index. Any curves which are classified differently between the two methods are then investigated again, favouring the results of the cut-off classification unless it is clear that the measure used is unsuitable for that curve.

Mini Peak

First, we aim to remove all thrombin generation curves with either a high initial thrombin concentration or a significant secondary peak. After filtering these curves by hand, the Mini Peak measure is defined as the relative height of the second highest local maximum as a ratio of the global maximum. If only one local maximum is present, then the measure is set to zero.

After the filtering by hand 116 curves have been proposed for removal and the optimal cut-off for removing curves is found to be a second peak larger than 24.5% the height of the largest peak. Using this cut-off would result in 106 curves being removed with fourteen curves being classified differently between the two methods. One of these fourteen curves was not filtered in the computed filtering as it did not completely make a local maximum but was removed by hand. Since the height of this bump is still large enough it was removed. The computed filtering was used for all other curves resulting in the removal of 107 curves.

No Lag

Next, we aim to remove the thrombin generation curves with no delay for the lagtime. The No Lag filtering was done by hand, then an optimal separation was found using the ratio between the initial gradient of the thrombin generation curve and the maximum gradient of the curve.

After filtering by hand, 60 of the remaining curves were proposed for removal. From this, the optimal cut-off was determined as an initial gradient larger than

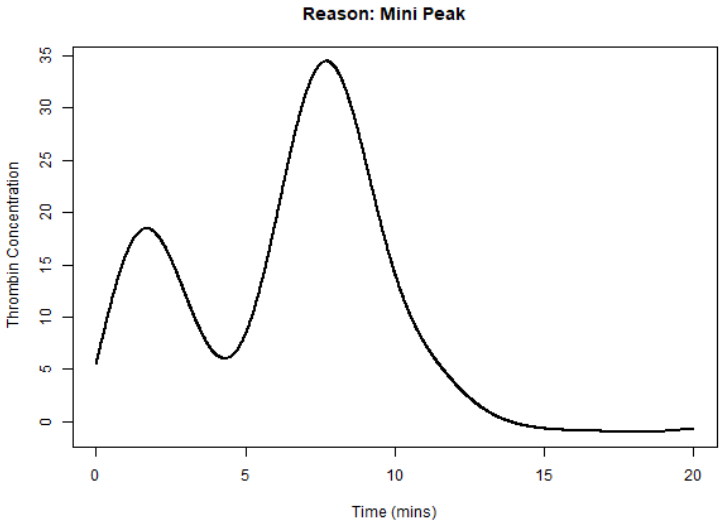

Figure 4.13: An example of a thrombin generation curve that was removed due to the presence of a mini peak.

30.5% of the maximum gradient. This cut-off gives a computed filtering which removes 66 curves with 20 discrepancies between the two filtering methods. In these 20 discrepancies, there were six curves which featured a small insignificant Mini Peak which provided a large enough initial gradient to trigger the computed filtering which have now been kept since they still offer a lagtime prior to large scale thrombin generation. The computed filtering was used for all other curves leading to 60 further curves being removed.

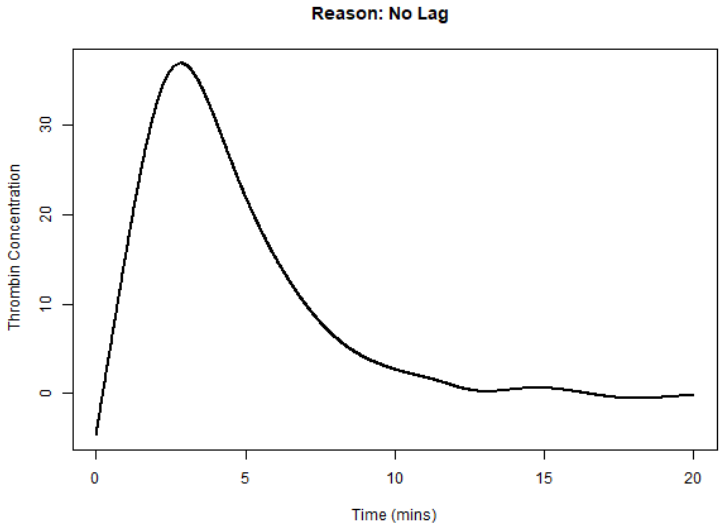

Figure 4.14: An example of a thrombin generation curve that was removed due to the lack of a lag time.

Other

Finally, the remaining curves were investigated by hand to search for any other non-physiological curves that should be removed. A total of fourteen further curves we removed, all of which featured large perturbations to otherwise normal thrombin generation curves.

The results of this data filtering leave 166 of the original 333 thrombin generation curves remaining (Removed curves are in Figure 4.16 and the remaining curves are in Figure 4.17). The demographics of the reduced population are similar to the full cohort (17% female and 51% controls after filtering compared with 14% female and 49% controls for the full cohort). Although this filtering does remove a significant portion of the data, there should still be a sufficient number of curves remaining for fitting. Additionally, if there is improvement seen in the fitting then we can investigate either a less stringent filtering or data cleaning to retain some of the curves.

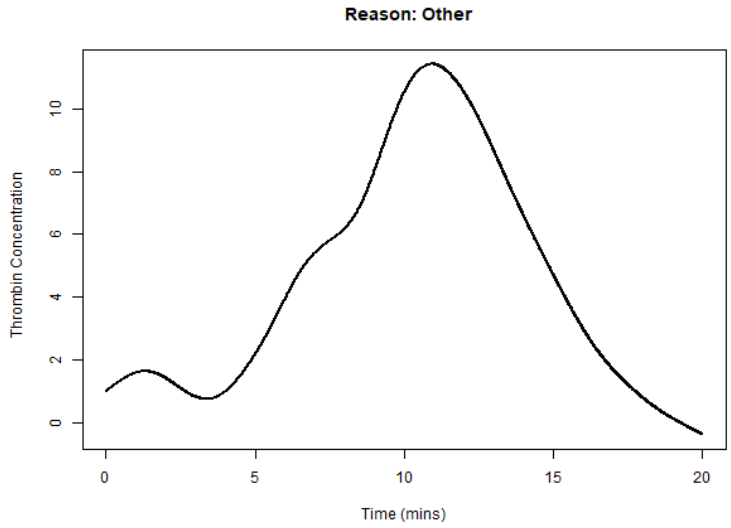

Figure 4.15: An example of a thrombin generation curve that was removed for other reasons, in this case because there was an unusual bump in the amplification.

4.7.3 Fitting

We fit the Reduced Unified Model given in the previous chapter, restricted to only fit to the filtered data curves. There are 49 reaction rates that are significant in their effect on OD for the Reduced Unified Model. The cost improves from 317 to 166 after fitting with only a minor improvement compared with the costs previously. ETP scatter plots before and after fitting are given in Figure 4.18 and thrombin generation curves for an average donor are given in Figure 4.20.

Figure 4.19 shows the OD curves for the individuals with the best and worst ETP predictions. All of the individuals that previously gave the worst predictions were removed by the filtering. However, the conclusions for this models worst

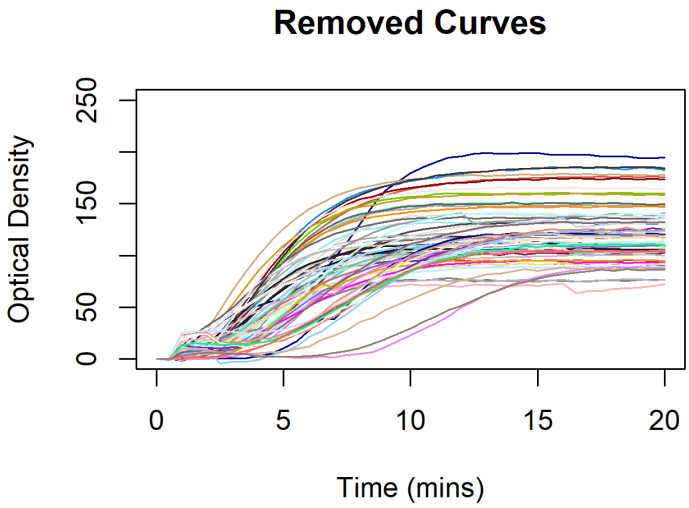

Figure 4.16: All of the OD curves (pre-smoothing) that have been removed by the data filtering.

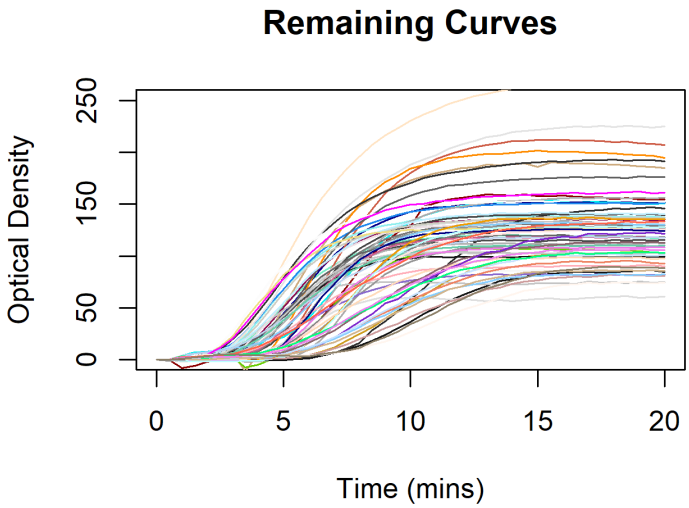

Figure 4.17: All of the OD curves (pre-smoothing) that remain after data filtering.

individual are generally similar (high factors levels, although not high FVIII, very large ETP, outside the general range that the model can seem to predict). The best predicted individual does not match on lagtime but the shape does seem similar.

The fitting does produce a slightly more realistic thrombin generation curve shape than seen with the other models or the previous versions of the Unified Model, however, the model is still a poor predictor of the data.

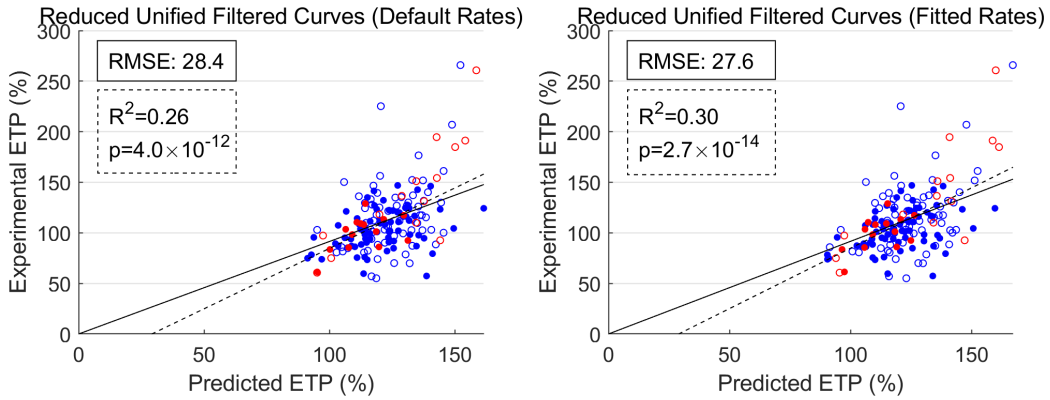

Figure 4.18: ETP correlation scatter graph for the Reduced Unified Model with the default rates and fitted rates for the filtered curves.

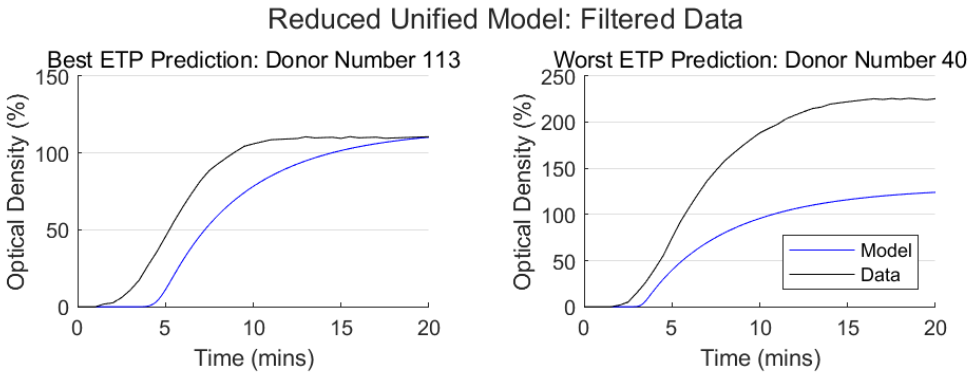

Figure 4.19: The Reduced Unified Model predicted OD curve and the experimental OD curve for the individuals with the best and worst predicted ETP for the gradient descent fitted rates. Both fitting and evaluating are restricted to the filtered data.

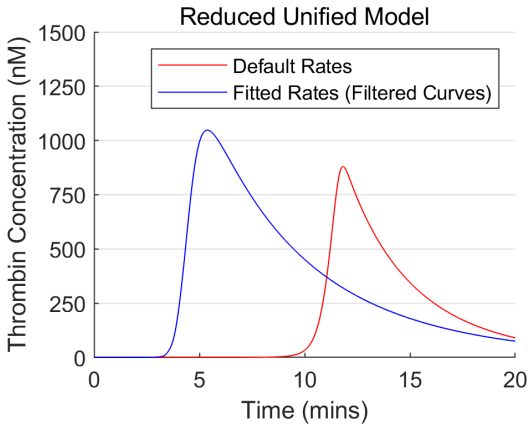

Figure 4.20: Thrombin generation curves for the Reduced Unified Model before and after fitting to the filtered curves.

4.8 Conclusions

While exploring the thrombin generation curves, we found that many curves had unusual shapes, with some featuring apparent high initial concentrations of thrombin and multiple peaks (Section 4.2). These are likely artefacts from the noise in the OD curves and we have verified that they did not interfere with the fitting (Section 4.7) by rerunning the fitting with curves presenting these artefacts removed. Additionally, the presence of these shapes is uncorrelated with the summary statistics of the thrombin generation curves (Figure 4.5), further suggesting they are the result of experimental noise.

We identified clusters in the thrombin generation curves and found that model accuracy varied between the clusters, with the models being a particularly poor predictor for the Big and Late Peak clusters (Section 4.3). Factor VIII varied significantly between the clusters and appeared to have a large influence over the amount of thrombin generated. This is contrary to the predictions of the models which all suggest FIX activation has the largest control over the magnitude of thrombin generation (Section 2.4).

It was also identified that model error is significantly lower in the samples where exogenous TF is added (Section 4.6). This does not seem to be accounted for just by the TF concentration as the addition of 5pM of exogenous TF has a larger impact on ETP than an average increase in endogenous TF would suggest.

Chapter 5

Improved Unified Model

5.1 Introduction

In Chapter 3, we were unable to produce a model that accurately reproduced experimental OD data. However, both through developing these models in Chapter 3 and analysis of the data in Chapter 4, we were able to identify a handful of issues in the versions of the Unified Model which we will attempt to address in this chapter. The issues we address are:

- Inhibition of the complexes Xa:Va, IXa:VIIIa, and TF:VIIa,
- Predicting partial prothrombin conversion without manual intervention,
- Identifying and improving upon the sources used for FXI activation,
- Continuing investigation into the long lagtime that is featured in the previous versions of the Unified Model and identifying why the long lagtime is not present in the previous models.

We begin by addressing the inhibition of the complexes, with a particular focus on prothrombinase. The goal of this section will be to identify mechanisms for fully inhibiting prothrombinase prior to the total conversion of prothrombin. We search the literature for new reaction rates for these reactions and explore any data which may help illuminate the mechanisms of complex inhibition that occur *in vitro*. Following this, we explore FXI activation, aiming to identify new sources for reaction rates. We then explore which reaction rates most significantly affect the lagtime, expanding on the work completed in Chapter 3; and update the module documents, introducing new modules to identify prior distributions not included in the Expanded Unified Model. Finally, we will use this new research to build a definitive Unified Model, named the Improved Unified Model, and use this model to explore uncertainty caused by variation between sources in the reaction rates.

5.2 Prothrombinase Inhibition

In this section, we explore the mechanisms for prothrombinase inhibition. We show the effects of the different mechanisms featured in the previous models. We

then demonstrate the influence of reaction rates over these inhibition mechanisms through the use of the previous versions of the Unified Model. Finally, we show other possible mechanisms for prothrombinase inhibition, one of which is able to predict partial prothrombin conversion.

5.2.1 Previous Models

Previous models have featured different schemes for prothrombinase inhibition. The Tyurin model features an inhibition of the form given below* and the other models only inhibit FXa, requiring Xa:Va to disassociate before it can be inhibited. Since the levels of prothrombinase dictate the shape of the thrombin generation curve, an accurate description of prothrombinase inhibition is required to construct a predictive model. Plots of prothrombinase concentration are given in Figure 5.1 for the previous models. As demonstrated previously in Section 2.4, four models (Chatterjee, Bungay, Tyurin, and Zhu) feature very rapid formation of Xa:Va which corresponds to FXI activation (or excess TF:VIIa in the case of Zhu). The remaining models do not form the maximum amount of Xa:Va of 20nM due to the lack of FXI.

$$\text{Xa:Va} + \text{AT} \rightarrow \text{Xa:AT} + \text{Va}$$

In Figure 5.2, we have extended the simulation time to explore the inhibition of prothrombinase. For a model to not fully convert prothrombin, it must fully inhibit prothrombinase prior to total prothrombin conversion. From this figure, it is clear that waiting for Xa:Va disassociation, the same mechanism utilised by all except the Tyurin model, would require dramatically different reaction rates to sufficiently inhibit prothrombinase. The Tyurin model is able to fully inhibit prothrombinase by around 10 minutes, demonstrating that this inhibition mechanism could be sufficient for partial prothrombin conversion.

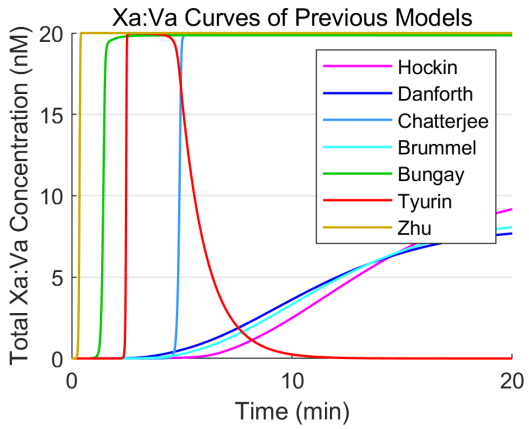

Figure 5.1: Plots of prothrombinase concentration for the previous models.

*The Panteleev model mimics a reaction of this form, however, it does not track Xa:Va concentration explicitly so is not featured in this section.

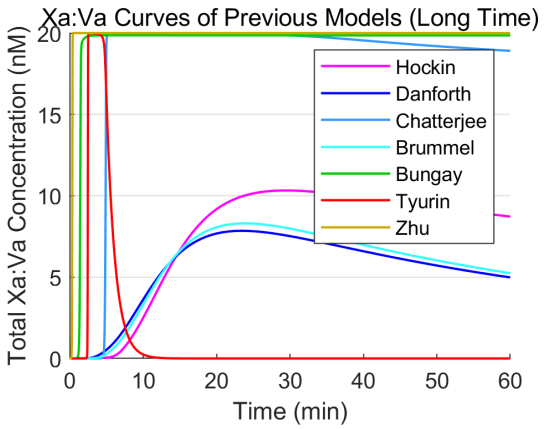

Figure 5.2: Plots of prothrombinase concentration for the previous models, featuring an extended simulation time of 60 minutes.

5.2.2 Unified Models

The previous versions of the Unified Model have all used the same mechanism for prothrombinase inhibition as the Tyurin model but with varying reaction rates. We can use these models to explore the effects of variation in the reaction rates on inhibition of prothrombinase. Figures 5.3 and 5.4 present plots of prothrombinase concentration over time for the Unified Model and the Reduced Unified Model, respectively. Results for the different versions of the Expanded Unified Model present similarly to the Reduced Unified Model, with the differences between the versions most influenced by the inclusion of $\alpha_1 - AT$ which is in all but the original Unified Model.

The Unified Model shows two styles of curves. The first is presented by the default rates and the gradient descent fitted rates, showing full activation after the lagtime with minimal inhibition occurring in the 20 minutes. The ABC-SMC fitted rates instead do not fully activate prothrombinase to the 20nM maximum and show significant inhibition in the 20 minutes, but still fail to fully inhibit quickly enough to make partial prothrombin conversion possible.

The Reduced Unified Model, and other version of the Unified Model, presents similar curves for the default rates as the Unified Model for the ABC-SMC rates, showing a peak activation below 20nM followed by inhibition. The gradient descent fitted rates show a smaller peak and we see complete inhibition of prothrombinase by 10 minutes.

5.2.3 Different Inhibition Schemes

We have seen two different mechanisms for inhibiting prothrombinase so far. The first of which requires prothrombinase to disassociate and then inhibits the FXa part. The second mechanism inhibits the prothrombinase complex in a reaction that releases the FVa, only inhibiting the FXa of the complex. We propose that, given there is significantly more FX in the assay than FV, inhibiting the full Xa:Va

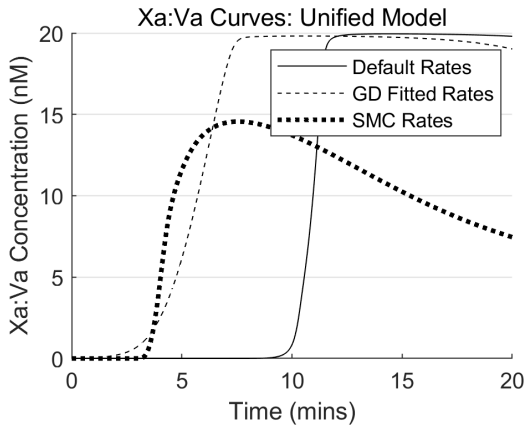

Figure 5.3: Plots of prothrombinase concentration for the Unified Model (using the default, gradient descent fitted, and ABC-SMC fitted rates).

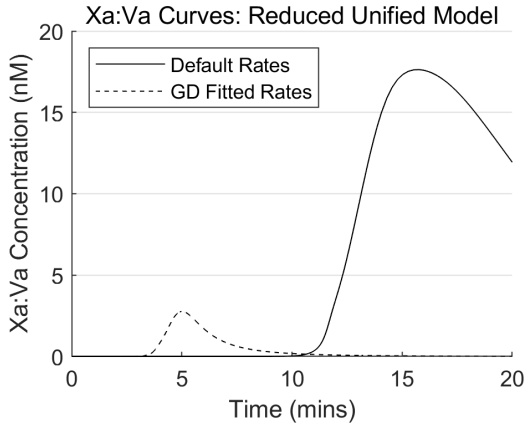

Figure 5.4: Plots of prothrombinase concentration for the Reduced Unified Model (using the default and gradient descent fitted rates).

complex could lead to a faster method of inhibition. We implement these three inhibition mechanisms, given below, into the Reduced Unified Model and Figures 5.5 and 5.6 give the resulting prothrombinase and prothrombin concentration curves, respectively.

- Xa:Va + AT $\rightarrow$ Xa:AT + Va, Xa + AT $\rightarrow$ Xa:AT
- Xa:Va + AT $\rightarrow$ Xa:Va:AT, Xa + AT $\rightarrow$ Xa:AT
- Xa + AT $\rightarrow$ Xa:AT only

We see the inhibition method has a strong influence on the prothrombinase concentration and the amount of prothrombin that is converted into thrombin. For the case where FVa is not released when the complex is inhibited, we see, for the first-time, partial prothrombin conversion without the need to manually alter the reaction rates. It is possible that finding the correct method for prothrombinase inhibition could resolve the mismatch between the models and the data regarding total prothrombin conversion.

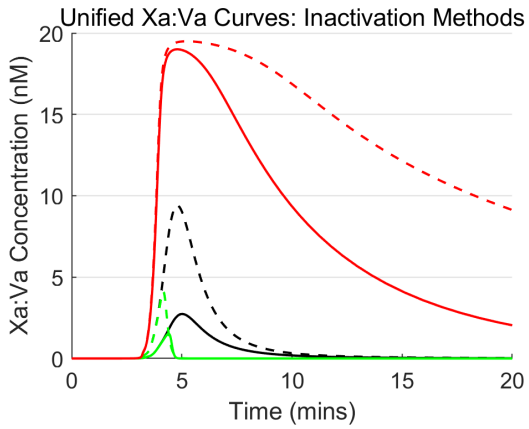

Figure 5.5: Plots of prothrombinase concentration for the Reduced Unified Model with the gradient descent fitted rates for three different inhibition mechanisms for prothrombinase.

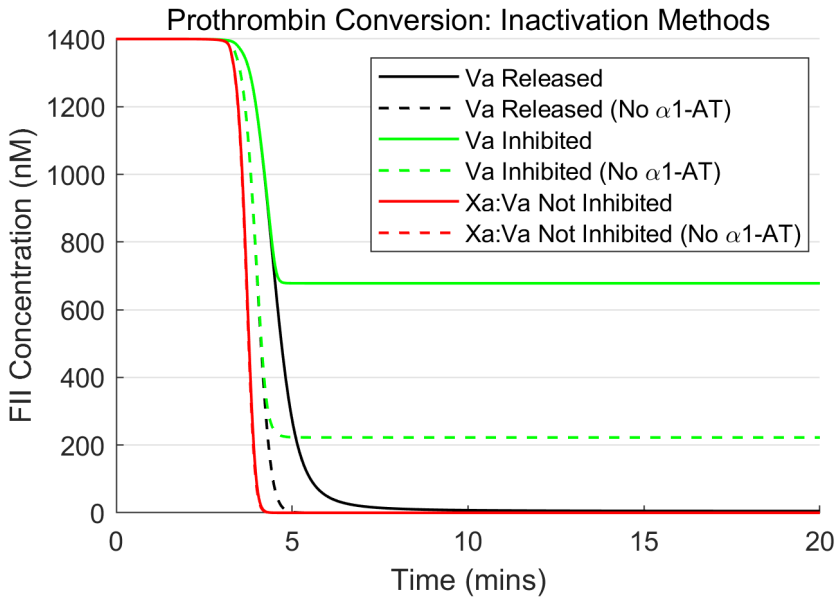

Figure 5.6: Plots of prothrombin concentration for the Reduced Unified Model with the gradient descent fitted rates for three different inhibition mechanisms for prothrombinase.

5.2.4 Changes to Prothrombinase Inhibition

After demonstrating that the mechanism of prothrombinase inhibition has significant influence over the rate of prothrombinase inhibition and over the possibility of partial prothrombin conversion, we investigate the original sources for the inhibition rates of prothrombinase, looking for any evidence which may suggest one of these mechanisms over the others.

There are two sources used for determining reaction rates of prothrombinase inhibition [114, 115]. Upon further investigation of one of these sources [114], it was revealed that the inhibition was of FXa and not Xa:Va, as FVa was later added in order to measure the activity of the remaining, non-inhibited FXa. Due

to this, the reaction rates given in [114] are no longer used for informing rates of inhibition of prothrombinase. The other source [115] does measure the inhibition of the full prothrombinase complex but gives no indication as to whether or not the FVa is released from the complex after inhibition.

Other papers studying prothrombinase inhibition, those that do not give reaction rates, were also searched but no indication as to the mechanism was found. Since inhibiting the FVa produces results more in line with experimental data, we implement this inhibition mechanism for Xa:Va and IXa:VIIIa.

5.3 Varying FXI Activation

In Section 2.4, we saw that the previous models differ greatly between those that feature FXI and those that do not. In this section, we investigate the differences between the models after accounting for the presence of FXI. To do this, we add FXI activation into the Danforth model (with the rates used in Tyurin, given in Table 5.1). In Figures 5.7 and 5.8, we show plots of the concentrations of factors XIa, IX, IXa, X, Xa, and IIa and the complexes Xa:Va and IXa:VIIIa, for the new Danforth model and the Tyurin model, respectively. In these plots, we gradually reduce the activation rates of FXI (k_{cat} for FXI activation by FIIa and FXIa are scaled by values given in the figure legend) to examine the remaining differences between the models.

There is faster inhibition of FXIa in the Tyurin model than in the Danforth model. There are a variety of inhibitors of FXIa in the Tyurin model that are not included in the Danforth model ($\alpha_1 - AT$, $\alpha_2 - AP$, C1-inh and PAI-1). In Figure 5.9, we present similar curves with the inhibitors $\alpha_1 - AT$ and $\alpha_2 - AP$ removed from the Tyurin model. This produces similar FXIa curves as the Danforth model.

Unlike the Tyurin model, the Danforth model is able to inhibit IXa:VIIIa significantly. This is due to the FVIIIa degradation also affecting IXa:VIIIa in the Danforth model, which gives a stronger inhibition than the sole AT reaction used by Tyurin. Removing this reaction from the Danforth model produces curves similar to the Tyurin model. This difference has a large impact on the level of FX with the Tyurin model predicting FX is all activated, even if the effect of FXI is removed.

It is clear that FXI has a strong effect in the models, however, it seems large changes to the reaction rates are needed before the effect of FXI starts to be reduced (on the order of a 1000-fold reduction). This suggests that we do not need to know the rates of FXI very accurately, assuming current values are reasonable. However, due to the lack of sources, it would be worth investigating further to decide if we believe the current sources provide reasonable values in comparison to our assay methods, and as such, further research into FXI is necessary.

Reaction	Rate
XI + IIa → XI:IIa	$1 \times 10^8 M^{-1}s^{-1}$
XI:IIa → XI + IIa	$3.57s^{-1}$
XI:IIa → XIa + IIa	$1.43s^{-1}$
XI + XIa → XI:XIa	$1 \times 10^8 M^{-1}s^{-1}$
XI:XIa → XI + XIa	$4.87s^{-1}$
XI:XIa → XIa + XIa	$0.13s^{-1}$
XIa + AT → XIa:AT	$167M^{-1}s^{-1}$
IX + XIa → IX:XIa	$1 \times 10^8 M^{-1}s^{-1}$
IX:XIa → IX + XIa	$34.25s^{-1}$
IX:XIa → IXa + XIa	$1.25s^{-1}$

Table 5.1: The FXI reactions and rates that were added to the Danforth model, using a mass action law version of the reaction scheme and rates from the Tyurin model.

5.3.1 Changes to FXI Activation

Factor XI was first discovered to be activated in the absence of FXIIa when in the presence of dextran sulphate, a non-physiological negatively charged surface. This was demonstrated to occur through both an auto-activation by FXIa and activation by FIIa [96, 116]. It was then later shown that other negative surfaces, such as polyphosphate (commonly shortened to polyP, released from platelets) and nucleic acids, can also stimulate FXI activation, with polyP believed to be the physiological activation surface [117, 118, 119, 120]. More recently it has been discovered that FIIa activation of FXI can be stimulated by negatively charged phospholipids such as PS (phosphatidylserine) [121], which are present in our assay. Due to the heavily surface dependent nature of FXI activation and the fact that neither of the sources we used measure this activation on phospholipid surfaces, we likely need updated reaction rates for FXI activation.

We will make use of two new sources for FXI activation [118, 121]. One of these sources [121] measures FXI activation by FIIa at a variety of phospholipid compositions and concentrations, and in the presence of polyP. The other source [118] measures FXI activation by FXIa in the presence of varying lengths and concentrations of polyP, which we will use to estimate the rates in the presence of phospholipids.

For the activation of FXI by FIIa, the data has been digitized using WebPlotDigitizer [122] and linearly interpolated to estimate the reaction rate for 4μM of 50:50 PC:PS vesicles. This source also gives data for different phospholipid compositions using 50μM of PC:PS with varying composition. Since our assay used 28.5% PS, we have then scaled this rate by the ratio between 50% PS composition and 28.5% PS composition (28.5% estimated through linear interpolation).

The linearly interpolated rate for $4\mu M$ of 50:50 PC:PS vesicles is estimated to be $8.55 \times 10^{-3} nM/min$ [121] for 1nM of FIIa and 30nM of FXI. The ratio

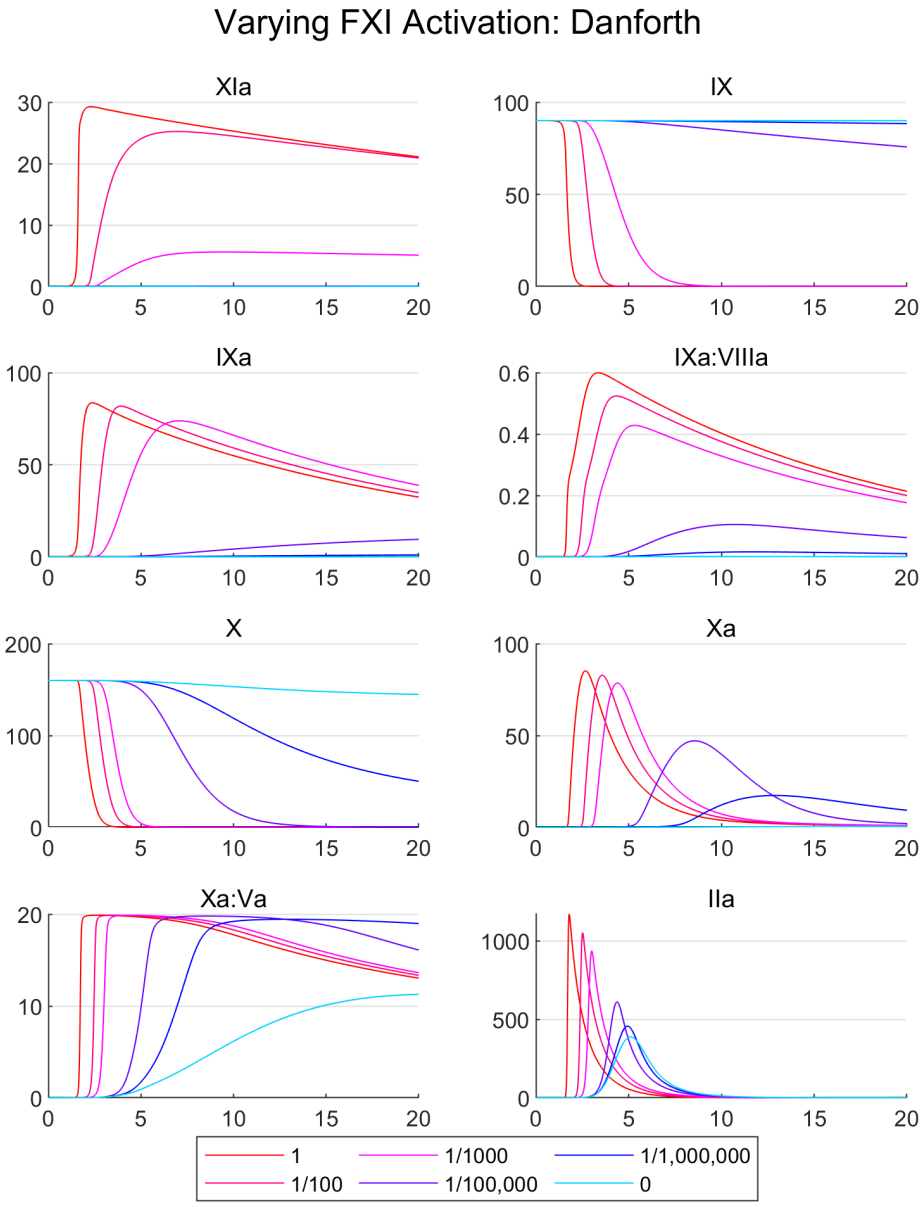

Figure 5.7: Plots of multiple coagulation factors for the Danforth model (with newly added FXI) for various FXI activation rates. Both the k_{cat} for FXI activation by FIIa and the k_{cat} for FXI activation by FXIa are scaled by the values given in the legend. Plots of various coagulation factors are then given using pooled plasma initial conditions. The values of k_+ and k_- are not adjusted to ensure the same K_m.

of 28.5% PS composition to 50% PS composition, for 50μM of PC:PS is estimated to be 23.9%. This gives an estimated second order rate for 4μM of PC:PS (71.5:28.5) of $\frac{k_{\text{cat}}}{K_m} = 1136 M^{-1}s^{-1}$. Using a typical $K_m = 5 \times 10^{-8} M$, we estimate $k_{\text{cat}} = 5.68 \times 10^{-5} s^{-1}$.

Reaction rates have been reported for FXI auto-activation [118] using 4μM of polyP at varying polymer lengths. This source also gives reaction rates for varying

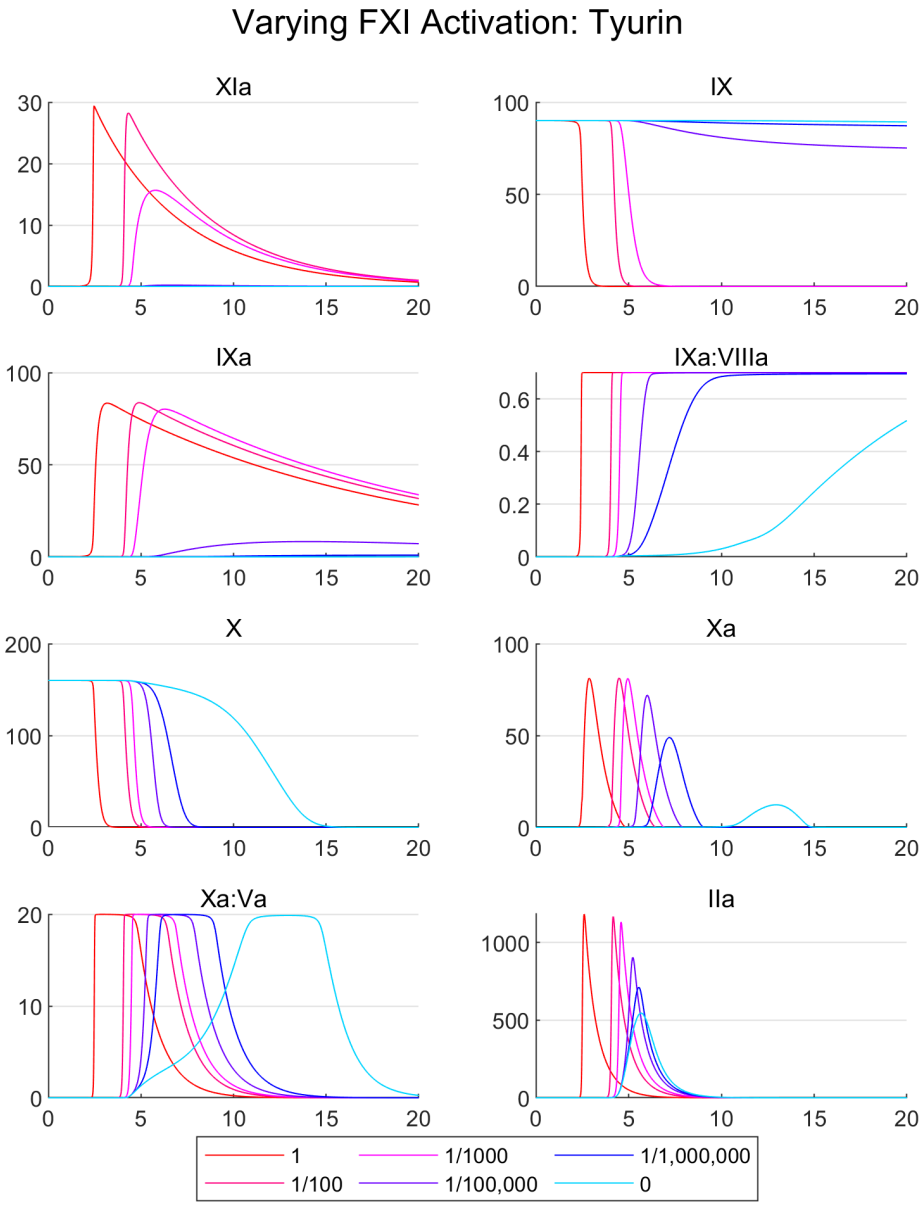

Figure 5.8: Plots of multiple coagulation factors for the Tyurin model for various FXI activation rates. Both the k_{cat} for FXI activation by FIIa and the k_{cat} for FXI activation by FXIa are scaled by the values given in the legend. Plots of various coagulation factors are then given using pooled plasma initial conditions.

concentrations of polyP at a handful of lengths for activation by FIIa.

We use this data to estimate both a ratio between 1μM of polyP and 4μM of polyP for activation by FIIa, and a ratio between 1μM of polyP at a length of 70mer and our estimated phospholipid composition for activation by FIIa. We combine these ratios with the reaction rate for activation by FXIa in the presence of 4μM of polyP to estimate a rate for activation by FXIa in our phospholipid composition.

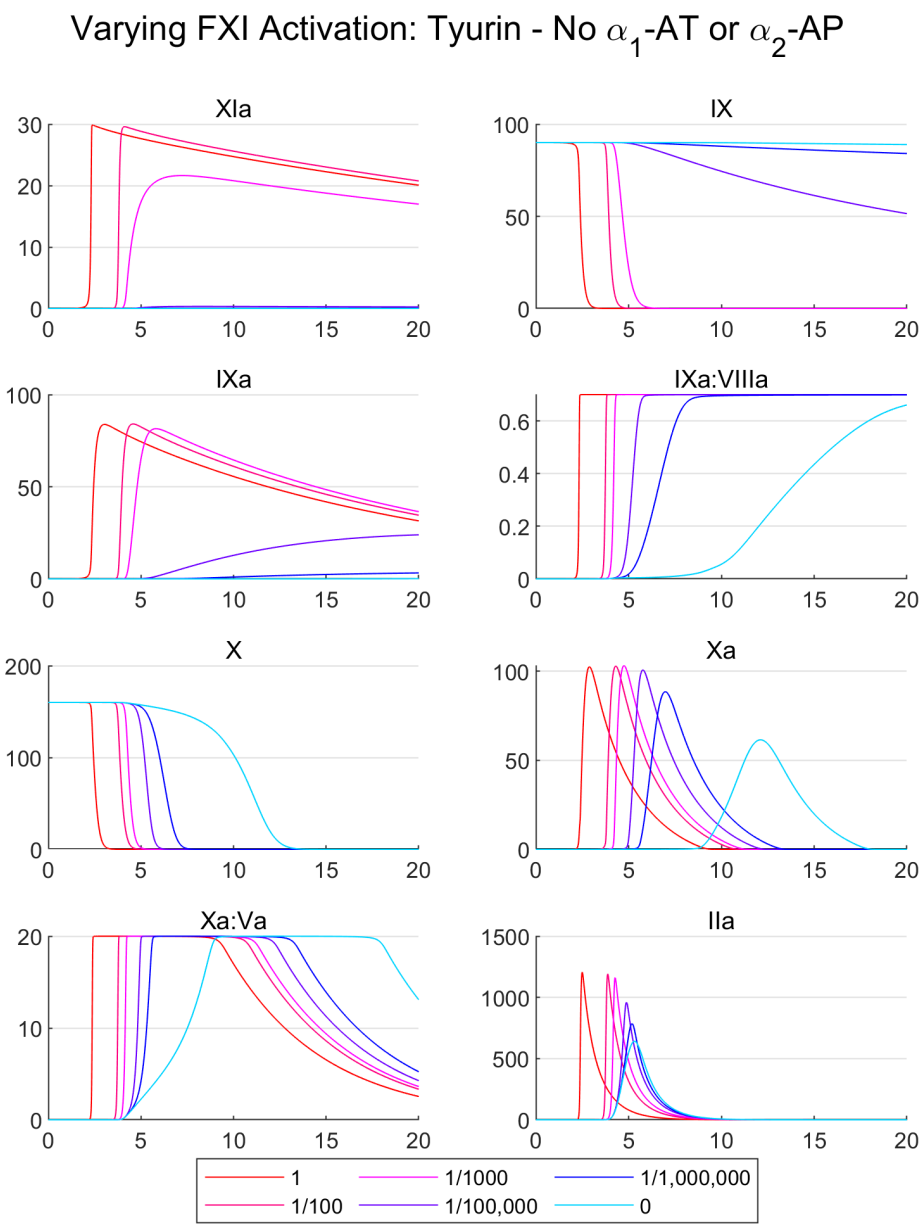

Figure 5.9: Plots of multiple coagulation factors for the Tyurin model for various FXI activation rates. The inhibitors $\alpha_1 - AT$ and $\alpha_2 - AP$ have been removed to better match the FXIa curves of the Danforth model. Both the k_{cat} for FXI activation by FIIa and the k_{cat} for FXI activation by FXIa are scaled by the values given in the legend. Plots of various coagulation factors are then given using pooled plasma initial conditions.

The second order rate constant for activation by FXIa, measured with 4μM of 70mer polyP, is $\frac{k_{\text{cat}}}{K_m} = 1.89 \times 10^5 M^{-1}s^{-1}$. The ratio between 1μM and 4μM of polyP for activation by FIIa, using 65mer polyP, is 33%. The ratio between 1μM of 70mer polyP and our phospholipid composition for activation by FIIa (calculated using data from [121]) is 5%. This gives an estimated second order rate for FXI auto-activation using our phospholipid composition of $\frac{k_{\text{cat}}}{K_m} = 3065 M^{-1}s^{-1}$. Using a typical $K_m = 5 \times 10^{-8} M$, this gives $k_{\text{cat}} = 1.53 \times 10^{-4} s^{-1}$.

These new rates for FXI activation can then be used in an updated model.

5.4 Shortening the Long Lagtime

The previous versions of the Unified Model all present a long lagtime but the previous models, those that the Unified Model is based on, do not all feature such a long lagtime. When we previously investigated this in Chapter 3, we found the interactions between TF:VIIa and FXa to be the most likely cause and specifically mentioned TF:VII activation by FXa as the likely cause. In this section, we have continued this work, expanding upon it to identify more possible reactions which influence the lagtime based on our prior distributions. We have compared the reaction rates of the Unified Model with those of the previous models for the reactions in the TF:VIIa, Xa:Va, and IIa modules. Of these reactions, the k_+ rates for TF:VII and TF:VIIa appear to be the key difference. Changing these rates to be more in line with the previous models reduces the lagtime from 10 minutes to 5 minutes.

This issue was also noticed in the Tyurin model (which has similar k_+ rates to the Unified models), demonstrated in Section 2.4, where activation by FVIIa, instead of TF:VIIa, was amplified relative to the other models to account for this. However, we have three sources for the TF:VIIa association rate which are fairly consistent in value and none of which reach the more extreme rates used by the other previous models. This suggests that, although the reason we have a longer lagtime than the previous models is due to using this lower association rate, there should be a more likely reaction rate which can be adjusted to fix this lagtime while maintaining realistic values. Figure 5.10 demonstrates the effect of increasing the association rates for TF:VII and TF:VIIa to match those used in the Hockin model.

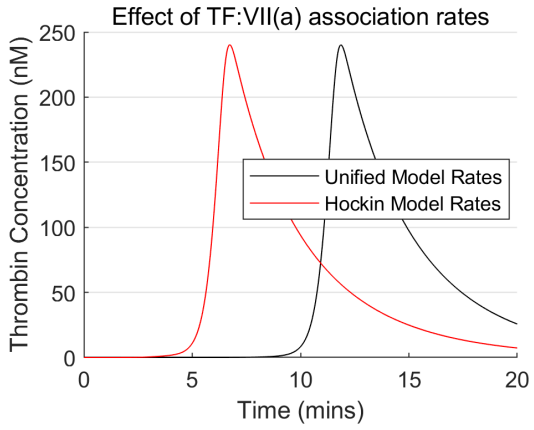

Figure 5.10: The thrombin generation curves for two different sets of reaction rates: the default rates, given in black; and the increased reaction rates for TF:VII and TF:VIIa association (using the Hockin models association rates), given in red.

To investigate other possible causes, we have varied the reaction rates in the

Reduced Unified Model along the priors (where defined for the Unified Model), using the 5th and 95th percentiles. This identified seven reactions which, when their rates were varied, could shorten the lagtime to 5 minutes or below. These reactions are given in Table 5.2, along with the smallest lagtime (out of the 5th or 95th percentiles for either k_{cat} or K_m) and the standard deviation used to define the priors. Five of the seven reactions use a wide prior standard deviation of 2.5 because we only have one source available for these reactions. The remaining two reactions have multiple sources and therefore use smaller prior standard deviations. It seems most likely that the inaccuracy comes from these two reactions rather than falling on the outer limits of the wide prior distributions. Figure 5.11 shows thrombin generation curves for these two reactions for the 5th and 95th percentile rates and the default rates. The first of these reactions, activation of TF:VII by FXa, was identified previously in Chapter 3. The second reaction is activation of FX by TF:VIIa, which we have many sources for, but still shows a similar magnitude of effect.

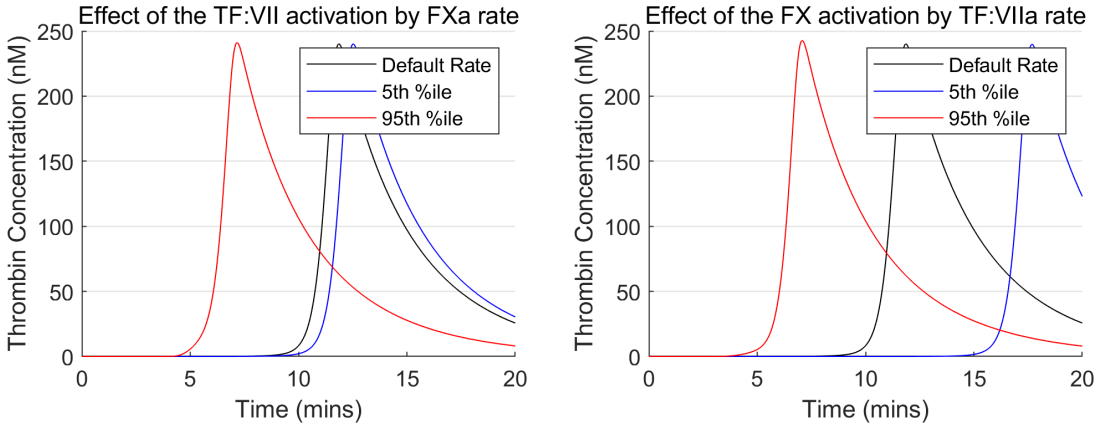

Figure 5.11: The thrombin generation curves for varying the activation of TF:VII by FXa and for varying the activation of FX by TF:VIIa.

Reaction	Smallest Lagtime (mins)	Prior Standard Deviation
VII $\overset{Xa}{\rightarrow}$ VIIa	4	2.5
TF:VII $\overset{Xa}{\rightarrow}$ TF:VIIa	4	1.49
TF:VII $\overset{IXa}{\rightarrow}$ TF:VIIa	5	2.5
X $\overset{TF:VIIa}{\rightarrow}$ Xa	4	0.63
XI $\overset{XIa}{\rightarrow}$ XIa	3	2.5
IX $\overset{VIIa}{\rightarrow}$ IXa	2	2.5

Table 5.2: The reactions which can produce a lagtime of under five minutes while maintaining realistic reaction rates.

5.5 New Modules

When new reactions were added to the Unified Model to form the Expanded Unified Model, the reaction rates were reused from the previous models. These reactions included many new inhibitors such as $\alpha_1 - AT$ and $\alpha_2 - AP$, which we have now found to be significant in their effect on factor XIa. To ensure the reaction rates are accurate for these reactions, we have created a new module, named the Other Inhibitors module. This module allows us to use multiple sources and investigate the original sources used for the reactions. We have also built the Fibrinogen module, although this has a slightly different structure compared to the other modules as the fibrinogen reactions are based off another model which has been well validated. We have still allowed variation of these rates in the priors, however, the standard deviations of these priors are reduced from 2.5 to 1.5 to account for the validation in this module.

5.6 Improved Unified Model

Applying these changes give us the Improved Unified Model. The updated module documents are given in Appendix E. The reactions, default reaction rates and prior distributions for the resulting model are given in Table 5.3.

5.6.1 Model Fitting

We fit the model through both Gradient Descent and ABC-SMC, with five-fold cross validation. The fitted reaction rates are given in Table 5.4. The fitting results, presented through the ETP metrics; cost (with cross validation); ETP correlation scatter graphs; and thrombin generation curves are given in Table 5.5, Table 5.6, Figure 5.12, and Figure 5.14, respectively. The Improved Unified Model ODEs and fitted reaction rates in mass action form are given in Appendices A and B.

Model performance is improved compared with previous version of the Unified Model in most metrics, but the model is still a poor predictive tool. Other conclusions, such as the change in the shape of the thrombin generation curves, are identical to the previous versions of the Unified Model.

Reaction	Rates	Priors
TF + VII $\leftrightarrow$ TF:VII	$k_+ = 1.25 \times 10^5 M^{-1}s^{-1}$, $k_- = 3.75 \times 10^{-4}s^{-1}$	$K_d \sim 10 \wedge N(-8.53, 0.58^2)$, $k_+ \sim 10 \wedge N(5.10, 0.56^2)$
TF + VIIa $\leftrightarrow$ TF:VIIa	$k_+ = 1.3 \times 10^5 M^{-1}s^{-1}$, $k_- = 4.16 \times 10^{-4}s^{-1}$	$K_d \sim 10 \wedge N(-8.50, 0.55^2)$, $k_+ \sim 10 \wedge N(5.11, 0.23^2)$
VII + Xa $\leftrightarrow$ VII:Xa	$k_+ = 1 \times 10^8 M^{-1}s^{-1}, k_- = 105s^{-1}$	$K_m \sim 10 \wedge N(-5.92, 2.5^2)$,
VII:Xa $\rightarrow$ VIIa + Xa	$k_{\text{cat}} = 15.2s^{-1}$	$k_{\text{cat}} \sim 10 \wedge N(1.18, 2.5^2)$
TF:VII + Xa $\leftrightarrow$ TF:VII:Xa	$k_+ = 1 \times 10^8 M^{-1}s^{-1}, k_- = 7.34s^{-1}$	$K_m \sim 10 \wedge N(-6.98, 1.49^2)$,
TF:VII:Xa $\rightarrow$ TF:VIIa + Xa	$k_{\text{cat}} = 3.16s^{-1}$	$k_{\text{cat}} \sim 10 \wedge N(0.5, 0.96^2)$
VII + IIa $\leftrightarrow$ VII:IIa	$k_+ = 1 \times 10^8 M^{-1}s^{-1}, k_- = 270s^{-1}$	$K_m \sim 10 \wedge N(-5.57, 2.5^2)$,
VII:IIa $\rightarrow$ VIIa + IIa	$k_{\text{cat}} = 6.1 \times 10^{-2}s^{-1}$	$k_{\text{cat}} \sim 10 \wedge N(-1.21, 2.5^2)$
TF:VII + IIa $\leftrightarrow$ TF:VII:IIa	$k_+ = 1 \times 10^8 M^{-1}s^{-1}, k_- = 270s^{-1}$	$K_m \sim 10 \wedge N(-5.57, 2.5^2)$,
TF:VII:IIa $\rightarrow$ TF:VIIa + IIa	$k_{\text{cat}} = 6.1 \times 10^{-2}s^{-1}$	$k_{\text{cat}} \sim 10 \wedge N(-1.21, 2.5^2)$
VII + IXa $\leftrightarrow$ VII:IXa	$k_+ = 1 \times 10^8 M^{-1}s^{-1}, k_- = 170s^{-1}$	$K_m \sim 10 \wedge N(-5.77, 2.5^2)$,
VII:IXa $\rightarrow$ VIIa + IXa	$k_{\text{cat}} = 0.32s^{-1}$	$k_{\text{cat}} \sim 10 \wedge N(-0.49, 2.5^2)$
TF:VII + IXa $\leftrightarrow$ TF:VII:IXa	$k_+ = 1 \times 10^8 M^{-1}s^{-1}, k_- = 170s^{-1}$	$K_m \sim 10 \wedge N(-5.77, 2.5^2)$,
TF:VII:IXa $\rightarrow$ TF:VIIa + IXa	$k_{\text{cat}} = 0.32s^{-1}$	$k_{\text{cat}} \sim 10 \wedge N(-0.49, 2.5^2)$
VII + TF:VIIa $\leftrightarrow$ VII:TF:VIIa	$k_+ = 1 \times 10^8 M^{-1}s^{-1}, k_- = 319s^{-1}$	$K_m \sim 10 \wedge N(-5.49, 2.5^2)$,
VII:TF:VIIa $\rightarrow$ VIIa + TF:VIIa	$k_{\text{cat}} = 1.4s^{-1}$	$k_{\text{cat}} \sim 10 \wedge N(0.15, 2.5^2)$
TF:VIIa + AT $\rightarrow$ TF:VIIa:AT	$k = 450M^{-1}s^{-1}$	$k \sim 10 \wedge N(2.65, 2.5^2)$
X + TF:VIIa $\leftrightarrow$ X:TF:VIIa	$k_+ = 1 \times 10^8 M^{-1}s^{-1}, k_- = 26s^{-1}$	$K_m \sim 10 \wedge N(-6.5, 0.58^2)$,
X:TF:VIIa $\rightarrow$ Xa + TF:VIIa	$k_{\text{cat}} = 6s^{-1}$	$k_{\text{cat}} \sim 10 \wedge N(0.78, 0.63^2)$
X + VIIa $\leftrightarrow$ X:VIIa	$k_+ = 1 \times 10^8 M^{-1}s^{-1}, k_- = 110s^{-1}$	$K_m \sim 10 \wedge N(-5.96, 0.91^2)$,
X:VIIa $\rightarrow$ Xa + VIIa	$k_{\text{cat}} = 3.2 \times 10^{-4}s^{-1}$	$k_{\text{cat}} \sim 10 \wedge N(-3.49, 0.13^2)$
X + IXa:VIIIa $\leftrightarrow$ X:IXa:VIIIa	$k_+ = 1 \times 10^8 M^{-1}s^{-1}, k_- = 6.31s^{-1}$	$K_m \sim 10 \wedge N(-7.07, 0.37^2)$,
X:IXa:VIIIa $\rightarrow$ Xa + IXa:VIIIa	$k_{\text{cat}} = 2.19s^{-1}$	$k_{\text{cat}} \sim 10 \wedge N(0.34, 0.82^2)$
X + IXa $\leftrightarrow$ X:IXa	$k_+ = 1 \times 10^8 M^{-1}s^{-1}, k_- = 8s^{-1}$	$K_m \sim 10 \wedge N(-7.10, 0.86^2)$,

X:IXa $\rightarrow$ Xa + IXa	$k_{\text{cat}} = 6.3 \times 10^{-4} s^{-1}$	$k_{\text{cat}} \sim 10 \wedge N(-3.20, 0.91^2)$
V + IIa $\leftrightarrow$ V:IIa	$k_+ = 1 \times 10^8 M^{-1} s^{-1}, k_- = 6.87 s^{-1}$	$K_m \sim 10 \wedge N(-7.14, 2.5^2)$,
V:IIa $\rightarrow$ Va + IIa	$k_{\text{cat}} = 0.3 s^{-1}$	$k_{\text{cat}} \sim 10 \wedge N(-0.53, 0.13^2)$
V + Xa $\leftrightarrow$ V:Xa	$k_+ = 1 \times 10^8 M^{-1} s^{-1}, k_- = 0.997 s^{-1}$	$K_m \sim 10 \wedge N(-7.98, 2.5^2)$,
V:Xa $\rightarrow$ Va + Xa	$k_{\text{cat}} = 4.3 \times 10^{-2} s^{-1}$	$k_{\text{cat}} \sim 10 \wedge N(-1.37, 2.5^2)$
Xa + Va $\leftrightarrow$ Xa:Va	$k_+ = 1.6 \times 10^9 M^{-1} s^{-1}$,	$K_d \sim 10 \wedge N(-10.5, 1.51^2)$,
	$k_- = 5.04 \times 10^{-2} s^{-1}$	$k_+ \sim 10 \wedge N(9.20, 2.5^2)$
Xa + AT $\rightarrow$ Xa:AT	$k = 2.1 \times 10^3 M^{-1} s^{-1}$	$k \sim 10 \wedge N(3.32, 0.39^2)$
Xa:Va + AT $\rightarrow$ Xa:Va:AT	$k = 367 M^{-1} s^{-1}$	$k \sim 10 \wedge N(2.56, 2.5^2)$
II + Xa $\leftrightarrow$ II:Xa	$k_+ = 1 \times 10^8 M^{-1} s^{-1}, k_- = 130 s^{-1}$	$K_m \sim 10 \wedge N(-5.88, 0.91^2)$,
II:Xa $\rightarrow$ IIa + Xa	$k_{\text{cat}} = 9.3 \times 10^{-3} s^{-1}$	$k_{\text{cat}} \sim 10 \wedge N(-2.03, 0.86^2)$
II + Xa:Va $\leftrightarrow$ II:Xa:Va	$k_+ = 1 \times 10^8 M^{-1} s^{-1}, k_- = 34 s^{-1}$	$K_m \sim 10 \wedge N(-6.16, 0.34^2)$,
II:Xa:Va $\rightarrow$ IIa + Xa:Va	$k_{\text{cat}} = 36 s^{-1}$	$k_{\text{cat}} \sim 10 \wedge N(1.55, 0.19^2)$
IIa + AT $\rightarrow$ IIa:AT	$k = 6.1 \times 10^3 M^{-1} s^{-1}$	$k \sim 10 \wedge N(3.79, 0.08^2)$
XI + IIa $\leftrightarrow$ XI:IIa	$k_+ = 1 \times 10^8 M^{-1} s^{-1}, k_- = 5 s^{-1}$	$K_m \sim 10 \wedge N(-7.3, 2.5^2)$,
XI:IIa $\rightarrow$ XIa + IIa	$k_{\text{cat}} = 5.68 \times 10^{-5} s^{-1}$	$k_{\text{cat}} \sim 10 \wedge N(-4.25, 2.5^2)$
XI + XIa $\leftrightarrow$ XI:XIa	$k_+ = 1 \times 10^8 M^{-1} s^{-1}, k_- = 5 s^{-1}$	$K_m \sim 10 \wedge N(-7.3, 2.5^2)$,
XI:XIa $\rightarrow$ XIa + XIa	$k_{\text{cat}} = 1.53 \times 10^{-4} s^{-1}$	$k_{\text{cat}} \sim 10 \wedge N(-3.82, 2.5^2)$
XIa + AT $\rightarrow$ XIa:AT	$k = 400 M^{-1} s^{-1}$	$k \sim 10 \wedge N(2.6, 0.14^2)$
IX + TF:VIIa $\leftrightarrow$ IX:TF:VIIa	$k_+ = 1 \times 10^8 M^{-1} s^{-1}, k_- = 11.3 s^{-1}$	$K_m \sim 10 \wedge N(-6.93, 0.49^2)$,
IX:TF:VIIa $\rightarrow$ IXa + TF:VIIa	$k_{\text{cat}} = 0.43 s^{-1}$	$k_{\text{cat}} \sim 10 \wedge N(-0.37, 0.30^2)$
IX + VIIa $\leftrightarrow$ IX:VIIa	$k_+ = 1 \times 10^8 M^{-1} s^{-1}, k_- = 0.8 s^{-1}$	$K_m \sim 10 \wedge N(-8.10, 2.5^2)$,
IX:VIIa $\rightarrow$ IXa + VIIa	$k_{\text{cat}} = 1.62 \times 10^{-4} s^{-1}$	$k_{\text{cat}} \sim 10 \wedge N(-3.79, 2.5^2)$
IX + XIa $\leftrightarrow$ IX:XIa	$k_+ = 1 \times 10^8 M^{-1} s^{-1}, k_- = 41.3 s^{-1}$	$K_m \sim 10 \wedge N(-6.38, 0.37^2)$,
IX:XIa $\rightarrow$ IXa + XIa	$k_{\text{cat}} = 0.74 s^{-1}$	$k_{\text{cat}} \sim 10 \wedge N(-0.13, 0.65^2)$
VIII + IIa $\leftrightarrow$ VIII:IIa	$k_+ = 1 \times 10^8 M^{-1} s^{-1}, k_- = 13.9 s^{-1}$	$K_m \sim 10 \wedge N(-6.83, 2.5^2)$,
VIII:IIa $\rightarrow$ VIIIa + IIa	$k_{\text{cat}} = 0.8 s^{-1}$	$k_{\text{cat}} \sim 10 \wedge N(-0.09, 0.06^2)$
VIII + Xa $\leftrightarrow$ VIII:Xa	$k_+ = 1 \times 10^8 M^{-1} s^{-1}, k_- = 14.5 s^{-1}$	$K_m \sim 10 \wedge N(-6.83, 2.5^2)$,

VIII:Xa $\rightarrow$ VIIIa + Xa	$k_{\text{cat}} = 0.16s^{-1}$	$k_{\text{cat}} \sim 10 \wedge N(-0.79, 2.5^2)$
VIIIa $\leftrightarrow$ VIIIa$_1$L + VIIIa$_2$	$k_+ = 5.85 \times 10^{-3}s^{-1}$,	$K_d \sim 10 \wedge N(-6.58, 0.02^2)$,
	$k_- = 2.19 \times 10^4 M^{-1}s^{-1}$	$k_+ \sim 10 \wedge N(-2.24, 2.5^2)^\dagger$
IXa:VIIIa $\rightarrow$ IXa + VIIIa$_1$L + VIIIa$_2$	$k = 1.4 \times 10^{-3}M^{-1}s^{-1}$	$k \sim 10 \wedge N(-2.85, 2.5^2)$
IXa + VIIIa $\leftrightarrow$ IXa:VIIIa	$k_+ = 1 \times 10^7 M^{-1}s^{-1}$,	$K_d \sim 10 \wedge N(-8.45, 0.22^2)$,
	$k_- = 3.5 \times 10^{-2}s^{-1}$	$k_+ \sim 10 \wedge N(7, 2.5^2)$
IXa + AT $\rightarrow$ IXa:AT	$k = 490M^{-1}s^{-1}$	$k \sim 10 \wedge N(2.69, 2.5^2)$
IXa:VIIIa + AT $\rightarrow$ IXa:VIIIa:AT	$k = 317M^{-1}s^{-1}$	$k \sim 10 \wedge N(2.5, 2.5^2)$
Xa + TFPI $\leftrightarrow$ Xa:TFPI	$k_+ = 3.8 \times 10^6 M^{-1}s^{-1}$,	$K_d \sim 10 \wedge N(-10.03, 0.9^2)$,
	$k_- = 3.5 \times 10^{-4}s^{-1}$	$k_+ \sim 10 \wedge N(6.58, 0.88^2)$
TF:VIIa + Xa:TFPI $\leftrightarrow$ TF:VIIa:Xa:TFPI	$k_+ = 8.9 \times 10^6 M^{-1}s^{-1}$,	$K_d \sim 10 \wedge N(-9.82, 2.5^2)$,
	$k_- = 1.34 \times 10^{-3}s^{-1}$	$k_+ \sim 10 \wedge N(6.95, 0.12^2)$
IIa + $\alpha_1 - AT \rightarrow$ IIa:$\alpha_1 - AT$	$k = 72M^{-1}s^{-1}$	$k \sim 10 \wedge N(1.86, 0.25^2)$
Xa + $\alpha_1 - AT \rightarrow$ Xa:$\alpha_1 - AT$	$k = 262M^{-1}s^{-1}$	$k \sim 10 \wedge N(2.42, 2.5^2)$
Xa:Va + $\alpha_1 - AT \rightarrow$ Xa:Va:$\alpha_1 - AT$	$k = 262M^{-1}s^{-1}$	$k \sim 10 \wedge N(2.42, 2.5^2)$
XIa + $\alpha_1 - AT \rightarrow$ XIa:$\alpha_1 - AT$	$k = 82M^{-1}s^{-1}$	$k \sim 10 \wedge N(1.91, 0.12^2)$
XIa + $\alpha_2 - AP \rightarrow$ XIa:$\alpha_2 - AP$	$k = 656M^{-1}s^{-1}$	$k \sim 10 \wedge N(2.82, 0.26^2)$
IIa + $\alpha_2 - M \rightarrow$ IIa:$\alpha_2 - M$	$k = 488M^{-1}s^{-1}$	$k \sim 10 \wedge N(2.69, 2.5^2)$
XIa + C1-inh $\rightarrow$ XIa:C1-inh	$k = 1.1 \times 10^3 M^{-1}s^{-1}$	$k \sim 10 \wedge N(3.04, 0.3^2)$
XIa + PAI-1 $\rightarrow$ XIa:PAI-1	$k = 2.1 \times 10^5 M^{-1}s^{-1}$	$k \sim 10 \wedge N(5.32, 2.5^2)$
Fbg + IIa $\leftrightarrow$ Fbg:IIa	$k_+ = 1 \times 10^8 M^{-1}s^{-1}$,	$k_+ \sim 10 \wedge N(8, 1.5^2)$,
	$k_- = 636s^{-1}$	$k_- \sim 10 \wedge N(2.8, 1.5^2)$
Fbg:IIa $\rightarrow$ Fbn1 + IIa + FPA	$k_{\text{cat}} = 84s^{-1}$	$k_{\text{cat}} \sim 10 \wedge N(1.92, 1.5^2)$
Fbn1 + IIa $\leftrightarrow$ Fbn1:IIa	$k_+ = 1 \times 10^8 M^{-1}s^{-1}$,	$k_+ \sim 10 \wedge N(8, 1.5^2)$,
	$k_- = 743s^{-1}$	$k_- \sim 10 \wedge N(2.87, 1.5^2)$
Fbn1:IIa $\rightarrow$ Fbn2 + IIa + FPB	$k_{\text{cat}} = 7.45s^{-1}$	$k_{\text{cat}} \sim 10 \wedge N(0.87, 1.5^2)$
Fbn2 + IIa $\leftrightarrow$ Fbn2:IIa	$k_+ = 1 \times 10^8 M^{-1}s^{-1}, k_- = 1 \times 10^3 s^{-1}$	$k_+ \sim 10 \wedge N(8, 1.5^2), k_- \sim 10 \wedge N(3, 1.5^2)$
Fbn1:IIa + AT $\rightarrow$ Fbn1:IIa:AT	$k = 6.1 \times 10^3 M^{-1}s^{-1}$	$k \sim 10 \wedge N(3.79, 1.5^2)$

Fbn2:IIa + AT → Fbn2:IIa:AT	$k = 3.8 \times 10^3 M^{-1}s^{-1}$	$k \sim 10 \wedge N(3.58, 1.5^2)$
Substrate + IIa ↔ Substrate:IIa	$k_+ = 1 \times 10^8 M^{-1}s^{-1}, k_- = 1.95 \times 10^5 s^{-1}$	$K_m \sim 10 \wedge N(-2.71, 0^2)$,
Substrate:IIa → Activated Substrate + IIa	$k_{\text{cat}} = 1.91 s^{-1}$	$k_{\text{cat}} \sim 10 \wedge N(0.28, 0^2)$

Table 5.3: The reactions used in the Improved Unified Model with their corresponding default reaction rates and priors.

Reaction	Gradient Descent Rates	ABC-SMC Rates
TF + VII ↔ TF:VII	$k_+ = 1.87 \times 10^6 M^{-1}s^{-1}$, $k_- = 5.62 \times 10^{-3} s^{-1}$	$k_+ = 1.22 \times 10^5 M^{-1}s^{-1}$, $k_- = 3.66 \times 10^{-4} s^{-1}$
TF + VIIa ↔ TF:VIIa	$k_+ = 1.01 \times 10^6 M^{-1}s^{-1}$, $k_- = 3.22 \times 10^{-3} s^{-1}$	$k_+ = 8.19 \times 10^4 M^{-1}s^{-1}$, $k_- = 2.62 \times 10^{-4} s^{-1}$
VII + Xa ↔ VII:Xa	$k_+ = 1 \times 10^8 M^{-1}s^{-1}, k_- = 109 s^{-1}$	$k_+ = 1 \times 10^{11} M^{-1}s^{-1}, k_- = 1.37 \times 10^3 s^{-1}$
VII:Xa → VIIa + Xa	$k_{\text{cat}} = 119 s^{-1}$	$k_{\text{cat}} = 681 s^{-1}$
TF:VII + Xa ↔ TF:VII:Xa	$k_+ = 1 \times 10^9 M^{-1}s^{-1}, k_- = 34.5 s^{-1}$	$k_+ = 1 \times 10^8 M^{-1}s^{-1}, k_- = 0.05 s^{-1}$
TF:VII:Xa → TF:VIIa + Xa	$k_{\text{cat}} = 23.4 s^{-1}$	$k_{\text{cat}} = 0.75 s^{-1}$
VII + IIa ↔ VII:IIa	$k_+ = 1 \times 10^8 M^{-1}s^{-1}, k_- = 270 s^{-1}$	$k_+ = 1 \times 10^8 M^{-1}s^{-1}, k_- = 270 s^{-1}$
VII:IIa → VIIa + IIa	$k_{\text{cat}} = 1.15 \times 10^{-4} s^{-1}$	$k_{\text{cat}} = 4.92 \times 10^{-3} s^{-1}$
TF:VII + IIa ↔ TF:VII:IIa	$k_+ = 1 \times 10^8 M^{-1}s^{-1}, k_- = 2.56 \times 10^3 s^{-1}$	$k_+ = 1 \times 10^{10} M^{-1}s^{-1}, k_- = 4.96 \times 10^3 s^{-1}$
TF:VII:IIa → TF:VIIa + IIa	$k_{\text{cat}} = 2.05 \times 10^{-4} s^{-1}$	$k_{\text{cat}} = 3.02 \times 10^3 s^{-1}$
VII + IXa ↔ VII:IXa	$k_+ = 1 \times 10^8 M^{-1}s^{-1}, k_- = 1.28 \times 10^3 s^{-1}$	$k_+ = 1 \times 10^8 M^{-1}s^{-1}, k_- = 3.13 s^{-1}$
VII:IXa → VIIa + IXa	$k_{\text{cat}} = 2.69 s^{-1}$	$k_{\text{cat}} = 1.53 s^{-1}$
TF:VII + IXa ↔ TF:VII:IXa	$k_+ = 1 \times 10^8 M^{-1}s^{-1}, k_- = 7.25 \times 10^2 s^{-1}$	$k_+ = 1 \times 10^8 M^{-1}s^{-1}, k_- = 12.3 s^{-1}$
TF:VII:IXa → TF:VIIa + IXa	$k_{\text{cat}} = 1.45 s^{-1}$	$k_{\text{cat}} = 0.026 s^{-1}$
VII + TF:VIIa ↔ VII:TF:VIIa	$k_+ = 1 \times 10^8 M^{-1}s^{-1}, k_- = 1.46 \times 10^3 s^{-1}$	$k_+ = 1 \times 10^8 M^{-1}s^{-1}, k_- = 4.3 \times 10^3 s^{-1}$
VII:TF:VIIa → VIIa + TF:VIIa	$k_{\text{cat}} = 1.4 s^{-1}$	$k_{\text{cat}} = 1.4 s^{-1}$
TF:VIIa + AT → TF:VIIa:AT	$k = 2.47 \times 10^3 M^{-1}s^{-1}$	$k = 5.56 \times 10^3 M^{-1}s^{-1}$

[†] k_+ here refers to the forward rate rather than the association/binding rate. This means that k_- is given by $\frac{k_+}{K_d}$.

X + TF:VIIa $\leftrightarrow$ X:TF:VIIa	$k_+ = 1 \times 10^{11} M^{-1}s^{-1}, k_- = 126 s^{-1}$	$k_+ = 1 \times 10^{8} M^{-1}s^{-1}, k_- = 94.4 s^{-1}$
X:TF:VIIa $\rightarrow$ Xa + TF:VIIa	$k_{\text{cat}} = 15.8 s^{-1}$	$k_{\text{cat}} = 2.81 s^{-1}$
X + VIIa $\leftrightarrow$ X:VIIa	$k_+ = 1 \times 10^{8} M^{-1}s^{-1}, k_- = 398 s^{-1}$	$k_+ = 1 \times 10^{8} M^{-1}s^{-1}, k_- = 15.5 s^{-1}$
X:VIIa $\rightarrow$ Xa + VIIa	$k_{\text{cat}} = 3.2 \times 10^{-4} s^{-1}$	$k_{\text{cat}} = 3.2 \times 10^{-4} s^{-1}$
X + IXa:VIIIa $\leftrightarrow$ X:IXa:VIIIa	$k_+ = 1 \times 10^{11} M^{-1}s^{-1}, k_- = 50.1 s^{-1}$	$k_+ = 1 \times 10^{9} M^{-1}s^{-1}, k_- = 59.4 s^{-1}$
X:IXa:VIIIa $\rightarrow$ Xa + IXa:VIIIa	$k_{\text{cat}} = 16.7 s^{-1}$	$k_{\text{cat}} = 6.96 s^{-1}$
X + IXa $\leftrightarrow$ X:IXa	$k_+ = 1 \times 10^{8} M^{-1}s^{-1}, k_- = 0.187 s^{-1}$	$k_+ = 1 \times 10^{8} M^{-1}s^{-1}, k_- = 0.96 s^{-1}$
X:IXa $\rightarrow$ Xa + IXa	$k_{\text{cat}} = 2.15 \times 10^{-4} s^{-1}$	$k_{\text{cat}} = 1.45 \times 10^{-3} s^{-1}$
V + IIa $\leftrightarrow$ V:IIa	$k_+ = 1 \times 10^{8} M^{-1}s^{-1}, k_- = 31.2 s^{-1}$	$k_+ = 1 \times 10^{10} M^{-1}s^{-1}, k_- = 1.20 s^{-1}$
V:IIa $\rightarrow$ Va + IIa	$k_{\text{cat}} = 3.18 s^{-1}$	$k_{\text{cat}} = 0.33 s^{-1}$
V + Xa $\leftrightarrow$ V:Xa	$k_+ = 1 \times 10^{8} M^{-1}s^{-1}, k_- = 6.14 s^{-1}$	$k_+ = 1 \times 10^{8} M^{-1}s^{-1}, k_- = 3.34 \times 10^{3} s^{-1}$
V:Xa $\rightarrow$ Va + Xa	$k_{\text{cat}} = 0.299 s^{-1}$	$k_{\text{cat}} = 1.33 s^{-1}$
Xa + Va $\leftrightarrow$ Xa:Va	$k_+ = 1.39 \times 10^{10} M^{-1}s^{-1}, k_- = 0.338 s^{-1}$	$k_+ = 9.24 \times 10^{10} M^{-1}s^{-1}, k_- = 0.35 s^{-1}$
Xa + AT $\rightarrow$ Xa:AT	$k = 5.23 \times 10^{3} M^{-1}s^{-1}$	$k = 1.36 \times 10^{3} M^{-1}s^{-1}$
Xa:Va + AT $\rightarrow$ Xa:Va:AT	$k = 3.52 \times 10^{3} M^{-1}s^{-1}$	$k = 0.27 M^{-1}s^{-1}$
II + Xa $\leftrightarrow$ II:Xa	$k_+ = 1 \times 10^{8} M^{-1}s^{-1}, k_- = 903 s^{-1}$	$k_+ = 1 \times 10^{8} M^{-1}s^{-1}, k_- = 31.7 s^{-1}$
II:Xa $\rightarrow$ IIa + Xa	$k_{\text{cat}} = 9.3 \times 10^{-3} s^{-1}$	$k_{\text{cat}} = 9.3 \times 10^{-3} s^{-1}$
II + Xa:Va $\leftrightarrow$ II:Xa:Va	$k_+ = 1 \times 10^{8} M^{-1}s^{-1}, k_- = 0.462 s^{-1}$	$k_+ = 1 \times 10^{8} M^{-1}s^{-1}, k_- = 145 s^{-1}$
II:Xa:Va $\rightarrow$ IIa + Xa:Va	$k_{\text{cat}} = 83.9 s^{-1}$	$k_{\text{cat}} = 41.1 s^{-1}$
IIa + AT $\rightarrow$ IIa:AT	$k = 4.02 \times 10^{3} M^{-1}s^{-1}$	$k = 5.39 \times 10^{3} M^{-1}s^{-1}$
XI + IIa $\leftrightarrow$ XI:IIa	$k_+ = 1 \times 10^{8} M^{-1}s^{-1}, k_- = 95 s^{-1}$	$k_+ = 1 \times 10^{8} M^{-1}s^{-1}, k_- = 2.13 s^{-1}$
XI:IIa $\rightarrow$ XIa + IIa	$k_{\text{cat}} = 9.83 \times 10^{-5} s^{-1}$	$k_{\text{cat}} = 1.65 \times 10^{-5} s^{-1}$
XI + XIa $\leftrightarrow$ XI:XIa	$k_+ = 1 \times 10^{8} M^{-1}s^{-1}, k_- = 22.4 s^{-1}$	$k_+ = 1 \times 10^{8} M^{-1}s^{-1}, k_- = 0.051 s^{-1}$
XI:XIa $\rightarrow$ XIa + XIa	$k_{\text{cat}} = 2.94 \times 10^{-4} s^{-1}$	$k_{\text{cat}} = 1.14 \times 10^{-4} s^{-1}$
XIa + AT $\rightarrow$ XIa:AT	$k = 400 M^{-1}s^{-1}$	$k = 400 M^{-1}s^{-1}$
IX + TF:VIIa $\leftrightarrow$ IX:TF:VIIa	$k_+ = 1 \times 10^{8} M^{-1}s^{-1}, k_- = 87.2 s^{-1}$	$k_+ = 1 \times 10^{8} M^{-1}s^{-1}, k_- = 4.02 s^{-1}$
IX:TF:VIIa $\rightarrow$ IXa + TF:VIIa	$k_{\text{cat}} = 0.43 s^{-1}$	$k_{\text{cat}} = 0.43 s^{-1}$
IX + VIIa $\leftrightarrow$ IX:VIIa	$k_+ = 1 \times 10^{8} M^{-1}s^{-1}, k_- = 0.817 s^{-1}$	$k_+ = 1 \times 10^{8} M^{-1}s^{-1}, k_- = 6.46 s^{-1}$

IX:VIIa $\rightarrow$ IXa + VIIa	$k_{\text{cat}} = 1.34 \times 10^{-4} s^{-1}$	$k_{\text{cat}} = 9.11 \times 10^{-5} s^{-1}$
IX + XIa $\leftrightarrow$ IX:XIa	$k_+ = 1 \times 10^8 M^{-1} s^{-1}, k_- = 689 s^{-1}$	$k_+ = 1 \times 10^8 M^{-1} s^{-1}, k_- = 24.3 s^{-1}$
IX:XIa $\rightarrow$ IXa + XIa	$k_{\text{cat}} = 0.924 s^{-1}$	$k_{\text{cat}} = 0.33 s^{-1}$
VIII + IIa $\leftrightarrow$ VIII:IIa	$k_+ = 1 \times 10^9 M^{-1} s^{-1}, k_- = 1.28 s^{-1}$	$k_+ = 1 \times 10^8 M^{-1} s^{-1}, k_- = 0.94 s^{-1}$
VIII:IIa $\rightarrow$ VIIIa + IIa	$k_{\text{cat}} = 0.8 s^{-1}$	$k_{\text{cat}} = 0.8 s^{-1}$
VIII + Xa $\leftrightarrow$ VIII:Xa	$k_+ = 1 \times 10^8 M^{-1} s^{-1}, k_- = 56.5 s^{-1}$	$k_+ = 1 \times 10^8 M^{-1} s^{-1}, k_- = 62.7 s^{-1}$
VIII:Xa $\rightarrow$ VIIIa + Xa	$k_{\text{cat}} = 1.26 s^{-1}$	$k_{\text{cat}} = 2.74 s^{-1}$
VIIIa $\leftrightarrow$ VIIIa_1L + VIIIa_2	$k_+ = 1.82 \times 10^{-2} s^{-1}$, $k_- = 6.86 \times 10^4 M^{-1} s^{-1}$	$k_+ = 3.88 \times 10^{-2} s^{-1}$, $k_- = 1.47 \times 10^5 M^{-1} s^{-1}$
IXa:VIIIa $\rightarrow$ IXa + VIIIa_1L + VIIIa_2	$k = 8.96 \times 10^{-3} M^{-1} s^{-1}$	$k = 0.037 M^{-1} s^{-1}$
IXa + VIIIa $\leftrightarrow$ IXa:VIIIa	$k_+ = 5.51 \times 10^7 M^{-1} s^{-1}, k_- = 0.306 s^{-1}$	$k_+ = 1.26 \times 10^{11} M^{-1} s^{-1}, k_- = 297 s^{-1}$
IXa + AT $\rightarrow$ IXa:AT	$k = 2.79 \times 10^3 M^{-1} s^{-1}$	$k = 1.66 M^{-1} s^{-1}$
IXa:VIIIa + AT $\rightarrow$ IXa:VIIIa:AT	$k = 2.45 \times 10^3 M^{-1} s^{-1}$	$k = 2.35 \times 10^3 M^{-1} s^{-1}$
Xa + TFPI $\leftrightarrow$ Xa:TFPI	$k_+ = 1.39 \times 10^7 M^{-1} s^{-1}$, $k_- = 1.28 \times 10^{-3} s^{-1}$	$k_+ = 1.11 \times 10^6 M^{-1} s^{-1}$, $k_- = 1.03 \times 10^{-4} s^{-1}$
TF:VIIa + Xa:TFPI $\leftrightarrow$ TF:VIIa:Xa:TFPI	$k_+ = 8.9 \times 10^6 M^{-1} s^{-1}$, $k_- = 1.34 \times 10^{-3} s^{-1}$	$k_+ = 8.9 \times 10^6 M^{-1} s^{-1}$, $k_- = 1.34 \times 10^{-3} s^{-1}$
IIa + $\alpha_1 - AT$ $\rightarrow$ IIa:$\alpha_1 - AT$	$k = 156 M^{-1} s^{-1}$	$k = 102 M^{-1} s^{-1}$
Xa + $\alpha_1 - AT$ $\rightarrow$ Xa:$\alpha_1 - AT$	$k = 87.5 M^{-1} s^{-1}$	$k = 124 M^{-1} s^{-1}$
Xa:Va + $\alpha_1 - AT$ $\rightarrow$ Xa:Va:$\alpha_1 - AT$	$k = 4.43 \times 10^3 M^{-1} s^{-1}$	$k = 4.24 M^{-1} s^{-1}$
XIa + $\alpha_1 - AT$ $\rightarrow$ XIa:$\alpha_1 - AT$	$k = 82 M^{-1} s^{-1}$	$k = 82 M^{-1} s^{-1}$
XIa + $\alpha_2 - AP$ $\rightarrow$ XIa:$\alpha_2 - AP$	$k = 656 M^{-1} s^{-1}$	$k = 656 M^{-1} s^{-1}$
IIa + $\alpha_2 - M$ $\rightarrow$ IIa:$\alpha_2 - M$	$k = 465 M^{-1} s^{-1}$	$k = 4.98 M^{-1} s^{-1}$
XIa + C1-inh $\rightarrow$ XIa:C1-inh	$k = 1.1 \times 10^3 M^{-1} s^{-1}$	$k = 1.1 \times 10^3 M^{-1} s^{-1}$
XIa + PAI-1 $\rightarrow$ XIa:PAI-1	$k = 1.09 \times 10^6 M^{-1} s^{-1}$	$k = 2.96 \times 10^5 M^{-1} s^{-1}$
Fbg + IIa $\leftrightarrow$ Fbg:IIa	$k_+ = 1.42 \times 10^8 M^{-1} s^{-1}$, $k_- = 6.57 \times 10^3 s^{-1}$	$k_+ = 1.10 \times 10^8 M^{-1} s^{-1}$, $k_- = 77.4 s^{-1}$
Fbg:IIa $\rightarrow$ Fbn1 + IIa + FPA	$k_{\text{cat}} = 299 s^{-1}$	$k_{\text{cat}} = 291 s^{-1}$

Fbn1 + IIa $\leftrightarrow$ Fbn1:IIa	$k_+ = 6.51 \times 10^8 M^{-1}s^{-1}$,	$k_+ = 1.15 \times 10^7 M^{-1}s^{-1}$,
	$k_- = 1.59 \times 10^3 s^{-1}$	$k_- = 1.61 \times 10^4 s^{-1}$
Fbn1:IIa $\rightarrow$ Fbn2 + IIa + FPB	$k_{\text{cat}} = 50 s^{-1}$	$k_{\text{cat}} = 17.8 s^{-1}$
Fbn2 + IIa $\leftrightarrow$ Fbn2:IIa	$k_+ = 9.62 \times 10^4 M^{-1}s^{-1}$,	$k_+ = 3.48 \times 10^7 M^{-1}s^{-1}$,
	$k_- = 2.93 \times 10^3 s^{-1}$	$k_- = 2.79 \times 10^3 s^{-1}$
Fbn1:IIa + AT $\rightarrow$ Fbn1:IIa:AT	$k = 864 M^{-1}s^{-1}$	$k = 3.13 \times 10^4 M^{-1}s^{-1}$
Fbn2:IIa + AT $\rightarrow$ Fbn2:IIa:AT	$k = 2.16 \times 10^4 M^{-1}s^{-1}$	$k = 106 M^{-1}s^{-1}$
Substrate + IIa $\leftrightarrow$ Substrate:IIa	$k_+ = 1 \times 10^8 M^{-1}s^{-1}, k_- = 1.95 \times 10^5 s^{-1}$	$k_+ = 1 \times 10^8 M^{-1}s^{-1}, k_- = 1.95 \times 10^5 s^{-1}$
Substrate:IIa $\rightarrow$ Activated Substrate + IIa	$k_{\text{cat}} = 1.91 s^{-1}$	$k_{\text{cat}} = 1.91 s^{-1}$

Table 5.4: The reactions used in the Improved Unified Model with their corresponding fitted reaction rates from both the Gradient Descent and the ABC-SMC algorithms.

	Fitting Method	R^2	RMSE_{fit}	$\text{RMSE}_{1:1}$
Improved Unified Model	No fitting	0.08	29.8	34.3
	Gradient Descent	0.24	26.9	29.7
	ABC-SMC	0.21	27.3	31.1

Table 5.5: The predictive accuracy of the Improved Unified Model, before fitting and after gradient descent and ABC-SMC fitting.

Fitting Method		Training Cost	Test Cost
No fitting		N/A	298
Gradient Descent	Cross Validation	167±6	164±22
	Full	167	N/A
ABC-SMC	Cross Validation	178±12	179±34
	Full	175	N/A

Table 5.6: The results from the Improved Unified Model fitting process. Cross validation costs are given as mean$\pm\frac{1}{2}\times$range from the five folds.

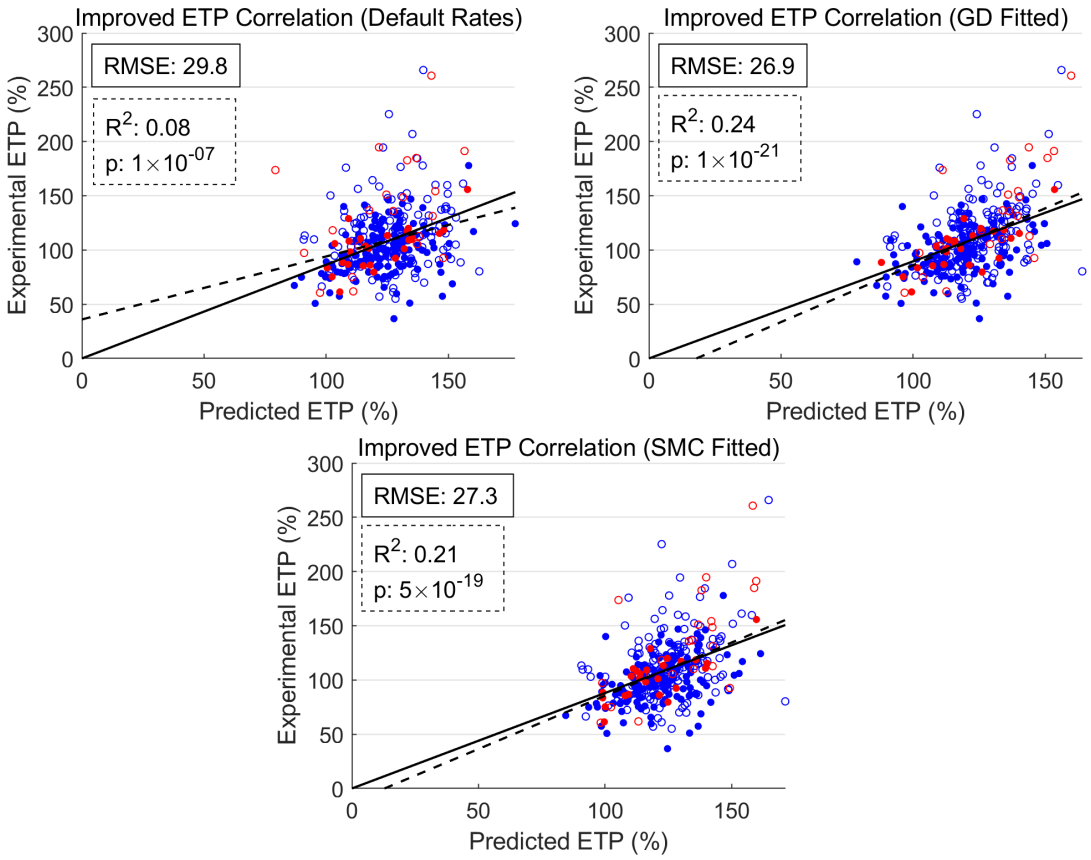

Figure 5.12: The ETP correlation scatter graphs for the Improved Unified Model for the default, gradient descent fitted, and ABC-SMC fitted reaction rates.

Figure 5.13 shows the OD curves for the individuals with the best and worst

ETP predictions, given for the gradient descent fitted rates and the ABC-SMC fitted rates. The worst predicted individuals draw similar conclusions to those seen previously, suggesting we may not have achieved partial prothrombin conversion. The best predicted individual for the gradient descent fitted rates matches well in both lagtime and shape, while the ABC-SMC fitted rates show a longer model predicted lagtime and smoother shape.

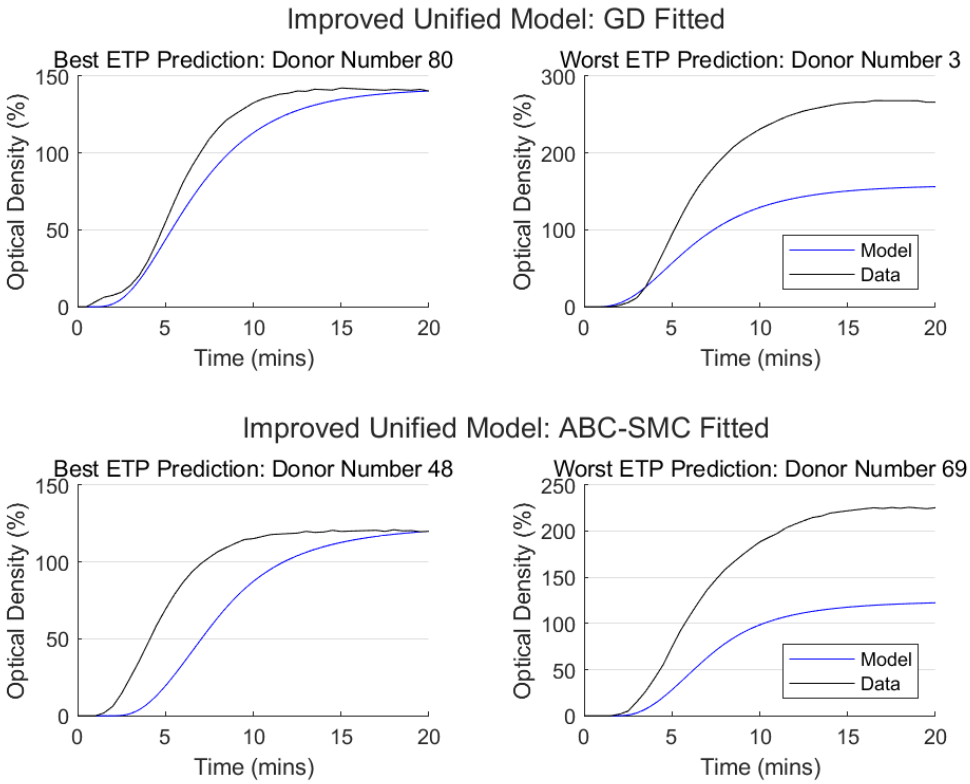

Figure 5.13: The Improved Unified Model predicted OD curve and the experimental OD curve for the individuals with the best and worst predicted ETP, separated by the Gradient Descent (top) and ABC-SMC (bottom) fitted rates.

5.6.2 Partial Prothrombin Conversion

One of the improvements we aimed to make with this new model was to build a model which can predict partial prothrombin conversion while using realistic reaction rates. To test if this has worked and to see if this property continues after fitting, prothrombin conversion curves are given in Figure 5.15.

We were unable to achieve partial prothrombin conversion in the Improved Unified Model. The reason for this was investigated by comparing the reaction rates in the Improved Unified Model to that of the Reduced Unified Model that the partial prothrombin conversion result was achieved with. It was found that the result from the Reduced Unified Model relied on the use of the fitted rates, specifically on the large k_- for the activation of FII by Xa:Va given in the fitted rates ($K_m = 3 \times 10^{-5} M, k_{\text{cat}} = 365 s^{-1} \Rightarrow k_- = 2.6 \times 10^3 s^{-1}$) compared with the

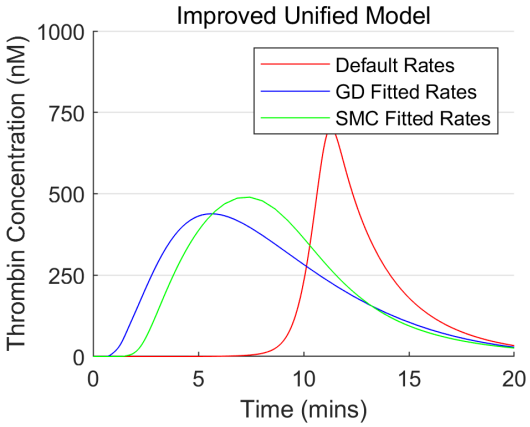

Figure 5.14: The thrombin generation curves for the Improved Unified Model, before fitting and after gradient descent and ABC-SMC fitting.

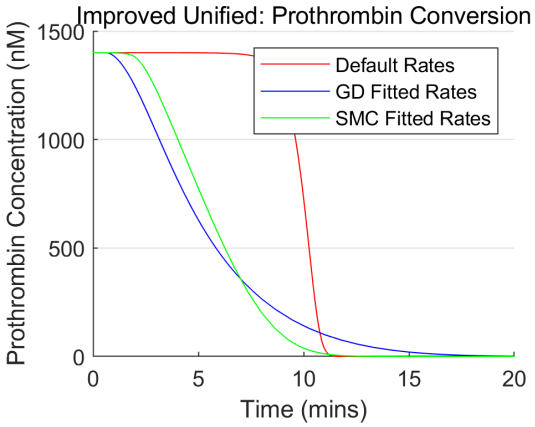

Figure 5.15: The prothrombin conversion curves are given for the Improved Unified Model with the default, gradient descent fitted, and ABC-SMC fitted reaction rates.

default rates ($K_m = 7 \times 10^{-7}M, k_{\text{cat}} = 36s^{-1} \Rightarrow k_- = 34s^{-1}$). It may be the case that either a high k_- for FII activation by Xa:Va or inhibition of the bound complex II:Xa:Va is needed to properly inhibit Xa:Va, however, it appears more data is needed on the inhibition of the complexes and on which factors are fully or partially converted before partial prothrombin conversion can be achieved by the models.

5.6.3 Model Uncertainty

Due to the large variation in reaction rates, Hemker proposed that the models may result in significant amounts of uncertainty in their predictions [76]. Most reaction rates in the previous models are defined using a single source, with only 10% of reaction rates using multiple sources, all of which then take an average value. Thanks to our prior distributions, allowing us to quantify variation between different sources for many reaction rates, we can provide an answer as to whether or not this variation results in significant model uncertainty.

To quantify the variation in the reaction rates, we use our prior distributions with one change. The variation in reaction rates that only have a single source or use approximated values, currently assumed to be a log-normal standard deviation of 2.5, is instead set to a log-normal standard deviation of 0.5 (the average log-normal standard deviation of the reaction rates with multiple sources). We then draw 2000 samples from these edited prior distributions and use them to generate 2000 OD curves in the Improved Unified Model.

Figure 5.16 presents the resulting variation in these OD curves, showing the median OD curve and both the central 50% and 90% of the variance in the OD curves. We see a significant amount of uncertainty in the model predictions and it is clear that identifying a single source for each reaction rate is insufficient if precautions are not made to reproduce a particular experimental setting. Figure 5.17 shows the resulting uncertainty after fitting. It shows the variation in the 2000 sampled reaction rates from the ABC-SMC posterior distributions and the variation is dramatically reduced compared with that before fitting. It appears fitting the reaction rates is a suitable method to manage this uncertainty.

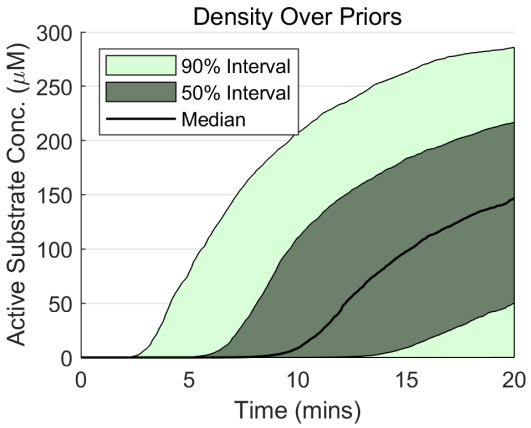

Figure 5.16: A measure of the uncertainty in model predictions through variation across the prior distributions.

5.6.4 Effect of Healthy Variation in Other Inhibitors

During the fitting process, there are a handful of factors for which we do not have patient specific data ($\alpha_1 - AT$, $\alpha_2 - AP$, $\alpha_2 - M$, PAI-1 and C1-inh). Due to this, we assume a fixed, healthy value for each of these inhibitors. It is possible that varying these factors across a healthy range could produce a significant change in the thrombin generation curves, suggesting that fitting without this data would be unlikely to work.

We have gathered data on each of these factors to find a healthy range, given in Table 5.7, and simulated thrombin generation curves using the Improved Unified Model for 500 randomly sampled initial concentrations of these inhibitors from the uniform hypercube defined by their healthy ranges. All model reaction rates were

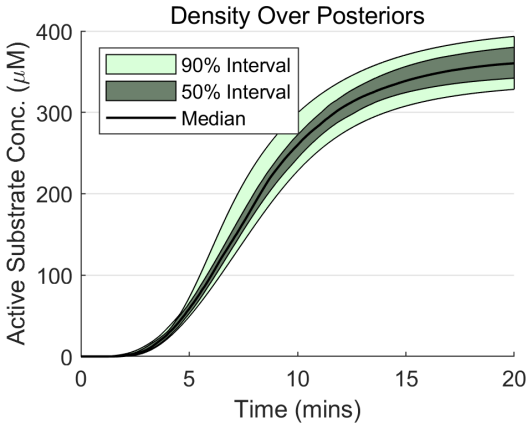

Figure 5.17: A measure of the uncertainty in model predictions, after fitting, through variation across the ABC-SMC posterior distributions.

fixed at their default values. Figure 5.18 gives the mean and median thrombin generation curves and 5th and 95th percentiles to show variation. We see that varying across a healthy range for these inhibitors does not produce a significant change in the thrombin generation curves, so it is unlikely that patient specific data for these would improve model predictions.

Inhibitor	Healthy Range	Sources
$\alpha_1 - AT$	$16\mu M$ to $32\mu M$	$0.9g/L$ to $1.75g/L$ [123]. 54kDa [124].
$\alpha_2 - AP$	$0.4\mu M$ to $1.2\mu M$	Range of 45% to 128% [125]. Using our default concentration of $0.95\mu M$ (other sources report similarly, $\sim 1\mu M$ [126]).
$\alpha_2 - M$	$2.365\mu M$ to $2.601\mu M$	$178.8 \pm 8.5mg/dl$ [127]. 720kDa [128].
PAI-1	$0.1pM$ to $0.4pM$	$5ng/ml$ to $20ng/ml$ [129]. 49kDa [130].
C1-inh	$1\mu M$ to $6\mu M$	Mean: $0.25g/L$, SD: $0.09g/L$ [131]. 71kDa [132].

Table 5.7: The healthy concentrations for the inhibitors $\alpha_1 - AT$, $\alpha_2 - AP$, $\alpha_2 - M$, PAI-1 and C1-inh.

5.7 Conclusions

After building the Improved Unified Model, we did not see significant improvement compared to the previous work in Chapter 3. However, we did introduce more qualitative improvements through more accurate rates for factor XI activation and the introduction of a new mechanism for complex inhibition which was shown in a previous version of the Unified Model to predict partial prothrombin conversion. We also further identified the cause for the long lagtime in the default rates (Section 5.4) and included more accurate reaction rates for FXI activation (Section 5.3). Finally, we showed that a model which uses a single source for each reaction rate results in high levels of uncertainty in model predictions if the

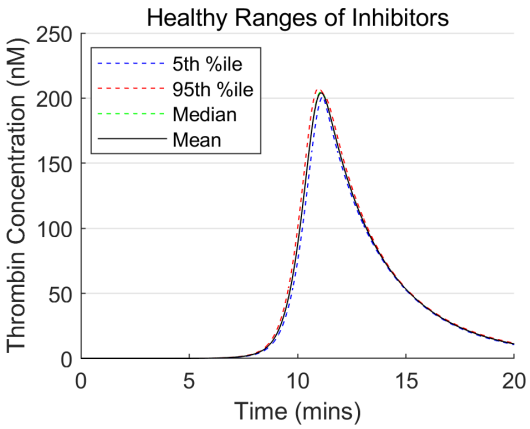

Figure 5.18: The distribution of thrombin generation curves under healthy variation of the inhibitors $\alpha_1 - AT$, $\alpha_2 - AP$, $\alpha_2 - M$, PAI-1 and C1-inh.

experimental conditions are not matched. In Section 5.6.3, we then showed that fitting to a data set is sufficient to significantly reduce this uncertainty.

One point that we have not addressed in the model uncertainty is the use of averaging multiple reaction rates to produce a single value. Some of the models make use of this as a way to include multiple sources for each reaction rate. While it is true that this would reduce the variation in the implemented reaction rates, this does not necessarily mean that model uncertainty is improved. The use of averaging the reaction rates requires variation between sources to be the result of experimental noise, however, given that each source shows small variation upon repeated measurements, and it is only between the different sources that large variation occurs, it seems more likely that this variation is due to differing experimental conditions, which cannot be improved by averaging across multiple sources. It is possible that, if the experimental conditions were sufficiently similar to one another, then the derived reaction rates could be used together without fitting. However, given that many reaction rates still have only one or two sources, this is not a viable method for the foreseeable future.

After showing that variation in the inhibitors that we do not have individual level concentrations for is not the cause for a poor model fit (Section 5.6.4), we now move ahead and begin a simulation study to assess the fitting methods we use. Hopefully, this will grant us insight into how the model fitting can be improved and if the model is lacking in its construction.

Chapter 6

Simulation Study

6.1 Introduction

Through the development of multiple versions of the Unified Model, we have been unable to accurately reproduce patient data across the cohort, including after fitting. This could be due to discrepancies between the reactions used in the model and the reactions involved in the assay that generated the data, or there could be issues with the parameter fitting methods we are using. We have explored the former through the use of different versions of the Unified Model in Chapters 3 and 5 and the previously completed data analysis in Section 4.4. In this chapter, we explore the latter through a simulation study.

We will complete our simulation study in batches, each focusing on answering a separate question about the fitting process. Each batch will complete the following steps (further detailed in Figure 6.1 and in the methods section of batch 1):

1. Generate Data Sets
2. Parameter Fitting
3. Performance Evaluation Metrics

6.2 Batch 1 - Exploration of Fitting Methods

The first batch will be a basic assessment of the fitting methods we use with the conclusions then informing the later batches.

6.2.1 Methods

Generate Data Sets

In order to generate the simulated data sets, we first require a set of reaction rates. For this batch, the set of reaction rates is randomly sampled from the prior distributions under the added condition that the shape of the resulting thrombin

generation curve (for pooled plasma initial factor concentrations) should be realistic*. Once we have the sampled set of reaction rates, which we term the *'true'* rates, we can simulate the Improved Unified Model, using these reaction rates, for the initial factor concentrations in the data set (measurements of TF, AT, TFPI and factors II, V, VII, VIII, IX, X and XI for 333 individuals). We then extract the chromogenic substrate concentrations and normalise them by the final concentration of the pooled plasma initial conditions to match the form of the data. We repeat this to generate five different, independent sets of reaction rates and their corresponding predicted OD curves to produce five repetitions (for brevity, referred to here as reps). We do not add noise to the simulated data based on the results in Section 3.3.2.

Parameter Fitting

We will use both the Gradient Descent and ABC-SMC fitting algorithms for our parameter fitting, using similar methods to our previous fitting of the Improved Unified Model. For this first batch, the reaction rates that would normally remain fixed during fitting, determined using the method described in Chapter 3, are set to the *'true'* rates. This ensures the parameter space explored by the fitting methods contains the *'true'* rates. We will then explore the consequences of using the default values for these instead of the *'true'* rates in the following batch. We use the cost metric defined previously, and given again below in Equation (6.1), for evaluating model fit in both fitting algorithms. The ABC-SMC algorithm uses the prior distributions given for the Improved Unified Model (the same ones that were used to sample the *'true'* rates) and the parameters $N = 2000$, $U = 200$, $\varepsilon_0 = 400$ (the same as for the Improved Unified Model fitting). Both fitting algorithms fit the prior form of the reaction rates ($K_m, k_{\text{cat}}, K_d, k_+$) and then convert these to the mass action law form of the reaction rates (k_+, k_-, k_{cat}, using $k_+ = 1 \times 10^8 M^{-1} s^{-1}$ for enzymatic reactions) to simulate the model. In addition to this, we only fit reaction rates which, when varied to the 5th and 95th percentiles of their priors, give a significant change in the output (as defined in Section 3.2.5), specifically in the chromogenic substrate concentration.

$$\text{cost} = \sqrt{\frac{\sum_{i=1}^{n}[\sum_{j=0}^{40}((modelOD_{i,j} - dataOD_{i,j})^2)]}{n}} \tag{6.1}$$

Performance Evaluation Metrics

To assess the quality of fit, we will utilise two performance evaluation metrics.

To assess how closely the model predictions are to the predictions made by the *'true'* rates, we use the cost metric which is used for the fitting process and is given in Equation (6.1). The variables $dataOD_{i,j}$ and $modelOD_{i,j}$ represent the values of the OD curve of individual i at time-point j (time-points are from 0 to 20 minutes in intervals of 30 seconds) predicted by the *'true'* rates and the fitted

*This removes curves that do not reach a peak, have unusual or extreme shapes, etc.

reaction rates, respectively.

To evaluate how close the fitted reaction rates are to the *'true'* rates, we use RMSLE (Root Mean Squared Log Error), given by Equation (6.2), where k_i is the i^{th} *'true'* reaction rate and $\hat{k}_i$ is the i^{th} fitted reaction rate, both given in prior form.

$$\text{RMSLE} = \sqrt{\frac{1}{N}\sum_{i=1}^{N}(\log_{10}(k_i) - \log_{10}(\hat{k}_i))^2} \tag{6.2}$$

An overview of these methods is provided in Figure 6.1.

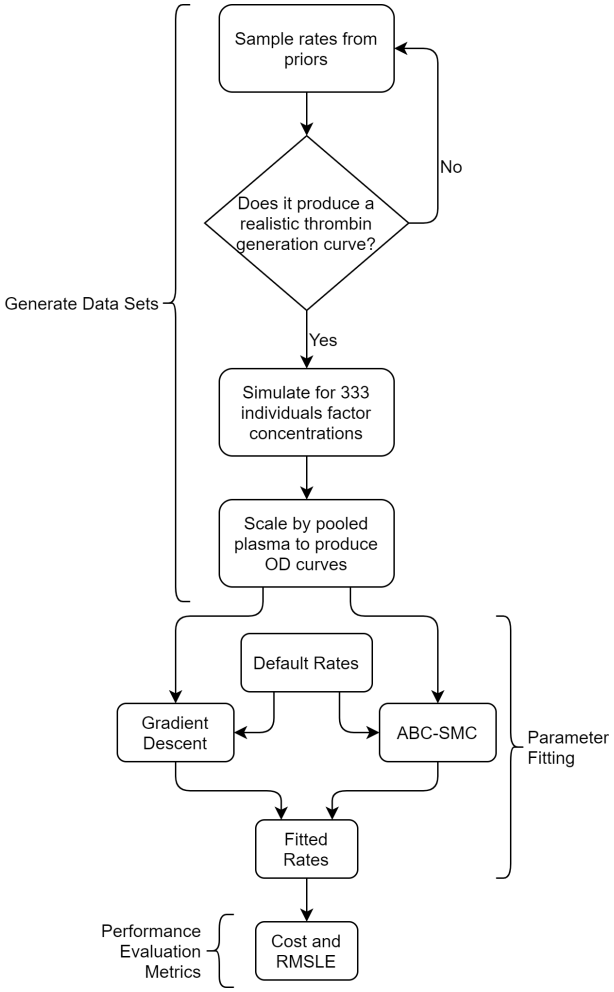

Figure 6.1: A flowchart outlining the steps in the first batch of the simulation study.

6.2.2 Results

The results of the first batch of the simulation study are shown in Table 6.1. There is a dramatic decrease in the cost after fitting, with four of the five reps achieving a cost below 30 in each of the fitting methods and all reps achieving a cost below

30 for at least one fitting method. The Improved Unified Model, when fitted to patient data, achieved a cost of 167, with all other versions of the Unified Model achieving similar costs. There appears to be a single repetition, rep 1, which the fitting struggled to reproduce. None of the repetitions were able to identify reaction rates that were similar to their respective *'true'* rates, with all fitted rates falling at around a RMSLE of 2 (on average the fitted reaction rates were a factor of 100 away from the true rates).

So while we were able to achieve a significantly lower cost, we were not able to recover the original parameters that were used to generate the data. In the following two batches, we will investigate assumptions that are made during the fitting process which may explain why this fitting achieves much lower cost than when fitting to patient data.

Rep	Default		Gradient Descent		ABC-SMC	
	Cost	RMSLE	Cost	RMSLE	Cost	RMSLE
1	497.1	1.80	235.2	2.18	25.2	2.06
2	255.8	1.92	28.4	2.02	18.7	1.96
3	348.7	2.04	23.1	2.05	12.5	1.72
4	245.4	1.63	9.2	1.62	16.1	1.80
5	115.2	1.90	18.2	1.92	46.9	2.20
Mean	292.4	1.86	62.8	1.96	23.9	1.95

Table 6.1: Performance metrics for the batch 1 fitting. Metrics are given for the default rates and the fitted reaction rates. The cost (Equation (6.1)) gives a measure of the difference in the OD curves and RMSLE (Equation (6.2)) measures the difference in the reaction rates (smaller is better for both metrics).

6.3 Batch 2 - Parameter Identifiability

In the previous batch, we included the *'true'* rates for the reaction rates that we do not fit. We did this to ensure that the parameter space the fitting methods could explore contained the *'true'* rates that were used to construct the data. In this batch, we instead fix these reaction rates at the default rates, as was done when fitting to patient data.

6.3.1 Methods

The methods used for this batch are identical to those used in batch 1, however, the reaction rates that are not varied through fitting are maintained at the default rate values (median of the prior distributions). Since the parameter space explored by the fitting methods now no longer contains the *'true'* rates, we also report the *'perfect'* cost and *'perfect'* RMSLE. These represent the metrics given when all reaction rates that are varied during fitting exactly match the *'true'* rates (those

used to generate the data) but those that are fixed during fitting are set to the default rates (different from the *'true'* rates used to generate the data).

This means that while the *'perfect'* RMSLE is the global minimum of the RMSLE metric (in the restricted parameter space where only some of the rates are fitted), the *'perfect'* cost will be non-zero (due to the differences in the rates that are not fitted). It is possible that the *'perfect'* cost is not even the global minimum of the cost metric in the restricted parameter space (since it may be the case that a lower cost can be achieved by accounting for the differences in parameters that cannot be fit by continuing to fit the parameters that can be fitted).

This batch reuses the data generated, and the *'true'* rates, from batch 1. This allows us to compare the results between these batches more easily without the effects of the random sampling of rates interfering with conclusions.

6.3.2 Results

Table 6.2 gives the cost and RMSLE for each set of fitted reaction rates. Interestingly, the cost is lower in this batch than in batch 1 in many cases, including rep 1 where the previous batch struggled to fit (235.2 and 25.2 in batch 1 vs 8.3 and 23.3 in batch 2).

The costs for both fitting methods are considerably lower than when fitting to the data (8-40 rather than 165-170), suggesting there is a significant difference between the data and the model predictions sampled from the prior. We will investigate a possible cause of this in batch 3.

The RMSLE is again around 2 for all reps (slight increase from batch 1), compared with *'perfect'* RMSLEs of 0.27-0.83, demonstrating that we are unable to identify the *'perfect'* reaction rates. Since the RMSLE for the default rates is lower than that of the fitted rates, the fitting method is not even converging towards the *'true'* rates.

Notably, the costs for some of the reps are below the *'perfect'* costs. This could only happen if the fitting is accounting for differences in the reaction rates that are fixed by further varying the reaction rates that are variable. This demonstrates that the set of reaction rates which cause a significant change in the model is changing throughout the fitting and resulting in the global minimum of the cost function not being the same as the global minimum in the RMSLE metric. We will further investigate this in batch 4.

This happens because the method for determining which parameters are significant is only locally determined (near the default rates). As the fitting progress and the algorithm moves away from the default rates other parameters can become significant and previously significant parameters can become insignificant.

Rep	Default		Gradient Descent		ABC-SMC		*'Perfect'*	
	Cost	RMSLE	Cost	RMSLE	Cost	RMSLE	Cost	RMSLE
1	497.1	1.80	8.3	2.38	23.3	1.88	127.2	0.83
2	255.8	1.92	28.5	2.14	39.6	2.23	4.4	0.27
3	348.7	2.04	19.3	2.37	16.5	2.32	16.6	0.70
4	245.4	1.63	8.0	1.71	16.1	2.21	15.0	0.47
5	115.2	1.90	13.7	1.95	17.1	1.86	123.3	0.47
Mean	292.4	1.86	15.6	2.11	22.5	2.10	57.3	0.55

Table 6.2: Performance metrics for the batch 2 fitting. Metrics are given for the default rates, the fitted reaction rates, both using Gradient Descent and ABC-SMC, followed by the *'perfect'* metrics. The cost (Equation (6.1)) gives a measure of the difference in the OD curves and RMSLE (Equation (6.2)) measures the difference in the reaction rates (smaller is better for both metrics).

6.4 Batch 3 - Assumption Testing

We have seen that for randomly sampled reaction rates from the prior, we are able to fit significantly better than for patient data. This would suggest that either the reaction rates that correspond to the data are far outside of the prior distributions[†] or the model structure does not match the data set. However, there is an assumption in how the reaction rates are generated that we have yet to test, the assumption that $k_+ = 1 \times 10^8 M^{-1}s^{-1}$ (the reaction is diffusion limited) for enzymatic reactions. There may be some variation in this rate for different reactions and this could explain why we are able to reproduce simulated data (which also uses this assumption) but not patient data (which may or may not follow this assumption).

6.4.1 Methods

This batch uses the data generating method outlined in batch 1 with one change. During the process of generating these data sets, when the reaction rates are converted from prior form $(K_m, k_{\text{cat}}, K_d, k_+)$ to the mass action law form $(k_+, k_-, k_{\text{cat}})$, as described in Section 3.2.3, instead of assuming $k_+ = 1 \times 10^8 M^{-1}s^{-1}$, we instead randomly choose a k_+ from a log-uniform distribution between $1 \times 10^4 M^{-1}s^{-1}$ and $1 \times 10^9 M^{-1}s^{-1}$[‡].

The fitting algorithm and performance evaluation methods are the same as in batch 2, including the fitting algorithms still assuming $k_+ = 1 \times 10^8 M^{-1}s^{-1}$ for enzymatic reactions. This allows us to see if, even under this assumption, we are

[†]This seems unlikely since we either have multiple sources giving us a known range where the reaction rates should fall or, where we only have a single rate, have assumed a very wide distribution around that point.

[‡]We still maintain the iterative increasing method for k_+ (described previously in Chapter 3) to ensure that $k_- > 0$. The values chosen for the bounds represent the upper and lower limits of values for k_+ used in the priors for the association reactions.

able to reproduce data which was generated without this assumption.

6.4.2 Results

Table 6.3 gives the cost and RMSLE for each set of fitted reaction rates. The achieved costs are higher than in batch 2 but still significantly lower than for fitting to patient data. The assumed value of the on rate appears to be sufficient to reproduce even data in which different values are used, although with a slight penalty to the achieved cost.

Rep	Default		Gradient Descent		ABC-SMC		*'Perfect'*	
	Cost	RMSLE	Cost	RMSLE	Cost	RMSLE	Cost	RMSLE
1	158.7	1.53	14.2	1.66	15.6	2.13	151.7	0.70
2	84.2	1.55	21.4	1.58	67.8	2.53	81.9	0.54
3	222.2	1.83	37.7	1.85	42.2	2.13	180.3	0.63
4	289.2	1.81	51.9	2.03	48.2	2.23	101.2	0.64
5	458.4	1.55	30.8	1.78	31.9	1.86	38.0	0.28
Mean	242.5	1.65	31.2	1.78	41.1	2.17	110.6	0.56

Table 6.3: Performance metrics for the batch 3 fitting. Metrics are given for the default rates, the fitted reaction rates, both using Gradient Descent and ABC-SMC, followed by the *'perfect'* metrics. The cost (Equation (6.1)) gives a measure of the difference in the OD curves and RMSLE (Equation (6.2)) measures the difference in the reaction rates (smaller is better for both metrics).

6.5 Batch 4 - Significant Rates

We saw in both batch 2 and batch 3 that the cost achieved by the fitting was frequently below the *'perfect'* cost. This suggests that there is a change in which reaction rates are significant during the fitting process and that the fitting is accounting for not being able to fit some of the reaction rates by changing others. This means that even if we were able to find the reaction rates which minimise the cost function (the global minimum), these rates would not necessarily minimise the RMSLE metric or be close to the *'true'* rates.

6.5.1 Methods

In this batch, we attempt to fix this problem by allowing all reaction rates[§] to vary during the fitting. This means we fit 86 reaction rates rather than the reduced number of 68. This means that the *'perfect'* cost and *'perfect'* RMSLE for this batch will both be zero. We will reuse the generated data sets from batch 1 so

that the cost and RMSLE can be compared directly.

6.5.2 Results

Table 6.4 gives the cost and RMSLE for each set of fitted reaction rates. We are able to achieve better costs for the gradient descent than we found in batches 1 and 2 but we still do not converge towards the *'true'* rates, ending up at rates that are a similar distance away as batches 1 and 2. We will now investigate the cost function to understand if changes can be made which further improve the fitting or aid in identifying the *'true'* rates.

Rep	Default		Gradient Descent		ABC-SMC	
	Cost	RMSLE	Cost	RMSLE	Cost	RMSLE
1	497.1	1.80	8.7	2.01	25.6	1.81
2	255.8	1.92	28.5	1.98	118.7	2.11
3	348.7	2.04	15.2	2.39	12.5	2.18
4	245.4	1.63	8.6	1.92	16.1	2.01
5	115.2	1.90	12.8	2.03	12.6	2.07
Mean	292.4	1.86	14.8	2.07	37.1	2.04

Table 6.4: Performance metrics for the batch 4 fitting. Metrics are given for the default rates and the fitted reaction rates only since the *'perfect'* metrics are all zero. The cost (Equation (6.1)) gives a measure of the difference in the OD curves and RMSLE (Equation (6.2)) measures the difference in the reaction rates (smaller is better for both metrics).

6.5.3 Cost Function

We have generated plots of the cost function as the reaction rates are linearly shifted from the fitted rates to the corresponding *'true'* rates (using the prior form of the reaction rates). The plots are given in Figures 6.2 and 6.3 for the Gradient Descent and ABC-SMC fitting, respectively.

The cost function is smooth with few, if any, local minima along the straight line in parameter space between the fitted rates and *'true'* rates, so it does not appear there is an issue of a large number of local minima which would be problematic for the gradient descent.

The cost functions do appear uninformative as to the direction of the global minimum. Figure 6.2 reports the cost function between the default and gradient descent fitted rates and Figure 6.3 reports the cost function between the default and ABC-SMC fitted rates. All the cost functions, except for rep 5 (GD and

[§]We still do not vary the rates for the activation of the substrate but since this is assumed to be fixed in the prior distribution then we still have the potential to fit to the *'true'* rates exactly.

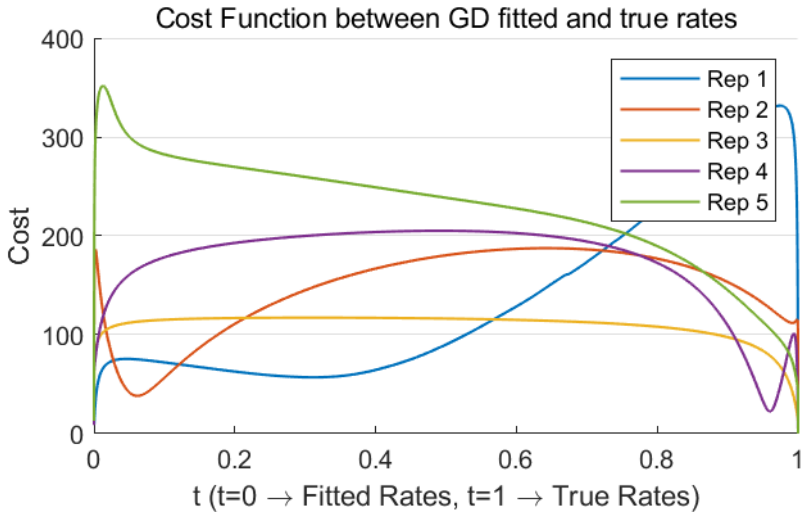

Figure 6.2: Evaluation of the cost function between the Gradient Descent fitted rates and the *'true'* rates for each repetition.

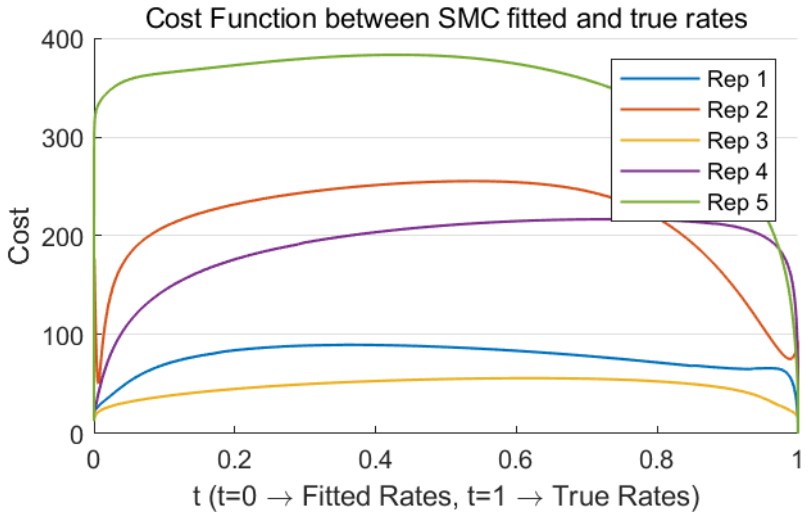

Figure 6.3: Evaluation of the cost function between the ABC-SMC fitted rates and the *'true'* rates for each repetition.

ABC-SMC), appear to have a poor radius of convergence for the global minimum, either featuring other nearby local minima (rep 4 GD; rep 2 ABC-SMC), sharp drops from an otherwise high-cost surface (rep 1 GD; reps 1, 3, and 4 ABC-SMC) or the surface has a clear gradient, but it is towards the fitted local minimum not the global minimum (reps 1 and 2 GD). Changing the cost function may help with making it more informative for fitting.

6.5.4 OD Curves

In order to better understand where the accuracy of the fitting is lacking and how we could make a more informative cost function, we have investigated fitted and *'true'* OD and thrombin generation curves. Some example curves are given in Figure 6.4.

The curves demonstrate that OD (particularly ETP) is fitted very well, with only the ABC-SMC fitting for rep 2 fitting poorly. However, the thrombin generation curves (given as dOD/dt) allow us to note some further issues. Peak height (in all reps), lagtime (in reps 2, 3 and 4), and maximum increasing rate (in reps 1, 2, 3 and 5) appear to be poorly predicted by both fitting methods. We may be able to use a cost function which evaluates, and places a larger emphasis on, these summary statistics to produce a more informative cost surface.

It is worth noting that these curves are still normalised by a pooled plasma ETP (as described in Section 3.1.1). As shown in Table 6.5, the values of pooled plasma ETP after fitting, compared with the *'true'* pooled plasma ETP, is typically off by 5% with some repetitions being off by as much as 33%. It may improve the fit if we remove this normalisation step (something we cannot do for these data but could be useful knowledge for future work), however, how much of an improvement we could achieve is unclear.

		Pooled Plasma ETP (M)		
Rep	Fitting Method	Fitted	True	Abs. Rel. Error (%)
1	Gradient Descent	6.2758×10^5	5.9610×10^5	5.28
1	ABC-SMC	5.2551×10^5	5.9610×10^5	11.84
2	Gradient Descent	1.7989×10^4	1.8371×10^4	2.08
2	ABC-SMC	2.4379×10^4	1.8371×10^4	32.70
3	Gradient Descent	3.0282×10^4	2.4148×10^4	25.40
3	ABC-SMC	2.3949×10^4	2.4148×10^4	0.82
4	Gradient Descent	3.1579×10^4	3.1728×10^4	0.47
4	ABC-SMC	3.3359×10^4	3.1728×10^4	5.14
5	Gradient Descent	2.5182×10^4	2.6830×10^4	6.14
5	ABC-SMC	2.6756×10^4	2.6830×10^4	0.28

Table 6.5: Predictions for the pooled plasma ETP (given as the concentration of activated substrate) and the absolute relative error (Abs. Rel. Error) between the fitted rates and *'true'* rates for batch 4.

6.6 Batch 5 - Cost Functions

We have seen that the cost function is uninformative as to the location of the global minimum and fits ETP well at the cost of lagtime and peak height. To investigate whether a cost function which explicitly evaluates these summary statistics to calculate model error may help to alleviate this problem, we have generated similar cost function curves as seen in Figures 6.2 and 6.3 for each summary statistic for the Gradient Descent fitted rates. These results are given in Figure 6.5.

No summary statistics seem to be any more informative as to the direction of the global minimum than the original cost function. Generally, the fitted local

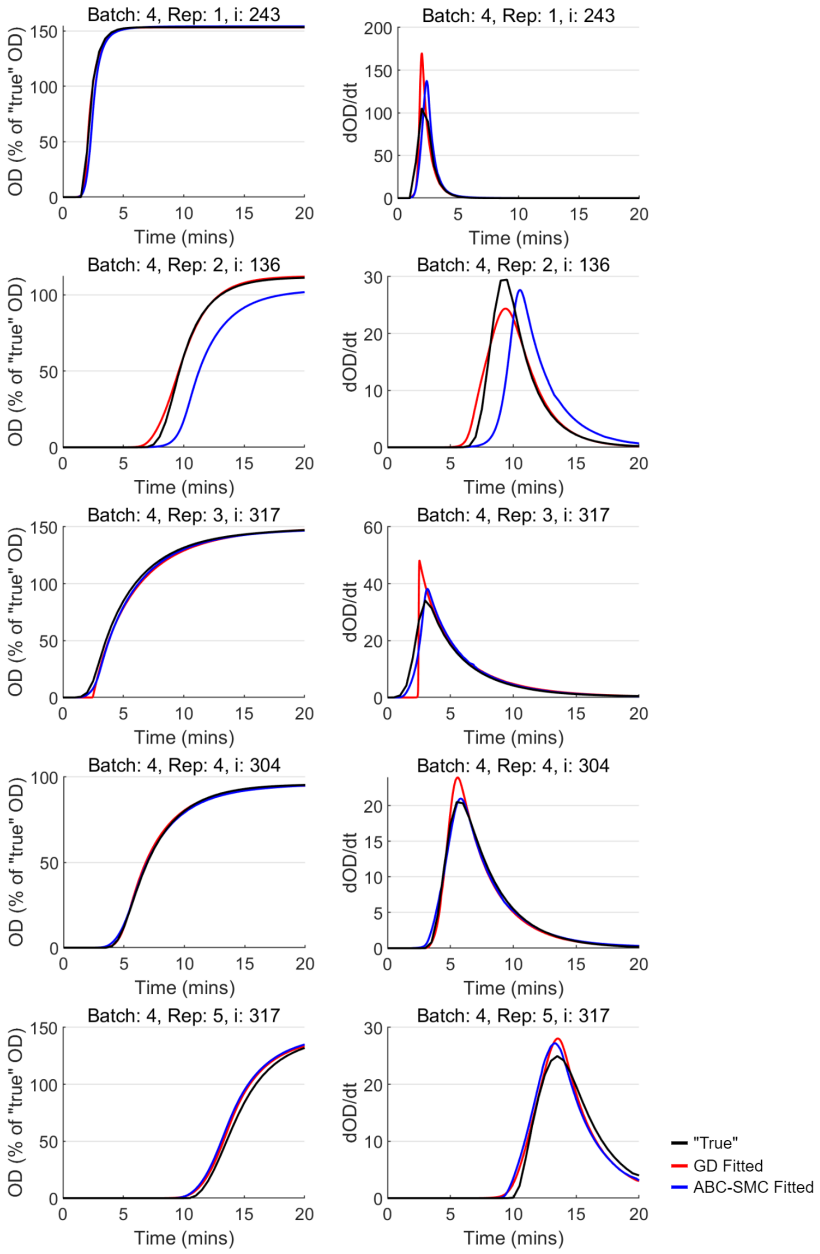

Figure 6.4: OD and Thrombin Generation (represented as derivative of OD) curves for randomly selected individuals for each repetition of batch 4.

minima are also local minima in each of the summary statistics, with a few exceptions such as rep 2 for ttP. Even though lagtime is a summary statistic that we do not fit as well as we would like, the lagtime cost function is very similar to the original cost function. It may instead be the case that the lagtime does have a large effect on the cost function but cannot be accurately fitted further due to the limited temporal resolution (0.5 minutes).

It seems that, although some summary statistics are more informative for some of the repetitions, the majority are either as equally informative as the original cost function or perform worse and any weighting of the summary statistics would be unlikely to fix this.

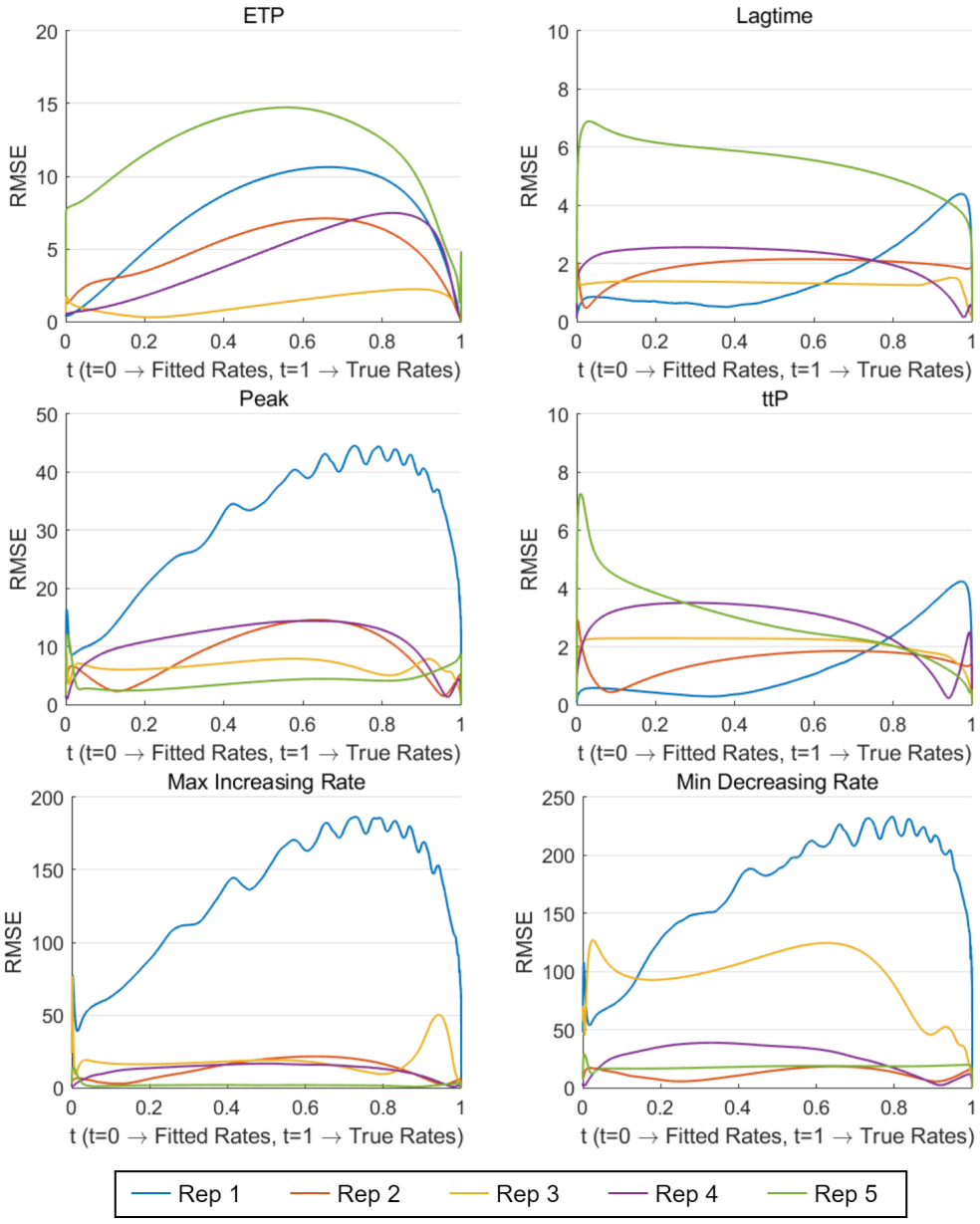

Figure 6.5: Plots of each summary statistics RMSE for linearly interpolated rates between the Gradient Descent rates and the *'true'* rates. Since there is no noise, the *'true'* rates define the global minimum at zero.

6.7 Batch 6 - Pooled Plasma Scaling

So far, we have demonstrated that the current fitting algorithms are sufficient to reproduce OD curves with a high degree of accuracy but are unable to identify the *'true'* rates. We saw in batch 4 that the predicted values of the pooled plasma ETP (that is used to scale the OD curves to convert the units to % of pooled plasma) were frequently different between the fitted rates and the *'true'* rates and this may be limiting the ability of the fitting to identify the *'true'* rates. It is possible that multiple sets of reaction rates produce concentration curves that are

proportional to one another and therefore, after scaling by pooled plasma, would be identical in their output. In this batch we remove the effect of pooled plasma scaling and investigate if this improves predictions of pooled plasma ETP and if this allows us to identify the *'true'* rates from fitting.

6.7.1 Methods

In order to implement this, we have used the same data as batch 1 (same *'true'* rates and OD curves), but during the fitting process, instead of scaling by the pooled plasma for those rates, we use the pooled plasma for the *'true'* rates. Originally, using the method described in Section 3.1.1, in order to evaluate the cost of a set of reaction rates, we would run the model with each patients initial concentrations to generate a patient specific OD curve, we would then also run the model with pooled plasma initial conditions and find the final value of the OD curve. We could then rescale the patient specific OD curves by this final value of the pooled OD curve in order to calculate the patient specific OD curves as a percentage of pooled plasma. This entire process used the same set of reaction rates to derive their cost. We now, instead of running the pooled plasma simulation with the rates we are evaluating, use the *'true'* rates. This ensures the cost function is on the same scale as the previously reported values but now we are only scaling by a fixed constant rather than one which depends on the current rates. This allows us to explore what the fitting would look like if the data was given as concentrations in moles rather than percentage of pooled plasma, while still allowing us to compare the costs between this batch and the other batches. This fitting varies all reaction rates as was identified as beneficial in the previous batches.

6.7.2 Results

Table 6.7 gives the cost and RMSLE for each set of fitted reaction rates. The costs are similar to batch 4, with a sizeable increase in cost for reps 1 and 4 for the Gradient Descent fitted rates and reps 2 and 5 for the ABC-SMC fitted rates. However, the pooled plasma predictions, presented in Table 6.6, are now considerably more accurate with below 4% relative error for all reps for both fitting methods. Removing the pooled plasma scaling does improve the predictions for pooled plasma ETP, as would be expected, but does not improve cost or RMSLE.

6.8 Batch 7 - Narrow Priors

Many of the reaction rates have multiple sources and therefore have an estimate for the log-normal standard deviation in the prior distributions. However, there are still a significant number of reaction rates for which we only have one source and so have assumed a large log-normal standard deviation of 2.5. We wish to

[¶]This repetition failed to converge when using the ABC-SMC algorithm.

Rep	Fitting Method	Pooled Plasma ETP (M) Fitted	True	Abs. Rel. Error (%)
1	Gradient Descent	5.9722×10^{-5}	5.9610×10^{-5}	0.19
1	ABC-SMC	N/A¶	5.9610×10^{-5}	N/A¶
2	Gradient Descent	1.8868×10^{-4}	1.8371×10^{-4}	2.71
2	ABC-SMC	1.9083×10^{-4}	1.8371×10^{-4}	3.88
3	Gradient Descent	2.4191×10^{-4}	2.4148×10^{-4}	0.18
3	ABC-SMC	2.4882×10^{-4}	2.4148×10^{-4}	3.04
4	Gradient Descent	3.1553×10^{-4}	3.1728×10^{-4}	0.55
4	ABC-SMC	3.0926×10^{-4}	3.1728×10^{-4}	2.53
5	Gradient Descent	2.7649×10^{-4}	2.6830×10^{-4}	3.05
5	ABC-SMC	2.7219×10^{-4}	2.6830×10^{-4}	1.45

Table 6.6: Predictions for the pooled plasma ETP (given as the concentration of activated substrate) and the absolute relative error (Abs. Rel. Error) between the fitted rates and *'true'* rates for batch 6.

Rep	Default		Gradient Descent		ABC-SMC	
	Cost	RMSLE	Cost	RMSLE	Cost	RMSLE
1	497.1	1.80	98.0	3.14	NA¶	NA¶
2	255.8	1.92	29.7	1.98	112.5	2.68
3	348.7	2.04	13.2	2.92	34.7	2.37
4	245.4	1.63	18.4	1.89	24.6	1.98
5	115.2	1.90	13.5	1.98	118.9	2.51
Mean	292.4	1.86	34.6	2.38	72.7	2.39

Table 6.7: Performance metrics for the batch 6 fitting. Metrics are given for the default rates and the fitted reaction rates only since the *'perfect'* metrics are all zero. The cost (Equation (6.1)) gives a measure of the difference in the OD curves and RMSLE (Equation (6.2)) measures the difference in the reaction rates (smaller is better for both metrics).

identify if in future, when the variation in these reaction rates is known similarly to the other rates, those that we have multiple sources for, will the fitting be able to identify the *'true'* rates.

6.8.1 Methods

We have set the prior standard deviations for all reaction rates with one source (or none) to 0.5 (the average log-normal standard deviation for reaction rates with multiple sources). We then generate a new set of reaction rates from this prior and a new data set from these rates. The Gradient Descent algorithm does not include a measure of uncertainty so is the same as for the previous batches, but the ABC-SMC algorithm uses the new narrower prior distributions.

6.8.2 Results

Table 6.8 gives the cost and RMSLE for each set of fitted reaction rates. The costs are similar to those seen in the previous batches. The RMSLE is significantly lower in this batch than seen previously, but this appears to be due to the narrower priors used for sampling since the default rates produce a RMSLE similar to the ABC-SMC and lower than Gradient Descent. Additionally, ABC-SMC outperforms Gradient Descent in RMSLE for all reps and performs similarly or better in cost, significantly outperforming for reps 1 and 5.

Rep	Default		Gradient Descent		ABC-SMC	
	Cost	RMSLE	Cost	RMSLE	Cost	RMSLE
1	427.3	0.61	84.1	1.17	42.3	0.83
2	140.5	0.55	17.2	1.11	17.2	0.67
3	247.3	0.56	15.8	0.98	16.3	0.64
4	120.0	0.56	56.2	0.94	56.5	0.59
5	353.0	0.51	66.2	3.03	28.6	0.71
Mean	257.6	0.56	47.9	1.45	32.2	0.69

Table 6.8: Performance metrics for the batch 7 fitting. Metrics are given for the default rates and the fitted reaction rates only since the *'perfect'* metrics are all zero. The cost (Equation (6.1)) gives a measure of the difference in the OD curves and RMSLE (Equation (6.2)) measures the difference in the reaction rates (smaller is better for both metrics).

6.9 Fitting to Patient Data

Since we have seen an improvement to our fitting methods by fitting all reaction rates rather than a reduced subset, we present here the results of fitting the Improved Unified Model to the PRAMIS cohort data when fitting all reaction rates (except the rates for the chromogenic substrate).

Figure 6.6 presents the ETP correlation, before and after fitting, and Figure 6.8 presents the thrombin generation curves for the reference concentrations before and after fitting. After fitting we achieve a cost of 164.5 for gradient descent and 177.4 for ABC-SMC.

The fitted thrombin generation curves when fitting to data are different between the Gradient Descent fitted rates and the ABC-SMC fitted rates. However, when fitting to the simulated data both algorithms produced similar curves (see Figure 6.4). It appears that there are many curves which can reproduce the data sufficiently accurately but since the simulated data can be reproduced much more accurately than the experimental data, there are fewer possibilities.

The fitted reaction rates for this can be found in Appendix B and the results of a sensitivity analysis on this final version of the model are given in Appendix

F.

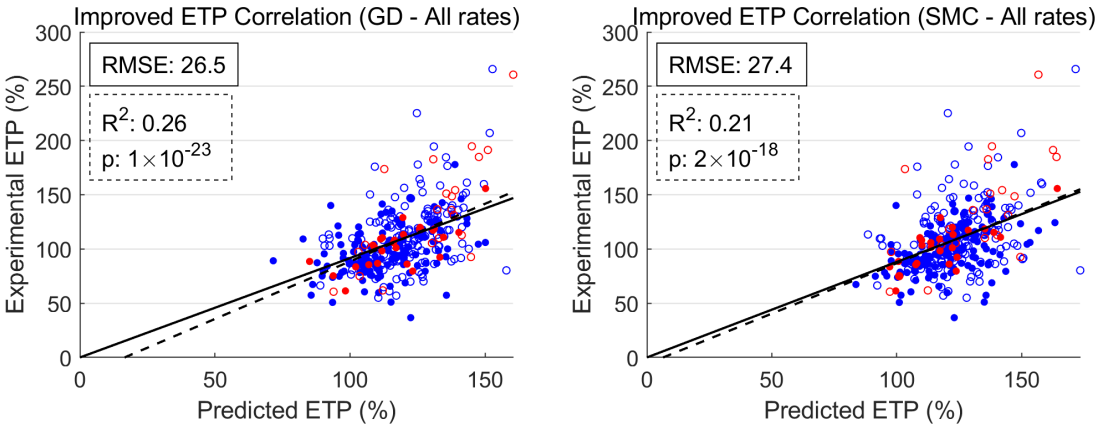

Figure 6.6: The ETP correlation scatter graphs for the Improved Unified Model for the default, gradient descent fitted, and ABC-SMC fitted reaction rates when fitting all reaction rates.

Figure 6.7 shows the OD curves for the individuals with the best and worst ETP predictions, given for the gradient descent fitted rates and the ABC-SMC fitted rates. The worst predicted individuals draw similar conclusions to those seen previously. The best predicted individual for the gradient descent fitted rates matches well, baring the bumps in the data. The ABC-SMC fitting results in a larger lagtime for both the best and worst individuals.

6.10 Conclusions

We have demonstrated than the fitting methods are sufficient to replicate OD and thrombin generation curves for reaction rates sampled from the prior distributions (Sections 6.2 and 6.3). Since we are unable to achieve this quality of fit for the patient data, it would suggest that either the prior distributions do not accurately reflect the reaction rates (which seems unlikely given our broad prior distributions) or the reaction scheme does not accurately reflect the reactions taking place in the assay, a possible source of model discrepancy.

We have validated the assumption of the diffusion limited association rate for enzymatic activations (Section 6.4). In Section 6.5, we found that our assumption that we only need to fit reaction rates that give a significant change in the output (originally described in Section 3.2.5) is not valid and all reaction rates should be fitted. We then showed that this fitting produces similar OD and thrombin generation curves but without identifying the *'true'* rates that were used to generate the data.

We have evaluated the performance of the fitting algorithms in settings that may be relevant in future work. We demonstrated that scaling the data by pooled plasma ETP does not interfere with the fitting (Section 6.7). We also saw that

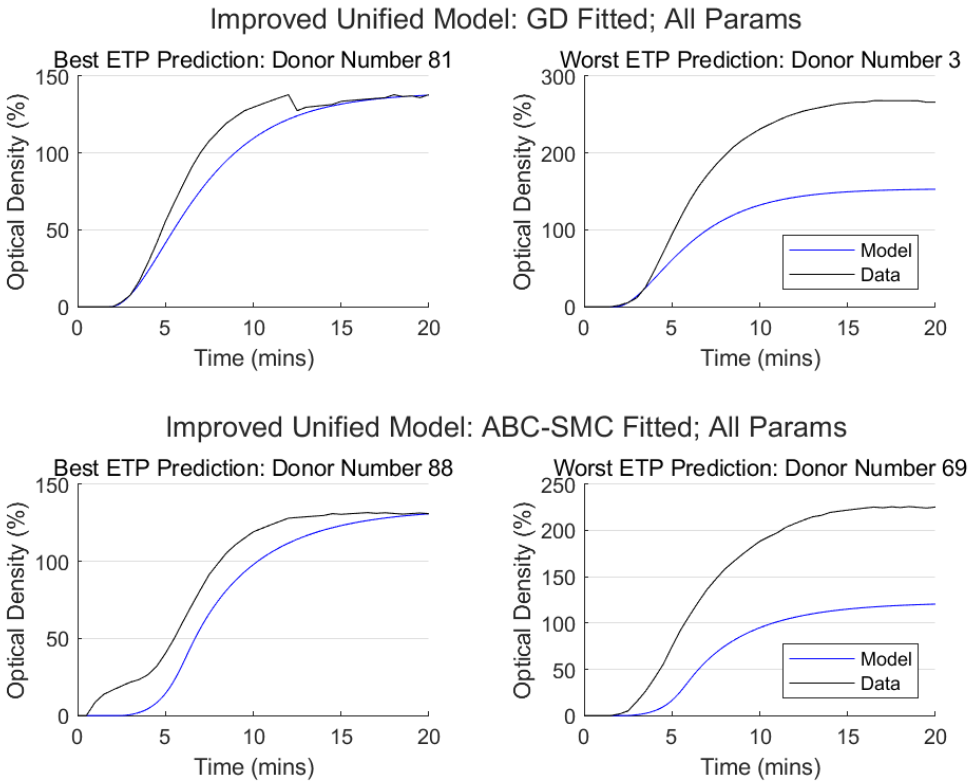

Figure 6.7: The Improved Unified Model predicted OD curve and the experimental OD curve for the individuals with the best and worst predicted ETP, separated by the Gradient Descent (top) and ABC-SMC (bottom) fitted rates when fitting all reaction rates.

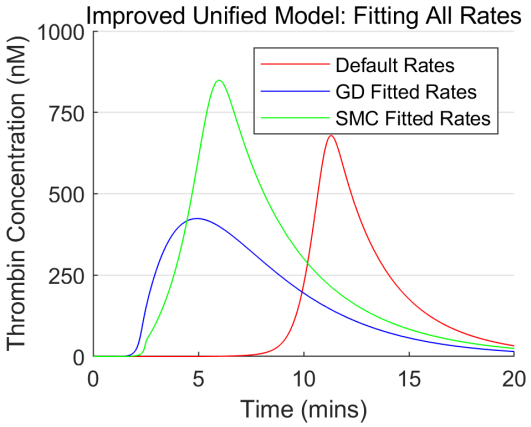

Figure 6.8: The thrombin generation curves for the Improved Unified Model, before fitting and after gradient descent and ABC-SMC fitting when fitting all reaction rates.

even if all reaction rates have multiple sources to produce a reasonable estimate for the log-normal standard deviation, we would still be unable to identify the *'true'* rates (Section 6.8). Additionally, as the prior distributions begin to narrow the ABC-SMC fitting begins to outperform the Gradient Descent fitting (Table 6.8).

Finally, we fitted the Improved Unified Model to the PRAMIS data with the updated fitting method (Section 6.9). This did not significantly improve the fitting (Figures 6.6 and 6.7), as would be expected if there is significant model discrepancy.

Chapter 7

Conclusion

7.1 Summary

We began this work by comparing eight mathematical models of thrombin generation, chosen to best match a data set of 348 individuals. All eight models showed poor predictive capabilities when used to simulate thrombin generation data across this large cohort (RMSE: 27.6-32.5), with the Panteleev model giving marginally the best result (Section 2.3, Figure 2.19). Interestingly, the ETP predicted by the models was much more strongly correlated between the models than it was with the data; however, the other summary statistics generally had a weaker correlation between the models (Figure 2.22).

When comparing the differences between the models in their predicted thrombin generation curves, we were able to identify two groups of models (Section 2.4). The Quick group, consisting of Bungay, Chatterjee, Tyurin, and Zhu, all showed rapid activation of thrombin. The Symmetrical group, consisting of Hockin, Danforth, Brummel, and Panteleev, all showed smoother, near symmetrical thrombin generation curves. We were able to identify the cause of this difference to be activation of FIX (Figure 2.30). Specifically, the Quick group activate significant amounts of FIX, with all models fully depleting it, leading to large concentrations of FXa and therefore Xa:Va. By contrast, the Symmetrical group activate very little FIX which results in lower levels of Xa:Va which are formed at a slower rate. The most common cause for this difference is the presence or absence of FXI (Figure 2.31), which determines the levels of FIXa in all but the Zhu and Panteleev models. The Zhu model activates most FIX through TF:VIIa and the Panteleev model uses a significantly weaker rate for FXIa activation of FIX (Panteleev: $\frac{k_{\text{cat}}}{K_m} = 4.9 \times 10^5 M^{-1}s^{-1}$, Chatterjee: $\frac{k_{\text{cat}}}{K_m} = 1.6 \times 10^7 M^{-1}s^{-1}$).

From the sensitivity analysis (Section 2.5), we were able to show a strong relationship between the Hockin-based models, with the only change between their sensitivities being the sensitivity of the Chatterjee model to FXI auto-activation. We identified AT inhibition of FIIa to be the most sensitive reaction in all models; however, other inhibitions by AT were generally much less sensitive.

We investigated the original sources for all reaction rates across the models (Section 2.6). As has been reported previously by Hemker [76], we observed a

large variation between experimental sources for the same reaction. Due to the low variation observed under repeated measurements in the same source, we expect this variation to be due to differing experimental conditions between the sources rather than experimental noise. Additionally, we identified that only 10% of reaction rates in the models utilised more than one experimental source to derive their values (Table 2.34).

As the final stage of exploratory analysis of the models, we conducted a timescale analysis of the Danforth and Tyurin models (Section 2.7). We showed than almost all reactions were significant on at least one timescale. The results of the timescale analysis also highlighted an issue seen previously in the models (Section 2.24). The Tyurin model is the only model to use an observed value for the association rate for TF:VII and TF:VIIa, with all other models using an assumed rate, or a fitted rate, with an experimentally determined $K_d = \frac{k_-}{k_+}$. However, all the assumed values were significantly higher than the values reported in the literature. This led to the Tyurin model generating very little TF:VIIa during the early stages when TF:VIIa is most useful and instead relied on its activation by FVIIa to initiate coagulation.

These results led us to develop a new model, the Unified Model, which places a heavy emphasis on the choice of reaction rates (Chapter 3). To manage the large variation between experimental sources, we constructed prior distributions for each reaction rate using multiple sources to define the amount of variation (Section 3.2.3). From this, we assume the experimental conditions used for the thrombin generation data on the PRAMIS cohort should result in reaction rates that lie in the area of high probability in the prior distributions, which we explored through parameter inference. The reaction scheme aims to cover all relevant reactions in the previous models (Section 3.2.2). Unfortunately, the resulting model failed to significantly improve upon the previous models. After making changes to the reaction scheme, expanding to incorporate other features, we were still unable to significantly improve. However, we did note that some of the changes made, such as the inclusion of fibrinogen (Section 3.3.6), were significant in their influence on the model and so should still be included.

In order to assess where further improvements could be made, we conducted a stage of data analysis (Chapter 4). The Functional Data Analysis demonstrated some curves which the model would be unable to reproduce (Section 4.2). However, removing these from the data set and refitting did not improve the model accuracy (Section 4.7). We were unable to identify any factors which could explain the large variation we saw in experimental ETP (Section 4.4), suggesting that there may be other proteins, varying on a patient specific level, which are heavily influencing coagulation. We found a discrepancy between the exogenous TF added in the assay and the endogenous TF in which the exogenous TF had a much larger effect over ETP than would be expected from just an increase in TF concentration (Section 4.6).

To continue model development, we constructed the Improved Unified Model (Chapter 5). The aim of this model was to improve upon the previous versions of

the Unified Model in a select few key areas. We aimed to get the model to achieve partial prothrombin conversion which we attempted to do through making changes to the inhibition scheme for prothrombinase (Section 5.2). Furthermore, we updated the reaction rates for FXI activation to be more in line with a phospholipid activation surface (Section 5.3). Unfortunately, this model did not significantly improve upon the previous versions of the Unified Model (Figures 5.12 and 5.13) nor predict partial prothrombin conversion (Figure 5.15). Finally, we assessed model uncertainty though both edited prior distributions and the posterior distributions (Section 5.6.3). From this uncertainty work, we were able to show that a model that uses only a single source for each reaction rate results in too much uncertainty for the model predictions to be reliable (Figure 5.16); however, after fitting, this uncertainty is massively reduced (Figure 5.17), both answering an open question posed by Hemker [76] about the variability in reaction rates and demonstrating a solution to this problem.

In order to verify if the poor fitting is a problem with the model or the fitting methods, we conducted a simulation study (Chapter 6). Section 6.2 showed that the current fitting methods were able to reproduce simulated data to a much higher degree of accuracy than for real data, although with poor parameter identifiability. We tested two assumptions used in the fitting methods, the diffusion limited association rate for enzymatic reactions (Section 6.4) and the percentage of pooled plasma scaling for the OD curves (Section 6.7). We showed that neither of these influence or disrupt the fitting methods. Even if the association rates are not diffusion limited, fitting is still able to reproduce the simulated data. Removing the pooled plasma scaling from the data does not improve on the accuracy after fitting. In Section 6.5, we were able to find an improvement on the fitting methods used previously by fitting all parameters rather than a reduced set. Finally, we showed that even if the reaction rates for which we only have one source, can be more accurately understood with further measurements, the current fitting methods will not be able to identify the true parameters (Section 6.8). This work led us to conclude that the low accuracy in model predictions is due to model discrepancy rather than as a result of the fitting methods used.

The progression of the cost function throughout this work is presented in Figure 7.1.

We believe that this model discrepancy is the main problem the models of thrombin generation currently face. Although the fitting methods we present here still present issues which will need to be resolved in the future, in particular poor parameter identifiability, they are sufficient for the current accuracy of the models. Further experimental investigation to address this model discrepancy will prove vital in future developments of mathematical models of thrombin generation. In the following section, we suggest possible methods and investigations which we believe are currently most useful.

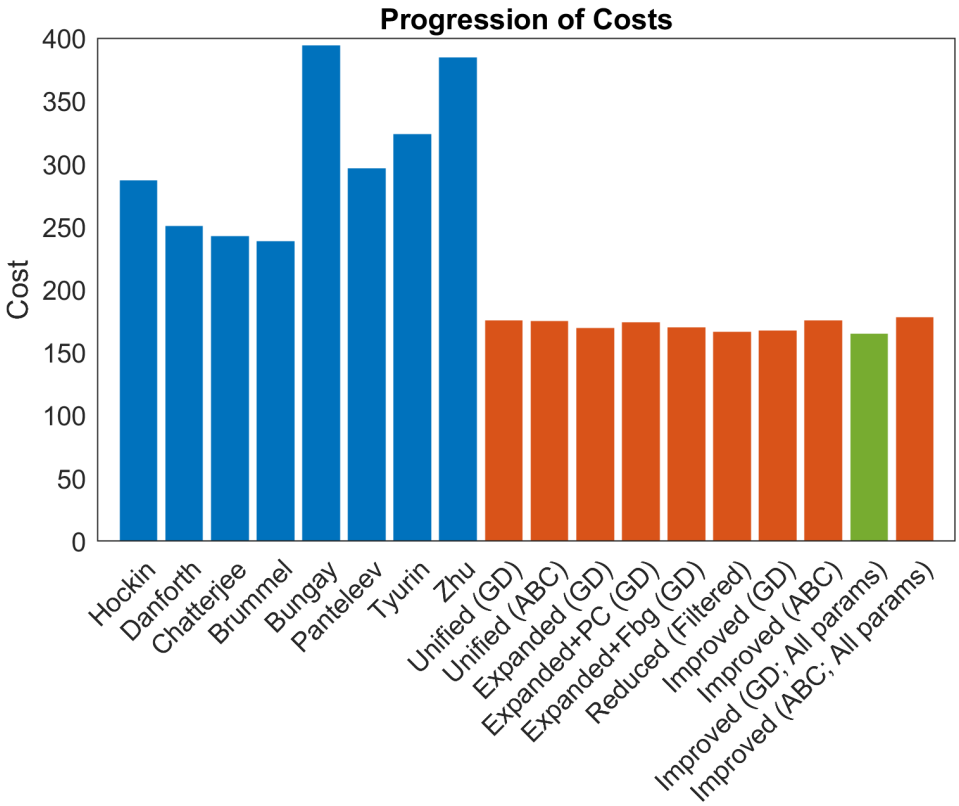

Figure 7.1: The progression of the cost function throughout this work. The previous models are given in blue, evaluated using their originally described reaction rates as detailed in Chapter 3. The Unified Models are given in orange and green. GD: The Gradient Descent fitted rates; ABC: The ABC-SMC fitted rates; Filtered: Fitting (and evaluating against) the reduced data set from Chapter 4; All params: Fitting all prior form parameters, as described in Chapter 6. The model parameterization that gives the lowest cost is shown in green.

7.2 Discussion

Our work on the previous models highlights why this kind of quantitative validation against a large cohort is so important. All models give unique predictions with similarities, such as that seen in the inter-model correlation, coming from their fundamentally similar structure. As these models have evolved, the standards for developing new models have increased. Quantitative validation against a large cohort, as we have done here, is now necessary in order to assess if changes to a model actually improve its predictions, something which qualitative validation against variation in only one or two factors can no longer do.

The focus of this work has been placed on the thrombin generation assay. In addition to this, there are mathematical models aiming to capture effects of coagulation varying from assays under flow to *in vivo* conditions [43, 80, 81, 84]. These models are able to capture many effects that are exclusive to this setting, including the large effect flow has over this system where it can act as an inhibitor in its own right [83] while also serving procoagulant roles, providing a fresh supply of coagulation factors in their zymogen form. The complications that arise from both modelling the system under flow and flow-based assays result in a lack of available data to grant quantitative validation across a variety of conditions. However, given these complications also result in a poorer understanding of the dynamics of coagulation under flow, these models do not need to be a perfect match to aid in new discoveries and have in fact already done so [44].

In addition to these flow-based models, there is also a wide variety of models for platelet aggregation. Due to the complex nature of platelets and their role in coagulation, there have been a variety of modelling techniques used to capture the different dynamics of platelets. These models range from chemical kinetic ODE models [133] to platelet ODE models under flow [44] or through a two-phase flow capturing the differences between flow through a platelet thrombus and free flow through a vessel [134]. There is also a range of multiscale models for platelet aggregation, including a molecular dynamics model for platelets using dissipative particle dynamics for fluid flow [135], or lattice kinetic Monte Carlo models for platelets coupled with neural networks for the platelet activating species, all under flow [136, 137].

As demonstrated from the simulation study, model discrepancy currently appears to be the largest problem with the models. This lack in the model structure could come from a number of things. We could be seeing a lack of important reactions and proteins in the system, or a violation of the model assumptions for chemical kinetic models. One possible violated assumption lies in the role of phospholipids. By acting as a surface for many of the reactions in the coagulation cascade, they may grant a local high-activity spatial effect that is not captured in a homogenised model. This has been explored previously for activation of FXa where it was found that a homogenised model was suitable to capture the kinetics on this reduced set of reactions [138]. If the model discrepancy is due to missing reactions between known factors, it may be possible to account for these unknown reactions through including a neural network, or more specifically a single layered

perceptron, into the ODEs as shown by Equation (7.1) below (where $\mathcal{NN}_{VIII}(S)$ is the neural network for FVIII, taking an input S of the current state of the system, represented as a vector of concentrations of factors that may be able to interact with FVIII) [139, 140]. However, this cannot account for reactions involving proteins we do not have concentration data for or are currently unknown. This may also present problems with over-fitting due to the large numbers of parameters introduced, which will need to be carefully managed to ensure the results are reproducible.

$$\frac{d[VIII]}{dt} = -k_1[VIII][IIa] - k_2[VIII][Xa] - [VIII]\mathcal{NN}_{VIII}(S) \tag{7.1}$$

One of the issues highlighted by the simulation study in Chapter 6 was parameter identifiability. None of the batches of the simulation study correctly identified the reaction rates after fitting. While the models still show signs of model discrepancy, this is not a major issue since parameter identifiability only makes sense when the model matches the underlying data generating process. However, in the future, parameter identifiability will be vital to use the models in pharmacokinetic settings. A possible path to achieve parameter identifiability would be through optimal experimental design [141]. Including data measuring the concentration of the other coagulation factors or constructing assays using coagulation factor concentrations optimised to improve parameter identifiability may aid in this situation. Another possibility would be to alter how the prior distributions function*. The current prior distributions work by understanding the variation between experimental sources, many of which use differing experimental conditions, and assuming our experimental conditions should be in line with this variation. A possible modification would be to construct weighted prior distributions, giving larger weights to experimental conditions that are similar to that of the thrombin generation data from the PRAMIS cohort. This would likely be a fairly simple change that would maintain the workflow we have used for the model construction. As an alternative to this, we could use our knowledge of the differing experimental conditions to construct a model which predicts the reaction rates for any experimental conditions. If we were able to predict reaction rates under any experimental conditions, then the uncertainty surrounding these reaction rates could be reduced or even removed entirely, possibly eliminating the need for fitting.

A viable method for further developing the models would be validation at the module level. This would consist of validating the reactions for say TF:VIIa formation under varying levels of TF, FXa, FIIa, FVII, and FVIIa. The same could be repeated for the other modules. After this, further differences can be accounted for by interactions between the modules, which can be assessed by including other coagulation factors that are expected to have little influence and comparing model predictions with experimental results. This method of using the models as a tool to describe current understanding and building upon this to derive an accurate

*Included in this are ways to reduce the uncertainty in the prior distributions.

model has already been implemented for fibrin formation [92]. This smaller scale of validation can help with both the interpretation of the results and parameter identifiability, greatly aiding the development of the models.

There are still known proteins that have not been included in the models. Two such proteins are protein Z and protein Z-dependent protease inhibitor (ZPI), ZPI being able to inhibit FXa, boosted by its cofactor protein Z, and FXIa, whose inhibition is unaffected by protein Z [142, 143, 144]. They were not included in the Unified Model due to a lack of reaction rates and patient level concentrations for both of these proteins, although we have already seen that some inhibitors ($\alpha_1 - AT$, $\alpha_2 - AP$, $\alpha_2 - M$, PAI-1, and C1-inh) can be included into the model at an average concentration and patient specific values do not always need to be known. As more proteins are discovered to be involved in coagulation, these models will continue to need updates and improvements.

There are also other reactions not currently captured between coagulation factors that are included in the models. Such reactions include II + Va $\leftrightarrow$ II:Va, which is included in the Brummel model. We choose not to include this reaction in the Unified Model as it was not clear if the complex II:Va could result in activation of prothrombin. There are also interactions such as that between TF:VIIa and FV [145] that are not included in the models due to the lack of available reaction rates.

Finally, an improved understanding of prothrombin conversion would prove useful to model development. We have been able to show it is possible to predict partial prothrombin conversion in a model, both with the Expanded Unified Model by tweaking reaction rates, the Expanded Protein C Model, and the Reduced Unified Model with the new prothrombinase inhibition scheme. Understanding how the remaining prothrombin concentration is influenced by the other coagulation factors and which other coagulation factors are still present at the end of the assay and which are fully depleted would provide further qualitative measures of model accuracy to test against. Currently, it appears that the lack of knowledge surrounding prothrombinase inhibition is the limiting factor in predicting partial prothrombin conversion.

We began this work aiming to explore the current mathematical models of thrombin generation. We have identified problems with these models and the root cause for these issues. We have provided solutions to resolve the issues with these models and used this to develop a new model. From this new model, we answered open questions surrounding the applicability of these models. Finally, we have identified future issues that may disrupt further improvements on the models and given possible methods for resolving each of these.

From the discoveries we have made, and the work suggested in this chapter, we believe models of the coagulation cascade will prove to be a useful tool in future thrombosis and haemostasis research. Initially, they are best suited as a 'quantifier of current knowledge' for comparison to experimental data to explore missing information in the current description of the coagulation cascade. Later, once these models have improved in accuracy, they can begin to be used as a

highly transparent proxy for biological experiments, allowing fast, thorough and in-depth information about potential drug candidates or personalised medicine with individually tailored treatments.

Glossary

α inhibitor

The collective name we use for the inhibitors α_1-AntiTrypsin, α_2-AntiPlasmin and α_2-Macroglobulin. See Chapter 1.

$\mathbb{N}_0$

Natural numbers including zero.

ABC-SMC

We utilise the ABC-SMC with Early Rejection algorithm from [100]. We use N=2000 particles, of which U=200 are unique, with an initial tolerance of ε_0=400 to define the first sample from the priors. Further tolerances are determined algorithmically to ensure there are 200 unique particles in each population. The final reaction rates are given as the mode of the posterior sampled reaction rates. See Chapter 3.

activated partial thromboplastin time

A clinical assay to measure the performance of the intrinsic pathway. See Chapter 1.

ADP

Adenosine DiPhosphate is a compound that is released by activated platelets that can activate more platelets.

amplification

The second stage of the cell-based model of haemostasis. See Chapter 1.

ANOVA

Analysis of Variance. A statistical method for comparing means between groups. See Chapter 4.

antithrombin

Antithrombin (AT) is a serpin (serine protease inhibitor) which inhibits many active coagulation factors. It acheives this by binding to these factors, blocking their active site and remains bound until removed from the blood. See Chapter 1.

approximate Bayesian computation

A class of algorithms using Bayesian statistics that approximate the posterior distribution through comparisons to data. See Chapters 1 and 3.

assay

A biological experiment for measuring a quantity or activity..

association

A reaction in which two species bind together.

asymptotic analysis

A group of methods that can be applied to a system or equation in which its terms are on different scales. See Chapter 1.

basis function

A family of functions with linear combinations of these functions forming a function space.

bilayer

The phospholipid bilayer is the natural form phospholipids take, in which two layers of phospholipids are stacked one on top of the other, with the bottom inverted so that both the top and bottom layers have the hydrophilic heads exposed. See Chapter 1.

blood plasma

The fluid part of blood. Blood plasma is what remains after red blood cells, white blood cells, and platelets are removed.

blood vessel

Blood vessels (including veins, arteries and capillaries) are used to transport blood around the body.

C-reactive protein

A protein whose concentration increases during and after inflammation.

calcium chloride

A salt used in the thrombin generation assay to supply calcium ions which are used by prothrombinase.

calibrated automated thrombogram

The name for the fluorogenic thrombin generation assay. It requires an additional sample of a fixed, constant thrombin concentration to calibrate the fluorescence signal. See Chapter 1.

cassette

A grouping of reactions with a particular goal. See Chapter 3.

cell-based model of haemostasis

A more up-to-date description haemostasis, taking into account the roles of surfaces such as platelets and how this influences coagulation. See Chapter 1.

chromogenic substrate

Used in the measurement of the thrombin concentration during the chromogenic thrombin generation assay. When the substrate is activated by thrombin, it exposes its chromophores which can be picked up by a light detector. See Chapter 1.

clustering

A class of methods used to group data into clusters where the data in each cluster is more similar to one another than to data in the other clusters. See Chapters 1 and 4.

coagulation

The third stage of haemostasis. Also called secondary haemostasis. This is a series of enzymatic reactions which result in production of a fibrin mesh which stabilises the blood clot. See Chapter 1.

coagulation cascade

The series of reactions which lead to production of thrombin. The name "cascade" comes from the structure of the reactions in which each coagulation factor activates the next one in the cascade. See Chapter 1.

coagulation factor

A protein which circulates in blood plasma and is involved in blood coagulation. See Chapter 1.

cofactor

In reference to coagulation factors, cofactors are proteins which increase the enzymatic activity of an enzyme. See Chapter 1.

collagen

A common protein that is found external to blood vessels. See Chapter 1.

competitive inhibition

A property of enzyme kinetics. During the process of an enzyme activating a substrate, its active site is likely blocked. This means that the enzyme is unable to activate other substrates so the effective concentration of the enzyme is temporarily decreased. See Chapter 1.

complex

A complex is a group of two or more proteins that are associated or bound together.

conservation law

A equation representing the conservation of a particular quantity in a chemical kinetic model.

contact activation

The mechanism for FXII activation through contact with collagen or other negatively charged surfaces. See Chapter 1.

corn trypsin inhibitor

An inhibitor of contact activation commonly used in thrombin generation assays.

cost

The metric used to compare model predicted and experimental optical density curves. See Chapter 3.

cross validation

A method in data analysis to diagnose over-fitting. This involves fitting the data to a subset of the full data set and then testing the resulting model against the remaining data. See Chapter 3.

cubic spline

A method of interpolation in which points are connected through cubic polynomials.

data filtering

Removing data that satisfy certain properties from a data set. See Chapter 4.

default rates

The default rates are the reaction rates given by the median of the prior distributions. This is equivalent to the geometric mean of the experimentally measured values used to construct the prior distribution. See Chapter 3.

defibrinated plasma

Blood plasma that has fibrinogen removed.

dextran sulphate

A surface for factor XI activation.

diffusion limited

A reaction rate is diffusion limited when its reaction rate is sufficiently rapid that it is capped by the time it takes to be transported around the solution through diffusion.

dissociation

A reaction in which a species breaks apart into two or more constituent parts.

endogenous tissue factor

Endogenous TF is TF that is already present in the plasma sample and is not added in. We have measured values of the endogenous TF concentration for each individual.

endothelial

The cells in the vessel wall that are in contact with the blood. Blocks contact between the sub-endothelial cells and the blood plasma. See Chapter 1.

enzymatic reaction

A reaction involving an enzyme in which it acts upon a substrate, cleaving it to change its form. See Chapter 1.

ETP

The integral of the thrombin generation curve. See Chapter 1.

exogenous tissue factor

Exogenous TF is TF that is added to our assay from external source as opposed to already present in the blood plasma from when the sample was taken. When exogenous TF is used in the assay that was used to collect our data set, it is always in a concentration of 5pM.

experimental noise

Random fluctuations due to an experimental apparatus.

extrinsic pathway

The coagulation cascade pathway which begins with tissue factor and the formation of TF:VIIa. See Chapter 1.

extrinsic tenase

The TF:VIIa complex which activates FX and FIX into FXa and FIXa, respectively. See Chapter 1.

factor V Leiden

A mutation in factor V which can stop its inhibition by activated protein C. See Chapter 1.

fibrin

The protein that is cleaved from its precursor fibrinogen by thrombin. Fibrin is a monomer which joins to other fibrin monomers to for a long polymer chain. See Chapter 1.

fibrin mesh

After fibrin has polymerised into long chains, it is cross-linked by factor XIII into a mesh. This mesh stabilizes the platelet plug, capturing red blood cells and more platelets. See Chapter 1.

fibrinogen

The precursor form of fibrin. See Chapter 1.

fibrinolysis

The fourht stage of haemostasis. In this stage, a series of enzymatic reactions, triggered by coagulation factors, lead to production of an enzyme plasmin, which breaks down the fibrin mesh to remove the blood clot. See Chapter 1.

first order reaction

A reaction with one reactant.

Fisher's exact test

A statistical test used to determine association between categorical variables, in our case a categorical variables and the group. See Chapter 4.

fluorogenic substrate

Used in the measurement of the thrombin concentration during the fluorogenic thrombin generation assay. When the substrate is activated by thrombin, it briefly fluoresces which can be picked up by a light detector. Unlike the chromogenic substrate, this fluorescence signal can not be easily converted to a thrombin concentration. See Chapter 1.

functional data analysis

A class of methods in data analysis for analysing functional data. See Chapters 1 and 4.

gap statistic

A metric to determine the optimal number of clusters in a data set. See Chapters 1 and 4.

Gini index

A metric to determine the optimal question for regression and decision trees. See Chapters 1 and 4.

Gradient Descent

The Gradient Descent fitting algorithm we use is the interior point algorithm (to provide a lower bound of zero on all reaction rates) implemented through MATLAB's fmincon using a finite difference step size of 0.001. See Chapters 1 and 3.

haemophilia

A bleeding disorder caused by deficiency in one of factors VIII, IX, or XI. See Chapter 1.

haemostasis

The name of the processes used in stopping or reducing the loss of blood after damage to a vessel wall. It consists of four stages, vasoconstriction, formation of a platelet plug, coagulation and fibrinolysis. See Chapter 1.

heparin

Increases the activity of antithrombin.

in vitro

Experiment performed external to the normal biological environment.

in vivo

Inside the body or other living organism.

inhibition

The process by which an enzyme has its activity removed, typically by blocking the active site.

initiation

The first stage of the cell-based model of haemostasis. See Chapter 1.

inter-model correlation

Assessing the correlation of predictions between two models. See Section 2.3.

interior point algorithm

A method for bounded gradient descent. See Chapters 1 and 3.

interpolation

Determining a function which passes through a series of data points.

intervals of influence

The time interval that a particular term in an ordinary differential equation has a significant influence on the value of the differential equation. See Section 2.7.

intractable

Not possible or difficult to calculate.

intrinsic pathway

The coagulation cascade pathway which begins with FXII, activated on contact with collagen or other negatively charged surfaces. See Chapter 1.

intrinsic tenase

The IXa:VIIIa complex which activates FX into FXa. See Chapter 1.

iterative increasing method

The iterative increasing method accounts for the possibility of identifying a K_m, k_{cat} pair that, when using $k_+ = 1 \times 10^8 M^{-1} s^{-1}$, can give $k_- \leq 0$. To avoid this we iteratively multiply k_+ by 10 until we find a k_+ that gives a $k_- > 0$. See Chapter 3.

kallikrein

The active form of prekallikrein. Part of a positive feedback loop with FXIIa in which they can activate each other. See Chapter 1.

kaolin

A mineral used in the Activated Partial Thromboplastin Time test..

knots

In the context of splines, a knot is where the individual components of the spline are joined together. For example, for linear splines the knots will be at the points where it is not differentiable.

lagtime

The time to reach 5% of the maximum concentration of thrombin from the thrombin generation curve. See Chapter 1.

lipoprotein

Lipoproteins, a mix of proteins and lipids (fats), carry cholesterol through the blood stream. They come in two types, high-density lipoproteins (HDLs) and low-density lipoproteins (LDLs).

log-normal distribution

A random variable X has log-normal distribution if $\log(X)$ has a normal distribution. We denote a log-normal distribution by $10 \wedge N(\mu, \sigma^2)$ where μ and σ^2 are mean and variance of $\log_{10}(X)$.

Markov chain

A stochastic model where future states depend only on the current state and not on earlier states.

mass action

A chemical kinetic rate law. It assumes reactions occur at a rate proportional to the product of their reactants. See Chapter 1.

mass action law form

The model simulates fully in mass action law kinetics, so the reaction rates need to be converted from prior form to mass action law form. This consists of, for complex binding using $k_+, k_- = K_d \times k_+$ and for enzymatic activations using $k_+ = 1 \times 10^8 M^{-1} s^{-1}, k_- = K_m \times k_+ - k_{\text{cat}}, k_{\text{cat}}$. See Chapter 3.

maximum increasing rate

The maximum value of the gradient of the thrombin generation curve. See Chapter 1.

Michaelis Menten

A chemical kinetic rate law commonly used for enzymatic reactions. See Chapter 1.

minimum decreasing rate

The minimum value (most negative) of the gradient of the thrombin generation curve. See Chapter 1.

model discrepancy

When the underlying structure of a model is different from the process it is attempting to reproduce.

monomer

a molecule which can bind to other identical molecules to form a long chain called a polymer.

myocardial infarction

A condition where a blood clot reduces or stops blood from supplying the heart with oxygen. Colloquially known as a heart attack.

negative feedback

Negative feedback is when a processes output is fed back into itself, where increases in the output result in future decreases. An example of negative feedback in coagulation is protein C, where increases in thrombin result in increases in protein C, leading to less FVa and FVIIIa which reduces thrombin formation.

nondimensionalization

The process of removing dimensions (units) from a mathematical system. See Chapter 1 and Section 2.7.

optical density

The chromophore concentration, and by extension the concentration of substrate that has been activated, is measured in units of optical density. The optical density curve at time t is proportional to the integral of the thrombin generation curve between time 0 and t. See Chapters 1 and 3.

ordinary differential equation

An equation involving one or more functions of a single variable and derivatives of these functions.

over-fitting

A consequence of fitting more parameters than can be informed by the data. It results in a model which is especially good at predicting the data it was trained on but performs considerably worse on data it was not trained on.

parameter determinability

The parameter determinability method we use determines the reaction rates we keep fixed during fitting. This method varies the reaction rates one-at-a-time to see if they have a significant influence on the optical density curve. See Chapter 3.

parameter identifiability

A property in which parameter fitting is able to correctly identify the parameters for the system.

PCPS

PCPS (PhosphatidylCholine-PhosphatidylSerine) are 2 types of phospholipids commonly used together for coagulation assays. See Chapter 1.

peak

The maximum concentration of thrombin from the thrombin generation curve. See Chapter 1.

peptide

A short chain of amino acids. Proteins, also called polypeptides, consist of many peptide sub-units.

perfect rate

The reaction rates that are closest to the true rates (measured in the RMSLE metric) that can be fitted by the fitting algorithms. See Chapter 6.

perturbation kernel

A perturbation kernel is a function used in ABC-SMC to perturb particles. See Chapter 1.

phospholipid

A protein consisting of a hydrophilic head and hydrophobic tail. Phospholipids act as a surface for coagulation factors to bind to. See Chapter 1.

plasmin

The enzyme which breaks down fibrin. Its precursor, plasminogen, is cleaved by FXIa, FXIIa, tPA (tissue plasminogen activation), and urokinase. See Chapter 1.

plasminogen activator inhibitor 1

An inhibitor in fibrinolysis. It also inhibits factor XIa.

platelet plug

The platelet plug is a collection of activated platelets which have aggregated together and forms part of the final blood clot. See Chapter 1.

platelets

A small cell fragment without a nucleus that is involved in clotting. See Chapter 1.

polymer

A long chain of monomer molecules. The length of a polymer is measured as the number of monomers, for example, a 70mer polymer consists of 70 monomers.

polyphosphate

A surface for factor XI activation.

pooled plasma

In the assay, pooled plasma refers to a technique for generating a standard plasma sample by pooling together the plasma samples of multiple individuals to average out the individual variation with our assay using a 20-donor pool. In the model, we use standard, averaged reference concentrations for each factor to emulate this and produce a standard thrombin generation curve. See Chapters 1 and 3.

positive feedback

Negative feedback is when a processes output is fed back into itself, where increases in the output result in future decreases. An example of positive feedback in coagulation is the cofactors. Higher levels of thrombin lead to higher levels of the cofactors FVa and FVIIIa which result in an increase in thrombin formation.

PRAMIS

Platelet Reactivity in Myocardial Infarction Study. The cohort on which the thrombin generation data we use was measured. See Chapter 1.

prekallikrein

The precursor to kallikrein. Involved in contact activation. See Chapter 1.

primary haemostasis

The second stage of haemostasis. Primary haemostasis is the formation of a platelet plug. See Chapter 1.

principal component analysis

A method of dimensionality reduction. See Chapter 1.

prior distribution

A prior distribution in Bayesian statistics summarises the current beliefs around the value of a parameter. See Chapter 1. The prior distributions in this work are log-normal distributions for each reaction rate, fitted to the reaction rate's experimentally measured values. See Chapters 3 and 5.

prior form

The experimentally measured values of the reaction rates are frequently given in terms of $K_d = \frac{k_-}{k_+}$ for complex binding and K_m, k_{cat} for enzymatic activation. As such, the prior distributions define reaction rates in terms of K_d, k_+ for complex binding and K_m, k_{cat} and the set of reaction rates are termed to be in prior form. The prior form is used for fitting reaction rates and transformed into mass action law form for model simulation. See Chapter 3.

propagation

The third stage of the cell-based model of haemostasis. See Chapter 1.

protein

A protein is a long chain of amino acids. Many bodily functions are controlled by proteins, including coagulation in which all coagulation factors, both zymogen and active forms, are all proteins.

protein C

Protein C (PC) is the precursor to Activated Protein C (APC). APC is a serine protease which is activated by the IIa:TM (thrombin-thrombomodulin complex) and degrades factors Va and VIIIa. See Chapter 1.

protein S

Protein S is the cofactor for protein C and has also been shown to serve as a cofactor for TFPI. See Chapter 1.

prothrombin

The zymogen form of the enzyme thrombin. See Chapter 1.

prothrombin conversion

Prothrombin conversion can either be total (in which all prothrombin is converted to thrombin) or partial (in which prothrombin is remaining at the end of the assay). The prothrombin conversion discrepancy is that the previous models, and many Union Models, predict total prothrombin conversion whereas experimental measures demonstrate partial prothrombin conversion. See Section 2.4 and Chapters 4 and 5.

prothrombin time

A clinical assay to measure the performance of the extrinsic pathway. See Chapter 1.

prothrombinase

The complex between FXa and FVa (Xa:Va) which is able to activate prothrombin into thrombin. See Chapter 1.

pseudopodia

The arm like tendrils that grow from a platelet when it is activated. See Chapter 1.

rate law

The method used to convert a set of reactions and reaction rates into an ordinary differential equation system. The two most common are Mass Action and Michaelis Menten. See Chapter 1.

reaction scheme

A set of reactions.

red blood cell

Disk-shaped cells in the blood that carry oxygen.

regression tree

A method in data analysis in which a variable is approximated from a data set through binary questions on the other variables. See Chapters 1 and 4.

relative error

The absolute error between a predicted value and its true value, as a percentage of the true value.

relipidated tissue factor

Tissue factor that has been removed from phospholipids (delipidated) and then expressed on another set of phospholipid vesicles so greater control can be placed over the composition and size of the phospholipid vesicles.

RMSE

Root Mean Squared Error. See Chapter 1.

RMSLE

Root Mean Squared Log Error. See Chapter 6.

roughness penalty

A penalty that can be applied when fitting curves to data to reduce high frequency oscillations resulting from over-fitting. See Chapters 1 and 4.

SBML

Systems Biology Markup Language. A data format for representing mathematical systems biology models including chemical kinetic models.

second order reaction

A reaction with two reactants.

sensitivity analysis

A method of uncertainty quantification. See Chapter 1 and Section 2.5.

serine protease

A protein, specifically an enzyme, which cleaves other proteins through its serine amino acid active site.

simulation study

A method in which a simulated data set is constructed to test a statistical method in a situation where the true data generating method is known. See Chapter 6.

species

A term in chemical kinetic modelling to describe each molecule. For example, in thrombin generation models, all of FX, FXa, FV, FVa, and Xa:Va are all species.

sub-endothelial cell

Cells found in an internal layer of blood vessels which normally does not come into contact with blood. These cells are smooth muscle cells and express tissue factor. See Chapter 1.

thrombin

The serine protease which is uniquely able to cleave fibrinogen into fibrin. This coagulation factor (factor IIa) is the focus of much of this and others work. See Chapter 1.

thrombin generation assay

The assay for measuring thrombin concentration over the course of its activation. This assay is initiated by tissue factor, phospholipids and calcium ions. See Chapter 1.

thrombin generation curve

A plot of thrombin concentration over time from a thrombin generation assay or mathematical model. See Chapter 1.

thrombomodulin

The surface bound protein (TM) serves as the cofactor to increase the rate of protein C activation by thrombin. See Chapter 1.

time to peak

The time to reach the maximum concentration of thrombin from the thrombin generation curve. See Chapter 1.

timescale analysis

The process of analysing a mathematical model on different timescales. See Chapter 1 and Section 2.7.

tissue factor

A protein that is expressed on sub-endothelial cells. See Chapter 1.

tissue factor pathway inhibitor

Tissue Factor Pathway Inhibitor (TFPI) is an inhibitor for FXa and TF:VIIa. It first inhibits FXa, forming the Xa:TFPI complex, which then may inhibit the TF:VIIa complex. See Chapter 1.

true rate

The reaction rates used to generate a simulated data set. See Chapter 6.

uncertainty quantification

A class of methods used to evaluate and quantify the uncertainty in parameters and their effects on model output. See Chapter 1.

unidentifiable

A model is unidentifiable if it is not possible to identify a unique set of parameters from some data. This is typically either because the model returns identical outputs for different parameter sets (true unidentifiability) or outputs that are sufficiently similar that it is not reasonable to separate them when acounting for experimental noise (practical unidentifiability).

uninformative prior

A form of prior distribution where a wide range of values have similar probability. Useful when very little information is known about the parameters.

varimax rotation

A rotation that can be applied to the principal components to emphasise the change in a few variables to aid interpretation. See Chapter 1.

vasoconstriction

The first stage of haemostasis. The muscular response in which a blood vessel constricts to reduce blood flow upon damage. See Chapter 1.

vesicle

A phosphilipid vesicle is a ball-shaped phospholipid bilayer..

vessel wall

The vessel wall, or endothelium, consists of many layers, two of which are relevant to this work. The layer which is typically exposed to the blood is a layer of endothelial cells. Beneath this layer are the sub-endothelial cells which are involved in coagulation. See Chapter 1.

von Willebrand Factor

A glycoprotein that can bind to plaletes and factor VIII.

zymogen

The precursor form of an enzyme.

Bibliography

[1] Boon GD. An overview of hemostasis. *Toxicologic Pathology*. 1993; 21(2): 170–179. DOI: 10.1177/019262339302100209.

[2] Versteeg HH, Heemskerk JW, Levi M, Reitsma PH. New fundamentals in hemostasis. *Physiological Reviews*. 2013; 93(1): 327–358. DOI: 10.1152/physrev.00016.2011.

[3] LaPelusa A, Dave HD. (2023, March 7) *Physiology, Hemostasis.* In: StatPearls. StatPearls Publishing. URL: https://www.ncbi.nlm.nih.gov/books/NBK545263/.

[4] Davie EW, Ratnoff OD. Waterfall sequence for intrinsic blood clotting. *Science*. 1964; 145(3638): 1310–1312. DOI: 10.1126/science.145.3638.1310.

[5] Macfarlane RG. An enzyme cascade in the blood clotting mechanism, and its function as a biochemical amplifier. *Nature*. 1964; 202(4931): 498–499. DOI: 10.1038/202498a0.

[6] Hoffman M, Monroe 3rd DM. A cell-based model of hemostasis. *Thrombosis and Haemostasis*. 2001; 85(6): 958–965. DOI: 10.1055/s-0037-1615947.

[7] Protty MB, Vince Jenkins P, Collins PW, O'Donnell VB. The role of procoagulant phospholipids on the surface of circulating blood cells in thrombosis and haemostasis. *Open Biology*. 2022; 12(4): 210318. DOI: 10.1098/rsob.210318.

[8] van Montfoort ML, Meijers JCM. Recent insights into the role of the contact pathway in thrombo-inflammatory disorders. *Hematology*. 2014; 2014(1): 60–65. DOI: 10.1182/asheducation.v2014.1.60.3882400.

[9] Vojacek JF. Should we replace the terms intrinsic and extrinsic coagulation pathways with tissue factor pathway? *Clinical and Applied Thrombosis/Hemostasis*. 2017; 23(8): 922–927. DOI: 10.1177/1076029616673733.

[10] Quick AJ. The development and use of the prothrombin tests. *Circulation*. 1959; 19(1): 92–96. DOI: 10.1161/01.CIR.19.1.92.

[11] White 2nd GC. The partial thromboplastin time: Defining an era in coagulation. *Journal of Thrombosis and Haemostasis*. 2003; 1(11): 2267–2270. DOI: 10.1046/j.1538-7836.2003.00459.x.

[12] Castoldi E, Rosing J. Thrombin generation tests. *Thrombosis Research*. 2011; 127(Suppl 3): S21–S25. DOI: 10.1016/S0049-3848(11)70007-X.

[13] Hemker HC, Willems GM, Béguin S. A computer assisted method to obtain the prothrombin activation velocity in whole plasma independent of thrombin decay processes. *Thrombosis and Haemostasis*. 1986; 56(1): 9–17. DOI: 10.1055/s-0038-1661594.

[14] Colucci G, Tsakiris DA. Thrombophilia screening revisited: An issue of personalized medicine. *Journal of Thrombosis and Thrombolysis*. 2020; 49(4): 618–629. DOI: 10.1007/s11239-020-02090-y.

[15] Ament L. Factor V Leiden: A review of the literature. *Journal of Perinatal and Neonatal Nursing*. 2003; 17(3): 190–195. DOI: 10.1097/00005237-200307000-00004.

[16] *Global Health Estimates 2020: Deaths by Cause, Age, Sex, by Country and by Region, 2000-2019*. 2020.

[17] Franchini M, Mannucci PM. The history of hemophilia. *Seminars in Thrombosis and Hemostasis*. 2014; 40(5): 571–576. DOI: 10.1055/s-0034-1381232.

[18] Bharati KP, Prashanth UR. Von Willebrand disease: An overview. *Indian Journal of Pharmaceutical Sciences*. 2011; 73(1): 7–16. DOI: 10.4103/0250-474x.89751.

[19] Iorio A, Stonebraker JS, Chambost H, Makris M, Coffin D, Herr C, Germini F. Establishing the Prevalence and Prevalence at Birth of Hemophilia in Males. *Annals of Internal Medicine*. 2019; 171(8): 540–546. DOI: 10.7326/M19-1208.

[20] Hassan S, Monahan RC, Mauser-Bunschoten EP, Vulpen LFD van, Eikenboom J, Beckers EAM, Hooimeijer L, Ypma PF, Nieuwenhuizen L, Coppens M, Schols SEM, Leebeek FWG, Smit C, Driessens MH, Cessie S le, Balen EC van, Rosendaal FR, Bom JG van der, Gouw SC. Mortality, life expectancy, and causes of death of persons with hemophilia in the Netherlands 2001–2018. *Journal of Thrombosis and Haemostasis*. 2021; 19(3): 645–653. DOI: 10.1111/jth.15182.

[21] Dunster JL, Wright JR, Samani NJ, Goodall AH. A system-wide investigation and stratification of the hemostatic proteome in premature myocardial infarction. *Frontiers in Cardiovascular Medicine*. 2022; 9: 919394. DOI: 10.3389/fcvm.2022.919394.

[22] Brouilette S, Singh RK, Thompson JR, Goodall AH, Samani NJ. White cell telomere length and risk of premature myocardial infarction. *Arteriosclerosis, Thrombosis, and Vascular Biology*. 2003; 23(5): 842–846. DOI: 10.1161/01.ATV.0000067426.96344.32.

[23] Feinberg M. *Foundations of Chemical Reaction Network Theory*. Applied Mathematical Sciences; vol 2. Cham, Switzerland: Springer; 2019.

[24] Horn F, Jackson R. General mass action kinetics. *Archive for Rational Mechanics and Analysis*. 1972; 47(2): 81–116. DOI: 10.1007/BF00251225.

[25] Chen WW, Niepel M, Sorger PK. Classic and contemporary approaches to modeling biochemical reactions. *Genes and Development*. 2010; 24(17): 1861–1875. DOI: 10.1101/gad.1945410.

[26] Johnson KA, Goody RS. The original Michaelis constant: Translation of the 1913 Michaelis-Menten Paper. *Biochemistry*. 2011; 50(39): 8264–8269. DOI: 10.1021/bi201284u.

[27] Navarro-Lozano MJ, Valero E, Varon R, Garcia-Carmona F. Kinetic study of an enzyme-catalysed reaction in the presence of novel irreversible-type inhibitors that react with the product of enzymatic catalysis. *Bulletin of Mathematical Biology*. 1995; 57(1): 157–168. DOI: 10.1007/BF02458321.

[28] Whiteley CG. Mechanistic and kinetic studies of inhibition of enzymes. *Cell Biochemistry and Biophysics*. 2000; 33(3): 217–225. DOI: 10.1385/CBB:33:3:217.

[29] Buckingham E. On physically similar systems; Illustrations of the use of dimensional equations. *Physical Review*. 1914; 4(4): 345–376. DOI: 10.1103/PhysRev.4.345.

[30] Dunster JL, King JR. Mathematical modelling of thrombin generation: asymptotic analysis and pathway characterization. *IMA Journal of Applied Mathematics*. 2017; 82(1): 60–96. DOI: 10.1093/imamat/hxw012.

[31] Hinch EJ. *Perturbation Methods*. Cambridge Texts in Applied Mathematics; vol 6. Cambridge, United Kingdom: Cambridge University Press; 1991.

[32] Kevorkian J, Cole JD. *Multiple Scale and Singular Perturbation Methods*. Applied Mathematical Sciences; vol 114. New York, USA: Springer; 1996.

[33] Watts RG. *Essentials of Applied Mathematics for Engineers and Scientists*. Synthesis Lectures on Mathematics & Statistics. 2nd ed. Cham, Switzerland: Springer; 2008. Chapter 10, Introduction to Perturbation Methods; p.153-162.

[34] Wolfe P. Convergence conditions for ascent methods. *SIAM Review*. 1969; 11(2): 226–235. DOI: 10.1137/1011036.

[35] Kiefer J, Wolfowitz J. Stochastic estimation of the maximum of a regression function. *The Annals of Mathematical Statistics*. 1952; 23(3): 462–466. DOI: 10.1214/aoms/1177729392.

[36] Qian N. On the momentum term in gradient descent learning algorithms. *Neural Networks*. 1999; 12(1): 145–151. DOI: 10.1016/S0893-6080(98)00116-6.

[37] Byrd RH, Gilbert JC, Nocedal J. A trust region method based on interior point techniques for nonlinear programming. *Mathematical Programming*. 2000; 89(1): 149–185. DOI: 10.1007/PL00011391.

[38] Toni T, Welch D, Strelkowa N, Ipsen A, Stumpf MPH. Approximate Bayesian computation scheme for parameter inference and model selection in dynamical systems. *Journal of the Royal Society Interface*. 2009; 6(31): 187–202. DOI: 10.1098/rsif.2008.0172.

[39] Chatterjee MS, Denney WS, Jing H, Diamond SL. Systems biology of coagulation initiation: Kinetics of thrombin generation in resting and activated human blood. *PLoS Computational Biology*. 2010; 6(9): e1000950. DOI: 10.1371/journal.pcbi.1000950.

[40] Chen J, Diamond SL. Sensitivity analysis of a reduced model of thrombosis under flow: Roles of factor IX, factor XI, and γ'-Fibrin. *PLoS ONE*. 2021; 16(11): e0260366. DOI: 10.1371/journal.pone.0260366.

[41] Danforth CM, Orfeo T, Everse SJ, Mann KG, Brummel-Ziedins KE. Defining the boundaries of normal thrombin generation: Investigations into hemostasis. *PLoS ONE*. 2012; 7(2): e30385. DOI: 10.1371/journal.pone.0030385.

[42] Danforth CM, Orfeo T, Mann KG, Brummel-Ziedins KE, Everse SJ. The impact of uncertainty in a blood coagulation model. *Mathematical Medicine and Biology*. 2009; 26(4): 323–336. DOI: 10.1093/imammb/dqp011.

[43] Link KG, Stobb MT, Di Paola J, Neeves KB, Fogelson AL, Sindi SS, Leiderman K. A local and global sensitivity analysis of a mathematical model of coagulation and platelet deposition under flow. *PLoS ONE*. 2018; 13(7): e0200917. DOI: 10.1371/journal.pone.0200917.

[44] Link KG, Stobb MT, Sorrells MG, Bortot M, Ruegg K, Manco-Johnson MJ, Di Paola JA, Sindi SS, Fogelson AL, Leiderman K, Neeves KB. A mathematical model of coagulation under flow identifies factor V as a modifier of thrombin generation in hemophilia A. *Journal of Thrombosis and Haemostasis*. 2020; 18(2): 306–317. DOI: 10.1111/jth.14653.

[45] Luan D, Zai M, Varner JD. Computationally derived points of fragility of a human cascade are consistent with current therapeutic strategies. *PLoS Computational Biology*. 2007; 3(7): e142. DOI: 10.1371/journal.pcbi.0030142.

[46] Jolliffe IT, Cadima J. Principal component analysis: a review and recent developments. *Philosophical Transactions. Series A, Mathematical, Physical and Engineering Sciences*. 2016; 374(2065): 20150202. DOI: 10.1098/rsta.2015.0202.

[47] Tibshirani R, Walther G, Hastie T. Estimating the number of clusters in a data set via the gap statistic. *Journal of the Royal Statistical Society. Series B: Statistical Methodology*. 2001; 63(2): 411–423. DOI: 10.1111/1467-9868.00293.

[48] Dudoit S, Fridlyand J. A prediction-based resampling method for estimating the number of clusters in a dataset. *Genome biology*. 2002; 3(7): research0036.1. DOI: 10.1186/GB-2002-3-7-RESEARCH0036.

[49] Krzywinski M, Altman N. Classification and regression trees. *Nature Methods*. 2017; 14(8): 757–758. DOI: 10.1038/nmeth.4370.

[50] Loh WY. Fifty years of classification and regression trees. *International Statistical Review*. 2014; 82(3): 329–348. DOI: 10.1111/insr.12016.

[51] Jacques J, Preda C. Functional data clustering: A survey. *Advances in Data Analysis and Classification*. 2014; 8(3): 231–255. DOI: 10.1007/s11634-013-0158-y.

[52] Ramsay JO, Silverman BW. *Functional Data Analysis*. Springer Series in Statistics. 2nd ed. New York, USA: Springer; 2005.

[53] Jones KC, Mann KG. A model for the tissue factor pathway to thrombin. II. A mathematical simulation. *Journal of Biological Chemistry*. 1994; 269(37): 23367–23373. DOI: 10.1016/S0021-9258(17)31662-9.

[54] Khanin MA, Semenov VV. A mathematical model of the kinetics of blood coagulation. *Journal of Theoretical Biology*. 1989; 136(2): 127–134. DOI: 10.1016/S0022-5193(89)80220-6.

[55] Willems GM, Lindhout T, Hermens WT, Hemker HC. Simulation model for thrombin generation in plasma. *Haemostasis*. 1991; 21(4): 197–207. DOI: 10.1159/000216229.

[56] Leipold RJ, Bozarth TA, Racanelli AL, Dicker IB. Mathematical model of serine protease inhibition in the tissue factor pathway to thrombin. *Journal of Biological Chemistry*. 1995; 270(43): 25383–25387. DOI: 10.1074/jbc.270.43.25383.

[57] Zarnitsina VI, Pokhilko AV, Ataullakhanov FI. A mathematical model for the spatio-temporal dynamics of intrinsic pathway of blood coagulation. I. The model description. *Thrombosis Research*. 1996; 84(4): 225–236. DOI: 10.1016/S0049-3848(96)00182-X.

[58] Khanin MA, Rakov DV, Kogan AE. Mathematical model for the blood coagulation prothrombin time test. *Thrombosis Research*. 1998; 89(5): 227–232. DOI: 10.1016/S0049-3848(97)00288-0.

[59] Hockin MF, Jones KC, Everse SJ, Mann KG. A model for the stoichiometric regulation of blood coagulation. *Journal of Biological Chemistry*. 2002; 277(21): 18322–18333. DOI: 10.1074/jbc.M201173200.

[60] Brummel-Ziedins KE, Orfeo T, Callas PW, Gissel M, Mann KG, Bovill EG. The prothrombotic phenotypes in familial protein C deficiency are differentiated by computational modeling of thrombin generation. *PLoS ONE*. 2012; 7(9): e44378. DOI: 10.1371/journal.pone.0044378.

[61] Mitrophanov AY, Szlam F, Sniecinski RM, Levy JH, Reifman J. A step toward balance: Thrombin generation improvement via procoagulant factor and antithrombin supplementation. *Anesthesia and Analgesia*. 2016; 123(3): 535–546. DOI: 10.1213/ANE.0000000000001361.

[62] Bungay SD, Gentry PA, Gentry RD. A mathematical model of lipid-mediated thrombin generation. *Mathematical Medicine and Biology*. 2003; 20(1): 105–129. DOI: 10.1093/imammb/20.1.105.

[63] Panteleev MA, Balandina AN, Lipets EN, Ovanesov MV, Ataullakhanov FI. Task-oriented modular decomposition of biological networks: Trigger mechanism in blood coagulation. *Biophysical Journal*. 2010; 98(9): 1751–1761. DOI: 10.1016/j.bpj.2010.01.027.

[64] Panteleev MA, Ovanesov MV, Kireev DA, Shibeko AM, Sinauridze EI, Ananyeva NM, Butylin AA, Saenko EL, Ataullakhanov FI. Spatial propagation and localization of blood coagulation are regulated by intrinsic and protein C pathways, respectively. *Biophysical Journal*. 2006; 90(5): 1489–1500. DOI: 10.1529/biophysj.105.069062.

[65] Qiao YH, Liu JL, Zeng YJ. A kinetic model for simulation of blood coagulation and inhibition in the intrinsic path. *Journal of Medical Engineering and Technology*. 2005; 29(2): 70–74. DOI: 10.1080/03091900410001709079.

[66] Tyurin KV, Khanin MA. Hemostasis as an optimal system. *Mathematical Biosciences*. 2006; 204(2): 167–184. DOI: 10.1016/j.mbs.2006.09.005.

[67] Xu C, Xu XH, Zeng Y, Chen YW. Simulation of a mathematical model of the role of the TFPI in the extrinsic pathway of coagulation. *Computers in Biology and Medicine*. 2005; 35(5): 435–445. DOI: 10.1016/S0010-4825(04)00043-5.

[68] Zhu D. Mathematical modeling of blood coagulation cascade: Kinetics of intrinsic and extrinsic pathways in normal and deficient conditions. *Blood Coagulation and Fibrinolysis*. 2007; 18(7): 637–646. DOI: 10.1097/MBC.0b013e3282a167bb.

[69] Kuharsky AL, Fogelson AL. Surface-mediated control of blood coagulation: The role of binding site densities and platelet deposition. *Biophysical Journal*. 2001; 80(3): 1050–1074. DOI: 10.1016/S0006-3495(01)76085-7.

[70] Xu CQ, Zeng YJ, Gregersen H. Dynamic model of the role of platelets in the blood coagulation system. *Medical Engineering and Physics*. 2002; 24(9): 587–593. DOI: 10.1016/S1350-4533(02)00047-4.

[71] Butenas S, Orfeo T, Gissel MT, Brummel KE, Mann KG. The significance of circulating factor IXa in blood. *Journal of Biological Chemistry*. 2004; 279(22): 22875–22882. DOI: 10.1074/jbc.M400531200.

[72] Brummel-Ziedins KE, Orfeo T, Gissel M, Mann KG, Rosendaal FR. Factor Xa generation by computational modeling: An additional discriminator to thrombin generation evaluation. *PLoS ONE*. 2012; 7(1): e29178. DOI: 10.1371/journal.pone.0029178.

[73] Hemker HC, Wielders S, Kessels H, Béguin S. Continuous registration of thrombin generation in plasma, its use for the determination of the thrombin potential. *Thrombosis and Haemostasis*. 1993; 70(4): 617–624. DOI: 10.1055/s-0038-1649638.

[74] Hemker HC, Giesen P, Al Dieri R, Regnault V, de Smedt E, Wagenvoord R, Lecompte T, Béguin S. Calibrated automated thrombin generation measurement in clotting plasma. *Pathophysiology of Haemostasis and Thrombosis*. 2003; 33(1): 4–15. DOI: 10.1159/000071636.

[75] Hemker HC, Kremers R. Data management in thrombin generation. *Thrombosis Research*. 2013; 131(1): 3–11. DOI: 10.1016/j.thromres.2012.10.011.

[76] Hemker HC, Kerdelo S, Kremers RMW. Is there value in kinetic modeling of thrombin generation? No (unless...) *Journal of Thrombosis and Haemostasis*. 2012; 10(8): 1470–1477. DOI: 10.1111/j.1538-7836.2012.04802.x.

[77] Mann KG. Is there value in kinetic modeling of thrombin generation? Yes. *Journal of Thrombosis and Haemostasis*. 2012; 10(8): 1463–1469. DOI: 10.1111/j.1538-7836.2012.04799.x.

[78] Chelle P, Morin C, Montmartin A, Piot M, Cournil M, Tardy-Poncet B. Evaluation and calibration of in silico models of thrombin generation using experimental data from healthy and haemophilic subjects. *Bulletin of Mathematical Biology*. 2018; 80(8): 1989–2025. DOI: 10.1007/s11538-018-0440-4.

[79] Wagenvoord R, Hemker PW, Hemker HC. The limits of simulation of the clotting system. *Journal of Thrombosis and Haemostasis*. 2006; 4(6): 1331–1338. DOI: 10.1111/j.1538-7836.2006.01967.x.

[80] Leiderman K, Fogelson A. An overview of mathematical modeling of thrombus formation under flow. *Thrombosis Research*. 2014; 133(Suppl 1): S12–S14. DOI: 10.1016/j.thromres.2014.03.005.

[81] Leiderman K, Fogelson AL. Grow with the flow: A spatial-temporal model of platelet deposition and blood coagulation under flow. *Mathematical Medicine and Biology*. 2011; 28(1): 47–84. DOI: 10.1093/imammb/dqq005.

[82] Link KG, Sorrells MG, Danes NA, Neeves KB, Leiderman K, Fogelson AL. A mathematical model of platelet aggregation in an extravascular injury under flow. *Multiscale Modeling and Simulation*. 2020; 18(4): 1489–1524. DOI: 10.1137/20M1317785.

[83] Lobanov AI, Starozhilova TK. The effect of convective flows on blood coagulation processes. *Pathophysiology of Haemostasis and Thrombosis*. 2006; 34(2-3): 121–134. DOI: 10.1159/000089932.

[84] Sequeira A, Santos RF, Bodnár T. Blood coagulation dynamics: Mathematical modeling and stability results. *Mathematical Biosciences and Engineering*. 2011; 8(2): 425–443. DOI: 10.3934/mbe.2011.8.425.

[85] Butenas S, van't Veer C, Mann KG. "Normal" thrombin heneration. *Blood*. 1999; 94(7): 2169–2178. DOI: 10.1182/blood.V94.7.2169.419k22_2169_2178.

[86] Bravo MC, Orfeo T, Mann KG, Everse SJ. Modeling of human factor Va inactivation by activated protein C. *BMC Systems Biology*. 2012; 6(1): 45. DOI: 10.1186/1752-0509-6-45.

[87] Chelliah V, Juty N, Ajmera I, Ali R, Dumousseau M, Glont M, Hucka M, Jalowicki G, Keating S, Knight-Schrijver V, Lloret-Villas A, Natarajan KN, Pettit JB, Rodriguez N, Schubert M, Wimalaratne SM, Zhao Y, Hermjakob H, Le Novère N, Laibe C. BioModels: Ten-year anniversary. *Nucleic Acids Research*. 2015; 43(D1): D542–D548. DOI: 10.1093/nar/gku1181.

[88] Kogan AE, Kardakov DV, Khanin MA. Analysis of the activated partial thromboplastin time test using mathematical modeling. *Thrombosis Research*. 2001; 101(4): 299–310. DOI: 10.1016/S0049-3848(00)00405-9.

[89] Kremers RMW, Peters TC, Wagenvoord RJ, Hemker HC. The balance of pro- and anticoagulant processes underlying thrombin generation. *Journal of Thrombosis and Haemostasis*. 2015; 13(3): 437–447. DOI: 10.1111/jth.12798.

[90] O'Brien DP, Kemball-Cook G, Hutchinson AM, Martin DMA, Johnson DJD, Byfield PGH, Takamiya O, Tuddenham EGD, McVey JH. Surface plasmon resonance studies of the interaction between factor VII and tissue factor. Demonstration of defective tissue factor binding in a variant FVII molecule (FVII-R79Q). *Biochemistry*. 1994; 33(47): 14162–14169. DOI: 10.1021/bi00251a027.

[91] Krishnaswamy S. The interaction of human factor VIIa with tissue factor. *Journal of Biological Chemistry*. 1992; 267(33): 23696–23706. DOI: 10.1016/S0021-9258(18)35894-0.

[92] Naski MC, Shafer JA. A kinetic model for the α-thrombin-catalyzed conversion of plasma levels of fibrinogen to fibrin in the presence of antithrombin III. *Journal of Biological Chemistry*. 1991; 266(20): 13003–13010. DOI: 10.1016/S0021-9258(18)98795-8.

[93] Hockin MF, Cawthern KM, Kalafatis M, Mann KG. A model describing the inactivation of factor Va by APC: Bond cleavage, fragment dissociation, and product inhibition. *Biochemistry*. 1999; 38(21): 6918–6934. DOI: 10.1021/bi981966e.

[94] Baglia FA, Walsh PN. Thrombin-mediated feedback activation of factor XI on the activated platelet surface is preferred over contact activation by factor XIIa or factor XIa. *Journal of Biological Chemistry*. 2000; 275(27): 20514–20519. DOI: 10.1074/jbc.M000464200.

[95] Baglia FA, Walsh PN. Thrombin-mediated feedback activation of factor XI on the activated platelet surface is preferred over contact activation by factor XIIa or factor XIa [retraction of: Baglia FA, Walsh PN. *J Biol Chem*. 2000; 275(27): 20514-9]. *Journal of Biological Chemistry*. 2007; 282(39): 29067. DOI: 10.1016/S0021-9258(20)58640-7.

[96] Gailani D, Broze Jr GJ. Factor XI activation in a revised model of blood coagulation. *Science*. 1991; 253(5022): 909–912. DOI: 10.1126/science.1652157.

[97] Doyle MF, Mann KG. Multiple active forms of thrombin. IV. Relative activities of meizothrombins. *Journal of Biological Chemistry*. 1990; 265(18): 10693–10701. DOI: 10.1016/S0021-9258(18)87002-8.

[98] Bach R, Gentry R, Nemerson Y. Factor VII binding to tissue factor in reconstituted phospholipid vesicles: Induction of cooperativity by phosphatidylserinet. *Biochemistry*. 1986; 25(14): 4007–4020. DOI: 10.1021/bi00362a005.

[99] Björquist P, Boström S. Determination of the kinetic constants of tissue factor/factor VII/factor VIIa and antithrombin/heparin using surface plasmon resonance. *Thrombosis Research*. 1997; 85(3): 225–236. DOI: 10.1016/S0049-3848(97)00007-8.

[100] Everitt RG, Rowińska PA. Delayed acceptance ABC-SMC. *Journal of Computational and Graphical Statistics*. 2021; 30(1): 55–66. DOI: 10.1080/10618600.2020.1775617.

[101] Hackeng TM, Maurissen LFA, Castoldi E, Rosing J. Regulation of TFPI function by protein S. *Journal of Thrombosis and Haemostasis*. 2009; 7(Suppl 1): 165–168. DOI: 10.1111/j.1538-7836.2009.03363.x.

[102] Peraramelli S, Rosing J, Hackeng TM. TFPI-dependent activities of Protein S. *Thrombosis Research*. 2012; 129(Suppl 2): S23–S26. DOI: 10.1016/j.thromres.2012.02.024.

[103] Castoldi E, Simioni P, Tormene D, Rosing J, Hackeng TM. Hereditary and acquired protein S deficiencies are associated with low TFPI levels in plasma. *Journal of Thrombosis and Haemostasis*. 2010; 8(2): 294–300. DOI: 10.1111/j.1538-7836.2009.03712.x.

[104] Reglińska-Matveyev N, Andersson HM, Rezende SM, Dahlbäck B, Crawley JTB, Lane DA, Ahnström J. TFPI cofactor function of protein S: Essential role of the protein S SHBG-like domain. *Blood*. 2014; 123(25): 3979–3987. DOI: 10.1182/blood-2014-01-551812.

[105] Ahnström J, Andersson HM, Hockey V, Meng Y, McKinnon TAJ, Hamuro T, Crawley JTB, Lane DA. Identification of functionally important residues in TFPI Kunitz domain 3 required for the enhancement of its activity by protein S. *Blood*. 2012; 120(25): 5059–5062. DOI: 10.1182/blood-2012-05-432005.

[106] Aso Y, Fujiwara Y, Tayama K, Takebayashi K, Inukai T, Takemura Y. Relationship between soluble thrombomodulin in plasma and coagulation or fibrinolysis in type 2 diabetes. *Clinica Chimica Acta*. 2000; 301(1-2): 135–145. DOI: 10.1016/S0009-8981(00)00335-1.

[107] Jackson DE, Tetaz TJ, Salem HH, Mitchell CA. Purification and characterization of two forms of soluble thrombomodulin from human urine. *European Journal of Biochemistry*. 1994; 221(3): 1079–1087. DOI: 10.1111/j.1432-1033.1994.tb18827.x.

[108] Lu G, Chhum S, Krishnaswamy S. The affinity of protein C for the thrombin-thrombomodulin complex is determined in a primary way by active site-dependent interactions. *Journal of Biological Chemistry*. 2005; 280(15): 15471–15478. DOI: 10.1074/jbc.M500881200.

[109] Parkinson JF, Grinnell BW, Moore RE, Hoskins J, Vlahos CJ, Bang NU. Stable expression of a secretable deletion mutant of recombinant human thrombomodulin in mammalian cells. *Journal of Biological Chemistry*. 1990; 265(21): 12602–12610. DOI: 10.1016/s0021-9258(19)38386-3.

[110] Bajzar L, Morser J, Nesheim M. TAFI, or plasma procarboxypeptidase B, couples the coagulation and fibrinolytic cascades through the thrombin-thrombomodulin complex. *Journal of Biological Chemistry*. 1996; 271(28): 16603–16608. DOI: 10.1074/jbc.271.28.16603.

[111] Weisel JW, Litvinov RI. Fibrin Formation, Structure and Properties. In: Parry DAD, Squire JM. (eds) *Fibrous Proteins: Structures and Mechanisms.* Subcellular Biochemistry; vol 82. Cham, Switzerland: Springer; 2017. p.405-456.

[112] Ramsay J, Graves S, Hooker G. *fda: Functional Data Analysis*. R package version 5.4.0. URL: https://CRAN.R-project.org/package=fda.

[113] Glass GV, Peckham PD, Sanders JR. Consequences of Failure to Meet Assumptions Underlying the Fixed Effects Analyses of Variance and Covariance. *Review of Educational Research*. 1972; 42(3): 237–288. DOI: 10.3102/00346543042003237.

[114] Jesty J. The kinetics of inhibition of thrombin by antithrombin in the presence of components of the hemostatic system. *Blood*. 1985; 66(5): 1189–1195. DOI: 10.1182/blood.v66.5.1189.bloodjournal6651189.

[115] Ellis V, Scully MF, Kakkar VV. Inhibition of prothrombinase complex by plasma proteinase inhibitors. *Biochemistry*. 1984; 23(24): 5882–5887. DOI: 10.1021/bi00319a030.

[116] Naito K, Fujikawa K. Activation of human blood coagulation factor XI independent of factor XII: Factor XI is activated by thrombin and factor XIa in the presence of negatively charged surfaces. *Journal of Biological Chemistry*. 1991; 266(12): 7353–7358. DOI: 10.1016/S0021-9258(20)89453-8.

[117] Mohammed BM, Matafonov A, Ivanov I, Sun MF, Cheng Q, Dickeson SK, Li C, Sun D, Verhamme IM, Emsley J, Gailani D. An update on factor XI structure and function. *Thrombosis Research*. 2018; 161: 94–105. DOI: 10.1016/j.thromres.2017.10.008.

[118] Choi SH, Smith SA, Morrissey JH. Polyphosphate is a cofactor for the activation of factor XI by thrombin. *Blood*. 2011; 118(26): 6963–6970. DOI: 10.1182/blood-2011-07-368811.

[119] Geng Y, Verhamme IM, Smith SA, Cheng Q, Sun M, Sheehan JP, Morrissey JH, Gailani D. Factor XI anion-binding sites are required for productive interactions with polyphosphate. *Journal of Thrombosis and Haemostasis*. 2013; 11(11): 2020–2028. DOI: 10.1111/jth.12414.

[120] Ivanov I, Shakhawat R, Sun MF, Dickeson SK, Puy C, McCarty OJT, Gruber A, Matafonov A, Gailani D. Nucleic acids as cofactors for factor XI and prekallikrein activation: Different roles for high-molecular-weight kininogen. *Thrombosis and Haemostasis*. 2017; 117(4): 671–681. DOI: 10.1160/TH16-09-0691.

[121] Omarova F, Rosing J, Bertina RM, Castoldi E. Negatively charged phospholipids stimulate factor XI activation by thrombin. *Thrombosis Update*. 2021; 2: 100022. DOI: 10.1016/j.tru.2020.100022.

[122] Rohatgi A. *WebPlotDigitizer: Version 4.5*. 2021. URL: https://automeris.io/WebPlotDigitizer.

[123] Janciauskiene SM, Bals R, Koczulla R, Vogelmeier C, Köhnlein T, Welte T. The discovery of α1-antitrypsin and its role in health and disease. *Respiratory Medicine*. 2011; 105(8): 1129–1139. DOI: 10.1016/J.RMED.2011.02.002.

[124] Pirooznia N, Hasannia S, Arab SS, Lotfi AS, Ghanei M, Shali A. The design of a new truncated and engineered alpha1-antitrypsin based on theoretical studies: An antiprotease therapeutics for pulmonary diseases. *Theoretical Biology and Medical Modelling*. 2013; 10(1): 36. DOI: 10.1186/1742-4682-10-36.

[125] Kager LM, Weehuizen TA, Wiersinga WJ, Roelofs JJTH, Meijers JCM, Dondorp AM, van't Veer C, van der Poll T. Endogenous α2-antiplasmin is protective during severe gram-negative sepsis (melioidosis). *American Journal of Respiratory and Critical Care Medicine*. 2013; 188(8): 967–975. DOI: 10.1164/rccm.201307-1344OC.

[126] Singh S, Saleem S, Reed GL. Alpha2-antiplasmin: The devil you don't know in cerebrovascular and cardiovascular disease. *Frontiers in Cardiovascular Medicine*. 2020; 7: 608899. DOI: 10.3389/fcvm.2020.608899.

[127] Mocchegiani E, Costarelli L, Giacconi R, Cipriano C, Muti E, Malavolta M. Zinc-binding proteins (metallothionein and alpha-2 macroglobulin) and immunosenescence. *Experimental Gerontology*. 2006; 41(11): 1094–1107. DOI: 10.1016/j.exger.2006.08.010.

[128] Zhu M, Zhao B, Wei L, Wang S. Alpha-2-macroglobulin, a native and powerful proteinase inhibitor, prevents cartilage degeneration disease by inhibiting majority of catabolic enzymes and cytokines. *Current Molecular Biology Reports*. 2021; 7(1): 1–7. DOI: 10.1007/s40610-020-00142-z.

[129] Tjärnlund-Wolf A, Brogren H, Lo EH, Wang X. Plasminogen activator inhibitor-1 and thrombotic cerebrovascular diseases. *Stroke*. 2012; 43(10): 2833–2839. DOI: 10.1161/STROKEAHA.111.622217.

[130] Le Magueresse-Battistoni B, Pernod G, Sigillo F, Kolodié L, Benahmed M. Plasminogen activator inhibitor-1 is expressed in cultured rat sertoli cells. *Biology of Reproduction*. 1998; 59(3): 591–598. DOI: 10.1095/biolreprod59.3.591.

[131] Gregorek H, Kokai M, Hidvégi T, Füst G, Sabbouh K, Madaliński K. Concentration of C1 inhibitor in sera of healthy blood donors as studied by immunoenzymatic assay. *Complement and Inflammation*. 1991; 8(5-6): 310–312. DOI: 10.1159/000463201.

[132] Kajdácsi E, Jandrasics Z, Veszeli N, Makó V, Koncz A, Gulyás D, Köhalmi KV, Temesszentandrási G, Cervenak L, Gál P, Dobó J, de Maat S, Maas C, Farkas H, Varga L. Patterns of C1-inhibitor/plasma serine protease complexes in healthy humans and in hereditary angioedema patients. *Frontiers in Immunology*. 2020; 11: 794. DOI: 10.3389/fimmu.2020.00794.

[133] Filkova AA, Martyanov AA, Garzon Dasgupta AK, Panteleev MA, Sveshnikova AN. Quantitative dynamics of reversible platelet aggregation: mathematical modelling and experiments. *Scientific Reports*. 2019; 9: 6217. DOI: 10.1038/s41598-019-42701-0.

[134] Du J, Fogelson AL. A two-phase mixture model of platelet aggregation. *Mathematical Medicine and Biology*. 2018; 35(2): 225–256. DOI: 10.1093/imammb/dqx001.

[135] Gupta P, Zhang P, Sheriff J, Bluestein D, Deng Y. A multiscale model for multiple platelet aggregation in shear flow. *Biomechanics and Modeling in Mechanobiology*. 2021; 20(3): 1013–1030. DOI: 10.1007/s10237-021-01428-6.

[136] Lu Y, Lee MY, Zhu S, Sinno T, Diamond SL. Multiscale simulation of thrombus growth and vessel occlusion triggered by collagen/tissue factor using a data-driven model of combinatorial platelet signalling. *Mathematical Medicine and Biology*. 2017; 34(4): 523–546. DOI: 10.1093/imammb/dqw015.

[137] Shankar KN, Zhang Y, Sinno T, Diamond SL. A three-dimensional multiscale model for the prediction of thrombus growth under flow with single-platelet resolution. *PLoS Computational Biology*. 2022; 18(1): e1009850. DOI: 10.1371/journal.pcbi.1009850.

[138] Kovalenko TA, Panteleev MA, Sveshnikova AN. Different modeling approaches in the simulation of extrinsic coagulation factor X activation: Limitations and areas of applicability [Special Issue]. *International Journal for Numerical Methods in Biomedical Engineering*. 2023: e3689. DOI: 10.1002/cnm.3689.

[139] Bonnaffé W, Sheldon BC, Coulson T. Neural ordinary differential equations for ecological and evolutionary time-series analysis. *Methods in Ecology and Evolution*. 2021; 12(7): 1301–1315. DOI: 10.1111/2041-210X.13606.

[140] Lei CL, Mirams GR. Neural network differential equations for ion channel modelling. *Frontiers in Physiology*. 2021; 12: 708944. DOI: 10.3389/fphys.2021.708944.

[141] Fedorov V. Optimal experimental design. *Wiley Interdisciplinary Reviews: Computational Statistics*. 2010; 2(5): 581–589. DOI: 10.1002/wics.100.

[142] Han X, Fiehler R, Broze Jr GJ. Isolation of a protein Z-dependent plasma protease inhibitor. *Proceedings of the National Academy of Sciences of the United States of America*. 1998; 95(16): 9250–9255. DOI: 10.1073/pnas.95.16.9250.

[143] Han X, Huang ZF, Fiehler R, Broze Jr GJ. The protein Z-dependent protease inhibitor is a serpin. *Biochemistry*. 1999; 38(34): 11073–11078. DOI: 10.1021/bi990641a.

[144] Wei Z, Yan Y, Carrell RW, Zhou A. Crystal structure of protein Z–dependent inhibitor complex shows how protein Z functions as a cofactor in the membrane inhibition of factor X. *Blood*. 2009; 114(17): 3662–3667. DOI: 10.1182/blood-2009-04-210021.

[145] Al Dieri R, Bloemen S, Kelchtermans H, Wagenvoord R, Hemker HC. A new regulatory function of activated factor V: Inhibition of the activation by tissue factor/factor VII(a) of factor X. *Journal of Thrombosis and Haemostasis*. 2013; 11(3): 503–511. DOI: 10.1111/jth.12126.

Appendix A

Models ODEs

This appendix presents the ODEs for all of the implemented models. It begins with the previous models, Hockin, Danforth, Brummel, Chatterjee, Panteleev, Bungay, Tyurin, and Zhu. Then presents the reduced ODEs corresponding to the timescale analysis in Section 2.7 for the Danforth model and the Tyurin model. Finally, it presents the ODEs for each version of the Unified Model (Unified Model, Expanded Unified Model, Expanded Unified Model with Protein C, Expanded Unified Model with Fibrinogen, Reduced Unified Model, and Improved Unified Model). In all cases the names of the parameters match those used to report the parameter values in Section 2.1 for the previous models and Appendix B for the Unified Models.

A.1 Previous Models

A.1.1 Hockin Model

$$\frac{d[TF]}{dt} = k_{-,1}[TF{:}VII] - k_{+,1}[TF][VII] + k_{-,2}[TF{:}VIIa] - k_{+,2}[TF][VIIa]$$

$$\frac{d[VII]}{dt} = k_{-,1}[TF{:}VII] - k_{+,1}[TF][VII] - k_{+,3}[VII][TF{:}VIIa] - k_{+,4}[VII][Xa] - k_{+,5}[VII][IIa]$$

$$\frac{d[TF{:}VII]}{dt} = -k_{-,1}[TF{:}VII] + k_{+,1}[TF][VII]$$

$$\frac{d[VIIa]}{dt} = k_{-,2}[TF{:}VIIa] - k_{+,2}[TF][VIIa] + k_{+,3}[VII][TF{:}VIIa] + k_{+,4}[VII][Xa] + k_{+,5}[VII][IIa]$$

$$\frac{d[TF{:}VIIa]}{dt} = -k_{-,2}[TF{:}VIIa] + k_{+,2}[TF][VIIa] + k_{-,6}[TF{:}VIIa{:}X] - k_{+,6}[TF{:}VIIa][X] + k_{-,8}[TF{:}VIIa{:}Xa] - k_{+,8}[TF{:}VIIa][Xa] + k_{-,9}[TF{:}VIIa{:}IX] - k_{+,9}[TF{:}VIIa][IX] + k_{-,10}[TF{:}VIIa{:}IX] - k_{+,25}[TF{:}VIIa][Xa{:}TFPI] - k_{+,30}[TF{:}VIIa][AT]$$

$$\frac{d[Xa]}{dt} = k_{-,8}[TF{:}VIIa{:}Xa] - k_{+,8}[TF{:}VIIa][Xa] + k_{-,15}[IXa{:}VIIIa{:}X] + k_{-,23}[Xa{:}TFPI] - k_{+,23}[Xa][TFPI] - k_{+,26}[Xa][AT] + k_{-,19}[Xa{:}Va] - k_{+,19}[Xa][Va]$$

$$\frac{d[IIa]}{dt} = k_{+,11}[II][Xa] + k_{+,22}[mIIa][Xa{:}Va] - k_{+,29}[IIa][AT]$$

$$\frac{d[X]}{dt} = k_{-,6}[TF{:}VIIa{:}X] - k_{+,6}[TF{:}VIIa][X] + k_{-,14}[IXa{:}VIIIa{:}X] - k_{+,14}[IXa{:}VIIIa][X] + k_{-,17}[IXa{:}VIIIa{:}X]$$

$$\frac{d[TF{:}VIIa{:}X]}{dt} = -k_{-,6}[TF{:}VIIa{:}X] + k_{+,6}[TF{:}VIIa][X] - k_{-,7}[TF{:}VIIa{:}X]$$

$$\frac{d[TF{:}VIIa{:}Xa]}{dt} = k_{-,7}[TF{:}VIIa{:}X] - k_{-,8}[TF{:}VIIa{:}Xa] + k_{+,8}[TF{:}VIIa][Xa] + k_{-,24}[TF{:}VIIa{:}Xa{:}TFPI] - k_{+,24}[TF{:}VIIa{:}Xa][TFPI]$$

$$\frac{d[IX]}{dt} = k_{-,9}[TF{:}VIIa{:}IX] - k_{+,9}[TF{:}VIIa][IX]$$

$$\frac{d[TF{:}VIIa{:}IX]}{dt} = -k_{-,9}[TF{:}VIIa{:}IX] + k_{+,9}[TF{:}VIIa][IX] - k_{-,10}[TF{:}VIIa{:}IX]$$

$$\frac{d[IXa]}{dt} = k_{-,10}[TF{:}VIIa{:}IX] + k_{-,13}[IXa{:}VIIIa] - k_{+,13}[IXa][VIIIa] + k_{-,17}[IXa{:}VIIIa{:}X] + k_{-,17}[IXa{:}VIIIa] - k_{+,28}[IXa][AT]$$

$$\frac{d[II]}{dt} = -k_{+,11}[II][Xa] + k_{-,20}[Xa{:}Va{:}II] - k_{+,20}[Xa{:}Va][II]$$

$$\frac{d[VIII]}{dt} = -k_{+,12}[VIII][IIa]$$

$$\frac{d[VIIIa]}{dt} = k_{+,12}[VIII][IIa] + k_{-,13}[IXa{:}VIIIa] - k_{+,13}[IXa][VIIIa] + k_{+,16}[VIIIa1L][VIIIa2] - k_{-,16}[VIIIa]$$

$$\frac{d[IXa{:}VIIIa]}{dt} = -k_{-,13}[IXa{:}VIIIa] + k_{+,13}[IXa][VIIIa] + k_{-,14}[IXa{:}VIIIa{:}X] - k_{+,14}[IXa{:}VIIIa][X] + k_{-,15}[IXa{:}VIIIa{:}X] - k_{-,17}[IXa{:}VIIIa]$$

$$\frac{d[IXa{:}VIIIa{:}X]}{dt} = -k_{-,14}[IXa{:}VIIIa{:}X] + k_{+,14}[IXa{:}VIIIa][X] - k_{-,15}[IXa{:}VIIIa{:}X] - k_{-,17}[IXa{:}VIIIa{:}X]$$

$$\frac{d[VIIIa1L]}{dt} = \frac{d[VIIIa2]}{dt} = -k_{+,16}[VIIIa1L][VIIIa2] + k_{-,16}[VIIIa] + k_{-,17}[IXa{:}VIIIa{:}X] + k_{-,17}[IXa{:}VIIIa]$$

$$\frac{d[V]}{dt} = -k_{+,18}[V][IIa]$$

$$\frac{d[Va]}{dt} = k_{+,18}[V][IIa] + k_{-,19}[Xa{:}Va] - k_{+,19}[Xa][Va]$$

$$\frac{d[Xa{:}Va]}{dt} = -k_{-,19}[Xa{:}Va] + k_{+,19}[Xa][Va] + k_{-,20}[Xa{:}Va{:}II] - k_{+,20}[Xa{:}Va][II] + k_{-,21}[Xa{:}Va{:}II]$$

$$\frac{d[Xa{:}Va{:}II]}{dt} = -k_{-,20}[Xa{:}Va{:}II] + k_{+,20}[Xa{:}Va][II] - k_{-,21}[Xa{:}Va{:}II]$$

$$\frac{d[mIIa]}{dt} = k_{-,21}[Xa{:}Va{:}II] - k_{+,22}[mIIa][Xa{:}Va] - k_{+,27}[mIIa][AT]$$

$$\frac{d[TFPI]}{dt} = k_{-,23}[Xa{:}TFPI] - k_{+,23}[Xa][TFPI] + k_{-,24}[TF{:}VIIa{:}Xa{:}TFPI] - k_{+,24}[TF{:}VIIa{:}Xa][TFPI]$$

$$\frac{d[Xa{:}TFPI]}{dt} = -k_{-,23}[Xa{:}TFPI] + k_{+,23}[Xa][TFPI] - k_{+,25}[TF{:}VIIa][Xa{:}TFPI]$$

$$\frac{d[TF{:}VIIa{:}Xa{:}TFPI]}{dt} = -k_{-,24}[TF{:}VIIa{:}Xa{:}TFPI] + k_{+,24}[TF{:}VIIa{:}Xa][TFPI] + k_{+,25}[TF{:}VIIa][Xa{:}TFPI]$$

$$\frac{d[AT]}{dt} = -k_{+,26}[Xa][AT] - k_{+,27}[mIIa][AT] - k_{+,28}[IXa][AT] - k_{+,29}[IIa][AT] - k_{+,30}[TF{:}VIIa][AT]$$

A.1.2 Danforth Model

$$\frac{d[Xa]}{dt} = k_{-,8}[TF{:}VIIa{:}Xa] - k_{+,8}[TF{:}VIIa][Xa] + k_{-,15}[IXa{:}VIIIa{:}X] + k_{-,23}[Xa{:}TFPI] - k_{+,23}[Xa][TFPI] - k_{+,26}[Xa][AT] + k_{+,31}[X][IXa] + k_{-,19}[Xa{:}Va] - k_{+,19}[Xa][Va]$$

$$\frac{d[X]}{dt} = k_{-,6}[TF{:}VIIa{:}X] - k_{+,6}[TF{:}VIIa][X] + k_{-,14}[IXa{:}VIIIa{:}X] - k_{+,14}[IXa{:}VIIIa][X] + k_{-,17}[IXa{:}VIIIa{:}X] - k_{+,31}[X][IXa]$$

$$\frac{d[V]}{dt} = -k_{+,18}[V][IIa] - k_{+,32}[V][mIIa]$$

$$\frac{d[Va]}{dt} = k_{+,18}[V][IIa] + k_{-,19}[Xa{:}Va] - k_{+,19}[Xa][Va] + k_{+,32}[V][mIIa]$$

A.1.3 Brummel Model

$$\frac{d[TF]}{dt} = k_1[TF{:}VII] - k_2[TF][VII] + k_3[TF{:}VIIa] - k_4[TF][VIIa]$$

$$\frac{d[VII]}{dt} = k_1[TF{:}VII] - k_2[TF][VII] - k_5[VII][TF{:}VIIa] - k_6[VII][Xa] - k_7[VII][IIa]$$

$$\frac{d[TF{:}VII]}{dt} = -k_1[TF{:}VII] + k_2[TF][VII]$$

$$\frac{d[VIIa]}{dt} = k_3[TF{:}VIIa] - k_4[TF][VIIa] + k_5[VII][TF{:}VIIa] + k_6[VII][Xa] + k_7[VII][IIa]$$

$$\frac{d[TF{:}VIIa]}{dt} = -k_3[TF{:}VIIa] + k_4[TF][VIIa] + k_8[TF{:}VIIa{:}X] - k_9[TF{:}VIIa][X] + k_{11}[TF{:}VIIa{:}Xa] - k_{12}[TF{:}VIIa][Xa] + k_{13}[TF{:}VIIa{:}IX] - k_{14}[TF{:}VIIa][IX] + k_{15}[TF{:}VIIa{:}IX] - k_{37}[TF{:}VIIa][Xa{:}TFPI] - k_{42}[TF{:}VIIa][AT]$$

$$\frac{d[Xa]}{dt} = k_{11}[TF{:}VIIa{:}Xa] - k_{12}[TF{:}VIIa][Xa] + k_{22}[IXa{:}VIIIa{:}X] + k_{27}[Xa{:}Va] - k_{28}[Xa][Va] + k_{33}[Xa{:}TFPI] - k_{34}[Xa][TFPI] - k_{38}[Xa][AT] + k_{54}[Xa{:}Va5] - k_{28}[Xa][Va5] + k_{54}[Xa{:}Va3] - k_{28}[Xa][Va3] + k_{59}[Xa{:}Va3] + k_{59}[Xa{:}Va3{:}II] + k_{60}[X][IXa] + k_{54}[Xa{:}Va53] - k_{28}[Xa][Va53] + k_{59}[Xa{:}Va53] + k_{59}[Xa{:}Va53{:}II]$$

$$\frac{d[IIa]}{dt} = k_{16}[II][Xa] + k_{32}[mIIa][Xa{:}Va] - k_{41}[IIa][AT] + k_{43}[TM{:}IIa] - k_{44}[TM][IIa] + k_{57}[mIIa][Xa{:}Va5] + k_{58}[mIIa][Xa{:}Va3] + k_{58}[mIIa][Xa{:}Va53]$$

$$\frac{d[X]}{dt} = k_8[TF{:}VIIa{:}X] - k_9[TF{:}VIIa][X] + k_{20}[IXa{:}VIIIa{:}X] - k_{21}[IXa{:}VIIIa][X] + k_{25}[IXa{:}VIIIa{:}X] - k_{60}[X][IXa]$$

$$\frac{d[TF{:}VIIa{:}X]}{dt} = -k_8[TF{:}VIIa{:}X] + k_9[TF{:}VIIa][X] - k_{10}[TF{:}VIIa{:}X]$$

$$\frac{d[TF{:}VIIa{:}Xa]}{dt} = k_{10}[TF{:}VIIa{:}X] - k_{11}[TF{:}VIIa{:}Xa] + k_{12}[TF{:}VIIa][Xa] + k_{35}[TF{:}VIIa{:}Xa{:}TFPI] - k_{36}[TF{:}VIIa{:}Xa][TFPI]$$

$$\frac{d[IX]}{dt} = k_{13}[TF{:}VIIa{:}IX] - k_{14}[TF{:}VIIa][IX]$$

$$\frac{d[TF{:}VIIa{:}IX]}{dt} = -k_{13}[TF{:}VIIa{:}IX] + k_{14}[TF{:}VIIa][IX] - k_{15}[TF{:}VIIa{:}IX]$$

$$\frac{d[IXa]}{dt} = k_{15}[TF{:}VIIa{:}IX] + k_{18}[IXa{:}VIIIa] - k_{19}[IXa][VIIIa] + k_{25}[IXa{:}VIIIa{:}X] + k_{25}[IXa{:}VIIIa] - k_{40}[IXa][AT]$$

$$\frac{d[II]}{dt} = -k_{16}[II][Xa] + k_{29}[Xa{:}Va{:}II] - k_{30}[Xa{:}Va][II] + k_{29}[Xa{:}Va5{:}II] - k_{30}[Xa{:}Va5][II] + k_{29}[Xa{:}Va3{:}II] - k_{30}[Xa{:}Va3][II] + k_{59}[Xa{:}Va3{:}II] + k_{29}[Xa{:}Va53{:}II] - k_{30}[II][Xa{:}Va53] + k_{59}[Xa{:}Va53{:}II] + k_{62}[II{:}Va] - k_{63}[II][Va]$$

$$\frac{d[VIII]}{dt} = -k_{17}[VIII][IIa]$$

$$\frac{d[VIIIa]}{dt} = k_{17}[VIII][IIa] + k_{18}[IXa{:}VIIIa] - k_{19}[IXa][VIIIa] + k_{23}[VIIIa1L][VIIIa2] - k_{24}[VIIIa]$$

$$\frac{d[IXa{:}VIIIa]}{dt} = -k_{18}[IXa{:}VIIIa] + k_{19}[IXa][VIIIa] + k_{20}[IXa{:}VIIIa{:}X] - k_{21}[IXa{:}VIIIa][X] + k_{22}[IXa{:}VIIIa{:}X] - k_{25}[IXa{:}VIIIa]$$

$$\frac{d[IXa{:}VIIIa{:}X]}{dt} = -k_{20}[IXa{:}VIIIa{:}X] + k_{21}[IXa{:}VIIIa][X] - k_{22}[IXa{:}VIIIa{:}X] - k_{25}[IXa{:}VIIIa{:}X]$$

$$\frac{d[VIIIa1L]}{dt} = \frac{d[VIIIa2]}{dt} = -k_{23}[VIIIa1L][VIIIa2] + k_{24}[VIIIa] + k_{25}[IXa{:}VIIIa{:}X] + k_{25}[IXa{:}VIIIa]$$

$$\frac{d[V]}{dt} = -k_{26}[V][IIa] - k_{61}[V][mIIa]$$

$$\frac{d[Va]}{dt} = k_{26}[V][IIa] + k_{27}[Xa{:}Va] - k_{28}[Xa][Va] + k_{49}[APC{:}Va] - k_{50}[APC][Va] + k_{61}[V][mIIa] + k_{62}[II{:}Va] - k_{63}[II][Va]$$

$$\frac{d[Xa{:}Va]}{dt} = -k_{27}[Xa{:}Va] + k_{28}[Xa][Va] + k_{29}[Xa{:}Va{:}II] - k_{30}[Xa{:}Va][II] + k_{31}[Xa{:}Va{:}II]$$

$$\frac{d[Xa{:}Va{:}II]}{dt} = -k_{29}[Xa{:}Va{:}II] + k_{30}[Xa{:}Va][II] - k_{31}[Xa{:}Va{:}II]$$

$$\frac{d[mIIa]}{dt} = k_{31}[Xa{:}Va{:}II] - k_{32}[mIIa][Xa{:}Va] - k_{39}[mIIa][AT] + k_{55}[Xa{:}Va5{:}II] + k_{56}[Xa{:}Va3{:}II] - k_{57}[mIIa][Xa{:}Va5] - k_{58}[mIIa][Xa{:}Va3] + k_{43}[TM{:}mIIa] - k_{44}[TM][mIIa] + k_{56}[Xa{:}Va53{:}II] - k_{58}[mIIa][Xa{:}Va53]$$

$$\frac{d[TFPI]}{dt} = k_{33}[Xa{:}TFPI] - k_{34}[Xa][TFPI] + k_{35}[TF{:}VIIa{:}Xa{:}TFPI] - k_{36}[TF{:}VIIa{:}Xa][TFPI]$$

$$\frac{d[Xa{:}TFPI]}{dt} = -k_{33}[Xa{:}TFPI] + k_{34}[Xa][TFPI] - k_{37}[TF{:}VIIa][Xa{:}TFPI]$$

$$\frac{d[TF{:}VIIa{:}Xa{:}TFPI]}{dt} = -k_{35}[TF{:}VIIa{:}Xa{:}TFPI] + k_{36}[TF{:}VIIa{:}Xa][TFPI] + k_{37}[TF{:}VIIa][Xa{:}TFPI]$$

$$\frac{d[AT]}{dt} = -k_{38}[Xa][AT] - k_{39}[mIIa][AT] - k_{40}[IXa][AT] - k_{41}[IIa][AT] - k_{42}[TF{:}VIIa][AT] - k_{48}[TM{:}IIa][AT] - k_{48}[TM{:}mIIa][AT]$$

$$\frac{d[TM]}{dt} = k_{43}[TM{:}IIa] - k_{44}[TM][IIa] + k_{48}[TM{:}IIa][AT] + k_{43}[TM{:}mIIa] - k_{44}[TM][mIIa] + k_{48}[TM{:}mIIa][AT]$$

$$\frac{d[TM{:}IIa]}{dt} = -k_{43}[TM{:}IIa] + k_{44}[TM][IIa] + k_{45}[TM{:}IIa{:}PC] - k_{46}[PC][TM{:}IIa] + k_{47}[TM{:}IIa{:}PC] - k_{48}[TM{:}IIa][AT] + k_{45}[TM{:}IIa{:}APC] - k_{46}[APC][TM{:}IIa]$$

$$\frac{d[PC]}{dt} = k_{45}[TM{:}IIa{:}PC] - k_{46}[PC][TM{:}IIa] + k_{45}[TM{:}mIIa{:}PC] - k_{46}[TM{:}mIIa][PC]$$

$$\frac{d[TM{:}IIa{:}PC]}{dt} = -k_{45}[TM{:}IIa{:}PC] + k_{46}[PC][TM{:}IIa] - k_{47}[TM{:}IIa{:}PC]$$

$$\frac{d[APC]}{dt} = k_{47}[TM{:}IIa{:}PC] + k_{49}[APC{:}Va] - k_{50}[APC][Va] + k_{51}[APC{:}Va] + k_{52}[APC{:}Va] + k_{49}[APC{:}Va5] - k_{50}[APC][Va5] + k_{49}[APC{:}Va3] - k_{50}[APC][Va3] + k_{51}[APC{:}Va3] + k_{52}[APC{:}Va5] + k_{49}[APC{:}LCA1] - k_{50}[APC][LCA1] + k_{45}[TM{:}IIa{:}APC] - k_{46}[APC][TM{:}IIa] + k_{47}[TM{:}mIIa{:}PC]$$

$$\frac{d[APC{:}Va]}{dt} = k_{49}[APC{:}Va] - k_{50}[APC][Va] - k_{51}[APC{:}Va] - k_{52}[APC{:}Va]$$

$$\frac{d[Va5]}{dt} = k_{51}[APC{:}Va] + k_{49}[APC{:}Va5] - k_{50}[APC][Va5] + k_{54}[Xa{:}Va5] - k_{28}[Xa][Va5]$$

$$\frac{d[Va3]}{dt} = k_{52}[APC{:}Va] + k_{49}[APC{:}Va3] - k_{50}[APC][Va3] - k_{53}[Va3] + k_{54}[Xa{:}Va3] - k_{28}[Xa][Va3]$$

$$\frac{d[APC{:}Va5]}{dt} = -k_{49}[APC{:}Va5] + k_{50}[APC][Va5] - k_{52}[APC{:}Va5]$$

$$\frac{d[APC{:}Va3]}{dt} = -k_{49}[APC{:}Va3] + k_{50}[APC][Va3] - k_{51}[APC{:}Va3]$$

$$\frac{d[Va53]}{dt} = k_{51}[APC{:}Va3] + k_{52}[APC{:}Va5] - k_{53}[Va53] + k_{54}[Xa{:}Va53] - k_{28}[Xa][Va53]$$

$$\frac{d[HCF]}{dt} = k_{53}[Va3] + k_{53}[Va53] + k_{59}[Xa{:}Va3] + k_{59}[Xa{:}Va3{:}II] + k_{59}[Xa{:}Va53] + k_{59}[Xa{:}Va53{:}II]$$

$$\frac{d[LCA1]}{dt} = k_{53}[Va3] + k_{53}[Va53] + k_{49}[APC{:}LCA1] - k_{50}[APC][LCA1] + k_{59}[Xa{:}Va3] + k_{59}[Xa{:}Va3{:}II] + k_{59}[Xa{:}Va53] + k_{59}[Xa{:}Va53{:}II]$$

$$\frac{d[APC{:}LCA1]}{dt} = -k_{49}[APC{:}LCA1] + k_{50}[APC][LCA1]$$

$$\frac{d[TM{:}IIa{:}APC]}{dt} = -k_{45}[TM{:}IIa{:}APC] + k_{46}[APC][TM{:}IIa]$$

$$\frac{d[Xa{:}Va5]}{dt} = -k_{54}[Xa{:}Va5] + k_{28}[Xa][Va5] + k_{29}[Xa{:}Va5{:}II] - k_{30}[Xa{:}Va5][II] + k_{55}[Xa{:}Va5{:}II] - k_{64}[Xa{:}Va5][APC]$$

$$\frac{d[Xa{:}Va3]}{dt} = -k_{54}[Xa{:}Va3] + k_{28}[Xa][Va3] + k_{29}[Xa{:}Va3{:}II] - k_{30}[Xa{:}Va3][II] + k_{56}[Xa{:}Va3{:}II] - k_{59}[Xa{:}Va3]$$

$$\frac{d[Xa{:}Va5{:}II]}{dt} = -k_{29}[Xa{:}Va5{:}II] + k_{30}[Xa{:}Va5][II] - k_{55}[Xa{:}Va5{:}II]$$

$$\frac{d[Xa{:}Va3{:}II]}{dt} = -k_{29}[Xa{:}Va3{:}II] + k_{30}[Xa{:}Va3][II] - k_{56}[Xa{:}Va3{:}II] - k_{59}[Xa{:}Va3{:}II]$$

$$\frac{d[TM{:}mIIa]}{dt} = -k_{43}[TM{:}mIIa] + k_{44}[TM][mIIa] + k_{45}[TM{:}mIIa{:}PC] - k_{46}[TM{:}mIIa][PC] + k_{47}[TM{:}mIIa{:}PC] - k_{48}[TM{:}mIIa][AT]$$

$$\frac{d[TM{:}mIIa{:}PC]}{dt} = -k_{45}[TM{:}mIIa{:}PC] + k_{46}[TM{:}mIIa][PC] - k_{47}[TM{:}mIIa{:}PC]$$

$$\frac{d[Xa{:}Va53]}{dt} = -k_{54}[Xa{:}Va53] + k_{28}[Xa][Va53] + k_{29}[Xa{:}Va53{:}II] - k_{30}[II][Xa{:}Va53] + k_{56}[Xa{:}Va53{:}II] - k_{59}[Xa{:}Va53] + k_{64}[Xa{:}Va5][APC]$$

$$\frac{d[Xa{:}Va53{:}II]}{dt} = -k_{29}[Xa{:}Va53{:}II] + k_{30}[II][Xa{:}Va53] - k_{56}[Xa{:}Va53{:}II] - k_{59}[Xa{:}Va53{:}II]$$

$$\frac{d[II{:}Va]}{dt} = -k_{62}[II{:}Va] + k_{63}[II][Va]$$

A.1.4 Chatterjee Model

$$\frac{d[TF]}{dt} = k_{-,1}[TF{:}VII] - k_{+,1}[TF][VII] + k_{-,2}[TF{:}VIIa] - k_{+,2}[TF][VIIa]$$

$$\frac{d[VII]}{dt} = k_{-,1}[TF{:}VII] - k_{+,1}[TF][VII] - k_{+,3}[VII][TF{:}VIIa] - k_{+,4}[VII][Xa] - k_{+,5}[VII][IIa]$$

$$\frac{d[TF{:}VII]}{dt} = -k_{-,1}[TF{:}VII] + k_{+,1}[TF][VII]$$

$$\frac{d[VIIa]}{dt} = k_{-,2}[TF{:}VIIa] - k_{+,2}[TF][VIIa] + k_{+,3}[VII][TF{:}VIIa] + k_{+,4}[VII][Xa] + k_{+,5}[VII][IIa] - k_{+,60}[VIIa][IX] + k_{-,60}[VIIa{:}IX] + k_{-,61}[VIIa{:}IX] - k_{+,62}[VIIa][X] + k_{-,62}[VIIa{:}X]/\epsilon + k_{-,63}[VIIa{:}X]$$

$$\frac{d[TF{:}VIIa]}{dt} = -k_{-,2}[TF{:}VIIa] + k_{+,2}[TF][VIIa] + k_{-,6}[TF{:}VIIa{:}X] - k_{+,6}[TF{:}VIIa][X] + k_{-,8}[TF{:}VIIa{:}Xa] - k_{+,8}[TF{:}VIIa][Xa] + k_{-,9}[TF{:}VIIa{:}IX] - k_{+,9}[TF{:}VIIa][IX] + k_{-,10}[TF{:}VIIa{:}IX] - k_{+,25}[TF{:}VIIa][Xa{:}TFPI] - k_{+,30}[TF{:}VIIa][AT]$$

$$\frac{d[Xa]}{dt} = k_{-,8}[TF{:}VIIa{:}Xa] - k_{+,8}[TF{:}VIIa][Xa] + k_{-,15}[IXa{:}VIIIa{:}X] + k_{-,19}[Xa{:}Va]/\epsilon - k_{+,19}[Xa][Va] + k_{-,23}[Xa{:}TFPI]/\epsilon - k_{+,23}[Xa][TFPI] - k_{+,26}[Xa][AT] + k_{-,57}[IXa{:}X] - k_{+,58}[Xa][VIII] + k_{-,58}[Xa{:}VIII]/\epsilon + k_{-,59}[Xa{:}VIII]] + k_{-,63}[VIIa{:}X]$$

$$\frac{d[IIa]}{dt} = k_{+,11}[II][Xa] + k_{+,22}[mIIa][Xa{:}Va] - k_{+,29}[IIa][AT] - k_{+,31}[Boc{-}VPR{-}MCA][IIa] + k_{-,31}[Boc{-}VPR{-}MCA{:}IIa] + k_{-,32}[Boc{-}VPR{-}MCA{:}IIa] - k_{+,45}[XI][IIa] + k_{-,45}[XI{:}IIa] + k_{-,46}[XI{:}IIa] - k_{+,64}[Fbg][IIa] + k_{-,64}[Fbg{:}IIa] + k_{-,65}[Fbg{:}IIa] - k_{+,66}[Fbn1][IIa] + k_{-,66}[Fbn1{:}IIa] + k_{-,67}[Fbn1{:}IIa] - k_{+,69}[Fbn12][IIa] + k_{-,69}[Fbn12{:}IIa] + k_{-,70}[Fbn12{:}IIa] - k_{+,71}[Fbn2][IIa] + k_{-,71}[Fbn2{:}IIa]$$

$$\frac{d[X]}{dt} = k_{-,6}[TF{:}VIIa{:}X] - k_{+,6}[TF{:}VIIa][X] + k_{-,14}[IXa{:}VIIIa{:}X]/\epsilon - k_{+,14}[IXa{:}VIIIa][X] + k_{-,17}[IXa{:}VIIIa{:}X] - k_{+,56}[IXa][X] + k_{-,56}[IXa{:}X]/\epsilon - k_{+,62}[VIIa][X] + k_{-,62}[VIIa{:}X]/\epsilon$$

$$\frac{d[TF{:}VIIa{:}X]}{dt} = -k_{-,6}[TF{:}VIIa{:}X] + k_{+,6}[TF{:}VIIa][X] - k_{-,7}[TF{:}VIIa{:}X]$$

$$\frac{d[TF{:}VIIa{:}Xa]}{dt} = k_{-,7}[TF{:}VIIa{:}X] - k_{-,8}[TF{:}VIIa{:}Xa] + k_{+,8}[TF{:}VIIa][Xa] + k_{-,24}[TF{:}VIIa{:}Xa{:}TFPI] - k_{+,24}[TF{:}VIIa{:}Xa][TFPI]$$

$$\frac{d[IX]}{dt} = k_{-,9}[TF{:}VIIa{:}IX] - k_{+,9}[TF{:}VIIa][IX] - k_{+,54}[XIa][IX] + k_{-,54}[XIa{:}IX]/\epsilon - k_{+,60}[VIIa][IX] + k_{-,60}[VIIa{:}IX]$$

$$\frac{d[TF{:}VIIa{:}IX]}{dt} = -k_{-,9}[TF{:}VIIa{:}IX] + k_{+,9}[TF{:}VIIa][IX] - k_{-,10}[TF{:}VIIa{:}IX]$$

$$\frac{d[IXa]}{dt} = k_{-,10}[TF{:}VIIa{:}IX] + k_{-,13}[IXa{:}VIIIa]/\epsilon - k_{+,13}[IXa][VIIIa] + k_{-,17}[IXa{:}VIIIa{:}X] + k_{-,17}[IXa{:}VIIIa] - k_{+,28}[IXa][AT] + k_{-,55}[XIa{:}IX] - k_{+,56}[IXa][X] + k_{-,56}[IXa{:}X]/\epsilon + k_{-,57}[IXa{:}X] + k_{-,61}[VIIa{:}IX]$$

$$\frac{d[II]}{dt} = -k_{+,11}[II][Xa] + k_{-,20}[Xa{:}Va{:}II]/\epsilon - k_{+,20}[Xa{:}Va][II]$$

$$\frac{d[VIII]}{dt} = -k_{+,12}[VIII][IIa] - k_{+,58}[Xa][VIII] + k_{-,58}[Xa{:}VIII]/\epsilon$$

$$\frac{d[VIIIa]}{dt} = k_{+,12}[VIII][IIa] + k_{-,13}[IXa{:}VIIIa]/\epsilon - k_{+,13}[IXa][VIIIa] + k_{+,16}[VIIIa1L][VIIIa2] - k_{-,16}[VIIIa]/\epsilon + k_{-,59}[Xa{:}VIII]$$

$$\frac{d[IXa{:}VIIIa]}{dt} = -k_{-,13}[IXa{:}VIIIa]/\epsilon + k_{+,13}[IXa][VIIIa] + k_{-,14}[IXa{:}VIIIa{:}X]/\epsilon - k_{+,14}[IXa{:}VIIIa][X] + k_{-,15}[IXa{:}VIIIa{:}X] - k_{-,17}[IXa{:}VIIIa]$$

$$\frac{d[IXa{:}VIIIa{:}X]}{dt} = -k_{-,14}[IXa{:}VIIIa{:}X]/\epsilon + k_{+,14}[IXa{:}VIIIa][X] - k_{-,15}[IXa{:}VIIIa{:}X] - k_{-,17}[IXa{:}VIIIa{:}X]$$

$$\frac{d[VIIIa1L]}{dt} = \frac{d[VIIIa2]}{dt} = -k_{+,16}[VIIIa1L][VIIIa2] + k_{-,16}[VIIIa]/\epsilon + k_{-,17}[IXa{:}VIIIa{:}X] + k_{-,17}[IXa{:}VIIIa]$$

$$\frac{d[V]}{dt} = -k_{+,18}[V][IIa]$$

$$\frac{d[Va]}{dt} = k_{+,18}[V][IIa] + k_{-,19}[Xa{:}Va]/\epsilon - k_{+,19}[Xa][Va]$$

$$\frac{d[Xa{:}Va]}{dt} = -k_{-,19}[Xa{:}Va]/\epsilon + k_{+,19}[Xa][Va] + k_{-,20}[Xa{:}Va{:}II]/\epsilon - k_{+,20}[Xa{:}Va][II] + k_{-,21}[Xa{:}Va{:}II]$$

$$\frac{d[Xa{:}Va{:}II]}{dt} = -k_{-,20}[Xa{:}Va{:}II]/\epsilon + k_{+,20}[Xa{:}Va][II] - k_{-,21}[Xa{:}Va{:}II]$$

$$\frac{d[mIIa]}{dt} = k_{-,21}[Xa{:}Va{:}II] - k_{+,22}[mIIa][Xa{:}Va] - k_{+,27}[mIIa][AT]$$

$$\frac{d[TFPI]}{dt} = k_{-,23}[Xa{:}TFPI]/\epsilon - k_{+,23}[Xa][TFPI] + k_{-,24}[TF{:}VIIa{:}Xa{:}TFPI] - k_{+,24}[TF{:}VIIa{:}Xa][TFPI]$$

$$\frac{d[Xa{:}TFPI]}{dt} = -k_{-,23}[Xa{:}TFPI]/\epsilon + k_{+,23}[Xa][TFPI] - k_{+,25}[TF{:}VIIa][Xa{:}TFPI]$$

$$\frac{d[TF{:}VIIa{:}Xa{:}TFPI]}{dt} = -k_{-,24}[TF{:}VIIa{:}Xa{:}TFPI] + k_{+,24}[TF{:}VIIa{:}Xa][TFPI] + k_{+,25}[TF{:}VIIa][Xa{:}TFPI]$$

$$\frac{d[AT]}{dt} = -k_{+,26}[Xa][AT] - k_{+,27}[mIIa][AT] - k_{+,28}[IXa][AT] - k_{+,29}[IIa][AT] - k_{+,30}[TF{:}VIIa][AT] - k_{+,44}[XIIa][AT] - k_{+,50}[XIa][AT] - k_{+,72}[Fbn12{:}IIa][AT] - k_{+,73}[Fbn1{:}IIa][AT] - k_{+,74}[Fbn2{:}IIa][AT]$$

$$\frac{d[Boc{-}VPR{-}MCA]}{dt} = -k_{+,31}[Boc{-}VPR{-}MCA][IIa] + k_{-,31}[Boc{-}VPR{-}MCA{:}IIa]$$

$$\frac{d[Boc{-}VPR{-}MCA{:}IIa]}{dt} = k_{+,31}[Boc{-}VPR{-}MCA][IIa] - k_{-,31}[Boc{-}VPR{-}MCA{:}IIa] - k_{-,32}[Boc{-}VPR{-}MCA{:}IIa]$$

$$\frac{d[Boc{-}VPR]}{dt} = k_{-,32}[Boc{-}VPR{-}MCA{:}IIa]$$

$$\frac{d[AMC]}{dt} = k_{-,32}[Boc{-}VPR{-}MCA{:}IIa]$$

$$\frac{d[XII]}{dt} = -k_{-,33}[XII] - k_{+,34}[XIIa][XII] + k_{-,34}[XIIa{:}XII]/\epsilon - k_{+,38}[XII][K] + k_{-,38}[XII{:}K]/\epsilon$$

$$\frac{d[XIIa]}{dt} = k_{-,33}[XII] - k_{+,34}[XIIa][XII] + k_{-,34}[XIIa{:}XII]/\epsilon + 2k_{-,35}[XIIa{:}XII] - k_{+,36}[XIIa][PK] + k_{-,36}[XIIa{:}PK]/\epsilon + k_{-,37}[XIIa{:}PK] + k_{-,39}[XII{:}K] - k_{+,42}[XIIa][CTI] + k_{-,42}[XIIa{:}CTI] - k_{-,43}[XIIa][C1{-}inh] - k_{+,44}[XIIa][AT] - k_{+,47}[XIIa][XI] + k_{-,47}[XIIa{:}XI]/\epsilon + k_{-,48}[XIIa{:}XI]$$

$$\frac{d[XIIa{:}XII]}{dt} = k_{+,34}[XIIa][XII] - k_{-,34}[XIIa{:}XII]/\epsilon - k_{-,35}[XIIa{:}XII]$$
$$\frac{d[PK]}{dt} = -k_{+,36}[XIIa][PK] + k_{-,36}[XIIa{:}PK]/\epsilon - k_{+,40}[PK][K]$$
$$\frac{d[XIIa{:}PK]}{dt} = k_{+,36}[XIIa][PK] - k_{-,36}[XIIa{:}PK]/\epsilon - k_{-,37}[XIIa{:}PK]$$
$$\frac{d[K]}{dt} = k_{-,37}[XIIa{:}PK] - k_{+,38}[XII][K] + k_{-,38}[XII{:}K]/\epsilon + k_{-,39}[XII{:}K] + k_{+,40}[PK][K] - k_{-,41}[K]$$
$$\frac{d[XII{:}K]}{dt} = k_{+,38}[XII][K] - k_{-,38}[XII{:}K]/\epsilon - k_{-,39}[XII{:}K]$$
$$\frac{d[CTI]}{dt} = -k_{+,42}[XIIa][CTI] + k_{-,42}[XIIa{:}CTI]$$
$$\frac{d[C1{-}inh]}{dt} = -k_{-,43}[XIIa][C1{-}inh] - k_{+,51}[XIa][C1{-}inh]$$
$$\frac{d[XI]}{dt} = -k_{+,45}[XI][IIa] + k_{-,45}[XI{:}IIa] - k_{+,47}[XIIa][XI] + k_{-,47}[XIIa{:}XI]/\epsilon - k_{+,49}[XIa][XI]$$
$$\frac{d[XI{:}IIa]}{dt} = k_{+,45}[XI][IIa] - k_{-,45}[XI{:}IIa] - k_{-,46}[XI{:}IIa]$$
$$\frac{d[XIa]}{dt} = k_{-,46}[XI{:}IIa] + k_{-,48}[XIIa{:}XI] + k_{+,49}[XIa][XI] - k_{+,50}[XIa][AT] - k_{+,51}[XIa][C1{-}inh] - k_{+,52}[XIa][\alpha_1{-}AT] - k_{+,53}[XIa][\alpha_2{-}AP] - k_{+,54}[XIa][IX] + k_{-,54}[XIa{:}IX]/\epsilon + k_{-,55}[XIa{:}IX]$$
$$\frac{d[XIIa{:}XI]}{dt} = k_{+,47}[XIIa][XI] - k_{-,47}[XIIa{:}XI]/\epsilon - k_{-,48}[XIIa{:}XI]$$
$$\frac{d[\alpha_1{-}AT]}{dt} = -k_{+,52}[XIa][\alpha_1{-}AT]$$
$$\frac{d[\alpha_2{-}AP]}{dt} = -k_{+,53}[XIa][\alpha_2{-}AP]$$
$$\frac{d[XIa{:}IX]}{dt} = k_{+,54}[XIa][IX] - k_{-,54}[XIa{:}IX]/\epsilon - k_{-,55}[XIa{:}IX]$$
$$\frac{d[IXa{:}X]}{dt} = k_{+,56}[IXa][X] - k_{-,56}[IXa{:}X]/\epsilon - k_{-,57}[IXa{:}X]$$
$$\frac{d[Xa{:}VIII]}{dt} = k_{+,58}[Xa][VIII] - k_{-,58}[Xa{:}VIII]/\epsilon - k_{-,59}[Xa{:}VIII]$$
$$\frac{d[VIIa{:}IX]}{dt} = k_{+,60}[VIIa][IX] - k_{-,60}[VIIa{:}IX] - k_{-,61}[VIIa{:}IX]$$
$$\frac{d[VIIa{:}X]}{dt} = k_{+,62}[VIIa][X] - k_{-,62}[VIIa{:}X]/\epsilon - k_{-,63}[VIIa{:}X]$$
$$\frac{d[Fbg]}{dt} = -k_{+,64}[Fbg][IIa] + k_{-,64}[Fbg{:}IIa]$$
$$\frac{d[Fbg{:}IIa]}{dt} = k_{+,64}[Fbg][IIa] - k_{-,64}[Fbg{:}IIa] - k_{-,65}[Fbg{:}IIa]$$
$$\frac{d[Fbn1]}{dt} = k_{-,65}[Fbg{:}IIa] - k_{+,66}[Fbn1][IIa] + k_{-,66}[Fbn1{:}IIa] - k_{+,68}[Fbn1]^2 + k_{-,68}[Fbn12]$$
$$\frac{d[FPA]}{dt} = k_{-,65}[Fbg{:}IIa]$$
$$\frac{d[Fbn2]}{dt} = k_{-,67}[Fbn1{:}IIa] - k_{+,71}[Fbn2][IIa] + k_{-,71}[Fbn2{:}IIa]$$
$$\frac{d[Fbn12]}{dt} = k_{+,68}[Fbn1]^2 - k_{-,68}[Fbn12] - k_{+,69}[Fbn12][IIa] + k_{-,69}[Fbn12{:}IIa]$$
$$\frac{d[Fbn22]}{dt} = k_{-,70}[Fbn12{:}IIa]$$

$$\frac{d[FPB]}{dt} = k_{-,67}[Fbn1{:}IIa] + k_{-,70}[Fbn12{:}IIa]$$
$$\frac{d[Fbn2{:}IIa]}{dt} = k_{+,71}[Fbn2][IIa] - k_{-,71}[Fbn2{:}IIa] - k_{+,74}[Fbn2{:}IIa][AT]$$
$$\frac{d[Fbn12{:}IIa]}{dt} = k_{+,69}[Fbn12][IIa] - k_{-,69}[Fbn12{:}IIa] - k_{-,70}[Fbn12{:}IIa] - k_{+,72}[Fbn12{:}IIa][AT]$$
$$\frac{d[Fbn1{:}IIa]}{dt} = k_{+,66}[Fbn1][IIa] - k_{-,66}[Fbn1{:}IIa] - k_{-,67}[Fbn1{:}IIa] - k_{+,73}[Fbn1{:}IIa][AT]$$

A.1.5 Panteleev Model

$$[IXaBF] = [IXa]pn_1/(K_{11} + [IXa])$$
$$[TF{:}VIIaF] = [TF{:}VIIa]/(1 + [IX]/K_1 + [X]/K_3)$$
$$[TF{:}VIIa{:}Xa] = k_6/(K_3k_{-3})[X][TF{:}VIIaF]$$
$$[VaB] = [Va]pn_4/(K_{18} + [Va])$$
$$[Xa{:}VaB] = [Xa][VaB]/(K_{14}(1 + [PS]/K_{15} + [Xa]/K_{14}) + [VaB])$$
$$[VaBF] = [VaB] - [Xa{:}VaB]$$
$$[XaF] = [Xa] - [Xa{:}VaB]$$
$$[IIB] = [II]pn_3/(K_{17}(1 + [X]/K_{16} + [II]/K_{17}))$$
$$[IIaF] = [IIa]/(1 + ([Ia] + [I])/K_8)$$
$$[XB] = [X]pn_3/(K_{16}(1 + [X]/K_{16} + [II]/K_{17}))$$
$$[VIIIaBF] = [VIIIa]pn_2/((K_{12} + [VIIIa])(1 + [XB]/(pK_7)(1 + [PS]/K_{13})))$$
$$\frac{d[TF{:}VIIa]}{dt} = k_1[VIIa][TF] - k_{-1}[TF{:}VIIaF] + k_2[TF : VII][IIaF] + k_3[TF : VII][XaF] - h_1[TF{:}VIIaF][Xa{:}TFPI] - h_2[TF{:}VIIa{:}Xa][TFPI]$$
$$\frac{d[TF{:}VII]}{dt} = k_1[VII][TF] - k_{-1}[TF : VII] - k_2[TF : VII][IIaF] - k_3[TF : VII][XaF]$$
$$\frac{d[TF]}{dt} = -k_1[VIIa][TF] + k_{-1}[TF{:}VIIaF] - k_1[VII][TF] + k_{-1}[TF : VII]$$
$$\frac{d[VIIa]}{dt} = -k_1[VIIa][TF] + k_{-1}[TF{:}VIIaF] + k_2[VII][IIaF]$$
$$\frac{d[VII]}{dt} = -k_1[VII][TF] + k_{-1}[TF : VII] - k_2[VII][IIaF]$$
$$\frac{d[IXa]}{dt} = k_4/K_1[IX][TF{:}VIIaF] + k_5[IX][XIa]/(K_2 + [IX]) - h_3[AT][IXa]$$
$$\frac{d[IX]}{dt} = -k_4/K_1[IX][TF{:}VIIaF] - k_5[IX][XIa]/(K_2 + [IX])$$
$$\frac{d[Xa]}{dt} = k_6/K_3[X][TF{:}VIIaF] + k_8[IXaBF][VIIIaBF][XB]/(p^2K_6K_5) + k_7[IXaBF][XB]/(pK_4) - k_9[XaF][TFPI] + k_{-2}[Xa{:}TFPI] - h_4[AT][XaF] - h_5[\alpha_2{-}M][XaF] - h_6[\alpha_1{-}AT][XaF] - h_7[PCI][XaF] - h_8[AT][Xa{:}VaB]$$
$$\frac{d[X]}{dt} = -k_6/K_3[X][TF{:}VIIaF] - k_7[IXaBF][XB]/(pK_4) - k_8[IXaBF][VIIIaBF][XB]/(p^2K_6K_5)$$
$$\frac{d[IIa]}{dt} = k_{10}p[XaF][II] + k_{11}[Xa{:}VaB][IIB]/p - h_9[AT][IIaF] - h_{10}[\alpha_2{-}M][IIaF] - h_{11}[\alpha_1{-}AT][IIaF] - h_{12}[PCI][IIaF] - h_{13}[hep][IIaF]$$
$$\frac{d[II]}{dt} = -k_{10}p[XaF][II] - k_{11}[Xa{:}VaB][IIB]/p$$
$$\frac{d[Ia]}{dt} = k_{12}/K_8[I][IIaF]$$

$$\frac{d[I]}{dt} = -k_{12}/K_8[I][IIaF]$$
$$\frac{d[VIIIa]}{dt} = k_{13}[VIII][IIaF]/(K_9 + [IIaF]) - h_{14}[VIIIa]$$
$$\frac{d[VIII]}{dt} = -k_{13}[VIII][IIaF]/(K_9 + [IIaF])$$
$$\frac{d[Va]}{dt} = k_{14}[V][IIaF]/(K_{10} + [IIaF]) - h_{15}[APC][VaBF]$$
$$\frac{d[V]}{dt} = -k_{14}[V][IIaF]/(K_{10} + [IIaF])$$
$$\frac{d[XIa]}{dt} = k_{15}p[XI][IIaF] - h_{16}[AT][XIa] - h_{17}[a1AP][XIa] - h_{18}[\alpha_1{-}AT][XIa] - h_{19}[PCI][XIa] - h_{20}[C1{-}inh][XIa]$$
$$\frac{d[XI]}{dt} = -k_{15}p[XI][IIaF]$$
$$\frac{d[AT]}{dt} = -h_3[IXa][AT] - h_4[XaF][AT] - h_8[Xa{:}VaB][AT] - h_9[IIaF][AT] - h_{16}[XIa][AT]$$
$$\frac{d[TFPI]}{dt} = -k_9[XaF][TFPI] + k_{-2}[Xa{:}TFPI] - h_2[TF{:}VIIa{:}Xa][TFPI]$$
$$\frac{d[Xa{:}TFPI]}{dt} = k_9[XaF][TFPI] - k_{-2}[Xa{:}TFPI] - h_1[TF{:}VIIaF][Xa{:}TFPI]$$
$$\frac{d[APC]}{dt} = k_{16}[PC][IIaF] - h_{21}[\alpha_2{-}M][APC] - h_{22}[a1AP][APC] - h_{23}[\alpha_1{-}AT][APC] - h_{24}[PCI][APC]$$
$$\frac{d[PC]}{dt} = -k_{16}[PC][IIaF]$$

A.1.6 Bungay Model

$$\frac{d[II_f]}{dt} = -k_{on_1}[II_f][LIPID]/n_{Va} + k_{off_1}[II_L]$$
$$\frac{d[II_L]}{dt} = k_{on_1}[II_f][LIPID]/n_{Va} - k_{off_1}[II_L] - k_{+,22}[Xa{:}Va_L][II_L] + k_{-,22}[Xa{:}Va{:}II_L]$$
$$\frac{d[mIIa_f]}{dt} = -k_{on_2}[mIIa_f][LIPID]/n_{Va} + k_{off_2}[mIIa_L] - k_{+,46}[mIIa_f][AT_f]$$
$$\frac{d[mIIa_L]}{dt} = k_{on_2}[mIIa_f][LIPID]/n_{Va} - k_{off_2}[mIIa_L] - k_{+,23}[Xa{:}Va_L][mIIa_L] + k_{-,23}[Xa{:}Va{:}mIIa_L] - k_{+,39}[V_L][mIIa_L] + k_{-,39}[V{:}mIIa_L] + k_{-,40}[V{:}mIIa_L] - k_{+,41}[VIII_L][mIIa_L] + k_{-,41}[VIII{:}mIIa_L] + k_{-,42}[VIII{:}mIIa_L]$$
$$\frac{d[V_f]}{dt} = -k_{on_3}[V_f][LIPID]/n_{Va} + k_{off_3}[V_L]$$
$$\frac{d[V_L]}{dt} = k_{on_3}[V_f][LIPID]/n_{Va} - k_{off_3}[V_L] - k_{+,14}[V_L][Xa_L] + k_{-,14}[V{:}Xa_L] - k_{+,18}[V_L][IIa_f] + k_{-,18}[V{:}IIa_L] - k_{+,39}[V_L][mIIa_L] + k_{-,39}[V{:}mIIa_L]$$
$$\frac{d[Va_f]}{dt} = -k_{on_4}[Va_f][LIPID]/n_{Va} + k_{off_4}[Va_L]$$
$$\frac{d[Va_L]}{dt} = k_{on_4}[Va_f][LIPID]/n_{Va} - k_{off_4}[Va_L] - k_{+,11}[Xa_L][Va_L] + k_{-,11}[Xa{:}Va_L] + k_{-,19}[V{:}IIa_L] - k_{+,32}[APC{:}PS_L][Va_L] + k_{-,32}[APC{:}PS{:}Va_L] + k_{-,40}[V{:}mIIa_L]$$
$$\frac{d[VII_f]}{dt} = -k_{on_5}[VII_f][LIPID]/n_{Va} + k_{off_5}[VII_L]$$
$$\frac{d[VII_L]}{dt} = k_{on_5}[VII_f][LIPID]/n_{Va} - k_{off_5}[VII_L] - k_{+,2}[TF_L][VII_L] + k_{-,2}[TF{:}VII_L] - k_{+,26}[VII_L][Xa_L] + k_{-,26}[VII{:}Xa_L]$$

$$\frac{d[VIIa_f]}{dt} = -k_{on_6}[VIIa_f][LIPID]/n_{Va} + k_{off_6}[VIIa_L]$$
$$\frac{d[VIIa_L]}{dt} = k_{on_6}[VIIa_f][LIPID]/n_{Va} - k_{off_6}[VIIa_L] - k_{+,1}[TF_L][VIIa_L] + k_{-,1}[TF{:}VIIa_L] + k_{-,27}[VII{:}Xa_L]$$
$$\frac{d[VIII_f]}{dt} = -k_{on_7}[VIII_f][LIPID]/n_{Va} + k_{off_7}[VIII_L]$$
$$\frac{d[VIII_L]}{dt} = k_{on_7}[VIII_f][LIPID]/n_{Va} - k_{off_7}[VIII_L] - k_{+,16}[VIII_L][Xa_L] + k_{-,16}[VIII{:}Xa_L] - k_{+,20}[VIII_L][IIa_f] + k_{-,20}[VIII{:}IIa_L] - k_{+,41}[VIII_L][mIIa_L] + k_{-,41}[VIII{:}mIIa_L]$$
$$\frac{d[VIIIa_f]}{dt} = -k_{on_8}[VIIIa_f][LIPID]/n_{Va} + k_{off_8}[VIIIa_L]$$
$$\frac{d[VIIIa_L]}{dt} = k_{on_8}[VIIIa_f][LIPID]/n_{Va} - k_{off_8}[VIIIa_L] - k_{+,10}[IXa_L][VIIIa_L] + k_{-,10}[IXa{:}VIIIa_L] + k_{-,17}[VIII{:}Xa_L] + k_{-,21}[VIII{:}IIa_L] - k_{+,30}[APC{:}PS_L][VIIIa_L] + k_{-,30}[APC{:}PS{:}VIIIa_L] + k_{-,42}[VIII{:}mIIa_L]$$
$$\frac{d[IX_f]}{dt} = -k_{on_9}[IX_f][LIPID]/n_{Va} + k_{off_9}[IX_L]$$
$$\frac{d[IX_L]}{dt} = k_{on_9}[IX_f][LIPID]/n_{Va} - k_{off_9}[IX_L] - k_{+,3}[TF{:}VIIa_L][IX_L] + k_{-,3}[TF{:}VIIa{:}IX_L] - k_{+,48}[XIa_f][IX_L] + k_{-,48}[XIa{:}IX_L]$$
$$\frac{d[IXa_f]}{dt} = -k_{on_{10}}[IXa_f][LIPID]/n_{Va} + k_{off_{10}}[IXa_L] - k_{+,36}[IXa_f][AT_f]$$
$$\frac{d[IXa_L]}{dt} = k_{on_{10}}[IXa_f][LIPID]/n_{Va} - k_{off_{10}}[IXa_L] + k_{-,4}[TF{:}VIIa{:}IX_L] - k_{+,10}[IXa_L][VIIIa_L] + k_{-,10}[IXa{:}VIIIa_L] + k_{-,49}[XIa{:}IX_L]$$
$$\frac{d[X_f]}{dt} = -k_{on_{11}}[X_f][LIPID]/n_{Va} + k_{off_{11}}[X_L]$$
$$\frac{d[X_L]}{dt} = k_{on_{11}}[X_f][LIPID]/n_{Va} - k_{off_{11}}[X_L] - k_{+,5}[TF{:}VIIa_L][X_L] + k_{-,5}[TF{:}VIIa{:}X_L] - k_{+,12}[IXa{:}VIIIa_L][X_L] + k_{-,12}[IXa{:}VIIIa{:}X_L]$$
$$\frac{d[Xa_f]}{dt} = -k_{on_{12}}[Xa_f][LIPID]/n_{Va} + k_{off_{12}}[Xa_L] - k_{+,34}[TFPI_f][Xa_f] + k_{-,34}[TFPI{:}Xa_f] - k_{+,37}[Xa_f][AT_f]$$
$$\frac{d[Xa_L]}{dt} = k_{on_{12}}[Xa_f][LIPID]/n_{Va} - k_{off_{12}}[Xa_L] - k_{-,7}[TF{:}VIIa{:}Xa_L] - k_{+,8}[TF{:}VII_L][Xa_L] + k_{-,8}[TF{:}VII{:}Xa_L] + k_{-,9}[TF{:}VII{:}Xa_L] - k_{+,11}[Xa_L][Va_L] + k_{-,11}[Xa{:}Va_L] + k_{-,13}[IXa{:}VIIIa{:}X_L] - k_{+,14}[V_L][Xa_L] + k_{-,14}[V{:}Xa_L] + k_{-,15}[V{:}Xa_L] - k_{+,16}[VIII_L][Xa_L] + k_{-,16}[VIII{:}Xa_L] + k_{-,17}[VIII{:}Xa_L] - k_{+,26}[VII_L][Xa_L] + k_{-,26}[VII{:}Xa_L] + k_{-,27}[VII{:}Xa_L]$$
$$\frac{d[APC_f]}{dt} = -k_{on_{13}}[APC_f][LIPID]/n_{Va} + k_{off_{13}}[APC_L]$$
$$\frac{d[APC_L]}{dt} = k_{on_{13}}[APC_f][LIPID]/n_{Va} - k_{off_{13}}[APC_L] + k_{-,45}[IIa{:}TM{:}PC_L] - k_{+,47}[APC_L][PS_L] + k_{-,47}[APC{:}PS_L]$$
$$\frac{d[PS_f]}{dt} = -k_{on_{14}}[PS_f][LIPID]/n_{Va} + k_{off_{14}}[PS_L]$$
$$\frac{d[PS_L]}{dt} = k_{on_{14}}[PS_f][LIPID]/n_{Va} - k_{off_{14}}[PS_L] - k_{+,47}[APC_L][PS_L] + k_{-,47}[APC{:}PS_L]$$
$$\frac{d[VIIIai_f]}{dt} = -k_{on_{15}}[VIIIai_f][LIPID]/n_{Va} + k_{off_{15}}[VIIIai_L]$$

$$\frac{d[VIIIai_L]}{dt} = k_{on_{15}}[VIIIai_f][LIPID]/n_{Va} - k_{off_{15}}[VIIIai_L] + k_{-,31}[APC{:}PS{:}VIIIa_L]$$
$$\frac{d[Vai_f]}{dt} = -k_{on_{16}}[Vai_f][LIPID]/n_{Va} + k_{off_{16}}[Vai_L]$$
$$\frac{d[Vai_L]}{dt} = k_{on_{16}}[Vai_f][LIPID]/n_{Va} - k_{off_{16}}[Vai_L] + k_{-,33}[APC{:}PS{:}Va_L]$$
$$\frac{d[PC_f]}{dt} = -k_{on_{17}}[PC_f][LIPID]/n_{Va} + k_{off_{17}}[PC_L]$$
$$\frac{d[PC_L]}{dt} = k_{on_{17}}[PC_f][LIPID]/n_{Va} - k_{off_{17}}[PC_L] - k_{+,44}[IIa{:}TM_L][PC_L] + k_{-,44}[IIa{:}TM{:}PC_L]$$
$$\frac{d[TF_L]}{dt} = -k_{+,1}[TF_L][VIIa_L] + k_{-,1}[TF{:}VIIa_L] - k_{+,2}[TF_L][VII_L] + k_{-,2}[TF{:}VII_L]$$
$$\frac{d[TF{:}VIIa_L]}{dt} = k_{+,1}[TF_L][VIIa_L] - k_{-,1}[TF{:}VIIa_L] - k_{+,3}[TF{:}VIIa_L][IX_L] + k_{-,3}[TF{:}VIIa{:}IX_L] + k_{-,4}[TF{:}VIIa{:}IX_L] - k_{+,5}[TF{:}VIIa_L][X_L] + k_{-,5}[TF{:}VIIa{:}X_L] + k_{-,7}[TF{:}VIIa{:}Xa_L] + k_{-,9}[TF{:}VII{:}Xa_L] - k_{+,35}[TFPI{:}Xa_f][TF{:}VIIa_L] + k_{-,35}[TFPI{:}Xa{:}TF{:}VIIa_L]$$
$$\frac{d[TF{:}VII_L]}{dt} = k_{+,2}[TF_L][VII_L] - k_{-,2}[TF{:}VII_L] - k_{+,8}[TF{:}VII_L][Xa_L] + k_{-,8}[TF{:}VII{:}Xa_L]$$
$$\frac{d[TF{:}VIIa{:}IX_L]}{dt} = k_{+,3}[TF{:}VIIa_L][IX_L] - k_{-,3}[TF{:}VIIa{:}IX_L] - k_{-,4}[TF{:}VIIa{:}IX_L]$$
$$\frac{d[TF{:}VIIa{:}X_L]}{dt} = k_{+,5}[TF{:}VIIa_L][X_L] - k_{-,5}[TF{:}VIIa{:}X_L] - k_{-,6}[TF{:}VIIa{:}X_L]$$
$$\frac{d[TF{:}VIIa{:}Xa_L]}{dt} = k_{-,6}[TF{:}VIIa{:}X_L] + k_{-,7}[TF{:}VIIa{:}Xa_L]$$
$$\frac{d[TF{:}VII{:}Xa_L]}{dt} = k_{+,8}[TF{:}VII_L][Xa_L] - k_{-,8}[TF{:}VII{:}Xa_L] - k_{-,9}[TF{:}VII{:}Xa_L]$$
$$\frac{d[IXa{:}VIIIa_L]}{dt} = k_{+,10}[IXa_L][VIIIa_L] - k_{-,10}[IXa{:}VIIIa_L] - k_{+,12}[IXa{:}VIIIa_L][X_L] + k_{-,12}[IXa{:}VIIIa{:}X_L] + k_{-,13}[IXa{:}VIIIa{:}X_L]$$
$$\frac{d[Xa{:}Va_L]}{dt} = k_{+,11}[Xa_L][Va_L] - k_{-,11}[Xa{:}Va_L] - k_{+,22}[Xa{:}Va_L][II_L] + k_{-,22}[Xa{:}Va{:}II_L] - k_{+,23}[Xa{:}Va_L][mIIa_L] + k_{-,23}[Xa{:}Va{:}mIIa_L] + k_{-,25}[Xa{:}Va{:}mIIa_L]$$
$$\frac{d[IXa{:}VIIIa{:}X_L]}{dt} = k_{+,12}[IXa{:}VIIIa_L][X_L] - k_{-,12}[IXa{:}VIIIa{:}X_L] - k_{-,13}[IXa{:}VIIIa{:}X_L]$$
$$\frac{d[V{:}Xa_L]}{dt} = k_{+,14}[V_L][Xa_L] - k_{-,14}[V{:}Xa_L] - k_{-,15}[V{:}Xa_L]$$
$$\frac{d[VIII{:}Xa_L]}{dt} = k_{+,16}[VIII_L][Xa_L] - k_{-,16}[VIII{:}Xa_L] - k_{-,17}[VIII{:}Xa_L]$$
$$\frac{d[IIa_f]}{dt} = -k_{+,18}[V_L][IIa_f] + k_{-,18}[V{:}IIa_L] + k_{-,19}[V{:}IIa_L] - k_{+,20}[VIII_L][IIa_f] + k_{-,20}[VIII{:}IIa_L] + k_{-,21}[VIII{:}IIa_L] + k_{-,25}[Xa{:}Va{:}mIIa_L] - k_{+,28}[XI_f][IIa_f] + k_{-,28}[XI{:}IIa_f] + k_{-,29}[XI{:}IIa_f] - k_{+,38}[IIa_f][AT_f] - k_{+,43}[IIa_f][TM_L] + k_{-,43}[IIa{:}TM_L]$$
$$\frac{d[V{:}IIa_L]}{dt} = k_{+,18}[V_L][IIa_f] - k_{-,18}[V{:}IIa_L] - k_{-,19}[V{:}IIa_L]$$
$$\frac{d[VIII{:}IIa_L]}{dt} = k_{+,20}[VIII_L][IIa_f] - k_{-,20}[VIII{:}IIa_L] - k_{-,21}[VIII{:}IIa_L]$$
$$\frac{d[Xa{:}Va{:}II_L]}{dt} = k_{+,22}[Xa{:}Va_L][II_L] - k_{-,22}[Xa{:}Va{:}II_L] - k_{-,24}[Xa{:}Va{:}II_L]$$
$$\frac{d[Xa{:}Va{:}mIIa_L]}{dt} = k_{+,23}[Xa{:}Va_L][mIIa_L] - k_{-,23}[Xa{:}Va{:}mIIa_L] + k_{-,24}[Xa{:}Va{:}II_L] - k_{-,25}[Xa{:}Va{:}mIIa_L]$$

$$\frac{d[XI_f]}{dt} = -k_{+,28}[XI_f][IIa_f] + k_{-,28}[XI{:}IIa_f]$$
$$\frac{d[XI{:}IIa_f]}{dt} = k_{+,28}[XI_f][IIa_f] - k_{-,28}[XI{:}IIa_f] - k_{-,29}[XI{:}IIa_f]$$
$$\frac{d[XIa_f]}{dt} = k_{-,29}[XI{:}IIa_f] - k_{+,48}[XIa_f][IX_L] + k_{-,48}[XIa{:}IX_L] + k_{-,49}[XIa{:}IX_L]$$
$$\frac{d[APC{:}PS_L]}{dt} = -k_{+,30}[APC{:}PS_L][VIIIa_L] + k_{-,30}[APC{:}PS{:}VIIIa_L] + k_{-,31}[APC{:}PS{:}VIIIa_L] - k_{+,32}[APC{:}PS_L][Va_L] + k_{-,32}[APC{:}PS{:}Va_L] + k_{-,33}[APC{:}PS{:}Va_L] + k_{+,47}[APC_L][PS_L] - k_{-,47}[APC{:}PS_L]$$
$$\frac{d[APC{:}PS{:}VIIIa_L]}{dt} = k_{+,30}[APC{:}PS_L][VIIIa_L] - k_{-,30}[APC{:}PS{:}VIIIa_L] - k_{-,31}[APC{:}PS{:}VIIIa_L]$$
$$\frac{d[TFPI_f]}{dt} = -k_{+,34}[TFPI_f][Xa_f] + k_{-,34}[TFPI{:}Xa_f]$$
$$\frac{d[AT_f]}{dt} = -k_{+,36}[IXa_f][AT_f] - k_{+,37}[Xa_f][AT_f] - k_{+,38}[IIa_f][AT_f] - k_{+,46}[mIIa_f][AT_f]$$
$$\frac{d[IIa{:}AT_f]}{dt} = k_{+,38}[IIa_f][AT_f]$$
$$\frac{d[TFPI{:}Xa_f]}{dt} = k_{+,34}[TFPI_f][Xa_f] - k_{-,34}[TFPI{:}Xa_f] - k_{+,35}[TFPI{:}Xa_f][TF{:}VIIa_L] + k_{-,35}[TFPI{:}Xa{:}TF{:}VIIa_L]$$
$$\frac{d[TFPI{:}Xa{:}TF{:}VIIa_L]}{dt} = k_{+,35}[TFPI{:}Xa_f][TF{:}VIIa_L] - k_{-,35}[TFPI{:}Xa{:}TF{:}VIIa_L]$$
$$\frac{d[APC{:}PS{:}Va_L]}{dt} = k_{+,32}[APC{:}PS_L][Va_L] - k_{-,32}[APC{:}PS{:}Va_L] - k_{-,33}[APC{:}PS{:}Va_L]$$
$$\frac{d[IXa{:}AT_f]}{dt} = k_{+,36}[IXa_f][AT_f]$$
$$\frac{d[Xa{:}AT_f]}{dt} = k_{+,37}[Xa_f][AT_f]$$
$$\frac{d[VII{:}Xa_L]}{dt} = k_{+,26}[VII_L][Xa_L] - k_{-,26}[VII{:}Xa_L] - k_{-,27}[VII{:}Xa_L]$$
$$\frac{d[V{:}mIIa_L]}{dt} = k_{+,39}[V_L][mIIa_L] - k_{-,39}[V{:}mIIa_L] - k_{-,40}[V{:}mIIa_L]$$
$$\frac{d[VIII{:}mIIa_L]}{dt} = k_{+,41}[VIII_L][mIIa_L] - k_{-,41}[VIII{:}mIIa_L] - k_{-,42}[VIII{:}mIIa_L]$$
$$\frac{d[TM_L]}{dt} = -k_{+,43}[IIa_f][TM_L] + k_{-,43}[IIa{:}TM_L]$$
$$\frac{d[IIa{:}TM_L]}{dt} = k_{+,43}[IIa_f][TM_L] - k_{-,43}[IIa{:}TM_L] - k_{+,44}[IIa{:}TM_L][PC_L] + k_{-,44}[IIa{:}TM{:}PC_L] + k_{-,45}[IIa{:}TM{:}PC_L]$$
$$\frac{d[IIa{:}TM{:}PC_L]}{dt} = k_{+,44}[IIa{:}TM_L][PC_L] - k_{-,44}[IIa{:}TM{:}PC_L] - k_{-,45}[IIa{:}TM{:}PC_L]$$
$$\frac{d[mIIa{:}AT_f]}{dt} = k_{+,46}[mIIa_f][AT_f]$$
$$\frac{d[XIa{:}IX_L]}{dt} = k_{+,48}[XIa_f][IX_L] - k_{-,48}[XIa{:}IX_L] - k_{-,49}[XIa{:}IX_L]$$

$$\frac{d[LIPID]}{dt} = k_{on_1}[II_f][LIPID] - k_{off_1}[II_L]/n_{Va} + k_{on_2}[mIIa_f][LIPID] - k_{off_2}[mIIa_L]/n_{Va} + k_{on_3}[V_f][LIPID] - k_{off_3}[V_L]/n_{Va} + k_{on_4}[Va_f][LIPID] - k_{off_4}[Va_L]/n_{Va} + k_{on_5}[VII_f][LIPID] - k_{off_5}[VII_L]/n_{Va} + k_{on_6}[VIIa_f][LIPID] - k_{off_6}[VIIa_L]/n_{Va} + k_{on_7}[VIII_f][LIPID] - k_{off_7}[VIII_L]/n_{Va} + k_{on_8}[VIIIa_f][LIPID] - k_{off_8}[VIIIa_L]/n_{Va} + k_{on_9}[IX_f][LIPID] - k_{off_9}[IX_L]/n_{Va} + k_{on_{10}}[IXa_f][LIPID] - k_{off_{10}}[IXa_L]/n_{Va} + k_{on_{11}}[X_f][LIPID] - k_{off_{11}}[X_L]/n_{Va} + k_{on_{12}}[Xa_f][LIPID] - k_{off_{12}}[Xa_L]/n_{Va} + k_{on_{13}}[APC_f][LIPID] - k_{off_{13}}[APC_L]/n_{Va} + k_{on_{14}}[PS_f][LIPID] - k_{off_{14}}[PS_L]/n_{Va} + k_{on_{15}}[VIIIai_f][LIPID] - k_{off_{15}}[VIIIai_L]/n_{Va} + k_{on_{16}}[Vai_f][LIPID] - k_{off_{16}}[Vai_L]/n_{Va} + k_{on_{17}}[PC_f][LIPID] - k_{off_{17}}[PC_L]$$

A.1.7 Tyurin Model

$$\frac{d[Va]}{dt} = -k_1[Va][Xa] + k_{16}[Xa{:}Va][\alpha_1{-}AT] + k_{17}[Xa{:}Va][AT] + k_{\mathrm{cat}_{13}}[IIa][V]/(K_{m_{13}}(1+[XI]/K_{m_2}+[VIII]/K_{m_{17}})+[V]) + k_{\mathrm{cat}_{14}}[Xa][V]/(K_{m_{14}}(1+[II]/K_{m_{11}}+[VII]/K_{m_{15}}+[TF{:}VII]/K_{m_{16}})+[V]) - k_{\mathrm{cat}_{19}}[APC][Va]/(K_{m_{19}}+[VIIIa]+[Va]+[Xa{:}Va]+[IXa{:}VIIIa])$$

$$\frac{d[Xa]}{dt} = -k_1[Va][Xa] - k_{13}[Xa][AT] - k_{14}[Xa][\alpha_1{-}AT] - k_{15}[Xa][TFPI] + k_{\mathrm{cat}_7}[IXa][X]/(K_{m_7}+[X]) + k_{\mathrm{cat}_{10}}[TF{:}VIIa][X]/(K_{m_{10}}(1+[IX]/K_{m_6})+[X]) + k_{\mathrm{cat}_9}[VIIa][X]/(K_{m_9}(1+[IX]/K_{m_5})+[X]) + k_{\mathrm{cat}_8}[IXa{:}VIIIa][X]/(K_{m_8}+[X]) + k_{\mathrm{cat}_{19}}[APC][Xa{:}Va]/(K_{m_{19}}+[VIIIa]+[Va]+[Xa{:}Va]+[IXa{:}VIIIa])$$

$$\frac{d[Xa{:}Va]}{dt} = k_1[Va][Xa] - k_{16}[Xa{:}Va][\alpha_1{-}AT] - k_{17}[Xa{:}Va][AT] - k_{\mathrm{cat}_{19}}[APC][Xa{:}Va]/(K_{m_{19}}+[VIIIa]+[Va]+[Xa{:}Va]+[IXa{:}VIIIa])$$

$$\frac{d[VIIIa]}{dt} = -k_2[VIIIa][IXa] + k_{19}[IXa{:}VIIIa][AT] + k_{\mathrm{cat}_{17}}[IIa][VIII]/(K_{m_{17}}(1+[XI]/K_{m_2}+[V]/K_{m_{13}})+[VIII]) - k_{\mathrm{cat}_{19}}[APC][VIIIa]/(K_{m_{19}}+[VIIIa]+[Va]+[Xa{:}Va]+[IXa{:}VIIIa])$$

$$\frac{d[IXa]}{dt} = -k_2[VIIIa][IXa] - k_{18}[IXa][AT] + k_{\mathrm{cat}_4}[XIa][IX]/(K_{m_4}(1+[XI]/K_{m_3})+[IX]) + k_{\mathrm{cat}_5}[VIIa][IX]/(K_{m_5}(1+[X]/K_{m_9})+[IX]) + k_{\mathrm{cat}_6}[TF{:}VIIa][IX]/(K_{m_6}(1+[X]/K_{m_{10}})+[IX]) + k_{\mathrm{cat}_{19}}[APC][IXa{:}VIIIa]/(K_{m_{19}}+[VIIIa]+[Va]+[Xa{:}Va]+[IXa{:}VIIIa])$$

$$\frac{d[IXa{:}VIIIa]}{dt} = k_2[VIIIa][IXa] - k_{19}[IXa{:}VIIIa][AT] - k_{\mathrm{cat}_{19}}[APC][IXa{:}VIIIa]/(K_{m_{19}}+[VIIIa]+[Va]+[Xa{:}Va]+[IXa{:}VIIIa])$$

$$\frac{d[VIIa]}{dt} = -k_3[VIIa][TF] + k_4[TF{:}VIIa] + k_{\mathrm{cat}_{15}}[Xa][VII]/(K_{m_{15}}(1+[II]/K_{m_{11}}+[V]/K_{m_{14}}+[TF{:}VII]/K_{m_{16}})+[VII])$$

$$\frac{d[TF]}{dt} = -k_3[VIIa][TF] - k_5[VII][TF] + k_4[TF{:}VIIa] + k_6[TF{:}VII]$$

$$\frac{d[TF{:}VIIa]}{dt} = k_3[VIIa][TF] - k_7[TF{:}VIIa][Xa{:}TFPI] - k_8[TF{:}VIIa][AT] - k_4[TF{:}VIIa] + k_{\mathrm{cat}_{16}}[Xa][TF{:}VII]/(K_{m_{16}}(1+[II]/K_{m_{11}}+[V]/K_{m_{14}}+[VII]/K_{m_{15}})+[TF{:}VII])$$

$$\frac{d[VII]}{dt} = -k_5[VII][TF] + k_6[TF{:}VII] - k_{\mathrm{cat}_{15}}[Xa][VII]/(K_{m_{15}}(1+[II]/K_{m_{11}}+[V]/K_{m_{14}}+[TF{:}VII]/K_{m_{16}})+[VII])$$

$$\frac{d[TF{:}VII]}{dt} = k_5[VII][TF] - k_6[TF{:}VII] - k_{\mathrm{cat}_{16}}[Xa][TF{:}VII]/(K_{m_{16}}(1+[II]/K_{m_{11}}+[V]/K_{m_{14}}+[VII]/K_{m_{15}})+[TF{:}VII])$$

$$\frac{d[AT]}{dt} = -k_8[TF{:}VIIa][AT] - k_9[IIa][AT] - k_{13}[Xa][AT] - k_{17}[Xa{:}Va][AT] - k_{18}[IXa][AT] - k_{19}[IXa{:}VIIIa][AT] - k_{22}[XIa][AT]$$

$$\frac{d[TF{:}VIIa{:}AT]}{dt} = k_8[TF{:}VIIa][AT]$$

$$\frac{d[IIa]}{dt} = -k_9[IIa][AT] - k_{10}[IIa][\alpha_1{-}AT] - k_{11}[IIa][\alpha_2{-}M] - k_{12}[IIa][PCI] + k_{\mathrm{cat}_{11}}[Xa][II]/(K_{m_{11}}(1+[V]/K_{m_{13}}+[VII]/K_{m_{15}}+[TF{:}VII]/K_{m_{16}})+[II]) + k_{\mathrm{cat}_{12}}[Xa{:}Va][II]/(K_{m_{12}}+[II]) - k_{25}[IIa][TM]$$

$$\frac{d[\alpha_1{-}AT]}{dt} = -k_{10}[IIa][\alpha_1{-}AT] - k_{14}[Xa][\alpha_1{-}AT] - k_{16}[Xa{:}Va][\alpha_1{-}AT] - k_{21}[XIa][\alpha_1{-}AT] - k_{28}[APC][\alpha_1{-}AT]$$

$$\frac{d[\alpha_2{-}M]}{dt} = -k_{11}[IIa][\alpha_2{-}M]$$

$$\frac{d[PCI]}{dt} = -k_{12}[IIa][PCI] - k_{26}[IIa{:}TM][PCI] - k_{27}[APC][PCI]$$

$$\frac{d[TFPI]}{dt} = -k_{15}[Xa][TFPI]$$

$$\frac{d[Xa{:}TFPI]}{dt} = -k_7[TF{:}VIIa][Xa{:}TFPI] + k_{15}[Xa][TFPI]$$

$$\frac{d[XIa]}{dt} = -k_{20}[XIa][C1{-}inh] - k_{21}[XIa][\alpha_1{-}AT] - k_{22}[XIa][AT] - k_{23}[XIa][\alpha_2{-}AP] - k_{24}[XIa][PAI1] + k_{\mathrm{cat}_1}[XIIa][XI]/(K_{m_1}+[XI]) + k_{\mathrm{cat}_2}[IIa][XI]/(K_{m_2}(1+[V]/K_{m_{13}}+[VIII]/K_{m_{17}})+[XI]) + k_{\mathrm{cat}_3}[XIa][XI]/(K_{m_3}(1+[IX]/K_{m_4})+[XI])$$

$$\frac{d[C1{-}inh]}{dt} = -k_{20}[XIa][C1{-}inh]$$

$$\frac{d[\alpha_2{-}AP]}{dt} = -k_{23}[XIa][\alpha_2{-}AP]$$

$$\frac{d[PAI1]}{dt} = -k_{24}[XIa][PAI1]$$

$$\frac{d[TM]}{dt} = -k_{25}[IIa][TM]$$

$$\frac{d[IIa{:}TM]}{dt} = k_{25}[IIa][TM] - k_{26}[IIa{:}TM][PCI]$$

$$\frac{d[APC]}{dt} = -k_{27}[APC][PCI] - k_{28}[APC][\alpha_1{-}AT] + k_{\mathrm{cat}_{18}}[IIa{:}TM][PC]/(K_{m_{18}}+[PC])$$

$$\frac{d[TF{:}VIIa{:}Xa{:}TFPI]}{dt} = k_7[TF{:}VIIa][Xa{:}TFPI]$$

$$\frac{d[XI]}{dt} = -k_{\mathrm{cat}_1}[XIIa][XI]/(K_{m_1}+[XI]) - k_{\mathrm{cat}_3}[XIa][XI]/(K_{m_3}(1+[IX]/K_{m_4})+[XI]) - k_{\mathrm{cat}_2}[IIa][XI]/(K_{m_2}(1+[V]/K_{m_{13}}+[VIII]/K_{m_{17}})+[XI])$$

$$\frac{d[IX]}{dt} = -k_{\mathrm{cat}_4}[XIa][IX]/(K_{m_4}(1+[XI]/K_{m_3})+[IX]) - k_{\mathrm{cat}_5}[VIIa][IX]/(K_{m_5}(1+[X]/K_{m_9})+[IX]) - k_{\mathrm{cat}_6}[TF{:}VIIa][IX]/(K_{m_6}(1+[X]/K_{m_{10}})+[IX])$$

$$\frac{d[X]}{dt} = -k_{\mathrm{cat}_7}[IXa][X]/(K_{m_7}+[X]) - k_{\mathrm{cat}_8}[IXa{:}VIIIa][X]/(K_{m_8}+[X]) - k_{\mathrm{cat}_9}[VIIa][X]/(K_{m_9}(1+[IX]/K_{m_5})+[X]) - k_{\mathrm{cat}_{10}}[TF{:}VIIa][X]/(K_{m_{10}}(1+[IX]/K_{m_6})+[X])$$

$$\frac{d[II]}{dt} = -k_{\text{cat}_{12}}[Xa{:}Va][II]/(K_{m_{12}} + [II]) \\ - k_{\text{cat}_{11}}[Xa][II]/(K_{m_{11}}(1 + [V]/K_{m_{13}} + [VII]/K_{m_{15}} + [TF{:}VII]/K_{m_{16}}) + [II])$$

$$\frac{d[V]}{dt} = -k_{\text{cat}_{13}}[IIa][V]/(K_{m_{13}}(1 + [XI]/K_{m_2} + [VIII]/K_{m_{17}}) + [V]) \\ - k_{\text{cat}_{14}}[Xa][V]/(K_{m_{14}}(1 + [II]/K_{m_{11}} + [VII]/K_{m_{15}} + [TF{:}VII]/K_{m_{16}}) + [V])$$

$$\frac{d[VIII]}{dt} = -k_{\text{cat}_{17}}[IIa][VIII]/(K_{m_{17}}(1 + [XI]/K_{m_2} + [V]/K_{m_{13}}) + [VIII])$$

$$\frac{d[PC]}{dt} = -k_{\text{cat}_{18}}[IIa{:}TM][PC]/(K_{m_{18}} + [PC])$$

A.1.8 Zhu Model

$$\frac{d[Va]}{dt} = -k_{30}[APC][Va] + k_{\text{cat}_{13}}[IIa][V]/(K_{m_{13}} + [V]) + k_{\text{cat}_{14}}[Xa][V]/(K_{m_{14}} + [V]) \\ - k_1[Va][Xa]$$

$$\frac{d[Xa]}{dt} = -k_6[Xa][AT] - k_7[Xa][\alpha_1{-}AT] - k_8[Xa][TFPI] + k_{\text{cat}_9}[IXa][X]/(K_{m_9} + [X]) \\ + k_{\text{cat}_{10}}[IXa{:}VIIIa][X]/(K_{m_{10}} + [X]) - k_1[Va][Xa] + k_{\text{cat}_{18}}[TF{:}VIIa][X]/(K_{m_{18}} + [X])$$

$$\frac{d[Xa{:}Va]}{dt} = -k_{32}[APC][Xa{:}Va] + k_1[Va][Xa]$$

$$\frac{d[VIIIa]}{dt} = -k_2[VIIIa][IXa] - k_{31}[APC][VIIIa] + k_{\text{cat}_{15}}[IIa][VIII]/(K_{m_{15}} + [VIII])$$

$$\frac{d[IXa]}{dt} = -k_2[VIIIa][IXa] - k_9[IXa][AT] + k_{\text{cat}_8}[XIa][IX]/(K_{m_8} + [IX]) \\ + k_{\text{cat}_{19}}[TF{:}VIIa][IX]/(K_{m_{19}} + [IX])$$

$$\frac{d[IIa]}{dt} = -k_3[IIa][AT] - k_4[IIa][\alpha_1{-}AT] - k_5[IIa][\alpha_2{-}M] - k_{34}[TM][IIa] \\ + k_{\text{cat}_{11}}[Xa][II]/(K_{m_{11}} + [II]) + k_{\text{cat}_{12}}[Xa{:}Va][II]/(K_{m_{12}} + [II])$$

$$\frac{d[AT]}{dt} = -k_3[IIa][AT] - k_6[Xa][AT] - k_9[IXa][AT] - k_{12}[XIa][AT] - k_{18}[XIIa][AT] \\ - k_{22}[XIIf][AT] - k_{26}[K][AT] - k_{28}[TF{:}VIIa][AT]$$

$$\frac{d[IXa{:}VIIIa]}{dt} = k_2[VIIIa][IXa] - k_{33}[APC][IXa{:}VIIIa]$$

$$\frac{d[\alpha_1{-}AT]}{dt} = -k_4[IIa][\alpha_1{-}AT] - k_7[Xa][\alpha_1{-}AT] - k_{11}[XIa][\alpha_1{-}AT]$$

$$\frac{d[\alpha_2{-}M]}{dt} = -k_5[IIa][\alpha_2{-}M] - k_{17}[XIIa][\alpha_2{-}M] - k_{24}[K][\alpha_2{-}M]$$

$$\frac{d[TFPI]}{dt} = -k_8[Xa][TFPI]$$

$$\frac{d[Xa{:}TFPI]}{dt} = k_8[Xa][TFPI] - k_{29}[TF{:}VIIa][Xa{:}TFPI]$$

$$\frac{d[XIa]}{dt} = -k_{10}[XIa][C1{-}inh] - k_{11}[XIa][\alpha_1{-}AT] - k_{12}[XIa][AT] - k_{13}[XIa][\alpha_2{-}AP] \\ - k_{14}[XIa][PAI1] + k_{\text{cat}_6}[XIIa][XI]/(K_{m_6} + [XI]) + k_{35}[XI]$$

$$\frac{d[C1{-}inh]}{dt} = -k_{10}[XIa][C1{-}inh] - k_{15}[XIIa][C1{-}inh] - k_{20}[XIIf][C1{-}inh] \\ - k_{23}[K][C1{-}inh]$$

$$\frac{d[\alpha_2{-}AP]}{dt} = -k_{13}[XIa][\alpha_2{-}AP] - k_{16}[XIIa][\alpha_2{-}AP] - k_{21}[XIIf][\alpha_2{-}AP]$$

$$\frac{d[PAI1]}{dt} = -k_{14}[XIa][PAI1] - k_{19}[XIIa][PAI1] - k_{25}[K][PAI1]$$

$$\frac{d[XIIa]}{dt} = -k_{15}[XIIa][C1{-}inh] - k_{16}[XIIa][\alpha_2{-}AP] - k_{17}[XIIa][\alpha_2{-}M] - k_{18}[XIIa][AT]$$
$$- k_{19}[XIIa][PAI1] + k_{\mathrm{cat}_1}[XIIa][XII]/(K_{m_1} + [XII]) + k_{\mathrm{cat}_4}[K][XII]/(K_{m_4} + [XII])$$
$$- k_{\mathrm{cat}_5}[K][XIIa]/(K_{m_5} + [XIIa]) + k_{\mathrm{cat}_7}[XIa][XII]/(K_{m_7} + [XII])$$

$$\frac{d[XIIf]}{dt} = -k_{20}[XIIf][C1{-}inh] - k_{21}[XIIf][\alpha_2{-}AP] - k_{22}[XIIf][AT]$$
$$+ k_{\mathrm{cat}_5}[K][XIIa]/(K_{m_5} + [XIIa])$$

$$\frac{d[K]}{dt} = -k_{23}[K][C1{-}inh] - k_{24}[K][\alpha_2{-}M] - k_{25}[K][PAI1] - k_{26}[K][AT]$$
$$+ k_{\mathrm{cat}_2}[XIIa][PK]/(K_{m_2} + [PK]) + k_{\mathrm{cat}_3}[XIIf][PK]/(K_{m_3} + [PK])$$

$$\frac{d[VII]}{dt} = -k_{27}[VII][TF]$$

$$\frac{d[TF]}{dt} = -k_{27}[VII][TF]$$

$$\frac{d[TF{:}VII]}{dt} = k_{27}[VII][TF] - k_{\mathrm{cat}_{17}}[Xa][TF{:}VII]/(K_{m_{17}} + [TF{:}VII])$$

$$\frac{d[TF{:}VIIa]}{dt} = -k_{28}[TF{:}VIIa][AT] - k_{29}[TF{:}VIIa][Xa{:}TFPI]$$
$$+ k_{\mathrm{cat}_{17}}[Xa][TF{:}VII]/(K_{m_{17}} + [TF{:}VII])$$

$$\frac{d[TF{:}VIIa{:}Xa{:}TFPI]}{dt} = k_{29}[TF{:}VIIa][Xa{:}TFPI]$$

$$\frac{d[APC]}{dt} = -k_{30}[APC][Va] - k_{31}[APC][VIIIa] - k_{32}[APC][Xa{:}Va]$$
$$- k_{33}[APC][IXa{:}VIIIa] + k_{\mathrm{cat}_{20}}[IIa{:}TM][PC]/(K_{m_{20}} + [PC])$$

$$\frac{d[APC{:}Va]}{dt} = k_{30}[APC][Va]$$

$$\frac{d[APC{:}VIIIa]}{dt} = k_{31}[APC][VIIIa]$$

$$\frac{d[APC{:}Xa{:}Va]}{dt} = k_{32}[APC][Xa{:}Va]$$

$$\frac{d[APC{:}IXa{:}VIIIa]}{dt} = k_{33}[APC][IXa{:}VIIIa]$$

$$\frac{d[TM]}{dt} = -k_{34}[TM][IIa]$$

$$\frac{d[IIa{:}TM]}{dt} = k_{34}[TM][IIa]$$

$$\frac{d[XII]}{dt} = -k_{\mathrm{cat}_1}[XIIa][XII]/(K_{m_1} + [XII]) - k_{\mathrm{cat}_4}[K][XII]/(K_{m_4} + [XII])$$
$$- k_{\mathrm{cat}_7}[XIa][XII]/(K_{m_7} + [XII])$$

$$\frac{d[PK]}{dt} = -k_{\mathrm{cat}_2}[XIIa][PK]/(K_{m_2} + [PK]) - k_{\mathrm{cat}_3}[XIIf][PK]/(K_{m_3} + [PK])$$

$$\frac{d[XI]}{dt} = -k_{\mathrm{cat}_6}[XIIa][XI]/(K_{m_6} + [XI]) - k_{35}[XI]$$

$$\frac{d[IX]}{dt} = -k_{\mathrm{cat}_8}[XIa][IX]/(K_{m_8} + [IX]) - k_{\mathrm{cat}_{19}}[TF{:}VIIa][IX]/(K_{m_{19}} + [IX])$$

$$\frac{d[X]}{dt} = -k_{\mathrm{cat}_9}[IXa][X]/(K_{m_9} + [X]) - k_{\mathrm{cat}_{10}}[IXa{:}VIIIa][X]/(K_{m_{10}} + [X])$$
$$- k_{\mathrm{cat}_{18}}[TF{:}VIIa][X]/(K_{m_{18}} + [X])$$

$$\frac{d[II]}{dt} = -k_{\mathrm{cat}_{11}}[Xa][II]/(K_{m_{11}} + [II]) - k_{\mathrm{cat}_{12}}[Xa{:}Va][II]/(K_{m_{12}} + [II])$$

$$\frac{d[V]}{dt} = -k_{\mathrm{cat}_{13}}[IIa][V]/(K_{m_{13}} + [V]) - k_{\mathrm{cat}_{14}}[Xa][V]/(K_{m_{14}} + [V])$$

$$\frac{d[VIII]}{dt} = -k_{\mathrm{cat}_{15}}[IIa][VIII]/(K_{m_{15}} + [VIII])$$

$$\frac{d[Fbg]}{dt} = -k_{\text{cat}_{16}}[IIa][Fbg]/(K_{m_{16}} + [Fbg])$$
$$\frac{d[Fbn]}{dt} = k_{\text{cat}_{16}}[IIa][Fbg]/(K_{m_{16}} + [Fbg])$$
$$\frac{d[PC]}{dt} = -k_{\text{cat}_{20}}[IIa{:}TM][PC]/(K_{m_{20}} + [PC])$$

A.2 Timescale Analysis

A.2.1 Danforth - First Timescale

$$\frac{d[TF]}{dt} = -k_{+,1}[TF][VII]$$
$$\frac{d[VII]}{dt} = -k_{+,1}[TF][VII]$$
$$\frac{d[TF{:}VII]}{dt} = k_{+,1}[TF][VII]$$
$$\frac{d[VIIa]}{dt} = -k_{+,2}[TF][VIIa] + k_{+,4}[VII][Xa]$$
$$\frac{d[TF{:}VIIa]}{dt} = k_{+,2}[TF][VIIa] + k_{-,6}[TF{:}VIIa{:}X] - k_{+,6}[TF{:}VIIa][X] + k_{-,8}[TF{:}VIIa{:}Xa] + k_{-,10}[TF{:}VIIa{:}IX]$$
$$\frac{d[Xa]}{dt} = k_{-,8}[TF{:}VIIa{:}Xa]$$
$$\frac{d[IIa]}{dt} = k_{+,11}[II][Xa]$$
$$\frac{d[X]}{dt} = -k_{+,6}[TF{:}VIIa][X]$$
$$\frac{d[TF{:}VIIa{:}X]}{dt} = -k_{-,6}[TF{:}VIIa{:}X] + k_{+,6}[TF{:}VIIa][X] - k_{-,7}[TF{:}VIIa{:}X]$$
$$\frac{d[TF{:}VIIa{:}Xa]}{dt} = k_{-,7}[TF{:}VIIa{:}X] - k_{-,8}[TF{:}VIIa{:}Xa] - k_{+,24}[TF{:}VIIa{:}Xa][TFPI]$$
$$\frac{d[IX]}{dt} = k_{-,9}[TF{:}VIIa{:}IX] - k_{+,9}[TF{:}VIIa][IX]$$
$$\frac{d[TF{:}VIIa{:}IX]}{dt} = -k_{-,9}[TF{:}VIIa{:}IX] + k_{+,9}[TF{:}VIIa][IX] - k_{-,10}[TF{:}VIIa{:}IX]$$
$$\frac{d[IXa]}{dt} = k_{-,10}[TF{:}VIIa{:}IX]$$
$$\frac{d[TFPI]}{dt} = -k_{+,24}[TF{:}VIIa{:}Xa][TFPI]$$
$$\frac{d[Xa{:}TFPI]}{dt} = +k_{+,23}[Xa][TFPI]$$
$$\frac{d[TF{:}VIIa{:}Xa{:}TFPI]}{dt} = k_{+,24}[TF{:}VIIa{:}Xa][TFPI]$$

A.2.2 Danforth - Second Timescale

$$\frac{d[TF]}{dt} = -k_{+,1}[TF][VII]$$
$$\frac{d[VII]}{dt} = -k_{+,1}[TF][VII] - k_{+,4}[VII][Xa]$$
$$\frac{d[TF{:}VII]}{dt} = k_{+,1}[TF][VII]$$
$$\frac{d[VIIa]}{dt} = k_{+,4}[VII][Xa]$$

$$\frac{d[TF{:}VIIa]}{dt} = -k_{-,2}[TF{:}VIIa] + k_{+,2}[TF][VIIa] + k_{-,6}[TF{:}VIIa{:}X] - k_{+,6}[TF{:}VIIa][X] + k_{-,8}[TF{:}VIIa{:}Xa] + k_{-,9}[TF{:}VIIa{:}IX] - k_{+,9}[TF{:}VIIa][IX] + k_{-,10}[TF{:}VIIa{:}IX]$$

$$\frac{d[Xa]}{dt} = k_{-,8}[TF{:}VIIa{:}Xa] - k_{+,8}[TF{:}VIIa][Xa] - k_{+,26}[Xa][AT] + k_{+,31}[X][IXa]$$

$$\frac{d[IIa]}{dt} = k_{+,11}[II][Xa] - k_{+,29}[IIa][AT]$$

$$\frac{d[X]}{dt} = -k_{+,6}[TF{:}VIIa][X]$$

$$\frac{d[TF{:}VIIa{:}X]}{dt} = -k_{-,6}[TF{:}VIIa{:}X] + k_{+,6}[TF{:}VIIa][X] - k_{-,7}[TF{:}VIIa{:}X]$$

$$\frac{d[TF{:}VIIa{:}Xa]}{dt} = k_{-,7}[TF{:}VIIa{:}X] - k_{-,8}[TF{:}VIIa{:}Xa] - k_{+,24}[TF{:}VIIa{:}Xa][TFPI]$$

$$\frac{d[IX]}{dt} = k_{-,9}[TF{:}VIIa{:}IX] - k_{+,9}[TF{:}VIIa][IX]$$

$$\frac{d[TF{:}VIIa{:}IX]}{dt} = -k_{-,9}[TF{:}VIIa{:}IX] + k_{+,9}[TF{:}VIIa][IX] - k_{-,10}[TF{:}VIIa{:}IX]$$

$$\frac{d[IXa]}{dt} = k_{-,10}[TF{:}VIIa{:}IX]$$

$$\frac{d[II]}{dt} = k_{-,20}[Xa{:}Va{:}II] - k_{+,20}[Xa{:}Va][II]$$

$$\frac{d[V]}{dt} = -k_{+,18}[V][IIa] - k_{+,32}[V][mIIa]$$

$$\frac{d[Va]}{dt} = k_{+,18}[V][IIa] - k_{+,19}[Xa][Va] + k_{+,32}[V][mIIa]$$

$$\frac{d[Xa{:}Va]}{dt} = -k_{-,19}[Xa{:}Va] + k_{+,19}[Xa][Va] + k_{-,20}[Xa{:}Va{:}II] - k_{+,20}[Xa{:}Va][II] + k_{-,21}[Xa{:}Va{:}II]$$

$$\frac{d[Xa{:}Va{:}II]}{dt} = -k_{-,20}[Xa{:}Va{:}II] + k_{+,20}[Xa{:}Va][II] - k_{-,21}[Xa{:}Va{:}II]$$

$$\frac{d[mIIa]}{dt} = k_{-,21}[Xa{:}Va{:}II]$$

$$\frac{d[TFPI]}{dt} = -k_{+,23}[Xa][TFPI] - k_{+,24}[TF{:}VIIa{:}Xa][TFPI]$$

$$\frac{d[Xa{:}TFPI]}{dt} = k_{+,23}[Xa][TFPI]$$

$$\frac{d[TF{:}VIIa{:}Xa{:}TFPI]}{dt} = k_{+,24}[TF{:}VIIa{:}Xa][TFPI]$$

A.2.3 Danforth - Third Timescale

$$\frac{d[TF]}{dt} = k_{-,1}[TF{:}VII] - k_{+,1}[TF][VII] - k_{+,2}[TF][VIIa]$$

$$\frac{d[VII]}{dt} = -k_{+,4}[VII][Xa] - k_{+,5}[VII][IIa]$$

$$\frac{d[TF{:}VII]}{dt} = -k_{-,1}[TF{:}VII] + k_{+,1}[TF][VII]$$

$$\frac{d[VIIa]}{dt} = k_{+,4}[VII][Xa] + k_{+,5}[VII][IIa]$$

$$\frac{d[TF{:}VIIa]}{dt} = -k_{-,2}[TF{:}VIIa] + k_{+,2}[TF][VIIa] + k_{-,6}[TF{:}VIIa{:}X] - k_{+,6}[TF{:}VIIa][X] + k_{-,8}[TF{:}VIIa{:}Xa] + k_{-,9}[TF{:}VIIa{:}IX] - k_{+,9}[TF{:}VIIa][IX] + k_{-,10}[TF{:}VIIa{:}IX] - k_{+,30}[TF{:}VIIa][AT]$$

$$\frac{d[Xa]}{dt} = k_{-,8}[TF{:}VIIa{:}Xa] + k_{-,15}[IXa{:}VIIIa{:}X] + k_{-,19}[Xa{:}Va] - k_{+,19}[Xa][Va] - k_{+,26}[Xa][AT]$$

$$\frac{d[IIa]}{dt} = k_{+,11}[II][Xa] + k_{+,22}[mIIa][Xa{:}Va] - k_{+,29}[IIa][AT]$$

$$\frac{d[X]}{dt} = -k_{+,6}[TF{:}VIIa][X] - k_{+,14}[IXa{:}VIIIa][X]$$

$$\frac{d[TF{:}VIIa{:}X]}{dt} = -k_{-,6}[TF{:}VIIa{:}X] + k_{+,6}[TF{:}VIIa][X] - k_{-,7}[TF{:}VIIa{:}X]$$

$$\frac{d[TF{:}VIIa{:}Xa]}{dt} = k_{-,7}[TF{:}VIIa{:}X] - k_{-,8}[TF{:}VIIa{:}Xa] + k_{-,24}[TF{:}VIIa{:}Xa{:}TFPI] - k_{+,24}[TF{:}VIIa{:}Xa][TFPI]$$

$$\frac{d[IX]}{dt} = k_{-,9}[TF{:}VIIa{:}IX] - k_{+,9}[TF{:}VIIa][IX]$$

$$\frac{d[TF{:}VIIa{:}IX]}{dt} = -k_{-,9}[TF{:}VIIa{:}IX] + k_{+,9}[TF{:}VIIa][IX] - k_{-,10}[TF{:}VIIa{:}IX]$$

$$\frac{d[IXa]}{dt} = k_{-,10}[TF{:}VIIa{:}IX] + k_{-,13}[IXa{:}VIIIa] - k_{+,13}[IXa][VIIIa] - k_{+,28}[IXa][AT]$$

$$\frac{d[II]}{dt} = k_{-,20}[Xa{:}Va{:}II] - k_{+,20}[Xa{:}Va][II]$$

$$\frac{d[VIII]}{dt} = -k_{+,12}[VIII][IIa]$$

$$\frac{d[VIIIa]}{dt} = k_{+,12}[VIII][IIa] - k_{-,16}[VIIIa]$$

$$\frac{d[IXa{:}VIIIa]}{dt} = -k_{-,13}[IXa{:}VIIIa] + k_{+,13}[IXa][VIIIa] - k_{+,14}[IXa{:}VIIIa][X] + k_{-,15}[IXa{:}VIIIa{:}X]$$

$$\frac{d[IXa{:}VIIIa{:}X]}{dt} = k_{+,14}[IXa{:}VIIIa][X] - k_{-,15}[IXa{:}VIIIa{:}X]$$

$$\frac{d[VIIIa1L]}{dt} = \frac{d[VIIIa2]}{dt} = k_{-,16}[VIIIa]$$

$$\frac{d[V]}{dt} = -k_{+,18}[V][IIa] - k_{+,32}[V][mIIa]$$

$$\frac{d[Va]}{dt} = k_{+,18}[V][IIa] + k_{+,32}[V][mIIa]$$

$$\frac{d[Xa{:}Va]}{dt} = -k_{-,19}[Xa{:}Va] + k_{+,19}[Xa][Va] + k_{-,20}[Xa{:}Va{:}II] - k_{+,20}[Xa{:}Va][II] + k_{-,21}[Xa{:}Va{:}II]$$

$$\frac{d[Xa{:}Va{:}II]}{dt} = -k_{-,20}[Xa{:}Va{:}II] + k_{+,20}[Xa{:}Va][II] - k_{-,21}[Xa{:}Va{:}II]$$

$$\frac{d[mIIa]}{dt} = k_{-,21}[Xa{:}Va{:}II] - k_{+,22}[mIIa][Xa{:}Va] - k_{+,27}[mIIa][AT]$$

$$\frac{d[TFPI]}{dt} = -k_{+,23}[Xa][TFPI] - k_{+,24}[TF{:}VIIa{:}Xa][TFPI]$$

$$\frac{d[Xa{:}TFPI]}{dt} = k_{+,23}[Xa][TFPI]$$

$$\frac{d[TF{:}VIIa{:}Xa{:}TFPI]}{dt} = k_{+,24}[TF{:}VIIa{:}Xa][TFPI]$$

$$\frac{d[AT]}{dt} = -k_{+,27}[mIIa][AT]$$

A.2.4 Danforth - Fourth Timescale

$$\frac{d[TF]}{dt} = k_{-,1}[TF{:}VII] - k_{+,1}[TF][VII] - k_{+,2}[TF][VIIa]$$

$$\frac{d[VII]}{dt} = -k_{+,4}[VII][Xa] - k_{+,5}[VII][IIa]$$
$$\frac{d[TF{:}VII]}{dt} = -k_{-,1}[TF{:}VII] + k_{+,1}[TF][VII]$$
$$\frac{d[VIIa]}{dt} = k_{+,4}[VII][Xa] + k_{+,5}[VII][IIa]$$
$$\frac{d[TF{:}VIIa]}{dt} = -k_{-,2}[TF{:}VIIa] + k_{+,2}[TF][VIIa] + k_{-,6}[TF{:}VIIa{:}X] - k_{+,6}[TF{:}VIIa][X]$$
$$+ k_{-,8}[TF{:}VIIa{:}Xa] - k_{+,8}[TF{:}VIIa][Xa] + k_{-,9}[TF{:}VIIa{:}IX] - k_{+,9}[TF{:}VIIa][IX]$$
$$+ k_{-,10}[TF{:}VIIa{:}IX] - k_{+,25}[TF{:}VIIa][Xa{:}TFPI] - k_{+,30}[TF{:}VIIa][AT]$$
$$\frac{d[Xa]}{dt} = k_{-,8}[TF{:}VIIa{:}Xa] + k_{-,15}[IXa{:}VIIIa{:}X] + k_{-,19}[Xa{:}Va] - k_{+,19}[Xa][Va]$$
$$- k_{+,26}[Xa][AT]$$
$$\frac{d[IIa]}{dt} = k_{+,22}[mIIa][Xa{:}Va] - k_{+,29}[IIa][AT]$$
$$\frac{d[X]}{dt} = -k_{+,14}[IXa{:}VIIIa][X]$$
$$\frac{d[TF{:}VIIa{:}X]}{dt} = -k_{-,6}[TF{:}VIIa{:}X] + k_{+,6}[TF{:}VIIa][X] - k_{-,7}[TF{:}VIIa{:}X]$$
$$\frac{d[TF{:}VIIa{:}Xa]}{dt} = k_{-,7}[TF{:}VIIa{:}X] - k_{-,8}[TF{:}VIIa{:}Xa] + k_{+,8}[TF{:}VIIa][Xa]$$
$$+ k_{-,24}[TF{:}VIIa{:}Xa{:}TFPI] - k_{+,24}[TF{:}VIIa{:}Xa][TFPI]$$
$$\frac{d[IX]}{dt} = k_{-,9}[TF{:}VIIa{:}IX] - k_{+,9}[TF{:}VIIa][IX]$$
$$\frac{d[TF{:}VIIa{:}IX]}{dt} = -k_{-,9}[TF{:}VIIa{:}IX] + k_{+,9}[TF{:}VIIa][IX] - k_{-,10}[TF{:}VIIa{:}IX]$$
$$\frac{d[IXa]}{dt} = k_{-,10}[TF{:}VIIa{:}IX] + k_{-,13}[IXa{:}VIIIa] - k_{+,13}[IXa][VIIIa]$$
$$+ k_{-,17}[IXa{:}VIIIa{:}X] + k_{-,17}[IXa{:}VIIIa] - k_{+,28}[IXa][AT]$$
$$\frac{d[II]}{dt} = k_{-,20}[Xa{:}Va{:}II] - k_{+,20}[Xa{:}Va][II]$$
$$\frac{d[VIIIa]}{dt} = -k_{-,16}[VIIIa]$$
$$\frac{d[IXa{:}VIIIa]}{dt} = -k_{-,13}[IXa{:}VIIIa] + k_{+,13}[IXa][VIIIa] + k_{-,14}[IXa{:}VIIIa{:}X]$$
$$- k_{+,14}[IXa{:}VIIIa][X] + k_{-,15}[IXa{:}VIIIa{:}X] - k_{-,17}[IXa{:}VIIIa]$$
$$\frac{d[IXa{:}VIIIa{:}X]}{dt} = -k_{-,14}[IXa{:}VIIIa{:}X] + k_{+,14}[IXa{:}VIIIa][X] - k_{-,15}[IXa{:}VIIIa{:}X]$$
$$- k_{-,17}[IXa{:}VIIIa{:}X]$$
$$\frac{d[VIIIa1L]}{dt} = \frac{d[VIIIa2]}{dt} = k_{-,16}[VIIIa]$$
$$\frac{d[Va]}{dt} = k_{-,19}[Xa{:}Va] - k_{+,19}[Xa][Va]$$
$$\frac{d[Xa{:}Va]}{dt} = -k_{-,19}[Xa{:}Va] + k_{+,19}[Xa][Va] + k_{-,20}[Xa{:}Va{:}II] - k_{+,20}[Xa{:}Va][II]$$
$$+ k_{-,21}[Xa{:}Va{:}II]$$
$$\frac{d[Xa{:}Va{:}II]}{dt} = -k_{-,20}[Xa{:}Va{:}II] + k_{+,20}[Xa{:}Va][II] - k_{-,21}[Xa{:}Va{:}II]$$
$$\frac{d[mIIa]}{dt} = k_{-,21}[Xa{:}Va{:}II] - k_{+,22}[mIIa][Xa{:}Va] - k_{+,27}[mIIa][AT]$$
$$\frac{d[TFPI]}{dt} = -k_{+,23}[Xa][TFPI] - k_{+,24}[TF{:}VIIa{:}Xa][TFPI]$$
$$\frac{d[Xa{:}TFPI]}{dt} = k_{+,23}[Xa][TFPI]$$

$$\frac{d[TF{:}VIIa{:}Xa{:}TFPI]}{dt} = k_{+,24}[TF{:}VIIa{:}Xa][TFPI]$$
$$\frac{d[AT]}{dt} = -k_{+,27}[mIIa][AT] - k_{+,29}[IIa][AT]$$

A.2.5 Danforth - Fifth Timescale

This timescale decouple thrombin from the majority of other species. The ODEs, and their solutions, are described in Section 2.7.

A.2.6 Tyurin - First Timescale

$$\frac{d[Va]}{dt} = k_{\text{cat}_{14}}[Xa][V]/(K_{m_{14}}(1 + [II]/K_{m_{11}} + [VII]/K_{m_{15}}) + [V])$$
$$\frac{d[Xa]}{dt} = k_{\text{cat}_9}[VIIa][X]/(K_{m_9}(1 + [IX]/K_{m_5}) + [X]) + k_{\text{cat}_{10}}[TF{:}VIIa][X]/(K_{m_{10}}(1 + [IX]/K_{m_6}) + [X])$$
$$\frac{d[Xa{:}Va]}{dt} = k_1[Va][Xa]$$
$$\frac{d[VIIIa]}{dt} = k_{\text{cat}_{17}}[IIa][VIII]/(K_{m_{17}}(1 + [XI]/K_{m_2} + [V]/K_{m_{13}}) + [VIII])$$
$$\frac{d[IXa]}{dt} = k_{\text{cat}_4}[XIa][IX]/(K_{m_4}(1 + [XI]/K_{m_3}) + [IX]) + k_{\text{cat}_5}[VIIa][IX]/(K_{m_5}(1 + [X]/K_{m_9}) + [IX])$$
$$\frac{d[VIIa]}{dt} = -k_3[VIIa][TF] + k_{\text{cat}_{15}}[Xa][VII]/(K_{m_{15}}(1 + [II]/K_{m_{11}} + [V]/K_{m_{14}} + [TF{:}VII]/K_{m_{16}}) + [VII])$$
$$\frac{d[TF]}{dt} = -k_5[VII][TF]$$
$$\frac{d[TF{:}VIIa]}{dt} = k_3[VIIa][TF]$$
$$\frac{d[VII]}{dt} = -k_5[VII][TF]$$
$$\frac{d[TF{:}VII]}{dt} = k_5[VII][TF]$$
$$\frac{d[IIa]}{dt} = -k_9[IIa][AT] + k_{\text{cat}_{12}}[Xa{:}Va][II]/(K_{m_{12}} + [II]) + k_{\text{cat}_{11}}[Xa][II]/(K_{m_{11}}(1 + [V]/K_{m_{13}} + [VII]/K_{m_{15}} + [TF{:}VII]/K_{m_{16}}) + [II])$$
$$\frac{d[Xa{:}TFPI]}{dt} = k_{15}[Xa][TFPI]$$
$$\frac{d[XIa]}{dt} = k_{\text{cat}_2}[IIa][XI]/(K_{m_2}(1 + [V]/K_{m_{13}} + [VIII]/K_{m_{17}}) + [XI]) + k_{\text{cat}_3}[XIa][XI]/(K_{m_3}(1 + [IX]/K_{m_4}) + [XI])$$
$$\frac{d[XI]}{dt} = -k_{\text{cat}_2}[IIa][XI]/(K_{m_2}(1 + [V]/K_{m_{13}} + [VIII]/K_{m_{17}}) + [XI]) - k_{\text{cat}_3}[XIa][XI]/(K_{m_3}(1 + [IX]/K_{m_4}) + [XI])$$
$$\frac{d[IX]}{dt} = -k_{\text{cat}_4}[XIa][IX]/(K_{m_4}(1 + [XI]/K_{m_3}) + [IX]) - k_{\text{cat}_5}[VIIa][IX]/(K_{m_5}(1 + [X]/K_{m_9}) + [IX])$$
$$\frac{d[X]}{dt} = -k_{\text{cat}_9}[VIIa][X]/(K_{m_9}(1 + [IX]/K_{m_5}) + [X])$$

$$\frac{d[II]}{dt} = -k_{\text{cat}_{12}}[Xa{:}Va][II]/(K_{m_{12}} + [II])$$
$$- k_{\text{cat}_{11}}[Xa][II]/(K_{m_{11}}(1 + [V]/K_{m_{13}} + [VII]/K_{m_{15}} + [TF{:}VII]/K_{m_{16}}) + [II])$$
$$\frac{d[V]}{dt} = -k_{\text{cat}_{14}}[Xa][V]/(K_{m_{14}}(1 + [II]/K_{m_{11}} + [VII]/K_{m_{15}} + [TF{:}VII]/K_{m_{16}}) + [V])$$
$$\frac{d[VIII]}{dt} = -k_{\text{cat}_{17}}[IIa][VIII]/(K_{m_{17}}(1 + [XI]/K_{m_2} + [V]/K_{m_{13}}) + [VIII])$$

A.2.7 Tyurin - Second Timescale

$$\frac{d[Va]}{dt} = k_{\text{cat}_{13}}[IIa][V]/(K_{m_{13}}(1 + [XI]/K_{m_2} + [VIII]/K_{m_{17}}) + [V])$$
$$+ k_{\text{cat}_{14}}[Xa][V]/(K_{m_{14}}(1 + [II]/K_{m_{11}} + [VII]/K_{m_{15}} + [TF{:}VII]/K_{m_{16}}) + [V])$$
$$\frac{d[Xa]}{dt} = -k_{13}[Xa][AT] - k_{15}[Xa][TFPI] + k_{\text{cat}_8}[IXa{:}VIIIa][X]/(K_{m_8} + [X])$$
$$+ k_{\text{cat}_9}[VIIa][X]/(K_{m_9}(1 + [IX]/K_{m_5}) + [X])$$
$$+ k_{\text{cat}_{10}}[TF{:}VIIa][X]/(K_{m_{10}}(1 + [IX]/K_{m_6}) + [X])$$
$$\frac{d[Xa{:}Va]}{dt} = k_1[Va][Xa]$$
$$\frac{d[VIIIa]}{dt} = k_{\text{cat}_{17}}[IIa][VIII]/(K_{m_{17}}(1 + [XI]/K_{m_2} + [V]/K_{m_{13}}) + [VIII])$$
$$- k_2[VIIIa][IXa]$$
$$\frac{d[IXa]}{dt} = k_{\text{cat}_4}[XIa][IX]/(K_{m_4}(1 + [XI]/K_{m_3}) + [IX])$$
$$\frac{d[IXa{:}VIIIa]}{dt} = k_2[VIIIa][IXa]$$
$$\frac{d[VIIa]}{dt} = -k_3[VIIa][TF]$$
$$+ k_{\text{cat}_{15}}[Xa][VII]/(K_{m_{15}}(1 + [II]/K_{m_{11}} + [V]/K_{m_{14}} + [TF{:}VII]/K_{m_{16}}) + [VII])$$
$$\frac{d[TF]}{dt} = -k_5[VII][TF]$$
$$\frac{d[TF{:}VIIa]}{dt} = k_3[VIIa][TF] - k_8[TF{:}VIIa][AT]$$
$$+ k_{\text{cat}_{16}}[Xa][TF{:}VII]/(K_{m_{16}}(1 + [II]/K_{m_{11}} + [V]/K_{m_{14}} + [VII]/K_{m_{15}}) + [TF{:}VII])$$
$$\frac{d[VII]}{dt} = -k_5[VII][TF]$$
$$\frac{d[TF{:}VII]}{dt} = k_5[VII][TF]$$
$$\frac{d[IIa]}{dt} = -k_9[IIa][AT] + k_{\text{cat}_{12}}[Xa{:}Va][II]/(K_{m_{12}} + [II])$$
$$\frac{d[Xa{:}TFPI]}{dt} = k_{15}[Xa][TFPI]$$
$$\frac{d[XIa]}{dt} = k_{\text{cat}_2}[IIa][XI]/(K_{m_2}(1 + [V]/K_{m_{13}} + [VIII]/K_{m_{17}}) + [XI])$$
$$+ k_{\text{cat}_3}[XIa][XI]/(K_{m_3}(1 + [IX]/K_{m_4}) + [XI])$$
$$\frac{d[XI]}{dt} = -k_{\text{cat}_2}[IIa][XI]/(K_{m_2}(1 + [V]/K_{m_{13}} + [VIII]/K_{m_{17}}) + [XI])$$
$$- k_{\text{cat}_3}[XIa][XI]/(K_{m_3}(1 + [IX]/K_{m_4}) + [XI])$$
$$\frac{d[IX]}{dt} = -k_{\text{cat}_4}[XIa][IX]/(K_{m_4}(1 + [XI]/K_{m_3}) + [IX])$$
$$\frac{d[X]}{dt} = -k_{\text{cat}_8}[IXa{:}VIIIa][X]/(K_{m_8} + [X]) - k_{\text{cat}_9}[VIIa][X]/(K_{m_9}(1 + [IX]/K_{m_5}) + [X])$$
$$\frac{d[II]}{dt} = -k_{\text{cat}_{12}}[Xa{:}Va][II]/(K_{m_{12}} + [II])$$

$$\frac{d[V]}{dt} = -k_{\text{cat}_{13}}[IIa][V]/(K_{m_{13}}(1+[XI]/K_{m_2}+[VIII]/K_{m_{17}})+[V]) \\ - k_{\text{cat}_{14}}[Xa][V]/(K_{m_{14}}(1+[II]/K_{m_{11}}+[VII]/K_{m_{15}}+[TF{:}VII]/K_{m_{16}})+[V])$$

$$\frac{d[VIII]}{dt} = -k_{\text{cat}_{17}}[IIa][VIII]/(K_{m_{17}}(1+[XI]/K_{m_2}+[V]/K_{m_{13}})+[VIII])$$

A.2.8 Tyurin - Third Timescale

$$\frac{d[Va]}{dt} = -k_1[Va][Xa] + k_{\text{cat}_{13}}[IIa][V]/(K_{m_{13}}(1+[XI]/K_{m_2}+[VIII]/K_{m_{17}})+[V]) \\ + k_{\text{cat}_{14}}[Xa][V]/(K_{m_{14}}(1+[II]/K_{m_{11}}+[VII]/K_{m_{15}}+[TF{:}VII]/K_{m_{16}})+[V]) \\ + k_{17}[Xa{:}Va][AT]$$

$$\frac{d[Xa]}{dt} = -k_1[Va][Xa] - k_{13}[Xa][AT] - k_{15}[Xa][TFPI] + k_{\text{cat}_8}[IXa{:}VIIIa][X]/(K_{m_8}+[X])$$

$$\frac{d[Xa{:}Va]}{dt} = k_1[Va][Xa] - k_{17}[Xa{:}Va][AT]$$

$$\frac{d[VIIIa]}{dt} = k_{\text{cat}_{17}}[IIa][VIII]/(K_{m_{17}}(1+[XI]/K_{m_2}+[V]/K_{m_{13}})+[VIII]) - k_2[VIIIa][IXa]$$

$$\frac{d[IXa]}{dt} = -k_{18}[IXa][AT] + k_{\text{cat}_4}[XIa][IX]/(K_{m_4}(1+[XI]/K_{m_3})+[IX])$$

$$\frac{d[IXa{:}VIIIa]}{dt} = k_2[VIIIa][IXa] - k_{19}[IXa{:}VIIIa][AT]$$

$$\frac{d[VIIa]}{dt} = k_{\text{cat}_{15}}[Xa][VII]/(K_{m_{15}}(1+[II]/K_{m_{11}}+[V]/K_{m_{14}}+[TF{:}VII]/K_{m_{16}})+[VII])$$

$$\frac{d[TF]}{dt} = -k_3[VIIa][TF] - k_5[VII][TF]$$

$$\frac{d[TF{:}VIIa]}{dt} = k_3[VIIa][TF] - k_7[TF{:}VIIa][Xa{:}TFPI] - k_8[TF{:}VIIa][AT] \\ + k_{\text{cat}_{16}}[Xa][TF{:}VII]/(K_{m_{16}}(1+[II]/K_{m_{11}}+[V]/K_{m_{14}}+[VII]/K_{m_{15}})+[TF{:}VII])$$

$$\frac{d[VII]}{dt} = -k_{\text{cat}_{15}}[Xa][VII]/(K_{m_{15}}(1+[II]/K_{m_{11}}+[V]/K_{m_{14}}+[TF{:}VII]/K_{m_{16}})+[VII])$$

$$\frac{d[TF{:}VII]}{dt} = k_5[VII][TF] \\ - k_{\text{cat}_{16}}[Xa][TF{:}VII]/(K_{m_{16}}(1+[II]/K_{m_{11}}+[V]/K_{m_{14}}+[VII]/K_{m_{15}})+[TF{:}VII])$$

$$\frac{d[AT]}{dt} = -k_9[IIa][AT]$$

$$\frac{d[IIa]}{dt} = -k_9[IIa][AT] + k_{\text{cat}_{12}}[Xa{:}Va][II]/(K_{m_{12}}+[II])$$

$$\frac{d[TFPI]}{dt} = -k_{15}[Xa][TFPI]$$

$$\frac{d[Xa{:}TFPI]}{dt} = -k_7[TF{:}VIIa][Xa{:}TFPI] + k_{15}[Xa][TFPI]$$

$$\frac{d[XIa]}{dt} = -k_{22}[XIa][AT] + k_{\text{cat}_3}[XIa][XI]/(K_{m_3}(1+[IX]/K_{m_4})+[XI]) \\ + k_{\text{cat}_2}[IIa][XI]/(K_{m_2}(1+[V]/K_{m_{13}}+[VIII]/K_{m_{17}})+[XI])$$

$$\frac{d[XI]}{dt} = -k_{\text{cat}_2}[IIa][XI]/(K_{m_2}(1+[V]/K_{m_{13}}+[VIII]/K_{m_{17}})+[XI]) \\ - k_{\text{cat}_3}[XIa][XI]/(K_{m_3}(1+[IX]/K_{m_4})+[XI])$$

$$\frac{d[IX]}{dt} = -k_{\text{cat}_4}[XIa][IX]/(K_{m_4}(1+[XI]/K_{m_3})+[IX])$$

$$\frac{d[X]}{dt} = -k_{\text{cat}_8}[IXa{:}VIIIa][X]/(K_{m_8}+[X])$$

$$\frac{d[II]}{dt} = -k_{\text{cat}_{12}}[Xa{:}Va][II]/(K_{m_{12}}+[II])$$

$$\frac{d[V]}{dt} = -k_{\text{cat}_{13}}[IIa][V]/(K_{m_{13}}(1+[XI]/K_{m_2}+[VIII]/K_{m_{17}})+[V]) \\ - k_{\text{cat}_{14}}[Xa][V]/(K_{m_{14}}(1+[II]/K_{m_{11}}+[VII]/K_{m_{15}}+[TF{:}VII]/K_{m_{16}})+[V])$$

$$\frac{d[VIII]}{dt} = -k_{\text{cat}_{17}}[IIa][VIII]/(K_{m_{17}}(1+[XI]/K_{m_2}+[V]/K_{m_{13}})+[VIII])$$

A.2.9 Tyurin - Fourth and Fifth Timescales

Both of these timescales decouple thrombin from the majority of other species. The ODEs, and their solutions, are described in Section 2.7.

A.3 Unified Models

A.3.1 Unified Model

$$\frac{d[TF]}{dt} = -k_1[TF][VII] + k_2[TF{:}VII] - k_3[TF][VIIa] + k_4[TF{:}VIIa]$$

$$\frac{d[VII]}{dt} = -k_1[TF][VII] + k_2[TF{:}VII] - k_5[VII][Xa] + k_6[VII{:}Xa] - k_{11}[VII][IIa] \\ + k_{12}[VII{:}IIa] - k_{17}[VII][IXa] + k_{18}[VII{:}IXa] - k_{23}[VII][TF{:}VIIa] + k_{24}[VII{:}TF{:}VIIa]$$

$$\frac{d[VIIa]}{dt} = -k_3[TF][VIIa] + k_4[TF{:}VIIa] + k_7[VII{:}Xa] + k_{13}[VII{:}IIa] + k_{19}[VII{:}IXa] \\ + k_{25}[VII{:}TF{:}VIIa] - k_{30}[X][VIIa] + k_{31}[X{:}VIIa] + k_{32}[X{:}VIIa] - k_{66}[IX][VIIa] \\ + k_{67}[IX{:}VIIa] + k_{68}[IX{:}VIIa]$$

$$\frac{d[TF{:}VII]}{dt} = k_1[TF][VII] - k_2[TF{:}VII] - k_8[TF{:}VII][Xa] + k_9[TF{:}VII{:}Xa] \\ - k_{14}[TF{:}VII][IIa] + k_{15}[TF{:}VII{:}IIa] - k_{20}[TF{:}VII][IXa] + k_{21}[TF{:}VII{:}IXa]$$

$$\frac{d[TF{:}VIIa]}{dt} = k_3[TF][VIIa] - k_4[TF{:}VIIa] + k_{10}[TF{:}VII{:}Xa] + k_{16}[TF{:}VII{:}IIa] \\ + k_{22}[TF{:}VII{:}IXa] - k_{23}[VII][TF{:}VIIa] + k_{24}[VII{:}TF{:}VIIa] + k_{25}[VII{:}TF{:}VIIa] \\ - k_{26}[TF{:}VIIa][AT] - k_{27}[X][TF{:}VIIa] + k_{28}[X{:}TF{:}VIIa] + k_{29}[X{:}TF{:}VIIa] \\ - k_{63}[IX][TF{:}VIIa] + k_{64}[IX{:}TF{:}VIIa] + k_{65}[IX{:}TF{:}VIIa] \\ - k_{84}[Xa{:}TFPI][TF{:}VIIa] + k_{85}[TF{:}VIIa{:}Xa{:}TFPI]$$

$$\frac{d[X]}{dt} = -k_{27}[X][TF{:}VIIa] + k_{28}[X{:}TF{:}VIIa] - k_{30}[X][VIIa] + k_{31}[X{:}VIIa] \\ - k_{33}[X][IXa{:}VIIIa] + k_{34}[X{:}IXa{:}VIIIa] - k_{36}[X][IXa] + k_{37}[X{:}IXa]$$

$$\frac{d[Xa]}{dt} = -k_5[VII][Xa] + k_6[VII{:}Xa] + k_7[VII{:}Xa] - k_8[TF{:}VII][Xa] + k_9[TF{:}VII{:}Xa] \\ + k_{10}[TF{:}VII{:}Xa] + k_{29}[X{:}TF{:}VIIa] + k_{32}[X{:}VIIa] + k_{35}[X{:}IXa{:}VIIIa] \\ + k_{38}[X{:}IXa] - k_{42}[V][Xa] + k_{43}[V{:}Xa] + k_{44}[V{:}Xa] - k_{45}[Xa][Va] + k_{46}[Xa{:}Va] \\ - k_{47}[Xa][AT] - k_{49}[II][Xa] + k_{50}[II{:}Xa] + k_{51}[II{:}Xa] - k_{75}[VIII][Xa] + k_{76}[VIII{:}Xa] \\ + k_{77}[VIII{:}Xa] - k_{82}[Xa][TFPI] + k_{83}[Xa{:}TFPI]$$

$$\frac{d[II]}{dt} = -k_{49}[II][Xa] + k_{50}[II{:}Xa] - k_{52}[II][Xa{:}Va] + k_{53}[II{:}Xa{:}Va]$$

$$\frac{d[IIa]}{dt} = -k_{11}[VII][IIa] + k_{12}[VII{:}IIa] + k_{13}[VII{:}IIa] - k_{14}[TF{:}VII][IIa] \\ + k_{15}[TF{:}VII{:}IIa] + k_{16}[TF{:}VII{:}IIa] - k_{39}[V][IIa] + k_{40}[V{:}IIa] + k_{41}[V{:}IIa] \\ + k_{51}[II{:}Xa] + k_{54}[II{:}Xa{:}Va] - k_{55}[IIa][AT] - k_{56}[XI][IIa] + k_{57}[XI{:}IIa] \\ + k_{58}[XI{:}IIa] - k_{72}[VIII][IIa] + k_{73}[VIII{:}IIa] + k_{74}[VIII{:}IIa] \\ - k_{86}[IIa][Substrate] + k_{87}[IIa{:}Substrate] + k_{88}[IIa{:}Substrate]$$

$$\frac{d[V]}{dt} = -k_{39}[V][IIa] + k_{40}[V{:}IIa] - k_{42}[V][Xa] + k_{43}[V{:}Xa]$$
$$\frac{d[Va]}{dt} = k_{41}[V{:}IIa] + k_{44}[V{:}Xa] - k_{45}[Xa][Va] + k_{46}[Xa{:}Va] + k_{48}[Xa{:}Va][AT]$$
$$\frac{d[VIII]}{dt} = -k_{72}[VIII][IIa] + k_{73}[VIII{:}IIa] - k_{75}[VIII][Xa] + k_{76}[VIII{:}Xa]$$
$$\frac{d[VIIIa]}{dt} = k_{74}[VIII{:}IIa] + k_{77}[VIII{:}Xa] - k_{78}[IXa][VIIIa] + k_{79}[IXa{:}VIIIa] + k_{81}[IXa{:}VIIIa][AT]$$
$$\frac{d[XI]}{dt} = -k_{56}[XI][IIa] + k_{57}[XI{:}IIa] - k_{59}[XI][XIa] + k_{60}[XI{:}XIa]$$
$$\frac{d[XIa]}{dt} = k_{58}[XI{:}IIa] - k_{59}[XI][XIa] + k_{60}[XI{:}XIa] + 2k_{61}[XI{:}XIa] - k_{62}[XIa][AT] - k_{69}[IX][XIa] + k_{70}[IX{:}XIa] + k_{71}[IX{:}XIa]$$
$$\frac{d[IX]}{dt} = -k_{63}[IX][TF{:}VIIa] + k_{64}[IX{:}TF{:}VIIa] - k_{66}[IX][VIIa] + k_{67}[IX{:}VIIa] - k_{69}[IX][XIa] + k_{70}[IX{:}XIa]$$
$$\frac{d[IXa]}{dt} = -k_{17}[VII][IXa] + k_{18}[VII{:}IXa] + k_{19}[VII{:}IXa] - k_{20}[TF{:}VII][IXa] + k_{21}[TF{:}VII{:}IXa] + k_{22}[TF{:}VII{:}IXa] - k_{36}[X][IXa] + k_{37}[X{:}IXa] + k_{38}[X{:}IXa] + k_{65}[IX{:}TF{:}VIIa] + k_{68}[IX{:}VIIa] + k_{71}[IX{:}XIa] - k_{78}[IXa][VIIIa] + k_{79}[IXa{:}VIIIa] - k_{80}[IXa][AT]$$
$$\frac{d[IXa{:}VIIIa]}{dt} = -k_{33}[X][IXa{:}VIIIa] + k_{34}[X{:}IXa{:}VIIIa] + k_{35}[X{:}IXa{:}VIIIa] + k_{78}[IXa][VIIIa] - k_{79}[IXa{:}VIIIa] - k_{81}[IXa{:}VIIIa][AT]$$
$$\frac{d[Xa{:}Va]}{dt} = k_{45}[Xa][Va] - k_{46}[Xa{:}Va] - k_{48}[Xa{:}Va][AT] - k_{52}[II][Xa{:}Va] + k_{53}[II{:}Xa{:}Va] + k_{54}[II{:}Xa{:}Va]$$
$$\frac{d[TFPI]}{dt} = -k_{82}[Xa][TFPI] + k_{83}[Xa{:}TFPI]$$
$$\frac{d[Xa{:}TFPI]}{dt} = k_{82}[Xa][TFPI] - k_{83}[Xa{:}TFPI] - k_{84}[Xa{:}TFPI][TF{:}VIIa] + k_{85}[TF{:}VIIa{:}Xa{:}TFPI]$$
$$\frac{d[TF{:}VIIa{:}Xa{:}TFPI]}{dt} = k_{84}[Xa{:}TFPI][TF{:}VIIa] - k_{85}[TF{:}VIIa{:}Xa{:}TFPI]$$
$$\frac{d[AT]}{dt} = -k_{26}[TF{:}VIIa][AT] - k_{47}[Xa][AT] - k_{48}[Xa{:}Va][AT] - k_{55}[IIa][AT] - k_{62}[XIa][AT] - k_{80}[IXa][AT] - k_{81}[IXa{:}VIIIa][AT]$$
$$\frac{d[VII{:}Xa]}{dt} = k_5[VII][Xa] - k_6[VII{:}Xa] - k_7[VII{:}Xa]$$
$$\frac{d[TF{:}VII{:}Xa]}{dt} = k_8[TF{:}VII][Xa] - k_9[TF{:}VII{:}Xa] - k_{10}[TF{:}VII{:}Xa]$$
$$\frac{d[VII{:}IIa]}{dt} = k_{11}[VII][IIa] - k_{12}[VII{:}IIa] - k_{13}[VII{:}IIa]$$
$$\frac{d[TF{:}VII{:}IIa]}{dt} = k_{14}[TF{:}VII][IIa] - k_{15}[TF{:}VII{:}IIa] - k_{16}[TF{:}VII{:}IIa]$$
$$\frac{d[VII{:}IXa]}{dt} = k_{17}[VII][IXa] - k_{18}[VII{:}IXa] - k_{19}[VII{:}IXa]$$
$$\frac{d[TF{:}VII{:}IXa]}{dt} = k_{20}[TF{:}VII][IXa] - k_{21}[TF{:}VII{:}IXa] - k_{22}[TF{:}VII{:}IXa]$$
$$\frac{d[VII{:}TF{:}VIIa]}{dt} = k_{23}[VII][TF{:}VIIa] - k_{24}[VII{:}TF{:}VIIa] - k_{25}[VII{:}TF{:}VIIa]$$
$$\frac{d[X{:}TF{:}VIIa]}{dt} = k_{27}[X][TF{:}VIIa] - k_{28}[X{:}TF{:}VIIa] - k_{29}[X{:}TF{:}VIIa]$$

$$\frac{d[X{:}VIIa]}{dt} = k_{30}[X][VIIa] - k_{31}[X{:}VIIa] - k_{32}[X{:}VIIa]$$
$$\frac{d[X{:}IXa{:}VIIIa]}{dt} = k_{33}[X][IXa{:}VIIIa] - k_{34}[X{:}IXa{:}VIIIa] - k_{35}[X{:}IXa{:}VIIIa]$$
$$\frac{d[X{:}IXa]}{dt} = k_{36}[X][IXa] - k_{37}[X{:}IXa] - k_{38}[X{:}IXa]$$
$$\frac{d[V{:}IIa]}{dt} = k_{39}[V][IIa] - k_{40}[V{:}IIa] - k_{41}[V{:}IIa]$$
$$\frac{d[V{:}Xa]}{dt} = k_{42}[V][Xa] - k_{43}[V{:}Xa] + k_{44}[V{:}Xa]$$
$$\frac{d[II{:}Xa]}{dt} = k_{49}[II][Xa] - k_{50}[II{:}Xa] - k_{51}[II{:}Xa]$$
$$\frac{d[II{:}Xa{:}Va]}{dt} = k_{52}[II][Xa{:}Va] - k_{53}[II{:}Xa{:}Va] - k_{54}[II{:}Xa{:}Va]$$
$$\frac{d[XI{:}IIa]}{dt} = k_{56}[XI][IIa] - k_{57}[XI{:}IIa] - k_{58}[XI{:}IIa]$$
$$\frac{d[XI{:}XIa]}{dt} = k_{59}[XI][XIa] - k_{60}[XI{:}XIa] - k_{61}[XI{:}XIa]$$
$$\frac{d[IX{:}TF{:}VIIa]}{dt} = k_{63}[IX][TF{:}VIIa] - k_{64}[IX{:}TF{:}VIIa] - k_{65}[IX{:}TF{:}VIIa]$$
$$\frac{d[IX{:}VIIa]}{dt} = k_{66}[IX][VIIa] - k_{67}[IX{:}VIIa] - k_{68}[IX{:}VIIa]$$
$$\frac{d[IX{:}XIa]}{dt} = k_{69}[IX][XIa] - k_{70}[IX{:}XIa] + k_{71}[IX{:}XIa]$$
$$\frac{d[VIII{:}IIa]}{dt} = k_{72}[VIII][IIa] - k_{73}[VIII{:}IIa] - k_{74}[VIII{:}IIa]$$
$$\frac{d[VIII{:}Xa]}{dt} = k_{75}[VIII][Xa] - k_{76}[VIII{:}Xa] - k_{77}[VIII{:}Xa]$$
$$\frac{d[Substrate]}{dt} = -k_{86}[IIa][Substrate] + k_{87}[IIa{:}Substrate]$$
$$\frac{d[ActiveSubstrate]}{dt} = k_{88}[IIa{:}Substrate]$$
$$\frac{d[IIa{:}Substrate]}{dt} = k_{86}[IIa][Substrate] - k_{87}[IIa{:}Substrate] - k_{88}[IIa{:}Substrate]$$

A.3.2 Expanded Unified Model

$$\frac{d[TF]}{dt} = -k_1[TF][VII] + k_2[TF{:}VII] - k_3[TF][VIIa] + k_4[TF{:}VIIa]$$
$$\begin{aligned}\frac{d[VII]}{dt} = &-k_1[TF][VII] + k_2[TF{:}VII] - k_5[VII][Xa] + k_6[VII{:}Xa] - k_{11}[VII][IIa] \\ &+ k_{12}[VII{:}IIa] - k_{17}[VII][IXa] + k_{18}[VII{:}IXa] - k_{23}[VII][TF{:}VIIa] + k_{24}[VII{:}TF{:}VIIa]\end{aligned}$$
$$\begin{aligned}\frac{d[VIIa]}{dt} = &-k_3[TF][VIIa] + k_4[TF{:}VIIa] + k_7[VII{:}Xa] + k_{13}[VII{:}IIa] + k_{19}[VII{:}IXa] \\ &+ k_{25}[VII{:}TF{:}VIIa] - k_{30}[X][VIIa] + k_{31}[X{:}VIIa] + k_{32}[X{:}VIIa] \\ &- k_{66}[IX][VIIa] + k_{67}[IX{:}VIIa] + k_{68}[IX{:}VIIa]\end{aligned}$$
$$\begin{aligned}\frac{d[TF{:}VII]}{dt} = &\ k_1[TF][VII] - k_2[TF{:}VII] - k_8[TF{:}VII][Xa] + k_9[TF{:}VII{:}Xa] \\ &- k_{14}[TF{:}VII][IIa] + k_{15}[TF{:}VII{:}IIa] - k_{20}[TF{:}VII][IXa] + k_{21}[TF{:}VII{:}IXa]\end{aligned}$$

$$\frac{d[TF{:}VIIa]}{dt} = k_3[TF][VIIa] - k_4[TF{:}VIIa] + k_{10}[TF{:}VII{:}Xa] + k_{16}[TF{:}VII{:}IIa] + k_{22}[TF{:}VII{:}IXa] - k_{23}[VII][TF{:}VIIa] + k_{24}[VII{:}TF{:}VIIa] + k_{25}[VII{:}TF{:}VIIa] - k_{26}[TF{:}VIIa][AT] - k_{27}[X][TF{:}VIIa] + k_{28}[X{:}TF{:}VIIa] + k_{29}[X{:}TF{:}VIIa] - k_{63}[IX][TF{:}VIIa] + k_{64}[IX{:}TF{:}VIIa] + k_{65}[IX{:}TF{:}VIIa] - k_{84}[Xa{:}TFPI][TF{:}VIIa] + k_{85}[TF{:}VIIa{:}Xa{:}TFPI] - k_{89}[TF{:}VIIa][Xa] + k_{90}[TF{:}VIIa{:}Xa] - k_{84}[Xa{=}TFPI][TF{:}VIIa] + k_{85}[TF{:}VIIa{:}Xa{=}TFPI] - k_{84}[Xa{:}TFPI{:}PS][TF{:}VIIa] + k_{85}[TF{:}VIIa{:}Xa{:}TFPI{:}PS] - k_{84}[Xa{=}TFPI{:}PS][TF{:}VIIa] + k_{85}[TF{:}VIIa{:}Xa{=}TFPI{:}PS]$$

$$\frac{d[X]}{dt} = -k_{27}[X][TF{:}VIIa] + k_{28}[X{:}TF{:}VIIa] - k_{30}[X][VIIa] + k_{31}[X{:}VIIa] - k_{33}[X][IXa{:}VIIIa] + k_{34}[X{:}IXa{:}VIIIa] - k_{36}[X][IXa] + k_{37}[X{:}IXa]$$

$$\frac{d[Xa]}{dt} = -k_5[VII][Xa] + k_6[VII{:}Xa] + k_7[VII{:}Xa] - k_8[TF{:}VII][Xa] + k_9[TF{:}VII{:}Xa] + k_{10}[TF{:}VII{:}Xa] + k_{29}[X{:}TF{:}VIIa] + k_{32}[X{:}VIIa] + k_{35}[X{:}IXa{:}VIIIa] + k_{38}[X{:}IXa] - k_{42}[V][Xa] + k_{43}[V{:}Xa] + k_{44}[V{:}Xa] - k_{45}[Xa][Va] + k_{46}[Xa{:}Va] - k_{47}[Xa][AT] - k_{49}[II][Xa] + k_{50}[II{:}Xa] + k_{51}[II{:}Xa] - k_{75}[VIII][Xa] + k_{76}[VIII{:}Xa] + k_{77}[VIII{:}Xa] - k_{82}[Xa][TFPI] + k_{83}[Xa{:}TFPI] - k_{89}[TF{:}VIIa][Xa] + k_{90}[TF{:}VIIa{:}Xa] - k_{92}[Xa][\alpha_1{-}AT] - k_{110}[TFPI{:}PS][Xa] + k_{111}[Xa{:}TFPI{:}PS]$$

$$\frac{d[II]}{dt} = -k_{49}[II][Xa] + k_{50}[II{:}Xa] - k_{52}[II][Xa{:}Va] + k_{53}[II{:}Xa{:}Va]$$

$$\frac{d[IIa]}{dt} = -k_{11}[VII][IIa] + k_{12}[VII{:}IIa] + k_{13}[VII{:}IIa] - k_{14}[TF{:}VII][IIa] + k_{15}[TF{:}VII{:}IIa] + k_{16}[TF{:}VII{:}IIa] - k_{39}[V][IIa] + k_{40}[V{:}IIa] + k_{41}[V{:}IIa] + k_{51}[II{:}Xa] + k_{54}[II{:}Xa{:}Va] - k_{55}[IIa][AT] - k_{56}[XI][IIa] + k_{57}[XI{:}IIa] + k_{58}[XI{:}IIa] - k_{72}[VIII][IIa] + k_{73}[VIII{:}IIa] + k_{74}[VIII{:}IIa] - k_{86}[IIa][Substrate] + k_{87}[IIa{:}Substrate] + k_{88}[IIa{:}Substrate] - k_{91}[IIa][\alpha_1{-}AT] - k_{96}[IIa][\alpha_2{-}M]$$

$$\frac{d[V]}{dt} = -k_{39}[V][IIa] + k_{40}[V{:}IIa] - k_{42}[V][Xa] + k_{43}[V{:}Xa]$$

$$\frac{d[Va]}{dt} = k_{41}[V{:}IIa] + k_{44}[V{:}Xa] - k_{45}[Xa][Va] + k_{46}[Xa{:}Va] + k_{48}[Xa{:}Va][AT] + k_{93}[Xa{:}Va][\alpha_1{-}AT]$$

$$\frac{d[VIII]}{dt} = -k_{72}[VIII][IIa] + k_{73}[VIII{:}IIa] - k_{75}[VIII][Xa] + k_{76}[VIII{:}Xa] - k_{102}[IXa][VIII] + k_{103}[IXa{:}VIII]$$

$$\frac{d[VIIIa]}{dt} = k_{74}[VIII{:}IIa] + k_{77}[VIII{:}Xa] - k_{78}[IXa][VIIIa] + k_{79}[IXa{:}VIIIa] + k_{81}[IXa{:}VIIIa][AT] - k_{99}[VIIIa] + k_{100}[VIIIa1L][VIIIa2] + k_{104}[IXa{:}VIII]$$

$$\frac{d[XI]}{dt} = -k_{56}[XI][IIa] + k_{57}[XI{:}IIa] - k_{59}[XI][XIa] + k_{60}[XI{:}XIa]$$

$$\frac{d[XIa]}{dt} = k_{58}[XI{:}IIa] - k_{59}[XI][XIa] + k_{60}[XI{:}XIa] + 2k_{61}[XI{:}XIa] - k_{62}[XIa][AT] - k_{69}[IX][XIa] + k_{70}[IX{:}XIa] + k_{71}[IX{:}XIa] - k_{94}[XIa][\alpha_1{-}AT] - k_{95}[XIa][\alpha_2{-}AP] - k_{97}[XIa][C1{-}inh] - k_{98}[XIa][PAI1]$$

$$\frac{d[IX]}{dt} = -k_{63}[IX][TF{:}VIIa] + k_{64}[IX{:}TF{:}VIIa] - k_{66}[IX][VIIa] + k_{67}[IX{:}VIIa] - k_{69}[IX][XIa] + k_{70}[IX{:}XIa]$$

$$\frac{d[IXa]}{dt} = -k_{17}[VII][IXa] + k_{18}[VII{:}IXa] + k_{19}[VII{:}IXa] - k_{20}[TF{:}VII][IXa] + k_{21}[TF{:}VII{:}IXa] + k_{22}[TF{:}VII{:}IXa] - k_{36}[X][IXa] + k_{37}[X{:}IXa] + k_{38}[X{:}IXa] + k_{65}[IX{:}TF{:}VIIa] + k_{68}[IX{:}VIIa] + k_{71}[IX{:}XIa] - k_{78}[IXa][VIIIa] + k_{79}[IXa{:}VIIIa] - k_{80}[IXa][AT] + k_{101}[IXa{:}VIIIa] - k_{102}[IXa][VIII] + k_{103}[IXa{:}VIII] + k_{104}[IXa{:}VIII]$$

$$\frac{d[IXa{:}VIIIa]}{dt} = -k_{33}[X][IXa{:}VIIIa] + k_{34}[X{:}IXa{:}VIIIa] + k_{35}[X{:}IXa{:}VIIIa] + k_{78}[IXa][VIIIa] - k_{79}[IXa{:}VIIIa] - k_{81}[IXa{:}VIIIa][AT] - k_{101}[IXa{:}VIIIa]$$

$$\frac{d[Xa{:}Va]}{dt} = k_{45}[Xa][Va] - k_{46}[Xa{:}Va] - k_{48}[Xa{:}Va][AT] - k_{52}[II][Xa{:}Va] + k_{53}[II{:}Xa{:}Va] + k_{54}[II{:}Xa{:}Va] - k_{93}[Xa{:}Va][\alpha_1 - AT]$$

$$\frac{d[TFPI]}{dt} = -k_{82}[Xa][TFPI] + k_{83}[Xa{:}TFPI] - k_{107}[TF{:}VIIa{:}Xa][TFPI] - k_{108}[PS][TFPI] + k_{109}[TFPI{:}PS]$$

$$\frac{d[Xa{:}TFPI]}{dt} = k_{82}[Xa][TFPI] - k_{83}[Xa{:}TFPI] - k_{84}[Xa{:}TFPI][TF{:}VIIa] + k_{85}[TF{:}VIIa{:}Xa{:}TFPI] - k_{105}[Xa{:}TFPI] + k_{106}[Xa{=}TFPI] - k_{105}[Xa{:}TFPI] + k_{106}[Xa{=}TFPI] - k_{108}[Xa{:}TFPI][PS] + k_{109}[Xa{:}TFPI{:}PS]$$

$$\frac{d[TF{:}VIIa{:}Xa{:}TFPI]}{dt} = k_{84}[Xa{:}TFPI][TF{:}VIIa] - k_{85}[TF{:}VIIa{:}Xa{:}TFPI] + k_{107}[TF{:}VIIa{:}Xa][TFPI] - k_{105}[TF{:}VIIa{:}Xa{:}TFPI] + k_{106}[TF{:}VIIa{:}Xa{=}TFPI] - k_{108}[TF{:}VIIa{:}Xa{:}TFPI][PS] + k_{109}[TF{:}VIIa{:}Xa{:}TFPI{:}PS]$$

$$\frac{d[AT]}{dt} = -k_{26}[TF{:}VIIa][AT] - k_{47}[Xa][AT] - k_{48}[Xa{:}Va][AT] - k_{55}[IIa][AT] - k_{62}[XIa][AT] - k_{80}[IXa][AT] - k_{81}[IXa{:}VIIIa][AT]$$

$$\frac{d[VII{:}Xa]}{dt} = k_5[VII][Xa] - k_6[VII{:}Xa] - k_7[VII{:}Xa]$$

$$\frac{d[TF{:}VII{:}Xa]}{dt} = k_8[TF{:}VII][Xa] - k_9[TF{:}VII{:}Xa] - k_{10}[TF{:}VII{:}Xa]$$

$$\frac{d[VII{:}IIa]}{dt} = k_{11}[VII][IIa] - k_{12}[VII{:}IIa] - k_{13}[VII{:}IIa]$$

$$\frac{d[TF{:}VII{:}IIa]}{dt} = k_{14}[TF{:}VII][IIa] - k_{15}[TF{:}VII{:}IIa] - k_{16}[TF{:}VII{:}IIa]$$

$$\frac{d[VII{:}IXa]}{dt} = k_{17}[VII][IXa] - k_{18}[VII{:}IXa] - k_{19}[VII{:}IXa]$$

$$\frac{d[TF{:}VII{:}IXa]}{dt} = k_{20}[TF{:}VII][IXa] - k_{21}[TF{:}VII{:}IXa] - k_{22}[TF{:}VII{:}IXa]$$

$$\frac{d[VII{:}TF{:}VIIa]}{dt} = k_{23}[VII][TF{:}VIIa] - k_{24}[VII{:}TF{:}VIIa] - k_{25}[VII{:}TF{:}VIIa]$$

$$\frac{d[X{:}TF{:}VIIa]}{dt} = k_{27}[X][TF{:}VIIa] - k_{28}[X{:}TF{:}VIIa] - k_{29}[X{:}TF{:}VIIa]$$

$$\frac{d[X{:}VIIa]}{dt} = k_{30}[X][VIIa] - k_{31}[X{:}VIIa] - k_{32}[X{:}VIIa]$$

$$\frac{d[X{:}IXa{:}VIIIa]}{dt} = k_{33}[X][IXa{:}VIIIa] - k_{34}[X{:}IXa{:}VIIIa] - k_{35}[X{:}IXa{:}VIIIa]$$

$$\frac{d[X{:}IXa]}{dt} = k_{36}[X][IXa] - k_{37}[X{:}IXa] - k_{38}[X{:}IXa]$$

$$\frac{d[V{:}IIa]}{dt} = k_{39}[V][IIa] - k_{40}[V{:}IIa] - k_{41}[V{:}IIa]$$

$$\frac{d[V{:}Xa]}{dt} = k_{42}[V][Xa] - k_{43}[V{:}Xa] + k_{44}[V{:}Xa]$$

$$\frac{d[II{:}Xa]}{dt} = k_{49}[II][Xa] - k_{50}[II{:}Xa] - k_{51}[II{:}Xa]$$

$$\frac{d[II{:}Xa{:}Va]}{dt} = k_{52}[II][Xa{:}Va] - k_{53}[II{:}Xa{:}Va] - k_{54}[II{:}Xa{:}Va]$$
$$\frac{d[XI{:}IIa]}{dt} = k_{56}[XI][IIa] - k_{57}[XI{:}IIa] - k_{58}[XI{:}IIa]$$
$$\frac{d[XI{:}XIa]}{dt} = k_{59}[XI][XIa] - k_{60}[XI{:}XIa] - k_{61}[XI{:}XIa]$$
$$\frac{d[IX{:}TF{:}VIIa]}{dt} = k_{63}[IX][TF{:}VIIa] - k_{64}[IX{:}TF{:}VIIa] - k_{65}[IX{:}TF{:}VIIa]$$
$$\frac{d[IX{:}VIIa]}{dt} = k_{66}[IX][VIIa] - k_{67}[IX{:}VIIa] - k_{68}[IX{:}VIIa]$$
$$\frac{d[IX{:}XIa]}{dt} = k_{69}[IX][XIa] - k_{70}[IX{:}XIa] + k_{71}[IX{:}XIa]$$
$$\frac{d[VIII{:}IIa]}{dt} = k_{72}[VIII][IIa] - k_{73}[VIII{:}IIa] - k_{74}[VIII{:}IIa]$$
$$\frac{d[VIII{:}Xa]}{dt} = k_{75}[VIII][Xa] - k_{76}[VIII{:}Xa] - k_{77}[VIII{:}Xa]$$
$$\frac{d[Substrate]}{dt} = -k_{86}[IIa][Substrate] + k_{87}[IIa{:}Substrate]$$
$$\frac{d[ActiveSubstrate]}{dt} = k_{88}[IIa{:}Substrate]$$
$$\frac{d[IIa{:}Substrate]}{dt} = k_{86}[IIa][Substrate] - k_{87}[IIa{:}Substrate] - k_{88}[IIa{:}Substrate]$$
$$\frac{d[TF{:}VIIa{:}Xa]}{dt} = k_{89}[TF{:}VIIa][Xa] - k_{90}[TF{:}VIIa{:}Xa] - k_{107}[TF{:}VIIa{:}Xa][TFPI] - k_{107}[TF{:}VIIa{:}Xa][TFPI{:}PS]$$
$$\frac{d[\alpha_1{-}AT]}{dt} = -k_{91}[IIa][\alpha_1{-}AT] - k_{92}[Xa][\alpha_1{-}AT] - k_{93}[Xa{:}Va][\alpha_1{-}AT] - k_{94}[XIa][\alpha_1{-}AT]$$
$$\frac{d[\alpha_2{-}AP]}{dt} = -k_{95}[XIa][\alpha_2{-}AP]$$
$$\frac{d[\alpha_2{-}M]}{dt} = -k_{96}[IIa][\alpha_2{-}M]$$
$$\frac{d[C1{-}inh]}{dt} = -k_{97}[XIa][C1{-}inh]$$
$$\frac{d[PAI1]}{dt} = -k_{98}[XIa][PAI1]$$
$$\frac{d[VIIIa1L]}{dt} = \frac{d[VIIIa2]}{dt} = k_{99}[VIIIa] - k_{100}[VIIIa1L][VIIIa2] + k_{101}[IXa{:}VIIIa]$$
$$\frac{d[IXa{:}VIII]}{dt} = k_{102}[IXa][VIII] - k_{103}[IXa{:}VIII] - k_{104}[IXa{:}VIII]$$
$$\frac{d[PS]}{dt} = -k_{108}[PS][TFPI] + k_{109}[TFPI{:}PS] - k_{108}[Xa{:}TFPI][PS] + k_{109}[Xa{:}TFPI{:}PS] - k_{108}[Xa{=}TFPI][PS] + k_{109}[Xa{=}TFPI{:}PS] - k_{108}[TF{:}VIIa{:}Xa{:}TFPI][PS] + k_{109}[TF{:}VIIa{:}Xa{:}TFPI{:}PS] - k_{108}[TF{:}VIIa{:}Xa{=}TFPI][PS] - k_{109}[TF{:}VIIa{:}Xa{=}TFPI{:}PS]$$
$$\frac{d[Xa{=}TFPI]}{dt} = k_{105}[Xa{:}TFPI] - k_{106}[Xa{=}TFPI] + k_{105}[Xa{:}TFPI] - k_{106}[Xa{=}TFPI] - k_{84}[Xa{=}TFPI][TF{:}VIIa] + k_{85}[TF{:}VIIa{:}Xa{=}TFPI] - k_{108}[Xa{=}TFPI][PS] + k_{109}[Xa{=}TFPI{:}PS]$$
$$\frac{d[TF{:}VIIa{:}Xa{=}TFPI]}{dt} = k_{84}[Xa{=}TFPI][TF{:}VIIa] - k_{85}[TF{:}VIIa{:}Xa{=}TFPI] + k_{105}[TF{:}VIIa{:}Xa{:}TFPI] - k_{106}[TF{:}VIIa{:}Xa{=}TFPI] - k_{108}[TF{:}VIIa{:}Xa{=}TFPI][PS] + k_{109}[TF{:}VIIa{:}Xa{=}TFPI{:}PS]$$

$$\frac{d[TFPI{:}PS]}{dt} = k_{108}[PS][TFPI] - k_{109}[TFPI{:}PS] - k_{110}[TFPI{:}PS][Xa] + k_{111}[Xa{:}TFPI{:}PS] - k_{107}[TF{:}VIIa{:}Xa][TFPI{:}PS]$$

$$\frac{d[Xa{:}TFPI{:}PS]}{dt} = k_{110}[TFPI{:}PS][Xa] - k_{111}[Xa{:}TFPI{:}PS] - k_{112}[Xa{:}TFPI{:}PS] + k_{113}[Xa{=}TFPI{:}PS] - k_{84}[Xa{:}TFPI{:}PS][TF{:}VIIa] + k_{85}[TF{:}VIIa{:}Xa{:}TFPI{:}PS] + k_{108}[Xa{:}TFPI][PS] - k_{109}[Xa{:}TFPI{:}PS]$$

$$\frac{d[Xa{=}TFPI{:}PS]}{dt} = k_{112}[Xa{:}TFPI{:}PS] - k_{113}[Xa{=}TFPI{:}PS] + k_{112}[Xa{:}TFPI{:}PS] - k_{113}[Xa{=}TFPI{:}PS] - k_{84}[Xa{=}TFPI{:}PS][TF{:}VIIa] + k_{85}[TF{:}VIIa{:}Xa{=}TFPI{:}PS] + k_{108}[Xa{=}TFPI][PS] - k_{109}[Xa{=}TFPI{:}PS]$$

$$\frac{d[TF{:}VIIa{:}Xa{:}TFPI{:}PS]}{dt} = k_{84}[Xa{:}TFPI{:}PS][TF{:}VIIa] - k_{85}[TF{:}VIIa{:}Xa{:}TFPI{:}PS] + k_{107}[TF{:}VIIa{:}Xa][TFPI{:}PS] - k_{112}[TF{:}VIIa{:}Xa{:}TFPI{:}PS] + k_{113}[TF{:}VIIa{:}Xa{=}TFPI{:}PS] + k_{108}[TF{:}VIIa{:}Xa{:}TFPI][PS] - k_{109}[TF{:}VIIa{:}Xa{:}TFPI{:}PS]$$

$$\frac{d[TF{:}VIIa{:}Xa{=}TFPI{:}PS]}{dt} = k_{84}[Xa{=}TFPI{:}PS][TF{:}VIIa] - k_{85}[TF{:}VIIa{:}Xa{=}TFPI{:}PS] + k_{112}[TF{:}VIIa{:}Xa{:}TFPI{:}PS] - k_{113}[TF{:}VIIa{:}Xa{=}TFPI{:}PS] + k_{108}[TF{:}VIIa{:}Xa{=}TFPI][PS] - k_{109}[TF{:}VIIa{:}Xa{=}TFPI{:}PS]$$

A.3.3 Expanded Unified Model with Protein C

$$\frac{d[TF]}{dt} = -k_1[TF][VII] + k_2[TF{:}VII] - k_3[TF][VIIa] + k_4[TF{:}VIIa]$$

$$\frac{d[VII]}{dt} = -k_1[TF][VII] + k_2[TF{:}VII] - k_5[VII][Xa] + k_6[VII{:}Xa] - k_{11}[VII][IIa] + k_{12}[VII{:}IIa] - k_{17}[VII][IXa] + k_{18}[VII{:}IXa] - k_{23}[VII][TF{:}VIIa] + k_{24}[VII{:}TF{:}VIIa]$$

$$\frac{d[VIIa]}{dt} = -k_3[TF][VIIa] + k_4[TF{:}VIIa] + k_7[VII{:}Xa] + k_{13}[VII{:}IIa] + k_{19}[VII{:}IXa] + k_{25}[VII{:}TF{:}VIIa] - k_{30}[X][VIIa] + k_{31}[X{:}VIIa] + k_{32}[X{:}VIIa] - k_{66}[IX][VIIa] + k_{67}[IX{:}VIIa] + k_{68}[IX{:}VIIa]$$

$$\frac{d[TF{:}VII]}{dt} = k_1[TF][VII] - k_2[TF{:}VII] - k_8[TF{:}VII][Xa] + k_9[TF{:}VII{:}Xa] - k_{14}[TF{:}VII][IIa] + k_{15}[TF{:}VII{:}IIa] - k_{20}[TF{:}VII][IXa] + k_{21}[TF{:}VII{:}IXa]$$

$$\frac{d[TF{:}VIIa]}{dt} = k_3[TF][VIIa] - k_4[TF{:}VIIa] + k_{10}[TF{:}VII{:}Xa] + k_{16}[TF{:}VII{:}IIa] + k_{22}[TF{:}VII{:}IXa] - k_{23}[VII][TF{:}VIIa] + k_{24}[VII{:}TF{:}VIIa] + k_{25}[VII{:}TF{:}VIIa] - k_{26}[TF{:}VIIa][AT] - k_{27}[X][TF{:}VIIa] + k_{28}[X{:}TF{:}VIIa] + k_{29}[X{:}TF{:}VIIa] - k_{63}[IX][TF{:}VIIa] + k_{64}[IX{:}TF{:}VIIa] + k_{65}[IX{:}TF{:}VIIa] - k_{84}[Xa{:}TFPI][TF{:}VIIa] + k_{85}[TF{:}VIIa{:}Xa{:}TFPI] - k_{89}[TF{:}VIIa][Xa] + k_{90}[TF{:}VIIa{:}Xa] - k_{84}[Xa{=}TFPI][TF{:}VIIa] + k_{85}[TF{:}VIIa{:}Xa{=}TFPI] - k_{84}[Xa{:}TFPI{:}PS][TF{:}VIIa] + k_{85}[TF{:}VIIa{:}Xa{:}TFPI{:}PS] - k_{84}[Xa{=}TFPI{:}PS][TF{:}VIIa] + k_{85}[TF{:}VIIa{:}Xa{=}TFPI{:}PS]$$

$$\frac{d[X]}{dt} = -k_{27}[X][TF{:}VIIa] + k_{28}[X{:}TF{:}VIIa] - k_{30}[X][VIIa] + k_{31}[X{:}VIIa] - k_{33}[X][IXa{:}VIIIa] + k_{34}[X{:}IXa{:}VIIIa] - k_{36}[X][IXa] + k_{37}[X{:}IXa]$$

$$\frac{d[Xa]}{dt} = -k_5[VII][Xa] + k_6[VII{:}Xa] + k_7[VII{:}Xa] - k_8[TF{:}VII][Xa] + k_9[TF{:}VII{:}Xa] + k_{10}[TF{:}VII{:}Xa] + k_{29}[X{:}TF{:}VIIa] + k_{32}[X{:}VIIa] + k_{35}[X{:}IXa{:}VIIIa] + k_{38}[X{:}IXa] - k_{42}[V][Xa] + k_{43}[V{:}Xa] + k_{44}[V{:}Xa] - k_{45}[Xa][Va] + k_{46}[Xa{:}Va] - k_{47}[Xa][AT] - k_{49}[II][Xa] + k_{50}[II{:}Xa] + k_{51}[II{:}Xa] - k_{75}[VIII][Xa] + k_{76}[VIII{:}Xa] + k_{77}[VIII{:}Xa] - k_{82}[Xa][TFPI] + k_{83}[Xa{:}TFPI] - k_{89}[TF{:}VIIa][Xa] + k_{90}[TF{:}VIIa{:}Xa] - k_{92}[Xa][\alpha_1{-}AT] - k_{110}[TFPI{:}PS][Xa] + k_{111}[Xa{:}TFPI{:}PS] + k_{124}[Xa{:}Va{:}APC]$$

$$\frac{d[II]}{dt} = -k_{49}[II][Xa] + k_{50}[II{:}Xa] - k_{52}[II][Xa{:}Va] + k_{53}[II{:}Xa{:}Va]$$

$$\frac{d[IIa]}{dt} = -k_{11}[VII][IIa] + k_{12}[VII{:}IIa] + k_{13}[VII{:}IIa] - k_{14}[TF{:}VII][IIa] + k_{15}[TF{:}VII{:}IIa] + k_{16}[TF{:}VII{:}IIa] - k_{39}[V][IIa] + k_{40}[V{:}IIa] + k_{41}[V{:}IIa] + k_{51}[II{:}Xa] + k_{54}[II{:}Xa{:}Va] - k_{55}[IIa][AT] - k_{56}[XI][IIa] + k_{57}[XI{:}IIa] + k_{58}[XI{:}IIa] - k_{72}[VIII][IIa] + k_{73}[VIII{:}IIa] + k_{74}[VIII{:}IIa] - k_{86}[IIa][Substrate] + k_{87}[IIa{:}Substrate] + k_{88}[IIa{:}Substrate] - k_{91}[IIa][\alpha_1{-}AT] - k_{96}[IIa][\alpha_2{-}M] - k_{114}[IIa][sTM] + k_{115}[IIa{:}sTM]$$

$$\frac{d[V]}{dt} = -k_{39}[V][IIa] + k_{40}[V{:}IIa] - k_{42}[V][Xa] + k_{43}[V{:}Xa]$$

$$\frac{d[Va]}{dt} = k_{41}[V{:}IIa] + k_{44}[V{:}Xa] - k_{45}[Xa][Va] + k_{46}[Xa{:}Va] + k_{48}[Xa{:}Va][AT] + k_{93}[Xa{:}Va][\alpha_1{-}AT] - k_{119}[Va][APC] + k_{120}[Va{:}APC]$$

$$\frac{d[VIII]}{dt} = -k_{72}[VIII][IIa] + k_{73}[VIII{:}IIa] - k_{75}[VIII][Xa] + k_{76}[VIII{:}Xa] - k_{102}[IXa][VIII] + k_{103}[IXa{:}VIII]$$

$$\frac{d[VIIIa]}{dt} = k_{74}[VIII{:}IIa] + k_{77}[VIII{:}Xa] - k_{78}[IXa][VIIIa] + k_{79}[IXa{:}VIIIa] + k_{81}[IXa{:}VIIIa][AT] - k_{99}[VIIIa] + k_{100}[VIIIa1L][VIIIa2] + k_{104}[IXa{:}VIII] - k_{125}[VIIIa][APC] + k_{126}[VIIIa{:}APC]$$

$$\frac{d[XI]}{dt} = -k_{56}[XI][IIa] + k_{57}[XI{:}IIa] - k_{59}[XI][XIa] + k_{60}[XI{:}XIa]$$

$$\frac{d[XIa]}{dt} = k_{58}[XI{:}IIa] - k_{59}[XI][XIa] + k_{60}[XI{:}XIa] + 2k_{61}[XI{:}XIa] - k_{62}[XIa][AT] - k_{69}[IX][XIa] + k_{70}[IX{:}XIa] + k_{71}[IX{:}XIa] - k_{94}[XIa][\alpha_1{-}AT] - k_{95}[XIa][\alpha_2{-}AP] - k_{97}[XIa][C1{-}inh] - k_{98}[XIa][PAI1]$$

$$\frac{d[IX]}{dt} = -k_{63}[IX][TF{:}VIIa] + k_{64}[IX{:}TF{:}VIIa] - k_{66}[IX][VIIa] + k_{67}[IX{:}VIIa] - k_{69}[IX][XIa] + k_{70}[IX{:}XIa]$$

$$\frac{d[IXa]}{dt} = -k_{17}[VII][IXa] + k_{18}[VII{:}IXa] + k_{19}[VII{:}IXa] - k_{20}[TF{:}VII][IXa] + k_{21}[TF{:}VII{:}IXa] + k_{22}[TF{:}VII{:}IXa] - k_{36}[X][IXa] + k_{37}[X{:}IXa] + k_{38}[X{:}IXa] + k_{65}[IX{:}TF{:}VIIa] + k_{68}[IX{:}VIIa] + k_{71}[IX{:}XIa] - k_{78}[IXa][VIIIa] + k_{79}[IXa{:}VIIIa] - k_{80}[IXa][AT] + k_{101}[IXa{:}VIIIa] - k_{102}[IXa][VIII] + k_{103}[IXa{:}VIII] + k_{104}[IXa{:}VIII] + k_{130}[IXa{:}VIIIa{:}APC]$$

$$\frac{d[IXa{:}VIIIa]}{dt} = -k_{33}[X][IXa{:}VIIIa] + k_{34}[X{:}IXa{:}VIIIa] + k_{35}[X{:}IXa{:}VIIIa] + k_{78}[IXa][VIIIa] - k_{79}[IXa{:}VIIIa] - k_{81}[IXa{:}VIIIa][AT] - k_{101}[IXa{:}VIIIa] - k_{128}[IXa{:}VIIIa][APC] + k_{129}[IXa{:}VIIIa{:}APC]$$

$$\frac{d[Xa{:}Va]}{dt} = k_{45}[Xa][Va] - k_{46}[Xa{:}Va] - k_{48}[Xa{:}Va][AT] - k_{52}[II][Xa{:}Va] + k_{53}[II{:}Xa{:}Va] + k_{54}[II{:}Xa{:}Va] - k_{93}[Xa{:}Va][\alpha_1{-}AT] - k_{122}[Xa{:}Va][APC] + k_{123}[Xa{:}Va{:}APC]$$

$$\frac{d[TFPI]}{dt} = -k_{82}[Xa][TFPI] + k_{83}[Xa{:}TFPI] - k_{107}[TF{:}VIIa{:}Xa][TFPI] - k_{108}[PS][TFPI] + k_{109}[TFPI{:}PS]$$

$$\frac{d[Xa{:}TFPI]}{dt} = k_{82}[Xa][TFPI] - k_{83}[Xa{:}TFPI] - k_{84}[Xa{:}TFPI][TF{:}VIIa] + k_{85}[TF{:}VIIa{:}Xa{:}TFPI] - k_{105}[Xa{:}TFPI] + k_{106}[Xa{=}TFPI] - k_{105}[Xa{:}TFPI] + k_{106}[Xa{=}TFPI] - k_{108}[Xa{:}TFPI][PS] + k_{109}[Xa{:}TFPI{:}PS]$$

$$\frac{d[TF{:}VIIa{:}Xa{:}TFPI]}{dt} = k_{84}[Xa{:}TFPI][TF{:}VIIa] - k_{85}[TF{:}VIIa{:}Xa{:}TFPI] + k_{107}[TF{:}VIIa{:}Xa][TFPI] - k_{105}[TF{:}VIIa{:}Xa{:}TFPI] + k_{106}[TF{:}VIIa{:}Xa{=}TFPI] - k_{108}[TF{:}VIIa{:}Xa{:}TFPI][PS] + k_{109}[TF{:}VIIa{:}Xa{:}TFPI{:}PS]$$

$$\frac{d[AT]}{dt} = -k_{26}[TF{:}VIIa][AT] - k_{47}[Xa][AT] - k_{48}[Xa{:}Va][AT] - k_{55}[IIa][AT] - k_{62}[XIa][AT] - k_{80}[IXa][AT] - k_{81}[IXa{:}VIIIa][AT]$$

$$\frac{d[VII{:}Xa]}{dt} = k_5[VII][Xa] - k_6[VII{:}Xa] - k_7[VII{:}Xa]$$

$$\frac{d[TF{:}VII{:}Xa]}{dt} = k_8[TF{:}VII][Xa] - k_9[TF{:}VII{:}Xa] - k_{10}[TF{:}VII{:}Xa]$$

$$\frac{d[VII{:}IIa]}{dt} = k_{11}[VII][IIa] - k_{12}[VII{:}IIa] - k_{13}[VII{:}IIa]$$

$$\frac{d[TF{:}VII{:}IIa]}{dt} = k_{14}[TF{:}VII][IIa] - k_{15}[TF{:}VII{:}IIa] - k_{16}[TF{:}VII{:}IIa]$$

$$\frac{d[VII{:}IXa]}{dt} = k_{17}[VII][IXa] - k_{18}[VII{:}IXa] - k_{19}[VII{:}IXa]$$

$$\frac{d[TF{:}VII{:}IXa]}{dt} = k_{20}[TF{:}VII][IXa] - k_{21}[TF{:}VII{:}IXa] - k_{22}[TF{:}VII{:}IXa]$$

$$\frac{d[VII{:}TF{:}VIIa]}{dt} = k_{23}[VII][TF{:}VIIa] - k_{24}[VII{:}TF{:}VIIa] - k_{25}[VII{:}TF{:}VIIa]$$

$$\frac{d[X{:}TF{:}VIIa]}{dt} = k_{27}[X][TF{:}VIIa] - k_{28}[X{:}TF{:}VIIa] - k_{29}[X{:}TF{:}VIIa]$$

$$\frac{d[X{:}VIIa]}{dt} = k_{30}[X][VIIa] - k_{31}[X{:}VIIa] - k_{32}[X{:}VIIa]$$

$$\frac{d[X{:}IXa{:}VIIIa]}{dt} = k_{33}[X][IXa{:}VIIIa] - k_{34}[X{:}IXa{:}VIIIa] - k_{35}[X{:}IXa{:}VIIIa]$$

$$\frac{d[X{:}IXa]}{dt} = k_{36}[X][IXa] - k_{37}[X{:}IXa] - k_{38}[X{:}IXa]$$

$$\frac{d[V{:}IIa]}{dt} = k_{39}[V][IIa] - k_{40}[V{:}IIa] - k_{41}[V{:}IIa]$$

$$\frac{d[V{:}Xa]}{dt} = k_{42}[V][Xa] - k_{43}[V{:}Xa] + k_{44}[V{:}Xa]$$

$$\frac{d[II{:}Xa]}{dt} = k_{49}[II][Xa] - k_{50}[II{:}Xa] - k_{51}[II{:}Xa]$$

$$\frac{d[II{:}Xa{:}Va]}{dt} = k_{52}[II][Xa{:}Va] - k_{53}[II{:}Xa{:}Va] - k_{54}[II{:}Xa{:}Va]$$

$$\frac{d[XI{:}IIa]}{dt} = k_{56}[XI][IIa] - k_{57}[XI{:}IIa] - k_{58}[XI{:}IIa]$$

$$\frac{d[XI{:}XIa]}{dt} = k_{59}[XI][XIa] - k_{60}[XI{:}XIa] - k_{61}[XI{:}XIa]$$

$$\frac{d[IX{:}TF{:}VIIa]}{dt} = k_{63}[IX][TF{:}VIIa] - k_{64}[IX{:}TF{:}VIIa] - k_{65}[IX{:}TF{:}VIIa]$$

$$\frac{d[IX{:}VIIa]}{dt} = k_{66}[IX][VIIa] - k_{67}[IX{:}VIIa] - k_{68}[IX{:}VIIa]$$

$$\frac{d[IX{:}XIa]}{dt} = k_{69}[IX][XIa] - k_{70}[IX{:}XIa] + k_{71}[IX{:}XIa]$$

$$\frac{d[VIII{:}IIa]}{dt} = k_{72}[VIII][IIa] - k_{73}[VIII{:}IIa] - k_{74}[VIII{:}IIa]$$
$$\frac{d[VIII{:}Xa]}{dt} = k_{75}[VIII][Xa] - k_{76}[VIII{:}Xa] - k_{77}[VIII{:}Xa]$$
$$\frac{d[Substrate]}{dt} = -k_{86}[IIa][Substrate] + k_{87}[IIa{:}Substrate]$$
$$\frac{d[ActiveSubstrate]}{dt} = k_{88}[IIa{:}Substrate]$$
$$\frac{d[IIa{:}Substrate]}{dt} = k_{86}[IIa][Substrate] - k_{87}[IIa{:}Substrate] - k_{88}[IIa{:}Substrate]$$
$$\frac{d[TF{:}VIIa{:}Xa]}{dt} = k_{89}[TF{:}VIIa][Xa] - k_{90}[TF{:}VIIa{:}Xa] - k_{107}[TF{:}VIIa{:}Xa][TFPI] - k_{107}[TF{:}VIIa{:}Xa][TFPI{:}PS]$$
$$\frac{d[\alpha_1{-}AT]}{dt} = -k_{91}[IIa][\alpha_1{-}AT] - k_{92}[Xa][\alpha_1{-}AT] - k_{93}[Xa{:}Va][\alpha_1{-}AT] - k_{94}[XIa][\alpha_1{-}AT]$$
$$\frac{d[\alpha_2{-}AP]}{dt} = -k_{95}[XIa][\alpha_2{-}AP]$$
$$\frac{d[\alpha_2{-}M]}{dt} = -k_{96}[IIa][\alpha_2{-}M]$$
$$\frac{d[C1{-}inh]}{dt} = -k_{97}[XIa][C1{-}inh]$$
$$\frac{d[PAI1]}{dt} = -k_{98}[XIa][PAI1]$$
$$\frac{d[VIIIa1L]}{dt} = \frac{d[VIIIa2]}{dt} = k_{99}[VIIIa] - k_{100}[VIIIa1L][VIIIa2] + k_{101}[IXa{:}VIIIa]$$
$$\frac{d[IXa{:}VIII]}{dt} = k_{102}[IXa][VIII] - k_{103}[IXa{:}VIII] - k_{104}[IXa{:}VIII]$$
$$\frac{d[PS]}{dt} = -k_{108}[PS][TFPI] + k_{109}[TFPI{:}PS] - k_{108}[Xa{:}TFPI][PS] + k_{109}[Xa{:}TFPI{:}PS] - k_{108}[Xa{=}TFPI][PS] + k_{109}[Xa{=}TFPI{:}PS] - k_{108}[TF{:}VIIa{:}Xa{:}TFPI][PS] + k_{109}[TF{:}VIIa{:}Xa{:}TFPI{:}PS] - k_{108}[TF{:}VIIa{:}Xa{=}TFPI][PS] - k_{109}[TF{:}VIIa{:}Xa{=}TFPI{:}PS]$$
$$\frac{d[Xa{=}TFPI]}{dt} = k_{105}[Xa{:}TFPI] - k_{106}[Xa{=}TFPI] + k_{105}[Xa{:}TFPI] - k_{106}[Xa{=}TFPI] - k_{84}[Xa{=}TFPI][TF{:}VIIa] + k_{85}[TF{:}VIIa{:}Xa{=}TFPI] - k_{108}[Xa{=}TFPI][PS] + k_{109}[Xa{=}TFPI{:}PS]$$
$$\frac{d[TF{:}VIIa{:}Xa{=}TFPI]}{dt} = k_{84}[Xa{=}TFPI][TF{:}VIIa] - k_{85}[TF{:}VIIa{:}Xa{=}TFPI] + k_{105}[TF{:}VIIa{:}Xa{:}TFPI] - k_{106}[TF{:}VIIa{:}Xa{=}TFPI] - k_{108}[TF{:}VIIa{:}Xa{=}TFPI][PS] + k_{109}[TF{:}VIIa{:}Xa{=}TFPI{:}PS]$$
$$\frac{d[TFPI{:}PS]}{dt} = k_{108}[PS][TFPI] - k_{109}[TFPI{:}PS] - k_{110}[TFPI{:}PS][Xa] + k_{111}[Xa{:}TFPI{:}PS] - k_{107}[TF{:}VIIa{:}Xa][TFPI{:}PS]$$
$$\frac{d[Xa{:}TFPI{:}PS]}{dt} = k_{110}[TFPI{:}PS][Xa] - k_{111}[Xa{:}TFPI{:}PS] - k_{112}[Xa{:}TFPI{:}PS] + k_{113}[Xa{=}TFPI{:}PS] - k_{84}[Xa{:}TFPI{:}PS][TF{:}VIIa] + k_{85}[TF{:}VIIa{:}Xa{:}TFPI{:}PS] + k_{108}[Xa{:}TFPI][PS] - k_{109}[Xa{:}TFPI{:}PS]$$
$$\frac{d[Xa{=}TFPI{:}PS]}{dt} = k_{112}[Xa{:}TFPI{:}PS] - k_{113}[Xa{=}TFPI{:}PS] + k_{112}[Xa{:}TFPI{:}PS] - k_{113}[Xa{=}TFPI{:}PS] - k_{84}[Xa{=}TFPI{:}PS][TF{:}VIIa] + k_{85}[TF{:}VIIa{:}Xa{=}TFPI{:}PS] + k_{108}[Xa{=}TFPI][PS] - k_{109}[Xa{=}TFPI{:}PS]$$

$$\frac{d[TF{:}VIIa{:}Xa{:}TFPI{:}PS]}{dt} = k_{84}[Xa{:}TFPI{:}PS][TF{:}VIIa] - k_{85}[TF{:}VIIa{:}Xa{:}TFPI{:}PS] + k_{107}[TF{:}VIIa{:}Xa][TFPI{:}PS] - k_{112}[TF{:}VIIa{:}Xa{:}TFPI{:}PS] + k_{113}[TF{:}VIIa{:}Xa{=}TFPI{:}PS] + k_{108}[TF{:}VIIa{:}Xa{:}TFPI][PS] - k_{109}[TF{:}VIIa{:}Xa{:}TFPI{:}PS]$$

$$\frac{d[TF{:}VIIa{:}Xa{=}TFPI{:}PS]}{dt} = k_{84}[Xa{=}TFPI{:}PS][TF{:}VIIa] - k_{85}[TF{:}VIIa{:}Xa{=}TFPI{:}PS] + k_{112}[TF{:}VIIa{:}Xa{:}TFPI{:}PS] - k_{113}[TF{:}VIIa{:}Xa{=}TFPI{:}PS] + k_{108}[TF{:}VIIa{:}Xa{=}TFPI][PS] - k_{109}[TF{:}VIIa{:}Xa{=}TFPI{:}PS]$$

$$\frac{[sTM]}{dt} = -k_{114}[IIa][sTM] + k_{115}[IIa{:}sTM]$$

$$\frac{[IIa{:}sTM]}{dt} = k_{114}[IIa][sTM] - k_{115}[IIa{:}sTM] - k_{116}[PC][IIa{:}sTM] + k_{117}[IIa{:}sTM{:}PC] + k_{118}[IIa{:}sTM{:}PC]$$

$$\frac{[PC]}{dt} = -k_{116}[PC][IIa{:}sTM] + k_{117}[IIa{:}sTM{:}PC]$$

$$\frac{[IIa{:}sTM{:}PC]}{dt} = k_{116}[PC][IIa{:}sTM] - k_{117}[IIa{:}sTM{:}PC] - k_{118}[IIa{:}sTM{:}PC]$$

$$\frac{[APC]}{dt} = k_{118}[IIa{:}sTM{:}PC] - k_{119}[Va][APC] + k_{120}[Va{:}APC] + k_{121}[Va{:}APC] - k_{122}[Xa{:}Va][APC] + k_{123}[Xa{:}Va{:}APC] + k_{124}[Xa{:}Va{:}APC] - k_{125}[VIIIa][APC] + k_{126}[VIIIa{:}APC] + k_{127}[VIIIa{:}APC] - k_{128}[IXa{:}VIIIa][APC] + k_{129}[IXa{:}VIIIa{:}APC] + k_{130}[IXa{:}VIIIa{:}APC]$$

$$\frac{[Va{:}APC]}{dt} = k_{119}[Va][APC] - k_{120}[Va{:}APC] - k_{121}[Va{:}APC]$$

$$\frac{[Xa{:}Va{:}APC]}{dt} = k_{122}[Xa{:}Va][APC] - k_{123}[Xa{:}Va{:}APC] - k_{124}[Xa{:}Va{:}APC]$$

$$\frac{[VIIIa{:}APC]}{dt} = k_{125}[VIIIa][APC] - k_{126}[VIIIa{:}APC] - k_{127}[VIIIa{:}APC]$$

$$\frac{[IXa{:}VIIIa{:}APC]}{dt} = k_{128}[IXa{:}VIIIa][APC] - k_{129}[IXa{:}VIIIa{:}APC] - k_{130}[IXa{:}VIIIa{:}APC]$$

A.3.4 Expanded Unified Model with Fibrinogen

$$\frac{d[TF]}{dt} = -k_1[TF][VII] + k_2[TF{:}VII] - k_3[TF][VIIa] + k_4[TF{:}VIIa]$$

$$\frac{d[VII]}{dt} = -k_1[TF][VII] + k_2[TF{:}VII] - k_5[VII][Xa] + k_6[VII{:}Xa] - k_{11}[VII][IIa] + k_{12}[VII{:}IIa] - k_{17}[VII][IXa] + k_{18}[VII{:}IXa] - k_{23}[VII][TF{:}VIIa] + k_{24}[VII{:}TF{:}VIIa]$$

$$\frac{d[VIIa]}{dt} = -k_3[TF][VIIa] + k_4[TF{:}VIIa] + k_7[VII{:}Xa] + k_{13}[VII{:}IIa] + k_{19}[VII{:}IXa] + k_{25}[VII{:}TF{:}VIIa] - k_{30}[X][VIIa] + k_{31}[X{:}VIIa] + k_{32}[X{:}VIIa] - k_{66}[IX][VIIa] + k_{67}[IX{:}VIIa] + k_{68}[IX{:}VIIa]$$

$$\frac{d[TF{:}VII]}{dt} = k_1[TF][VII] - k_2[TF{:}VII] - k_8[TF{:}VII][Xa] + k_9[TF{:}VII{:}Xa] - k_{14}[TF{:}VII][IIa] + k_{15}[TF{:}VII{:}IIa] - k_{20}[TF{:}VII][IXa] + k_{21}[TF{:}VII{:}IXa]$$

$$\frac{d[TF{:}VIIa]}{dt} = k_3[TF][VIIa] - k_4[TF{:}VIIa] + k_{10}[TF{:}VII{:}Xa] + k_{16}[TF{:}VII{:}IIa]$$
$$+ k_{22}[TF{:}VII{:}IXa] - k_{23}[VII][TF{:}VIIa] + k_{24}[VII{:}TF{:}VIIa] + k_{25}[VII{:}TF{:}VIIa]$$
$$- k_{26}[TF{:}VIIa][AT] - k_{27}[X][TF{:}VIIa] + k_{28}[X{:}TF{:}VIIa] + k_{29}[X{:}TF{:}VIIa]$$
$$- k_{63}[IX][TF{:}VIIa] + k_{64}[IX{:}TF{:}VIIa] + k_{65}[IX{:}TF{:}VIIa]$$
$$- k_{84}[Xa{:}TFPI][TF{:}VIIa] + k_{85}[TF{:}VIIa{:}Xa{:}TFPI] - k_{89}[TF{:}VIIa][Xa]$$
$$+ k_{90}[TF{:}VIIa{:}Xa] - k_{84}[Xa{=}TFPI][TF{:}VIIa] + k_{85}[TF{:}VIIa{:}Xa{=}TFPI]$$
$$- k_{84}[Xa{:}TFPI{:}PS][TF{:}VIIa] + k_{85}[TF{:}VIIa{:}Xa{:}TFPI{:}PS]$$
$$- k_{84}[Xa{=}TFPI{:}PS][TF{:}VIIa] + k_{85}[TF{:}VIIa{:}Xa{=}TFPI{:}PS]$$

$$\frac{d[X]}{dt} = -k_{27}[X][TF{:}VIIa] + k_{28}[X{:}TF{:}VIIa] - k_{30}[X][VIIa] + k_{31}[X{:}VIIa]$$
$$- k_{33}[X][IXa{:}VIIIa] + k_{34}[X{:}IXa{:}VIIIa] - k_{36}[X][IXa] + k_{37}[X{:}IXa]$$

$$\frac{d[Xa]}{dt} = -k_5[VII][Xa] + k_6[VII{:}Xa] + k_7[VII{:}Xa] - k_8[TF{:}VII][Xa] + k_9[TF{:}VII{:}Xa]$$
$$+ k_{10}[TF{:}VII{:}Xa] + k_{29}[X{:}TF{:}VIIa] + k_{32}[X{:}VIIa] + k_{35}[X{:}IXa{:}VIIIa]$$
$$+ k_{38}[X{:}IXa] - k_{42}[V][Xa] + k_{43}[V{:}Xa] + k_{44}[V{:}Xa] - k_{45}[Xa][Va]$$
$$+ k_{46}[Xa{:}Va] - k_{47}[Xa][AT] - k_{49}[II][Xa] + k_{50}[II{:}Xa] + k_{51}[II{:}Xa]$$
$$- k_{75}[VIII][Xa] + k_{76}[VIII{:}Xa] + k_{77}[VIII{:}Xa] - k_{82}[Xa][TFPI]$$
$$+ k_{83}[Xa{:}TFPI] - k_{89}[TF{:}VIIa][Xa] + k_{90}[TF{:}VIIa{:}Xa] - k_{92}[Xa][\alpha_1{-}AT]$$
$$- k_{110}[TFPI{:}PS][Xa] + k_{111}[Xa{:}TFPI{:}PS]$$

$$\frac{d[II]}{dt} = -k_{49}[II][Xa] + k_{50}[II{:}Xa] - k_{52}[II][Xa{:}Va] + k_{53}[II{:}Xa{:}Va]$$

$$\frac{d[IIa]}{dt} = -k_{11}[VII][IIa] + k_{12}[VII{:}IIa] + k_{13}[VII{:}IIa] - k_{14}[TF{:}VII][IIa]$$
$$+ k_{15}[TF{:}VII{:}IIa] + k_{16}[TF{:}VII{:}IIa] - k_{39}[V][IIa] + k_{40}[V{:}IIa] + k_{41}[V{:}IIa]$$
$$+ k_{51}[II{:}Xa] + k_{54}[II{:}Xa{:}Va] - k_{55}[IIa][AT] - k_{56}[XI][IIa] + k_{57}[XI{:}IIa]$$
$$+ k_{58}[XI{:}IIa] - k_{72}[VIII][IIa] + k_{73}[VIII{:}IIa] + k_{74}[VIII{:}IIa]$$
$$- k_{86}[IIa][Substrate] + k_{87}[IIa{:}Substrate] + k_{88}[IIa{:}Substrate] - k_{91}[IIa][\alpha_1{-}AT]$$
$$- k_{96}[IIa][\alpha_2{-}M] - k_{114}[Fbg][IIa] + k_{115}[Fbg{:}IIa] + k_{116}[Fbg{:}IIa] - k_{117}[Fbn1][IIa]$$
$$+ k_{118}[Fbn1{:}IIa] + k_{119}[Fbn1{:}IIa] - k_{120}[Fbn2][IIa] + k_{121}[Fbn2{:}IIa]$$

$$\frac{d[V]}{dt} = -k_{39}[V][IIa] + k_{40}[V{:}IIa] - k_{42}[V][Xa] + k_{43}[V{:}Xa]$$

$$\frac{d[Va]}{dt} = k_{41}[V{:}IIa] + k_{44}[V{:}Xa] - k_{45}[Xa][Va] + k_{46}[Xa{:}Va] + k_{48}[Xa{:}Va][AT]$$
$$+ k_{93}[Xa{:}Va][\alpha_1{-}AT]$$

$$\frac{d[VIII]}{dt} = -k_{72}[VIII][IIa] + k_{73}[VIII{:}IIa] - k_{75}[VIII][Xa] + k_{76}[VIII{:}Xa]$$
$$- k_{102}[IXa][VIII] + k_{103}[IXa{:}VIII]$$

$$\frac{d[VIIIa]}{dt} = k_{74}[VIII{:}IIa] + k_{77}[VIII{:}Xa] - k_{78}[IXa][VIIIa] + k_{79}[IXa{:}VIIIa]$$
$$+ k_{81}[IXa{:}VIIIa][AT] - k_{99}[VIIIa] + k_{100}[VIIIa1L][VIIIa2] + k_{104}[IXa{:}VIII]$$

$$\frac{d[XI]}{dt} = -k_{56}[XI][IIa] + k_{57}[XI{:}IIa] - k_{59}[XI][XIa] + k_{60}[XI{:}XIa]$$

$$\frac{d[XIa]}{dt} = k_{58}[XI{:}IIa] - k_{59}[XI][XIa] + k_{60}[XI{:}XIa] + 2k_{61}[XI{:}XIa] - k_{62}[XIa][AT]$$
$$- k_{69}[IX][XIa] + k_{70}[IX{:}XIa] + k_{71}[IX{:}XIa] - k_{94}[XIa][\alpha_1{-}AT] - k_{95}[XIa][\alpha_2{-}AP]$$
$$- k_{97}[XIa][C1{-}inh] - k_{98}[XIa][PAI1]$$

$$\frac{d[IX]}{dt} = -k_{63}[IX][TF{:}VIIa] + k_{64}[IX{:}TF{:}VIIa] - k_{66}[IX][VIIa] + k_{67}[IX{:}VIIa]$$
$$- k_{69}[IX][XIa] + k_{70}[IX{:}XIa]$$

$$\frac{d[IXa]}{dt} = -k_{17}[VII][IXa] + k_{18}[VII{:}IXa] + k_{19}[VII{:}IXa] - k_{20}[TF{:}VII][IXa] + k_{21}[TF{:}VII{:}IXa] + k_{22}[TF{:}VII{:}IXa] - k_{36}[X][IXa] + k_{37}[X{:}IXa] + k_{38}[X{:}IXa] + k_{65}[IX{:}TF{:}VIIa] + k_{68}[IX{:}VIIa] + k_{71}[IX{:}XIa] - k_{78}[IXa][VIIIa] + k_{79}[IXa{:}VIIIa] - k_{80}[IXa][AT] + k_{101}[IXa{:}VIIIa] - k_{102}[IXa][VIII] + k_{103}[IXa{:}VIII] + k_{104}[IXa{:}VIII]$$

$$\frac{d[IXa{:}VIIIa]}{dt} = -k_{33}[X][IXa{:}VIIIa] + k_{34}[X{:}IXa{:}VIIIa] + k_{35}[X{:}IXa{:}VIIIa] + k_{78}[IXa][VIIIa] - k_{79}[IXa{:}VIIIa] - k_{81}[IXa{:}VIIIa][AT] - k_{101}[IXa{:}VIIIa]$$

$$\frac{d[Xa{:}Va]}{dt} = k_{45}[Xa][Va] - k_{46}[Xa{:}Va] - k_{48}[Xa{:}Va][AT] - k_{52}[II][Xa{:}Va] + k_{53}[II{:}Xa{:}Va] + k_{54}[II{:}Xa{:}Va] - k_{93}[Xa{:}Va][\alpha_1 - AT]$$

$$\frac{d[TFPI]}{dt} = -k_{82}[Xa][TFPI] + k_{83}[Xa{:}TFPI] - k_{107}[TF{:}VIIa{:}Xa][TFPI] - k_{108}[PS][TFPI] + k_{109}[TFPI{:}PS]$$

$$\frac{d[Xa{:}TFPI]}{dt} = k_{82}[Xa][TFPI] - k_{83}[Xa{:}TFPI] - k_{84}[Xa{:}TFPI][TF{:}VIIa] + k_{85}[TF{:}VIIa{:}Xa{:}TFPI] - k_{105}[Xa{:}TFPI] + k_{106}[Xa{=}TFPI] - k_{105}[Xa{:}TFPI] + k_{106}[Xa{=}TFPI] - k_{108}[Xa{:}TFPI][PS] + k_{109}[Xa{:}TFPI{:}PS]$$

$$\frac{d[TF{:}VIIa{:}Xa{:}TFPI]}{dt} = k_{84}[Xa{:}TFPI][TF{:}VIIa] - k_{85}[TF{:}VIIa{:}Xa{:}TFPI] + k_{107}[TF{:}VIIa{:}Xa][TFPI] - k_{105}[TF{:}VIIa{:}Xa{:}TFPI] + k_{106}[TF{:}VIIa{:}Xa{=}TFPI] - k_{108}[TF{:}VIIa{:}Xa{:}TFPI][PS] + k_{109}[TF{:}VIIa{:}Xa{:}TFPI{:}PS]$$

$$\frac{d[AT]}{dt} = -k_{26}[TF{:}VIIa][AT] - k_{47}[Xa][AT] - k_{48}[Xa{:}Va][AT] - k_{55}[IIa][AT] - k_{62}[XIa][AT] - k_{80}[IXa][AT] - k_{81}[IXa{:}VIIIa][AT]$$

$$\frac{d[VII{:}Xa]}{dt} = k_5[VII][Xa] - k_6[VII{:}Xa] - k_7[VII{:}Xa]$$

$$\frac{d[TF{:}VII{:}Xa]}{dt} = k_8[TF{:}VII][Xa] - k_9[TF{:}VII{:}Xa] - k_{10}[TF{:}VII{:}Xa]$$

$$\frac{d[VII{:}IIa]}{dt} = k_{11}[VII][IIa] - k_{12}[VII{:}IIa] - k_{13}[VII{:}IIa]$$

$$\frac{d[TF{:}VII{:}IIa]}{dt} = k_{14}[TF{:}VII][IIa] - k_{15}[TF{:}VII{:}IIa] - k_{16}[TF{:}VII{:}IIa]$$

$$\frac{d[VII{:}IXa]}{dt} = k_{17}[VII][IXa] - k_{18}[VII{:}IXa] - k_{19}[VII{:}IXa]$$

$$\frac{d[TF{:}VII{:}IXa]}{dt} = k_{20}[TF{:}VII][IXa] - k_{21}[TF{:}VII{:}IXa] - k_{22}[TF{:}VII{:}IXa]$$

$$\frac{d[VII{:}TF{:}VIIa]}{dt} = k_{23}[VII][TF{:}VIIa] - k_{24}[VII{:}TF{:}VIIa] - k_{25}[VII{:}TF{:}VIIa]$$

$$\frac{d[X{:}TF{:}VIIa]}{dt} = k_{27}[X][TF{:}VIIa] - k_{28}[X{:}TF{:}VIIa] - k_{29}[X{:}TF{:}VIIa]$$

$$\frac{d[X{:}VIIa]}{dt} = k_{30}[X][VIIa] - k_{31}[X{:}VIIa] - k_{32}[X{:}VIIa]$$

$$\frac{d[X{:}IXa{:}VIIIa]}{dt} = k_{33}[X][IXa{:}VIIIa] - k_{34}[X{:}IXa{:}VIIIa] - k_{35}[X{:}IXa{:}VIIIa]$$

$$\frac{d[X{:}IXa]}{dt} = k_{36}[X][IXa] - k_{37}[X{:}IXa] - k_{38}[X{:}IXa]$$

$$\frac{d[V{:}IIa]}{dt} = k_{39}[V][IIa] - k_{40}[V{:}IIa] - k_{41}[V{:}IIa]$$

$$\frac{d[V{:}Xa]}{dt} = k_{42}[V][Xa] - k_{43}[V{:}Xa] + k_{44}[V{:}Xa]$$

$$\frac{d[II{:}Xa]}{dt} = k_{49}[II][Xa] - k_{50}[II{:}Xa] - k_{51}[II{:}Xa]$$

$$\frac{d[II{:}Xa{:}Va]}{dt} = k_{52}[II][Xa{:}Va] - k_{53}[II{:}Xa{:}Va] - k_{54}[II{:}Xa{:}Va]$$
$$\frac{d[XI{:}IIa]}{dt} = k_{56}[XI][IIa] - k_{57}[XI{:}IIa] - k_{58}[XI{:}IIa]$$
$$\frac{d[XI{:}XIa]}{dt} = k_{59}[XI][XIa] - k_{60}[XI{:}XIa] - k_{61}[XI{:}XIa]$$
$$\frac{d[IX{:}TF{:}VIIa]}{dt} = k_{63}[IX][TF{:}VIIa] - k_{64}[IX{:}TF{:}VIIa] - k_{65}[IX{:}TF{:}VIIa]$$
$$\frac{d[IX{:}VIIa]}{dt} = k_{66}[IX][VIIa] - k_{67}[IX{:}VIIa] - k_{68}[IX{:}VIIa]$$
$$\frac{d[IX{:}XIa]}{dt} = k_{69}[IX][XIa] - k_{70}[IX{:}XIa] + k_{71}[IX{:}XIa]$$
$$\frac{d[VIII{:}IIa]}{dt} = k_{72}[VIII][IIa] - k_{73}[VIII{:}IIa] - k_{74}[VIII{:}IIa]$$
$$\frac{d[VIII{:}Xa]}{dt} = k_{75}[VIII][Xa] - k_{76}[VIII{:}Xa] - k_{77}[VIII{:}Xa]$$
$$\frac{d[Substrate]}{dt} = -k_{86}[IIa][Substrate] + k_{87}[IIa{:}Substrate]$$
$$\frac{d[ActiveSubstrate]}{dt} = k_{88}[IIa{:}Substrate]$$
$$\frac{d[IIa{:}Substrate]}{dt} = k_{86}[IIa][Substrate] - k_{87}[IIa{:}Substrate] - k_{88}[IIa{:}Substrate]$$
$$\frac{d[TF{:}VIIa{:}Xa]}{dt} = k_{89}[TF{:}VIIa][Xa] - k_{90}[TF{:}VIIa{:}Xa] - k_{107}[TF{:}VIIa{:}Xa][TFPI] - k_{107}[TF{:}VIIa{:}Xa][TFPI{:}PS]$$
$$\frac{d[\alpha_1{-}AT]}{dt} = -k_{91}[IIa][\alpha_1{-}AT] - k_{92}[Xa][\alpha_1{-}AT] - k_{93}[Xa{:}Va][\alpha_1{-}AT] - k_{94}[XIa][\alpha_1{-}AT]$$
$$\frac{d[\alpha_2{-}AP]}{dt} = -k_{95}[XIa][\alpha_2{-}AP]$$
$$\frac{d[\alpha_2{-}M]}{dt} = -k_{96}[IIa][\alpha_2{-}M]$$
$$\frac{d[C1{-}inh]}{dt} = -k_{97}[XIa][C1{-}inh]$$
$$\frac{d[PAI1]}{dt} = -k_{98}[XIa][PAI1]$$
$$\frac{d[VIIIa1L]}{dt} = \frac{d[VIIIa2]}{dt} = k_{99}[VIIIa] - k_{100}[VIIIa1L][VIIIa2] + k_{101}[IXa{:}VIIIa]$$
$$\frac{d[IXa{:}VIII]}{dt} = k_{102}[IXa][VIII] - k_{103}[IXa{:}VIII] - k_{104}[IXa{:}VIII]$$
$$\frac{d[PS]}{dt} = -k_{108}[PS][TFPI] + k_{109}[TFPI{:}PS] - k_{108}[Xa{:}TFPI][PS] + k_{109}[Xa{:}TFPI{:}PS] - k_{108}[Xa{=}TFPI][PS] + k_{109}[Xa{=}TFPI{:}PS] - k_{108}[TF{:}VIIa{:}Xa{:}TFPI][PS] + k_{109}[TF{:}VIIa{:}Xa{:}TFPI{:}PS] - k_{108}[TF{:}VIIa{:}Xa{=}TFPI][PS] - k_{109}[TF{:}VIIa{:}Xa{=}TFPI{:}PS]$$
$$\frac{d[Xa{=}TFPI]}{dt} = k_{105}[Xa{:}TFPI] - k_{106}[Xa{=}TFPI] + k_{105}[Xa{:}TFPI] - k_{106}[Xa{=}TFPI] - k_{84}[Xa{=}TFPI][TF{:}VIIa] + k_{85}[TF{:}VIIa{:}Xa{=}TFPI] - k_{108}[Xa{=}TFPI][PS] + k_{109}[Xa{=}TFPI{:}PS]$$
$$\frac{d[TF{:}VIIa{:}Xa{=}TFPI]}{dt} = k_{84}[Xa{=}TFPI][TF{:}VIIa] - k_{85}[TF{:}VIIa{:}Xa{=}TFPI] + k_{105}[TF{:}VIIa{:}Xa{:}TFPI] - k_{106}[TF{:}VIIa{:}Xa{=}TFPI] - k_{108}[TF{:}VIIa{:}Xa{=}TFPI][PS] + k_{109}[TF{:}VIIa{:}Xa{=}TFPI{:}PS]$$

$$\frac{d[TFPI{:}PS]}{dt} = k_{108}[PS][TFPI] - k_{109}[TFPI{:}PS] - k_{110}[TFPI{:}PS][Xa] + k_{111}[Xa{:}TFPI{:}PS] - k_{107}[TF{:}VIIa{:}Xa][TFPI{:}PS]$$

$$\frac{d[Xa{:}TFPI{:}PS]}{dt} = k_{110}[TFPI{:}PS][Xa] - k_{111}[Xa{:}TFPI{:}PS] - k_{112}[Xa{:}TFPI{:}PS] + k_{113}[Xa{=}TFPI{:}PS] - k_{84}[Xa{:}TFPI{:}PS][TF{:}VIIa] + k_{85}[TF{:}VIIa{:}Xa{:}TFPI{:}PS] + k_{108}[Xa{:}TFPI][PS] - k_{109}[Xa{:}TFPI{:}PS]$$

$$\frac{d[Xa{=}TFPI{:}PS]}{dt} = k_{112}[Xa{:}TFPI{:}PS] - k_{113}[Xa{=}TFPI{:}PS] + k_{112}[Xa{:}TFPI{:}PS] - k_{113}[Xa{=}TFPI{:}PS] - k_{84}[Xa{=}TFPI{:}PS][TF{:}VIIa] + k_{85}[TF{:}VIIa{:}Xa{=}TFPI{:}PS] + k_{108}[Xa{=}TFPI][PS] - k_{109}[Xa{=}TFPI{:}PS]$$

$$\frac{d[TF{:}VIIa{:}Xa{:}TFPI{:}PS]}{dt} = k_{84}[Xa{:}TFPI{:}PS][TF{:}VIIa] - k_{85}[TF{:}VIIa{:}Xa{:}TFPI{:}PS] + k_{107}[TF{:}VIIa{:}Xa][TFPI{:}PS] - k_{112}[TF{:}VIIa{:}Xa{:}TFPI{:}PS] + k_{113}[TF{:}VIIa{:}Xa{=}TFPI{:}PS] + k_{108}[TF{:}VIIa{:}Xa{:}TFPI][PS] - k_{109}[TF{:}VIIa{:}Xa{:}TFPI{:}PS]$$

$$\frac{d[TF{:}VIIa{:}Xa{=}TFPI{:}PS]}{dt} = k_{84}[Xa{=}TFPI{:}PS][TF{:}VIIa] - k_{85}[TF{:}VIIa{:}Xa{=}TFPI{:}PS] + k_{112}[TF{:}VIIa{:}Xa{:}TFPI{:}PS] - k_{113}[TF{:}VIIa{:}Xa{=}TFPI{:}PS] + k_{108}[TF{:}VIIa{:}Xa{=}TFPI][PS] - k_{109}[TF{:}VIIa{:}Xa{=}TFPI{:}PS]$$

$$\frac{[Fbg]}{dt} = -k_{114}[Fbg][IIa] + k_{115}[Fbg{:}IIa]$$

$$\frac{[Fbg{:}IIa]}{dt} = k_{114}[Fbg][IIa] - k_{115}[Fbg{:}IIa] - k_{116}[Fbg{:}IIa]$$

$$\frac{[Fbn1]}{dt} = k_{116}[Fbg{:}IIa] - k_{117}[Fbn1][IIa] + k_{118}[Fbn1{:}IIa]$$

$$\frac{[Fbn1{:}IIa]}{dt} = k_{117}[Fbn1][IIa] - k_{118}[Fbn1{:}IIa] - k_{119}[Fbn1{:}IIa]$$

$$\frac{[Fbn2]}{dt} = k_{119}[Fbn1{:}IIa] - k_{120}[Fbn2][IIa] + k_{121}[Fbn2{:}IIa]$$

$$\frac{[Fbn2{:}IIa]}{dt} = k_{120}[Fbn2][IIa] - k_{121}[Fbn2{:}IIa]$$

$$\frac{[FPA]}{dt} = k_{116}[Fbg{:}IIa]$$

$$\frac{[FPB]}{dt} = k_{119}[Fbn1{:}IIa]$$

A.3.5 Reduced Unified Model

$$\frac{d[TF]}{dt} = -k_1[TF][VII] + k_2[TF{:}VII] - k_3[TF][VIIa] + k_4[TF{:}VIIa]$$

$$\frac{d[VII]}{dt} = -k_1[TF][VII] + k_2[TF{:}VII] - k_5[VII][Xa] + k_6[VII{:}Xa] - k_{11}[VII][IIa] + k_{12}[VII{:}IIa] - k_{17}[VII][IXa] + k_{18}[VII{:}IXa]$$

$$\frac{d[VIIa]}{dt} == k_3[TF][VIIa] + k_4[TF{:}VIIa] - k_7[VII{:}Xa] + k_{13}[VII{:}IIa] - k_{19}[VII{:}IXa] - k_{27}[X][VIIa] + k_{28}[X{:}VIIa] + k_{29}[X{:}VIIa] - k_{63}[IX][VIIa] + k_{64}[IX{:}VIIa] + k_{65}[IX{:}VIIa]$$

$$\frac{d[TF{:}VII]}{dt} = k_1[TF][VII] - k_2[TF{:}VII] - k_8[TF{:}VII][Xa] + k_9[TF{:}VII{:}Xa] - k_{14}[TF{:}VII][IIa] + k_{15}[TF{:}VII{:}IIa] - k_{20}[TF{:}VII][IXa] + k_{21}[TF{:}VII{:}IXa]$$

$$\frac{d[TF{:}VIIa]}{dt} = k_3[TF][VIIa] - k_4[TF{:}VIIa] + k_{10}[TF{:}VII{:}Xa] + k_{16}[TF{:}VII{:}IIa] + k_{22}[TF{:}VII{:}IXa] - k_{23}[TF{:}VIIa][AT] - k_{24}[X][TF{:}VIIa] + k_{25}[X{:}TF{:}VIIa] + k_{26}[X{:}TF{:}VIIa] - k_{60}[IX][TF{:}VIIa] + k_{61}[IX{:}TF{:}VIIa] + k_{62}[IX{:}TF{:}VIIa] - k_{81}[Xa{:}TFPI][TF{:}VIIa] + k_{82}[TF{:}VIIa{:}Xa{:}TFPI] - k_{86}[TF{:}VIIa][Xa] + k_{87}[TF{:}VIIa{:}Xa]$$

$$\frac{d[X]}{dt} = -k_{24}[X][TF{:}VIIa] + k_{25}[X{:}TF{:}VIIa] - k_{27}[X][VIIa] + k_{28}[X{:}VIIa] - k_{30}[X][IXa{:}VIIIa] + k_{31}[X{:}IXa{:}VIIIa] - k_{33}[X][IXa] + k_{34}[X{:}IXa]$$

$$\frac{d[Xa]}{dt} = -k_5[VII][Xa] + k_6[VII{:}Xa] + k_7[VII{:}Xa] - k_8[TF{:}VII][Xa] + k_9[TF{:}VII{:}Xa] + k_{10}[TF{:}VII{:}Xa] + k_{26}[X{:}TF{:}VIIa] + k_{29}[X{:}VIIa] + k_{32}[X{:}IXa{:}VIIIa] + k_{35}[X{:}IXa] - k_{39}[V][Xa] + k_{40}[V{:}Xa] + k_{41}[V{:}Xa] - k_{42}[Xa][Va] + k_{43}[Xa{:}Va] - k_{44}[Xa][AT] - k_{46}[II][Xa] + k_{47}[II{:}Xa] + k_{48}[II{:}Xa] - k_{72}[VIII][Xa] + k_{73}[VIII{:}Xa] + k_{74}[VIII{:}Xa] - k_{79}[Xa][TFPI] + k_{80}[Xa{:}TFPI] - k_{86}[TF{:}VIIa][Xa] + k_{87}[TF{:}VIIa{:}Xa] - k_{89}[Xa][\alpha_1{-}AT]$$

$$\frac{d[II]}{dt} = -k_{46}[II][Xa] + k_{47}[II{:}Xa] - k_{49}[II][Xa{:}Va] + k_{50}[II{:}Xa{:}Va]$$

$$\frac{d[IIa]}{dt} = -k_{11}[VII][IIa] + k_{12}[VII{:}IIa] + k_{13}[VII{:}IIa] - k_{14}[TF{:}VII][IIa] + k_{15}[TF{:}VII{:}IIa] + k_{16}[TF{:}VII{:}IIa] - k_{36}[V][IIa] + k_{37}[V{:}IIa] + k_{38}[V{:}IIa] + k_{48}[II{:}Xa] + k_{51}[II{:}Xa{:}Va] - k_{52}[IIa][AT] - k_{53}[XI][IIa] + k_{54}[XI{:}IIa] - k_{69}[VIII][IIa] + k_{70}[VIII{:}IIa] + k_{71}[VIII{:}IIa] - k_{83}[IIa][Substrate] + k_{84}[IIa{:}Substrate] + k_{85}[IIa{:}Substrate] - k_{88}[IIa][\alpha_1{-}AT] - k_{93}[IIa][\alpha_2{-}M] - k_{98}[Fbg][IIa] + k_{99}[Fbg{:}IIa] + k_{100}[Fbg{:}IIa] - k_{101}[Fbn1][IIa] + k_{102}[Fbn1{:}IIa] + k_{103}[Fbn1{:}IIa] - k_{104}[Fbn2][IIa] + k_{105}[Fbn2{:}IIa]$$

$$\frac{d[V]}{dt} = -k_{36}[V][IIa] + k_{37}[V{:}IIa] - k_{39}[V][Xa] + k_{40}[V{:}Xa] + k_{55}[XI{:}IIa]$$

$$\frac{d[Va]}{dt} = k_{38}[V{:}IIa] + k_{41}[V{:}Xa] - k_{42}[Xa][Va] + k_{43}[Xa{:}Va] + k_{45}[Xa{:}Va][AT] + k_{90}[Xa{:}Va][\alpha_1{-}AT]$$

$$\frac{d[VIII]}{dt} = -k_{69}[VIII][IIa] + k_{70}[VIII{:}IIa] - k_{72}[VIII][Xa] + k_{73}[VIII{:}Xa]$$

$$\frac{d[VIIIa]}{dt} = k_{71}[VIII{:}IIa] + k_{74}[VIII{:}Xa] - k_{75}[IXa][VIIIa] + k_{76}[IXa{:}VIIIa] + k_{78}[IXa{:}VIIIa][AT] - k_{95}[VIIIa]$$

$$\frac{d[XI]}{dt} = -k_{53}[XI][IIa] + k_{54}[XI{:}IIa] - k_{56}[XI][XIa] + k_{57}[XI{:}XIa]$$

$$\frac{d[XIa]}{dt} = k_{55}[XI{:}IIa] - k_{56}[XI][XIa] + k_{57}[XI{:}XIa] + 2k_{58}[XI{:}XIa] - k_{59}[XIa][AT] - k_{66}[IX][XIa] + k_{67}[IX{:}XIa] + k_{68}[IX{:}XIa] - k_{91}[XIa][\alpha_1{-}AT] - k_{92}[XIa][\alpha_2{-}AP] - k_{94}[XIa][PAI1]$$

$$\frac{d[IX]}{dt} = -k_{60}[IX][TF{:}VIIa] + k_{61}[IX{:}TF{:}VIIa] - k_{63}[IX][VIIa] + k_{64}[IX{:}VIIa] - k_{66}[IX][XIa] + k_{67}[IX{:}XIa]$$

$$\frac{d[IXa]}{dt} = -k_{17}[VII][IXa] + k_{18}[VII{:}IXa] + k_{19}[VII{:}IXa] - k_{20}[TF{:}VII][IXa] + k_{21}[TF{:}VII{:}IXa] + k_{22}[TF{:}VII{:}IXa] - k_{33}[X][IXa] + k_{34}[X{:}IXa] + k_{35}[X{:}IXa] + k_{62}[IX{:}TF{:}VIIa] + k_{65}[IX{:}VIIa] + k_{68}[IX{:}XIa] - k_{75}[IXa][VIIIa] + k_{76}[IXa{:}VIIIa] - k_{77}[IXa][AT] + k_{96}[IXa{:}VIIIa]$$

$$\frac{d[IXa{:}VIIIa]}{dt} = -k_{30}[X][IXa{:}VIIIa] + k_{31}[X{:}IXa{:}VIIIa] + k_{32}[X{:}IXa{:}VIIIa] + k_{75}[IXa][VIIIa] - k_{76}[IXa{:}VIIIa] - k_{78}[IXa{:}VIIIa][AT] - k_{96}[IXa{:}VIIIa]$$

$$\frac{d[Xa{:}Va]}{dt} = k_{42}[Xa][Va] - k_{43}[Xa{:}Va] - k_{45}[Xa{:}Va][AT] - k_{49}[II][Xa{:}Va] + k_{50}[II{:}Xa{:}Va] + k_{51}[II{:}Xa{:}Va] - k_{90}[Xa{:}Va][\alpha_1 - AT]$$

$$\frac{d[TFPI]}{dt} = -k_{79}[Xa][TFPI] + k_{80}[Xa{:}TFPI] - k_{97}[TF{:}VIIa{:}Xa][TFPI]$$

$$\frac{d[Xa{:}TFPI]}{dt} = k_{79}[Xa][TFPI] - k_{80}[Xa{:}TFPI] - k_{81}[Xa{:}TFPI][TF{:}VIIa] + k_{82}[TF{:}VIIa{:}Xa{:}TFPI]$$

$$\frac{d[TF{:}VIIa{:}Xa{:}TFPI]}{dt} = k_{81}[Xa{:}TFPI][TF{:}VIIa] - k_{82}[TF{:}VIIa{:}Xa{:}TFPI] + k_{97}[TF{:}VIIa{:}Xa][TFPI]$$

$$\frac{d[AT]}{dt} = -k_{23}[TF{:}VIIa][AT] - k_{44}[Xa][AT] - k_{45}[Xa{:}Va][AT] - k_{52}[IIa][AT] - k_{59}[XIa][AT] - k_{77}[IXa][AT] - k_{78}[IXa{:}VIIIa][AT]$$

$$\frac{d[VII{:}Xa]}{dt} = k_5[VII][Xa] - k_6[VII{:}Xa] - k_7[VII{:}Xa]$$

$$\frac{d[TF{:}VII{:}Xa]}{dt} = k_8[TF{:}VII][Xa] - k_9[TF{:}VII{:}Xa] - k_{10}[TF{:}VII{:}Xa]$$

$$\frac{d[VII{:}IIa]}{dt} = k_{11}[VII][IIa] - k_{12}[VII{:}IIa] - k_{13}[VII{:}IIa]$$

$$\frac{d[TF{:}VII{:}IIa]}{dt} = k_{14}[TF{:}VII][IIa] - k_{15}[TF{:}VII{:}IIa] - k_{16}[TF{:}VII{:}IIa]$$

$$\frac{d[VII{:}IXa]}{dt} = k_{17}[VII][IXa] - k_{18}[VII{:}IXa] - k_{19}[VII{:}IXa]$$

$$\frac{d[TF{:}VII{:}IXa]}{dt} = k_{20}[TF{:}VII][IXa] - k_{21}[TF{:}VII{:}IXa] - k_{22}[TF{:}VII{:}IXa]$$

$$\frac{d[X{:}TF{:}VIIa]}{dt} = k_{24}[X][TF{:}VIIa] - k_{25}[X{:}TF{:}VIIa] - k_{26}[X{:}TF{:}VIIa]$$

$$\frac{d[X{:}VIIa]}{dt} = k_{27}[X][VIIa] - k_{28}[X{:}VIIa] - k_{29}[X{:}VIIa]$$

$$\frac{d[X{:}IXa{:}VIIIa]}{dt} = k_{30}[X][IXa{:}VIIIa] - k_{31}[X{:}IXa{:}VIIIa] - k_{32}[X{:}IXa{:}VIIIa]$$

$$\frac{d[X{:}IXa]}{dt} = k_{33}[X][IXa] - k_{34}[X{:}IXa] - k_{35}[X{:}IXa]$$

$$\frac{d[V{:}IIa]}{dt} = k_{36}[V][IIa] - k_{37}[V{:}IIa] - k_{38}[V{:}IIa]$$

$$\frac{d[V{:}Xa]}{dt} = k_{39}[V][Xa] - k_{40}[V{:}Xa] - k_{41}[V{:}Xa]$$

$$\frac{d[II{:}Xa]}{dt} = k_{46}[II][Xa] - k_{47}[II{:}Xa] - k_{48}[II{:}Xa]$$

$$\frac{d[II{:}Xa{:}Va]}{dt} = k_{49}[II][Xa{:}Va] - k_{50}[II{:}Xa{:}Va] - k_{51}[II{:}Xa{:}Va]$$

$$\frac{d[XI{:}IIa]}{dt} = k_{53}[XI][IIa] - k_{54}[XI{:}IIa] - k_{55}[XI{:}IIa]$$

$$\frac{d[XI{:}XIa]}{dt} = k_{56}[XI][XIa] - k_{57}[XI{:}XIa] - k_{58}[XI{:}XIa]$$

$$\frac{d[IX{:}TF{:}VIIa]}{dt} = k_{60}[IX][TF{:}VIIa] - k_{61}[IX{:}TF{:}VIIa] - k_{62}[IX{:}TF{:}VIIa]$$

$$\frac{d[IX{:}VIIa]}{dt} = k_{63}[IX][VIIa] - k_{64}[IX{:}VIIa] - k_{65}[IX{:}VIIa]$$

$$\frac{d[IX{:}XIa]}{dt} = k_{66}[IX][XIa] - k_{67}[IX{:}XIa] - k_{68}[IX{:}XIa]$$

$$\frac{d[VIII{:}IIa]}{dt} = k_{69}[VIII][IIa] - k_{70}[VIII{:}IIa] - k_{71}[VIII{:}IIa]$$
$$\frac{d[VIII{:}Xa]}{dt} = k_{72}[VIII][Xa] - k_{73}[VIII{:}Xa] - k_{74}[VIII{:}Xa]$$
$$\frac{d[Substrate]}{dt} = -k_{83}[IIa][Substrate] + k_{84}[IIa{:}Substrate]$$
$$\frac{d[ActiveSubstrate]}{dt} = k_{85}[IIa{:}Substrate]$$
$$\frac{d[IIa{:}Substrate]}{dt} = k_{83}[IIa][Substrate] - k_{84}[IIa{:}Substrate] - k_{85}[IIa{:}Substrate]$$
$$\frac{d[TF{:}VIIa{:}Xa]}{dt} = k_{86}[TF{:}VIIa][Xa] - k_{87}[TF{:}VIIa{:}Xa] - k_{97}[TF{:}VIIa{:}Xa][TFPI]$$
$$\frac{d[\alpha_1{-}AT]}{dt} = -k_{88}[IIa][\alpha_1{-}AT] - k_{89}[Xa][\alpha_1{-}AT] - k_{90}[Xa{:}Va][\alpha_1{-}AT] - k_{91}[XIa][\alpha_1{-}AT]$$
$$\frac{d[IIa{:}\alpha_1{-}AT]}{dt} = k_{88}[IIa][\alpha_1{-}AT]$$
$$\frac{d[Xa{:}\alpha_1{-}AT]}{dt} = k_{89}[Xa][\alpha_1{-}AT] + k_{90}[Xa{:}Va][\alpha_1{-}AT]$$
$$\frac{d[XIa{:}\alpha_1{-}AT]}{dt} = k_{91}[XIa][\alpha_1{-}AT]$$
$$\frac{d[\alpha_2{-}AP]}{dt} = -k_{92}[XIa][\alpha_2{-}AP]$$
$$\frac{d[XIa{:}\alpha_2{-}AP]}{dt} = k_{92}[XIa][\alpha_2{-}AP]$$
$$\frac{d[\alpha_2{-}M]}{dt} = -k_{93}[IIa][\alpha_2{-}M]$$
$$\frac{d[IIa{:}\alpha_2{-}M]}{dt} = k_{93}[IIa][\alpha_2{-}M]$$
$$\frac{d[PAI1]}{dt} = -k_{94}[XIa][PAI1]$$
$$\frac{d[XIa{:}PAI1]}{dt} = k_{94}[XIa][PAI1]$$
$$\frac{d[VIIIa1L]}{dt} = \frac{d[VIIIa2]}{dt} = k_{95}[VIIIa] + k_{96}[IXa{:}VIIIa]$$
$$\frac{d[Fbg]}{dt} = -k_{98}[Fbg][IIa] + k_{99}[Fbg{:}IIa]$$
$$\frac{d[Fbg{:}IIa]}{dt} = k_{98}[Fbg][IIa] - k_{99}[Fbg{:}IIa] - k_{100}[Fbg{:}IIa]$$
$$\frac{d[Fbn1]}{dt} = k_{100}[Fbg{:}IIa] - k_{101}[Fbn1][IIa] + k_{102}[Fbn1{:}IIa]$$
$$\frac{d[Fbn1{:}IIa]}{dt} = k_{101}[Fbn1][IIa] - k_{102}[Fbn1{:}IIa] - k_{103}[Fbn1{:}IIa]$$
$$\frac{d[Fbn2]}{dt} = k_{103}[Fbn1{:}IIa] - k_{104}[Fbn2][IIa] + k_{105}[Fbn2{:}IIa]$$
$$\frac{d[Fbn2{:}IIa]}{dt} = k_{104}[Fbn2][IIa] - k_{105}[Fbn2{:}IIa]$$
$$\frac{d[FPA]}{dt} = k_{100}[Fbg{:}IIa]$$
$$\frac{d[FPB]}{dt} = k_{103}[Fbn1{:}IIa]$$

A.3.6 Improved Unified Model

$$\frac{d[TF]}{dt} = -k_1[TF][VII] + k_2[TF{:}VII] - k_3[TF][VIIa] + k_4[TF{:}VIIa]$$

$$\frac{d[VII]}{dt} = -k_1[TF][VII] + k_2[TF{:}VII] - k_5[VII][Xa] + k_6[VII{:}Xa] - k_{11}[VII][IIa] + k_{12}[VII{:}IIa] - k_{17}[VII][IXa] + k_{18}[VII{:}IXa] - k_{23}[VII][TF{:}VIIa] + k_{24}[VII{:}TF{:}VIIa]$$

$$\frac{d[VIIa]}{dt} = -k_3[TF][VIIa] + k_4[TF{:}VIIa] + k_7[VII{:}Xa] + k_{13}[VII{:}IIa] + k_{19}[VII{:}IXa] + k_{25}[VII{:}TF{:}VIIa] - k_{30}[X][VIIa] + k_{31}[X{:}VIIa] + k_{32}[X{:}VIIa] - k_{66}[IX][VIIa] + k_{67}[IX{:}VIIa] + k_{68}[IX{:}VIIa]$$

$$\frac{d[TF{:}VII]}{dt} = k_1[TF][VII] - k_2[TF{:}VII] - k_8[TF{:}VII][Xa] + k_9[TF{:}VII{:}Xa] - k_{14}[TF{:}VII][IIa] + k_{15}[TF{:}VII{:}IIa] - k_{20}[TF{:}VII][IXa] + k_{21}[TF{:}VII{:}IXa]$$

$$\frac{d[TF{:}VIIa]}{dt} = k_3[TF][VIIa] - k_4[TF{:}VIIa] + k_{10}[TF{:}VII{:}Xa] + k_{16}[TF{:}VII{:}IIa] + k_{22}[TF{:}VII{:}IXa] - k_{23}[VII][TF{:}VIIa] + k_{24}[VII{:}TF{:}VIIa] + k_{25}[VII{:}TF{:}VIIa] - k_{26}[TF{:}VIIa][AT] - k_{27}[X][TF{:}VIIa] + k_{28}[X{:}TF{:}VIIa] + k_{29}[X{:}TF{:}VIIa] - k_{63}[IX][TF{:}VIIa] + k_{64}[IX{:}TF{:}VIIa] + k_{65}[IX{:}TF{:}VIIa] - k_{87}[Xa{:}TFPI][TF{:}VIIa] + k_{88}[TF{:}VIIa{:}Xa{:}TFPI]$$

$$\frac{d[X]}{dt} = -k_{27}[X][TF{:}VIIa] + k_{28}[X{:}TF{:}VIIa] - k_{30}[X][VIIa] + k_{31}[X{:}VIIa] - k_{33}[X][IXa{:}VIIIa] + k_{34}[X{:}IXa{:}VIIIa] - k_{36}[X][IXa] + k_{37}[X{:}IXa]$$

$$\frac{d[Xa]}{dt} = -k_5[VII][Xa] + k_6[VII{:}Xa] + k_7[VII{:}Xa] - k_8[TF{:}VII][Xa] + k_9[TF{:}VII{:}Xa] + k_{10}[TF{:}VII{:}Xa] + k_{29}[X{:}TF{:}VIIa] + k_{32}[X{:}VIIa] + k_{35}[X{:}IXa{:}VIIIa] + k_{38}[X{:}IXa] - k_{42}[V][Xa] + k_{43}[V{:}Xa] + k_{44}[V{:}Xa] - k_{45}[Xa][Va] + k_{46}[Xa{:}Va] - k_{47}[Xa][AT] - k_{49}[II][Xa] + k_{50}[II{:}Xa] + k_{51}[II{:}Xa] - k_{75}[VIII][Xa] + k_{76}[VIII{:}Xa] + k_{77}[VIII{:}Xa] - k_{85}[Xa][TFPI] + k_{86}[Xa{:}TFPI] - k_{90}[Xa][\alpha_1{-}AT]$$

$$\frac{d[II]}{dt} = -k_{49}[II][Xa] + k_{50}[II{:}Xa] - k_{52}[II][Xa{:}Va] + k_{53}[II{:}Xa{:}Va]$$

$$\frac{d[IIa]}{dt} = -k_{11}[VII][IIa] + k_{12}[VII{:}IIa] + k_{13}[VII{:}IIa] - k_{14}[TF{:}VII][IIa] + k_{15}[TF{:}VII{:}IIa] + k_{16}[TF{:}VII{:}IIa] - k_{39}[V][IIa] + k_{40}[V{:}IIa] + k_{41}[V{:}IIa] + k_{51}[II{:}Xa] + k_{54}[II{:}Xa{:}Va] - k_{55}[IIa][AT] - k_{56}[XI][IIa] + k_{57}[XI{:}IIa] + k_{58}[XI{:}IIa] - k_{72}[VIII][IIa] + k_{73}[VIII{:}IIa] + k_{74}[VIII{:}IIa] - k_{89}[IIa][\alpha_1{-}AT] - k_{94}[IIa][\alpha_2{-}M] - k_{97}[Fbg][IIa] + k_{98}[Fbg{:}IIa] + k_{99}[Fbg{:}IIa] - k_{100}[Fbn1][IIa] + k_{101}[Fbn1{:}IIa] + k_{102}[Fbn1{:}IIa] - k_{103}[Fbn2][IIa] + k_{104}[Fbn2{:}IIa] - k_{107}[IIa][Substrate] + k_{108}[IIa{:}Substrate] + k_{109}[IIa{:}Substrate]$$

$$\frac{d[V]}{dt} = -k_{39}[V][IIa] + k_{40}[V{:}IIa] - k_{42}[V][Xa] + k_{43}[V{:}Xa]$$

$$\frac{d[Va]}{dt} = k_{41}[V{:}IIa] + k_{44}[V{:}Xa] - k_{45}[Xa][Va] + k_{46}[Xa{:}Va]$$

$$\frac{d[VIII]}{dt} = -k_{72}[VIII][IIa] + k_{73}[VIII{:}IIa] - k_{75}[VIII][Xa] + k_{76}[VIII{:}Xa]$$

$$\frac{d[VIIIa]}{dt} = k_{74}[VIII{:}IIa] + k_{77}[VIII{:}Xa] - k_{78}[VIIIa] + k_{79}[VIIIa1L][VIIIa2] - k_{81}[IXa][VIIIa] + k_{82}[IXa{:}VIIIa]$$

$$\frac{d[XI]}{dt} = -k_{56}[XI][IIa] + k_{57}[XI{:}IIa] - k_{59}[XI][XIa] + k_{60}[XI{:}XIa]$$

$$\frac{d[XIa]}{dt} = k_{58}[XI{:}IIa] - k_{59}[XI][XIa] + k_{60}[XI{:}XIa] + 2k_{61}[XI{:}XIa] - k_{62}[XIa][AT] - k_{69}[IX][XIa] + k_{70}[IX{:}XIa] + k_{71}[IX{:}XIa] - k_{92}[XIa][\alpha_1{-}AT] - k_{93}[XIa][\alpha_2{-}AP] - k_{95}[XIa][C1{-}inh] - k_{96}[XIa][PAI1]$$

$$\frac{d[IX]}{dt} = -k_{63}[IX][TF{:}VIIa] + k_{64}[IX{:}TF{:}VIIa] - k_{66}[IX][VIIa] + k_{67}[IX{:}VIIa] - k_{69}[IX][XIa] + k_{70}[IX{:}XIa]$$

$$\frac{d[IXa]}{dt} = -k_{17}[VII][IXa] + k_{18}[VII{:}IXa] + k_{19}[VII{:}IXa] - k_{20}[TF{:}VII][IXa] + k_{21}[TF{:}VII{:}IXa] + k_{22}[TF{:}VII{:}IXa] - k_{36}[X][IXa] + k_{37}[X{:}IXa] + k_{38}[X{:}IXa] + k_{65}[IX{:}TF{:}VIIa] + k_{68}[IX{:}VIIa] + k_{71}[IX{:}XIa] + k_{80}[IXa{:}VIIIa] - k_{81}[IXa][VIIIa] + k_{82}[IXa{:}VIIIa] - k_{83}[IXa][AT]$$

$$\frac{d[IXa{:}VIIIa]}{dt} = -k_{33}[X][IXa{:}VIIIa] + k_{34}[X{:}IXa{:}VIIIa] + k_{35}[X{:}IXa{:}VIIIa] - k_{80}[IXa{:}VIIIa] + k_{81}[IXa][VIIIa] - k_{82}[IXa{:}VIIIa] - k_{84}[IXa{:}VIIIa][AT]$$

$$\frac{d[Xa{:}Va]}{dt} = k_{45}[Xa][Va] - k_{46}[Xa{:}Va] - k_{48}[Xa{:}Va][AT] - k_{52}[II][Xa{:}Va] + k_{53}[II{:}Xa{:}Va] + k_{54}[II{:}Xa{:}Va] - k_{91}[Xa{:}Va][\alpha_1 - AT]$$

$$\frac{d[TFPI]}{dt} = -k_{85}[Xa][TFPI] + k_{86}[Xa{:}TFPI]$$

$$\frac{d[Xa{:}TFPI]}{dt} = k_{85}[Xa][TFPI] - k_{86}[Xa{:}TFPI] - k_{87}[Xa{:}TFPI][TF{:}VIIa] + k_{88}[TF{:}VIIa{:}Xa{:}TFPI]$$

$$\frac{d[TF{:}VIIa{:}Xa{:}TFPI]}{dt} = k_{87}[Xa{:}TFPI][TF{:}VIIa] - k_{88}[TF{:}VIIa{:}Xa{:}TFPI]$$

$$\frac{d[AT]}{dt} = -k_{26}[TF{:}VIIa][AT] - k_{47}[Xa][AT] - k_{48}[Xa{:}Va][AT] - k_{55}[IIa][AT] - k_{62}[XIa][AT] - k_{83}[IXa][AT] - k_{84}[IXa{:}VIIIa][AT] - k_{105}[Fbn1{:}IIa][AT] - k_{106}[Fbn2{:}IIa][AT]$$

$$\frac{d[VII{:}Xa]}{dt} = k_5[VII][Xa] - k_6[VII{:}Xa] - k_7[VII{:}Xa]$$

$$\frac{d[TF{:}VII{:}Xa]}{dt} = k_8[TF{:}VII][Xa] - k_9[TF{:}VII{:}Xa] - k_{10}[TF{:}VII{:}Xa]$$

$$\frac{d[VII{:}IIa]}{dt} = k_{11}[VII][IIa] - k_{12}[VII{:}IIa] - k_{13}[VII{:}IIa]$$

$$\frac{d[TF{:}VII{:}IIa]}{dt} = k_{14}[TF{:}VII][IIa] - k_{15}[TF{:}VII{:}IIa] - k_{16}[TF{:}VII{:}IIa]$$

$$\frac{d[VII{:}IXa]}{dt} = k_{17}[VII][IXa] - k_{18}[VII{:}IXa] - k_{19}[VII{:}IXa]$$

$$\frac{d[TF{:}VII{:}IXa]}{dt} = k_{20}[TF{:}VII][IXa] - k_{21}[TF{:}VII{:}IXa] - k_{22}[TF{:}VII{:}IXa]$$

$$\frac{d[VII{:}TF{:}VIIa]}{dt} = k_{23}[VII][TF{:}VIIa] - k_{24}[VII{:}TF{:}VIIa] - k_{25}[VII{:}TF{:}VIIa]$$

$$\frac{d[X{:}TF{:}VIIa]}{dt} = k_{27}[X][TF{:}VIIa] - k_{28}[X{:}TF{:}VIIa] - k_{29}[X{:}TF{:}VIIa]$$

$$\frac{d[X{:}VIIa]}{dt} = k_{30}[X][VIIa] - k_{31}[X{:}VIIa] - k_{32}[X{:}VIIa]$$

$$\frac{d[X{:}IXa{:}VIIIa]}{dt} = k_{33}[X][IXa{:}VIIIa] - k_{34}[X{:}IXa{:}VIIIa] - k_{35}[X{:}IXa{:}VIIIa]$$

$$\frac{d[X{:}IXa]}{dt} = k_{36}[X][IXa] - k_{37}[X{:}IXa] - k_{38}[X{:}IXa]$$

$$\frac{d[V{:}IIa]}{dt} = k_{39}[V][IIa] - k_{40}[V{:}IIa] - k_{41}[V{:}IIa]$$

$$\frac{d[V{:}Xa]}{dt} = k_{42}[V][Xa] - k_{43}[V{:}Xa] - k_{44}[V{:}Xa]$$

$$\frac{d[II{:}Xa]}{dt} = k_{49}[II][Xa] - k_{50}[II{:}Xa] - k_{51}[II{:}Xa]$$

$$\frac{d[II{:}Xa{:}Va]}{dt} = k_{52}[II][Xa{:}Va] - k_{53}[II{:}Xa{:}Va] - k_{54}[II{:}Xa{:}Va]$$
$$\frac{d[XI{:}IIa]}{dt} = k_{56}[XI][IIa] - k_{57}[XI{:}IIa] - k_{58}[XI{:}IIa]$$
$$\frac{d[XI{:}XIa]}{dt} = k_{59}[XI][XIa] - k_{60}[XI{:}XIa] - k_{61}[XI{:}XIa]$$
$$\frac{d[IX{:}TF{:}VIIa]}{dt} = k_{63}[IX][TF{:}VIIa] - k_{64}[IX{:}TF{:}VIIa] - k_{65}[IX{:}TF{:}VIIa]$$
$$\frac{d[IX{:}VIIa]}{dt} = k_{66}[IX][VIIa] - k_{67}[IX{:}VIIa] - k_{68}[IX{:}VIIa]$$
$$\frac{d[IX{:}XIa]}{dt} = k_{69}[IX][XIa] - k_{70}[IX{:}XIa] - k_{71}[IX{:}XIa]$$
$$\frac{d[VIII{:}IIa]}{dt} = k_{72}[VIII][IIa] - k_{73}[VIII{:}IIa] - k_{74}[VIII{:}IIa]$$
$$\frac{d[VIII{:}Xa]}{dt} = k_{75}[VIII][Xa] - k_{76}[VIII{:}Xa] - k_{77}[VIII{:}Xa]$$
$$\frac{d[Substrate]}{dt} = -k_{107}[IIa][Substrate] + k_{108}[IIa{:}Substrate]$$
$$\frac{d[ActiveSubstrate]}{dt} = k_{109}[IIa{:}Substrate]$$
$$\frac{d[IIa{:}Substrate]}{dt} = k_{107}[IIa][Substrate] - k_{108}[IIa{:}Substrate] - k_{109}[IIa{:}Substrate]$$
$$\frac{d[\alpha_1{-}AT]}{dt} = -k_{89}[IIa][\alpha_1{-}AT] - k_{90}[Xa][\alpha_1{-}AT] - k_{91}[Xa{:}Va][\alpha_1{-}AT] - k_{92}[XIa][\alpha_1{-}AT]$$
$$\frac{d[\alpha_2{-}AP]}{dt} = -k_{93}[XIa][\alpha_2{-}AP]$$
$$\frac{d[\alpha_2{-}M]}{dt} = -k_{94}[IIa][\alpha_2{-}M]$$
$$\frac{d[C1{-}inh]}{dt} = -k_{95}[XIa][C1{-}inh]$$
$$\frac{d[PAI1]}{dt} = -k_{96}[XIa][PAI1]$$
$$\frac{d[VIIIa1L]}{dt} = \frac{d[VIIIa2]}{dt} = k_{78}[VIIIa] - k_{79}[VIIIa1L][VIIIa2] + k_{80}[IXa{:}VIIIa]$$
$$\frac{d[Fbg]}{dt} = -k_{97}[Fbg][IIa] + k_{98}[Fbg{:}IIa]$$
$$\frac{d[Fbg{:}IIa]}{dt} = k_{97}[Fbg][IIa] - k_{98}[Fbg{:}IIa] - k_{99}[Fbg{:}IIa]$$
$$\frac{d[Fbn1]}{dt} = k_{99}[Fbg{:}IIa] - k_{100}[Fbn1][IIa] + k_{101}[Fbn1{:}IIa]$$
$$\frac{d[Fbn1{:}IIa]}{dt} = k_{100}[Fbn1][IIa] - k_{101}[Fbn1{:}IIa] - k_{102}[Fbn1{:}IIa] - k_{105}[Fbn1{:}IIa][AT]$$
$$\frac{d[Fbn2]}{dt} = k_{102}[Fbn1{:}IIa] - k_{103}[Fbn2][IIa] + k_{104}[Fbn2{:}IIa]$$
$$\frac{d[Fbn2{:}IIa]}{dt} = k_{103}[Fbn2][IIa] - k_{104}[Fbn2{:}IIa] - k_{106}[Fbn2{:}IIa][AT]$$
$$\frac{d[FPA]}{dt} = k_{99}[Fbg{:}IIa]$$
$$\frac{d[FPB]}{dt} = k_{102}[Fbn1{:}IIa]$$

Appendix B

Fitted Reaction Rates

This appendix presents the fitted reaction rates for Chapters 3, 4, 5, and 6. First order rates are given in units of s^{-1} and second order rates are given in units of $M^{-1}s^{-1}$.

B.1 Unified Model

Tables 3.6 and 3.7 present the fitted reaction rates in prior form. They are presented here in mass action form for simulation with the ODEs.

Rate	GD Fitted	ABC-SMC Fitted	GD ETP Fitted	GD Bounded
k_1	1.26×10^5	1.26×10^5	1.26×10^5	1.26×10^5
k_2	3.72×10^{-4}	3.72×10^{-4}	3.72×10^{-4}	3.72×10^{-4}
k_3	1.49×10^7	1.33×10^5	2.47×10^8	2.47×10^8
k_4	4.70×10^{-2}	4.20×10^{-4}	7.80×10^{-1}	7.80×10^{-1}
k_5	1.00×10^8	1.00×10^8	1.00×10^8	1.00×10^8
k_6	2.73×10^4	2.67	1.17×10^5	1.17×10^5
k_7	4.10×10^3	1.82×10^{-2}	2.31×10^4	2.31×10^4
k_8	1.00×10^{10}	1.00×10^8	1.00×10^9	1.00×10^9
k_9	1.99×10^4	1.15×10^4	4.61×10^4	4.61×10^4
k_{10}	2.21×10^3	5.49×10^1	6.01×10^3	6.01×10^3
k_{11}	1.00×10^8	1.00×10^8	1.00×10^8	1.00×10^8
k_{12}	9.62×10^4	5.95	3.37×10^5	3.37×10^5
k_{13}	8.08	1.65×10^{-1}	8.33×10^1	8.33×10^1
k_{14}	1.00×10^8	1.00×10^8	1.00×10^8	1.00×10^8
k_{15}	1.35×10^5	1.93×10^{-1}	4.23×10^5	4.23×10^5
k_{16}	1.04×10^1	2.67×10^{-1}	8.62×10^1	8.62×10^1
k_{17}	1.00×10^8	1.00×10^{11}	1.00×10^8	1.00×10^8
k_{18}	4.67×10^4	1.62×10^6	2.07×10^5	2.07×10^5
k_{19}	7.93×10^1	2.04×10^5	4.49×10^2	4.49×10^2
k_{20}	1.00×10^8	1.00×10^8	1.00×10^8	1.00×10^8
k_{21}	4.34×10^4	3.46×10^6	2.00×10^5	2.00×10^5
k_{22}	8.86×10^1	4.86×10^{-3}	4.81×10^2	4.81×10^2
k_{23}	1.00×10^8	1.00×10^9	1.00×10^8	1.00×10^8

k_{24}	7.93×10^{4}	1.12×10^{1}	4.76×10^{5}	4.76×10^{5}
k_{25}	1.41	1.41	1.41	1.41
k_{26}	3.78×10^{5}	2.71×10^{2}	1.29×10^{6}	1.29×10^{6}
k_{27}	1.00×10^{9}	1.00×10^{9}	1.00×10^{9}	1.00×10^{9}
k_{28}	3.36×10^{2}	4.16×10^{1}	4.46×10^{4}	4.46×10^{4}
k_{29}	5.54×10^{2}	6.81	1.55×10^{4}	1.55×10^{4}
k_{30}	1.00×10^{8}	1.00×10^{8}	1.00×10^{8}	1.00×10^{8}
k_{31}	2.46×10^{4}	2.36×10^{2}	1.72×10^{5}	1.72×10^{5}
k_{32}	3.24×10^{-4}	3.24×10^{-4}	3.24×10^{-4}	3.24×10^{-4}
k_{33}	1.00×10^{10}	1.00×10^{8}	1.00×10^{10}	1.00×10^{10}
k_{34}	5.51×10^{2}	4.06	1.57×10^{2}	1.57×10^{2}
k_{35}	3.00×10^{2}	4.45	6.94×10^{2}	6.94×10^{2}
k_{36}	1.00×10^{8}	1.00×10^{8}	1.00×10^{8}	1.00×10^{8}
k_{37}	1.04×10^{3}	3.57×10^{1}	9.97×10^{2}	9.97×10^{2}
k_{38}	2.82×10^{-4}	2.82×10^{-4}	2.82×10^{-4}	2.82×10^{-4}
k_{39}	1.00×10^{8}	1.00×10^{8}	1.00×10^{8}	1.00×10^{8}
k_{40}	1.18×10^{3}	1.34×10^{2}	8.80×10^{3}	8.80×10^{3}
k_{41}	2.95×10^{-1}	2.95×10^{-1}	2.95×10^{-1}	2.95×10^{-1}
k_{42}	1.00×10^{10}	1.00×10^{8}	1.00×10^{10}	1.00×10^{10}
k_{43}	9.05×10^{1}	8.78×10^{-1}	5.70×10^{1}	5.70×10^{1}
k_{44}	1.42×10^{1}	1.70×10^{-1}	4.77×10^{1}	4.77×10^{1}
k_{45}	1.58×10^{9}	1.58×10^{9}	1.58×10^{9}	1.58×10^{9}
k_{46}	3.58×10^{-4}	1.62	5.13×10^{-2}	5.13×10^{-2}
k_{47}	3.26×10^{5}	5.06×10^{3}	1.82×10^{5}	1.82×10^{5}
k_{48}	1.07×10^{3}	1.07×10^{3}	1.07×10^{3}	1.07×10^{3}
k_{49}	1.00×10^{8}	1.00×10^{8}	1.00×10^{8}	1.00×10^{8}
k_{50}	5.45×10^{4}	2.50×10^{2}	1.58×10^{5}	1.58×10^{5}
k_{51}	9.33×10^{-3}	9.33×10^{-3}	9.33×10^{-3}	9.33×10^{-3}
k_{52}	1.00×10^{8}	1.00×10^{8}	1.00×10^{9}	1.00×10^{9}
k_{53}	3.75×10^{4}	1.44×10^{2}	6.24×10^{4}	6.24×10^{4}
k_{54}	4.46×10^{3}	2.55×10^{1}	5.16×10^{4}	5.16×10^{4}
k_{55}	3.04×10^{3}	4.28×10^{3}	9.28×10^{2}	9.28×10^{2}
k_{56}	1.00×10^{8}	1.00×10^{8}	1.00×10^{8}	1.00×10^{8}
k_{57}	2.21×10^{3}	5.57×10^{-3}	8.67×10^{3}	8.67×10^{3}
k_{58}	1.11×10^{-4}	1.88×10^{-3}	1.75×10^{-1}	1.75×10^{-1}
k_{59}	1.00×10^{8}	1.00×10^{8}	1.00×10^{8}	1.00×10^{8}
k_{60}	1.48×10^{3}	8.98×10^{-1}	6.95×10^{3}	6.95×10^{3}
k_{61}	3.34×10^{-2}	1.85×10^{-1}	1.40×10^{-1}	1.40×10^{-1}
k_{62}	3.98×10^{2}	3.98×10^{2}	3.98×10^{2}	3.98×10^{2}
k_{63}	1.00×10^{8}	1.00×10^{8}	1.00×10^{8}	1.00×10^{8}
k_{64}	1.57×10^{1}	1.57×10^{1}	1.57×10^{1}	1.57×10^{1}
k_{65}	5.37×10^{-1}	5.37×10^{-1}	5.37×10^{-1}	5.37×10^{-1}
k_{66}	1.00×10^{8}	1.00×10^{8}	1.00×10^{8}	1.00×10^{8}
k_{67}	1.52×10^{2}	1.97×10^{-3}	1.70×10^{3}	1.70×10^{3}
k_{68}	5.55×10^{-5}	7.75×10^{-3}	4.67×10^{-2}	4.67×10^{-2}
k_{69}	1.00×10^{8}	1.00×10^{8}	1.00×10^{8}	1.00×10^{8}
k_{70}	9.80×10^{3}	6.90×10^{1}	3.19×10^{4}	3.19×10^{4}
k_{71}	6.00×10^{1}	1.99	6.26×10^{2}	6.26×10^{2}

k_{72}	1.00×10^{8}	1.00×10^{9}	1.00×10^{8}	1.00×10^{8}
k_{73}	4.63×10^{2}	1.33	2.54×10^{4}	2.54×10^{4}
k_{74}	3.02×10^{2}	5.32×10^{-1}	1.19×10^{3}	1.19×10^{3}
k_{75}	1.00×10^{8}	1.00×10^{9}	1.00×10^{8}	1.00×10^{8}
k_{76}	5.33×10^{3}	6.08	2.21×10^{4}	2.21×10^{4}
k_{77}	5.79×10^{1}	4.86	2.73×10^{2}	2.73×10^{2}
k_{78}	1.71×10^{9}	8.45×10^{6}	8.73×10^{9}	8.73×10^{9}
k_{79}	2.77	1.37×10^{-2}	1.42×10^{1}	1.42×10^{1}
k_{80}	1.11×10^{5}	9.48×10^{5}	6.93×10^{5}	6.93×10^{5}
k_{81}	1.24×10^{5}	3.93	4.16×10^{5}	4.16×10^{5}
k_{82}	5.33×10^{8}	1.36×10^{6}	4.20×10^{9}	4.20×10^{9}
k_{83}	4.97×10^{-2}	1.27×10^{-4}	3.92×10^{-1}	3.92×10^{-1}
k_{84}	8.91×10^{6}	8.91×10^{6}	8.91×10^{6}	8.91×10^{6}
k_{85}	1.35×10^{-3}	1.35×10^{-3}	1.35×10^{-3}	1.35×10^{-3}
k_{86}	1.00×10^{8}	1.00×10^{8}	1.00×10^{8}	1.00×10^{8}
k_{87}	1.95×10^{5}	1.95×10^{5}	1.95×10^{5}	1.95×10^{5}
k_{88}	1.91	1.91	1.91	1.91

Table B.1: The fitted reaction rates for the Unified Model, given in mass action form.

B.2 Chatterjee Model

Reaction rate	Fitted value	Reaction rate	Fitted value
$k_{-,1}$	0.031	$k_{+,1}$	3.2×10^{6}
$k_{-,2}$	3.1×10^{-5}	$k_{+,2}$	1.13×10^{8}
$k_{+,3}$	4.4×10^{5}	$k_{+,4}$	1.3×10^{7}
$k_{+,5}$	2.3×10^{4}	$k_{-,6}$	0.0105
$k_{+,6}$	2.5×10^{7}	$k_{-,7}$	6
$k_{-,8}$	231.6	$k_{+,8}$	2.2×10^{7}
$k_{-,9}$	2.4	$k_{+,9}$	1×10^{7}
$k_{-,10}$	1.8	$k_{+,11}$	2.63×10^{4}
$k_{+,12}$	1.18×10^{8}	$k_{-,13}$	1×10^{-4}
$k_{+,13}$	3.4×10^{7}	$k_{-,14}$	1×10^{-5}
$k_{+,14}$	9.7×10^{8}	$k_{-,15}$	11.2
$k_{+,16}$	2.2×10^{4}	$k_{-,16}$	6×10^{-5}
$k_{-,17}$	1×10^{-3}	$k_{+,18}$	1.6×10^{7}
$k_{-,19}$	0.008	$k_{+,19}$	4×10^{8}
$k_{-,20}$	29.8	$k_{+,20}$	3.37×10^{8}
$k_{-,21}$	3.99	$k_{+,22}$	2.24×10^{8}
$k_{-,23}$	3.6×10^{-4}	$k_{+,23}$	9×10^{5}
$k_{-,24}$	0.011	$k_{+,24}$	2.8×10^{9}
$k_{+,25}$	5×10^{7}	$k_{+,26}$	1.39×10^{4}
$k_{+,27}$	4.33×10^{4}	$k_{+,28}$	490
$k_{+,29}$	4.07×10^{3}	$k_{+,30}$	230
$k_{+,31}$	1×10^{8}	$k_{-,31}$	6100

$k_{-,32}$	53.8	$k_{-,33}$	0.0035
$k_{+,34}$	1×10^8	$k_{-,34}$	750
$k_{-,35}$	0.033	$k_{+,36}$	1×10^8
$k_{-,36}$	3600	$k_{-,37}$	40
$k_{+,38}$	1×10^8	$k_{-,38}$	45.3
$k_{-,39}$	5.7	$k_{+,40}$	2.7×10^4
$k_{-,41}$	0.011	$k_{+,42}$	1×10^8
$k_{-,42}$	2.4	$k_{+,43}$	3600
$k_{+,44}$	21.6	$k_{+,45}$	1×10^8
$k_{-,45}$	5	$k_{-,46}$	1.3×10^{-4}
$k_{+,47}$	7.9×10^8	$k_{-,47}$	1.8×10^3
$k_{-,48}$	0.0029	$k_{+,49}$	6.66×10^7
$k_{+,50}$	320	$k_{+,51}$	2.58×10^4
$k_{+,52}$	1.75×10^3	$k_{+,53}$	6.3×10^4
$k_{+,54}$	5.24×10^7	$k_{-,54}$	679
$k_{-,55}$	3.32	$k_{+,56}$	1.17×10^9
$k_{-,56}$	0.92	$k_{-,57}$	7×10^{-4}
$k_{+,58}$	1×10^8	$k_{-,58}$	2.1
$k_{-,59}$	0.023	$k_{+,60}$	2.88×10^5
$k_{-,60}$	8.34	$k_{-,61}$	3.6×10^{-5}
$k_{+,62}$	1×10^8	$k_{-,62}$	210
$k_{-,63}$	1.6×10^{-6}	$k_{+,64}$	1×10^8
$k_{-,64}$	636	$k_{-,65}$	84
$k_{+,66}$	1×10^8	$k_{-,66}$	742.6
$k_{-,67}$	7.4	$k_{+,68}$	1×10^6
$k_{-,68}$	0.064	$k_{+,69}$	1×10^8
$k_{-,69}$	701	$k_{-,70}$	49
$k_{+,71}$	1×10^8	$k_{-,71}$	1×10^3
$k_{+,72}$	1.6×10^4	$k_{+,73}$	1.6×10^4
$k_{+,74}$	1×10^4	ε_{max_0}	0.0116
k	0.0141		

Table B.2: The fitted reaction rates for the Chatterjee model.

B.3 Expanded Unified Model

Reaction rate	Fitted value	Reaction rate	Fitted value
k_1	1.26×10^5	k_2	3.72×10^{-4}
k_3	1.12×10^6	k_4	3.55×10^{-3}
k_5	1.00×10^8	k_6	1.05×10^2
k_7	1.51×10^1	k_8	1.00×10^{10}
k_9	9.40×10^1	k_{10}	4.59×10^1
k_{11}	1.00×10^8	k_{12}	2.69×10^2
k_{13}	6.17×10^{-2}	k_{14}	1.00×10^8
k_{15}	2.69×10^2	k_{16}	6.17×10^{-2}
k_{17}	1.00×10^8	k_{18}	1.70×10^2
k_{19}	3.24×10^{-1}	k_{20}	1.00×10^8

k_{21}	1.70×10^{2}	k_{22}	3.24×10^{-1}
k_{23}	1.00×10^{8}	k_{24}	3.22×10^{2}
k_{25}	1.41	k_{26}	8.43×10^{3}
k_{27}	1.00×10^{10}	k_{28}	6.23×10^{1}
k_{29}	4.24×10^{1}	k_{30}	1.00×10^{8}
k_{31}	1.85×10^{3}	k_{32}	2.63×10^{-3}
k_{33}	1.00×10^{13}	k_{34}	5.41×10^{1}
k_{35}	5.00×10^{1}	k_{36}	1.00×10^{8}
k_{37}	2.53	k_{38}	1.54×10^{-3}
k_{39}	1.00×10^{8}	k_{40}	2.01×10^{1}
k_{41}	3.01	k_{42}	1.00×10^{8}
k_{43}	9.66	k_{44}	5.60×10^{-1}
k_{45}	2.46×10^{10}	k_{46}	1.46
k_{47}	1.28×10^{4}	k_{48}	1.90×10^{4}
k_{49}	1.00×10^{8}	k_{50}	1.75×10^{3}
k_{51}	9.33×10^{-3}	k_{52}	1.00×10^{8}
k_{53}	1.03×10^{3}	k_{54}	8.95×10^{1}
k_{55}	3.12×10^{3}	k_{56}	1.00×10^{8}
k_{57}	9.24×10^{1}	k_{58}	1.14×10^{-3}
k_{59}	1.00×10^{8}	k_{60}	6.57×10^{1}
k_{61}	1.30×10^{-4}	k_{62}	3.98×10^{2}
k_{63}	1.00×10^{8}	k_{64}	1.85×10^{2}
k_{65}	5.37×10^{-1}	k_{66}	1.00×10^{8}
k_{67}	2.35×10^{-1}	k_{68}	5.30×10^{-4}
k_{69}	1.00×10^{8}	k_{70}	7.01×10^{2}
k_{71}	1.04×10^{1}	k_{72}	1.00×10^{8}
k_{73}	1.04×10^{2}	k_{74}	1.43×10^{1}
k_{75}	1.00×10^{8}	k_{76}	1.97×10^{1}
k_{77}	2.19×10^{-1}	k_{78}	6.98×10^{7}
k_{79}	6.39×10^{-1}	k_{80}	4.90×10^{2}
k_{81}	4.90×10^{2}	k_{82}	3.80×10^{6}
k_{83}	1.67×10^{-2}	k_{84}	8.91×10^{6}
k_{85}	1.35×10^{-3}	k_{86}	1.00×10^{8}
k_{87}	1.95×10^{5}	k_{88}	1.91
k_{89}	2.20×10^{7}	k_{90}	1.90×10^{1}
k_{91}	5.48×10^{1}	k_{92}	1.77×10^{3}
k_{93}	3.79×10^{3}	k_{94}	6.67×10^{1}
k_{95}	5.00×10^{2}	k_{96}	5.52×10^{2}
k_{97}	1.67×10^{1}	k_{98}	2.10×10^{5}
k_{99}	7.72×10^{-2}	k_{100}	2.01×10^{-8}
k_{101}	1.40×10^{-3}	k_{102}	1.00×10^{8}
k_{103}	1.98×10^{1}	k_{104}	2.20×10^{-1}
k_{105}	4.15×10^{-2}	k_{106}	5.00×10^{-4}
k_{107}	8.91×10^{6}	k_{108}	1.00×10^{8}
k_{109}	5.00×10^{-1}	k_{100}	3.03×10^{7}
k_{111}	1.51×10^{-2}	k_{112}	1.20×10^{-2}
k_{113}	4.67×10^{-4}		

Table B.3: The fitted reaction rates for the Expanded Unified Model, given in mass action form.

B.4 Expanded Unified Model with Protein C

Reaction rate	Fitted value	Reaction rate	Fitted value
k_1	5.21×10^{5}	k_2	1.54×10^{-3}
k_3	1.62×10^{6}	k_4	5.11×10^{-3}
k_5	1.00×10^{8}	k_6	1.05×10^{2}
k_7	1.51×10^{1}	k_8	1.00×10^{9}
k_9	6.74×10^{1}	k_{10}	1.55×10^{1}
k_{11}	1.00×10^{8}	k_{12}	2.69×10^{2}
k_{13}	6.17×10^{-2}	k_{14}	1.00×10^{8}
k_{15}	2.05×10^{2}	k_{16}	2.70×10^{-1}
k_{17}	1.00×10^{8}	k_{18}	1.70×10^{2}
k_{19}	3.24×10^{-1}	k_{20}	1.00×10^{8}
k_{21}	1.70×10^{2}	k_{22}	3.24×10^{-1}
k_{23}	1.00×10^{8}	k_{24}	3.22×10^{2}
k_{25}	1.41	k_{26}	3.00×10^{2}
k_{27}	1.00×10^{10}	k_{28}	1.49×10^{2}
k_{29}	1.21×10^{2}	k_{30}	1.00×10^{8}
k_{31}	2.01×10^{1}	k_{32}	9.22×10^{-4}
k_{33}	1.00×10^{8}	k_{34}	4.08
k_{35}	3.51×10^{-2}	k_{36}	1.00×10^{8}
k_{37}	4.62×10^{-1}	k_{38}	3.03×10^{-4}
k_{39}	1.00×10^{9}	k_{40}	1.48×10^{1}
k_{41}	1.73	k_{42}	1.00×10^{8}
k_{43}	6.05	k_{44}	9.43×10^{-2}
k_{45}	1.33×10^{10}	k_{46}	2.02×10^{-1}
k_{47}	3.84×10^{2}	k_{48}	2.65×10^{2}
k_{49}	1.00×10^{8}	k_{50}	4.00×10^{2}
k_{51}	9.33×10^{-3}	k_{52}	1.00×10^{13}
k_{53}	2.50×10^{2}	k_{54}	2.15×10^{2}
k_{55}	1.89×10^{3}	k_{56}	1.00×10^{8}
k_{57}	6.15×10^{1}	k_{58}	6.89×10^{-6}
k_{59}	1.00×10^{8}	k_{60}	2.31
k_{61}	1.30×10^{-4}	k_{62}	1.19×10^{3}
k_{63}	1.00×10^{8}	k_{64}	8.77×10^{1}
k_{65}	1.90	k_{66}	1.00×10^{8}
k_{67}	1.30×10^{1}	k_{68}	9.36×10^{-5}
k_{69}	1.00×10^{8}	k_{70}	2.77×10^{2}
k_{71}	1.38×10^{-4}	k_{72}	1.00×10^{9}
k_{73}	1.14×10^{1}	k_{74}	6.21
k_{75}	1.00×10^{8}	k_{76}	1.97×10^{1}
k_{77}	2.19×10^{-1}	k_{78}	9.04×10^{5}
k_{79}	9.33×10^{-4}	k_{80}	3.78×10^{1}

k_{81}	7.78×10^{2}	k_{82}	3.80×10^{6}
k_{83}	1.67×10^{-2}	k_{84}	8.91×10^{6}
k_{85}	1.35×10^{-3}	k_{86}	1.00×10^{8}
k_{87}	1.95×10^{5}	k_{88}	1.91
k_{89}	2.20×10^{7}	k_{90}	1.90×10^{1}
k_{91}	8.29×10^{1}	k_{92}	1.10×10^{2}
k_{93}	2.19×10^{2}	k_{94}	2.80×10^{1}
k_{95}	5.00×10^{2}	k_{96}	2.49×10^{2}
k_{97}	1.67×10^{1}	k_{98}	2.10×10^{5}
k_{99}	2.29×10^{-2}	k_{100}	5.96×10^{-9}
k_{101}	1.40×10^{-3}	k_{102}	1.00×10^{8}
k_{103}	1.98×10^{1}	k_{104}	2.20×10^{-1}
k_{105}	4.15×10^{-2}	k_{106}	5.00×10^{-4}
k_{107}	8.91×10^{6}	k_{108}	1.00×10^{8}
k_{109}	5.00×10^{-1}	k_{110}	2.72×10^{6}
k_{111}	1.36×10^{-3}	k_{112}	1.20×10^{-2}
k_{113}	4.67×10^{-4}	k_{114}	7.47×10^{8}
k_{115}	9.35×10^{-3}	k_{116}	1.00×10^{11}
k_{117}	4.21×10^{2}	k_{118}	4.15×10^{2}
k_{119}	1.00×10^{10}	k_{120}	4.52×10^{1}
k_{121}	1.08×10^{1}	k_{122}	1.00×10^{9}
k_{123}	6.32	k_{124}	2.43
k_{125}	1.00×10^{12}	k_{126}	2.03×10^{1}
k_{127}	2.58	k_{128}	1.00×10^{8}
k_{129}	9.29	k_{130}	1.98×10^{-2}

Table B.4: The fitted reaction rates for the Expanded Unified Model with Protein C, given in mass action form.

B.5 Expanded Unified Model with Fibrinogen

Reaction rate	Fitted value	Reaction rate	Fitted value
k_1	2.47×10^{6}	k_2	7.30×10^{-3}
k_3	1.19×10^{6}	k_4	1.25×10^{-2}
k_5	1.00×10^{8}	k_6	1.05×10^{2}
k_7	1.51×10^{1}	k_8	1.00×10^{11}
k_9	8.36×10^{2}	k_{10}	1.24×10^{2}
k_{11}	1.00×10^{8}	k_{12}	2.69×10^{2}
k_{13}	6.17×10^{-2}	k_{14}	1.00×10^{8}
k_{15}	2.69×10^{2}	k_{16}	6.17×10^{-2}
k_{17}	1.00×10^{8}	k_{18}	1.70×10^{2}
k_{19}	3.24×10^{-1}	k_{20}	1.00×10^{8}
k_{21}	1.70×10^{2}	k_{22}	3.24×10^{-1}
k_{23}	1.00×10^{8}	k_{24}	3.23×10^{2}
k_{25}	1.41	k_{26}	9.18×10^{3}
k_{27}	1.00×10^{8}	k_{28}	7.10×10^{2}
k_{29}	1.13×10^{2}	k_{30}	1.00×10^{8}

k_{31}	2.72×10^{3}	k_{32}	4.87×10^{-3}
k_{33}	1.00×10^{12}	k_{34}	5.05×10^{2}
k_{35}	9.65×10^{1}	k_{36}	1.00×10^{8}
k_{37}	6.93×10^{-2}	k_{38}	4.43×10^{-3}
k_{39}	1.00×10^{8}	k_{40}	9.26×10^{1}
k_{41}	8.34	k_{42}	1.00×10^{8}
k_{43}	1.30×10^{1}	k_{44}	8.17×10^{-1}
k_{45}	4.91×10^{10}	k_{46}	1.23
k_{47}	2.78×10^{4}	k_{48}	3.54×10^{4}
k_{49}	1.00×10^{8}	k_{50}	3.64×10^{3}
k_{51}	9.33×10^{-3}	k_{52}	1.00×10^{8}
k_{53}	1.75×10^{3}	k_{54}	7.77×10^{2}
k_{55}	2.94×10^{3}	k_{56}	1.00×10^{8}
k_{57}	2.06×10^{2}	k_{58}	1.36×10^{-3}
k_{59}	1.00×10^{8}	k_{60}	1.26×10^{2}
k_{61}	1.30×10^{-4}	k_{62}	3.98×10^{2}
k_{63}	1.00×10^{8}	k_{64}	1.18×10^{2}
k_{65}	5.37×10^{-1}	k_{66}	1.00×10^{8}
k_{67}	7.28	k_{68}	1.13×10^{-3}
k_{69}	1.00×10^{8}	k_{70}	1.86×10^{3}
k_{71}	1.59	k_{72}	1.00×10^{8}
k_{73}	4.23×10^{2}	k_{74}	1.95×10^{1}
k_{75}	1.00×10^{8}	k_{76}	1.98×10^{1}
k_{77}	2.19×10^{-1}	k_{78}	8.05×10^{7}
k_{79}	1.35×10^{-2}	k_{80}	4.90×10^{2}
k_{81}	4.90×10^{2}	k_{82}	3.80×10^{6}
k_{83}	1.67×10^{-2}	k_{84}	8.91×10^{6}
k_{85}	1.35×10^{-3}	k_{86}	1.00×10^{8}
k_{87}	1.95×10^{5}	k_{88}	1.91
k_{89}	2.20×10^{7}	k_{90}	1.90×10^{1}
k_{91}	3.28×10^{1}	k_{92}	7.21×10^{2}
k_{93}	9.08×10^{2}	k_{94}	6.67×10^{1}
k_{95}	5.00×10^{2}	k_{96}	7.87×10^{2}
k_{97}	1.67×10^{1}	k_{98}	2.10×10^{5}
k_{99}	2.26×10^{-2}	k_{100}	5.88×10^{-9}
k_{101}	1.40×10^{-3}	k_{102}	1.00×10^{8}
k_{103}	1.98×10^{1}	k_{104}	2.20×10^{-1}
k_{105}	4.15×10^{-2}	k_{106}	5.00×10^{-4}
k_{107}	8.91×10^{6}	k_{108}	1.00×10^{8}
k_{109}	5.00×10^{-1}	k_{110}	9.92×10^{7}
k_{111}	4.96×10^{-2}	k_{112}	1.20×10^{-2}
k_{113}	4.67×10^{-4}	k_{114}	1.00×10^{8}
k_{115}	3.75×10^{2}	k_{116}	8.40×10^{1}
k_{117}	1.00×10^{8}	k_{118}	7.00×10^{3}
k_{119}	7.45	k_{120}	1.00×10^{8}
k_{121}	5.75×10^{4}		

Table B.5: The fitted reaction rates for the Expanded Unified Model with Fibrinogen, given in mass action form.

B.6 Reduced Unified Model

This section presents the rates found in Chapter 4 when fitting to the reduced set of OD curves.

Reaction rate	Fitted value	Reaction rate	Fitted value
k_1	3.35×10^{6}	k_2	9.88×10^{-3}
k_3	3.61×10^{4}	k_4	2.34×10^{-3}
k_5	1.00×10^{8}	k_6	1.05×10^{2}
k_7	1.51×10^{1}	k_8	1.00×10^{12}
k_9	7.17×10^{1}	k_{10}	1.01×10^{2}
k_{11}	1.00×10^{8}	k_{12}	2.69×10^{2}
k_{13}	6.17×10^{-2}	k_{14}	1.00×10^{8}
k_{15}	1.34×10^{4}	k_{16}	6.18×10^{-1}
k_{17}	1.00×10^{8}	k_{18}	1.70×10^{2}
k_{19}	3.24×10^{-1}	k_{20}	1.00×10^{8}
k_{21}	1.70×10^{2}	k_{22}	3.24×10^{-1}
k_{23}	2.35×10^{4}	k_{24}	1.00×10^{8}
k_{25}	1.06×10^{3}	k_{26}	4.74×10^{1}
k_{27}	1.00×10^{8}	k_{28}	3.79×10^{3}
k_{29}	8.60×10^{-3}	k_{30}	1.00×10^{9}
k_{31}	2.75×10^{2}	k_{32}	1.51×10^{2}
k_{33}	1.00×10^{8}	k_{34}	1.29×10^{2}
k_{35}	8.03×10^{-3}	k_{36}	1.00×10^{8}
k_{37}	1.45×10^{2}	k_{38}	8.43
k_{39}	1.00×10^{11}	k_{40}	3.99
k_{41}	1.69	k_{42}	7.32×10^{8}
k_{43}	1.06	k_{44}	4.43×10^{3}
k_{45}	4.09×10^{4}	k_{46}	1.00×10^{8}
k_{47}	3.77×10^{3}	k_{48}	9.33×10^{-3}
k_{49}	1.00×10^{8}	k_{50}	2.56×10^{3}
k_{51}	3.65×10^{2}	k_{52}	3.97×10^{3}
k_{53}	1.00×10^{8}	k_{54}	2.72×10^{2}
k_{55}	4.96×10^{-3}	k_{56}	1.00×10^{8}
k_{57}	1.63×10^{2}	k_{58}	1.30×10^{-4}
k_{59}	3.98×10^{2}	k_{60}	1.00×10^{8}
k_{61}	3.24×10^{2}	k_{62}	5.37×10^{-1}
k_{63}	1.00×10^{8}	k_{64}	8.87×10^{-1}
k_{65}	1.70×10^{-3}	k_{66}	1.00×10^{8}
k_{67}	2.00×10^{3}	k_{68}	3.95×10^{1}
k_{69}	1.00×10^{8}	k_{70}	5.33×10^{2}
k_{71}	3.00×10^{1}	k_{72}	1.00×10^{8}
k_{73}	1.98×10^{1}	k_{74}	2.19×10^{-1}

k_{75}	2.20×10^{8}	k_{76}	1.48
k_{77}	4.90×10^{2}	k_{78}	4.90×10^{2}
k_{79}	1.15×10^{7}	k_{80}	1.07×10^{-3}
k_{81}	8.91×10^{6}	k_{82}	1.35×10^{-3}
k_{83}	1.00×10^{8}	k_{84}	1.95×10^{5}
k_{85}	1.91	k_{86}	2.20×10^{7}
k_{87}	1.90×10^{1}	k_{88}	1.61×10^{1}
k_{89}	7.27×10^{2}	k_{90}	5.19×10^{3}
k_{91}	6.67×10^{1}	k_{92}	5.00×10^{2}
k_{93}	1.57×10^{2}	k_{94}	2.10×10^{5}
k_{95}	2.51×10^{-2}	k_{96}	1.40×10^{-3}
k_{97}	8.91×10^{6}	k_{98}	1.00×10^{8}
k_{99}	2.84×10^{4}	k_{100}	8.40×10^{1}
k_{101}	1.00×10^{8}	k_{102}	2.99×10^{4}
k_{103}	7.45	k_{104}	1.00×10^{8}
k_{105}	6.09×10^{4}		

Table B.6: The fitted reaction rates for the Reduced Unified Model, given in mass action form.

B.7 Improved Unified Model

Table 5.4 presents the fitting reaction rates in prior form. They are presented here in mass action form for simulation with the ODEs.

Rate	GD	ABC-SMC	GD - All Rates	ABC-SMC - All Rates
k_1	1.87×10^{6}	1.22×10^{5}	1.59×10^{6}	5.17×10^{4}
k_2	5.62×10^{-3}	3.66×10^{-4}	1.33×10^{-4}	2.65×10^{-5}
k_3	1.01×10^{6}	8.19×10^{4}	5.54×10^{5}	1.47×10^{5}
k_4	3.22×10^{-3}	2.62×10^{-4}	3.97×10^{-3}	1.37×10^{-4}
k_5	1.00×10^{8}	1.00×10^{11}	1.00×10^{8}	1.00×10^{8}
k_6	1.09×10^{2}	1.37×10^{3}	5.89×10^{2}	2.53
k_7	1.19×10^{2}	6.81×10^{2}	2.46×10^{1}	1.06×10^{-2}
k_8	1.00×10^{9}	1.00×10^{8}	1.00×10^{8}	1.00×10^{8}
k_9	3.45×10^{1}	4.85×10^{-2}	1.49×10^{1}	1.24×10^{1}
k_{10}	2.34×10^{1}	7.52×10^{-1}	3.71	5.25
k_{11}	1.00×10^{8}	1.00×10^{8}	1.00×10^{8}	1.00×10^{8}
k_{12}	2.70×10^{2}	2.70×10^{2}	1.85×10^{3}	1.10×10^{4}
k_{13}	1.15×10^{-4}	4.92×10^{-3}	1.96×10^{-3}	5.18×10^{-3}
k_{14}	1.00×10^{8}	1.00×10^{10}	1.00×10^{8}	1.00×10^{8}
k_{15}	2.56×10^{3}	4.96×10^{3}	1.88×10^{3}	2.70×10^{3}
k_{16}	2.05×10^{-4}	3.02×10^{3}	1.66×10^{-4}	4.09×10^{2}
k_{17}	1.00×10^{8}	1.00×10^{8}	1.00×10^{8}	1.00×10^{13}
k_{18}	1.28×10^{3}	3.13	1.73×10^{2}	1.10×10^{4}
k_{19}	2.69	1.53	1.03	1.48×10^{3}
k_{20}	1.00×10^{8}	1.00×10^{8}	1.00×10^{8}	1.00×10^{8}

k_{21}	7.25×10^{2}	1.23×10^{1}	1.12×10^{3}	1.07
k_{22}	1.45	2.58×10^{-2}	5.54×10^{-1}	6.20×10^{-2}
k_{23}	1.00×10^{8}	1.00×10^{8}	1.00×10^{8}	1.00×10^{11}
k_{24}	1.46×10^{3}	4.33×10^{3}	1.19×10^{3}	4.97×10^{2}
k_{25}	1.40	1.40	7.91×10^{-1}	2.84×10^{4}
k_{26}	2.47×10^{3}	5.56×10^{3}	9.85×10^{2}	1.99×10^{2}
k_{27}	1.00×10^{11}	1.00×10^{8}	1.00×10^{11}	1.00×10^{8}
k_{28}	1.26×10^{2}	9.44×10^{1}	9.76×10^{1}	1.68×10^{2}
k_{29}	1.58×10^{1}	2.81	1.69×10^{1}	1.19
k_{30}	1.00×10^{8}	1.00×10^{8}	1.00×10^{8}	1.00×10^{8}
k_{31}	3.98×10^{2}	1.55×10^{1}	3.04×10^{2}	2.55×10^{1}
k_{32}	3.20×10^{-4}	3.20×10^{-4}	6.83×10^{-4}	3.12×10^{-4}
k_{33}	1.00×10^{11}	1.00×10^{9}	1.00×10^{11}	1.00×10^{9}
k_{34}	5.01×10^{1}	5.94×10^{1}	5.73×10^{1}	2.16×10^{1}
k_{35}	1.67×10^{1}	6.96	2.57×10^{1}	3.70
k_{36}	1.00×10^{8}	1.00×10^{8}	1.00×10^{8}	1.00×10^{8}
k_{37}	1.87×10^{-1}	9.56×10^{-1}	2.90×10^{-1}	2.21
k_{38}	2.15×10^{-4}	1.45×10^{-3}	5.48×10^{-4}	1.28×10^{-4}
k_{39}	1.00×10^{8}	1.00×10^{10}	1.00×10^{8}	1.00×10^{8}
k_{40}	3.12×10^{1}	1.20	5.94×10^{1}	1.87×10^{1}
k_{41}	3.18	3.28×10^{-1}	3.82×10^{-2}	2.58×10^{-1}
k_{42}	1.00×10^{8}	1.00×10^{8}	1.00×10^{8}	1.00×10^{11}
k_{43}	6.14	3.34×10^{3}	5.68	4.33×10^{1}
k_{44}	2.99×10^{-1}	1.33	1.07×10^{-1}	1.58×10^{1}
k_{45}	1.39×10^{10}	9.24×10^{10}	1.62×10^{10}	1.02×10^{11}
k_{46}	3.38×10^{-1}	3.54×10^{-1}	8.09×10^{-2}	5.30
k_{47}	5.23×10^{3}	1.36×10^{3}	5.67×10^{2}	2.38×10^{3}
k_{48}	3.52×10^{3}	2.72×10^{-1}	1.32×10^{3}	3.51×10^{-1}
k_{49}	1.00×10^{8}	1.00×10^{8}	1.00×10^{8}	1.00×10^{8}
k_{50}	9.03×10^{2}	3.17×10^{1}	6.80×10^{2}	1.20×10^{2}
k_{51}	9.30×10^{-3}	9.30×10^{-3}	7.65×10^{-3}	2.43×10^{-3}
k_{52}	1.00×10^{8}	1.00×10^{8}	1.00×10^{8}	1.00×10^{8}
k_{53}	4.62×10^{-1}	1.45×10^{2}	3.31×10^{2}	2.02×10^{1}
k_{54}	8.39×10^{1}	4.11×10^{1}	2.70×10^{2}	4.56×10^{1}
k_{55}	4.02×10^{3}	5.39×10^{3}	4.31×10^{3}	5.53×10^{3}
k_{56}	1.00×10^{8}	1.00×10^{8}	1.00×10^{8}	1.00×10^{8}
k_{57}	9.50×10^{1}	2.13	5.18×10^{1}	1.22×10^{2}
k_{58}	9.83×10^{-5}	1.65×10^{-5}	2.09×10^{-5}	1.22×10^{-12}
k_{59}	1.00×10^{8}	1.00×10^{8}	1.00×10^{8}	1.00×10^{8}
k_{60}	2.24×10^{1}	5.13×10^{-2}	2.07×10^{1}	1.95×10^{5}
k_{61}	2.94×10^{-4}	1.14×10^{-4}	8.90×10^{-4}	1.44×10^{-3}
k_{62}	4.00×10^{2}	4.00×10^{2}	4.59×10^{2}	5.44×10^{2}
k_{63}	1.00×10^{8}	1.00×10^{8}	1.00×10^{8}	1.00×10^{8}
k_{64}	8.72×10^{1}	4.02	7.19×10^{1}	1.84×10^{1}
k_{65}	4.30×10^{-1}	4.30×10^{-1}	1.10	4.73×10^{-1}
k_{66}	1.00×10^{8}	1.00×10^{8}	1.00×10^{8}	1.00×10^{8}
k_{67}	8.17×10^{-1}	6.46	1.18	2.77×10^{1}
k_{68}	1.34×10^{-3}	9.11×10^{-5}	1.54×10^{-3}	4.09×10^{-7}

k_{69}	1.00×10^{8}	1.00×10^{8}	1.00×10^{8}	1.00×10^{8}
k_{70}	6.89×10^{2}	2.43×10^{1}	2.66×10^{2}	3.77×10^{1}
k_{71}	9.24×10^{-1}	3.29×10^{-1}	4.13×10^{-1}	2.05
k_{72}	1.00×10^{9}	1.00×10^{8}	1.00×10^{10}	1.00×10^{8}
k_{73}	1.28	9.41×10^{-1}	1.11×10^{1}	9.98×10^{1}
k_{74}	8.00×10^{-1}	8.00×10^{-1}	4.05	7.25×10^{-1}
k_{75}	1.00×10^{8}	1.00×10^{8}	1.00×10^{8}	1.00×10^{8}
k_{76}	5.65×10^{1}	6.27×10^{1}	2.22×10^{1}	2.02
k_{77}	1.26	2.74	3.01×10^{-1}	5.31×10^{-1}
k_{78}	1.82×10^{-2}	3.88×10^{-2}	2.41×10^{-2}	4.57×10^{-8}
k_{79}	6.86×10^{4}	1.47×10^{5}	8.92×10^{3}	1.67×10^{-1}
k_{80}	8.96×10^{-3}	3.67×10^{-2}	2.27×10^{-3}	1.90×10^{-2}
k_{81}	5.51×10^{7}	1.26×10^{11}	3.04×10^{7}	1.07×10^{7}
k_{82}	3.06×10^{-1}	2.97×10^{2}	1.86×10^{-1}	3.15×10^{-2}
k_{83}	2.79×10^{3}	1.66	5.48×10^{2}	2.26
k_{84}	2.45×10^{3}	2.35×10^{3}	1.22×10^{3}	2.27×10^{4}
k_{85}	1.39×10^{7}	1.11×10^{6}	3.80×10^{6}	9.17×10^{5}
k_{86}	1.28×10^{-3}	1.03×10^{-4}	1.69×10^{-3}	4.81×10^{-5}
k_{87}	8.90×10^{6}	8.90×10^{6}	3.19×10^{7}	8.79×10^{6}
k_{88}	1.34×10^{-3}	1.34×10^{-3}	1.38×10^{-2}	5.17×10^{-2}
k_{89}	1.56×10^{2}	1.02×10^{2}	2.81×10^{2}	4.11×10^{1}
k_{90}	8.75×10^{1}	1.24×10^{2}	4.59×10^{1}	5.77×10^{-2}
k_{91}	4.43×10^{3}	4.24	3.03×10^{3}	1.02×10^{1}
k_{92}	8.20×10^{1}	8.20×10^{1}	4.76×10^{2}	9.54×10^{1}
k_{93}	6.56×10^{2}	6.56×10^{2}	2.86×10^{3}	9.91×10^{2}
k_{94}	4.65×10^{2}	4.98	1.99×10^{2}	1.03×10^{1}
k_{95}	1.10×10^{3}	1.10×10^{3}	3.49×10^{3}	1.50×10^{3}
k_{96}	1.09×10^{6}	2.96×10^{5}	6.48×10^{5}	8.11×10^{3}
k_{97}	1.42×10^{8}	1.10×10^{8}	4.24×10^{8}	5.80×10^{7}
k_{98}	6.57×10^{3}	7.74×10^{1}	5.48×10^{2}	5.81
k_{99}	2.99×10^{2}	2.91×10^{2}	3.96×10^{2}	1.08×10^{1}
k_{100}	6.51×10^{8}	1.15×10^{7}	7.75×10^{8}	7.76×10^{6}
k_{101}	1.59×10^{3}	1.61×10^{4}	2.70×10^{3}	4.90×10^{4}
k_{102}	5.00×10^{1}	1.78×10^{1}	3.30×10^{1}	3.31×10^{1}
k_{103}	9.62×10^{4}	3.48×10^{7}	3.49×10^{7}	3.37×10^{6}
k_{104}	2.93×10^{3}	2.79×10^{3}	9.79×10^{3}	1.50×10^{4}
k_{105}	8.64×10^{2}	3.13×10^{4}	9.81×10^{2}	4.12×10^{3}
k_{106}	2.16×10^{4}	1.06×10^{2}	2.04×10^{2}	1.23×10^{5}
k_{107}	1.00×10^{8}	1.00×10^{8}	1.00×10^{8}	1.00×10^{8}
k_{108}	1.95×10^{5}	1.95×10^{5}	1.95×10^{5}	1.95×10^{5}
k_{109}	1.91	1.91	1.91	1.91

Table B.7: The fitted reaction rates for the Improved Unified Model, given in mass action form.

Appendix C

Model Comparison

This appendix presents the remaining reactions not described in the comparison between the models in Section 2.4, given in Table C.1. These reactions all have at least two models they are included in and two models in which they are not included.

Reaction	Hockin?	Danforth?	Brummel?	Bungay?	Tyurin?	Zhu?	Chatterjee?	Panteleev?
XI $\overset{XIa}{\rightarrow}$ XIa	N	N	N	N	Y	N	Y	N
XIa + AT $\rightarrow$ XIa:AT	N	N	N	N	Y	Y	Y	Y
XI $\overset{IIa}{\rightarrow}$ XIa	N	N	N	Y	Y	N	Y	Y
IX $\overset{XIa}{\rightarrow}$ IXa	N	N	N	Y	Y	Y	Y	Y
IXa + VIIIa $\leftarrow$ IXa:VIIIa	Y	Y	Y	Y	N	N	Y	N
Xa + Va $\leftarrow$ Xa:Va	Y	Y	Y	Y	N	N	Y	Y
Xa + TFPI $\leftarrow$ Xa:TFPI	Y	Y	Y	Y	N	N	Y	Y
Xa:Va + AT $\rightarrow$ Xa:AT + Va	N	N	N	N	Y	N	N	Y
II $\overset{Xa:Va}{\rightarrow}$ mIIa	Y	Y	Y	Y	N	N	Y	N
mIIa $\overset{Xa:Va}{\rightarrow}$ IIa	Y	Y	Y	Y	N	N	Y	N

II $\overset{Xa:Va}{\rightarrow}$ IIa	N	N	N	N	Y	Y	N	Y
X $\overset{VIIa}{\rightarrow}$ Xa	N	N	N	N	Y	N	Y	N
IX $\overset{VIIa}{\rightarrow}$ IXa	N	N	N	N	Y	N	Y	N
X $\overset{IXa}{\rightarrow}$ Xa	N	Y	Y	N	Y	Y	Y	Y
VIIIa $\leftrightarrow$ VIIIa1L + VIIIa2	Y	Y	Y	N	N	N	Y	Y
IXa:VIIIa $\rightarrow$ IXa + VIIIa1L + VIIIa2	Y	Y	Y	N	N	N	Y	N
IXa:VIIIa:X $\rightarrow$ IXa + X + VIIIa1L + VIIIa2	Y	Y	Y	N	N	N	Y	N
TF:VIIa:Xa + TFPI $\rightarrow$ TF:VIIa:Xa:TFPI	Y	Y	Y	N	N	N	Y	Y
TF:VIIa:Xa + TFPI $\leftarrow$ TF:VIIa:Xa:TFPI	Y	Y	Y	N	N	N	Y	N
TF:VIIa + AT $\rightarrow$ TF:VIIa:AT	Y	Y	Y	N	Y	Y	Y	N
VII $\overset{IIa}{\rightarrow}$ VIIa	Y	Y	Y	N	N	N	Y	Y
VII $\overset{TF:VIIa}{\rightarrow}$ VIIa	Y	Y	Y	N	N	N	Y	N
VII $\overset{Xa}{\rightarrow}$ VIIa	Y	Y	Y	Y	Y	N	Y	N
TF:VII $\overset{Xa}{\rightarrow}$ TF:VIIa	N	N	N	Y	Y	Y	N	Y
VIII $\overset{Xa}{\rightarrow}$ VIIIa	N	N	N	Y	N	N	Y	N
V $\overset{Xa}{\rightarrow}$ Va	N	N	N	Y	Y	Y	N	N
V $\overset{mIIa}{\rightarrow}$ Va	N	Y	Y	Y	N	N	N	N
mIIa + AT $\rightarrow$ mIIa:AT	Y	Y	Y	Y	N	N	Y	N

Table C.1: The remaining reduced reactions and whether they are contained in each of the models.

Appendix D

Parameter Sources

This appendix provides the parameter source tables that we used for the results in Section 2.6. Each row gives the parameter name, as given in Section 2.1, the reaction that the parameter influences, the value used by the model, a citation to the source, and any notes on that source, for example a source might not measure a rate for that specific reaction but instead measures a similar reaction.

D.1 Hockin Model

Parameter	Reaction	Value	Sources	Notes
$k_{+,1}$	TF + VII $\rightarrow$ TF:VII	$3.2 \times 10^{6} M^{-1} s^{-1}$	[1]	$K_d = 2 \times 10^{-9} M$ [1] used as a base and fitted using data from [2]. In the model $K_d = 9.7 \times 10^{-10} M$.
$k_{-,1}$	TF + VII $\leftarrow$ TF:VII	$3.1 \times 10^{-3} s^{-1}$	[1]	See above

$k_{+,2}$	TF + VIIa $\rightarrow$ TF:VIIa	$2.3 \times 10^7 M^{-1}s^{-1}$	[1]	$K_d = 5.47 \times 10^{-9}M$ [1] used as a base and fitted using data from [3]. In the model $K_d = 1.35 \times 10^{-10}M$.
$k_{-,2}$	TF + VIIa $\leftarrow$ TF:VIIa	$3.1 \times 10^{-3}s^{-1}$	[1]	See above
$k_{+,3}$	TF:VIIa + VII $\rightarrow$ TF:VIIa + VIIa	$4.45 \times 10^5 M^{-1}s^{-1}$	[4]	[4] gives $K_m = 3.2 \times 10^{-6}M, k_{cat} = 1.4s^{-1}$
$k_{+,4}$	Xa + VII $\rightarrow$ Xa + VIIa	$1.3 \times 10^7 M^{-1}s^{-1}$	[4]	[4] gives $K_m = 1.2 \times 10^{-6}M, k_{cat} = 15.2s^{-1}$
$k_{+,5}$	IIa + VII $\rightarrow$ IIa + VIIa	$2.3 \times 10^4 M^{-1}s^{-1}$	[4]	[4] gives $K_m = 2.7 \times 10^{-6}M, k_{cat} = 0.061s^{-1}$
$k_{+,6}$	TF:VIIa + X $\rightarrow$ TF:VIIa:X	$2.5 \times 10^7 M^{-1}s^{-1}$	[5, 3, 6]	[5] gives $K_m = 2.38 \times 10^{-7}M$ and $k_{\text{cat}} = 7s^{-1}$, [3] gives $K_m = 6.9 \times 10^{-8}M$ and $k_{\text{cat}} = 7.4s^{-1}$, [6] gives $K_m = 4.35 \times 10^{-6}M$ and $k_{\text{cat}} = 5.69s^{-1}$, [6] suggest Xa binds similarly to X
$k_{-,6}$	TF:VIIa + X $\leftarrow$ TF:VIIa:X	$1.05s^{-1}$	[5, 3, 6]	See above
$k_{+,7}$	TF:VIIa:X $\rightarrow$ TF:VIIa:Xa	$6s^{-1}$	[5, 3, 6]	See above
$k_{+,8}$	TF:VIIa + Xa $\rightarrow$ TF:VIIa:Xa	$2.2 \times 10^7 M^{-1}s^{-1}$	[5, 6]	[6, 5] suggest that Xa binds similarly to X
$k_{-,8}$	TF:VIIa + Xa $\leftarrow$ TF:VIIa:Xa	$19s^{-1}$	[5, 6]	See above
$k_{+,9}$	TF:VIIa + IX $\rightarrow$ TF:VIIa:IX	$1.0 \times 10^7 M^{-1}s^{-1}$	[7]	From Jones model [8], [7] gives $K_m = 2.43 \times 10^{-7}M, k_{\text{cat}} = 0.34s^{-1}$, changed by Hockin based on [9] ratios for X and IX activation by TF:VIIa.
$k_{-,9}$	TF:VIIa + IX $\leftarrow$ TF:VIIa:IX	$2.45s^{-1}$	[7]	See above
$k_{+,10}$	TF:VIIa:IX $\rightarrow$ TF:VIIa + IXa	$1.8s^{-1}$	[7]	See above

$k_{+,11}$	Xa + II $\rightarrow$ Xa + IIa	$7.5 \times 10^3 M^{-1}s^{-1}$	[10]	[10] gives $K_m = 3 \times 10^{-7}M, k_{\text{cat}} = 2.3 \times 10^{-3}s^{-1}$
$k_{+,12}$	IIa + VIII $\rightarrow$ IIa + VIIIa	$2.0 \times 10^7 M^{-1}s^{-1}$	-	Assumed to be same as IIa activation of V
$k_{+,13}$	VIIIa + IXa $\rightarrow$ IXa:VIIIa	$1.0 \times 10^7 M^{-1}s^{-1}$	[11]	Used in Jones model [8], [11] gives $K_d = 2 \times 10^{-9}M$
$k_{-,13}$	VIIIa + IXa $\leftarrow$ IXa:VIIIa	$5.0 \times 10^{-3}s^{-1}$	[11]	See above
$k_{+,14}$	IXa:VIIIa + X $\rightarrow$ IXa:VIIIa:X	$1.0 \times 10^8 M^{-1}s^{-1}$	[12]	Used in Jones model [8], [12] gives $K_m = 6.3 \times 10^{-8}M$ and $k_{\text{cat}} = 8.3s^{-1}$
$k_{-,14}$	IXa:VIIIa + X $\leftarrow$ IXa:VIIIa:X	$1.0 \times 10^{-3}s^{-1}$	[12]	See above
$k_{+,15}$	IXa:VIIIa:X $\rightarrow$ IXa:VIIIa + Xa	$8.2s^{-1}$	[12]	See above
$k_{+,16}$	VIIIa $\rightarrow$ VIIIa1L + VIIIa2	$6.0 \times 10^{-3}s^{-1}$	[13, 14]	[13] gives $K_d = 2.73 \times 10^{-7}M, k_+ = 5.85 \times 10^{-3}s^{-1}$, [14] gives $K_d = 2.58 \times 10^{-7}M$.
$k_{-,16}$	VIIIa $\leftarrow$ VIIIa1L + VIIIa2	$2.2 \times 10^4 M^{-1}s^{-1}$	[13, 14]	See above
$k_{+,17}$	IXa:VIIIa $\rightarrow$ VIIIa1L + VIIIa2 + IXa*	$1.0 \times 10^{-3}s^{-1}$	[15]	[15] gives $k = 1.4 \times 10^{-3}M^{-1}s^{-1}$
$k_{+,18}$	IIa + V $\rightarrow$ IIa + Va	$2.0 \times 10^7 M^{-1}s^{-1}$	[16]	Used in Jones[8], [16] gives $K_m = 7.17 \times 10^{-8}M$ and $k_{\text{cat}} = 0.23s^{-1}$
$k_{+,19}$	Xa + Va $\rightarrow$ Xa:Va	$4.0 \times 10^8 M^{-1}s^{-1}$	[17]	Used in Jones[8], [17] gives $k_+ > 1 \times 10^9 M^{-1}s^{-1}$
$k_{-,19}$	Xa + Va $\leftarrow$ Xa:Va	$0.2s^{-1}$	-	[12, 11] gives $K_d = 1 - 2 \times 10^{-9}M$ for IXa:VIIIa, used in Jones[8]

$k_{+,20}$	Xa:Va + II $\rightarrow$ Xa:Va:II	$1.0 \times 10^8 M^{-1}s^{-1}$	-	Used in Jones model [8]. Original source unclear, [12],[7],[18] are all cited but none report rates. Changed from $70s^{-1}$ to $103s^{-1}$ by Hockin
$k_{-,20}$	Xa:Va + II $\leftarrow$ Xa:Va:II	$103s^{-1}$	-	See above
$k_{+,21}$	Xa:Va:II $\rightarrow$ Xa:Va + mIIa	$63.5s^{-1}$	-	See above
$k_{+,22}$	mIIa + Xa:Va $\rightarrow$ IIa + Xa:Va	$1.5 \times 10^7 M^{-1}s^{-1}$	-	Used in Jones model [8], fitted from data in Lawson[19]
$k_{+,23}$	Xa + TFPI $\rightarrow$ Xa:TFPI	$9.0 \times 10^5 M^{-1}s^{-1}$	[20]	[20] gives $k_+ = 9 \times 10^5 M^{-1}s^{-1}, k_- = 3.6 \times 10^{-4}s^{-1}$
$k_{-,23}$	Xa + TFPI $\leftarrow$ Xa:TFPI	$3.6 \times 10^{-4}s^{-1}$	[20]	See above
$k_{+,24}$	TF:VIIa:Xa + TFPI $\rightarrow$ TF:VIIa:Xa:TFPI	$3.2 \times 10^8 M^{-1}s^{-1}$	[20]	[20] gives $2.72 \times 10^8 M^{-1}s^{-1}$
$k_{-,24}$	TF:VIIa:Xa + TFPI $\leftarrow$ TF:VIIa:Xa:TFPI	$1.1 \times 10^{-4}s^{-1}$	[20]	[20] gives $k_- = 1.1 \times 10^{-3}s^{-1}$
$k_{+,25}$	TF:VIIa + Xa:TFPI $\rightarrow$ TF:VIIa:Xa:TFPI	$5.0 \times 10^7 M^{-1}s^{-1}$	[20]	[20] gives $k_+ = 5.0 \times 10^7 M^{-1}s^{-1}$
$k_{+,26}$	Xa + AT $\rightarrow$ Xa:AT	$1.5 \times 10^3 M^{-1}s^{-1}$	[21]	[21] gives $k = 4.9 \times 10^3 M^{-1}s^{-1}$ and $k = 2.9 \times 10^3 M^{-1}s^{-1}$
$k_{+,27}$	mIIa + AT $\rightarrow$ mIIa:AT	$7.1 \times 10^3 M^{-1}s^{-1}$	[22]	[22] gives $k = 6.2 \times 10^3 s^{-1}$
$k_{+,28}$	IXa + AT $\rightarrow$ IXa:AT	$4.9 \times 10^2 M^{-1}s^{-1}$	[23]	[21] appears to be an incorrect citation. Likely used [23] which gives $k = 490 M^{-1}s^{-1}$
$k_{+,29}$	IIa + AT $\rightarrow$ IIa:AT	$7.1 \times 10^3 M^{-1}s^{-1}$	[22]	[22] gives $k = 6.2 \times 10^3 s^{-1}$
$k_{+,30}$	TF:VIIa + AT $\rightarrow$ TF:VIIa:AT	$2.3 \times 10^2 M^{-1}s^{-1}$	[24]	[24] gives $k_+ = 450 M^{-1}s^{-1}$

Table D.1: Sources for the parameter values used in the Hockin model. Any experimental sources that are used to inform a reaction rate are given in the Source column. Any additional information, including the original measured values and any changes that were made are given in the Notes column. If the rate is reused from another model then this is stated and both the model it was used in and the original experimental source are given.

D.2 Danforth Model

*This reaction rate also covers a similar reaction for IXa:VIIIa:X but the source only measures for IXa:VIIIa.

Parameter	Reaction	Value	Sources	Notes
$k_{+,22}$	mIIa + Xa:Va → IIa + Xa:Va	$2.3 \times 10^8 M^{-1}s^{-1}$	-	No citation given
$k_{+,26}$	Xa + AT → Xa:AT	$4.2 \times 10^3 M^{-1}s^{-1}$	-	No citation given
$k_{+,31}$	IXa + X → IXa + Xa	$5.7 \times 10^3 M^{-1}s^{-1}$	[25]	Introduced to the model by Butenas[26], [25] gives $K_m = 1.4 \times 10^{-7} M$ and $k_{\text{cat}} = 8 \times 10^{-4} s^{-1}$
$k_{+,32}$	mIIa + V → mIIa + Va	$3.0 \times 10^6 M^{-1}s^{-1}$	[10]	[10] gives $3.5 \times 10^6 M^{-1}s^{-1}$ and $2.4 \times 10^6 M^{-1}s^{-1}$ for different methods

Table D.2: Sources for the parameter values used in the changes for the Danforth model. Any experimental sources that are used to inform a reaction rate are given in the Source column. Any additional information, including the original measured values and any changes that were made are given in the Notes column. If the rate is reused from another model then this is stated and both the model it was used in and the original experimental source are given.

D.3 Chatterjee Model

The parameters up to (and including) $k_{+,30}$ are from the Hockin model and the original sources can be found in the parameter sources for the Hockin model section. Any changes that are made from the original values will be referenced here.

Parameter	Reaction	Value	Sources	Notes
$k_{+,1}$	TF + VII → TF:VII	$3.2 \times 10^6 M^{-1}s^{-1}$	[27]	-
$k_{-,1}$	TF + VII ← TF:VII	$3.1 \times 10^{-2} s^{-1}$	[27]	Original value multiplied by 10 based on: Decrease in K_d from $14.9nM$ to $0.58nM$ as % phosphatidylserine (PS) increases from 0 to 40[28], $K_d = 2nM$ [1]

$k_{+,2}$	TF + VIIa $\rightarrow$ TF:VIIa	$2.3 \times 10^7 M^{-1}s^{-1}$	[27]	-
$k_{-,2}$	TF + VIIa $\leftarrow$ TF:VIIa	$3.1 \times 10^{-5}s^{-1}$	[27]	Original value multiplied by 0.01 based on: K_d decreases from 60pM to 10pM as PS % increases from 10-40 on TF liposomes and from 90pM to 10pM as PS % increases from 10-70 on TF nanodiscs (figure 5 in [29])
$k_{+,3}$	TF:VIIa + VII $\rightarrow$ TF:VIIa + VIIa	$4.45 \times 10^5 M^{-1}s^{-1}$	[27]	-
$k_{+,4}$	Xa + VII $\rightarrow$ Xa + VIIa	$1.3 \times 10^7 M^{-1}s^{-1}$	[27]	-
$k_{+,5}$	IIa + VII $\rightarrow$ IIa + VIIa	$2.3 \times 10^4 M^{-1}s^{-1}$	[27]	-
$k_{+,6}$	TF:VIIa + X $\rightarrow$ TF:VIIa:X	$2.5 \times 10^7 M^{-1}s^{-1}$	[27]	-
$k_{-,6}$	TF:VIIa + X $\leftarrow$ TF:VIIa:X	$0.0105s^{-1}$	[27]	Original value multiplied by 0.01 based on: [29] reported a decrease in K_m from 400nM to 20nM as PS % increases from 10 to 40 (figure 6), [5] reported a K_m of 238nM
$k_{+,7}$	TF:VIIa:X $\rightarrow$ TF:VIIa:Xa	$6s^{-1}$	[27]	-
$k_{+,8}$	TF:VIIa + Xa $\rightarrow$ TF:VIIa:Xa	$2.2 \times 10^7 M^{-1}s^{-1}$	[27]	-
$k_{-,8}$	TF:VIIa + Xa $\leftarrow$ TF:VIIa:Xa	$19s^{-1}$	[27]	-
$k_{+,9}$	TF:VIIa + IX $\rightarrow$ TF:VIIa:IX	$1.0 \times 10^7 M^{-1}s^{-1}$	[27]	-
$k_{-,9}$	TF:VIIa + IX $\leftarrow$ TF:VIIa:IX	$2.45s^{-1}$	[27]	-
$k_{+,10}$	TF:VIIa:IX $\rightarrow$ TF:VIIa + IXa	$1.8s^{-1}$	[27]	-
$k_{+,11}$	II + Xa $\rightarrow$ IIa + Xa	$7.5 \times 10^3 s^{-1}$	[27]	-

$k_{+,12}$	IIa + VIII $\rightarrow$ IIa + VIIIa	$2.0 \times 10^{7} M^{-1} s^{-1}$	[27]	-
$k_{+,13}$	VIIIa + IXa $\rightarrow$ IXa:VIIIa	$1.0 \times 10^{7} M^{-1} s^{-1}$	[27]	-
$k_{-,13}$	VIIIa + IXa $\leftarrow$ IXa:VIIIa	$1.0 \times 10^{-4} s^{-1}$	[27]	Original value multiplied by 0.02 based on: K_d decreases from 351nM to 4nM on PCPS vesicles [30], a K_d of 74pM was found on activated platelet surfaces compared to 550pM on equimolar PSPC vesicles [31]
$k_{+,14}$	IXa:VIIIa + X $\rightarrow$ IXa:VIIIa:X	$1.0 \times 10^{8} M^{-1} s^{-1}$	[27]	-
$k_{-,14}$	IXa:VIIIa + X $\leftarrow$ IXa:VIIIa:X	$1.0 \times 10^{-5} s^{-1}$	[27]	Original value multiplied by 0.01 based on: K_m decreases from 45μM to 160nM when using activated platelets rather than unactivated platelets [25]
$k_{+,15}$	IXa:VIIIa:X $\rightarrow$ IXa:VIIIa + Xa	$8.2 s^{-1}$	[27]	-
$k_{+,16}$	VIIIa $\rightarrow$ VIIIa1L + VIIIa2	$6.0 \times 10^{-5} s^{-1}$	[27]	Original value multiplied by 0.01 based on: K_d of 260nM in the absence of phopholipids [14], this reaction is stabilized in the presence of phospholipids [32]
$k_{-,16}$	VIIIa $\leftarrow$ VIIIa1L + VIIIa2	$2.2 \times 10^{4} M^{-1} s^{-1}$	[27]	-
$k_{+,17}$	IXa:VIIIa $\rightarrow$ VIIIa1L + VIIIa2 + IXa	$1.0 \times 10^{-3} s^{-1}$	[27]	-
$k_{+,18}$	IIa + V $\rightarrow$ IIa + Va	$2.0 \times 10^{7} M^{-1} s^{-1}$	[27]	-
$k_{+,19}$	Xa + Va $\rightarrow$ Xa:Va	$4.0 \times 10^{8} M^{-1} s^{-1}$	[27]	-

$k_{-,19}$	Xa + Va ← Xa:Va	$0.008s^{-1}$	[27]	Original value multiplied by 0.04 based on: K_d decreases from 3.3nM to 30pM when using 10μM 40% PS [33]
$k_{+,20}$	Xa:Va + II → Xa:Va:II	$1.0 \times 10^8 M^{-1}s^{-1}$	[27]	-
$k_{-,20}$	Xa:Va + II ← Xa:Va:II	$2.06s^{-1}$	[27]	Original value multiplied by 0.02 based on: K_m decreases from 34μM to 0.21μM when using 7.5μM phospholipids [34]
$k_{+,21}$	Xa:Va:II → Xa:Va + mIIa	$63.5s^{-1}$	[27]	-
$k_{+,22}$	Xa:Va + mIIa → Xa:Va + IIa	$1.5 \times 10^7 M^{-1}s^{-1}$	[27]	-
$k_{+,23}$	Xa + TFPI → Xa:TFPI	$9.0 \times 10^5 M^{-1}s^{-1}$	[27]	-
$k_{-,23}$	Xa + TFPI ← Xa:TFPI	$3.6 \times 10^{-4}s^{-1}$	[27]	-
$k_{+,24}$	TF:VIIa:Xa + TFPI → TF:VIIa:Xa:TFPI	$3.2 \times 10^8 M^{-1}s^{-1}$	[27]	-
$k_{-,24}$	TF:VIIa:Xa + TFPI ← TF:VIIa:Xa:TFPI	$1.1 \times 10^{-2}s^{-1}$	[27]	Original value multiplied by 100 based on: Data from [20] suggests that the original data fitting for the reaction produces a complex that binds too strongly
$k_{+,25}$	TF:VIIa + Xa:TFPI → TF:VIIa:Xa:TFPI	$5.0 \times 10^7 M^{-1}s^{-1}$	[27]	-
$k_{+,26}$	Xa + AT → Xa:AT	$1.5 \times 10^3 M^{-1}s^{-1}$	[27]	-
$k_{+,27}$	mIIa + AT → mIIa:AT	$7.1 \times 10^3 M^{-1}s^{-1}$	[27]	-
$k_{+,28}$	IXa + AT → IXa:AT	$4.9 \times 10^2 M^{-1}s^{-1}$	[27]	-
$k_{+,29}$	IIa + AT → IIa:AT	$7.1 \times 10^3 M^{-1}s^{-1}$	[27]	-
$k_{+,30}$	TF:VIIa + AT → TF:VIIa:AT	$2.3 \times 10^2 M^{-1}s^{-1}$	[27]	-

$k_{+,31}$	Boc-VPR-MCA + IIa $\rightarrow$ Boc-VPR-MCA:IIa	$1.0 \times 10^8 M^{-1}s^{-1}$	[35]	Determined experimentally by Chatterjee
$k_{-,31}$	Boc-VPR-MCA + IIa $\leftarrow$ Boc-VPR-MCA:IIa	$6.1 \times 10^3 s^{-1}$	[35]	See above
$k_{+,32}$	Boc-VPR-MCA:IIa $\rightarrow$ Boc-VPR + AMC + IIa	$53.8 s^{-1}$	[35]	See above
$k_{+,33}$	XII $\rightarrow$ XIIa	$5.0 \times 10^{-4} s^{-1}$	-	Estimated to better link Hockin model to experimental data
$k_{+,34}$	XIIa + XII $\rightarrow$ XIIa:XII	$1.0 \times 10^8 M^{-1}s^{-1}$	[36]	[36] gives $K_m = 7.5 \times 10^{-6} M$ and $k_{\text{cat}} = 0.033 s^{-1}$, $k_{+,34}$ is assumed to be diffusion limited [37]
$k_{-,34}$	XIIa + XII $\leftarrow$ XIIa:XII	$750 s^{-1}$	[36]	See above
$k_{+,35}$	XIIa:XII $\rightarrow$ XIIa + XIIa	$3.3 \times 10^{-2} s^{-1}$	[36]	See above
$k_{+,36}$	XIIa + PK $\rightarrow$ XIIa:PK	$1.0 \times 10^8 M^{-1}s^{-1}$	[36]	[36] gives $K_m = 3.7 \times 10^{-5} M$ and $k_{\text{cat}} = 40 s^{-1}$, $k_{+,36}$ is assumed to be diffusion limited [37]
$k_{-,36}$	XIIa + PK $\leftarrow$ XIIa:PK	$3.6 \times 10^3 s^{-1}$	[36]	See above
$k_{+,37}$	XIIa:PK $\rightarrow$ XIIa + K	$40 s^{-1}$	[36]	See above
$k_{+,38}$	XII + K $\rightarrow$ XII:K	$1.0 \times 10^8 M^{-1}s^{-1}$	[36]	[36] gives $K_m = 5.1 \times 10^{-7} M$ and $k_{\text{cat}} = 5.7 s^{-1}$, $k_{+,36}$ is assumed to be diffusion limited [37]
$k_{-,38}$	XII + K $\leftarrow$ XII:K	$45.3 s^{-1}$	[36]	See above
$k_{+,39}$	XII:K $\rightarrow$ XIIa + K	$5.7 s^{-1}$	[36]	See above
$k_{+,40}$	PK + K $\rightarrow$ K + K	$2.7 \times 10^4 M^{-1}s^{-1}$	[38]	[38] gives $2.7 \times 10^4 M^{-1}s^{-1}$

$k_{+,41}$	K $\rightarrow$ Kinh	$1.1 \times 10^{-2} s^{-1}$	-	[39] gives an approximation based on inactivation by C1-inh, α_2-M and AT
$k_{+,42}$	XIIa + CTI $\rightarrow$ XIIa:CTI	$1.0 \times 10^{8} M^{-1} s^{-1}$	[40]	[40] gives $K_d = 2.4 \times 10^{-8} M$, $k_{+,42}$ is assumed to be diffusion limited [37]
$k_{-,42}$	XIIa + CTI $\leftarrow$ XIIa:CTI	$2.45 s^{-1}$	[40]	See above
$k_{+,43}$	XIIa + C1-inh $\rightarrow$ XIIa:C1-inh	$3.6 \times 10^{3} M^{-1} s^{-1}$	[41]	[41] gives $3.6 \times 10^{3} M^{-1} s^{-1}$
$k_{+,44}$	XIIa + AT $\rightarrow$ XIIa:AT	$21.6 M^{-1} s^{-1}$	[41]	[41] gives $21.6 M^{-1} s^{-1}$
$k_{+,45}$	XI + IIa $\rightarrow$ XI:IIa	$1.0 \times 10^{8} M^{-1} s^{-1}$	[42]	[42] gives $K_m = 5 \times 10^{-8} M$ and $k_{\text{cat}} = 1.3 \times 10^{-4} s^{-1}$, $k_{+,45}$ is assumed to be diffusion limited [37]
$k_{-,45}$	XI + IIa $\leftarrow$ XI:IIa	$5 s^{-1}$	[42]	See above
$k_{+,46}$	XI:IIa $\rightarrow$ XIa + IIa	$1.3 \times 10^{-4} s^{-1}$	[42]	See above
$k_{+,47}$	XIIa + XI $\rightarrow$ XIIa:XI	$1.0 \times 10^{8} M^{-1} s^{-1}$	[42]	[42] gives $K_m = 2 \times 10^{-6} M$ and $k_{\text{cat}} = 5.3 \times 10^{-4} s^{-1}$, $k_{+,47}$ is assumed to be diffusion limited [37]
$k_{-,47}$	XIIa + XI $\leftarrow$ XIIa:XI	$200 s^{-1}$	[42]	See above
$k_{+,48}$	XIIa:XI $\rightarrow$ XIIa + XIa	$5.7 \times 10^{-4} s^{-1}$	[42]	See above
$k_{+,49}$	XIa + XI $\rightarrow$ XIa + XIa	$3.19 \times 10^{6} M^{-1} s^{-1}$	-	Fitted using the model of [43] but that model does not include IIa activation of XI
$k_{+,50}$	XIa + AT $\rightarrow$ XIa:AT	$3.2 \times 10^{2} M^{-1} s^{-1}$	[44]	[44] gives $k = 320 M^{-1} s^{-1}$
$k_{+,51}$	XIa + C1-inh $\rightarrow$ XIa:C1-inh	$1.8 \times 10^{3} M^{-1} s^{-1}$	[44]	[44] gives $1.8 \times 10^{3} M^{-1} s^{-1}$

$k_{+,52}$	XIa + α_1AT $\rightarrow$ XIa:α_1AT	$1.0 \times 10^2 M^{-1}s^{-1}$	[44]	[44] gives $100 M^{-1}s^{-1}$
$k_{+,53}$	XIa + α_2AP $\rightarrow$ XIa:α_2AP	$4.3 \times 10^3 M^{-1}s^{-1}$	[44]	[44] gives $4.3 \times 10^2 M^{-1}s^{-1}$
$k_{+,54}$	XIa + IX $\rightarrow$ XIa:IX	$1.0 \times 10^8 M^{-1}s^{-1}$	[45]	[45] gives $K_m = 4.9 \times 10^{-7} M$ and $k_{\text{cat}} = 7.7 s^{-1}$, $k_{+,54}$ is assumed to be diffusion limited [37]
$k_{-,54}$	XIa + IX $\leftarrow$ XIa:IX	$41 s^{-1}$	[45]	See above
$k_{+,55}$	XIa:IX $\rightarrow$ XIa + IXa	$7.7 s^{-1}$	[45]	See above
$k_{+,56}$	IXa + X $\rightarrow$ IXa:X	$1.0 \times 10^8 M^{-1}s^{-1}$	[46]	[46] gives $K_m = 6.45 \times 10^{-9} M$ and $k_{cat} = 7.0 \times 10^{-4} s^{-1}$, $k_{+,56}$ is assumed to be diffusion limited [37]
$k_{-,56}$	IXa + X $\leftarrow$ IXa:X	$0.64 s^{-1}$	[46]	See above
$k_{+,57}$	IXa:X $\rightarrow$ IXa + Xa	$7.0 \times 10^{-4} s^{-1}$	[46]	See above
$k_{+,58}$	Xa + VIII $\rightarrow$ Xa:VIII	$1.0 \times 10^8 M^{-1}s^{-1}$	[47]	Used in model [48], [47] gives $\frac{k_{\text{cat}}}{K_m} = 1.1 \times 10^6 M^{-1}s^{-1}$
$k_{-,58}$	Xa + VIII $\leftarrow$ Xa:VIII	$2.1 s^{-1}$	[47]	See above
$k_{+,59}$	Xa:VIII $\rightarrow$ Xa + VIIIa	$0.023 s^{-1}$	[47]	See above
$k_{+,60}$	VIIa + IX $\rightarrow$ VIIa:IX	$1.0 \times 10^8 M^{-1}s^{-1}$	[49]	[49] gives $K_m = 9 \times 10^{-9} M$ and $k_{\text{cat}} = 3.7 \times 10^{-5} s^{-1}$, $k_{+,60}$ is assumed to be diffusion limited [37]
$k_{-,60}$	VIIa + IX $\leftarrow$ VIIa:IX	$0.9 s^{-1}$	[49]	See above
$k_{+,61}$	VIIa:IX $\rightarrow$ VIIa + IXa	$3.6 \times 10^{-5} s^{-1}$	[49]	See above

$k_{+,62}$	VIIa + X $\rightarrow$ VIIa:X	$1.0 \times 10^8 M^{-1}s^{-1}$	[49]	[49] gives $K_m = 2.1 \times 10^{-6}M$ and $k_{\text{cat}} = 1.7 \times 10^{-6}s^{-1}$, $k_{+,62}$ is assumed to be diffusion limited [37]
$k_{-,62}$	VIIa + X $\leftarrow$ VIIa:X	$210s^{-1}$	[49]	See above
$k_{+,63}$	VIIa:X $\rightarrow$ VIIa + Xa	$1.6 \times 10^{-6}s^{-1}$	[49]	See above
$k_{+,64}$	Fbg + IIa $\rightarrow$ Fbg:IIa	$1.0 \times 10^8 M^{-1}s^{-1}$	[50]	[50] gives $K_m = 7.2 \times 10^{-6}M$ and $k_{\text{cat}} = 84s^{-1}$, Used in a fibrin model [51], $k_{+,64}$ is assumed to be diffusion limited [37]
$k_{-,64}$	Fbg + IIa $\leftarrow$ Fbg:IIa	$636s^{-1}$	[50]	See above
$k_{+,65}$	Fbg:IIa $\rightarrow$ Fbn1 + IIa + FPA	$84s^{-1}$	[50]	See above
$k_{+,66}$	Fbn1 + IIa $\rightarrow$ Fbn1:IIa	$1.0 \times 10^8 M^{-1}s^{-1}$	[52]	Used in model [51], $K_m = 7.5 \times 10^{-6}M$ and $k_{\text{cat}} = 49s^{-1}$ from [52], k_{cat} adjusted based on specificity constant in [53], $k_{+,66}$ is assumed to be diffusion limited [37]
$k_{-,66}$	Fbn1 + IIa $\leftarrow$ Fbn1:IIa	$742.6s^{-1}$	[52]	See above
$k_{+,67}$	Fbn1:IIa $\rightarrow$ Fbn2 + IIa + FPB	$7.45s^{-1}$	[52]	See above
$k_{+,68}$	Fbn1 + Fbn1 $\rightarrow (Fbn1)_2$	$1.0 \times 10^6 M^{-1}s^{-1}$	[53]	[53] gives $k_+ = 1 \times 10^6 M^{-1}s^{-1}$ and $k_- = 0.064s^{-1}$, Used in a fibrin model [51]
$k_{-,68}$	Fbn1 + Fbn1 $\leftarrow (Fbn1)_2$	$6.45 \times 10^{-2}s^{-1}$	[53]	See above
$k_{+,69}$	$(Fbn1)_2$ + IIa $\rightarrow (Fbn1)_2$:IIa	$1.0 \times 10^8 M^{-1}s^{-1}$	[52]	[52] gives $K_m = 7.5 \times 10^{-6}M$ and $k_{\text{cat}} = 49s^{-1}$, Used in a fibrin model [51], $k_{+,69}$ is assumed to be diffusion limited [37]
$k_{-,69}$	$(Fbn1)_2$ + IIa $\leftarrow (Fbn1)_2$:IIa	$701s^{-1}$	[52]	See above

$k_{+,70}$	$(Fbn1)_2$:IIa $\rightarrow$ $(Fbn2)_2$ + IIa + FPB	$49s^{-1}$	[52]	See above
$k_{+,71}$	Fbn2 + IIa $\rightarrow$ Fbn2:IIa	$1.0 \times 10^8 M^{-1}s^{-1}$	[51]	$K_d = 1 \times 10^{-5}M$ experimentally determined in [51], $k_{+,71}$ is assumed to be diffusion limited
$k_{-,71}$	Fbn2 + IIa $\leftarrow$ Fbn2:IIa	$1.0 \times 10^3 s^{-1}$	[51]	See above
$k_{+,72}$	$(Fbn1)_2$:IIa + AT $\rightarrow$ $(Fbn1)_2$:IIa:AT	$1.6 \times 10^4 M^{-1}s^{-1}$	[54]	$k_+ = 1.6 \times 10^4 M^{-1}s^{-1}$ experimentally determined in [51]
$k_{+,73}$	Fbn1:IIa + AT $\rightarrow$ Fbn1:IIa:AT	$1.6 \times 10^4 M^{-1}s^{-1}$	[54]	See above
$k_{+,74}$	Fbn2:IIa + AT $\rightarrow$ Fbn2:IIa:AT	$1.0 \times 10^4 M^{-1}s^{-1}$	[54]	[54] says it is 1.6 times slower than for free IIa and AT

Table D.3: Sources for the parameter values used in the Chatterjee model. Any experimental sources that are used to inform a reaction rate are given in the Source column. Any additional information, including the original measured values and any changes that were made are given in the Notes column. If the rate is reused from another model then this is stated and both the model it was used in and the original experimental source are given.

D.4 Brummel Model

Parameter	Reaction	Value	Sources	Notes
k_{43}	TM + IIa $\leftarrow$ TM:IIa	$0.33s^{-1}$	[55, 56]	[55] gives $K_d = 9.7 \times 10^{-10}M$, [56] gives $K_d = 2.4 \times 10^{-8}M$
k_{44}	TM + IIa $\rightarrow$ TM:IIa	$1 \times 10^8 M^{-1}s^{-1}$	[55, 56]	See above
k_{45}	TM:IIa + PC $\leftarrow$ TM:IIa:PC	$100s^{-1}$	[55]	[55] gives $K_m = 1.43 \times 10^{-5}M$ and $k_{\text{cat}} = 0.83s^{-1}$

k_{46}	TM:IIa + PC $\rightarrow$ TM:IIa:PC	$1 \times 10^8 M^{-1}s^{-1}$	[55]	See above
k_{47}	TM:IIa:PC $\rightarrow$ TM:IIa + APC	$0.41s^{-1}$	[55]	See above
k_{48}	TM:IIa + AT $\rightarrow$ IIa:AT + TM	$7.1 \times 10^3 M^{-1}s^{-1}$	[55, 56]	[55] gives $k_+ = 1.4 \times 10^4$, [56] gives $k_+ = 4 \times 10^3$ (both without TM)
k_{49}	APC + Va $\leftarrow$ APC:Va	$0.7s^{-1}$	-	Used in models[57, 58]. [57] cites [17] but this paper does not concern protein C, nor does it give the value of 0.7
k_{50}	APC + Va $\rightarrow$ APC:Va	$1 \times 10^8 M^{-1}s^{-1}$	-	Used in models[57, 58]. [57] cites [59] but this paper does not concern protein C, nor does it give the value of 1×10^8
k_{51}	APC:Va $\rightarrow$ APC + Va5	$1s^{-1}$	[60, 61]	[60] gives $k = 3 \times 10^7 M^{-1}s^{-1}$, [61] gives $k = 4.3 \times 10^7 M^{-1}s^{-1}$, [57] converts to first order rate of $k = 1s^{-1}$
k_{52}	APC:Va $\rightarrow$ APC + Va3	$0.192s^{-1}$	[58]	Determined experimentally in [58]
k_{53}	Va3 $\rightarrow$ HCF + LCA1	$0.028s^{-1}$	[57]	Determined experimentally in [57]
k_{54}	Xa + Va5 $\leftarrow$ Xa:Va5	$0.15s^{-1}$	[58]	Determined experimentally in [58]
k_{55}	Xa:Va5:II $\rightarrow$ Xa:Va5 + mIIa	$10.3s^{-1}$	-	Cited as [58] but this does not include any mIIa reactions.
k_{56}	Xa:Va3:II $\rightarrow$ Xa:Va3 + mIIa	$10.3s^{-1}$	-	See above
k_{57}	Xa:Va5 + mIIa $\rightarrow$ IIa + Xa:Va5	$4.6 \times 10^7 M^{-1}s^{-1}$	-	See above
k_{58}	Xa:Va3 + mIIa $\rightarrow$ IIa + Xa:Va3	$4.6 \times 10^7 M^{-1}s^{-1}$	-	See above
k_{59}	Xa:Va3 $\rightarrow$ HCF + LCA1 + Xa	$0.0035s^{-1}$	-	Used in model [58], no source given

k_{60}	IXa + X → IXa + Xa	$5.7 \times 10^3 M^{-1}s^{-1}$	[25]	Used in Butenas model [26], [25] gives $K_m = 1.4 \times 10^{-7}M$ and $k_{\text{cat}} = 8 \times 10^{-4}s^{-1}$
k_{61}	mIIa + V → mIIa + Va	$3 \times 10^6 M^{-1}s^{-1}$	[10]	[10] gives $3.5 \times 10^6 M^{-1}s^{-1}$ and $2.4 \times 10^6 M^{-1}s^{-1}$ for different methods
k_{62}	II + Va ← II:Va	$70s^{-1}$	[62]	Used in model [58], [62] gives $K_d = 8.8 \times 10^{-6}M$
k_{63}	II + Va → II:Va	$1 \times 10^8 M^{-1}s^{-1}$	[62]	See above
k_{64}	Xa:Va5 + APC → Xa:Va53 + APC	$4.05 \times 10^6 M^{-1}s^{-1}$	-	Cited as [58] but not used in that model

Table D.4: Sources for the parameter values used in the changes for the Brummel model. Any experimental sources that are used to inform a reaction rate are given in the Source column. Any additional information, including the original measured values and any changes that were made are given in the Notes column. If the rate is reused from another model then this is stated and both the model it was used in and the original experimental source are given.

D.5 Bungay Model

Parameter	Reaction	Value	Sources	Notes
$k_{+,1}$	TF_L + $VIIa_L$ → $TF{:}VIIa_L$	$5 \times 10^8 M^{-1}s^{-1}$	[63]	[63] gives $K_d = 1 \times 10^{-11}M$, struggled with precision
$k_{-,1}$	TF_L + $VIIa_L$ ← $TF{:}VIIa_L$	$0.005s^{-1}$	[63]	See above
$k_{+,2}$	TF_L + VII_L → $TF{:}VII_L$	$5 \times 10^6 M^{-1}s^{-1}$	-	Estimated by Bungay
$k_{-,2}$	TF_L + VII_L ← $TF{:}VII_L$	$0.005s^{-1}$	-	Estimated by Bungay
$k_{+,3}$	$TF{:}VIIa_L$ + IX_L → $TF{:}VIIa{:}IX_L$	$1 \times 10^7 M^{-1}s^{-1}$	[7]	[7] gives $K_m = 2.43 \times 10^{-7}M, k_{\text{cat}} = 0.34s^{-1}$.

$k_{-,3}$	$\text{TF:VIIa}_L + \text{IX}_L \leftarrow \text{TF:VIIa:IX}_L$	$2.09s^{-1}$	[7]	See above
$k_{+,4}$	$\text{TF:VIIa:IX}_L \rightarrow \text{TF:VIIa}_L + \text{IXa}_L$	$0.34s^{-1}$	[7]	See above
$k_{+,5}$	$\text{TF:VIIa}_L + \text{X}_L \rightarrow \text{TF:VIIa:X}_L$	$1 \times 10^8 M^{-1}s^{-1}$	[18, 64]	[18] gives $K_m = 4.5 \times 10^{-7}M$, $k_{\text{cat}} = 1.15s^{-1}$, [64] gives $K_m = 5.5 \times 10^{-8}M$, $k_{\text{cat}} = 81s^{-1}$
$k_{-,5}$	$\text{TF:VIIa}_L + \text{X}_L \leftarrow \text{TF:VIIa:X}_L$	$32.5s^{-1}$	[18, 64]	See above
$k_{+,6}$	$\text{TF:VIIa:X}_L \rightarrow \text{TF:VIIa:Xa}_L$	$1.5s^{-1}$	[18, 64]	See above
$k_{+,7}$	$\text{TF:VIIa:Xa}_L \rightarrow \text{TF:VIIa}_L + \text{Xa}_L$	$1s^{-1}$	[18, 64]	See above
$k_{+,8}$	$\text{TF:VII}_L + \text{Xa}_L \rightarrow \text{TF:VII:Xa}_L$	$5 \times 10^7 M^{-1}s^{-1}$	[4]	[4] gives $K_m = 1.2 \times 10^{-6}M$, $k_{\text{cat}} = 15.2s^{-1}$
$k_{-,8}$	$\text{TF:VII}_L + \text{Xa}_L \leftarrow \text{TF:VII:Xa}_L$	$44.8s^{-1}$	[4]	See above
$k_{+,9}$	$\text{TF:VII:Xa}_L \rightarrow \text{TF:VIIa}_L + \text{Xa}_L$	$15.2s^{-1}$	[4]	See above
$k_{+,10}$	$\text{IXa}_L + \text{VIIIa}_L \rightarrow \text{IXa:VIIIa}_L$	$1 \times 10^8 M^{-1}s^{-1}$	[11]	[11] gives $K_d = 2 \times 10^{-9}M$
$k_{-,10}$	$\text{IXa}_L + \text{VIIIa}_L \leftarrow \text{IXa:VIIIa}_L$	$0.2s^{-1}$	[11]	See above
$k_{+,11}$	$\text{Xa}_L + \text{Va}_L \rightarrow \text{Xa:Va}_L$	$1 \times 10^9 M^{-1}s^{-1}$	[65]	[65] gave $K_d = 1.04 \times 10^{-9}M$
$k_{-,11}$	$\text{Xa}_L + \text{Va}_L \leftarrow \text{Xa:Va}_L$	$1s^{-1}$	[65]	See above
$k_{+,12}$	$\text{IXa:VIIIa}_L + \text{X}_L \rightarrow \text{IXa:VIIIa:X}_L$	$1 \times 10^8 M^{-1}s^{-1}$	[12, 25]	[12] gives $K_m = 6.3 \times 10^{-8}M$ and $k_{\text{cat}} = 8.3s^{-1}$, [25] gives $K_m = 1.9 \times 10^{-7}M$, $k_{\text{cat}} = 29s^{-1}$
$k_{-,12}$	$\text{IXa:VIIIa}_L + \text{X}_L \leftarrow \text{IXa:VIIIa:X}_L$	$10.7s^{-1}$	[12, 25]	See above
$k_{+,13}$	$\text{IXa:VIIIa:X}_L \rightarrow \text{IXa:VIIIa}_L + \text{Xa}_L$	$8.3s^{-1}$	[12, 25]	See above

$k_{+,14}$	$\mathrm{V}_L + \mathrm{Xa}_L \rightarrow \mathrm{V{:}Xa}_L$	$1 \times 10^8 M^{-1}s^{-1}$	[16]	[16] gives $K_m = 1.04 \times 10^{-8}M$, $k_{\mathrm{cat}} = 0.043s^{-1}$
$k_{-,14}$	$\mathrm{V}_L + \mathrm{Xa}_L \leftarrow \mathrm{V{:}Xa}_L$	$1s^{-1}$	[16]	See above
$k_{+,15}$	$\mathrm{V{:}Xa}_L \rightarrow \mathrm{Va}_L + \mathrm{Xa}_L$	$0.043s^{-1}$	[16]	See above
$k_{+,16}$	$\mathrm{VIII}_L + \mathrm{Xa}_L \rightarrow \mathrm{VIII{:}Xa}_L$	$1 \times 10^8 M^{-1}s^{-1}$	[47]	[47] gives $\frac{k_{\mathrm{cat}}}{K_m} = 1.1 \times 10^{-6}M^{-1}s^{-1}$
$k_{-,16}$	$\mathrm{VIII}_L + \mathrm{Xa}_L \leftarrow \mathrm{VIII{:}Xa}_L$	$2.1s^{-1}$	[47]	See above
$k_{+,17}$	$\mathrm{VIII{:}Xa}_L \rightarrow \mathrm{VIIIa}_L + \mathrm{Xa}_L$	$0.023s^{-1}$	[47]	See above
$k_{+,18}$	$\mathrm{V}_L + \mathrm{IIa}_f \rightarrow \mathrm{V{:}IIa}_L$	$1 \times 10^8 M^{-1}s^{-1}$	[16]	[16] gives $K_m = 7.17 \times 10^{-8}M$ and $k_{\mathrm{cat}} = 0.23s^{-1}$
$k_{-,18}$	$\mathrm{V}_L + \mathrm{IIa}_f \leftarrow \mathrm{V{:}IIa}_L$	$6.94s^{-1}$	[16]	See above
$k_{+,19}$	$\mathrm{V{:}IIa}_L \rightarrow \mathrm{Va}_L + \mathrm{IIa}_f$	$0.23s^{-1}$	[16]	See above
$k_{+,20}$	$\mathrm{VIII}_L + \mathrm{IIa}_f \rightarrow \mathrm{VIII{:}IIa}_L$	$1 \times 10^8 M^{-1}s^{-1}$	[66]	[66] gives multiple values around $K_m = 2 \times 10^{-7}M, k_{\mathrm{cat}} = 1s^{-1}$ for different types of VIII
$k_{-,20}$	$\mathrm{VIII}_L + \mathrm{IIa}_f \leftarrow \mathrm{VIII{:}IIa}_L$	$13.8s^{-1}$	[66]	See above
$k_{+,21}$	$\mathrm{VIII{:}IIa}_L \rightarrow \mathrm{VIIIa}_L + \mathrm{IIa}_f$	$0.9s^{-1}$	[66]	See above
$k_{+,22}$	$\mathrm{Xa{:}Va}_L + \mathrm{II}_L \rightarrow \mathrm{Xa{:}Va{:}II}_L$	$1 \times 10^8 M^{-1}s^{-1}$	[65]	[65] gives $K_m = 4.6 \times 10^{-7}M, k_{\mathrm{cat}} = 13.5s^{-1}$
$k_{-,22}$	$\mathrm{Xa{:}Va}_L + \mathrm{II}_L \leftarrow \mathrm{Xa{:}Va{:}II}_L$	$100s^{-1}$	[65]	See above
$k_{+,23}$	$\mathrm{Xa{:}Va}_L + \mathrm{mIIa}_L \rightarrow \mathrm{Xa{:}Va{:}mIIa}_L$	$1 \times 10^8 M^{-1}s^{-1}$	[65]	[65] gives $K_m = 6.6 \times 10^{-7}M, k_{\mathrm{cat}} = 15.1s^{-1}$
$k_{-,23}$	$\mathrm{Xa{:}Va}_L + \mathrm{mIIa}_L \leftarrow \mathrm{Xa{:}Va{:}mIIa}_L$	$66s^{-1}$	[65]	See above

$k_{+,24}$	$\text{Xa:Va:II}_L \rightarrow \text{Xa:Va:mIIa}_L$	$13s^{-1}$	[65]	See $k_{+,22}$
$k_{+,25}$	$\text{Xa:Va:mIIa}_L \rightarrow \text{Xa:Va}_L + \text{IIa}_f$	$15s^{-1}$	[65]	See $k_{+,23}$
$k_{+,26}$	$\text{VII}_L + \text{Xa}_L \rightarrow \text{VII:Xa}_L$	$5 \times 10^7 M^{-1}s^{-1}$	[4]	[4] gives $K_m = 1.2 \times 10^{-6}M$, $k_{\text{cat}} = 15.2s^{-1}$
$k_{-,26}$	$\text{VII}_L + \text{Xa}_L \leftarrow \text{VII:Xa}_L$	$44.8s^{-1}$	[4]	See above
$k_{+,27}$	$\text{VII:Xa}_L \rightarrow \text{VIIa}_L + \text{Xa}_L$	$15.2s^{-1}$	[4]	See above
$k_{+,28}$	$\text{XI}_f + \text{IIa}_f \rightarrow \text{XI:IIa}_f$	$1 \times 10^8 M^{-1}s^{-1}$	[67]	[67] gives $k_{\text{cat}} = 1.43s^{-1}$, retracted in 2007 [68]
$k_{-,28}$	$\text{XI}_f + \text{IIa}_f \leftarrow \text{XI:IIa}_f$	$10s^{-1}$	[67]	See above
$k_{+,29}$	$\text{XI:IIa}_f \rightarrow \text{XIa}_f + \text{IIa}_f$	$1.453s^{-1}$	[67]	See above
$k_{+,30}$	$\text{APC:PS}_L + \text{VIIIa}_L \rightarrow \text{APC:PS:VIIIa}_L$	$1 \times 10^8 M^{-1}s^{-1}$	-	Assumed the same as for FVa_L
$k_{-,30}$	$\text{APC:PS}_L + \text{VIIIa}_L \leftarrow \text{APC:PS:VIIIa}_L$	$1.6s^{-1}$	-	See above
$k_{+,31}$	$\text{APC:PS:VIIIa}_L \rightarrow \text{APC:PS}_L + \text{VIIIai}_L$	$0.45s^{-1}$	-	See above
$k_{+,32}$	$\text{APC:PS}_L + \text{Va}_L \rightarrow \text{APC:PS:Va}_L$	$1 \times 10^8 M^{-1}s^{-1}$	[69]	[69] gives $K_m = 1.97 \times 10^{-8}M$, $k_{\text{cat}} = 0.79s^{-1}$
$k_{-,32}$	$\text{APC:PS}_L + \text{Va}_L \leftarrow \text{APC:PS:Va}_L$	$1.6s^{-1}$	[69]	See above
$k_{+,33}$	$\text{APC:PS:Va}_L \rightarrow \text{APC:PS}_L + \text{Vai}_L$	$0.45s^{-1}$	[69]	See above
$k_{+,34}$	$\text{TFPI}_f + \text{Xa}_f \rightarrow \text{TFPI:Xa}_f$	$1.6 \times 10^7 M^{-1}s^{-1}$	[70]	[70] gives $k_+ = 1.6 \times 10^7 M^{-1}s^{-1}, k_- = 3.3 \times 10^{-4}s^{-1}$
$k_{-,34}$	$\text{TFPI}_f + \text{Xa}_f \leftarrow \text{TFPI:Xa}_f$	$0.00033s^{-1}$	[70]	See above

$k_{+,35}$	TFPI:Xa$_f$ + TF:VIIa$_L$ $\rightarrow$ TFPI:Xa:TF:VIIa$_L$	$1 \times 10^7 M^{-1}s^{-1}$	[70, 20]	[70] gives $k_+ = 1.07 \times 10^7 M^{-1}s^{-1}$ and [20] gives $k_+ = 7.34 \times 10^6 M^{-1}s^{-1}, k_- = 1.1 \times 10^{-3}s^{-1}$
$k_{-,35}$	TFPI:Xa$_f$ + TF:VIIa$_L$ $\leftarrow$ TFPI:Xa:TF:VIIa$_L$	$0.0011s^{-1}$	[20]	See above
$k_{+,36}$	IXa$_f$ + AT$_f$ $\rightarrow$ IXa:AT$_f$	$4.9 \times 10^2 M^{-1}s^{-1}$	[23]	[23] gives $k = 490 M^{-1}s^{-1}$
$k_{+,37}$	Xa$_f$ + AT$_f$ $\rightarrow$ Xa:AT$_f$	$2.3 \times 10^3 M^{-1}s^{-1}$	[71]	[71] gives $k = 2.3 \times 10^3 M^{-1}s^{-1}$
$k_{+,38}$	IIa$_f$ + AT$_f$ $\rightarrow$ IIa:AT$_f$	$6.83 \times 10^4 M^{-1}s^{-1}$	[72]	[72] gives $6.83 \times 10^3 M^{-1}s^{-1}$
$k_{+,39}$	V$_L$ + mIIa$_L$ $\rightarrow$ V:mIIa$_L$	$1 \times 10^8 M^{-1}s^{-1}$	[16]	[16] gives $K_m = 7.17 \times 10^{-8}M$ and $k_{\text{cat}} = 0.23s^{-1}$ for thrombin, k_{cat} made 4.5 times larger, [73] gives $\frac{k_{\text{cat}}}{K_m} = 0.22 \times 10^6 M^{-1}s^{-1}$
$k_{-,39}$	V$_L$ + mIIa$_L$ $\leftarrow$ V:mIIa$_L$	$6.94s^{-1}$	[73, 16]	See above
$k_{+,40}$	V:mIIa$_L$ $\rightarrow$ Va$_L$ + mIIa$_L$	$1.035s^{-1}$	[73, 16]	See above
$k_{+,41}$	VIII$_L$ + mIIa$_L$ $\rightarrow$ VIII:mIIa$_L$	$1 \times 10^8 M^{-1}s^{-1}$	-	Assumed same as IIa
$k_{-,41}$	VIII$_L$ + mIIa$_L$ $\leftarrow$ VIII:mIIa$_L$	$13.8s^{-1}$	-	See above
$k_{+,42}$	VIII:mIIa$_L$ $\rightarrow$ VIIIa$_L$ + mIIa$_L$	$0.9s^{-1}$	-	See above
$k_{+,43}$	IIa$_f$ + TM$_L$ $\rightarrow$ TM:IIa$_L$	$1 \times 10^9 M^{-1}s^{-1}$	-	[74] gives $K_d \approx 0.5 \times 10^{-9}M$ without a source
$k_{-,43}$	IIa$_f$ + TM$_L$ $\leftarrow$ TM:IIa$_L$	$0.5s^{-1}$	-	See above
$k_{+,44}$	TM:IIa$_L$ + PC$_L$ $\rightarrow$ TM:IIa:PC$_L$	$1 \times 10^8 M^{-1}s^{-1}$	[75]	[75] gives $K_m = 1 \times 10^{-7}M$, $k_{\text{cat}} = 3.6s^{-1}$
$k_{-,44}$	TM:IIa$_L$ + PC$_L$ $\leftarrow$ TM:IIa:PC$_L$	$6.45s^{-1}$	[75]	See above
$k_{+,45}$	TM:IIa:PC$_L$ $\rightarrow$ TM:IIa$_L$ + APC$_L$	$3.6s^{-1}$	[75]	See above

$k_{+,46}$	$\text{mIIa}_f + \text{AT}_f \rightarrow \text{mIIa:AT}_f$	$6.83 \times 10^3 M^{-1}s^{-1}$	[72]	[72] gives $6.83 \times 10^3 M^{-1}s^{-1}$
$k_{+,47}$	$\text{APC}_L + \text{PS}_L \rightarrow \text{APC:PS}_L$	$1 \times 10^8 M^{-1}s^{-1}$	-	Reported as "Not available" in Bungay[76]
$k_{-,47}$	$\text{APC}_L + \text{PS}_L \leftarrow \text{APC:PS}_L$	$0.5s^{-1}$	-	See above
$k_{+,48}$	$\text{XIa}_f + \text{IX}_L \rightarrow \text{XIa:IX}_L$	$1 \times 10^7 M^{-1}s^{-1}$	[77]	[77] gives $K_m = 1.6 \times 10^{-7}M, k_{cat} = 0.183s^{-1}$
$k_{-,48}$	$\text{XIa}_f + \text{IX}_L \leftarrow \text{XIa:IX}_L$	$1.4517s^{-1}$	[77]	See above
$k_{+,49}$	$\text{XIa:IX}_L \rightarrow \text{XIa}_f + \text{IXa}_L$	$0.183s^{-1}$	[77]	See above
k_{on_1}	$\text{II}_f \rightarrow \text{II}_L$	$4.3 \times 10^6 M^{-1}s^{-1}$	[78]	[78] gives $k_+ = 4.3 \times 10^6 M^{-1}s^{-1}$ and $k_- = 1s^{-1}$
k_{off_1}	$\text{II}_f \leftarrow \text{II}_L$	$1s^{-1}$	[78]	See above
k_{on_2}	$\text{mIIa}_f \rightarrow \text{mIIa}_L$	$5 \times 10^7 M^{-1}s^{-1}$	-	Cited as [79] which gives $K_d = 9.5 \times 10^{-9}M$ for thrombin, does not measure for mIIa
k_{off_2}	$\text{mIIa}_f \leftarrow \text{mIIa}_L$	$0.4575s^{-1}$	-	See above
k_{on_3}	$\text{V}_f \rightarrow \text{V}_L$	$5 \times 10^7 M^{-1}s^{-1}$	[80]	[80] gives $K_d = 2.9 \times 10^{-9}M$
k_{off_3}	$\text{V}_f \leftarrow \text{V}_L$	$0.145s^{-1}$	[80]	See above
k_{on_4}	$\text{Va}_f \rightarrow \text{Va}_L$	$5.7 \times 10^7 M^{-1}s^{-1}$	[17]	[17] gives $k_+ = 5.7 \times 10^7 M^{-1}s^{-1}$ and $k_- = 0.17s^{-1}$
k_{off_4}	$\text{Va}_f \leftarrow \text{Va}_L$	$0.17s^{-1}$	[17]	See above
k_{on_5}	$\text{VII}_f \rightarrow \text{VII}_L$	$5 \times 10^7 M^{-1}s^{-1}$	[28]	[28] gives $K_d = 1.32 \times 10^{-8}M$, Includes TF in the vesicles.
k_{off_5}	$\text{VII}_f \leftarrow \text{VII}_L$	$0.66s^{-1}$	[28]	See above

k_{on_6}	$\text{VIIa}_f \rightarrow \text{VIIa}_L$	$5 \times 10^7 M^{-1} s^{-1}$	[28]	[28] gives $K_d = 4.54 \times 10^{-9} M$, Includes TF in the vesicles.
k_{off_6}	$\text{VIIa}_f \leftarrow \text{VIIa}_L$	$0.227 s^{-1}$	[28]	See above
k_{on_7}	$\text{VIII}_f \rightarrow \text{VIII}_L$	$5 \times 10^7 M^{-1} s^{-1}$	[80]	[80] gives $K_d = 2 \times 10^{-9} M$
k_{off_7}	$\text{VIII}_f \leftarrow \text{VIII}_L$	$0.1 s^{-1}$	[80]	See above
k_{on_8}	$\text{VIIIa}_f \rightarrow \text{VIIIa}_L$	$5 \times 10^7 M^{-1} s^{-1}$	[81]	[81] gives $K_d = 6.7 \times 10^{-9} M$, FIXa is bound to the lipids.
k_{off_8}	$\text{VIIIa}_f \leftarrow \text{VIIIa}_L$	$0.335 s^{-1}$	[81]	See above
k_{on_9}	$\text{IX}_f \rightarrow \text{IX}_L$	$5 \times 10^7 M^{-1} s^{-1}$	[82]	[82] gives $K_d = 2.3 \times 10^{-9} M$
k_{off_9}	$\text{IX}_f \leftarrow \text{IX}_L$	$0.115 s^{-1}$	[82]	See above
$k_{on_{10}}$	$\text{IXa}_f \rightarrow \text{IXa}_L$	$5 \times 10^7 M^{-1} s^{-1}$	[82]	[82] gives $K_d = 2.3 \times 10^{-9} M$
$k_{off_{10}}$	$\text{IXa}_f \leftarrow \text{IXa}_L$	$0.115 s^{-1}$	[82]	See above
$k_{on_{11}}$	$\text{X}_f \rightarrow \text{X}_L$	$1 \times 10^7 M^{-1} s^{-1}$	[83]	[83] gives $K_d = 1.9 \times 10^{-7} M$
$k_{off_{11}}$	$\text{X}_f \leftarrow \text{X}_L$	$1.9 s^{-1}$	[83]	See above
$k_{on_{12}}$	$\text{Xa}_f \rightarrow \text{Xa}_L$	$2.9 \times 10^7 M^{-1} s^{-1}$	[17]	[17] gives $k_+ = 2.9 \times 10^7 M^{-1} s^{-1}$ and $k_- = 3.3 s^{-1}$
$k_{off_{12}}$	$\text{Xa}_f \leftarrow \text{Xa}_L$	$3.3 s^{-1}$	[17]	See above
$k_{on_{13}}$	$\text{APC}_f \rightarrow \text{APC}_L$	$5 \times 10^7 M^{-1} s^{-1}$	[84]	[84] gives $K_d = 7.34 \times 10^{-8} M$ which decreases to $K_d = 7 \times 10^{-9} M$ in the presence of FVa
$k_{off_{13}}$	$\text{APC}_f \leftarrow \text{APC}_L$	$3.5 s^{-1}$	[84]	See above

$k_{on_{14}}$	$\text{PS}_f \rightarrow \text{PS}_L$	$5 \times 10^7 M^{-1} s^{-1}$	[85]	[85] gives $K_d = 4 \times 10^{-9} M$
$k_{off_{14}}$	$\text{PS}_f \leftarrow \text{PS}_L$	$0.2 s^{-1}$	[85]	See above
$k_{on_{15}}$	$\text{VIIIai}_f \rightarrow \text{VIIIai}_L$	$5 \times 10^7 M^{-1} s^{-1}$	-	Assumed to be the same as VIIIa
$k_{off_{15}}$	$\text{VIIIai}_f \leftarrow \text{VIIIai}_L$	$0.335 s^{-1}$	-	See above
$k_{on_{16}}$	$\text{Vai}_f \rightarrow \text{Vai}_L$	$5.7 \times 10^7 M^{-1} s^{-1}$	-	Assumed to be the same as Va
$k_{off_{16}}$	$\text{Vai}_f \leftarrow \text{Vai}_L$	$0.17 s^{-1}$	-	See above
$k_{on_{17}}$	$\text{PC}_f \rightarrow \text{PC}_L$	$5 \times 10^7 M^{-1} s^{-1}$	[86]	[86] gives $K_d = 2.3 \times 10^{-7} M$
$k_{off_{17}}$	$\text{PC}_f \leftarrow \text{PC}_L$	$11.5 s^{-1}$	[86]	See above

Table D.5: Sources for the parameter values used in the Bungay model. Any experimental sources that are used to inform a reaction rate are given in the Source column. Any additional information, including the original measured values and any changes that were made are given in the Notes column. If the rate is reused from another model then this is stated and both the model it was used in and the original experimental source are given.

D.6 Tyurin Model

Parameter	Reaction	Value	Sources	Notes
k_{cat_1}	XI $\overset{XIIa}{\rightarrow}$ XIa	$0.35 s^{-1}$	[67]	[67] gives $k_{\text{cat}} = 0.35 s^{-1}$, retracted in 2007 [68]
k_{m_1}	XI $\overset{XIIa}{\rightarrow}$ XIa	$5 \times 10^{-8} M$	-	Estimate by Tyurin
k_{cat_2}	XI $\overset{IIa}{\rightarrow}$ XIa	$1.43 s^{-1}$	[67]	[67] gives $k_{\text{cat}} = 1.43 s^{-1}$, retracted in 2007 [68]
k_{m_2}	XI $\overset{IIa}{\rightarrow}$ XIa	$5 \times 10^{-8} M$	-	Estimate by Tyurin

k_{cat_3}	XI $\overset{XIa}{\rightarrow}$ XIa	$0.13s^{-1}$	[67]	[67] gives $k_{\text{cat}} = 0.13s^{-1}$, retracted in 2007 [68]
k_{m_3}	XI $\overset{XIa}{\rightarrow}$ XIa	$5 \times 10^{-8}M$	-	Estimate by Tyurin
k_{cat_4}	IX $\overset{XIa}{\rightarrow}$ IXa	$1.25s^{-1}$	[87, 88, 89, 90, 45]	Averaged: [87] gives $K_m = 2 \times 10^{-6}M, k_{\text{cat}} = 0.173s^{-1}$, [88] gives $K_m = 3.1 \times 10^{-7}M, k_{\text{cat}} = 0.417s^{-1}$, [89] gives $K_m = 3.7 \times 10^{-7}M, k_{\text{cat}} = 0.66s^{-1}$, [90] gives $K_m = 3 \times 10^{-7}M, k_{\text{cat}} = 2.4s^{-1}$, [45] gives $K_m = 4.9 \times 10^{-7}M, k_{\text{cat}} = 7.7s^{-1}$
k_{m_4}	IX $\overset{XIa}{\rightarrow}$ IXa	$3.55 \times 10^{-7}M$	[87, 88, 89, 90, 45]	See above
k_{cat_5}	IX $\overset{VIIa}{\rightarrow}$ IXa	$1.8 \times 10^{-4}s^{-1}$	[49]	[49] gives $K_m = 9 \times 10^{-9}M, k_{\text{cat}} = 3.67 \times 10^{-5}s^{-1}$ and $K_m = 1.7 \times 10^{-8}M, k_{\text{cat}} = 1.8 \times 10^{-4}s^{-1}$ for different phospholipid concentrations
k_{m_5}	IX $\overset{VIIa}{\rightarrow}$ IXa	$9 \times 10^{-9}M$	[49]	See above
k_{cat_6}	IX $\overset{TF:VIIa}{\rightarrow}$ IXa	$0.7s^{-1}$	[49, 64, 88, 7]	Averaged: [49] gives $K_m = 8.2 \times 10^{-8}M, k_{\text{cat}} = 1.8s^{-1}$, [64] gives $K_m = 5.5 \times 10^{-8}M, k_{\text{cat}} = 1.35s^{-1}$ (uses X not IX), [88] gives $K_m = 2.1 \times 10^{-7}M, k_{\text{cat}} = 0.25s^{-1}$, [7] gives $K_m = 7 \times 10^{-8}M, k_{\text{cat}} = 0.4s^{-1}$
k_{m_6}	IX $\overset{TF:VIIa}{\rightarrow}$ IXa	$1 \times 10^{-7}M$	[49, 64, 88, 7]	See above
k_{cat_7}	X $\overset{IXa}{\rightarrow}$ Xa	$6.7 \times 10^{-4}s^{-1}$	[91, 25]	[91] gives $K_m = 8.1 \times 10^{-7}M$ and $k_{\text{cat}} = 6.8 \times 10^{-3}s^{-1}$, [25] gives $K_m = 1.4 \times 10^{-7}M$ and $k_{\text{cat}} = 8 \times 10^{-4}s^{-1}$
k_{m_7}	X $\overset{IXa}{\rightarrow}$ Xa	$1 \times 10^{-6}M$	[91, 25]	See above

k_{cat_8}	X $\overset{IXa:VIIIa}{\rightarrow}$ Xa	$25s^{-1}$	[25]	[25] gives $K_m = 1.9 \times 10^{-7}M$, $k_{\text{cat}} = 29s^{-1}$
k_{m_8}	X $\overset{IXa:VIIIa}{\rightarrow}$ Xa	$1.6 \times 10^{-7}M$	[25]	See above
k_{cat_9}	X $\overset{VIIa}{\rightarrow}$ Xa	$2.45 \times 10^{-3}s^{-1}$	[49]	[49] (mixed data) gives $K_m = 2.5 \times 10^{-7}M$, $k_{\text{cat}} = 2.6 \times 10^{-4}s^{-1}$
k_{m_9}	X $\overset{VIIa}{\rightarrow}$ Xa	$2.5 \times 10^{-7}M$	[49]	See above
$k_{cat_{10}}$	X $\overset{TF:VIIa}{\rightarrow}$ Xa	$1.8s^{-1}$	[49, 64, 88]	[49] gives $K_m = 2.3 \times 10^{-7}M$, $k_{\text{cat}} = 3.1s^{-1}$, [64] gives $K_m = 5.5 \times 10^{-8}M$, $k_{\text{cat}} = 81s^{-1}$, [88] gives $K_m = 2.05 \times 10^{-7}M$, $k_{\text{cat}} = 1.17s^{-1}$
$k_{m_{10}}$	X $\overset{TF:VIIa}{\rightarrow}$ Xa	$2.2 \times 10^{-7}M$	[49, 64, 88]	See above
$k_{cat_{11}}$	II $\overset{Xa}{\rightarrow}$ IIa	$0.0375s^{-1}$	[34]	[34] gives $K_m = 5.8 \times 10^{-6}M, k_{\text{cat}} = 0.0375s^{-1}$
$k_{m_{11}}$	II $\overset{Xa}{\rightarrow}$ IIa	$5.8 \times 10^{-6}M$	[34]	See above
$k_{cat_{12}}$	II $\overset{Xa:Va}{\rightarrow}$ IIa	$28.3s^{-1}$	[65, 92]	Used in Khanin[93], averaged from [65] which gives $K_m = 1.06 \times 10^{-6}M$, $k_{\text{cat}} = 22.4s^{-1}$ and [92] which gives $K_m = 1 \times 10^{-6}M$, $k_{\text{cat}} = 35s^{-1}$
$k_{m_{12}}$	II $\overset{Xa:Va}{\rightarrow}$ IIa	$1.03 \times 10^{-6}M$	[65, 92]	See above
$k_{cat_{13}}$	V $\overset{IIa}{\rightarrow}$ Va	$0.23s^{-1}$	[16]	[16] gives $K_m = 7.17 \times 10^{-8}M$ and $k_{\text{cat}} = 0.23s^{-1}$
$k_{m_{13}}$	V $\overset{IIa}{\rightarrow}$ Va	$7.17 \times 10^{-8}M$	[16]	See above
$k_{cat_{14}}$	V $\overset{Xa}{\rightarrow}$ Va	$0.043s^{-1}$	[16]	[16] gives $K_m = 1.04 \times 10^{-8}M$, $k_{\text{cat}} = 0.043s^{-1}$
$k_{m_{14}}$	V $\overset{Xa}{\rightarrow}$ Va	$1.04 \times 10^{-8}M$	[16]	See above

$k_{cat_{15}}$	VII $\overset{Xa}{\rightarrow}$ VIIa	$0.05s^{-1}$	-	No source given
$k_{m_{15}}$	VII $\overset{Xa}{\rightarrow}$ VIIa	$5 \times 10^{-8}M$	-	No source given
$k_{cat_{16}}$	TF:VII $\overset{Xa}{\rightarrow}$ TF:VIIa	$0.66s^{-1}$	[94]	[94] gives $K_m = 9.3 \times 10^{-9}M$, $k_{\text{cat}} = 0.66s^{-1}$
$k_{m_{16}}$	TF:VII $\overset{Xa}{\rightarrow}$ TF:VIIa	$9.3 \times 10^{-9}M$	[94]	See above
$k_{cat_{17}}$	VIII $\overset{IIa}{\rightarrow}$ VIIIa	$0.36s^{-1}$	[66]	[66] gives multiple values around $K_m = 2 \times 10^{-7}M, k_{\text{cat}} = 1s^{-1}$ for VIII cleavage at different positions
$k_{m_{17}}$	VIII $\overset{IIa}{\rightarrow}$ VIIIa	$2.0 \times 10^{-8}M$	[66]	See above
$k_{cat_{18}}$	PC $\overset{TM:IIa}{\rightarrow}$ APC	$88.3s^{-1}$	[95]	[95] gives $K_m = 5.9 \times 10^{-6}M$, $k_{\text{cat}} = 88.3s^{-1}$
$k_{m_{18}}$	PC $\overset{TM:IIa}{\rightarrow}$ APC	$5.9 \times 10^{-6}M$	[95]	See above
$k_{cat_{19}}$	Va $\overset{APC}{\rightarrow}$ Vai	$0.4s^{-1}$	[69]	[69] gives $K_m = 2 \times 10^{-8}M$, $k_{\text{cat}} = 0.4s^{-1}$
$k_{m_{19}}$	Va $\overset{APC}{\rightarrow}$ Vai	$2.0 \times 10^{-8}M$	[69]	See above
$k_{cat_{20}}$	VIIIa $\overset{APC}{\rightarrow}$ VIIIai	$0.4s^{-1}$	-	Estimated using data from [42]
$k_{m_{20}}$	VIIIa $\overset{APC}{\rightarrow}$ VIIIai	$2.0 \times 10^{-8}M$	-	Estimated using data from [42]
$k_{cat_{21}}$	IXa:VIIIa $\overset{APC}{\rightarrow}$ VIIIai + IXa	$0.4s^{-1}$	-	Estimated using data from [42]
$k_{m_{21}}$	IXa:VIIIa $\overset{APC}{\rightarrow}$ VIIIai + IXa	$2.0 \times 10^{-8}M$	-	Estimated using data from [42]
$k_{cat_{22}}$	Xa:Va $\overset{APC}{\rightarrow}$ Vai + Xa	$0.4s^{-1}$	-	Estimated using data from [42]
$k_{m_{22}}$	Xa:Va $\overset{APC}{\rightarrow}$ Vai + Xa	$2.0 \times 10^{-8}M$	-	Estimated using data from [42]

Table D.6: Sources for the parameter values used in the Tyurin model for the enzymatic reactions. Any experimental sources that are used to inform a reaction rate are given in the Source column. Any additional information, including the original measured values and any changes that were made are given in the Notes column. If the rate is reused from another model then this is stated and both the model it was used in and the original experimental source are given.

Parameter	Reaction	Value	Sources	Notes
k_1	Va + Xa $\rightarrow$ Xa:Va	$1.67 \times 10^8 M^{-1}s^{-1}$	[96]	Used in Willems model [97], [96] gives $k = 1.6 \times 10^9 M^{-1}s^{-1}$
k_2	VIIIa + IXa $\rightarrow$ VIIIa:IXa	$1.67 \times 10^8 M^{-1}s^{-1}$	-	Fitted from data in [65]
k_3	VIIa + TF $\rightarrow$ TF:VIIa	$5 \times 10^4 M^{-1}s^{-1}$	[98]	[98] gives $k_+ = 7 \times 10^4 M^{-1}s^{-1}$, $k_- = 3 \times 10^{-5}s^{-1}$, $K_d = 0.5 \times 10^{-9}M$
k_4	TF:VIIa $\rightarrow$ VIIa + TF	$3.33 \times 10^{-5}s^{-1}$	[98]	See above
k_5	VII + TF $\rightarrow$ TF:VII	$3.33 \times 10^4 M^{-1}s^{-1}$	[98]	[98] gives $k_+ = 5 \times 10^4 M^{-1}s^{-1}$, $k_- = 6 \times 10^{-5}s^{-1}$, $K_d = 1 \times 10^{-9}M$
k_6	TF:VII $\rightarrow$ VII + TF	$3.33 \times 10^{-6}s^{-1}$	[98]	See above
k_7	TF:VIIa + TFPI:Xa $\rightarrow$ TF:VIIa:TFPI:Xa	$1.08 \times 10^7 M^{-1}s^{-1}$	[70]	[70] gives $k_+ = 1.07 \times 10^7 M^{-1}s^{-1}$
k_8	TF:VIIa + AT $\rightarrow$ TF:VIIa:AT	$450 M^{-1}s^{-1}$	[24]	[24] gives $k_+ = 450 M^{-1}s^{-1}$
k_9	IIa + AT $\rightarrow$ IIa:AT	$7.08 \times 10^3 M^{-1}s^{-1}$	[23]	[23] gives $7.08 \times 10^3 M^{-1}s^{-1}$
k_{10}	IIa + α1AT $\rightarrow$ IIa:α1AT	$78.3 M^{-1}s^{-1}$	[99, 100]	Used in model [101]. Averaged: [99] gives $108.5 M^{-1}s^{-1}$, [100] gives $48 M^{-1}s^{-1}$
k_{11}	IIa + α2M $\rightarrow$ IIa:α2M	$488 M^{-1}s^{-1}$	[99]	[99] gives $488 M^{-1}s^{-1}$
k_{12}	IIa + PCI $\rightarrow$ IIa:PCI	$1.67 \times 10^4 M^{-1}s^{-1}$	[102]	[102] gives $1.7 \times 10^4 M^{-1}s^{-1}$

k_{13}	Xa + AT → Xa:AT	$3.13 \times 10^3 M^{-1}s^{-1}$	[23, 103]	[23] gives $k = 3.13 \times 10^3 M^{-1}s^{-1}$, [103] gives $k = 567 M^{-1}s^{-1}$
k_{14}	Xa + α1AT → Xa:α1AT	$262 M^{-1}s^{-1}$	[103]	[103] gives $262 M^{-1}s^{-1}$
k_{15}	Xa + TFPI → Xa:TFPI	$1.6 \times 10^7 M^{-1}s^{-1}$	[70]	[70] gives $k_+ = 1.6 \times 10^7 M^{-1}s^{-1}, k_- = 3.3 \times 10^{-4} s^{-1}$
k_{16}	Xa:Va + α1AT → Xa:α1AT + Va	$262 M^{-1}s^{-1}$	[103]	[103] reports same as for Xa
k_{17}	Xa:Va + AT → Xa:AT + Va	$1.67 \times 10^3 M^{-1}s^{-1}$	[23, 103]	[23] gives $k = 3.13 \times 10^3 M^{-1}s^{-1}$, [103] gives $k = 367 M^{-1}s^{-1}$
k_{18}	IXa + AT → IXa:AT	$490 M^{-1}s^{-1}$	[23]	[23] gives $k = 490 M^{-1}s^{-1}$
k_{19}	VIIIa:IXa + AT → IXa:AT + VIIIa	$500 M^{-1}s^{-1}$	-	Reported as [23] but this does not measure in the presence of VIIIa
k_{20}	XIa + C1-inh → XIa:C1-inh	$16.7 M^{-1}s^{-1}$	[104]	[104] gives $667 M^{-1}s^{-1}$, and also reports a reduction in rate of inhibition when in the presence of HMWK (at a factor of around 1/2 for C1-inh). [101] reduced this rate more than others when accounting for HMWK.
k_{21}	XIa + α1AT → XIa:α1AT	$66.7 M^{-1}s^{-1}$	[104]	[104] gives $68 M^{-1}s^{-1}$
k_{22}	XIa + AT → XIa:AT	$167 M^{-1}s^{-1}$	[104]	[104] gives $k = 167 M^{-1}s^{-1}$
k_{23}	XIa + α2AP → XIa:α2AP	$500 M^{-1}s^{-1}$	[104]	[104] gives $1000 M^{-1}s^{-1}$, and also reports a reduced in rate of inhibition when in the presence of HMWK (at a factor of around 1/2 for C1-inh)

k_{24}	XIa + PAI-1 $\rightarrow$ XIa:PAI-1	$2.1 \times 10^5 M^{-1}s^{-1}$	[105]	[105] gives $2.1 \times 10^5 M^{-1}s^{-1}$
k_{25}	IIa + TM $\rightarrow$ TM:IIa	$5 \times 10^5 M^{-1}s^{-1}$	-	Estimated by Tyurin
k_{26}	TM:IIa + PCI $\rightarrow$ TM:IIa:PCI	$1 \times 10^6 M^{-1}s^{-1}$	[102]	Average used which included non-TM bound IIa
k_{27}	APC + PCI $\rightarrow$ APC:PCI	$2.5 \times 10^3 M^{-1}s^{-1}$	[106]	[106] gives $2.5 \times 10^3 M^{-1}s^{-1}$
k_{28}	APC + α1AT $\rightarrow$ APC:α1AT	$10 M^{-1}s^{-1}$	[107]	[107] gives $10 M^{-1}s^{-1}$

Table D.7: Sources for the parameter values used in the Tyurin model for the mass action reactions. Any experimental sources that are used to inform a reaction rate are given in the Source column. Any additional information, including the original measured values and any changes that were made are given in the Notes column. If the rate is reused from another model then this is stated and both the model it was used in and the original experimental source are given.

D.7 Zhu Model

Parameter	Reaction	Value	Sources	Notes
k_{cat_1}	XII $\overset{XIIa}{\rightarrow}$ XIIa	$0.033 s^{-1}$	[36]	[36] gives $K_m = 7.5 \times 10^{-6} M$, $k_{\text{cat}} = 0.033 s^{-1}$
k_{m_1}	XII $\overset{XIIa}{\rightarrow}$ XIIa	$1.1 \times 10^{-5} M$	[36]	See above
k_{cat_2}	PK $\overset{XIIa}{\rightarrow}$ K	$3.6 s^{-1}$	[36]	[36] gives $K_m = 9.1 \times 10^{-8} M$, $k_{\text{cat}} = 3.6 s^{-1}$
k_{m_2}	PK $\overset{XIIa}{\rightarrow}$ K	$9.1 \times 10^{-8} M$	[36]	See above
k_{cat_3}	PK $\overset{XIIf}{\rightarrow}$ K	$40 s^{-1}$	[36]	[36] gives $K_m = 3.7 \times 10^{-5} M$, $k_{\text{cat}} = 40 s^{-1}$
k_{m_3}	PK $\overset{XIIf}{\rightarrow}$ K	$3.7 \times 10^{-5} M$	[36]	See above

k_{cat_4}	XII $\overset{K}{\rightarrow}$ XIIa	$5.7s^{-1}$	[36]	[36] gives $K_m = 5.1 \times 10^{-7}M$, $k_{\text{cat}} = 5.7s^{-1}$
k_{m_4}	XII $\overset{K}{\rightarrow}$ XIIa	$5.1 \times 10^{-7}M$	[36]	See above
k_{cat_5}	XIIa $\overset{K}{\rightarrow}$ XIIf	$5.7 \times 10^{-3}s^{-1}$	-	Used in model [101], estimated using data of [108]
k_{m_5}	XIIa $\overset{K}{\rightarrow}$ XIIf	$5 \times 10^{-7}M$	-	Estimated in model [101]
k_{cat_6}	XI $\overset{XIIa}{\rightarrow}$ XIa	$5.7 \times 10^{-4}s^{-1}$	[42]	[42] gives $K_m = 2 \times 10^{-6}M$, $k_{\text{cat}} = 5.7 \times 10^{-4}s^{-1}$
k_{m_6}	XI $\overset{XIIa}{\rightarrow}$ XIa	$2 \times 10^{-6}M$	[42]	See above
k_{cat_7}	XII $\overset{XIa}{\rightarrow}$ XIIa	$0.57s^{-1}$	-	Used in model [101], estimated using data of [109]
k_{m_7}	XII $\overset{XIa}{\rightarrow}$ XIIa	$5 \times 10^{-5}M$	-	Estimated in model [101]
k_{cat_8}	IX $\overset{XIa}{\rightarrow}$ IXa	$3.75s^{-1}$	[87, 88, 89, 90, 45, 110]	Averaged: [87] gives $K_m = 2 \times 10^{-6}M, k_{\text{cat}} = 0.173s^{-1}$, [88] gives $K_m = 3.1 \times 10^{-7}M, k_{\text{cat}} = 0.417s^{-1}$, [89] gives $K_m = 3.7 \times 10^{-7}M, k_{\text{cat}} = 0.66s^{-1}$, [90] gives $K_m = 3 \times 10^{-7}M, k_{\text{cat}} = 2.4s^{-1}$, [45] gives $K_m = 4.9 \times 10^{-7}M, k_{\text{cat}} = 7.7s^{-1}$, [110] says k_{cat} increases in the presence of phospholipids
k_{m_8}	IX $\overset{XIa}{\rightarrow}$ IXa	$3.5 \times 10^{-7}M$	[87, 88, 89, 90, 45, 110]	See above
k_{cat_9}	X $\overset{IXa}{\rightarrow}$ Xa	$6.7 \times 10^{-4}s^{-1}$	[91, 25]	Used in model [101], [91] gives $K_m = 8.1 \times 10^{-7}M$ and $k_{\text{cat}} = 6.8 \times 10^{-3}s^{-1}$, [25] gives $K_m = 1.4 \times 10^{-7}M$ and $k_{\text{cat}} = 8 \times 10^{-4}s^{-1}$
k_{m_9}	X $\overset{IXa}{\rightarrow}$ Xa	$2 \times 10^{-6}M$	[91, 25]	See above
$k_{cat_{10}}$	X $\overset{IXa:VIIIa}{\rightarrow}$ Xa	$29s^{-1}$	[25]	[25] gives $K_m = 1.9 \times 10^{-7}M$, $k_{\text{cat}} = 29s^{-1}$

$k_{m_{10}}$	X $\overset{IXa:VIIIa}{\rightarrow}$ Xa	$1.9 \times 10^{-7} M$	[25]	See above
$k_{cat_{11}}$	II $\overset{Xa}{\rightarrow}$ IIa	$0.0375 s^{-1}$	[34]	[34] gives $K_m = 5.8 \times 10^{-6} M, k_{\text{cat}} = 0.0375 s^{-1}$
$k_{m_{11}}$	II $\overset{Xa}{\rightarrow}$ IIa	$5.8 \times 10^{-8} M$	[34]	See above
$k_{cat_{12}}$	II $\overset{Xa:Va}{\rightarrow}$ IIa	$28.3 s^{-1}$	[65, 92]	Used in Khanin[93], averaged from [65] which gives $K_m = 1.06 \times 10^{-6} M$, $k_{\text{cat}} = 22.4 s^{-1}$ and [92] which gives $K_m = 1 \times 10^{-6} M$, $k_{\text{cat}} = 35 s^{-1}$
$k_{m_{12}}$	II $\overset{Xa:Va}{\rightarrow}$ IIa	$1 \times 10^{-6} M$	[65, 92]	See above
$k_{cat_{13}}$	V $\overset{IIa}{\rightarrow}$ Va	$0.23 s^{-1}$	[16]	[16] gives $K_m = 7.17 \times 10^{-8} M$ and $k_{\text{cat}} = 0.23 s^{-1}$
$k_{m_{13}}$	V $\overset{IIa}{\rightarrow}$ Va	$7.17 \times 10^{-8} M$	[16]	See above
$k_{cat_{14}}$	V $\overset{Xa}{\rightarrow}$ Va	$0.043 s^{-1}$	[16]	[16] gives $K_m = 1.04 \times 10^{-8} M$, $k_{\text{cat}} = 0.043 s^{-1}$
$k_{m_{14}}$	V $\overset{Xa}{\rightarrow}$ Va	$1.04 \times 10^{-8} M$	[16]	See above
$k_{cat_{15}}$	VIII $\overset{IIa}{\rightarrow}$ VIIIa	$1 s^{-1}$	[66]	[66] gives multiple values around $K_m = 2 \times 10^{-7} M, k_{\text{cat}} = 1 s^{-1}$ for VIII cleavage at different positions (Zhu used average)
$k_{m_{15}}$	VIII $\overset{IIa}{\rightarrow}$ VIIIa	$2 \times 10^{-8} M$	[66]	See above
$k_{cat_{16}}$	Fbg $\overset{IIa}{\rightarrow}$ Fbn	$84 s^{-1}$	[50]	[50] gives $K_m = 7.2 \times 10^{-6} M$, $k_{\text{cat}} = 84 s^{-1}$
$k_{m_{16}}$	Fbg $\overset{IIa}{\rightarrow}$ Fbn	$7.2 \times 10^{-6} M$	[50]	See above
$k_{cat_{17}}$	TF:VII $\overset{Xa}{\rightarrow}$ TF:VIIa	$0.66 s^{-1}$	[94]	[94] gives $K_m = 9.3 \times 10^{-9} M$, $k_{\text{cat}} = 0.66 s^{-1}$
$k_{m_{17}}$	TF:VII $\overset{Xa}{\rightarrow}$ TF:VIIa	$9.3 \times 10^{-9} M$	[94]	See above

$k_{cat_{18}}$	X $\overset{TF:VIIa}{\rightarrow}$ Xa	$1.72s^{-1}$	[49, 64, 88, 111]	Used in model [93], [49] (mixed data, varied concentrations) gives $K_m = 2.3 \times 10^{-7}M$, $k_{\text{cat}} = 3.1s^{-1}$, [64] gives $K_m = 5.5 \times 10^{-8}M$, $k_{\text{cat}} = 81s^{-1}$, [88] gives $K_m = 2.05 \times 10^{-7}M$, $k_{\text{cat}} = 1.17s^{-1}$, [111] gives $K_m = 1.04 \times 10^{-6}M$, $k_{\text{cat}} = 37.5s^{-1}$
$k_{m_{18}}$	X $\overset{TF:VIIa}{\rightarrow}$ Xa	$3.8 \times 10^{-7}M$	[49, 64, 88, 111]	See above
$k_{cat_{19}}$	IX $\overset{TF:VIIa}{\rightarrow}$ IXa	$0.57s^{-1}$	[49, 88, 64, 7]	[34] incorrectly cited. Value used appears to be from [93] which uses multiple sources: [49] (mixed data) gives $K_m = 8.2 \times 10^{-8}M, k_{\text{cat}} = 1.8s^{-1}$, [88] gives $K_m = 2.1 \times 10^{-7}M, k_{\text{cat}} = 0.25s^{-1}$, [64] gives $K_m = 5.5 \times 10^{-8}M, k_{\text{cat}} = 1.35s^{-1}$ (uses X not IX), [7] gives $K_m = 7 \times 10^{-8}M, k_{\text{cat}} = 0.4s^{-1}$
$k_{m_{19}}$	IX $\overset{TF:VIIa}{\rightarrow}$ IXa	$1.33 \times 10^{-7}M$	[49, 88, 64, 7]	See above
$k_{cat_{20}}$	PC $\overset{TM:IIa}{\rightarrow}$ APC	$0.33s^{-1}$	[112]	[112] gives $K_m = 7.7 \times 10^{-6}M$, $k_{\text{cat}} = 0.33s^{-1}$
$k_{m_{20}}$	PC $\overset{TM:IIa}{\rightarrow}$ APC	$7.7 \times 10^{-6}M$	[112]	See above

Table D.8: Sources for the parameter values used in the Zhu model for the enzymatic reactions. Any experimental sources that are used to inform a reaction rate are given in the Source column. Any additional information, including the original measured values and any changes that were made are given in the Notes column. If the rate is reused from another model then this is stated and both the model it was used in and the original experimental source are given.

Parameter	Reaction	Value	Sources	Notes
k_1	Xa + Va $\rightarrow$ Xa:Va	$1.67 \times 10^8 M^{-1}s^{-1}$	[96]	[96] gives $k = 1.6 \times 10^9 M^{-1}s^{-1}$, used in Willems[97] model

k_2	VIIIa + IXa → VIIIa:IXa	$1.67 \times 10^8 M^{-1}s^{-1}$	-	Estimated in model [93]
k_3	IIa + AT → IIa:AT	$5833 M^{-1}s^{-1}$	[23, 113]	Used in model [93]. Averaged: [23] gives $7.08 \times 10^3 M^{-1}s^{-1}$, [113] gives $2.07 \times 10^3 M^{-1}s^{-1}$
k_4	IIa + α_1AT → IIa:α_1AT	$78.3 M^{-1}s^{-1}$	[99, 100]	Used in model [101]. Averaged: [99] gives $108.5 M^{-1}s^{-1}$, [100] gives $48 M^{-1}s^{-1}$
k_5	IIa + α_2M → IIa:α_2M	$488 M^{-1}s^{-1}$	[99]	[99] gives $488 M^{-1}s^{-1}$ (Zhu reports using [100] however this source does not provide a value for α2-M on IIa and Zhu likely used [99] instead)
k_6	Xa + AT → Xa:AT	$1833 M^{-1}s^{-1}$	[23, 103]	Used in model [101], [23] gives $k = 3.13 \times 10^3 M^{-1}s^{-1}$, [103] gives $k = 567 M^{-1}s^{-1}$
k_7	Xa + α_1AT → Xa:α_1AT	$262 M^{-1}s^{-1}$	[103]	[103] gives $262 M^{-1}s^{-1}$
k_8	Xa + TFPI → Xa:TFPI	$1.6 \times 10^7 M^{-1}s^{-1}$	[70]	[70] gives $k_+ = 1.6 \times 10^7 M^{-1}s^{-1}, k_- = 3.3 \times 10^{-4} s^{-1}$
k_9	IXa + AT → IXa:AT	$490 M^{-1}s^{-1}$	[23]	[23] gives $k = 490 M^{-1}s^{-1}$
k_{10}	XIa + C1-inh → XIa:C1-inh	$16.7 M^{-1}s^{-1}$	[104]	Used in model [101], [104] gives $667 M^{-1}s^{-1}$, and also reports a reduction in rate of inhibition when in the presence of HMWK (at a factor of around 1/2 for C1-inh). [101] reduced this rate more than others when accounting for HMWK.

k_{11}	XIa + α_1AT → XIa:α_1AT	$66.7 M^{-1}s^{-1}$	[104]	Used in model [101], [104] gives $68 M^{-1}s^{-1}$
k_{12}	XIa + AT → XIa:AT	$167 M^{-1}s^{-1}$	[104]	[104] gives $k = 167 M^{-1}s^{-1}$
k_{13}	XIa + α_2AP → XIa:α_2AP	$500 M^{-1}s^{-1}$	[104]	Used in model [101], [104] gives $1000 M^{-1}s^{-1}$, and also reports a reduced in rate of inhibition when in the presence of HMWK (at a factor of around 1/2 for C1-inh)
k_{14}	XIa + PAI-1 → XIa:PAI-1	$2.1 \times 10^5 M^{-1}s^{-1}$	[105]	[105] gives $2.1 \times 10^5 M^{-1}s^{-1}$
k_{15}	XIIa + C1-inh → XIIa:C1-inh	$3667 M^{-1}s^{-1}$	[41]	[41] gives $3667 M^{-1}s^{-1}$
k_{16}	XIIa + α_2AP → XIIa:α_2AP	$183 M^{-1}s^{-1}$	[41]	[41] gives $183 M^{-1}s^{-1}$
k_{17}	XIIa + α_2M → XIIa:α_2M	$83 M^{-1}s^{-1}$	[41]	[41] gives $83 M^{-1}s^{-1}$
k_{18}	XIIa + AT → XIIa:AT	$21.7 M^{-1}s^{-1}$	[41]	[41] gives $21.7 M^{-1}s^{-1}$
k_{19}	XIIa + PAI-1 → XIIa:PAI-1	$1.6 \times 10^4 M^{-1}s^{-1}$	[105]	[105] gives $1.6 \times 10^4 M^{-1}s^{-1}$
k_{20}	XIIf + C1-inh → XIIf:C1-inh	$3083 M^{-1}s^{-1}$	[114]	[114] gives $3083 M^{-1}s^{-1}$
k_{21}	XIIf + α_2AP → XIIf:α_2AP	$152 M^{-1}s^{-1}$	[114]	[114] gives $152 M^{-1}s^{-1}$
k_{22}	XIIf + AT → XIIf:AT	$53.3 M^{-1}s^{-1}$	[114]	[114] gives $53.3 M^{-1}s^{-1}$
k_{23}	K + C1-inh → K:C1-inh	$1.67 \times 10^4 M^{-1}s^{-1}$	[115]	[114] was cited by Zhu but [115] appears to be the correct citation, [115] gives $1.7 \times 10^4 M^{-1}s^{-1}$
k_{24}	K + α_2M → K:α_2M	$4833 M^{-1}s^{-1}$	[115]	[115] gives $4.9 \times 10^3 M^{-1}s^{-1}$
k_{25}	K + PAI-1 → K:PAI-1	$6 \times 10^4 M^{-1}s^{-1}$	[105]	[105] gives $6 \times 10^4 M^{-1}s^{-1}$

k_{26}	K + AT → K:AT	$160M^{-1}s^{-1}$	[115]	[115] gives $160M^{-1}s^{-1}$
k_{27}	VII + TF → TF:VII	$3.3 \times 10^4 M^{-1}s^{-1}$	[116]	Used in model [93], [116] gives $k_+ = 3.4 \times 10^4 M^{-1}s^{-1}, k_- = 4 \times 10^{-6} M^{-1}s^{-1}$
k_{28}	TF:VIIa + AT → TF:VIIa:AT	$450M^{-1}s^{-1}$	[24]	$k_+ = 450M^{-1}s^{-1}$ [24]
k_{29}	TF:VIIa + Xa:TFPI → TF:VIIa:Xa:TFPI	$1.1 \times 10^7 M^{-1}s^{-1}$	[70]	[70] gives $k_+ = 1.07 \times 10^7 M^{-1}s^{-1}$
k_{30}	APC + Va → APC:Va	$2 \times 10^7 M^{-1}s^{-1}$	[69]	Used in model [117], [69] gives $K_m = 1.97 \times 10^{-8} M$, $k_{\text{cat}} = 0.395 s^{-1}$
k_{31}	APC + VIIIa → APC:VIIIa	$2 \times 10^7 M^{-1}s^{-1}$	-	Used in model [117], Assumed same as k_{30}
k_{32}	APC + Xa:Va → APC:Xa:Va	$2 \times 10^7 M^{-1}s^{-1}$	-	See above
k_{33}	APC + VIIIa:IXa → APC:VIIIa:IXa	$2 \times 10^7 M^{-1}s^{-1}$	-	See above
k_{34}	TM + IIa → TM:IIa	$6.7 \times 10^6 M^{-1}s^{-1}$	[118]	[118] gives $6.7 \times 10^6 M^{-1}s^{-1}$
k_{35}	XI → XIa	$1.3 \times 10^{-4} s^{-1}$	[42]	1st order, Used in model [117], Used value of $k_{cat} = 1.3 \times 10^{-4} s^{-1}$ from [42], representing IIa activation of XI

Table D.9: Sources for the parameter values used in the Zhu model for the mass action reactions. Any experimental sources that are used to inform a reaction rate are given in the Source column. Any additional information, including the original measured values and any changes that were made are given in the Notes column. If the rate is reused from another model then this is stated and both the model it was used in and the original experimental source are given.

Appendix E

Unified Model Modules

This appendix presents the Unified model module documents. The first six modules contain details for both the original Unified Model from Chapter 3 and the Improved Unified Model from Chapter 5. The final two module documents, convering the Other Inhibitors and Fibrinogen are only relevant to the Improved Unified Model.

E.1 TF:VIIa Module

Model Reactions

This module comprises the reactions from stimulation with TF through to the formation of TF:VIIa, including both association of TF to FVII or FVIIa and activation of FVII. The reactions included in previous mathematical models and those included in the Unified Model are described in Table E.1, while the former are depicted in Figure E.1 and the latter in Figure E.2.

Models	Reactions
Hockin, Danforth, Brummel and Chatterjee	$TF + VII \leftrightarrow TF{:}VII$
	$TF + VIIa \leftrightarrow TF{:}VIIa$
	$TF{:}VIIa + VII \rightarrow TF{:}VIIa + VIIa$
	$Xa + VII \rightarrow Xa + VIIa$
	$IIa + VII \rightarrow IIa + VIIa$
	$TF{:}VIIa + AT \rightarrow TF{:}VIIa{:}AT$
Bungay	$TF_L + VIIa_L \leftrightarrow TF{:}VIIa_L$
	$TF_L + VII_L \leftrightarrow TF{:}VII_L$
	$TF{:}VII_L + Xa_L \leftrightarrow TF{:}VIIa{:}Xa_L$
	$TF{:}VIIa{:}Xa_L \rightarrow TF{:}VIIa_L + Xa_L$
	$Xa_L + VII_L \leftrightarrow Xa{:}VII_L$
	$Xa{:}VII_L \rightarrow VIIa_L + Xa_L$
Tyurin	$VII \overset{Xa}{\rightarrow} VIIa$
	$TF{:}VII \overset{Xa}{\rightarrow} TF{:}VIIa$
	$TF + VII \leftrightarrow TF{:}VII$

	$\text{TF} + \text{VIIa} \leftrightarrow \text{TF:VIIa}$ $\text{TF:VIIa} + \text{AT} \rightarrow \text{TF:VIIa:AT}$
Zhu	$\text{TF:VII} \overset{Xa}{\rightarrow} \text{TF:VIIa}$ $\text{TF} + \text{VII} \leftrightarrow \text{TF:VII}$ $\text{TF:VIIa} + \text{AT} \rightarrow \text{TF:VIIa:AT}$
Unified	$\text{TF} + \text{VII} \leftrightarrow \text{TF:VII}$ $\text{TF} + \text{VIIa} \leftrightarrow \text{TF:VIIa}$ $\text{VII} \overset{Xa}{\rightarrow} \text{VIIa}$ $\text{TF:VII} \overset{Xa}{\rightarrow} \text{TF:VIIa}$ $\text{VII} \overset{IIa}{\rightarrow} \text{VIIa}$ $\text{TF:VII} \overset{IIa}{\rightarrow} \text{TF:VIIa}$ $\text{VII} \overset{TF:VIIa}{\rightarrow} \text{VIIa}$ $\text{TF:VIIa} + \text{AT} \rightarrow \text{TF:VIIa:AT}$
Improved Unified	$\text{TF} + \text{VII} \leftrightarrow \text{TF:VII}$ $\text{TF} + \text{VIIa} \leftrightarrow \text{TF:VIIa}$ $\text{VII} \overset{Xa}{\rightarrow} \text{VIIa}$ $\text{TF:VII} \overset{Xa}{\rightarrow} \text{TF:VIIa}$ $\text{VII} \overset{IIa}{\rightarrow} \text{VIIa}$ $\text{TF:VII} \overset{IIa}{\rightarrow} \text{TF:VIIa}$ $\text{VII} \overset{TF:VIIa}{\rightarrow} \text{VIIa}$ $\text{TF:VIIa} + \text{AT} \rightarrow \text{TF:VIIa:AT}$

Table E.1: The reactions that are used in the different models and our choice of reactions for the TF:VIIa module.

Network Diagrams

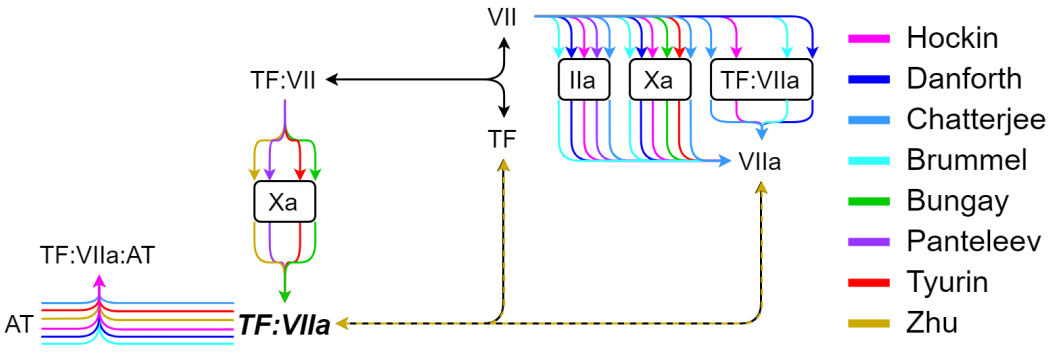

Figure E.1: A network diagram for the TF:VIIa module reactions that are included in previous mathematical models. Black lines represent a reaction that is included in all models. A dashed, black and coloured line represents a line that is included in all but the correspondingly coloured model.

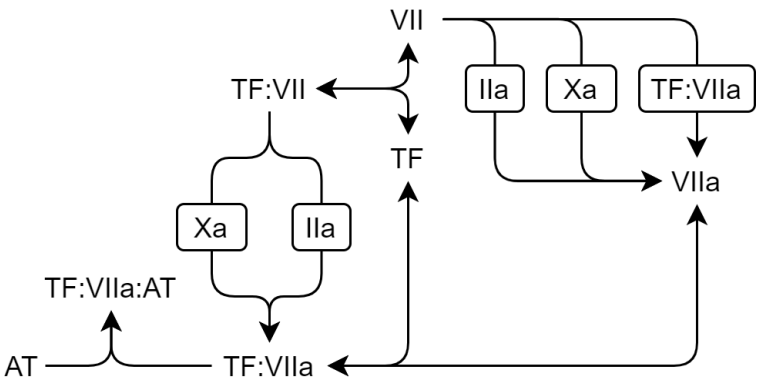

Figure E.2: A reaction diagram for our chosen reactions to be included in the Unified Model and Improved Unified Model for the TF:VIIa module.

Reaction rates for previous models

Reaction	Model	Model values	Data values
TF + VII $\leftrightarrow$ TF:VII	Hockin, Danforth, Brummel	$k_+ = 3.2 \times 10^6 M^{-1}s^{-1}$, $k_- = 3.1 \times 10^{-3}s^{-1}$, $K_d = 9.7 \times 10^{-10}M$	$K_d = 2 \times 10^{-9}M$ [1] used as a base and fitted using data from [2].
	Bungay	$k_+ = 5 \times 10^6 M^{-1}s^{-1}$, $k_- = 0.005s^{-1}$, $K_d = 1 \times 10^{-9}M$	Estimated.
	Tyurin	$k_+ = 3.33 \times 10^4 M^{-1}s^{-1}$, $k_- = 3.33 \times 10^{-6}s^{-1}$, $K_d = 1 \times 10^{-10}M$	$k_+ = 5 \times 10^4 M^{-1}s^{-1}$, $k_- = 6 \times 10^{-5}s^{-1}$, $K_d = 1 \times 10^{-9}M$ [98].
	Chatterjee	$k_+ = 3.2 \times 10^6 M^{-1}s^{-1}$, $k_- = 3.1 \times 10^{-2}s^{-1}$, $K_d = 9.7 \times 10^{-9}M$	Scaled $K_d = 2 \times 10^{-9}M$ [1] based on [28].
TF + VII $\rightarrow$ TF:VII	Zhu	$k_+ = 3.3 \times 10^4 M^{-1}s^{-1}$	Used in [93], [116] gives $k_+ = 3.4 \times 10^4 M^{-1}s^{-1}, k_- = 4 \times 10^{-6}M^{-1}s^{-1}$.
TF + VIIa $\leftrightarrow$ TF:VIIa	Hockin, Danforth, Brummel	$k_+ = 2.3 \times 10^7 M^{-1}s^{-1}$, $k_- = 3.1 \times 10^{-3}s^{-1}$, $K_d = 1.35 \times 10^{-10}M$	$K_d = 5.47 \times 10^{-9}M$ [1] used as a base and fitted using data from [3].
	Bungay	$k_+ = 5 \times 10^8 M^{-1}s^{-1}$, $k_- = 0.005s^{-1}$, $K_d = 1 \times 10^{-11}M$	$K_d = 1 \times 10^{-11}M$ [63].
	Tyurin	$k_+ = 5 \times 10^4 M^{-1}s^{-1}$, $k_- = 3.33 \times 10^{-5}s^{-1}$, $K_d = 6.66 \times 10^{-10}M$	$k_+ = 7 \times 10^4 M^{-1}s^{-1}$, $k_- = 3 \times 10^{-5}s^{-1}$, $K_d = 0.5 \times 10^{-9}M$ [98].

	Chatterjee	$k_+ = 2.3 \times 10^7 M^{-1}s^{-1}$, $k_- = 3.1 \times 10^{-5}s^{-1}$, $K_d = 1.3 \times 10^{-12}M$	Scaled $K_d = 5.47 \times 10^{-9}M$ [1] based on [29].
VII $\overset{Xa}{\rightarrow}$ VIIa	Hockin, Danforth, Brummel, Chatterjee	$\frac{K_m}{k_{\text{cat}}} = 1.3 \times 10^7 M^{-1}s^{-1}$	$K_m = 1.2 \times 10^{-6}M$, $k_{\text{cat}} = 15.2s^{-1}$, $\frac{k_{\text{cat}}}{K_m} = 1.3 \times 10^7 M^{-1}s^{-1}$ [4].
	Bungay	$k_+ = 5 \times 10^7 M^{-1}s^{-1}$, $k_- = 44.8s^{-1}$, $k_{\text{cat}} = 15.2s^{-1}$, $K_m = 1.2 \times 10^{-6}M$	$K_m = 1.2 \times 10^{-6}M$, $k_{\text{cat}} = 15.2s^{-1}$ [4].
	Tyurin	$K_m = 5 \times 10^{-8}M$, $k_{\text{cat}} = 0.05s^{-1}$	No source given.
TF:VII $\overset{Xa}{\rightarrow}$ TF:VIIa	Bungay	$k_+ = 5 \times 10^7 M^{-1}s^{-1}$, $k_- = 44.8s^{-1}$, $k_{\text{cat}} = 15.2s^{-1}$, $K_m = 1.2 \times 10^{-6}M$	$K_m = 1.2 \times 10^{-6}M$, $k_{\text{cat}} = 15.2s^{-1}$ [4].
	Tyurin, Zhu	$K_m = 9.3 \times 10^{-9}M$, $k_{\text{cat}} = 0.66s^{-1}$	$K_m = 9.3 \times 10^{-9}M$, $k_{\text{cat}} = 0.66s^{-1}$ [94].
VII $\overset{IIa}{\rightarrow}$ VIIa	Hockin, Danforth, Brummel, Chatterjee	$\frac{K_m}{k_{\text{cat}}} = 2.3 \times 10^4 M^{-1}s^{-1}$	$K_m = 2.7 \times 10^{-6}M$, $k_{\text{cat}} = 0.061s^{-1}$, $\frac{k_{\text{cat}}}{K_m} = 2.3 \times 10^4 M^{-1}s^{-1}$ [4].
VII $\overset{TF:VIIa}{\rightarrow}$ VIIa	Hockin, Danforth, Brummel, Chatterjee	$\frac{K_m}{k_{\text{cat}}} = 4.45 \times 10^5 M^{-1}s^{-1}$	$K_m = 3.2 \times 10^{-6}M$, $k_{\text{cat}} = 1.4s^{-1}$, $\frac{k_{\text{cat}}}{K_m} = 4.4 \times 10^5 M^{-1}s^{-1}$ [4].
	Hockin, Danforth,	$k_+ = 230M^{-1}s^{-1}$	$k_+ = 450M^{-1}s^{-1}$ [24].

TF:VIIa + AT → TF:VIIa:AT	Brummel, Chatterjee		
	Tyurin, Zhu	$k_+ = 450M^{-1}s^{-1}$	$k_+ = 450M^{-1}s^{-1}$ [24].

Table E.2: The parameter values used by each of the models along with the accompanying reference and original data value for each of the reactions in the TF:VIIa module.

Choosing Parameters

TF + VII $\leftrightarrow$ TF:VII		
Citation	Rates	Notes
[28]	$K_d = 13.2nM$	Temperature: 37°C. Bovine FVII. Purified bovine brain TF. Egg PC lipid from Supleco, Bellefonte, PA. pH: 7.5. Measures with different binding schemes for varying PS% (not taken into account here for consistency with other binding/unbinding reactions).
[98]	$K_d = 1nM$, $k_+ = 5 \times 10^4 M^{-1}s^{-1}$, $k_- = 6 \times 10^{-5}s^{-1}$	Room temp. Human FVII. Human TF from American Diagnostic Inc, Greenwich, CT, USA. pH: 7.4. Phospholipids not used as the surface. Separate association and dissociation rates are given. Also gives rates for AT.
[1]	$K_d = 2nM$, $k_+ = 3.14 \times 10^5 M^{-1}s^{-1}$, $k_- = 6.29 \times 10^{-4}s^{-1}$	Soluble truncated TF_{1-219} gift from Dr. D. L. Eaton, Greentech Inc., South San Francisco, CA. Separate association and disassociation rates are given. Also gives activation of FX. pH: 7.3.
Chosen values: $K_d = 3nM(10 \wedge N(-8.55, 0.58^2), 5\% = 3.28 \times 10^{-10}, 95\% = 2.66 \times 10^{-8}), k_+ = 1.25 \times 10^5 M^{-1}s^{-1}(10 \wedge N(5.10, 0.56^2), 5\% = 1.51 \times 10^4, 95\% = 1.05 \times 10^6)$ therefore $k_- = 3.75 \times 10^{-4}s^{-1}$		

Table E.3: The prior distributions and reaction rates used to inform the prior distributions for both the Unified Model and the Improved Unified Model for TF and FVII association/dissociation.

TF + VIIa $\leftrightarrow$ TF:VIIa		
Citation	Rates	Notes
[28]	$K_d = 4.54nM$	Temperature: 37°C. Bovine FVII. Purified bovine brain TF. Egg PC lipid from Supleco, Bellefonte, PA. pH: 7.5. Measures with different binding schemes for varying PS% (not taken into account here for consistency with other binding/unbinding reactions).
[98]	$K_d = 0.5nM$, $k_+ = 7 \times 10^4 M^{-1}s^{-1}$, $k_- = 3 \times 10^{-5}s^{-1}$	Room temp. Human FVII. Human TF from American Diagnostic Inc, Greenwich, CT, USA. pH: 7.4. Phospholipids not used as the surface. Separate association and disassociation rates are given. Also gives rates for AT.
[63]	$K_d = 10pM$	Full length TF in PC vesicles. Lacks clarification on other details. Excluded from calculation of priors due to large difference in rate compared with other sources.
[1]	$K_d = 5.47nM$, $k_+ = 1.6 \times 10^5 M^{-1}s^{-1}$, $k_- = 8.76 \times 10^{-4}s^{-1}$	Soluble truncated TF_{1-219} gift from Dr. D. L. Eaton, Greentech Inc., South San Francisco, CA. Separate association and disassociation rates are given. Also gives activation of FX. pH: 7.3.
[3]	$K_d = 8.4nM$, $k_+ = 1.9 \times 10^5 M^{-1}s^{-1}$, $k_- = 1.6 \times 10^{-3}s^{-1}$	Full length human TF. Gives separate association and disassociation rates. Also gives activation of FX. pH: 7.4.
Chosen values: $K_d = 3.2nM (10 \wedge N(-8.50, 0.55^2), 5\% = 3.94 \times 10^{-10}, 95\% = 2.54 \times 10^{-8})$, $k_+ = 1.3 \times 10^5 M^{-1}s^{-1} (10 \wedge N(5.11, 0.23^2), 5\% = 5.39 \times 10^4, 95\% = 3.08 \times 10^5)$ therefore $k_- = 4.16 \times 10^{-4}s^{-1}$		

Table E.4: The prior distributions and reaction rates used to inform the prior distributions for both the Unified Model and the Improved Unified Model for TF and FVIIa association/dissociation.

VII $\overset{Xa}{\rightarrow}$ VIIa / TF:VII $\overset{Xa}{\rightarrow}$ TF:VIIa		
Citation	Rates	Notes
[4]	$K_m = 1.2\mu M$, $k_{\text{cat}} = 15.2s^{-1}$	Temperature: 25°C. 20μM PCPS (75/25) purchased from Sigma. Human TF_{1-242} from Shu-Len Liu (Hyland Division, Baxter Healthcare Corp. Human FVII and Xa from Haematologic Technologies Inc. pH: 7.4. Same with and without TF.
[94]	$K_m = 9.3nM$, $k_{\text{cat}} = 0.66s^{-1}$	Only measures with TF. Human TF from Dr. T. S. Edgington, Department of Immunology, Scripps Research Institute, La Jolla, CA. Purified X from Sigma and activated by RVV. PC/PS: 70/30. Temperature: 37°C.
Chosen values: +TF: $K_m = 105nM(10 \wedge N(-6.98, 1.49^2), 5\% = 3.71 \times 10^{-10}, 95\% = 2.96 \times 10^{-5}), k_{\text{cat}} = 3.16s^{-1}(10 \wedge N(0.50, 0.96^2), 5\% = 8.24 \times 10^{-2}, 95\% = 1.22 \times 10^{2})$, -TF: $K_m = 1.2\mu M(10 \wedge N(-5.92, 2.5^2), 5\% = 9.28 \times 10^{-11}, 95\% = 1.56 \times 10^{-2}), k_{\text{cat}} = 15.2s^{-1}(10 \wedge N(1.18, 2.5^2), 5\% = 1.17 \times 10^{-3}, 95\% = 1.96 \times 10^{5})$		

Table E.5: The prior distributions and reaction rates used to inform the prior distributions for both the Unified Model and the Improved Unified Model for FVII and TF:VII activation by FXa.

VII $\overset{IIa}{\rightarrow}$ VIIa / TF:VII $\overset{IIa}{\rightarrow}$ TF:VIIa		
Citation	Rates	Notes
[4]	$K_m = 2.7\mu M$, $k_{\text{cat}} = 0.061s^{-1}$	Temperature: 25°C. 200μM PCPS (75/25) purchased from Sigma. Human TF_{1-242} from Shu-Len Liu (Hyland Division, Baxter Healthcare Corp. Human FIIa and FVII from Haematologic Technologies Inc. pH: 7.4. Same with and without TF.
Chosen values: +/-TF: $K_m = 2.7\mu M(10 \wedge N(-5.55, 2.5^2), 5\% = 2.08 \times 10^{-10}, 95\% = 3.49 \times 10^{-2}), k_{\text{cat}} = 0.061s^{-1}(10 \wedge N(-1.21, 2.5^2), 5\% = 4.76 \times 10^{-6}, 95\% = 7.99 \times 10^{2})$		

Table E.6: The prior distributions and reaction rates used to inform the prior distributions for both the Unified Model and the Improved Unified Model for FVII and TF:VII activation by FIIa.

VII $\overset{IXa}{\rightarrow}$ VIIa / TF:VII $\overset{IXa}{\rightarrow}$ TF:VIIa		
Citation	Rates	Notes
[4]	$K_m = 1.7\mu M$, $k_{\text{cat}} = 0.32s^{-1}$	Temperature: 25°C. 200μM PCPS (75/25) purchased from Sigma. Human TF_{1-242} from Shu-Len Liu (Hyland Division, Baxter Healthcare Corp. Human FVII and FIXa from Haematologic Technologies Inc. pH: 7.4. Same with and without TF.
Chosen values: +/-TF: $K_m = 1.7\mu M(10 \wedge N(-5.77, 2.5^2), 5\% = 1.31 \times 10^{-10}, 95\% = 2.20 \times 10^{-2}), k_{\text{cat}} = 0.32s^{-1}(10 \wedge N(-0.49, 2.5^2), 5\% = 2.50 \times 10^{-5}, 95\% = 4.19 \times 10^{3})$		

Table E.7: The prior distributions and reaction rates used to inform the prior distributions for both the Unified Model and the Improved Unified Model for FVII and TF:VII activation by FIXa.

VII $\overset{TF:VIIa}{\rightarrow}$ VIIa		
Citation	Rates	Notes
[4]	$K_m = 3.2\mu M$, $k_{\text{cat}} = 1.4s^{-1}$	Temperature: 25°C. 200μM PCPS (75/25) purchased from Sigma. Human TF_{1-242} from Shu-Len Liu (Hyland Division, Baxter Healthcare Corp. Human FVIIa and FVII from Haematologic Technologies Inc. pH: 7.4.
Chosen values: $K_m = 3.2\mu M(10 \wedge N(-5.49, 2.5^2), 5\% = 2.50 \times 10^{-10}, 95\% = 4.19 \times 10^{-2}), k_{\text{cat}} = 1.4s^{-1}(10 \wedge N(0.15, 2.5^2), 5\% = 1.09 \times 10^{-4}, 95\% = 1.83 \times 10^{4})$		

Table E.8: The prior distributions and reaction rates used to inform the prior distributions for both the Unified Model and the Improved Unified Model for FVII activation by TF:VIIa.

TF:VIIa + AT → TF:VIIa:AT		
Citation	Rates	Notes
[98]	$k_+ = 2 \times 10^3 M^{-1}s^{-1}$	Room temp. Human VII. Human TF from American Diagnostic Inc. AT from human plasma was from Chromogenic AB, Molndal, Sweden. pH: 7.4. Also gives rates for TF:VIIa binding/ unbinding.
[24]	$k_+ = 450 M^{-1}s^{-1}$	PCPS (75/25) from Sigma. AT purified from Human plasma. Human FVIIa from Novo Pharmaceuticals. Human TF from Dr. Shu-Len Liu, Hyland Division, Baxter Healthcare Corp. Temperature: 37°C. pH: 7.4.
Chosen values: $k_+ = 9.5 \times 10^2 M^{-1}s^{-1}(10 \wedge N(2.98, 0.46^2), 5\% = 1.67 \times 10^2, 95\% = 5.45 \times 10^3)$		

Table E.9: The prior distributions and reaction rates used to inform the prior distributions for the Unified Model for TF:VIIa inhibition by AT.

Changes for Improved Unified Model

The only change for the Improved Unified Model in this module is the removal of one source for TF:VIIa inhibition by AT as it includes heparin in its measurement.

TF:VIIa + AT → TF:VIIa:AT		
Citation	Rates	Notes
[98]	$k_+ = 2 \times 10^3 M^{-1}s^{-1}$	Room temp. Human VII. Human TF from American Diagnostic Inc. AT from human plasma was from Chromogenix AB, Molndal, Sweden. pH: 7.4. Also gives rates for TF:VIIa binding/ unbinding. Excluded from prior calculation as it includes heparin.
[24]	$k_+ = 450 M^{-1}s^{-1}$	PCPS (75/25) from Sigma. AT purified from Human plasma. Human FVIIa from Novo Pharmaceuticals. Human TF from Dr. Shu-Len Liu, Hyland Division, Baxter Healthcare Corp. Temperature: 37°C. pH: 7.4.
Chosen values: $k_+ = 4.5 \times 10^2 M^{-1}s^{-1}(10 \wedge N(2.65, 2.5^2), 5\% = 3.45 \times 10^{-2}, 95\% = 5.79 \times 10^6)$		

Table E.10: The prior distributions and reaction rates used to inform the prior distributions for the Improved Unified Model for TF:VIIa inhibition by AT.

E.2 Xa:Va Module

Model Reactions

This module comprises of the reactions that lead up to Xa:Va formation including both association of FXa to FVa and activation of FXa and of FVa. The reactions used in the models we have examined are given in Table E.11 as well as the reactions that we have chosen for the Unified and Improved Unified Models. The reactions for the previous models, the Unified Model and the Improved Unified Model are then demonstrated in Figures E.3, E.4, and E.5, respectively.

Models	Reactions
Hockin	$TF{:}VIIa + X \leftrightarrow TF{:}VIIa{:}X$ $TF{:}VIIa{:}X \rightarrow TF{:}VIIa{:}Xa$ $TF{:}VIIa{:}Xa \leftrightarrow TF{:}VIIa + Xa$ $IXa{:}VIIIa + X \leftrightarrow IXa{:}VIIIa{:}X$ $IXa{:}VIIIa{:}X \rightarrow IXa{:}VIIIa + Xa$ $IIa + V \rightarrow IIa + Va$ $Xa + Va \leftrightarrow Xa{:}Va$ $Xa + AT \rightarrow Xa{:}AT$
Danforth and Brummel	$TF{:}VIIa + X \leftrightarrow TF{:}VIIa{:}X$ $TF{:}VIIa{:}X \rightarrow TF{:}VIIa{:}Xa$ $TF{:}VIIa{:}Xa \leftrightarrow TF{:}VIIa + Xa$ $IXa{:}VIIIa + X \leftrightarrow IXa{:}VIIIa{:}X$ $IXa{:}VIIIa{:}X \rightarrow IXa{:}VIIIa + Xa$ $IXa + X \rightarrow IXa + Xa$ $IIa + V \rightarrow IIa + Va$ $mIIa + V \rightarrow mIIa + Va$ $Xa + Va \leftrightarrow Xa{:}Va$ $Xa + AT \rightarrow Xa{:}AT$
Bungay	$TF{:}VIIa_L + X_L \leftrightarrow TF{:}VIIa{:}X_L$ $TF{:}VIIa{:}X_L \rightarrow TF{:}VIIa{:}Xa_L$ $TF{:}VIIa{:}Xa_L \rightarrow TF{:}VIIa + Xa_L$ $IXa{:}VIIIa_L + X_L \leftrightarrow IXa{:}VIIIa{:}X_L$ $IXa{:}VIIIa{:}X_L \rightarrow IXa{:}VIIIa_L + Xa_L$ $V_L + Xa_L \leftrightarrow V{:}Xa_L$ $V{:}Xa_L \rightarrow Va_L + Xa_L$ $V_L + IIa_L \leftrightarrow V{:}IIa_L$ $V{:}IIa_L \rightarrow Va_L + IIa_L$ $V_L + mIIa_L \leftrightarrow V{:}mIIa_L$ $V{:}mIIa_L \rightarrow Va_L + mIIa_L$ $Xa_L + Va_L \leftrightarrow Xa{:}Va_L$ $Xa_f + AT_f \rightarrow Xa{:}AT_f$
Tyurin	$X \overset{IXa}{\rightarrow} Xa$ $X \overset{IXa{:}VIIIa}{\rightarrow} Xa$

	$X \overset{VIIa}{\rightarrow} Xa$
	$X \overset{TF:VIIa}{\rightarrow} Xa$
	$V \overset{IIa}{\rightarrow} Va$
	$V \overset{Xa}{\rightarrow} Va$
	$Xa + Va \rightarrow Xa{:}Va$
	$Xa + AT \rightarrow Xa{:}AT$
	$Xa{:}Va + AT \rightarrow Xa{:}AT + Va$
Zhu	$X \overset{IXa}{\rightarrow} Xa$
	$X \overset{IXa:VIIIa}{\rightarrow} Xa$
	$X \overset{TF:VIIa}{\rightarrow} Xa$
	$V \overset{IIa}{\rightarrow} Va$
	$V \overset{Xa}{\rightarrow} Va$
	$Xa + Va \rightarrow Xa{:}Va$
	$Xa + AT \rightarrow Xa{:}AT$
Chatterjee	$TF{:}VIIa + X \leftrightarrow TF{:}VIIa{:}X$
	$TF{:}VIIa{:}X \rightarrow TF{:}VIIa{:}Xa$
	$TF{:}VIIa{:}Xa \leftrightarrow TF{:}VIIa + Xa$
	$VIIa + X \leftrightarrow VIIa{:}X$
	$VIIa{:}X \rightarrow VIIa + Xa$
	$IXa{:}VIIIa + X \leftrightarrow IXa{:}VIIIa{:}X$
	$IXa{:}VIIIa{:}X \rightarrow IXa{:}VIIIa + Xa$
	$IXa + X \leftrightarrow IXa{:}X$
	$IXa{:}X \rightarrow IXa + Xa$
	$IIa + V \rightarrow IIa + Va$
	$Xa + Va \leftrightarrow Xa{:}Va$
	$Xa + AT \rightarrow Xa{:}AT$
Unified	$X \overset{TF:VIIa}{\rightarrow} Xa$
	$X \overset{VIIa}{\rightarrow} Xa$
	$X \overset{IXa:VIIIa}{\rightarrow} Xa$
	$X \overset{IXa}{\rightarrow} Xa$
	$V \overset{IIa}{\rightarrow} Va$
	$V \overset{Xa}{\rightarrow} Va$
	$Xa + Va \leftrightarrow Xa{:}Va$
	$Xa + AT \rightarrow Xa{:}AT$
	$Xa{:}Va + AT \rightarrow Xa{:}AT + Va$
Improved Unified	$X \overset{TF:VIIa}{\rightarrow} Xa$
	$X \overset{VIIa}{\rightarrow} Xa$
	$X \overset{IXa:VIIIa}{\rightarrow} Xa$
	$X \overset{IXa}{\rightarrow} Xa$
	$V \overset{IIa}{\rightarrow} Va$
	$V \overset{Xa}{\rightarrow} Va$
	$Xa + Va \leftrightarrow Xa{:}Va$

$Xa + AT \rightarrow Xa{:}AT$	
$Xa{:}Va + AT \rightarrow Xa{:}Va{:}AT$	

Table E.11: The reactions that are used in the different models and our choice of reactions.

Network Diagrams

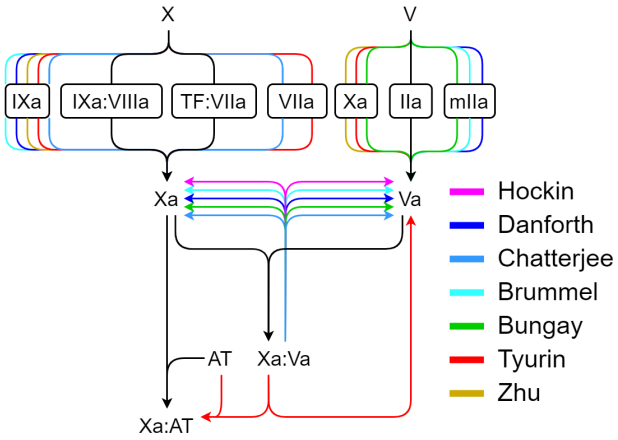

Figure E.3: A network diagram for the Xa:Va module reactions that are included in previous mathematical models. Black lines represent a reaction that is included in all models. A dashed, black and coloured line represents a line that is included in all but the correspondingly coloured model.

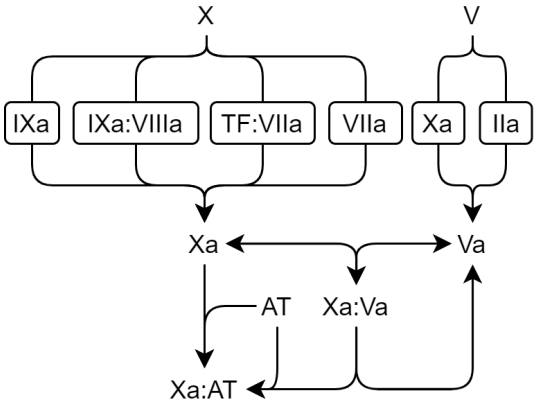

Figure E.4: A reaction diagram for our chosen reactions in the Unified Model for the Xa:Va module.

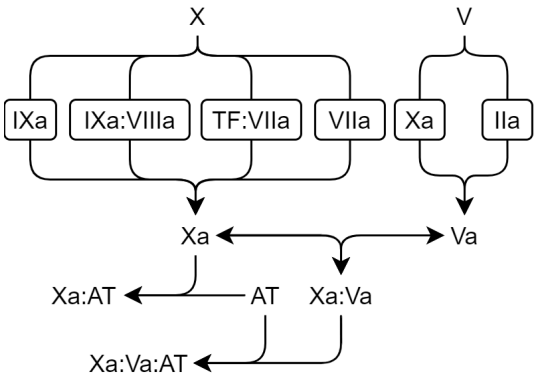

Figure E.5: A reaction diagram for our chosen reactions in the Improved Unified Model for the Xa:Va module.

Reaction rates for previous models

Reaction	Model	Model values	Data values
X $\overset{TF:VIIa}{\rightarrow}$ Xa	Hockin, Danforth, Brummel	$k_+ = 2.5 \times 10^7 M^{-1}s^{-1}, k_- = 1.05s^{-1}, k_{\text{cat}} = 6s^{-1}, k_{d,+} = 2.2 \times 10^7 M^{-1}s^{-1}, k_{d,-} = 19s^{-1}$	[5] gives $K_m = 2.38 \times 10^{-7}M$ and $k_{\text{cat}} = 7s^{-1}$, [3] gives $K_m = 6.9 \times 10^{-8}M$ and $k_{\text{cat}} = 7.4s^{-1}$, [6] gives $K_m = 4.35 \times 10^{-6}M$ and $k_{\text{cat}} = 5.69s^{-1}$, [6] suggest FXa binds similarly to FX.
	Bungay	$k_+ = 1 \times 10^8 M^{-1}s^{-1}, k_- = 32.5s^{-1}, k_{\text{cat}} = 1.5s^{-1}, k_{d,-} = 1s^{-1}$	[18] gives $K_m = 4.5 \times 10^{-7}M$, $k_{\text{cat}} = 1.15s^{-1}$, [64] gives $K_m = 5.5 \times 10^{-8}M$, $k_{\text{cat}} = 81s^{-1}$.
	Tyurin	$K_m = 2.2 \times 10^{-7}M, k_{\text{cat}} = 1.8s^{-1}$	[49] (mixed data, varied concentrations) gives $K_m = 2.3 \times 10^{-7}M$, $k_{\text{cat}} = 3.1s^{-1}$, [64] gives $K_m = 5.5 \times 10^{-8}M$, $k_{\text{cat}} = 81s^{-1}$, [88] gives $K_m = 2.05 \times 10^{-7}M$, $k_{\text{cat}} = 1.17s^{-1}$.
	Zhu	$K_m = 3.8 \times 10^{-7}M, k_{\text{cat}} = 1.72s^{-1}$	[49] (mixed data, varied concentrations) gives $K_m = 2.3 \times 10^{-7}M$, $k_{\text{cat}} = 3.1s^{-1}$, [64] gives $K_m = 5.5 \times 10^{-8}M$, $k_{\text{cat}} = 81s^{-1}$, [88] gives $K_m = 2.05 \times 10^{-7}M$, $k_{\text{cat}} = 1.17s^{-1}$, [111] gives $K_m = 1.04 \times 10^{-6}M$, $k_{\text{cat}} = 37.5s^{-1}$.
	Chatterjee	$k_+ = 2.5 \times 10^7 M^{-1}s^{-1}, k_- = 0.0105s^{-1}, k_{\text{cat}} = 6s^{-1}, k_{d,+} = 2.2 \times 10^7 M^{-1}s^{-1}, k_{d,-} = 19s^{-1}$	Hockin multiplied by 0.01 based on: [29] reported a decrease in K_m from 400nM to 20nM as PS % increases from 10 to 40 (figure 6), [5] reported a K_m of 238nM.
X $\overset{VIIa}{\rightarrow}$ Xa	Tyurin	$K_m = 2.5 \times 10^{-7}M, k_{\text{cat}} = 2.45 \times 10^{-3}s^{-1}$	[49] (mixed data) gives $K_m = 2.5 \times 10^{-7}M$, $k_{\text{cat}} = 2.6 \times 10^{-4}s^{-1}$.

	Chatterjee	$k_+ = 1 \times 10^8 M^{-1}s^{-1}, k_- = 210s^{-1}, k_{\text{cat}} = 1.6 \times 10^{-6}s^{-1}$	[49] (mixed data) gives $K_m = 2.5 \times 10^{-7}M$, $k_{\text{cat}} = 2.6 \times 10^{-4}s^{-1}$.
X $\overset{IXa:VIIIa}{\rightarrow}$ Xa	Hockin, Danforth, Brummel	$k_+ = 1 \times 10^8 M^{-1}s^{-1}, k_- = 1 \times 10^{-3}s^{-1}, k_{\text{cat}} = 8.2s^{-1}$	[12] gives $K_m = 6.3 \times 10^{-8}M$ and $k_{\text{cat}} = 8.3s^{-1}$, used in Jones [8].
	Bungay	$k_+ = 1 \times 10^8 M^{-1}s^{-1}, k_- = 10.7s^{-1}, k_{\text{cat}} = 8.3s^{-1}$	[12] gives $K_m = 6.3 \times 10^{-8}M$ and $k_{\text{cat}} = 8.3s^{-1}$, [25] gives $K_m = 1.9 \times 10^{-7}M$, $k_{\text{cat}} = 29s^{-1}$.
	Tyurin	$K_m = 1.6 \times 10^{-7}M, k_{\text{cat}} = 25s^{-1}$	[25] gives $K_m = 1.9 \times 10^{-7}M$, $k_{\text{cat}} = 29s^{-1}$.
	Zhu	$K_m = 1.9 \times 10^{-7}M, k_{\text{cat}} = 29s^{-1}$	[25] gives $K_m = 1.9 \times 10^{-7}M$, $k_{\text{cat}} = 29s^{-1}$.
	Chatterjee	$k_+ = 1 \times 10^8 M^{-1}s^{-1}, k_- = 1 \times 10^{-5}s^{-1}, k_{\text{cat}} = 8.2s^{-1}$	Hockin multiplied by 0.01 based on: K_m decreases from 45μM to 160nM when using activated platelets rather than inactive platelets [25].
X $\overset{IXa}{\rightarrow}$ Xa	Danforth, Brummel	$\frac{k_{\text{cat}}}{K_m} = 5.7 \times 10^3 M^{-1}s^{-1}$	[25] gives $K_m = 1.4 \times 10^{-7}M$ and $k_{\text{cat}} = 8 \times 10^{-4}s^{-1}$.
	Tyurin	$K_m = 1 \times 10^{-6}M, k_{\text{cat}} = 6.7 \times 10^{-4}s^{-1}$	[91] gives $K_m = 8.1 \times 10^{-7}M$ and $k_{\text{cat}} = 6.8 \times 10^{-3}s^{-1}$, [25] gives $K_m = 1.4 \times 10^{-7}M$ and $k_{\text{cat}} = 8 \times 10^{-4}s^{-1}$.
	Zhu	$K_m = 2 \times 10^{-6}M, k_{\text{cat}} = 6.7 \times 10^{-4}s^{-1}$	[91] gives $K_m = 8.1 \times 10^{-7}M$ and $k_{\text{cat}} = 6.8 \times 10^{-3}s^{-1}$, [25] gives $K_m = 1.4 \times 10^{-7}M$ and $k_{\text{cat}} = 8 \times 10^{-4}s^{-1}$.

	Chatterjee	$k_+ = 1 \times 10^8 M^{-1}s^{-1}, k_- = 0.64s^{-1}, k_{\text{cat}} = 7 \times 10^{-4}s^{-1}$	$K_m = 6.45nM$ and $k_{\text{cat}} = 7 \times 10^{-4}s^{-1}$ was used from [46].
V $\overset{IIa}{\rightarrow}$ Va	Hockin, Danforth, Brummel, Chatterjee	$\frac{k_{\text{cat}}}{K_m} = 2 \times 10^7 M^{-1}s^{-1}$	[16] gives $K_m = 7.17 \times 10^{-8}M$ and $k_{\text{cat}} = 0.23s^{-1}$, used in Jones [8].
	Bungay	$k_+ = 1 \times 10^8 M^{-1}s^{-1}, k_- = 6.94s^{-1}, k_{\text{cat}} = 0.23s^{-1}$	[16] gives $K_m = 7.17 \times 10^{-8}M$ and $k_{\text{cat}} = 0.23s^{-1}$.
	Tyurin	$K_m = 7.17 \times 10^{-8}M, k_{\text{cat}} = 0.23s^{-1}$	[16] gives $K_m = 7.17 \times 10^{-8}M$ and $k_{\text{cat}} = 0.23s^{-1}$.
	Zhu	$K_m = 7.17 \times 10^{-8}M, k_{\text{cat}} = 0.23s^{-1}$	[16] gives $K_m = 7.17 \times 10^{-8}M$ and $k_{\text{cat}} = 0.23s^{-1}$.
V $\overset{mIIa}{\rightarrow}$ Va	Danforth, Brummel	$\frac{k_{\text{cat}}}{K_m} = 3 \times 10^6 M^{-1}s^{-1}$	[10] gives $3.5 \times 10^6 M^{-1}s^{-1}$ and $2.4 \times 10^6 M^{-1}s^{-1}$ for different methods.
	Bungay	$k_+ = 1 \times 10^8 M^{-1}s^{-1}, k_- = 6.94s^{-1}, k_{\text{cat}} = 1.035s^{-1}$	[16] gives $K_m = 7.17 \times 10^{-8}M$ and $k_{\text{cat}} = 0.23s^{-1}$ for thrombin k_{cat} made 4.5 times larger, [73] gives $\frac{k_{\text{cat}}}{K_m} = 0.22 \times 10^6 M^{-1}s^{-1}$.
V $\overset{Xa}{\rightarrow}$ Va	Bungay	$k_+ = 1 \times 10^8 M^{-1}s^{-1}, k_- = 1s^{-1}, k_{\text{cat}} = 0.043s^{-1}$	[16] gives $K_m = 1.04 \times 10^{-8}M$, $k_{\text{cat}} = 0.043s^{-1}$.
	Tyurin	$K_m = 1.04 \times 10^{-8}M, k_{\text{cat}} = 0.043s^{-1}$	[16] gives $K_m = 1.04 \times 10^{-8}M$, $k_{\text{cat}} = 0.043s^{-1}$.
	Zhu	$K_m = 1.04 \times 10^{-7}M, k_{\text{cat}} = 0.043s^{-1}$	[16] gives $K_m = 1.04 \times 10^{-8}M$, $k_{\text{cat}} = 0.043s^{-1}$.
	Hockin,	$k = 4 \times 10^8 M^{-1}s^{-1}$	[17] ($> 1 \times 10^9 M^{-1}s^{-1}$), used in Jones [8].

Xa + Va → Xa:Va	Danforth, Brummel, Chatterjee		
	Bungay	$k = 1 \times 10^9 M^{-1}s^{-1}$	[65] gave $K_d = 1.04 \times 10^{-9} M$.
	Tyurin, Zhu	$k = 1.67 \times 10^8 M^{-1}s^{-1}$	[96] gives $k = 1.6 \times 10^9 M^{-1}s^{-1}$, used in Willems model [97].
Xa + Va ← Xa:Va	Hockin, Danforth, Brummel	$k = 0.2s^{-1}$	[12] gave $K_d = 1 - 2nM$ for IXa:VIIIa, used in Jones [8].
	Bungay	$k = 1s^{-1}$	[65] gave $K_d = 1.04 \times 10^{-9} M$.
	Chatterjee	$k = 0.008s^{-1}$	Hockin multiplied by 0.04 based on: K_d decreases from 3.3nM to 30pM when using 10μM 40% PS [33].
Xa + AT → Xa:AT	Hockin, Chatterjee	$k = 1.5 \times 10^3 M^{-1}s^{-1}$	[21] gives $k = 4.9 \times 10^3 M^{-1}s^{-1}$ and $k = 2.9 \times 10^3 M^{-1}s^{-1}$.
	Danforth, Brummel	$k = 4.2 \times 10^3 M^{-1}s^{-1}$	No citation for reaction rate in either Brummel or Danforth.
	Bungay	$k = 2.3 \times 10^3 M^{-1}s^{-1}$	[71] gives $k = 2.3 \times 10^3 M^{-1}s^{-1}$.
	Tyurin	$k = 3.13 \times 10^3 M^{-1}s^{-1}$	[23] gives $k = 3.13 \times 10^3 M^{-1}s^{-1}$, [103] gives $k = 567 M^{-1}s^{-1}$.
	Zhu	$k = 1.833 \times 10^3 M^{-1}s^{-1}$	[23] gives $k = 3.13 \times 10^3 M^{-1}s^{-1}$, [103] gives $k = 567 M^{-1}s^{-1}$.

Xa:Va + AT → Xa:AT + Va	Tyurin	$k = 1.67 \times 10^3 M^{-1}s^{-1}$	[23] gives $k = 3.13 \times 10^3 M^{-1}s^{-1}$, [103] gives $k = 367 M^{-1}s^{-1}$.

Table E.12: The parameter values used by each of the models along with the accompanying reference and original data value for each of the reactions in the Xa:Va module.

Choosing Parameters

X $\overset{VIIa}{\rightarrow}$ Xa		
Citation	Rates	Notes
[49]	$K_m = 2.5 \times 10^{-7} M$, $k_{\text{cat}} = 2.6 \times 10^{-4} s^{-1}$	PCPS (70/30), PC type V-E, bovine brain PS, both from Sigma. FX purified from human plasma. Human FVIIa. Temperature: 37°C. With and without TF. Measures activation of FX and FIX.
[18]	$K_m = 4.87 \times 10^{-6} M$, $k_{\text{cat}} = 3.95 \times 10^{-4} s^{-1}$	TF from Bovine brain thromboplastin. FX purified from bovine plasma. Temperature: 37°C. pH: 7.5. Gives with and without TF. Measured in the presence of benzamidine hydrochloride.
Chosen values: $K_m = 1.1 \mu M (10 \wedge N(-5.96, 0.91^2), 5\% = 3.49 \times 10^{-8}, 95\% = 3.44 \times 10^{-5}), k_{\text{cat}} = 3.2 \times 10^{-4} s^{-1} (10 \wedge N(-3.49, 0.13^2), 5\% = 1.98 \times 10^{-4}, 95\% = 5.29 \times 10^{-4})$		

Table E.13: The prior distributions and reaction rates used to inform the prior distributions for the Unified Model for FX activation by FVIIa.

$X \overset{TF:VIIa}{\rightarrow} Xa$		
Citation	Rates	Notes
[5]	$K_m = 2.38 \times 10^{-7} M$, $k_{\text{cat}} = 7.25 s^{-1}$	Human factor VII from Novo-Nordisk, Gentofte, Denmark. Human TF from Genentech, South San Francisco, CA. Human factor X purified from plasma. PCPS: (75/25), Hen egg PC and Bovine brain PS from Sigma. pH: 7.4. Temperature: 37°C.
[3]	$K_m = 6.9 \times 10^{-8} M$, $k_{\text{cat}} = 7.4 s^{-1}$	Full length human TF. FX purified from plasma. 200pM PCPS (70/30). Temperature: 37°C. pH: 7.4.
[6]	$K_m = 4.35 \times 10^{-6} M$, $k_{\text{cat}} = 5.69 s^{-1}$	Suggests FXa binds similarly to FX. Human FX from plasma. Human FVIIa purchased form Novo-Nordisc, Gentofte, Denmark. Human TF gift from Genentech, South San Francisco, CA.
[18]	$K_m = 4.5 \times 10^{-7} M$, $k_{\text{cat}} = 1.15 s^{-1}$	TF from Bovine brain thromboplastin. FX purified from bovine plasma. Temperature: 37°C. pH: 7.5. Gives with and without TF. Measured in the presence of benzamidine hydrochloride.
[64]	$K_m = 5.5 \times 10^{-8} M$, $k_{\text{cat}} = 81 s^{-1}$	Human FVII and FX from plasma. TF purified from human brain. PCPS (50/50). Temperature: 37°C. pH: 7.45.
[49]	$K_m = 2.3 \times 10^{-7} M$, $k_{\text{cat}} = 3.1 s^{-1}$	PCPS (70/30), PC type V-E, bovine brain PS, both from Sigma. FX purified from human plasma. Human brain TF. Human FVIIa. Temperature: 37°C. With and without TF. Measures activation of FX and FIX.
[88]	$K_m = 2.05 \times 10^{-7} M$, $k_{\text{cat}} = 1.17 s^{-1}$	Human brain TF. Human FVII and X. pH: 7.5. Activation of FX and FIX by: FXIa (FIX only), TF:VIIa (both) and IXa:VIIIa (FX only).
[111]	$K_m = 1.04 \times 10^{-6} M$, $k_{\text{cat}} = 37.5 s^{-1}$	Human FX from plasma. Human FVIIa. TF isolated from human brains. PCPS (75/25) from Sigma using bovine brain PC and hen egg PS. Temperature: 37°C. pH: 7.4.
[29]	$K_m = 4 \times 10^{-7} M$, $k_{\text{cat}} = 2.5 s^{-1}$	PCPS from Avanti Polar Lipids, Alabaster, AL. FVIIa from American Diagnostica, Greenwich, CT. X from Enzyme Research Laboratories, South Bend, IN. Human TF. Values stated are approximated from graphs.
Chosen values: $K_m = 0.32 \mu M (10 \wedge N(-6.50, 0.58^2), 5\% = 3.51 \times 10^{-8}, 95\% = 2.85 \times 10^{-6})$, $k_{\text{cat}} = 6 s^{-1} (10 \wedge N(0.78, 0.63^2), 5\% = 5.54 \times 10^{-1}, 95\% = 6.55 \times 10^{1})$		

Table E.14: The prior distributions and reaction rates used to inform the prior distributions for the Unified Model for FX activation by TF:VIIa.

X $\overset{IXa:VIIIa}{\rightarrow}$ Xa		
Citation	Rates	Notes
[12]	$K_m = 6.3 \times 10^{-8} M$, $k_{\text{cat}} = 8.3 s^{-1}$	Bovine FIX, FVIII and FX purified from plasma. 10μM DOPC/DOPSE (75/25). Temperature: 37°C. pH: 7.9. With and without FVIIIa.
[25]	$K_m = 1.9 \times 10^{-7} M$, $k_{\text{cat}} = 29 s^{-1}$	Human FIX, FVIII and FX. 25μM PCPS (75/25). Temperature: 37°C. pH: 7.4. With and without FVIIIa.
[88]	$K_m = 1.4 \times 10^{-7} M$, $k_{\text{cat}} = 0.42 s^{-1}$	Human brain TF. Human FIX and FX. pH: 7.5. Activation of FX and FIX by FXIa (FIX only), TF:VIIa (both) and IXa:VIIIa (FX only).
[91]	$K_m = 1.2 \times 10^{-7} M$, $V_{max} = 7.9 \times 10^{-13} M s^{-1}$	Human FVIII from Dr. William Thomas, Hyland Diagnostics Div., Travenol Laboratories, Inc., Costa Mesa, CA. Human FIX and FX were purified from factor IX concentrate from Cutter Laboratories, Inc., Berkeley, CA. PCPS, synthetic PS and bovine PC, both from Supelco, Inc., Bellefonte, PA. pH: 7.5 With and without FVIIIa.
[46]	$K_m = 2.26 \times 10^{-8} M$, $k_{\text{cat}} = 1.25 s^{-1}$	Human FIX and FX from Enzyme Research Laboratories, South Bend, IN. FVIII from Baxter Healthcare Corp., Duarte, CA. Temperature: 37°C. pH: 7.4. Values for wild type and normal (derived from plasma) are given. With and without FVIIIa.
Chosen values: $K_m = 85nM(10 \wedge N(-7.07, 0.37^2), 5\% = 2.10 \times 10^{-8}, 95\% = 3.46 \times 10^{-7}), k_{\text{cat}} = 3.35 s^{-1}(10 \wedge N(0.53, 0.82^2), 5\% = 1.52 \times 10^{-1}, 95\% = 7.57 \times 10^{1})$		

Table E.15: The prior distributions and reaction rates used to inform the prior distributions for the Unified Model for FX activation by IXa:VIIIa.

X $\overset{IXa}{\rightarrow}$ Xa		
Citation	Rates	Notes
[91]	$K_m = 7.6 \times 10^{-7} M$, $V_{max} = 1.4 \times 10^{-14} M s^{-1}$	Human FIX and FX were purified from Factor IX concentrate from Cutter Laboratories, Inc., Berkeley, CA. PCPS, synthetic PS and bovine PC, both from Supelco, Inc., Bellefonte, PA. pH: 7.5. With and without FVIIIa.
[46]	$K_m = 6.4 \times 10^{-9} M$, $k_{\text{cat}} = 7 \times 10^{-4} s^{-1}$	Human FIX and FX from Enzyme Research Laboratories, South Bend, IN. Temperature: 37°C. pH: 7.4. Values for wild type and normal (derived from plasma) are given. With and without FVIIIa.
[12]	$K_m = 5.8 \times 10^{-8} M$, $k_{\text{cat}} = 4.1 \times 10^{-5} s^{-1}$	Bovine FIX and FX purified from plasma. 10μM DOPC/DOPSE (75/25). Temperature: 37°C. pH: 7.9. With and without FVIIIa.
[25]	$K_m = 1.4 \times 10^{-7} M$, $k_{\text{cat}} = 8 \times 10^{-4} s^{-1}$	Human FIX and FX. 5μM PCPS (75/25). Temperature: 37°C. pH: 7.4. With and without FVIIIa.
Chosen values: $K_m = 80nM(10 \wedge N(-7.10, 0.86^2), 5\% = 3.06 \times 10^{-9}, 95\% = 2.06 \times 10^{-6}), k_{\text{cat}} = 2.8 \times 10^{-4} s^{-1}(10 \wedge N(-3.55, 0.73^2), 5\% = 1.77 \times 10^{-5}, 95\% = 4.48 \times 10^{-3})$		

Table E.16: The prior distributions and reaction rates used to inform the prior distributions for the Unified Model for FX activation by FIXa.

V $\overset{IIa}{\rightarrow}$ Va		
Citation	Rates	Notes
[16]	$K_m = 7.17 \times 10^{-8} M$, $k_{\text{cat}} = 0.23 s^{-1}$	20μM PCPS (75/25), Hen egg PC and bovine brain PS from Sigma. Human FV and FII from fresh frozen plasma. Temperature: 25°C. pH: 7.4. Also does activation by FXa.
[73]	$\frac{k_{\text{cat}}}{K_m} = 3.6 \times 10^6 M^{-1} s^{-1}$	60μM DOPC/DOPS (90/10) from Avanti Polar Lipids, Inc., Pelham, AL. Human FII and FV. Temperature: 37°C. pH: 7.5.
[10]	$\frac{k_{\text{cat}}}{K_m} = 6.4 \times 10^6 M^{-1} s^{-1}$, $\frac{k_{\text{cat}}}{K_m} = 4 \times 10^6 M^{-1} s^{-1}$	Different methods. DOPC/DOPS (75/25) from Avanti Polar Lipids, Inc., Pelham, AL. Human FII and FV purified from plasma. Temperature: 25°C. pH: 7.4. Also gives activation of FII by FXa and Xa:Va.
Chosen values: $K_m = 71.7 nM (10 \wedge N(-7.14, 2.5^2), 5\% = 5.59 \times 10^{-12}, 95\% = 9.39 \times 10^{-4}), k_{\text{cat}} = 0.3 s^{-1} (10 \wedge N(-0.53, 0.13^2), 5\% = 1.80 \times 10^{-1}, 95\% = 4.83 \times 10^{-1})^*$		

Table E.17: The prior distributions and reaction rates used to inform the prior distributions for the Unified Model for FV activation by FIIa.

V $\overset{Xa}{\rightarrow}$ Va		
Citation	Rates	Notes
[16]	$K_m = 1.04 \times 10^{-8} M$, $k_{\text{cat}} = 0.043 s^{-1}$	$20\mu M$ 20μM PCPS (75/25), Hen egg PC and bovine brain PS from Sigma. Human FV and FX from fresh frozen plasma. FX activated by RVV. Temperature: 25°C. pH: 7.4. Also does activation by FIIa.
Chosen values: $K_m = 10.4 nM (10 \wedge N(-7.98, 2.5^2), 5\% = 8.08 \times 10^{-13}, 95\% = 1.36 \times 10^{-4}), k_{\text{cat}} = 0.043 s^{-1} (10 \wedge N(-1.37, 2.5^2), 5\% = 3.29 \times 10^{-6}, 95\% = 5.53 \times 10^2)$		

Table E.18: The prior distributions and reaction rates used to inform the prior distributions for the Unified Model for FV activation by FXa.

*K_m uses a single source, this K_m is then used to find k_{cat} from the other sources.

Xa + Va → Xa:Va		
Citation	Rates	Notes
[17]	$> 1 \times 10^9 M^{-1} s^{-1}$	PCPS (75/25), Hen egg PC and bovine brain PS from Sigma. Details for binding rates with PCPS given. Bovine FV and FX purified from plasma. Once bound to PCPS reaction is very rapid. Temperature: 25°C. pH: 7.4.
[65]	$K_d = 1.04 \times 10^{-9} M$	PCPS (75/25), Hen egg PC and bovine brain PS from Sigma. Human FV and FX purified from plasma. FXa activated by RVV. Gives activation of FII. Temperature: 25°C. pH: 7.4.
[96]	$k_+ = 1.6 \times 10^9 M^{-1} s^{-1}$	DOPC/DOPS (80/20) both purchased from Sigma. 60-80nm diameter vesicles (also gives 20-30nm). Bovine FX and FV. FX activated by RVV from Sigma. Temperature: 37°C. pH: 7.5.
Chosen values: $K_d = 177pM (10 \wedge N(-9.75, 1.09^2), 5\% = 2.86 \times 10^{-12}, 95\% = 1.10 \times 10^{-8}), k_+ = 1.6 \times 10^9 M^{-1} s^{-1} (10 \wedge N(9.20, 2.5^2), 5\% = 1.22 \times 10^5, 95\% = 2.05 \times 10^{13})$ therefore $k_- = 0.28 s^{-1}$		

Table E.19: The prior distributions and reaction rates used to inform the prior distributions for the Unified Model for FXa and FVa association.

Xa + Va ← Xa:Va		
Citation	Rates	Notes
[65]	$K_d = 1.04 \times 10^{-9} M$	PCPS (75/25), Hen egg PC and bovine brain PS from Sigma. Human FV and FX purified from plasma. FXa activated by RVV. Gives activation of FII. Temperature: 25°C. pH: 7.4.
[33]	$K_d = 3 \times 10^{-11} M$	Many varying phospholipid concentrations and mix ratios. 10 μM DOPC/DOPS (60/40). Bovine FX and FV. FX activated by RVV. Temperature: 37°C. pH: 7.5.
[96]	$k_+ = 1.6 \times 10^{-3} s^{-1}$	DOPC/DOPS (80/20) both purchased from Sigma. 60-80nm diameter vesicles (also gives 20-30nm). Bovine FX and FV. FX activated by RVV from Sigma. Temperature: 37°C. pH: 7.5.
Chosen values: given above		

Table E.20: The prior distributions and reaction rates used to inform the prior distributions for the Unified Model for FXa and FVa dissociation.

Xa + AT → Xa:AT		
Citation	Rates	Notes
[21]	$k_+ = 8.9 \times 10^5 M^{-1}s^{-1}$, $k = 4.5 \times 10^3 M^{-1}s^{-1}$	Human FX purified from plasma. Human AT. Temperature: 25°C. pH: 7.4. With and without saturating levels of Heparin. Also includes thrombin.
-	$k_+ = 4.2 \times 10^3 M^{-1}s^{-1}$	Used in Danforth and Brummel. No citation given.
[71]	$k_+ = 2.3 \times 10^3 M^{-1}s^{-1}$	Human AT was purified from outdated plasma obtained from the Henry Ford Hospital blood bank. Human FX purified from plasma and activated by RVV. Temperature: 25°C. pH: 7.4.
[103]	$k_+ = 567 M^{-1}s^{-1}$	$20\mu M$ DOPC and Bovine brain PS (60/40) and from Sigma. Human FX and AT. X activated by RVV from Sigma. Temperature: 37°C. Also does in presence of FVa.
Chosen values: $k_+ = 1.8 \times 10^3 M^{-1}s^{-1}(10 \wedge N(3.26, 0.46^2), 5\% = 3.19 \times 10^2, 95\% = 1.04 \times 10^4)$		

Table E.21: The prior distributions and reaction rates used to inform the prior distributions for the Unified Model for FXa inhibition by AT.

Xa:Va + AT → Xa:AT + Va		
Citation	Rates	Notes
[23]	$k_+ = 3.13 \times 10^3 M^{-1}s^{-1}$	Rabbit brain thromboplastin from Ortho Diagnostics, Raritan, NJ (used for measuring FXa through FIIa activation). Human FXa, FVa and AT. Absence of heparin ($k = 4 \times 10^6 M^{-1}s^{-1}$ in presence of heparin). Also gives FIXa and FIIa. Temperature: 37°C. pH: 7.5. Measures in presence of FVa but not clear how this was handled.
[103]	$k_+ = 367 M^{-1}s^{-1}$	$20\mu M$ DOPC and Bovine brain PS (60/40) and from Sigma. Human FX and AT. Bovine FV purified from fresh bovine blood. FX activated by RVV from Sigma. Temperature: 37°C. Also does in absence of FVa.
Chosen values: $k_+ = 1.1 \times 10^3 M^{-1}s^{-1}(10 \wedge N(3.03, 0.66^2), 5\% = 8.80 \times 10^1, 95\% = 1.31 \times 10^4)$		

Table E.22: The prior distributions and reaction rates used to inform the prior distributions for the Unified Model for Xa:Va inhibition by AT.

Improved Unified Model - Choosing Parameters

Following the changes made for the Improved Unified Model, this section outlines the updated reaction rate sources and prior distributions with minor changes made to the notes on each source.

Inhibition of Xa:Va by AT is only given in one model, the Tyurin model, which cites two sources [23]† and [103]. This reaction would be strongly related to the ability of a model to be able to predict prothrombin not being fully converted into thrombin (data shows only around 90% of prothrombin is converted into thrombin [119]) since prothrombinase needs to be fully inhibited if prothrombin is going to be stopped from converted into thrombin. Other than in the Tyurin model, the only way in which Xa:Va is inhibited is first through disassociation into Xa + Va and then inhibition of FXa, however, since Xa:Va binds so tightly, this is too slow to fully inhibit before all prothrombin is activated.

In addition to the inclusion of this reaction, we have changed the reaction scheme to also inhibit the FVa rather than disassociation as used in the Tyurin model. We have done this in order to encourage prothrombinase to be inhibited earlier (since there is far less FV in the assay). For the sake of consistency, we do the same change to IXa:VIIIa inhibition by AT and Xa:Va inhibition of Xa:Va by α1-AT.

†This source is used to inform the reaction rate in the Tyurin model but measures FXa inhibition and only uses FVa after inhibition to measure the amount of remaining FXa through prothrombin activation.

$X \overset{TF:VIIa}{\rightarrow} Xa$		
Citation	Rates	Notes
[5]	$K_m = 2.38 \times 10^{-7} M$, $k_{\text{cat}} = 7.25 s^{-1}$	Human factor VII from Novo-Nordisk, Gentofte, Denmark. Human TF from Genentech, South San Francisco, CA. Human factor X purified from plasma. PCPS: (75/25), Hen egg PC and Bovine brain PS from Sigma. pH: 7.4. Temperature: 37°C.
[3]	$K_m = 6.9 \times 10^{-8} M$, $k_{\text{cat}} = 7.4 s^{-1}$	Full length human TF. FX purified from plasma. 200pM PCPS (70/30). Temperature: 37°C. pH: 7.4.
[6]	$K_m = 4.35 \times 10^{-6} M$, $k_{\text{cat}} = 5.69 s^{-1}$	Suggests FXa binds similarly to FX. Human FX from plasma. Human FVIIa purchased form Novo-Nordisc, Gentofte, Denmark. Human TF gift from Genentech, South San Francisco, CA.
[18]	$K_m = 4.5 \times 10^{-7} M$, $k_{\text{cat}} = 1.15 s^{-1}$	TF from Bovine brain thromboplastin. FX purified from bovine plasma. Temperature: 37°C. pH: 7.5. Gives with and without TF. Measured in the presence of benzamidine hydrochloride.
[64]	$K_m = 5.5 \times 10^{-8} M$, $k_{\text{cat}} = 81 s^{-1}$	Human FVII and X from plasma. TF purified from human brain. PCPS (50/50). Temperature: 37°C. pH: 7.45.
[49]	$K_m = 2.3 \times 10^{-7} M$, $k_{\text{cat}} = 3.1 s^{-1}$	PCPS (70/30), PC type V-E, bovine brain PS, both from Sigma. FX purified from human plasma. Human brain TF. Human FVIIa. Temperature: 37°C. With and without TF. Measures activation of FX and FIX.
[88]	$K_m = 2.05 \times 10^{-7} M$, $k_{\text{cat}} = 1.17 s^{-1}$	Human brain TF. Human FVII and FX. pH: 7.5. Activation of FX and FIX by: FXIa (FIX only), TF:VIIa (both) and IXa:VIIIa (FX only).
[111]	$K_m = 1.04 \times 10^{-6} M$, $k_{\text{cat}} = 37.5 s^{-1}$	Human FX from plasma. Human FVIIa. TF isolated from human brains. PCPS (75/25) from Sigma using bovine brain PC and hen egg PS. Temperature: 37°C. pH: 7.4.
[29]	$K_m = 4 \times 10^{-7} M$, $k_{\text{cat}} = 2.5 s^{-1}$	PCPS from Avanti Polar Lipids, Alabaster, AL. FVIIa from American Diagnostica, Greenwich, CT. FX from Enzyme Research Laboratories, South Bend, IN. Human TF. Values stated are approximated from graphs.
Chosen values: $K_m = 0.32 \mu M (10 \wedge N(-6.50, 0.58^2), 5\% = 3.51 \times 10^{-8}, 95\% = 2.85 \times 10^{-6})$, $k_{\text{cat}} = 6 s^{-1} (10 \wedge N(0.78, 0.63^2), 5\% = 5.54 \times 10^{-1}, 95\% = 6.55 \times 10^{1})$		

Table E.23: The prior distributions and reaction rates used to inform the prior distributions for the Improved Unified Model for FX activation by TF:VIIa.

X $\overset{VIIa}{\rightarrow}$ Xa		
Citation	Rates	Notes
[49]	$K_m = 2.5 \times 10^{-7} M$, $k_{\text{cat}} = 2.6 \times 10^{-4} s^{-1}$	PCPS (70/30), PC type V-E, bovine brain PS, both from Sigma. FX purified from human plasma. Human FVIIa. Temperature: 37°C. With and without TF. Measures activation of FX and FIX.
[18]	$K_m = 4.87 \times 10^{-6} M$, $k_{\text{cat}} = 3.95 \times 10^{-4} s^{-1}$	TF from Bovine brain thromboplastin. FX purified from bovine plasma. Temperature: 37°C. pH: 7.5. Gives with and without TF. Measured in the presence of benzamidine hydrochloride.
Chosen values: $K_m = 1.1 \mu M (10 \wedge N(-5.96, 0.91^2), 5\% = 3.49 \times 10^{-8}, 95\% = 3.44 \times 10^{-5})$, $k_{\text{cat}} = 3.2 \times 10^{-4} s^{-1} (10 \wedge N(-3.49, 0.13^2), 5\% = 1.98 \times 10^{-4}, 95\% = 5.29 \times 10^{-4})$		

Table E.24: The prior distributions and reaction rates used to inform the prior distributions for the Improved Unified Model for FX activation by FVIIa.

X $\overset{IXa:VIIIa}{\rightarrow}$ Xa		
Citation	Rates	Notes
[12]	$K_m = 6.3 \times 10^{-8} M$, $k_{\text{cat}} = 8.3 s^{-1}$	Bovine FIX, FVIII and FX purified from plasma. 10μM DOPC/DOPSE (75/25). Temperature: 37°C. pH: 7.9. With and without FVIIIa.
[25]	$K_m = 1.9 \times 10^{-7} M$, $k_{\text{cat}} = 29 s^{-1}$	Human FIX, FVIII and FX. 25μM PCPS (75/25). Temperature: 37°C. pH: 7.4. With and without FVIIIa.
[88]	$K_m = 1.4 \times 10^{-7} M$, $k_{\text{cat}} = 0.42 s^{-1}$	Human FIX and FX. pH: 7.5. Activation of FX and FIX by: FXIa (FIX only), TF:VIIa (both) and IXa:VIIIa (FX only).
[91]	$K_m = 1.2 \times 10^{-7} M$, $k_{\text{cat}} = 0.4 s^{-1}$	Human FVIII from Dr. William Thomas, Hyland Diagnostics Div., Travenol Laboratories, Inc., Costa Mesa, CA. Human FIX and FX were purified from factor IX concentrate from Cutter Laboratories, Inc., Berkeley, CA. PCPS, synthetic PS and bovine PC, both from Supelco, Inc., Bellefonte, PA. With and without VIIIa.
[46]	$K_m = 2.26 \times 10^{-8} M$, $k_{\text{cat}} = 1.25 s^{-1}$	Human FIX and FX from Enzyme Research Laboratories, South Bend, IN. FVIII from Baxter Healthcare Corp., Duarte, CA. Temperature: 37°C. pH: 7.4. Measured in the presence of platelets. With and without FVIIIa.
Chosen values: $K_m = 85nM(10 \wedge N(-7.07, 0.37^2), 5\% = 2.10 \times 10^{-8}, 95\% = 3.46 \times 10^{-7}), k_{\text{cat}} = 2.19 s^{-1}(10 \wedge N(0.34, 0.82^2), 5\% = 7.23 \times 10^{-2}, 95\% = 8.80 \times 10^{1})$		

Table E.25: The prior distributions and reaction rates used to inform the prior distributions for the Improved Unified Model for FX activation by IXa:VIIIa.

X $\overset{IXa}{\rightarrow}$ Xa		
Citation	Rates	Notes
[91]	$K_m = 7.6 \times 10^{-7} M$, $k_{\text{cat}} = 6.8 \times 10^{-3} s^{-1}$	Human FIX and FX were purified from factor IX concentrate from Cutter Laboratories, Inc., Berkeley, CA. PCPS, synthetic PS and bovine PC, both from Supelco, Inc., Bellefonte, PA. With and without FVIIIa.
[46]	$K_m = 6.4 \times 10^{-9} M$, $k_{\text{cat}} = 7 \times 10^{-4} s^{-1}$	Human FIX and FX from Enzyme Research Laboratories, South Bend, IN. Temperature: 37°C. pH: 7.4. Measured in the presence of platelets. With and without FVIIIa.
[12]	$K_m = 5.8 \times 10^{-8} M$, $k_{\text{cat}} = 4.1 \times 10^{-5} s^{-1}$	Bovine FIX and FX purified from plasma. 10μM DOPC/DOPSE (75/25). Temperature: 37°C. pH: 7.9. With and without FVIIIa.
[25]	$K_m = 1.4 \times 10^{-7} M$, $k_{\text{cat}} = 8 \times 10^{-4} s^{-1}$	Human FIX, FVIII and FX. 25μM PCPS (75/25). Temperature: 37°C. pH: 7.4. With and without FVIIIa.
Chosen values: $K_m = 80nM(10 \wedge N(-7.10, 0.86^2), 5\% = 3.06 \times 10^{-9}, 95\% = 2.06 \times 10^{-6}), k_{\text{cat}} = 6.3 \times 10^{-4} s^{-1}(10 \wedge N(-3.20, 0.91^2), 5\% = 2.00 \times 10^{-5}, 95\% = 1.98 \times 10^{-2})$		

Table E.26: The prior distributions and reaction rates used to inform the prior distributions for the Improved Unified Model for FX activation by FIXa.

V $\overset{IIa}{\rightarrow}$ Va		
Citation	Rates	Notes
[16]	$K_m = 7.17 \times 10^{-8} M$, $k_{\text{cat}} = 0.23 s^{-1}$	20μM PCPS (75/25), Hen egg PC and bovine brain PS from Sigma. Human FV and FII from fresh frozen plasma. Temperature: 25°C. pH: 7.4. Also does activation by FXa.
[73]	$\frac{k_{\text{cat}}}{K_m} = 3.6 \times 10^6 M^{-1} s^{-1}$	60μM DOPC/DOPS (90/10) from Avanti Polar Lipids, Inc., Pelham, AL. Human FII and FV. Temperature: 37°C. pH: 7.5.
[10]	$\frac{k_{\text{cat}}}{K_m} = 6.4 \times 10^6 M^{-1} s^{-1}$, $\frac{k_{\text{cat}}}{K_m} = 4 \times 10^6 M^{-1} s^{-1}$	Different methods. DOPC/DOPS (75/25) from Avanti Polar Lipids, Inc., Pelham, AL. Human FII and FV purified from plasma. Temperature: 25°C. pH: 7.4. Also gives activation of prothrombin by FXa and Xa:Va.
Chosen values: $K_m = 71.7nM(10 \wedge N(-7.14, 2.5^2), 5\% = 5.59 \times 10^{-12}, 95\% = 9.39 \times 10^{-4}), k_{\text{cat}} = 0.3 s^{-1}(10 \wedge N(-0.53, 0.13^2), 5\% = 1.80 \times 10^{-1}, 95\% = 4.83 \times 10^{-1})^{\ddagger}$		

Table E.27: The prior distributions and reaction rates used to inform the prior distributions for the Improved Unified Model for FV activation by FIIa.

V $\overset{Xa}{\rightarrow}$ Va		
Citation	Rates	Notes
[16]	$K_m = 1.04 \times 10^{-8} M$, $k_{\text{cat}} = 0.043 s^{-1}$	$20\mu M$ 20μM PCPS (75/25), Hen egg PC and bovine brain PS from Sigma. Human FV and FX from fresh frozen plasma. FX activated by RVV. Temperature: 25°C. pH: 7.4. Also does activation by FIIa.
Chosen values: $K_m = 10.4nM(10 \wedge N(-7.98, 2.5^2), 5\% = 8.08 \times 10^{-13}, 95\% = 1.36 \times 10^{-4}), k_{\text{cat}} = 0.043 s^{-1}(10 \wedge N(-1.37, 2.5^2), 5\% = 3.29 \times 10^{-6}, 95\% = 5.53 \times 10^2)$		

Table E.28: The prior distributions and reaction rates used to inform the prior distributions for the Improved Unified Model for FV activation by FXa.

[‡] K_m uses a single source, this K_m is then used to find k_{cat} from the other sources.

Xa + Va ↔ Xa:Va		
Citation	Rates	Notes
[17]	$k_+ > 1 \times 10^9 M^{-1} s^{-1}$	PCPS (75/25), Hen egg PC and bovine brain PS from Sigma. Bovine FV and FX purified from plasma. Temperature: 25°C. pH: 7.4. Binding rates are separated into binding FXa and FVa with PCPS and then rapid binding together. This makes is challenging to include with other sources (which do not consider rates of binding to lipids) so we do not include this source in prior calculations.
[65]	$K_d = 1.04 \times 10^{-9} M$	PCPS (75/25), Hen egg PC and bovine brain PS from Sigma. Human FV and FX purified from plasma. FXa activated by RVV. Gives activation of FII.
[96]	$K_d = 1 \times 10^{-12} M$, $k_+ = 1.6 \times 10^9 M^{-1} s^{-1}$	DOPC/DOPS (80/20) both purchased from Sigma. 60-80nm diameter vesicles (also gives 20-30nm). Bovine FX and FV. FX activated by RVV from Sigma. Temperature: 25°C. pH: 7.5.
[33]	$K_d = 3 \times 10^{-11} M$	Many varying phospholipid concentrations and mix ratios. 10 μM DOPC/DOPS (60/40). Bovine FX and FV. FX activated by RVV. Temperature: 37°C. pH: 7.5.
Chosen values: $K_d = 31.5pM(10 \wedge N(-10.5, 1.51^2), 5\% = 1.04 \times 10^{-13}, 95\% = 9.54 \times 10^{-9}), k_+ = 1.6 \times 10^9 M^{-1} s^{-1} (10 \wedge N(9.20, 2.5^2), 5\% = 1.22 \times 10^5, 95\% = 2.05 \times 10^{13})$ therefore $k_- = 5.04 \times 10^{-2} s^{-1}$		

Table E.29: The prior distributions and reaction rates used to inform the prior distributions for the Improved Unified Model for FXa and FVa association/dissociation.

Xa + AT → Xa:AT		
Citation	Rates	Notes
[21]	$k = 4.5 \times 10^3 M^{-1}s^{-1}$	Human FX purified from plasma. Human AT. Temperature: 25°C. pH: 7.4. Also measures thrombin.
-	$k_+ = 4.2 \times 10^3 M^{-1}s^{-1}$	Used in Danforth and Brummel. No citation given. Value not used for prior distributions.
[71]	$k_+ = 2.3 \times 10^3 M^{-1}s^{-1}$	Human AT was purified from outdated plasma obtained from the Henry Ford Hospital blood bank. Human FX purified from plasma and activated by RVV. Temperature: 25°C. pH: 7.4. Also gives inhibition of thrombin.
[103]	$k_+ = 567 M^{-1}s^{-1}$	$20\mu M$ 20μM DOPC and Bovine brain PS (60/40) and from Sigma. Human FX and AT. FX activated by RVV from Sigma. 37°C. pH: 7.4. Also does in presence of FVa and inhibition by α1-AT.
[23]	$k_+ = 3.13 \times 10^3 M^{-1}s^{-1}$	Rabbit brain thromboplastin from Ortho Diagnostics, Raritan, NJ (used for measuring FXa through FIIa activation). Human FXa, FVa and AT. Also gives FIXa and FIIa. Temperature: 37°C. pH: 7.5.
Chosen values: $k_+ = 2.1 \times 10^3 M^{-1}s^{-1}(10 \wedge N(3.32, 0.39^2), 5\% = 4.66 \times 10^2, 95\% = 9.19 \times 10^3)$		

Table E.30: The prior distributions and reaction rates used to inform the prior distributions for the Improved Unified Model for FXa inhibition by AT.

Xa:Va + AT → Xa:Va:AT		
Citation	Rates	Notes
[103]	$k_+ = 367 M^{-1}s^{-1}$	$20\mu M$ DOPC and Bovine brain PS (60/40) and from Sigma. Human FX and AT. Bovine FV purified from fresh bovine blood. FX activated by RVV from Sigma. Temperature: 37°C. Also does in absence of FVa.
Chosen values: $k_+ = 367 M^{-1}s^{-1}(10 \wedge N(2.56, 2.5^2), 5\% = 2.8 \times 10^{-2}, 95\% = 4.7 \times 10^6)$		

Table E.31: The prior distributions and reaction rates used to inform the prior distributions for the Improved Unified Model for Xa:Va inhibition by AT.

E.3 IIa Module

Model Reactions

This module comprises of the reactions that lead up to FIIa formation, including activation by both Xa and Xa:Va. The reactions used in the models we have examined are given in Table E.32 as well as the reactions that we have chosen for the Unified and Improved Unified Models. The reactions for the previous models and the Unified Model are then demonstrated in Figures E.6 and E.7, respectively. The reactions for the Improved Unified Model are identical to the reactions for the Unified Model for the FIIa module.

We have chosen not to include mIIa in the model as it makes the choices for reaction rates limited, particularly for the second step mIIa $\overset{Xa:Va}{\rightarrow}$ IIa, where as sources which measure II $\overset{Xa:Va}{\rightarrow}$ IIa are much more plentiful.

Models	Reactions
Hockin, Danforth and Chatterjee	$\text{II} + \text{Xa} \rightarrow \text{IIa} + \text{Xa}$ $\text{II} + \text{Xa:Va} \leftrightarrow$ $\text{II:Xa:Va} \rightarrow \text{Xa:Va} + \text{mIIa}$ $\text{Xa:Va} + \text{mIIa} \rightarrow \text{Xa:Va} + \text{IIa}$ $\text{mIIa} + \text{AT} \rightarrow \text{mIIa:AT}$ $\text{IIa} + \text{AT} \rightarrow \text{IIa:AT}$
Brummel	$\text{II} + \text{Xa} \rightarrow \text{IIa} + \text{Xa}$ $\text{II} + \text{Xa:Va} \leftrightarrow \text{II:Xa:Va}$ $\text{II:Xa:Va} \rightarrow \text{Xa:Va} + \text{mIIa}$ $\text{Va} + \text{II} \leftrightarrow \text{Va:II}$ $\text{mIIa} + \text{AT} \rightarrow \text{mIIa:AT}$ $\text{IIa} + \text{AT} \rightarrow \text{IIa:AT}$
Bungay	$\text{II}_L + \text{Xa:Va}_L \leftrightarrow \text{II:Xa:Va}_L$ $\text{II:Xa:Va}_L \rightarrow \text{Xa:Va:mIIa}_L$ $\text{Xa:Va:mIIa}_L \leftrightarrow \text{Xa:Va}_L + \text{mIIa}_L$ $\text{Xa:Va:mIIa}_L \rightarrow \text{Xa:Va}_L + \text{IIa}_f$ $\text{mIIa}_f + \text{AT}_f \rightarrow \text{mIIa:AT}_f$ $\text{IIa}_f + \text{AT}_f \rightarrow \text{IIa:AT}_f$
Tyurin and Zhu	$\text{II} \overset{Xa}{\rightarrow} \text{IIa}$ $\text{II} \overset{Xa:Va}{\rightarrow} \text{IIa}$ $\text{IIa} + \text{AT} \rightarrow \text{IIa:AT}$
Unified	$\text{II} \overset{Xa}{\rightarrow} \text{IIa}$ $\text{II} \overset{Xa:Va}{\rightarrow} \text{IIa}$ $\text{IIa} + \text{AT} \rightarrow \text{IIa:AT}$
Improved Unified	$\text{II} \overset{Xa}{\rightarrow} \text{IIa}$ $\text{II} \overset{Xa:Va}{\rightarrow} \text{IIa}$

IIa + AT → IIa:AT

Table E.32: The reactions that are used in the different models and our choice of reactions for the IIa module.

Network Diagrams

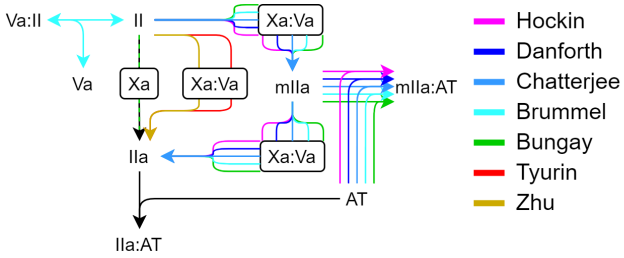

Figure E.6: A network diagram for the IIa module reactions that are included in previous models.

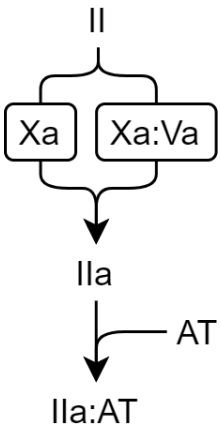

Figure E.7: A reaction diagram for our chosen reactions to be included in the Unified Model and Improved Unified Model for the IIa module.

Reaction rates for previous models

Reaction	Model	Model values	Data values
II $\overset{Xa}{\rightarrow}$ IIa	Hockin, Danforth, Brummel, Chatterjee	$\frac{k_{\text{cat}}}{K_m} = 7.5 \times 10^3 M^{-1}s^{-1}$	[10] gives $K_m = 3 \times 10^{-7}M, k_{\text{cat}} = 2.3 \times 10^{-3}s^{-1}, \frac{k_{\text{cat}}}{K_m} = 7.5 \times 10^3 M^{-1}s^{-1}$.
	Tyurin, Zhu	$K_m = 5.8 \times 10^{-6}M, k_{\text{cat}} = 0.0375s^{-1}$	[34] gives $K_m = 5.8 \times 10^{-6}M, k_{\text{cat}} = 0.0375s^{-1}$.
II $\overset{Xa:Va}{\rightarrow}$ mIIa	Hockin, Danforth, Brummel	$k_+ = 1 \times 10^8 M^{-1}s^{-1}, k_- = 103s^{-1}, k_{\text{cat}} = 63.5s^{-1}$	Used in Jones [8] with a change to the rates. Jones cites three sources, [12]; [7]; [18], as the source of four reaction rates (including the rate relevant to this reaction) however none of these sources concern FII activation. [12] gives FX activation by IXa:VIIIa, [7] gives FIX and FX activation by TF:VIIa and [18] gives FX activation by TF:VIIa as well.
	Bungay	$k_+ = 1 \times 10^8 M^{-1}s^{-1}, k_- = 100s^{-1}, k_{\text{cat}} = 13s^{-1}$	[65] gives $K_m = 6.6 \times 10^{-7}M, k_{\text{cat}} = 15.1s^{-1}$.
	Chatterjee	$k_+ = 1 \times 10^8 M^{-1}s^{-1}, k_- = 2.06s^{-1}, k_{\text{cat}} = 63.5s^{-1}$	Original value multiplied by 0.02 based on: K_m decreases from 34μM to 0.21μM when using 7.5μM phospholipids [34].
mIIa $\overset{Xa:Va}{\rightarrow}$ IIa	Hockin, Danforth, Brummel, Chatterjee	$\frac{k_{\text{cat}}}{K_m} = 1.5 \times 10^7 M^{-1}s^{-1}$	Jones [8], fitted from data in Lawson [19].

	Bungay	$k_+ = 1 \times 10^8 M^{-1}s^{-1}, k_- = 66s^{-1}, k_{\text{cat}} = 15s^{-1}$	[65] gives $K_m = 6.6 \times 10^{-7}M, k_{\text{cat}} = 15.1s^{-1}$.
II $\overset{Xa:Va}{\rightarrow}$ IIa	Tyurin, Zhu	$K_m = 1 \times 10^{-6}M, k_{\text{cat}} = 28.3s^{-1}$	Used in Khanin [93], averaged from [65] which gives $K_m = 1.06 \times 10^{-6}M$, $k_{\text{cat}} = 22.4s^{-1}$ and [92] which gives $K_m = 1 \times 10^{-6}M$, $k_{\text{cat}} = 35s^{-1}$.
IIa + AT $\rightarrow$ IIa:AT	Hockin, Danforth, Brummel, Chatterjee	$7.1 \times 10^3 M^{-1}s^{-1}$	[22] gives $k = 6.2 \times 10^3 M^{-1}s^{-1}$.
	Bungay	$6.83 \times 10^4 M^{-1}s^{-1}$	[72] gives $6.83 \times 10^3 M^{-1}s^{-1}$.
	Tyurin	$7.08 \times 10^3 M^{-1}s^{-1}$	[23] gives $7.08 \times 10^3 M^{-1}s^{-1}$.
	Zhu	$5.83 \times 10^3 M^{-1}s^{-1}$	Used in [93]. Averaged: [23] gives $7.08 \times 10^3 M^{-1}s^{-1}$, [113] gives $2.07 \times 10^3 M^{-1}s^{-1}$.

Table E.33: The parameter values used by each of the models along with the accompanying reference and original data value for each of the reactions in the IIa module.

Choosing Parameters

There are no changes between the Unified Model reaction rates and the Improved Unified Model reaction rates for this module. Below gives the sources and prior distributions for both models.

II $\overset{Xa}{\rightarrow}$ IIa		
Citation	Rates	Notes
[10]	$K_m = 3 \times 10^{-7} M$, $k_{\text{cat}} = 2.3 \times 10^{-3} s^{-1}$	200μM DOPC/DOPS (75/25) from Avanti Polar Lipids Inc., Alabaster, AL. Human Xa was a gift from Hematologic Technologies. Human FII. Temperature: 37°C. pH: 7.4. Gives in presence of FVa and activation of FV by FIIa.
[34]	$K_m = 5.8 \times 10^{-6} M$, $k_{\text{cat}} = 0.0375 s^{-1}$	Bovine FII and FX. FX activated by RVV. 7.5μM DOPC/DOPS. Temperature: 37°C. pH: 7.5. Gives activation in presence of FVa as well.
Chosen values: $K_m = 1.3\mu M (10 \wedge N(-5.88, 0.91^2), 5\% = 4.20 \times 10^{-8}, 95\% = 4.14 \times 10^{-5})$, $k_{\text{cat}} = 9.3 \times 10^{-3} s^{-1} (10 \wedge N(-2.03, 0.86^2), 5\% = 3.59 \times 10^{-4}, 95\% = 2.42 \times 10^{-1})$		

Table E.34: The prior distributions and reaction rates used to inform the prior distributions for both the Unified Model and the Improved Unified Model for FII activation by FXa.

II $\overset{Xa:Va}{\rightarrow}$ IIa		
Citation	Rates	Notes
[10]	$K_m = 1 \times 10^{-6} M$, $k_{\text{cat}} = 63.5 s^{-1}$	200μM DOPC/DOPS (75/25) from Avanti Polar Lipids Inc., Alabaster, AL. Human Xa was a gift from Hematologic Technologies. Human II. Human V from plasma. Temperature: 37°C. pH: 7.4. Gives in presence of FVa and activation of FV by FIIa.
[65]	$K_m = 1.06 \times 10^{-6} M$, $k_{\text{cat}} = 22.4 s^{-1}$	PCPS (75/25) Hen egg PC and bovine brain PS from Sigma. Human FV, FX and FII from plasma. FX activated by RVV. Temperature: 25°C. pH: 7.4.
[92]	$K_m = 1 \times 10^{-6} M$, $k_{\text{cat}} = 35 s^{-1}$	PCPS. Factors X, II and V purified from human plasma. FX activated by RVV. Temperature: 22°C. pH: 7.4.
[34]	$K_m = 2.1 \times 10^{-7} M$, $k_{\text{cat}} = 32 s^{-1}$	Bovine FII and FX. FX activated by RVV. 7.5μM DOPC/DOPS. Temperature: 37°C. pH: 7.5. Gives activation in absence of FVa as well.
Chosen values: $K_m = 0.7\mu M (10 \wedge N(-6.16, 0.34^2), 5\% = 1.91 \times 10^{-7}, 95\% = 2.51 \times 10^{-6}), k_{\text{cat}} = 36 s^{-1} (10 \wedge N(1.55, 0.19^2), 5\% = 1.73 \times 10^{1}, 95\% = 7.29 \times 10^{1})$		

Table E.35: The prior distributions and reaction rates used to inform the prior distributions for both the Unified Model and the Improved Unified Model for FII activation by Xa:Va.

IIa + AT $\rightarrow$ IIa:AT		
Citation	Rates	Notes
[72]	$k_+ = 6.83 \times 10^3 M^{-1} s^{-1}$	PCPS (50/50) from Supelco, Bellafonte, Pa. Human AT and FIIa from plasma. Temperature: 37°C. pH: 7.4.
[23]	$k_+ = 7.08 \times 10^3 M^{-1} s^{-1}$	Human FIIa and AT. Absence of heparin. Also gives FIXa and FXa. Temperature: 37°C. pH: 7.5.
[113]	$k_+ = 4.62 \times 10^3 M^{-1} s^{-1}$	Human FIIa from plasma. Human AT. pH: 7.5. Temperature: 24°C.
[22]	$k_+ = 6.2 \times 10^3 M^{-1} s^{-1}$	PCPS (75/25). Human thrombin and AT. Absence of heparin. Temperature: 37°C. pH: 7.9.
Chosen values: $k_+ = 6.1 \times 10^3 M^{-1} s^{-1} (10 \wedge N(3.79, 0.08^2), 5\% = 4.55 \times 10^3, 95\% = 8.35 \times 10^3)$		

Table E.36: The prior distributions and reaction rates used to inform the prior distributions for both the Unified Model and the Improved Unified Model for FIIa inhibition by AT.

E.4 XIa Module

Model Reactions

This module comprises only the reactions that activate FXI though the TF pathway. The reactions included in previous mathematical models and those in the Unified Model are described in Table E.37 while the former are depicted in Figure E.8 and the latter in Figure E.9. The Improved Unified Model uses identical reactions with different reaction rates.

Models	Reactions
Bungay	$XI_f + IIa_f \leftrightarrow XI{:}IIa_f$ $XI{:}IIa_f \rightarrow XIa_f + IIa_f$
Tyurin	$XI \overset{IIa}{\rightarrow} XIa$ $XI \overset{XIa}{\rightarrow} XIa$ $XIa + AT \rightarrow XIa{:}AT$
Zhu	$XI \rightarrow XIa^{\dagger}$ $XIa + AT \rightarrow XIa{:}AT$
Chatterjee	$XI + IIa \leftrightarrow XI{:}IIa$ $XI{:}IIa \rightarrow XIa + IIa$ $XIa + XI \rightarrow XIa + XIa$ $XIa + AT \rightarrow XIa{:}AT$
Unified	$XI \overset{IIa}{\rightarrow} XIa$ $XI \overset{XIa}{\rightarrow} XIa$ $XIa + AT \rightarrow XIa{:}AT$
Improved Unified	$XI \overset{IIa}{\rightarrow} XIa$ $XI \overset{XIa}{\rightarrow} XIa$ $XIa + AT \rightarrow XIa{:}AT$

Table E.37: The reactions that are used in the different models and our choice of reactions for the XIa module.

[†]This reaction hasn't been analysed as observations of this will be likely down to $XI \overset{XIa}{\rightarrow} XIa$

Network Diagrams

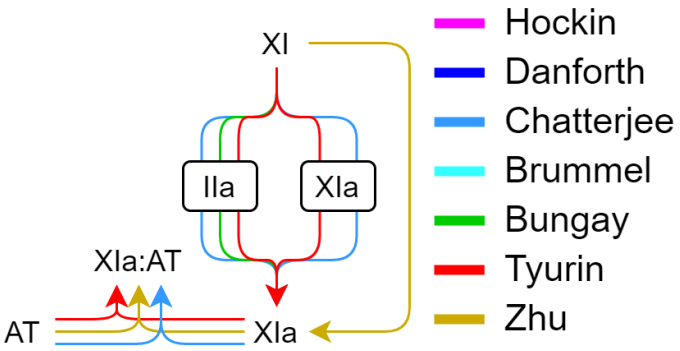

Figure E.8: A network diagram for the XIa module reactions that are included in previous mathematical models.

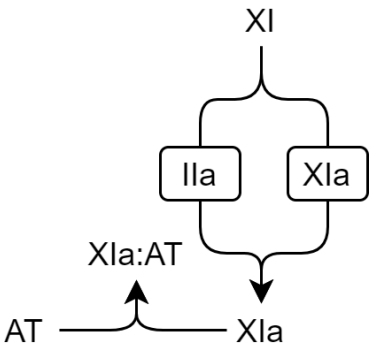

Figure E.9: A reaction diagram for our chosen reactions to be included in the Unified Model and Improved Unified Model for the XIa module.

Reaction rates for previous models

Reaction	Model	Model values	Data values
XI $\overset{IIa}{\rightarrow}$ XIa	Bungay	$k_+ = 1 \times 10^8 M^{-1}s^{-1}, k_- = 10s^{-1}, k_{\text{cat}} = 1.453s^{-1}$	[67] gives $k_{\text{cat}} = 1.43s^{-1}$, retracted in 2007 [68].
	Tyurin	$K_m = 5 \times 10^{-8}M, k_{\text{cat}} = 1.43s^{-1}$	K_m estimated by Tyurin, k_{cat} from [67] which gives $k_{\text{cat}} = 1.43s^{-1}$, retracted in 2007 [68].
	Chatterjee	$k_+ = 1 \times 10^8 M^{-1}s^{-1}, k_- = 5s^{-1}, k_{\text{cat}} = 1.3 \times 10^{-4}s^{-1}$	[42] gives $K_m = 5 \times 10^{-8}M, k_{\text{cat}} = 1.3 \times 10^{-4}s^{-1}$.
XI $\overset{XIa}{\rightarrow}$ XIa	Tyurin	$K_m = 5 \times 10^{-8}M, k_{\text{cat}} = 0.13s^{-1}$	K_m estimated by Tyurin, k_{cat} from [67] which gives $k_{\text{cat}} = 0.13s^{-1}$, retracted in 2007 [68].
	Chatterjee	$k = 3.19 \times 10^6 M^{-1}s^{-1}$	Fitted in [43] but that model doesn't include FIIa activation of FXI, Chatterjee reported that due to this they used a value 4 fold lower however they did not use a scaled value.
XIa + AT $\rightarrow$ XIa:AT	Tyurin	$k = 167M^{-1}s^{-1}$	[104] gives $k = 500M^{-1}s^{-1}$ ($k = 167M^{-1}s^{-1}$ for 23°C).
	Zhu	$k = 167M^{-1}s^{-1}$	[104] gives $k = 500M^{-1}s^{-1}$ ($k = 167M^{-1}s^{-1}$ for 23°C).
	Chatterjee	$k = 320M^{-1}s^{-1}$	[44] gives $k = 320M^{-1}s^{-1}$.

Table E.38: The parameter values used by each of the models along with the accompanying reference and original data value for each of the reactions in the XIa module.

XI $\overset{IIa}{\rightarrow}$ XIa		
Citation	Rates	Notes
[67]	$k_{cat} = 1.43s^{-1}$	Human FIIa from Enzyme Research Laboratories, South Bend, IN. FXI purified from human plasma. Temperature: 37°C. pH: 7.3. Retracted in 2007 [68].
[42]	$K_m = 5 \times 10^{-8}M$, $k_{cat} = 1.3 \times 10^{-4}s^{-1}$	Human FXI and FII from plasma. Temperature: 37°C. pH: 7.5.
Chosen values: $K_m = 50nM(10 \wedge N(-7.30, 2.5^2), 5\% = 3.87 \times 10^{-12}, 95\% = 6.49 \times 10^{-4}), k_{cat} = 1.3 \times 10^{-4}s^{-1}(10 \wedge N(-3.89, 2.5^2), 5\% = 9.94 \times 10^{-9}, 95\% = 1.67)$		

Table E.39: The prior distributions and reaction rates used to inform the prior distributions for the Unified Model for FXI activation by FIIa.

XI $\overset{XIa}{\rightarrow}$ XIa		
Citation	Rates	Notes
[67]	$k_{cat} = 0.13s^{-1}$	Human FXIa from Hematologic Technologies Inc., Essex Junction, VT. FXI purified from human plasma. Temperature: 37°C. pH: 7.3. Retracted in 2007 [68].
[43]	$k = 3.19 \times 10^6 M^{-1}s^{-1}$	Model fitted. Not biological measurement. Fitted without modelling FIIa activation of FXI.
Chosen values: $K_m = 50nM(10 \wedge N(-7.30, 2.5^2), 5\% = 3.87 \times 10^{-12}, 95\% = 6.49 \times 10^{-4}), k_{cat} = 1.3 \times 10^{-4}s^{-1}(10 \wedge N(-3.89, 2.5^2), 5\% = 9.94 \times 10^{-9}, 95\% = 1.67)$. Values assumed to be same as IIa		

Table E.40: The prior distributions and reaction rates used to inform the prior distributions for the Unified Model for FXI activation by FXIa.

XIa + AT → XIa:AT		
Citation	Rates	Notes
[104]	$k = 500M^{-1}s^{-1}$	AT purchased from Kabi (AB), Stockholm, Sweden. FXI from human plasma. Temperature: 37°C.
[44]	$k = 320M^{-1}s^{-1}$	Purified human FXIa was obtained from Kordia Laboratory Supplies, Leiden, The Netherlands. Human AT from Calbiochem. Temperature: 37°C. pH: 7.4. Also gives in presence of dextran sulfate, heparin, heparan sulfate, dermatan sulfate.
Chosen values: $k_+ = 400s^{-1}(10 \wedge N(2.60, 0.14^2), 5\% = 2.34 \times 10^2, 95\% = 6.77 \times 10^2)$		

Table E.41: The prior distributions and reaction rates used to inform the prior distributions for the Unified Model for FXIa inhibition by AT.

Improved Unified Model - Choosing Parameters

Sources for FXI activation are clearly very limited with two reactions using a retracted source and one reaction using a model fitting for the reaction rate. It has also been demonstrated that this reaction is very surface dependent [42]. Due to this we have tried to use other sources to estimate the reaction rates for our specific phospholipid composition*.

Utilising values from [120] we infer a rate for FIIa activation of FXI of $\frac{k_{\text{cat}}}{K_m} = 1136M^{-1}s^{-1}$ for 4μM PCPS (with 28.5% PS) using linear interpolation for 4μM 50:50 PCPS and the ratio of 50% PS to 28.5% PS (estimated by linear interpolation) for 50μM of PCPS. The $K_m = 50nM$ is used from [42] to estimate $k_{\text{cat}} = 5.68 \times 10^{-5}s^{-1}$.

To estimate the rates for FXI autoactivation we have used values from [121]. We use linear interpolation to estimate the rate for 4μM of polyphosphate at lengths of 70mer at $\frac{k_{\text{cat}}}{K_m} = 1.89 \times 10^5 M^{-1}s^{-1}$. The ratio of 33% between 1μM of polyphosphate and 4μM of polyphosphate (using lengths of 65mer) to estimate the rate for 1μM of polyphosphate at lengths of 70mer. This was then scaled using the ratio for 1μM of 70mer polyphosphate and 4μM PCPS (28.5% PS) for activation by FIIa given in [120] (ratio is 4.97%). This gives us our estimate of FXI autoactivation for 4μM PCPS (28.5% PS) of $\frac{k_{\text{cat}}}{K_m} = 3065M^{-1}s^{-1}$. Using the same K_m as for activation by FIIa [42] gives us $K_m = 50nM, k_{\text{cat}} = 1.53 \times 10^{-4}s^{-1}$.

*The phospholipid composition in our assay is: 24.7% phosphatidylcholine, 38.9% phosphatidylethanolamine, 28.5% phosphatidylserine, 5.7% phosphatidylinositol, 2.2% sphingomyelin.

XIa + AT → XIa:AT		
Citation	Rates	Notes
[104]	$k = 500M^{-1}s^{-1}$	AT purchased from Kabi (AB), Stockholm, Sweden. FXI from human plasma. Temperature: 37°C.
[44]	$k = 320M^{-1}s^{-1}$	Purified human FXIa was obtained from Kordia Laboratory Supplies, Leiden, The Netherlands. Human AT from Calbiochem. Temperature: 37°C. pH: 7.4. Also gives in presence of dextran sulfate, heparin, heparan sulfate, dermatan sulfate.
Chosen values: $k_+ = 400s^{-1}(10 \wedge N(2.60, 0.14^2), 5\% = 2.34 \times 10^2, 95\% = 6.77 \times 10^2)$		

Table E.42: The prior distributions and reaction rates used to inform the prior distributions for the Improved Unified Model for FXIa inhibition by AT.

E.5 IXa:VIIIa Module

Model Reactions

This module comprises of the reactions that lead up to IXa:VIIIa formation including activation of both FIXa and FVIIIa and binding/unbinding to form IXa:VIIIa. The reactions used in the models we have examined are given in Table E.43 as well as the reactions that we have chosen for the Unified and Improved Unified Models. The reactions for the previous models, the Unified Model and the Improved Unified Model are then demonstrated in Figures E.10, E.11, and E.12, respectively.

Models	Reactions
Hockin, Danforth and Brummel	TF:VIIa + IX ↔ TF:VIIa:IX TF:VIIa:IX → TF:VIIa + IXa IIa + VIII → IIa + VIIIa VIIIa ↔ VIIIa1L + VIIIa2 IXa:VIIIa:X → VIIIa1L + VIIIa2 + IXa + X IXa:VIIIa → VIIIa1L + VIIIa2 + IXa IXa + VIIIa ↔ IXa:VIIIa IXa + AT → IXa:AT
Bungay	$TF{:}VIIa_L + IX_L \leftrightarrow TF{:}VIIa{:}IX_L$ $TF{:}VIIa{:}IX_L \rightarrow TF{:}VIIa_L + IXa_L$ $XIa_f + IX_L \leftrightarrow XIa{:}IX_L$ $XIa{:}IX_L \rightarrow XIa_f + IXa_L$ $VIII_L + IIa_f \leftrightarrow VIII{:}IIa_L$ $VIII{:}IIa_L \rightarrow VIIIa_L + IIa_f$ $VIII_L + Xa_L \leftrightarrow VIII{:}Xa_L$ $VIII{:}Xa_L \rightarrow VIIIa_L + Xa_L$

	$VIII_L + mIIa_L \leftrightarrow VIII{:}mIIa_L$
	$VIII{:}mIIa_L \rightarrow VIIIa_L + mIIa_L$
	$IXa_L + VIIIa_L \leftrightarrow IXa{:}VIIIa_L$
	$IXa_f + AT_f \rightarrow IXa{:}AT_f$
Tyurin	$IX \xrightarrow{TF:VIIa} IXa$
	$IX \xrightarrow{VIIa} IXa$
	$IX \xrightarrow{XIa} IXa$
	$VIII \xrightarrow{IIa} VIIIa$
	$IXa + VIIIa \rightarrow IXa{:}VIIIa$
	$IXa + AT \rightarrow IXa{:}AT$
	$IXa{:}VIIIa + AT \rightarrow IXa{:}AT + VIIIa$
Zhu	$IX \xrightarrow{TF:VIIa} IXa$
	$IX \xrightarrow{XIa} IXa$
	$VIII \xrightarrow{IIa} VIIIa$
	$IXa + VIIIa \rightarrow IXa{:}VIIIa$
	$IXa + AT \rightarrow IXa{:}AT$
Chatterjee	$TF{:}VIIa + IX \leftrightarrow TF{:}VIIa{:}IX$
	$TF{:}VIIa{:}IX \rightarrow TF{:}VIIa + IXa$
	$XIa + IX \leftrightarrow XIa{:}IX$
	$XIa{:}IX \rightarrow XIa + IXa$
	$VIIa + IX \leftrightarrow VIIa{:}IX$
	$VIIa{:}IX \rightarrow VIIa + IXa$
	$IIa + VIII \rightarrow IIa + VIIIa$
	$VIIIa \leftrightarrow VIIIa1L + VIIIa2$
	$IXa{:}VIIIa{:}X \rightarrow VIIIa1L + VIIIa2 + IXa + X$
	$IXa{:}VIIIa \rightarrow VIIIa1L + VIIIa2 + IXa$
	$Xa + VIII \leftrightarrow Xa{:}VIII$
	$Xa{:}VIII \rightarrow Xa + VIIIa$
	$IXa + VIIIa \leftrightarrow IXa{:}VIIIa$
	$IXa + AT \rightarrow IXa{:}AT$
Unified	$IX \xrightarrow{TF:VIIa} IXa$
	$IX \xrightarrow{VIIa} IXa$
	$IX \xrightarrow{XIa} IXa$
	$VIII \xrightarrow{IIa} VIIIa$
	$VIII \xrightarrow{Xa} VIIIa$
	$IXa + VIIIa \leftrightarrow IXa{:}VIIIa$
	$IXa + AT \rightarrow IXa{:}AT$
	$IXa{:}VIIIa + AT \rightarrow IXa{:}AT + VIIIa$
Improved Unified	$IX \xrightarrow{TF:VIIa} IXa$
	$IX \xrightarrow{VIIa} IXa$
	$IX \xrightarrow{XIa} IXa$
	$VIII \xrightarrow{IIa} VIIIa$

$$\begin{gathered}
\text{VIII} \xrightarrow{Xa} \text{VIIIa} \\
\text{VIIIa} \leftrightarrow \text{VIIIa}_1\text{L} + \text{VIIIa}_2 \\
\text{IXa:VIIIa} \leftrightarrow \text{IXa} + \text{VIIIa}_1\text{L} + \text{VIIIa}_2 \\
\text{IXa} + \text{VIIIa} \leftrightarrow \text{IXa:VIIIa} \\
\text{IXa} + \text{AT} \rightarrow \text{IXa:AT} \\
\text{IXa:VIIIa} + \text{AT} \rightarrow \text{IXa:VIIIa:AT}
\end{gathered}$$

Table E.43: The reactions that are used in the different models and our choice of reactions for the IXa:VIIIa module.

Network Diagrams

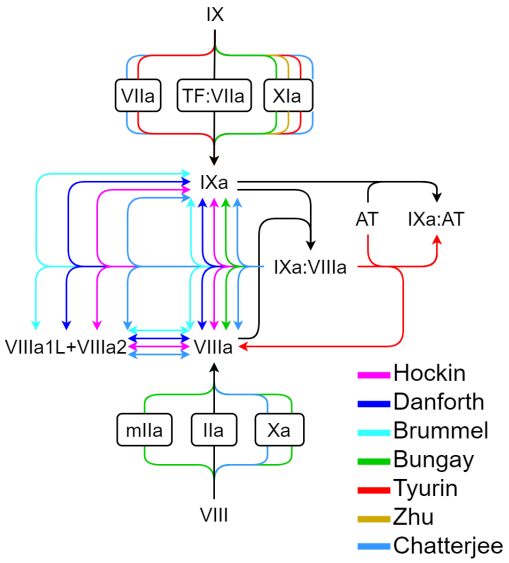

Figure E.10: A network diagram for the IXa:VIIIa module reactions that are included in previous models.

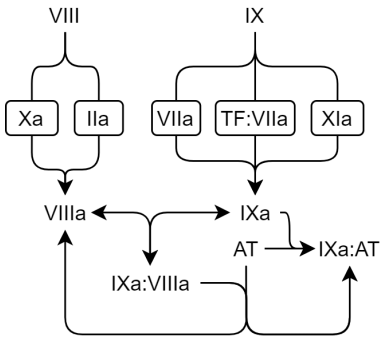

Figure E.11: A reaction diagram for our chosen reactions in the Unified Model for the IXa:VIIIa module.

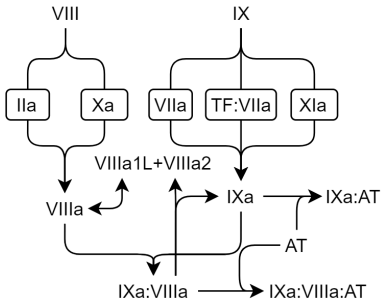

Figure E.12: A reaction diagram for our chosen reactions in the Improved Unified Model for the IXa:VIIIa module.

Reaction rates for previous models

Reaction	Model	Model values	Data values
IX $\overset{TF:VIIa}{\rightarrow}$ IXa	Hockin, Danforth, Brummel, Chatterjee	$k_+ = 1 \times 10^7 M^{-1}s^{-1}, k_- = 2.45s^{-1}, k_{\text{cat}} = 1.8s^{-1}$	[7] gives $K_m = 2.43 \times 10^{-7}M, k_{\text{cat}} = 0.34s^{-1}$, changed by Hockin based on [9] ratios for FX and FIX activation by TF:VIIa.
	Bungay	$k_+ = 1 \times 10^7 M^{-1}s^{-1}, k_- = 2.09s^{-1}, k_{\text{cat}} = 0.34s^{-1}$	[7] gives $K_m = 2.43 \times 10^{-7}M, k_{\text{cat}} = 0.34s^{-1}$.
	Tyurin	$K_m = 1 \times 10^{-7}M, k_{\text{cat}} = 0.7s^{-1}$	Averaged: [49] (mixed data) gives $K_m = 8.2 \times 10^{-8}M, k_{\text{cat}} = 1.8s^{-1}$, [64] gives $K_m = 5.5 \times 10^{-8}M, k_{\text{cat}} = 1.35s^{-1}$ (uses FX not FIX), [88] gives $K_m = 2.1 \times 10^{-7}M, k_{\text{cat}} = 0.25s^{-1}$, [87] gives $K_m = 7 \times 10^{-8}M, k_{\text{cat}} = 0.4s^{-1}$ (cited from [7]).
	Zhu	$K_m = 1.33 \times 10^{-7}M, k_{\text{cat}} = 0.57s^{-1}$	[34] incorrectly cited. Values used appear to be from [93] which uses multiple sources: [49] (mixed data) gives $K_m = 8.2 \times 10^{-8}M, k_{\text{cat}} = 1.8s^{-1}$, [88] gives $K_m = 2.1 \times 10^{-7}M, k_{\text{cat}} = 0.25s^{-1}$, [64] gives $K_m = 5.5 \times 10^{-8}M, k_{\text{cat}} = 1.35s^{-1}$ (uses FX not FIX), [87] gives $K_m = 7 \times 10^{-8}M, k_{\text{cat}} = 0.4s^{-1}$ (cited from [7]).
IX $\overset{VIIa}{\rightarrow}$ IXa	Tyurin	$K_m = 9 \times 10^{-9}M, k_{\text{cat}} = 1.8 \times 10^{-4}s^{-1}$	[49] gives $K_m = 9 \times 10^{-9}M, k_{\text{cat}} = 3.67 \times 10^{-5}s^{-1}$.

	Chatterjee	$k_+ = 1 \times 10^8 M^{-1}s^{-1}, k_- = 0.9s^{-1}, k_{\text{cat}} = 3.6 \times 10^{-5}s^{-1}$	[49] gives $K_m = 9 \times 10^{-9}M, k_{\text{cat}} = 3.67 \times 10^{-5}s^{-1}$.
IX $\overset{XIa}{\rightarrow}$ IXa	Bungay	$k_+ = 1 \times 10^7 M^{-1}s^{-1}, k_- = 1.4517s^{-1}, k_{\text{cat}} = 0.183s^{-1}$	[77] gives $K_m = 1.6 \times 10^{-7}M, k_{\text{cat}} = 0.183s^{-1}$.
	Tyurin	$K_m = 3.55 \times 10^{-7}M, k_{\text{cat}} = 1.25s^{-1}$	Averaged: [87] gives $K_m = 2 \times 10^{-6}M, k_{\text{cat}} = 0.173s^{-1}$, [88] gives $K_m = 3.1 \times 10^{-7}M, k_{\text{cat}} = 0.417s^{-1}$, [89] gives $K_m = 3.7 \times 10^{-7}M, k_{\text{cat}} = 0.66s^{-1}$, [90] gives $K_m = 3 \times 10^{-7}M, k_{\text{cat}} = 2.4s^{-1}$, [45] gives $K_m = 4.9 \times 10^{-7}M, k_{\text{cat}} = 7.7s^{-1}$.
	Zhu	$K_m = 3.5 \times 10^{-7}M, k_{\text{cat}} = 3.75s^{-1}$	Averaged: [87] gives $K_m = 2 \times 10^{-6}M, k_{\text{cat}} = 0.173s^{-1}$, [88] gives $K_m = 3.1 \times 10^{-7}M, k_{\text{cat}} = 0.417s^{-1}$, [89] gives $K_m = 3.7 \times 10^{-7}M, k_{\text{cat}} = 0.66s^{-1}$, [90] gives $K_m = 3 \times 10^{-7}M, k_{\text{cat}} = 2.4s^{-1}$, [45] gives $K_m = 4.9 \times 10^{-7}M, k_{\text{cat}} = 7.7s^{-1}$, [110] says k_{cat} increases in the presence of phospholipids.
	Chatterjee	$k_+ = 1 \times 10^8 M^{-1}s^{-1}, k_- = 41s^{-1}, k_{\text{cat}} = 7.7s^{-1}$	[45] gives $K_m = 4.9 \times 10^{-7}M, k_{\text{cat}} = 7.7s^{-1}$.
VIII $\overset{IIa}{\rightarrow}$ VIIIa	Hockin, Danforth, Brummel, Chatterjee	$\frac{k_{\text{cat}}}{K_m} = 2 \times 10^7 M^{-1}s^{-1}$	Assumed to be same as FIIa activation of FV.

	Bungay	$k_+ = 1 \times 10^8 M^{-1}s^{-1}, k_- = 13.8s^{-1}, k_{\text{cat}} = 0.9s^{-1}$	[66] gives multiple values around $K_m = 2\times10^{-7}M, k_{\text{cat}} = 1s^{-1}$ for different types of FVIII.
	Tyurin	$K_m = 2 \times 10^{-8}M, k_{\text{cat}} = 0.36s^{-1}$	[66] gives multiple values around $K_m = 2\times10^{-7}M, k_{\text{cat}} = 1s^{-1}$ for FVIII cleavage at different positions.
	Zhu	$K_m = 2\times10^{-8}M, k_{\text{cat}} = 1s^{-1}$	[66] gives multiple values around $K_m = 2\times10^{-7}M, k_{\text{cat}} = 1s^{-1}$ for FVIII cleavage at different positions (Zhu used average).
VIII $\overset{mIIa}{\rightarrow}$ VIIIa	Bungay	$k_+ = 1 \times 10^8 M^{-1}s^{-1}, k_- = 13.8s^{-1}, k_{\text{cat}} = 0.9s^{-1}$	Assumed same as FIIa.
VIII $\overset{Xa}{\rightarrow}$ VIIIa	Bungay	$k_+ = 1 \times 10^8 M^{-1}s^{-1}, k_- = 2.1s^{-1}, k_{\text{cat}} = 0.023s^{-1}$	[47] gives $\frac{k_{\text{cat}}}{K_m} = 1.1 \times 10^{-6}M^{-1}s^{-1}$.
	Chatterjee	$k_+ = 1 \times 10^8 M^{-1}s^{-1}, k_- = 2.1s^{-1}, k_{\text{cat}} = 0.023s^{-1}$	Rate constants from [48] (model uses $k_+ = 1 \times 10^8 M^{-1}s^{-1}, k_- = 2.1s^{-1}, k_{\text{cat}} = 0.023s^{-1}$) which use catalytic efficiencies from [47] (gives $\frac{k_{\text{cat}}}{K_m} = 1.1\times10^{-6}M^{-1}s^{-1}$) and based on ratios between FV and FVIII activation by Xa.
VIIIa $\leftrightarrow$ VIIIa1L + VIIIa2	Hockin, Danforth, Brummel	$k_+ = 6 \times 10^{-3}s^{-1}, k_- = 2.2 \times 10^4 M^{-1}s^{-1}$	[13] gives $k_+ = 5.85\times10^{-3}s^{-1}, K_d = 2.73\times10^{-7}M$, [14] gives $K_d = 2.58 \times 10^{-7}M$.

	Chatterjee	$k_+ = 6\times10^{-5}s^{-1}, k_- = 2.2\times 10^4 M^{-1}s^{-1}$	Hockin scaled by 0.01 based on: K_d of 260nM in the absence of phospholipids [14], this reaction is stabilised in the presence of phospholipids [32].
IXa:VIIIa $\rightarrow$ VIIIa1L + VIIIa2 + IXa	Hockin, Danforth, Brummel, Chatterjee	$1 \times 10^{-3}s^{-1}$	[15] gives $k = 1.4 \times 10^{-3}M^{-1}s^{-1}$.
IXa + VIIIa $\leftrightarrow$ IXa:VIIIa	Hockin, Danforth, Brummel	$k_+ = 1 \times 10^7 M^{-1}s^{-1}, k_- = 5 \times 10^{-3}s^{-1}$	[11] gives $K_d = 2 \times 10^{-9}M$ adjusted based on analogy to Xa:Va for k_+.
	Chatterjee	$k_+ = 1 \times 10^7 M^{-1}s^{-1}, k_- = 1 \times 10^{-4}s^{-1}$	Hockin scaled by 0.02 based on: K_d decreases from 351nM to 4nM on PCPS vesicles [30], a K_d of 74pM was found on activated platelet surfaces compared to 550pM on equimolar PSPC vesicles [31].
	Bungay	$k_+ = 1 \times 10^8 M^{-1}s^{-1}, k_- = 0.2s^{-1}$	[11] gives $K_d = 2 \times 10^{-9}M$.
	Tyurin	$k_+ 1.67 \times 10^{-8}M^{-1}s^{-1}$	Fitted from data in [65].
	Zhu	$k_+ 1.67 \times 10^{-8}M^{-1}s^{-1}$	Estimated in [93].
IXa + AT $\rightarrow$ IXa:AT	Hockin, Danforth, Brummel, Chatterjee	$4.9 \times 10^2 M^{-1}s^{-1}$	[21] incorrect citation. Likely used [23] which gives $k = 490M^{-1}s^{-1}$.
	Bungay	$4.9 \times 10^2 M^{-1}s^{-1}$	
	Tyurin	$4.9 \times 10^2 M^{-1}s^{-1}$	[23] gives $k = 490M^{-1}s^{-1}$.

	Zhu	$4.9 \times 10^2 M^{-1}s^{-1}$	
IXa:VIIIa + AT $\rightarrow$ IXa:AT + VIIIa	Tyurin	$500 M^{-1}s^{-1}$	[23] gives $k = 490 M^{-1}s^{-1}$.

Table E.44: The parameter values used by each of the models along with the accompanying reference and original data value for each of the reactions in the IXa:VIIIa module.

IX $\overset{TF:VIIa}{\rightarrow}$ IXa		
Citation	Rates	Notes
[7]	$K_m = 2.43 \times 10^{-7} M$, $k_{\text{cat}} = 0.34 s^{-1}$	Bovine FVIIa and FIX from plasma. 40% brain thromboplastin by volume extracted from bovine brain acetone powder. Mixed brain phospholipids. Temperature: 37°C. pH: 7.5.
[49]	$K_m = 8.2 \times 10^{-8} M$, $k_{\text{cat}} = 1.8 s^{-1}$	(mixed data) 300pM recombinant TF relipidated with PCPS (70/30) using Bovine brain PS and PC (type V-E) from Sigma. Human factor IX from plasma. Recombinant human factor VIIa. Temperature: 37°C. Without TF also given.
[88]	$K_m = 2.1 \times 10^{-7} M$, $k_{\text{cat}} = 0.25 s^{-1}$	Human brain TF. Human FVII and FIX. pH: 7.5. Activation of FX and FIX by FXIa (FIX only), TF:VIIa (both) and IXa:VIIIa (FX only).
Chosen values: $K_m = 0.16 \mu M (10 \wedge N(-6.79, 0.26^2), 5\% = 6.06 \times 10^{-8}, 95\% = 4.34 \times 10^{-7})$, $k_{\text{cat}} = 0.54 s^{-1} (10 \wedge N(-0.27, 0.46^2), 5\% = 9.40 \times 10^{-2}, 95\% = 3.07)$		

Table E.45: The prior distributions and reaction rates used to inform the prior distributions for the Unified Model for FIX activation by TF:VIIa.

IX $\overset{VIIa}{\rightarrow}$ IXa		
Citation	Rates	Notes
[49]	$K_m = 9 \times 10^{-9} M$, $k_{\text{cat}} = 3.67 \times 10^{-5} s^{-1}$	$1.4 \mu M$ PCPS (70/30) using Bovine brain PS and PC (type V-E) from Sigma. Human factor IX from plasma. Recombinant human factor VIIa. Temperature: 37°C. With TF also given. Other phospholipid concentrations given.
Chosen values: $K_m = 9 nM (10 \wedge N(-8.05, 2.5^2), 5\% = 6.88 \times 10^{-13}, 95\% = 1.15 \times 10^{-4})$, $k_{\text{cat}} = 3.67 \times 10^{-5} s^{-1} (10 \wedge N(-4.44, 2.5^2), 5\% = 2.80 \times 10^{-9}, 95\% = 0.47)$		

Table E.46: The prior distributions and reaction rates used to inform the prior distributions for the Unified Model for FIX activation by FVIIa.

IX $\overset{XIa}{\rightarrow}$ IXa		
Citation	Rates	Notes
[77]	$K_m = 1.6 \times 10^{-7} M$, $k_{\text{cat}} = 0.183 s^{-1}$	Factor XI from plasma. Purified factor IX was purchased from Enzyme Research Laboratories, South Bend, IN. Temperature: 37°C.
[87]	$K_m = 2 \times 10^{-6} M$, $k_{\text{cat}} = 0.173 s^{-1}$	Human factors IX and XI from plasma. Temperature: 37°C. pH: 7.5.
[88]	$K_m = 3.1 \times 10^{-7} M$, $k_{\text{cat}} = 0.417 s^{-1}$	Human FXI and FIX. pH: 7.5. Activation of FX and FIX by FXIa (FIX only), TF:VIIa (both) and IXa:VIIIa (FX only).
[89]	$K_m = 3.7 \times 10^{-7} M$, $k_{\text{cat}} = 0.66 s^{-1}$	Human factor XI from plasma activated by bovine FXIIa. Human FIX from plasma. Temperature: 37°C. pH: 7.4.
[90]	$K_m = 3 \times 10^{-7} M$, $k_{\text{cat}} = 2.4 s^{-1}$	PCPS (60/40). Human factors IX and XI. Temperature: 37°C. pH: 7.5.
[45]	$K_m = 4.9 \times 10^{-7} M$, $k_{\text{cat}} = 7.7 s^{-1}$	Human FXI purified from plasma activated by bovine FXIIa. Human factor IX. Temperature: 37°C. pH: 7.5.
Chosen values: $K_m = 0.42 \mu M (10 \wedge N(-6.38, 0.37^2), 5\% = 1.03 \times 10^{-7}, 95\% = 1.69 \times 10^{-6}), k_{\text{cat}} = 0.74 s^{-1} (10 \wedge N(-0.13, 0.65^2), 5\% = 6.32 \times 10^{-2}, 95\% = 8.69)$		

Table E.47: The prior distributions and reaction rates used to inform the prior distributions for the Unified Model for FIX activation by FXIa.

VIII $\overset{IIa}{\rightarrow}$ VIIIa		
Citation	Rates	Notes
[66]	Multiple values around $K_m = 2 \times 10^{-7} M$, $k_{\text{cat}} = 1 s^{-1}$	PCPS (75/25). Porcine factor VIII from plasma. Porcine FIIa. Room temperature. pH: 7.
[47]	$\frac{k_{\text{cat}}}{K_m} = 5 \times 10^6 M^{-1} s^{-1}$	PCPS (25/75) PC (type III-E) and PS purchased from Sigma. Porcine FVIII and FIIa. Temperature: 22°C. pH: 7.4. Also gives activation by FXa.
Chosen values: $K_m = 0.2 \mu M (10 \wedge N(-6.70, 2.5^2), 5\% = 1.54 \times 10^{-11}, 95\% = 2.59 \times 10^{-3}), k_{\text{cat}} = 1 s^{-1} (10 \wedge N(0, 0.5^2), 5\% = 0.105, 95\% = 6.65)$		

Table E.48: The prior distributions and reaction rates used to inform the prior distributions for the Unified Model for FVIII activation by FIIa.

VIII $\overset{Xa}{\rightarrow}$ VIIIa		
Citation	Rates	Notes
[47]	$\frac{k_{\text{cat}}}{K_m} = 1.1 \times 10^6 M^{-1} s^{-1}$	PCPS (25/75) PC (type III-E) and PS purchased from Sigma. Porcine FVIII and FXa. Temperature: 22°C. pH: 7.4. Also gives activation by FIIa.
Chosen values: $K_m = 0.2\mu M(10 \wedge N(-6.70, 2.5^2), 5\% = 1.54 \times 10^{-11}, 95\% = 2.59 \times 10^{-3}), k_{\text{cat}} = 0.22 s^{-1}(10 \wedge N(-0.66, 2.5^2), 5\% = 1.69 \times 10^{-5}, 95\% = 2.83 \times 10^3)$. K_m assumed same as for FIIa		

Table E.49: The prior distributions and reaction rates used to inform the prior distributions for the Unified Model for FVIII activation by FXa.

IXa + VIIIa $\leftrightarrow$ IXa:VIIIa		
Citation	Rates	Notes
[11]	$K_d = 2 \times 10^{-9} M$	PCPS (75/25) from PC and PS purchased from Sigma. Porcine FIXa and FVIIIa. Temperature: 25°C. pH: 7.4.
[30]	$K_d = 4 \times 10^{-9} M$	PCPSPE (40/20/40) from Sigma. Recombinant factor VIII gift of the Bayer Corporation. Factor IX from Enzyme Research Laboratories.
[31]	$K_d = 5.5 \times 10^{-10} M$	PCPS (50/50) using synthetic PC and PS purchased from Supelco Inc, Bellefonte, PA. Human FIXa. Human FVIIIa from plasma. Temperature: 37°C. pH: 7.4.
Chosen values: $K_d = 1.6nM(10 \wedge N(-8, 79, 0.44^2), 5\% = 3.06 \times 10^{-10}, 95\% = 8.59 \times 10^{-9}), k_+ = 1 \times 10^7 M^{-1} s^{-1}(10 \wedge N(7, 2.5^2), 5\% = 7.72 \times 10^2, 95\% = 1.30 \times 10^{11})$ therefore $k_- = 0.016 s^{-1}$		

Table E.50: The prior distributions and reaction rates used to inform the prior distributions for the Unified Model for FIXa and FVIIIa association/dissociation.

IXa + AT → IXa:AT		
Citation	Rates	Notes
[23]	$k = 490M^{-1}s^{-1}$	Human FIXa, FVIIIa and AT. Absence of heparin ($k = 5 \times 10^6 M^{-1}s^{-1}$ in presence of heparin). Measured in presence of FVIIIa. Also gives FIIa and FXa. Temperature: 37°C. pH: 7.5.
Chosen values: $k_+ = 490M^{-1}s^{-1}(10 \wedge N(2.69, 2.5^2), 5\% = 3.78 \times 10^{-2}, 95\% = 6.35 \times 10^6)$		

Table E.51: The prior distributions and reaction rates used to inform the prior distributions for the Unified Model for FIXa inhibition by AT.

IXa:VIIIa + AT → IXa:AT + VIIIa		
Citation	Rates	Notes
[23]	$k = 490M^{-1}s^{-1}$	Human FIXa, FVIIIa and AT. Absence of heparin ($k = 5 \times 10^6 M^{-1}s^{-1}$ in presence of heparin). Measured in presence of FVIIIa. Also gives FIIa and FXa. Temperature: 37°C. pH: 7.5.
Chosen values: $k_+ = 490M^{-1}s^{-1}(10 \wedge N(2.69, 2.5^2), 5\% = 3.78 \times 10^{-2}, 95\% = 6.35 \times 10^6)$		

Table E.52: The prior distributions and reaction rates used to inform the prior distributions for the Unified Model for IXa:VIIIa inhibition by AT.

Improved Unified Model - Choosing Parameters

Following the changes made for the Improved Unified Model, this section outlines the updated reaction rate sources and prior distributions with minor changes made to the notes on each source.

IX $\overset{TF:VIIa}{\rightarrow}$ IXa		
Citation	Rates	Notes
[7]	$K_m = 2.43 \times 10^{-7} M$, $k_{\text{cat}} = 0.34 s^{-1}$	Bovine FVIIa and FIX from plasma. TF from bovine brain thromboplastin. Mixed brain phospholipids. Temperature: 37°C. pH: 7.5.
[49]	$K_m = 3.2 \times 10^{-8} M$, $k_{\text{cat}} = 0.92 s^{-1}$	PCPS (70/30), PC type V-E, bovine brain PS, both from Sigma. Human factor IX from plasma. Human FVIIa. Human TF. Temperature: 37°C. Without TF also given.
[88]	$K_m = 2.1 \times 10^{-7} M$, $k_{\text{cat}} = 0.25 s^{-1}$	Human brain TF. Human FVII and FIX. pH: 7.5. Activation of FX and FIX by: FXIa (FIX only), TF:VIIa (both) and IXa:VIIIa (FX only).
Chosen values: $K_m = 117nM(10 \wedge N(-6.93, 0.49^2), 5\% = 1.83 \times 10^{-8}, 95\% = 7.56 \times 10^{-7}), k_{\text{cat}} = 0.43 s^{-1}(10 \wedge N(-0.37, 0.30^2), 5\% = 1.39 \times 10^{-1}, 95\% = 1.31)$		

Table E.53: The prior distributions and reaction rates used to inform the prior distributions for the Improved Unified Model for FIX activation by TF:VIIa.

IX $\overset{VIIa}{\rightarrow}$ IXa		
Citation	Rates	Notes
[49]	$K_m = 8 \times 10^{-9} M$, $k_{\text{cat}} = 1.62 \times 10^{-4} s^{-1}$	21μM PCPS (70/30) using Bovine brain PS and PC (type VE) from Sigma. Human factor IX from plasma. Recombinant human factor VIIa. Temperature: 37°C. With TF also given.
Chosen values: $K_m = 8nM(10 \wedge N(-8.10, 2.5^2), 5\% = 6.17 \times 10^{-13}, 95\% = 1.04 \times 10^{-4}), k_{\text{cat}} = 1.62 \times 10^{-4} s^{-1}(10 \wedge N(-3.79, 2.5^2), 5\% = 1.25 \times 10^{-8}, 95\% = 2.10)$		

Table E.54: The prior distributions and reaction rates used to inform the prior distributions for the Improved Unified Model for FIX activation by FVIIa.

IX $\overset{XIa}{\rightarrow}$ IXa		
Citation	Rates	Notes
[77]	$K_m = 1.6 \times 10^{-7} M$, $k_{\text{cat}} = 0.183 s^{-1}$	Human factor XI from plasma. Purified factor IX was purchased from Enzyme Research Laboratories, South Bend, IN. Temperature: 37°C.
[87]	$K_m = 2 \times 10^{-6} M$, $k_{\text{cat}} = 0.173 s^{-1}$	Human factors IX and XI from plasma. Temperature: 37°C. pH: 7.5.
[88]	$K_m = 3.1 \times 10^{-7} M$, $k_{\text{cat}} = 0.417 s^{-1}$	Human FXI and FIX. pH: 7.5. Activation of FX and FIX by FXIa (FIX only), TF:VIIa (both) and IXa:VIIIa (FX only).
[89]	$K_m = 3.7 \times 10^{-7} M$, $k_{\text{cat}} = 0.66 s^{-1}$	Human factor XI from plasma activated by bovine FXIIa. Human FIX from plasma. Temperature: 37°C. pH: 7.4.
[90]	$K_m = 3 \times 10^{-7} M$, $k_{\text{cat}} = 2.4 s^{-1}$	Human factors IX and XI. Temperature: 37°C. pH: 7.5.
[45]	$K_m = 4.9 \times 10^{-7} M$, $k_{\text{cat}} = 7.7 s^{-1}$	Human FXI purified from plasma activated by bovine FXIIa. Human factor IX. Temperature: 37°C. pH: 7.5.
Chosen values: $K_m = 0.42 \mu M (10 \wedge N(-6.38, 0.37^2), 5\% = 1.03 \times 10^{-7}, 95\% = 1.70 \times 10^{-6})$, $k_{\text{cat}} = 0.74 s^{-1} (10 \wedge N(-0.13, 0.65^2), 5\% = 6.24 \times 10^{-2}, 95\% = 8.72)$		

Table E.55: The prior distributions and reaction rates used to inform the prior distributions for the Improved Unified Model for FIX activation by FXIa.

VIII $\overset{IIa}{\rightarrow}$ VIIIa		
Citation	Rates	Notes
[66]	$K_m = 1.47 \times 10^{-7} M$, $k_{\text{cat}} = 0.9 s^{-1}$	PCPS (75/25). Porcine factor VIII from plasma. Porcine FIIa. Room temperature. pH: 7. Values given are for cleavage at position 372 which is the rate limiting step.
[47]	$\frac{k_{\text{cat}}}{K_m} = 5 \times 10^6 M^{-1} s^{-1}$	PCPS (25/75) PC (type III-E) and PS purchased from Sigma. Porcine FVIII and FIIa. Temperature: 22°C. pH: 7.4. Also gives activation by Xa.
Chosen values: $K_m = 147 nM (10 \wedge N(-6.83, 2.5^2), 5\% = 1.13 \times 10^{-11}, 95\% = 1.90 \times 10^{-3})$, $k_{\text{cat}} = 0.8 s^{-1} (10 \wedge N(-0.09, 0.06^2), 5\% = 0.64, 95\% = 1.03)$		

Table E.56: The prior distributions and reaction rates used to inform the prior distributions for the Improved Unified Model for FVIII activation by FIIa.

VIII $\overset{Xa}{\rightarrow}$ VIIIa		
Citation	Rates	Notes
[47]	$\frac{k_{\text{cat}}}{K_m} = 1.1 \times 10^6 M^{-1}s^{-1}$	PCPS (25/75) PC (type III-E) and PS purchased from Sigma. Porcine FVIII and FXa. Temperature: 22°C. pH: 7.4. Also gives activation by IIa.
Chosen values: $K_m = 147nM(10 \wedge N(-6.83, 2.5^2), 5\% = 1.13 \times 10^{-11}, 95\% = 1.90 \times 10^{-3}), k_{\text{cat}} = 0.16s^{-1}(10 \wedge N(-0.79, 2.5^2), 5\% = 1.25 \times 10^{-5}, 95\% = 2.10 \times 10^3)$. K_m assumed same as for IIa		

Table E.57: The prior distributions and reaction rates used to inform the prior distributions for the Improved Unified Model for FVIII activation by FXa.

VIIIa $\leftrightarrow$ VIIIa1L + VIIIa2		
Citation	Rates	Notes
[13]	$k_+ = 5.8 \times 10^{-3}s^{-1}$, $K_d = 2.73 \times 10^{-7}M$	PCPS (75/25). Human FVIIIa. Temperature: 22°C. pH: 7.4.
[14]	$K_d = 2.58 \times 10^{-7}M$	Human FVIII from Cutter Division of Miles Laboratories. Temperature: 22°C. pH: 7.4. K_d is heavily pH dependent.
Chosen values: $K_d = 265nM(10 \wedge N(-6.58, 0.02^2), 5\% = 2.49 \times 10^{-7}, 95\% = 2.83 \times 10^{-7}), k_+ = 5.8 \times 10^{-3}s^{-1}(10 \wedge N(-2.24, 2.5^2), 5\% = 4.48 \times 10^{-7}, 95\% = 7.51 \times 10^1)$ therefore $k_- = 2.19 \times 10^4 M^{-1}s^{-1}$ *		

Table E.58: The prior distributions and reaction rates used to inform the prior distributions for the Improved Unified Model for FVIIIa breaking into its long and short sub-units.

IXa:VIIIa $\rightarrow$ VIIIa1L + VIIIa2 + IXa		
Citation	Rates	Notes
[15]	$k = 1.4 \times 10^{-3}s^{-1}$	Fitted using a small model for FIX, FVIII and FX. Recombinant FVIII from Dr. Jim Brown of Bayer Corp. and Debra Pittman of the Genetics Institute. Factors IXa and X from Enzyme Research Laboratories. pH: 7.2.
Chosen values: $k_+ = 1.4 \times 10^{-3}s^{-1}(10 \wedge N(-2.85, 2.5^2), 5\% = 1.09 \times 10^{-7}, 95\% = 1.83 \times 10^1)$		

Table E.59: The prior distributions and reaction rates used to inform the prior distributions for the Improved Unified Model for FVIIIa breaking into its long and short sub-units while it is in the complex IXa:VIIIa.

*k_+ refers to the forwards rate which in this case is the disassociation. This means $K_d = \frac{k_+}{k_-}$.

IXa + VIIIa ↔ IXa:VIIIa		
Citation	Rates	Notes
[11]	$K_d = 2 \times 10^{-9} M$	PCPS (75/25) from PC and PS purchased from Sigma. Porcine FIXa and FVIIIa. Temperature: 25°C. pH: 7.4.
[30]	$K_d = 4 \times 10^{-9} M$	PCPSPE (40/20/40) from Sigma. Recombinant factor VIII gift of the Bayer Corporation. Factor IX from Enzyme Research Laboratories.
[31]	$K_d = 5.5 \times 10^{-10} M$	PCPS (50/50) using synthetic PC and PS purchased from Supelco Inc, Bellefonte, PA. Human FIXa. Human FVIIIa from plasma. Temperature: 37°C. pH: 7.4.
Chosen values: $K_d = 3.5nM(10 \wedge N(-8.45, 0.22^2), 5\% = 1.51 \times 10^{-9}, 95\% = 8.27 \times 10^{-9}), k_+ = 1 \times 10^7 M^{-1}s^{-1}(10 \wedge N(7, 2.5^2), 5\% = 7.72 \times 10^2, 95\% = 1.30 \times 10^{11})^\dagger$ therefore $k_- = 0.035 s^{-1}$		

Table E.60: The prior distributions and reaction rates used to inform the prior distributions for the Improved Unified Model for FIXa and FVIIIa association/dissociation.

IXa + AT → IXa:AT		
Citation	Rates	Notes
[23]	$k = 490 M^{-1}s^{-1}$	Human FIXa, FVIIIa and AT. Absence of heparin ($k = 5 \times 10^6 M^{-1}s^{-1}$ in presence of heparin). Also gives FIIa and FXa. Temperature: 37°C. pH: 7.5.
Chosen values: $k_+ = 490 M^{-1}s^{-1}(10 \wedge N(2.69, 2.5^2), 5\% = 3.78 \times 10^{-2}, 95\% = 6.35 \times 10^6)$		

Table E.61: The prior distributions and reaction rates used to inform the prior distributions for the Improved Unified Model for FIXa inhibition by AT.

$^\dagger k_+$ assumed value of $1 \times 10^7 M^{-1}s^{-1}$.

IXa:VIIIa + AT → IXa:VIIIa:AT		
Citation	Rates	Notes
-	-	No source. Assumed rate using IXa+AT reaction and the ratio of Xa+AT and Xa:Va+AT from [103].
Chosen values: $k_+ = 317M^{-1}s^{-1}(10 \wedge N(2.50, 2.5^2), 5\% = 2.45 \times 10^{-2}, 95\% = 4.11 \times 10^6)$		

Table E.62: The prior distributions and reaction rates used to inform the prior distributions for the Improved Unified Model for IXa:VIIIa inhibition by AT.

E.6 TFPI Module

Model Reactions

This module comprises of the reactions that cover the inhibition of FXa and TF:VIIa by TFPI. The reactions included in previous mathematical models and those in the Unified Model are described in Table E.63 while the former are depicted in Figure E.13 and the latter in Figure E.14. The Improved Unified Model uses identical reactions and reaction rates.

Models	Reactions
Hockin, Danforth, Brummel and Chatterjee	Xa + TFPI ↔ Xa:TFPI TF:VIIa:Xa + TFPI ↔ TF:VIIa:Xa:TFPI TF:VIIa + Xa:TFPI → TF:VIIa:Xa:TFPI
Bungay	Xa_f + $TFPI_f$ ↔ Xa:$TFPI_f$ TF:$VIIa_L$ + Xa:$TFPI_f$ ↔ TF:VIIa:Xa:$TFPI_L$
Tyurin and Zhu	Xa + TFPI → Xa:TFPI TF:VIIa + Xa:TFPI → TF:VIIa:Xa:TFPI
Unified	Xa + TFPI ↔ Xa:TFPI TF:VIIa + Xa:TFPI ↔ TF:VIIa:Xa:TFPI
Improved Unified	Xa + TFPI ↔ Xa:TFPI TF:VIIa + Xa:TFPI ↔ TF:VIIa:Xa:TFPI

Table E.63: The reactions that are used in the different models and our choice of reactions for the TFPI module.

Network Diagrams

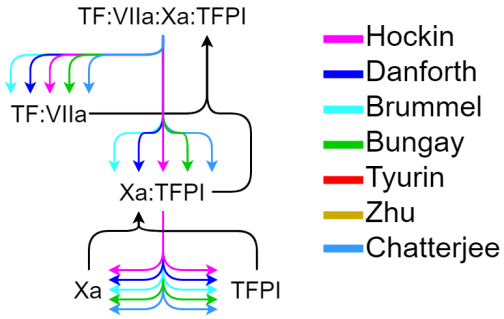

Figure E.13: A network diagram for the TFPI module reactions that are included in previous models.

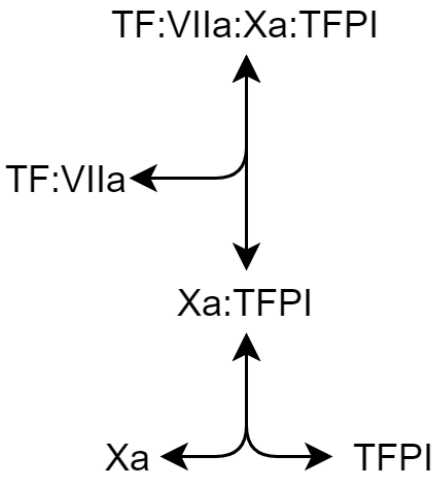

Figure E.14: A reaction diagram for our chosen reactions to be included in the Unified Model and Improved Unified Model for the TFPI module.

Reaction rates for previous models

Reaction	Model	Model values	Data values
Xa + TFPI ↔ Xa:TFPI	Hockin, Danforth, Brummel, Chatterjee	$k_+ = 9 \times 10^5 M^{-1}s^{-1}, k_- = 3.6 \times 10^{-4}s^{-1}$	[20] gives $k_+ = 9 \times 10^5 M^{-1}s^{-1}, k_- = 3.6 \times 10^{-4}s^{-1}$.
	Bungay	$k_+ = 1.6 \times 10^7 M^{-1}s^{-1}, k_- = 3.3 \times 10^{-4}s^{-1}$	[70] gives $k_+ = 1.6 \times 10^7 M^{-1}s^{-1}, k_- = 3.3 \times 10^{-4}s^{-1}$.
	Tyurin, Zhu	$k_+ = 1.6 \times 10^7 M^{-1}s^{-1}$	[70] gives $k_+ = 1.6 \times 10^7 M^{-1}s^{-1}, k_- = 3.3 \times 10^{-4}s^{-1}$.
TF:VIIa + Xa:TFPI ↔ TF:VIIa:Xa:TFPI	Hockin, Danforth, Brummel, Chatterjee	$k_+ = 5 \times 10^7 M^{-1}s^{-1}$	[20] gives $k_+ = 7.34 \times 10^6 M^{-1}s^{-1}, k_- = 1.1 \times 10^{-3}s^{-1}$.
	Bungay-	$k_+ = 1 \times 10^7 M^{-1}s^{-1}, k_- = 1.1 \times 10^{-3}s^{-1}$	[70] gives $k_+ = 1.07 \times 10^7 M^{-1}s^{-1}$ and [20] gives $k_+ = 7.34 \times 10^6 M^{-1}s^{-1}, k_- = 1.1 \times 10^{-3}s^{-1}$.
	Tyurin Zhu	$k_+ = 1.1 \times 10^7 M^{-1}s^{-1}$	[70] gives $k_+ = 1.07 \times 10^7 M^{-1}s^{-1}$.
TF:VIIa:Xa + TFPI ↔ TF:VIIa:Xa:TFPI	Hockin, Danforth, Brummel	$k_+ = 3.2 \times 10^8 M^{-1}s^{-1}, k_- = 1.1 \times 10^{-4}s^{-1}$	Unclear how these rates were chosen. The cited source, [20], suggests equivalent to Xa and TFPI binding ie $k_+ = 9 \times 10^5 M^{-1}s^{-1}, k_- = 3.6 \times 10^{-4}s^{-1}$ based on scheme 2 description.

Chatterjee	$k_+ = 3.2 \times 10^8 M^{-1} s^{-1}, k_- = 1.1 \times 10^{-2} s^{-1}$	Hockin value multiplied by 100 based on: Data from [20] suggests that the original data fitting for the reaction produces a complex that binds too strongly.

Table E.64: The parameter values used by each of the models along with the accompanying reference and original data value for each of the reactions in the TFPI module.

Choosing Parameters

There are no changes between the Unified Model reaction rates and the Improved Unified Model reaction rates for this module. Below gives the sources and prior distributions for both models.

Xa + TFPI ↔ Xa:TFPI		
Citation	Rates	Notes
[20]	$K_d = 0.4nM$, $k_+ = 9 \times 10^5 M^{-1}s^{-1}$, $k_- = 3.6 \times 10^{-4}s^{-1}$	Human factor X from plasma activated by RVV. Recombinant full length TFPI. Ambient temperature (estimated at 23±2°C). pH: 7.5.
[70]	$K_d = 21pM$, $k_+ = 1.6 \times 10^7 M^{-1}s^{-1}$, $k_- = 3.3 \times 10^{-4}s^{-1}$	Human factor X from Charles Heldebrant of Alpha Therapeutics. Recombinant TFPI. Temperature: 25°C. pH: 7.5.
Chosen values: $K_d = 92pM(10 \wedge N(-10.03, 0.90^2), 5\% = 3.09 \times 10^{-12}, 95\% = 2.82 \times 10^{-9}), k_+ = 3.8 \times 10^6 M^{-1}s^{-1}(10 \wedge N(6.58, 0.88^2), 5\% = 1.36 \times 10^5, 95\% = 1.07 \times 10^8)$ therefore $k_- = 3.5 \times 10^{-4}s^{-1}$		

Table E.65: The prior distributions and reaction rates used to inform the prior distributions for both the Unified Model and the Improved Unified Model for FXa and TFPI association/dissociation.

TF:VIIa + Xa:TFPI ↔ TF:VIIa:Xa:TFPI		
Citation	Rates	Notes
[20]	$K_d = 0.15nM$, $k_+ = 7.34 \times 10^6 M^{-1}s^{-1}$, $k_- = 1.1 \times 10^{-3}s^{-1}$	Recombinant human TF a gift from from Genentech, South San Francisco, CA reconstituted into PCPS (75/25) hen egg PC and bovine brain PS purchased from Sigma. Human factor X from plasma activated by RVV. Recombinant human factor VIIa purchased from Novo-Nordisk, Gentofte, Denmark. Recombinant full length TFPI. Ambient temperature (estimated at 23±2°C). pH: 7.5.
[70]	$k_+ = 1.07 \times 10^7 M^{-1}s^{-1}$	Recombinant human TF relipidated into PCPS (70/30) from Sigma. PCPS (50/50) vesicles. Human factor X Charles Heldebrant of Alpha Therapeutics. Recombinant human factor VIIa was supplied by Novo Nordisk, Bagsvaerd, Denmark. Recombinant TFPI. Temperature: 37°C. pH: 7.5.
Chosen values: $K_d = 0.15nM(10 \wedge N(-9.82, 2.5^2), 5\% = 1.17 \times 10^{-14}, 95\% = 1.96 \times 10^{-6}), k_+ = 8.9 \times 10^6 M^{-1}s^{-1}(10 \wedge N(6.95, 0.12^2), 5\% = 5.66 \times 10^6, 95\% = 1.40 \times 10^7)$ therefore $k_- = 1.3 \times 10^{-3}s^{-1}$		

Table E.66: The prior distributions and reaction rates used to inform the prior distributions for both the Unified Model and the Improved Unified Model for Xa:TFPI and TF:VIIa association/dissociation.

E.7 Other Inhibitors Module

Model Reactions

This module is only relevant for the Improved Unified Model and is not included in the previous versions. This module comprises of the reactions of inhibitors (other than AT and TFPI). The reactions used in the models we have examined are given in Table E.67 as well as the reactions that we have chosen to try to encompass all the effects.

Models	Reactions
Tyurin	IIa + α1-AT → IIa:α1-AT
	Xa + α1-AT → Xa:α1-AT
	Xa:Va + α1-AT → Xa:α1-AT + Va
	XIa + α1-AT → XIa:α1-AT
	XIa + α2-AP → XIa:α2-AP
	IIa + α2-M → IIa:α2-M
	XIa + PAI-1 → XIa:PAI-1

	XIa + C1-inh → XIa:C1-inh
Zhu	IIa + α1-AT → IIa:α1-AT
	Xa + α1-AT → Xa:α1-AT
	XIa + α1-AT → XIa:α1-AT
	XIa + α2-AP → XIa:α2-AP
	IIa + α2-M → IIa:α2-M
	XIa + PAI-1 → XIa:PAI-1
	XIa + C1-inh → XIa:C1-inh
Chatterjee	XIa + α1-AT → XIa:α1-AT
	XIa + α2-AP → XIa:α2-AP
	XIa + C1-inh → XIa:C1-inh
Improved Unified	IIa + α1-AT → IIa:α1-AT
	Xa + α1-AT → Xa:α1-AT
	Xa:Va + α1-AT → Xa:α1-AT + Va
	XIa + α1-AT → XIa:α1-AT
	XIa + α2-AP → XIa:α2-AP
	IIa + α2-M → IIa:α2-M
	XIa + PAI-1 → XIa:PAI-1
	XIa + C1-inh → XIa:C1-inh

Table E.67: The reactions that are used in the different models and our choice of reactions for the Inhibitors module.

Reaction rates for previous models

Reaction	Model	Model values	Data values
IIa + α1-AT $\rightarrow$ IIa:α1-AT	Tyurin, Zhu	$78.3 M^{-1}s^{-1}$	Used in [101]. Averaged: [99] gives $108.5 M^{-1}s^{-1}$, [100] gives $48 M^{-1}s^{-1}$.
Xa + α1-AT $\rightarrow$ Xa:α1-AT	Tyurin, Zhu	$262 M^{-1}s^{-1}$	[103] gives $262 M^{-1}s^{-1}$.
Xa:Va + α1-AT $\rightarrow$ Xa:α1-AT + Va	Tyurin	$262 M^{-1}s^{-1}$	[103] reports same as for FXa.
XIa + α1-AT $\rightarrow$ XIa:α1-AT	Tyurin, Zhu	$66.7 M^{-1}s^{-1}$	[104] gives $68 M^{-1}s^{-1}$.
	Chatterjee	$100 M^{-1}s^{-1}$	[44] gives $100 M^{-1}s^{-1}$.
XIa + α2-AP $\rightarrow$ XIa:α2-AP	Tyurin, Zhu	$500 M^{-1}s^{-1}$	[104] gives $1000 M^{-1}s^{-1}$, and also reports a reduced in rate of inhibition when in the presence of HMWK (at a factor of around 1/2 for C1-inh).
	Chatterjee	$4.3 \times 10^3 M^{-1}s^{-1}$	[44] gives $4.3 \times 10^2 M^{-1}s^{-1}$.
IIa + α2-M $\rightarrow$ IIa:α2-M	Tyurin, Zhu	$488 M^{-1}s^{-1}$	[99] gives $488 M^{-1}s^{-1}$ (Zhu reports using [100] however this source does not provide a value for α2-M on IIa and Zhu likely used [99] instead).
XIa + PAI-1 $\rightarrow$ XIa:PAI-1	Tyurin, Zhu	$2.1 \times 10^5 M^{-1}s^{-1}$	[105] gives $2.1 \times 10^5 M^{-1}s^{-1}$.

XIa + C1-inh → XIa:C1-inh	Tyurin, Zhu	$16.7 M^{-1}s^{-1}$	[104] gives $667 M^{-1}s^{-1}$, and also reports a reduced in rate of inhibition when in the presence of HMWK (at a factor of around 1/2 for C1-inh). [101] reduced this rate more than others when accounting for HMWK but it is not clear why.
	Chatterjee	$1.8 \times 10^3 M^{-1}s^{-1}$	[44] gives $1.8 \times 10^3 M^{-1}s^{-1}$.

Table E.68: The parameter values used by each of the models along with the accompanying reference and original data value for each of the reactions in the Inhibitors module.

Choosing Parameters

IIa + α1-AT $\rightarrow$ IIa:α1-AT		
Citation	Rates	Notes
[99]	$108.5 M^{-1}s^{-1}$	Human thrombin activated by a mixture of human and bovine factors. pH: 7.4. Temperature: 37°C.
[100]	$48 M^{-1}s^{-1}$	Human α1-AT and FIIa. pH: 8. Temperature: 25°C.
Chosen values: $k_+ = 72 M^{-1}s^{-1}(10 \wedge N(1.86, 0.25^2), 5\% = 23, 95\% = 223)$		

Table E.69: The prior distributions and reaction rates used to inform the prior distributions for the Improved Unified Model for FIIa inhibition by α1-AT. These reactions are not part of the Unified Model.

Xa + α1-AT $\rightarrow$ Xa:α1-AT		
Citation	Rates	Notes
[103]	$262 M^{-1}s^{-1}$	RVV from Sigma. Human FX and α1-AT with FX being activated by RVV. pH: 7.4. Temperature: 37°C.
Chosen values: $k_+ = 262 M^{-1}s^{-1}(10 \wedge N(2.42, 2.5^2), 5\% = 3 \times 10^{-3}, 95\% = 2.1 \times 10^7)$		

Table E.70: The prior distributions and reaction rates used to inform the prior distributions for the Improved Unified Model for FXa inhibition by α1-AT. These reactions are not part of the Unified Model.

Xa:Va + α1-AT $\rightarrow$ Xa:α1-AT + Va		
Citation	Rates	Notes
[103]	$262 M^{-1}s^{-1}$	Bovine brain PS, PC and RVV from Sigma. Human FX and α1-AT with FX being activated by RVV. Bovine FV activated by human FIIa. pH: 7.4. Temperature: 37°C.
Chosen values: $k_+ = 262 M^{-1}s^{-1}(10 \wedge N(2.42, 2.5^2), 5\% = 3 \times 10^{-3}, 95\% = 2.1 \times 10^7)$		

Table E.71: The prior distributions and reaction rates used to inform the prior distributions for the Improved Unified Model for Xa:Va inhibition by α1-AT. These reactions are not part of the Unified Model.

XIa + α1-AT $\rightarrow$ XIa:α1-AT		
Citation	Rates	Notes
[104]	$66.7 M^{-1}s^{-1}$	Human FXI from plasma. Temperature: 37°C.
[44]	$100 M^{-1}s^{-1}$	Purified FXIa from Kordia Laboratory Supplies, Leiden, The Netherlands. α1-AT from Calbiochem. pH: 7.4. Temperature: 37°C.
Chosen values: $k_+ = 82 M^{-1}s^{-1}(10 \wedge N(1.91, 0.12^2), 5\% = 47, 95\% = 143)$		

Table E.72: The prior distributions and reaction rates used to inform the prior distributions for the Improved Unified Model for FXIa inhibition by α1-AT. These reactions are not part of the Unified Model.

XIa + α2-AP $\rightarrow$ XIa:α2-AP		
Citation	Rates	Notes
[104]	$1000 M^{-1}s^{-1}$	[122] (pH: 7.5. Temperature: 37°C) reported that at physiological concentrations α2-AP inhibits the same amount of FXIa as C1-inh. [104] then calculates what value this should be using their value for C1-inh inhibition of FXIa.
[44]	$4.3 \times 10^2 M^{-1}s^{-1}$	Purified FXIa from Kordia Laboratory Supplies, Leiden, The Netherlands. α2-AP from Calbiochem. pH: 7.4. Temperature: 37°C.
Chosen values: $k_+ = 656 M^{-1}s^{-1}(10 \wedge N(2.82, 0.26^2), 5\% = 204, 95\% = 2112)$		

Table E.73: The prior distributions and reaction rates used to inform the prior distributions for the Improved Unified Model for FXIa inhibition by α2-AP. These reactions are not part of the Unified Model.

IIa + α2-M $\rightarrow$ IIa:α2-M		
Citation	Rates	Notes
[99]	$488 M^{-1}s^{-1}$	Human thrombin activated by a mixture of human and bovine factors. Human α2-M from Dr. Margaret Hunter (Institute of Science and Technology, University of Michigan). pH: 7.4. Temperature: 37°C.
Chosen values: $k_+ = 488 M^{-1}s^{-1}(10 \wedge N(2.69, 2.5^2), 5\% = 6.1 \times 10^{-3}, 95\% = 3.9 \times 10^7)$		

Table E.74: The prior distributions and reaction rates used to inform the prior distributions for the Improved Unified Model for FIIa inhibition by α2-M. These reactions are not part of the Unified Model.

XIa + PAI-1 → XIa:PAI-1		
Citation	Rates	Notes
[105]	$2.1 \times 10^5 M^{-1}s^{-1}$	Purified human PAI-1 and FXIa. pH: 8.2. Temperature: 37°C.
Chosen values: $k_+ = 2.1 \times 10^5 M^{-1}s^{-1}(10 \wedge N(5.32, 2.5^2), 5\% = 2.64, 95\% = 1.67 \times 10^{10})$		

Table E.75: The prior distributions and reaction rates used to inform the prior distributions for the Improved Unified Model for FXIa inhibition by PAI-1. These reactions are not part of the Unified Model.

XIa + C1-inh → XIa:C1-inh		
Citation	Rates	Notes
[104]	$667 M^{-1}s^{-1}$	C1-inh from Dr. Milan Wickerhauser. Human FXI from plasma. Temperature: 37°C.
[44]	$1.8 \times 10^3 M^{-1}s^{-1}$	Purified FXIa from Kordia Laboratory Supplies, Leiden, The Netherlands. C1-inh from Behringwerke AG, Marburg, Germany. pH: 7.4. Temperature: 37°C.
Chosen values: $k_+ = 1096 M^{-1}s^{-1}(10 \wedge N(3.04, 0.30^2), 5\% = 277, 95\% = 4337)$		

Table E.76: The prior distributions and reaction rates used to inform the prior distributions for the Improved Unified Model for FXIa inhibition by C1-inh. These reactions are not part of the Unified Model.

E.8 Fibrinogen Module

Model Reactions

This module is only relevant for the Improved Unified Model and is not included in the previous versions. This module comprises of the reactions that cover the activation of fibrinogen (FI) by FIIa. The reactions used in the models we have examined are given in Table E.77 as well as the reactions that we have chosen to try to encompass all the effects. Only 2 models use fibrinogen, with only the Chatterjee model using Mass Action law to incorporate the competitive inhibition effect. The implementation of fibrinogen given in the Chatterjee model is derived from another model [51]. Our assay restricts fibrin monomers from binding together so reactions involving $(Fbn1)_2$ and $(Fbn2)_2$ are dropped for our model.

Models	Reactions
	Fbg + IIa ↔ Fbg:IIa
	Fbg:IIa → Fbn1 + IIa + FPA
	Fbn1 + IIa ↔ Fbn1:IIa
	Fbn1:IIa → Fbn2 + IIa + FPB
Chatterjee	

	Fbn1 + Fbn1 $\leftrightarrow$ $(Fbn1)_2$
	$(Fbn1)_2$ + IIa $\leftrightarrow$ $(Fbn1)_2$:IIa
	$(Fbn1)_2$:IIa $\rightarrow$ $(Fbn2)_2$ + IIa + FPB
	Fbn2 + IIa $\leftrightarrow$ Fbn2:IIa
	$(Fbn1)_2$:IIa + AT $\rightarrow$ $(Fbn1)_2$:IIa:AT
	Fbn1:IIa + AT $\rightarrow$ Fbn1:IIa:AT
	Fbn2:IIa + AT $\rightarrow$ Fbn2:IIa:AT
Zhu	I $\overset{IIa}{\rightarrow}$ Ia
	Fbg + IIa $\leftrightarrow$ Fbg:IIa
	Fbg:IIa $\rightarrow$ Fbn1 + IIa + FPA
	Fbn1 + IIa $\leftrightarrow$ Fbn1:IIa
Improved Unified	Fbn1:IIa $\rightarrow$ Fbn2 + IIa + FPB
	Fbn2 + IIa $\leftrightarrow$ Fbn2:IIa
	Fbn1:IIa + AT $\rightarrow$ Fbn1:IIa:AT
	Fbn2:IIa + AT $\rightarrow$ Fbn2:IIa:AT

Table E.77: The reactions that are used in the different models and our choice of reactions.

Reaction rates for previous models

The fibrinogen model [51] features fibrinogen activation which can be included directly into the model as well as inhibition of fibrin-bound FIIa by AT. For the inhibition, the model describes a reduction in reaction rate for inhibition of Fbn2:IIa compared to the others, but because the models free inhibition of FIIa by AT is larger than that used by our models, the rate cannot be directly included (this is the reason AT inhibitions of the fibrin-IIa complexes are not included in the Expanded Fibrinogen model). The original source for this discovery [54] found that the inhibition of Fbn2:IIa is 1.6× slower than that of free FIIa so we have used this ratio instead to derive our own rate. The original sources for these reaction rates are reported in Table D.3.

Reaction	Rate	Prior	5%	95%
Fbg + IIa $\rightarrow$ Fbg:IIa	$1 \times 10^8 M^{-1}s^{-1}$	$10 \wedge N(8, 1.5^2)$	1.15×10^5	8.71×10^{10}
Fbg + IIa $\leftarrow$ Fbg:IIa	$636s^{-1}$	$10 \wedge N(2.80, 1.5^2)$	0.724	5.50×10^5
Fbg:IIa $\rightarrow$ Fbn1 + IIa + FPA	$84s^{-1}$	$10 \wedge N(1.92, 1.5^2)$	9.55×10^5	7.24×10^4
Fbn1 + IIa $\rightarrow$ Fbn1:IIa	$1 \times 10^8 M^{-1}s^{-1}$	$10 \wedge N(8, 1.5^2)$	1.15×10^5	8.71×10^{10}
Fbn1 + IIa $\leftarrow$ Fbn1:IIa	$742.6s^{-1}$	$10 \wedge N(2.87, 1.5^2)$	0.851	6.46×10^5
Fbn1:IIa $\rightarrow$ Fbn2 + IIa + FPB	$7.45s^{-1}$	$10 \wedge N(0.87, 1.5^2)$	8.51×10^{-3}	6.46×10^3
Fbn2 + IIa $\rightarrow$ Fbn2:IIa	$1 \times 10^8 M^{-1}s^{-1}$	$10 \wedge N(8, 1.5^2)$	1.15×10^5	8.71×10^{10}
Fbn2 + IIa $\leftarrow$ Fbn2:IIa	$1 \times 10^3 M^{-1}s^{-1}$	$10 \wedge N(3, 1.5^2)$	1.15	8.71×10^5
Fbn1:IIa + AT $\rightarrow$ Fbn1:IIa:AT	$6.1 \times 10^3 M^{-1}s^{-1}$	$10 \wedge N(3.79, 1.5^2)$	7.08	5.37×10^6
Fbn2:IIa + AT $\rightarrow$ Fbn2:IIa:AT	$3.8 \times 10^3 M^{-1}s^{-1}$	$10 \wedge N(3.58, 1.5^2)$	4.37	3.31×10^6

Table E.78: The reaction rates, with priors, 5th and 95th percentiles, for the fibrinogen module reactions.

Appendix F

Unified Model Sensitivity Analysis

We have conducted the reaction rate sensitivity described in Section 2.5 on the Improved Unified Model with the gradient descent fitted rates found at the end of Chapter 6 (when all reaction rates were fitted). In order to implement the original sensitivity analysis method, the reactions in the Fibrinogen and Other Inhibitor modules were removed, as was done with similar reactions in Section 2.5. The rates are perturbed in the mass action form and the sensitivity of enzymatic activations is taken as the maximum sensitivity of the mass action reactions of which it is comprised. We did keep in the reactions for the chromogenic substrate, since removing it dramatically alters model predictions to the point of making sensitivity analysis results without it uninformative. Due to this, the thrombin generation curve on which we calculate the summary statistics was given as the thrombin concentration plus the additional thrombin which is bound to the chromogenic substrate. The resulting sensitivity distribution is given by Figure F.1.

Compared with the results from the previous models, described in Section 2.5, the main points that stand out for the Improved Unified Model are:

- Initiation is predominantly driven by the feedback loop between TF:VIIa and FXa, the same reactions explored in Section 5.4.
- The model is incredibly sensitive to the reaction rates for the chromogenic substrate.
- The model is very insensitive to reactions involving FXI, in particular, its auto-activation.

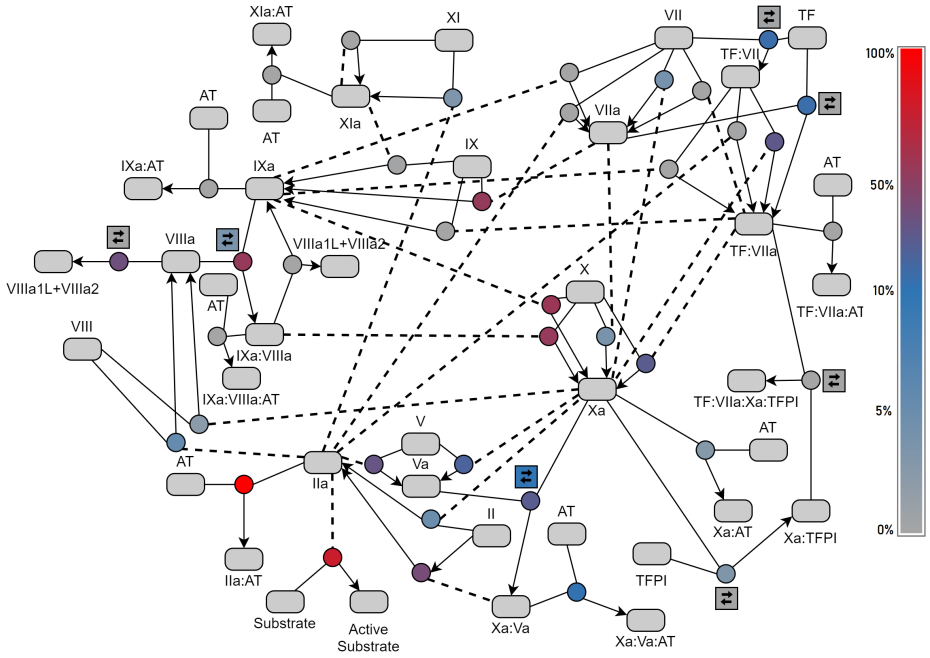

Figure F.1: The reaction rate sensitivity analysis results for the Improved Unified Model, given as a network diagram coloured by sensitivity as a proportion of the most sensitive reaction rate. Sensitive reactions are coloured in red, while insensitive reactions are given in grey. Reactions with an average level of sensitivity ($\approx 10\%$) are coloured in blue.

Bibliography

[1] O'Brien DP, Kemball-Cook G, Hutchinson AM, Martin DMA, Johnson DJD, Byfield PGH, Takamiya O, Tuddenham EGD, McVey JH. Surface plasmon resonance studies of the interaction between factor VII and tissue factor. Demonstration of defective tissue factor binding in a variant FVII molecule (FVII-R79Q). *Biochemistry*. 1994; 33(47): 14162–14169. DOI: 10.1021/bi00251a027.

[2] Krishnaswamy S. The interaction of human factor VIIa with tissue factor. *Journal of Biological Chemistry*. 1992; 267(33): 23696–23706. DOI: 10.1016/S0021-9258(18)35894-0.

[3] Shobe J, Dickinson CD, Edgington TS, Ruf W. Macromolecular substrate affinity for the tissue factor-factor VIIa complex is independent of scissile bond docking. *Journal of Biological Chemistry*. 1999; 274(34): 24171–24175. DOI: 10.1074/jbc.274.34.24171.

[4] Butenas S, Mann KG. Kinetics of human factor VII activation. *Biochemistry*. 1996; 35(6): 1904–1910. DOI: 10.1021/bi951768c.

[5] Baugh RJ, Krishnaswamy S. Role of the activation peptide domain in human factor X activation by the extrinsic Xase complex. *Journal of Biological Chemistry*. 1996; 271(27): 16126–16134. DOI: 10.1074/jbc.271.27.16126.

[6] Baugh RJ, Dickinson CD, Ruf W, Krishnaswamy S. Exosite interactions determine the affinity of factor X for the extrinsic Xase complex. *Journal of Biological Chemistry*. 2000; 275(37): 28826–28833. DOI: 10.1074/jbc.M005266200.

[7] Zur M, Nemerson Y. Kinetics of factor IX activation via the extrinsic pathway: Dependence on Km on tissue factor. *Journal of Biological Chemistry*. 1980; 255(12): 5703–5707. DOI: 10.1016/S0021-9258(19)70686-3.

[8] Jones KC, Mann KG. A model for the tissue factor pathway to thrombin. II. A mathematical simulation. *Journal of Biological Chemistry*. 1994; 269(37): 23367–23373. DOI: 10.1016/S0021-9258(17)31662-9.

[9] Bom VJ, van Hinsbergh VW, Reinalda-Poot HH, Mohanlal RW, Bertina RM. Extrinsic activation of human coagulation factors IX and X on the endothelial surface. *Thrombosis and Haemostasis*. 1991; 66(3): 283–291. DOI: 10.1055/s-0038-1646408.

[10] Orfeo T, Brufatto N, Nesheim ME, Xu H, Butenas S, Mann KG. The factor V activation paradox. *Journal of Biological Chemistry*. 2004; 279(19): 19580–19591. DOI: 10.1074/jbc.M400727200.

[11] Duffy E, Parker E, Mutucumarana V, Johnson A, Lollar P. Binding of factor VIIIa and factor VIII to factor IXa on phospholipid vesicles. *Journal of Biological Chemistry*. 1992; 267(24): 17006–17011. DOI: 10.1016/S0021-9258(18)41885-6.

[12] van Dieijen G, Tans G, Rosing J, Hemker H. The role of phospholipid and factor VIIIa in the activation of bovine factor X. *Journal of Biological Chemistry*. 1981; 256(7): 3433–3442. DOI: 10.1016/S0021-9258(19)69627-4.

[13] Lollar P, Parker ET, Fay PJ. Coagulant properties of hybrid human/porcine factor VIII molecules. *Journal of Biological Chemistry*. 1992; 267(33): 23652–23657. DOI: 10.1016/S0021-9258(18)35888-5.

[14] Fay PJ, Smudzin TM. Characterization of the interaction between the A2 subunit and A1/A3-C1-C2 dimer in human factor VIII(a). *Journal of Biological Chemistry*. 1992; 267(19): 13246–13250. DOI: 10.1016/S0021-9258(18)42201-6.

[15] Fay PJ, Beattie TL, Regan LM, O'Brien LM, Kaufman RJ. Model for the factor VIIIa-dependent decay of the intrinsic factor Xase: Role of subunit dissociation and factor IXa-catalyzed proteolysis. *Journal of Biological Chemistry*. 1996; 271(11): 6027–6032. DOI: 10.1074/jbc.271.11.6027.

[16] Monkovic DD, Tracy PB. Activation of human factor V by factor Xa and thrombin. *Biochemistry*. 1990; 29(5): 1118–1128. DOI: 10.1021/bi00457a004.

[17] Krishnaswamy S, Jones KC, Mann KG. Prothrombinase complex assembly. Kinetic mechanism of enzyme assembly on phospholipid vesicles. *Journal of Biological Chemistry*. 1988; 263(8): 3823–3834. DOI: 10.1016/S0021-9258(18)68999-9.

[18] Silverberg SA, Nemerson Y, Zur M. Kinetics of the activation of bovine coagulation factor X by components of the extrinsic pathway. Kinetic behavior of two-chain factor VII in the presence and absence of tissue factor. *Journal of Biological Chemistry*. 1977; 252(23): 8481–8488. DOI: 10.1016/S0021-9258(19)75245-4.

[19] Lawson JH, Kalafatis M, Stram S, Mann KG. A model for the tissue factor pathway to thrombin. I. An empirical study. *Journal of Biological Chemistry*. 1994; 269(37): 23357–23366. DOI: 10.1016/S0021-9258(17)31661-7.

[20] Baugh RJ, Broze Jr GJ, Krishnaswamy S. Regulation of extrinsic pathway factor Xa formation by tissue factor pathway inhibitor. *Journal of Biological Chemistry*. 1998; 273(8): 4378–4386. DOI: 10.1074/jbc.273.8.4378.

[21] Chuang YJ, Swanson R, Raja SM, Olson ST. Heparin enhances the specificity of antithrombin for thrombin and factor Xa independent of the reactive center loop sequence. Evidence for an exosite determinant of factor Xa specificity in heparin-activated antithrombin. *Journal of Biological Chemistry*. 2001; 276(18): 14961–14971. DOI: 10.1074/jbc.M011550200.

[22] Schoen P, Lindhout T. The in situ inhibition of prothrombinase-formed human α-thrombin and meizothrombin(des F1) by antithrombin III and heparin. *Journal of Biological Chemistry*. 1987; 262(23): 11268–11274. DOI: 10.1016/S0021-9258(18)60954-8.

[23] Jordan RE, Oosta GM, Gardner WT, Rosenberg RD. The kinetics of hemostatic enzyme-antithrombin interactions in the presence of low molecular weight heparin. *Journal of Biological Chemistry*. 1980; 255(21): 10081–10090. DOI: 10.1016/S0021-9258(19)70431-1.

[24] Lawson JH, Butenas S, Ribarik N, Mann KG. Complex-dependent inhibition of factor VIIa by antithrombin III and heparin. *Journal of Biological Chemistry*. 1993; 268(2): 767–770. DOI: 10.1016/S0021-9258(18)53998-3.

[25] Rawala-Sheikh R, Ahmad SS, Ashby B, Walsh PN. Kinetics of coagulation factor X activation of platelet-bound factor IXa. *Biochemistry*. 1990; 29(10): 2606–2611. DOI: 10.1021/bi00462a025.

[26] Butenas S, Orfeo T, Gissel MT, Brummel KE, Mann KG. The significance of circulating factor IXa in blood. *Journal of Biological Chemistry*. 2004; 279(22): 22875–22882. DOI: 10.1074/jbc.M400531200.

[27] Hockin MF, Jones KC, Everse SJ, Mann KG. A model for the stoichiometric regulation of blood coagulation. *Journal of Biological Chemistry*. 2002; 277(21): 18322–18333. DOI: 10.1074/jbc.M201173200.

[28] Bach R, Gentry R, Nemerson Y. Factor VII binding to tissue factor in reconstituted phospholipid vesicles: Induction of cooperativity by phosphatidylserinet. *Biochemistry*. 1986; 25(14): 4007–4020. DOI: 10.1021/bi00362a005.

[29] Shaw AW, Pureza VS, Sligar SG, Morrissey JH. The local phospholipid environment modulates the activation of blood clotting. *Journal of Biological Chemistry*. 2007; 282(9): 6556–6563. DOI: 10.1074/jbc.M607973200.

[30] Jenkins PV, Dill JL, Zhou Q, Fay PJ. Contribution of factor VIIIa A2 and A3-C1-C2 subunits to the affinity for factor IXa in factor Xase. *Biochemistry*. 2004; 43(17): 5094–5101. DOI: 10.1021/bi036289p.

[31] Neuenschwander P, Jesty J. A comparison of phospholipid and platelets in the activation of human factor VIII by thrombin and factor Xa, and in the activation of factor X. *Blood*. 1988; 72(5): 1761–1770. DOI: 10.1182/blood.v72.5.1761.bloodjournal7251761.

[32] Fay PJ, Mastri M, Koszelak ME. Factor VIIIa cofactor activity shows enhanced ionic strength sensitivity in the absence of phospholipid. *Biochimica et Biophysica Acta*. 2001; 1548(1): 159–168. DOI: 10.1016/S0167-4838(01)00225-4.

[33] Lindhout T, Govers-Riemslag JW, van de Waart P, Hemker HC, Rosing J. Factor Va-factor Xa interaction. effects of phospholipid vesicles of varying composition. *Biochemistry*. 1982; 21(22): 5494–5502. DOI: 10.1021/bi00265a018.

[34] Rosing J, Tans G, Govers-Riemslag JW, Zwaal RF, Hemker HC. The role of phospholipids and factor Va in the prothrombinase complex. *Journal of Biological Chemistry*. 1980; 255(1): 274–283. DOI: 10.1016/S0021-9258(19)86294-4.

[35] Chatterjee MS, Denney WS, Jing H, Diamond SL. Systems biology of coagulation initiation: Kinetics of thrombin generation in resting and activated human blood. *PLoS Computational Biology*. 2010; 6(9): e1000950. DOI: 10.1371/journal.pcbi.1000950.

[36] Tankersley DL, Finlayson JS. Kinetics of activation and autoactivation of human factor XII. *Biochemistry*. 1984; 23(2): 273–279. DOI: 10.1021/bi00297a016.

[37] Kuharsky AL, Fogelson AL. Surface-mediated control of blood coagulation: The role of binding site densities and platelet deposition. *Biophysical Journal*. 2001; 80(3): 1050–1074. DOI: 10.1016/S0006-3495(01)76085-7.

[38] Tans G, Rosing J, Berrettini M, Lämmle B, Griffin JH. Autoactivation of human plasma prekallikrein. *Journal of Biological Chemistry*. 1987; 262(23): 11308–11314. DOI: 10.1016/S0021-9258(18)60960-3.

[39] van der Graaf F, Kodedam JA, Bouma BN. Inactivation of kallikrein in human plasma. *Journal of Clinical Investigation*. 1983; 71(1): 149–158. DOI: 10.1172/JCI110743.

[40] Hojima Y, Pierce JV, Pisano JJ. Hageman factor fragment inhibitor in corn seeds: Purification and characterization. *Thrombosis Research*. 1980; 20(2): 149–162. DOI: 10.1016/0049-3848(80)90381-3.

[41] Pixley RA, Schapira M, Colman RW. The regulation of human factor XIIa by plasma proteinase inhibitors. *Journal of Biological Chemistry*. 1985; 260(3): 1723–1729. DOI: 10.1016/S0021-9258(18)89653-3.

[42] Gailani D, Broze Jr GJ. Factor XI activation in a revised model of blood coagulation. *Science*. 1991; 253(5022): 909–912. DOI: 10.1126/science.1652157.

[43] Kramoroff A, Nigretto JM. In vitro factor XI activation mechanism according to an optimized model of activated partial thromboplastin time test. *Blood Coagulation and Fibrinolysis*. 2001; 12(4): 289–299. DOI: 10.1097/00001721-200106000-00010.

[44] Wuillemin WA, Eldering E, Citarella F, de Ruig CP, ten Cate H, Hack CE. Modulation of contact system proteases by glycosaminoglycans: Selective enhancement of the inhibition of factor XIa. *Journal of Biological Chemistry*. 1996; 271(22): 12913–12918. DOI: 10.1074/jbc.271.22.12913.

[45] Walsh PN, Bradford H, Sinha D, Piperno JR, Tuszynski GP. Kinetics of the factor XIa catalyzed activation of human blood coagulation factor IX. *Journal of Clinical Investigation*. 1984; 73(5): 1392–1399. DOI: 10.1172/JCI111343.

[46] Wilkinson FH, Ahmad SS, Walsh PN. The factor IXa second epidermal growth factor (EGF2) domain mediates platelet binding and assembly of the factor X activating complex. *Journal of Biological Chemistry*. 2002; 277(8): 5734–5741. DOI: 10.1074/jbc.M107753200.

[47] Lollar P, Knutson GJ, Fass DN. Activation of porcine factor VIII:C by thrombin and factor Xa. *Biochemistry*. 1985; 24(27): 8056–8064. DOI: 10.1021/bi00348a033.

[48] Leipold RJ, Bozarth TA, Racanelli AL, Dicker IB. Mathematical model of serine protease inhibition in the tissue factor pathway to thrombin. *Journal of Biological Chemistry*. 1995; 270(43): 25383–25387. DOI: 10.1074/jbc.270.43.25383.

[49] Komiyama Y, Pedersen AH, Kisiel W. Proteolytic activation of human factors IX and X by recombinant human factor VIIa: Effects of calcium, phospholipids, and tissue factor. *Biochemistry*. 1990; 29(40): 9418–9425. DOI: 10.1021/bi00492a016.

[50] Higgins DL, Lewis SD, Shafer JA. Steady state kinetic parameters for the thrombin-catalyzed conversion of human fibrinogen to fibrin. *Journal of Biological Chemistry*. 1983; 258(15): 9276–9282. DOI: 10.1016/S0021-9258(17)44663-1.

[51] Naski MC, Shafer JA. A kinetic model for the α-thrombin-catalyzed conversion of plasma levels of fibrinogen to fibrin in the presence of antithrombin III. *Journal of Biological Chemistry*. 1991; 266(20): 13003–13010. DOI: 10.1016/S0021-9258(18)98795-8.

[52] Naski MC, Shafer JA. α-thrombin-catalyzed hydrolysis of fibrin I. Alternative binding modes and the accessibility of the active site in fibrin I-bound α-thrombin. *Journal of Biological Chemistry*. 1990; 265(3): 1401–1407. DOI: 10.1016/S0021-9258(19)40028-8.

[53] Lewis SD, Shields PP, Shafer JA. Characterization of the kinetic pathway for liberation of fibrinopeptides during assembly of fibrin. *Journal of Biological Chemistry*. 1985; 260(18): 10192–10199. DOI: 10.1016/S0021-9258(17)39231-1.

[54] Hogg PJ, Jackson CM. Fibrin monomer protects thrombin from inactivation by heparin-antithrombin III: implications for heparin efficacy. *Proceedings of the National Academy of Sciences of the United States of America*. 1989; 86(10): 3619–3623. DOI: 10.1073/pnas.86.10.3619.

[55] Doyle MF, Mann KG. Multiple active forms of thrombin. IV. Relative activities of meizothrombins. *Journal of Biological Chemistry*. 1990; 265(18): 10693–10701. DOI: 10.1016/S0021-9258(18)87002-8.

[56] Côté HC, Bajzar L, Stevens WK, Samis JA, Morser J, MacGillivray RT, Nesheim ME. Functional characterization of recombinant human meizothrombin and meizothrombin(desF1): Thrombomodulin-dependent activation of protein C and thrombin-activatable fibrinolysis inhibitor (TAFI), platelet aggregation, antithrombin-III inhibition. *Journal of Biological Chemistry*. 1997; 272(10): 6194–6200. DOI: 10.1074/jbc.272.10.6194.

[57] Hockin MF, Cawthern KM, Kalafatis M, Mann KG. A model describing the inactivation of factor Va by APC: Bond cleavage, fragment dissociation, and product inhibition. *Biochemistry*. 1999; 38(21): 6918–6934. DOI: 10.1021/bi981966e.

[58] Bravo MC, Orfeo T, Mann KG, Everse SJ. Modeling of human factor Va inactivation by activated protein C. *BMC Systems Biology*. 2012; 6(1): 45. DOI: 10.1186/1752-0509-6-45.

[59] Krishnaswamy S, Russell GD, Mann KG. The reassociation of factor Va from its isolated subunits. *Journal of Biological Chemistry*. 1989; 264(6): 3160–3168. DOI: 10.1016/S0021-9258(18)94045-7.

[60] Egan JO, Kalafatis M, Mann KG. The effect of Arg306 → Ala and Arg506 → Gln substitutions in the inactivation of recombinant human factor Va by activated protein C and protein S. *Protein Science*. 1997; 6(9): 2016–2027. DOI: 10.1002/pro.5560060922.

[61] Nicolaes GA, Tans G, Thomassen MCLGD, Hemker HC, Pabinger I, Varadi K, Schwarz HP, Rosing J. Peptide bond cleavages and loss of functional activity during inactivation of factor Va and factor Va(R506Q) by activated protein C. *Journal of Biological Chemistry*. 1995; 270(36): 21158–21166. DOI: 10.1074/jbc.270.36.21158.

[62] Boskovic DS, Giles AR, Nesheim ME. Studies of the role of factor Va in the factor Xa-catalyzed activation of prothrombin, fragment 1.2-prethrombin-2, and dansyl-L-glutamyl-glycyl-L-arginine-meizothrombin in the absence of phospholipid. *Journal of Biological Chemistry*. 1990; 265(18): 10497–10505. DOI: 10.1016/S0021-9258(18)86975-7.

[63] Nemerson Y. The tissue factor pathway of blood coagulation. *Seminars in Hematology*. 1992; 29(3): 170–176.

[64] Bom VJ, Bertina RM. The contributions of Ca2+, phospholipids and tissue-factor apoprotein to the activation of human blood-coagulation factor X by activated factor VII. *Biochemical Journal*. 1990; 265(2): 327–336. DOI: 10.1042/bj2650327.

[65] Krishnaswamy S, Church WR, Nesheim ME, Mann KG. Activation of human prothrombin by human prothrombinase. Influence of factor Va on the reaction mechanism. *Journal of Biological Chemistry*. 1987; 262(7): 3291–3299. DOI: 10.1016/S0021-9258(18)61503-0.

[66] Hill-Eubanks DC, Lollar P. von Willebrand factor is a cofactor for thrombin-catalyzed cleavage of the factor VIII light chain. *Journal of Biological Chemistry*. 1990; 265(29): 17854–17858. DOI: 10.1016/S0021-9258(18)38242-5.

[67] Baglia FA, Walsh PN. Thrombin-mediated feedback activation of factor XI on the activated platelet surface is preferred over contact activation by factor XIIa or factor XIa. *Journal of Biological Chemistry*. 2000; 275(27): 20514–20519. DOI: 10.1074/jbc.M000464200.

[68] Baglia FA, Walsh PN. Thrombin-mediated feedback activation of factor XI on the activated platelet surface is preferred over contact activation by factor XIIa or factor XIa [retraction of: Baglia FA, Walsh PN. *J Biol Chem.* 2000; 275(27): 20514-9]. *Journal of Biological Chemistry*. 2007; 282(39): 29067. DOI: 10.1016/S0021-9258(20)58640-7.

[69] Solymoss S, Tucker MM, Tracy PB. Kinetics of inactivation of membrane-bound factor Va by activated protein C. Protein S modulates factor Xa protection. *Journal of Biological Chemistry*. 1988; 263(29): 14884–14890. DOI: 10.1016/S0021-9258(18)68121-9.

[70] Jesty J, Wun TC, Lorenz A. Kinetics of the inhibition of factor Xa and the tissue factor-factor VIIa complex by the tissue factor pathway inhibitor in the presence and absence of heparin. *Biochemistry*. 1994; 33(42): 12686–12694. DOI: 10.1021/bi00208a020.

[71] Olson ST, Björk I, Sheffer R, Craig PA, Shore JD, Choay J. Role of the antithrombin-binding pentasaccharide in heparin acceleration of antithrombin-proteinase reactions. Resolution of the antithrombin conformational change contribution to heparin rate enhancement. *Journal of Biological Chemistry*. 1992; 267(18): 12528–12538. DOI: 10.1016/S0021-9258(18)42309-5.

[72] Jesty J. The kinetics of inhibition of thrombin by antithrombin in the presence of components of the hemostatic system. *Blood*. 1985; 66(5): 1189–1195. DOI: 10.1182/blood.v66.5.1189.bloodjournal6651189.

[73] Tans G, Nicolaes GA, Thomassen MC, Hemker HC, van Zonneveld AJ, Pannekoek H, Rosing J. Activation of human factor V by meizothrombin. *Journal of Biological Chemistry*. 1994; 269(23): 15969–15972. DOI: 10.1016/S0021-9258(17)33957-1.

[74] Zwaal RF, Comfurius P, Bevers EM. Lipid-protein interactions in blood coagulation. *Biochimica et Biophysica Acta*. 1998; 1376(3): 433–453. DOI: 10.1016/S0304-4157(98)00018-5.

[75] Galvin JB, Kurosawa S, Moore K, Esmon CT, Esmon NL. Reconstitution of rabbit thrombomodulin into phospholipid vesicles. *Journal of Biological Chemistry*. 1987; 262(5): 2199–2205. DOI: 10.1016/S0021-9258(18)61639-4.

[76] Bungay SD, Gentry PA, Gentry RD. A mathematical model of lipid-mediated thrombin generation. *Mathematical Medicine and Biology*. 2003; 20(1): 105–129. DOI: 10.1093/imammb/20.1.105.

[77] Sun Y, Gailani D. Identification of a factor IX binding site on the third apple domain of activated factor XI. *Journal of Biological Chemistry*. 1996; 271(46): 29023–29028. DOI: 10.1074/jbc.271.46.29023.

[78] Lu Y, Nelsestuen GL. Dynamic features of prothrombin interaction with phospholipid vesicles of different size and composition: Implications for protein-membrane contact. *Biochemistry*. 1996; 35(25): 8193–8200. DOI: 10.1021/bi960280o.

[79] Goldsmith JC, Jafvert CT, Lollar P, Owen WG, Hoak JC. Prostacyclin release from cultured and ex vivo bovine vascular endothelium. Studies with thrombin, arachidonic acid, and ionophore A23187. *Laboratory Investigation*. 1981; 45(2): 191–197.

[80] Gilbert GE, Furie BC, Furie B. Binding of human factor VIII to phospholipid vesicles. *Journal of Biological Chemistry*. 1990; 265(2): 815–822. DOI: 10.1016/S0021-9258(19)40122-1.

[81] van Dieijen G, van Rijn JL, Govers-Riemslag JW, Hemker HC, Rosing J. Assembly of the intrinsic factor X activating complex - Interactions between factor IXa, factor VIIIa and phospholipid. *Thrombosis and Haemostasis*. 1985; 53(3): 396–400. DOI: 10.1055/s-0038-1661322.

[82] Stern DM, Drillings M, Nossel HL, Hurlet-Jensen A, LaGamma KS, Owen J. Binding of factors IX and IX(a) to cultured vascular endothelial cells. *Proceedings of the National Academy of Sciences of the United States of America*. 1983; 80(13): 4119–4123. DOI: 10.1073/pnas.80.13.4119.

[83] van de Waart P, Bruls H, Hemker HC, Lindhout T. Interaction of bovine blood clotting factor Va and its subunits with phospholipid vesicles. *Biochemistry*. 1983; 22(10): 2427–2432. DOI: 10.1021/bi00279a019.

[84] Krishnaswamy S, Williams EB, Mann KG. The binding of activated protein C to factors V and Va. *Journal of Biological Chemistry*. 1986; 261(21): 9684–9693. DOI: 10.1016/S0021-9258(18)67569-6.

[85] Long GL, Lu D, Xie RL, Kalafatis M. Human protein S cleavage and inactivation by coagulation factor Xa. *Journal of Biological Chemistry*. 1998; 273(19): 11521–11526. DOI: 10.1074/jbc.273.19.11521.

[86] Walker FJ. Regulation of activated protein C by protein S. The role of phospholipid in factor Va inactivation. *Journal of Biological Chemistry*. 1981; 256(21): 11128–11131. DOI: 10.1016/S0021-9258(19)68566-2.

[87] Bajaj SP. Cooperative Ca2+ binding to human factor IX. Effects of Ca2+ on the kinetic parameters of the activation of factor IX by factor XIa. *Journal of Biological Chemistry*. 1982; 257(8): 4127–4132. DOI: 10.1016/S0021-9258(18)34695-7.

[88] Warn-Cramer BJ, Bajaj SP. Intrinsic versus extrinsic coagulation. Kinetic considerations. *Biochemical Journal*. 1986; 239(3): 757–762. DOI: 10.1042/bj2390757.

[89] Sinha D, Seaman FS, Walsh PN. Role of calcium ions and the heavy chain of factor XIa in the activation of human coagulation factor IX. *Biochemistry*. 1987; 26(13): 3768–3775. DOI: 10.1021/bi00387a005.

[90] Soons H, Janssen-Claessen T, Hemker HC, Tans G. The effect of platelets in the activation of human blood coagulation factor IX by factor XIa. *Blood*. 1986; 68(1): 140–148. DOI: 10 . 1182 / blood . v68 . 1 . 140 . bloodjournal681140.

[91] Hultin MB. Role of human factor VIII in factor X activation. *Journal of Clinical Investigation*. 1982; 69(4): 950–958. DOI: 10.1172/JCI110534.

[92] Tracy PB, Eide LL, Mann KG. Human prothrombinase complex assembly and function on isolated peripheral blood cell populations. *Journal of Biological Chemistry*. 1985; 260(4): 2119–2124. DOI: 10.1016/S0021-9258(18)89525-4.

[93] Khanin MA, Rakov DV, Kogan AE. Mathematical model for the blood coagulation prothrombin time test. *Thrombosis Research*. 1998; 89(5): 227–232. DOI: 10.1016/S0049-3848(97)00288-0.

[94] Matsushita T, Kojima T, Emi N, Takahashi I, Saito H. Impaired human tissue factor-mediated activity in blood clotting factor VII(Nagoya) (Arg304 → Trp). Evidence that a region in the catalytic domain of factor VII is important for the association with tissue factor. *Journal of Biological Chemistry*. 1994; 269(10): 7355–7363. DOI: 10.1016/S0021-9258(17)37292-7.

[95] Le Bonniec BF, Guinto ER, MacGillivray RT, Stone SR, Esmon CT. The role of thrombin's Tyr-Pro-Pro-Trp motif in the interaction with fibrinogen, thrombomodulin, protein C, antithrombin III, and the Kunitz inhibitors. *Journal of Biological Chemistry*. 1993; 268(25): 19055–19061. DOI: 10.1016/S0021-9258(17)46734-2.

[96] Giesen PL, Willems GM, Hemker HC, Hermens WT. Membrane-mediated assembly of the prothrombinase complex. *Journal of Biological Chemistry*. 1991; 266(28): 18720–18725. DOI: 10.1016/S0021-9258(18)55122-X.

[97] Willems GM, Lindhout T, Hermens WT, Hemker HC. Simulation model for thrombin generation in plasma. *Haemostasis*. 1991; 21(4): 197–207. DOI: 10.1159/000216229.

[98] Björquist P, Boström S. Determination of the kinetic constants of tissue factor/factor VII/factor VIIa and antithrombin/heparin using surface plasmon resonance. *Thrombosis Research*. 1997; 85(3): 225–236. DOI: 10.1016/S0049-3848(97)00007-8.

[99] Downing MR, Bloom JW, Mann KG. Comparison of the inhibition of thrombin by three plasma protease inhibitors. *Biochemistry*. 1978; 17(13): 2649–2653. DOI: 10.1021/bi00606a030.

[100] Beatty K, Bieth J, Travis J. Kinetics of association of serine proteinases with native and oxidized alpha-1-proteinase inhibitor and alpha-1-antichymotrypsin. *Journal of Biological Chemistry*. 1980; 255(9): 3931–3934. DOI: 10.1016/S0021-9258(19)85615-6.

[101] Kogan AE, Kardakov DV, Khanin MA. Analysis of the activated partial thromboplastin time test using mathematical modeling. *Thrombosis Research*. 2001; 101(4): 299–310. DOI: 10.1016/S0049-3848(00)00405-9.

[102] Rezaie AR, Cooper ST, Church FC, Esmon CT. Protein C inhibitor is a potent inhibitor of the thrombin-thrombomodulin complex. *Journal of Biological Chemistry*. 1995; 270(43): 25336–25339. DOI: 10.1074/jbc.270.43.25336.

[103] Ellis V, Scully MF, Kakkar VV. Inhibition of prothrombinase complex by plasma proteinase inhibitors. *Biochemistry*. 1984; 23(24): 5882–5887. DOI: 10.1021/bi00319a030.

[104] Scott CF, Schapira M, James HL, Cohen AB, Colman RW. Inactivation of factor XIa by plasma protease inhibition. Predominant role of α1-protease inhibitor and protective effect of high molecular weight kininogen. *Journal of Clinical Investigation*. 1982; 69(4): 844–852. DOI: 10.1172/JCI110524.

[105] Berrettini M, Schleef RR, España F, Loskutoff DJ, Griffin JH. Interaction of type 1 plasminogen activator inhibitor with the enzymes of the contact activation system. *Journal of Biological Chemistry*. 1989; 264(20): 11738–11743. DOI: 10.1016/S0021-9258(18)80127-2.

[106] Suzuki K, Nishioka J, Kusumoto H, Hashimoto S. Mechanism of inhibition of activated protein C by protein C inhibitor. *Journal of Biochemistry*. 1984; 95(1): 187–195. DOI: 10.1093/oxfordjournals.jbchem.a134583.

[107] Heeb MJ, Griffin JH. Physiologic inhibition of human activated protein C by α1-antitrypsin. *Journal of Biological Chemistry*. 1988; 263(24): 11613–11616. DOI: 10.1016/S0021-9258(18)37825-6.

[108] Dunn J, Silverberg M, Kaplan A. The cleavage and formation of activated human Hageman factor by autodigestion and by kallikrein. *Journal of Biological Chemistry*. 1982; 257(4): 1779–1784. DOI: 10.1016/S0021-9258(19)68105-6.

[109] Griffin JH. Role of surface in surface-dependent activation of Hageman factor (blood coagulation Factor XII). *Proceedings of the National Academy of Sciences of the United States of America*. 1978; 75(4): 1998–2002. DOI: 10.1073/pnas.75.4.1998.

[110] Mannhalter C, Schiffman S, Deutsch E. Phospholipids accelerate factor IX activation by surface bound factor XIa. *British Journal of Haematology*. 1984; 56(2): 261–271. DOI: 10.1111/j.1365-2141.1984.tb03954.x.

[111] Krishnaswamy S, Field KA, Edgington TS, Morrissey JH, Mann KG. Role of the membrane surface in the activation of human coagulation factor X. *Journal of Biological Chemistry*. 1992; 267(36): 26110–26120. DOI: 10.1016/S0021-9258(18)35724-7.

[112] Yang L, Manithody C, Rezaie AR. Activation of protein C by the thrombin-thrombomodulin complex: Cooperative roles of Arg-35 of thrombin and Arg-67 of protein C. *Proceedings of the National Academy of Sciences of the United States of America*. 2006; 103(4): 879–884. DOI: 10.1073/pnas.0507700103.

[113] Lau HK, Rosenberg RD. The isolation and characterization of a specific antibody population directed against the thrombin antithrombin complex. *Journal of Biological Chemistry*. 1980; 255(12): 5885–5893. DOI: 10.1016/S0021-9258(19)70713-3.

[114] de Agostini A, Lijnen HR, Pixley RA, Colman RW, Schapira M. Inactivation of factor XII active fragment in normal plasma. Predominant role of C-1-inhibitor. *Journal of Clinical Investigation*. 1984; 73(6): 1542–1549. DOI: 10.1172/JCI111360.

[115] Olson ST, Sheffer R, Francis AM. High molecular weight kininogen potentiates the heparin-accelerated inhibition of plasma kallikrein by antithrombin: Role for antithrombin in the regulation of kallikrein. *Biochemistry*. 1993; 32(45): 12136–12147. DOI: 10.1021/bi00096a026.

[116] Boström S, Björquist P. Determination of the kinetic constants for the interaction of factor VII/VIIa and tissue factor (TF) using two different methods [Abstract]. *Thrombosis and Haemostasis*. 1995; 73: 1234.

[117] Zarnitsina VI, Pokhilko AV, Ataullakhanov FI. A mathematical model for the spatio-temporal dynamics of intrinsic pathway of blood coagulation. I. The model description. *Thrombosis Research*. 1996; 84(4): 225–236. DOI: 10.1016/S0049-3848(96)00182-X.

[118] Baerga-Ortiz A, Rezaie AR, Komives EA. Electrostatic dependence of the thrombin-thrombomodulin interaction. *Journal of Molecular Biology*. 2000; 296(2): 651–658. DOI: 10.1006/jmbi.1999.3447.

[119] Kremers RMW, Peters TC, Wagenvoord RJ, Hemker HC. The balance of pro- and anticoagulant processes underlying thrombin generation. *Journal of Thrombosis and Haemostasis*. 2015; 13(3): 437–447. DOI: 10.1111/jth.12798.

[120] Omarova F, Rosing J, Bertina RM, Castoldi E. Negatively charged phospholipids stimulate factor XI activation by thrombin. *Thrombosis Update*. 2021; 2: 100022. DOI: 10.1016/j.tru.2020.100022.

[121] Choi SH, Smith SA, Morrissey JH. Polyphosphate is a cofactor for the activation of factor XI by thrombin. *Blood*. 2011; 118(26): 6963–6970. DOI: 10.1182/blood-2011-07-368811.

[122] Saito H, Goldsmith GH, Moroi M, Aoki N. Inhibitory spectrum of α2-plasmin inhibitor. *Proceedings of the National Academy of Sciences of the United States of America*. 1979; 76(4): 2013–2017. DOI: 10.1073/pnas.76.4.2013.